Beta Cell Stress and Heparan Sulfate Proteoglycans in Type 2 Diabetes

Sarita Dhounchak

December 2018

A thesis submitted for the degree of Doctor of Philosophy at
The Australian National University

Declaration

Immunohistochemistry for heparan sulfate, for some heparan sulfate proteoglycan core proteins and islet endocrine hormones (insulin and glucagon) as well as some islet isolations and intraperitoneal injections were performed by Ms Debra Brown. Localisation of FITC-labelled heparin and FITC-labelled PI-88 by confocal microscopy was performed by Ms Sarah Popp. Circulating free fatty acids in the plasma was analysed by Dr Viviane Delghingaro-Augusto. With these exceptions, the data presented in this thesis constitute the original work of the author unless otherwise stated. This thesis contains no material which has been accepted for the award of any other degree or diploma in any university.

Sarita Dhounchak

December 2018

Acknowledgments

I would like to express my sincerest gratitude to my supervisor, A/Prof Charmaine Simeonovic, for providing me with the opportunity to work on such a wonderful project. I would like to provide my thanks for her continuous guidance, support and patience during my research. Her supervision has provided me with research skills, as well as assistance with scientific writing and public speaking. I have greatly appreciated the wealth of feedback I have received from her during my PhD candidature. I would also to like to thank my PhD advisors, Prof Christopher Parish, Prof Christopher Nolan and Dr Harpreet Vohra for their valuable feedback and advice.

I would like to thank all the past and present members of The Simeonovic Group - Diabetes/Transplantation Immunology for creating such a friendly and supportive environment to work in. Ms Sarah Popp and Ms Debra Brown in particular have provided invaluable instruction in the technical skills required for this project. Sarah provided instruction on molecular techniques and performed confocal microscopy for my project. Thanks Sarah for proof reading the Materials and Methods chapter of this thesis. I am grateful to Deb for all of her support and assistance with islet isolations, intraperitoneal injections and immunohistochemistry assays, especially HS staining. Both Sarah and Deb have been very helpful throughout my PhD experience.

Thank you to Ms Cathy Gillespie for her assistance in microscopy, Dr Harpreet Vohra and Mr Michael Devoy for their valuable assistance in flow cytometry techniques. In addition, my thanks go to Ms Anne Prins for her help in histology. This project involved a large amount of flow cytometry experiments and histology work, and without their support my task would have been very difficult. Many thanks to the Australian Phenomics Facility staff for monitoring and taking good care of the mouse strains used in this project.

I would like to thank ANU for awarding me with the Australian Government Research Training Program (RTP) Scholarship. This scholarship has supported me financially during my PhD studies. I would also wish to thank my casual work employers at ANU Medical School, Research School of Biology, Examinations Office and the Australian

Phenomics Facility (Animal Facility and Scientific Projects Team). This employment helped to support me financially in my final year.

I also could not have completed my PhD without the continuous support and encouragement of my friends, Dr Fui Jiun Choong and Dr Mayank Khanna, whom I met during my Master's Year. Fui Jiun and Mayank provided valuable advice based on their PhD experience and proof-read chapters of this thesis. Thilaga, my writing buddy, was always there to listen to my challenges and encourage me to write. I would like to thank my Graduate House friends (especially Yasmin and Belinda), my JCSMR friends and my friends in India (especially Ashima) for their wonderful support in times of need.

Most importantly, I would like to express my sincere gratitude to my family (Papa, Mummy, Situ and Montu) and my partner Robert for their unconditional care and encouragement during my study. My family have gone to great lengths to support my academic endeavours throughout my life, and I will always be grateful for this. Many thanks to Robert for being there for me in all the ups and downs faced during my PhD. I could not have finished without his continuous moral support and encouragement. I appreciate their patience and understanding during my PhD journey.

Last, but not least, I would like to thank everyone who has directly or indirectly helped me in the successful completion of my thesis.

Abstract

Heparan sulfate proteoglycan (HSPG) core proteins and highly sulfated heparan sulfate (HS) are expressed at unusually high levels inside islet beta cells. Intracellular HS plays a critical role in the survival of beta cells and acts as a constitutive non-enzymatic quencher of reactive oxygen species (ROS). Heparanase (Hpse)-mediated degradation of intracellular HS in the beta cells of non-obese diabetic (NOD) mice has been shown to contribute to the development of type 1 diabetes (T1D). This project examines the role of beta cell HS and HSPG core proteins in obese db/db mice during the progression of type 2 diabetes (T2D).

Endoplasmic reticulum (ER) stress contributes to beta cell failure in T2D. Our studies demonstrate that ER stress in the islets of db/db mice correlates with a progressive loss of intra-islet HSPG core proteins and HS during T2D development. The isolation of islets *in vitro* leads to loss of intracellular HS but not HSPG core proteins from islet beta cells. Replacement of the lost HS in the wildtype and db/db beta cells *in vitro* using heparin (a highly sulfated HS analogue) improved cell viability and protected the beta cells from culture- and ROS-induced death (i.e., oxidative stress). Significantly, treatment of db/db mice with the chemical chaperone TUDCA relieved ER stress, improved intra-islet HSPG core proteins, HS and insulin levels, and impaired T2D progression. Similarly, $Ins2^{WT/C96Y}$ Akita mice, an established model of ER stress-mediated diabetes, demonstrated a decline in intra-islet HSPG core proteins, HS and insulin in islet beta cells. In addition, *in vitro* induction of ER stress in MIN6 cells reduced levels of intracellular HSPG core proteins, HS and Hpse (a HS-degrading enzyme) and increased beta cell death. ER stress-induced HS loss was therefore Hpse-independent. Since HS is synthesised directly onto HSPG core proteins, the novel findings in this project indicate that ER stress in db/db beta cells downregulates the production of HSPG core proteins, leading to diminished HS synthesis. As a consequence, beta cells are rendered more highly susceptible to oxidative stress and death.

A chronic low grade inflammation is associated with obesity, insulin resistance and beta cell stress in T2D. An increased proportion of monocytes/inflammatory macrophages in white adipose tissue, confirmed the heightened inflammatory status of db/db mice,

compared to wildtype controls. Importantly, increased cell surface expression of Hpse on myeloid cells was observed in wildtype white adipose tissue (homeostatic inflammation) and db/db white adipose tissue (T2D obesity-induced inflammation) compared to corresponding levels in the circulation. This finding suggests that Hpse plays an important role in the migration of leukocytes from the circulation and across sub-endothelial basement membranes to establish the enhanced adipose tissue inflammation in T2D.

This project has identified the potential for treatment with a heparin-like HS replacer/Hpse inhibitor, chemical chaperone or a combination of both for rescuing T2D beta cell HS, reducing adipose tissue inflammation and promoting beta cell survival/function.

List of Abbreviations

7AAD	7-aminoactinomycin D
AARE	Amino acid response element
AD	Alzheimer's disease
AKT	Protein kinase B
ANOVA	Analysis of variance
APF	Australian Phenomics Facility
ASKI	Apoptosis signal-regulating kinase 1
AT	Adipose tissue
ATF3	Activating transcription factor 3
ATF4	Activating transcription factor 4
ATF6	Activating transcription factor 6
ATM	Adipose tissue macrophage
ATP	Adenosine triphosphate
AUC	Area under the curve
Aβ	Amyloid β
BAP	BiP-associated protein
BCL2	B cell leukemia 2
Bg	Blood glucose
BiP	Immunoglobulin binding protein
BM	Basement membrane
BM	Basement membrane
BSA	Bovine serum albumin
bZIP	Basic leucine zipper domain
C	Control
Ca^{2+}	Calcium
Cal	Calcein
cAMP	Cyclic adenosine monophosphate
CCL2	Chemokine (C-C motif) ligand 2
CCR2	C-C chemokine receptor type 2
cDC	Conventional dendritic cells
cDNA	Complementary DNA

CHOP	C/EBP-homologous protein
CLS	Crown-like structure
Col18	Collagen type XVIII
CPE	Carboxypeptidase E
DC	Dendritic cell
DCF	Dichlorofluorescein
DIO	Diet induced obesity
DR5	Death receptor 5
DTT	Dithiothreitol
ECM	Extracellular matrix
EDEM	ER degradation-enhancing α-mannosidase-like protein
eIF2α	Eukaryotic translational initiation factor 2
ELISA	Enzyme-linked immunosorbent assay
EPAC	Exchange protein directly activated by cAMP
ER	Endoplasmic reticulum
ERAD	ER-associated degradation
ERO1	ER oxidoreductin
ERSE	ER stress response element
EXT	Exostosin
EXTL	Exostosin-like
FA	Fatty acid
FFA	Free fatty acid
FGF	Fibroblast growth factor
FGFR	Fibroblast growth factor receptor
FITC	Fluorescein isothiocyanate
FPG	Fasting plasma glucose
GADD34	Growth arrest and DNA damage 34
GAPDH	Glyceraldehyde 3-phosphate dehydrogenase
GBM	Glomerular basement membrane
GlcA	Glucuronic acid
GlcNAc	N-acetylglycosamine
GLP-1	Glucagon-like peptide 1
GLUT	Glucose transporter

GLUT2	Glucose transporter 2
Gm	Grams
GMFI	Geometric mean fluorescence intensity
GMFR	Geometric mean fluorescence ratio
GPI	Glycosyl phosphatidyl inositol
Grp94	Glucose-regulated protein 94
GSH	Glutathione
GSIS	Glucose stimulated insulin secretion
GTT	Glucose tolerance test
H_2O_2	Hydrogen peroxide
HA	Hylauronic acid
HbA1c	Haemoglobin A1c, glycated haemoglobin
HERP	Homocysteine-induced ER protein
HFD	High fat diet
HGF	Hepatocyte growth factor
hi	High
HMOX1	heme oxygenase (decycling) 1
Hpse	Heparanase
HRD1	HMG-CoA reductase degradation protein-1
Hrs	Hours
HS	Heparan sulfate
HS	Heparan sulfate
HSPG	Heparan sulfate proteoglycan
i.p.	Intraperitoneal
IAPP	Islet amyloid polypeptide
IdoA	Iduronic acid
IFG	Insulin-like growth Factor
IGT	Insulin glucose tolerance
IKkB	Inhibitor of nuclear factor kappa-B kinase subunit beta
IL	Interleukin
IL-RA1	Interleukin-receptor antagonist 1
IM	Interstitial matrix
Inf Mf	Inflammatory macrophage

iNOS	Inducible nitric oxide synthase
Ins	Insulin
INS1	Insulin gene 1
IP3R	Inositol 1,4,5-trisphosphate receptor
IR	Insulin resistance
IRE1	Inositol requirement 1
IRS	Insulin receptor substrate
JNK	c-Jun N-terminal kinase
Kg	Kilogram
KO	Knock-out
lo	Low
LSD	Least significant difference
mAb	Mouse antibody
MAPK	Mitogen-activated protein kinase
MCP1	Monocyte chemoattractant protein 1
mg	Milligram
MGL-1	Macrophage galactose-type lectin 1
MIN6	Mouse insulinoma 6
Mins	Minutes
mM	Milli molar
MPR	Mannose 6-phosphate receptor
NAD(P)H	Nicotinamide adenine dinucleotide phosphate
NDST	N-deacetylase/N-sulfotransferase
NF-kB	Nuclear factor kappa-light-chain-enhancer of activated B cells
NLRP3	Nucleotide-binding oligomerization domain leucine rich repeat and pyrin domain containing 3
NMJ	Neuromuscular junction
NOD	Non-obese diabetic
Npl4	Nuclear protein localization 4
Nrf1	Nuclear respiratory factor 1
NRF2	Nuclear respiratory factor 2
Ns	Not significant
OGTT	Oral glucose tolerance test

PB	Peripheral blood
PBA	Sodium phenylbutyrate
PC	Prohormone convertase
PCR	Polymerase chain reaction
PDGF	Platelet-derived growth factor
PDI	Protein disulfide isomerase
PDKI	Pancreatic and duodenal homeobox 1
PERK	PKR-like endoplasmic reticulum kinase
PI	Propidium iodide
PI-88	Phosphomannopentaose sulfate
PIP2	Phosphatidylinositol 4,5-bisphosphate
PIP3	Phosphatidylinositol 3,4,5 trisphosphate
PKA	Protein kinase A
PKC	Protein kinase
PP	Poly pancreatic
PPAR	Peroxisome proliferator-activated receptors
Q	Quadrant
Res Mf	Resident macrophage
RIDD	Regulated IRE1-dependent decay of mRNA
RIP	Regulated intramembrane proteolysis
RNA	Ribonucleic acid
RNAse	Ribonuclease
RNS	Reactive nitrogen species
ROS	Reactive oxygen species
RRP	Readily releasable pools
RT	Reverse transcription
S1P	Site 1 protease
S2P	Site 2 protease
Sdc1	Sydecan-1
SEL1L	Suppressor/Enhancer of Lin-12-like
SEM	Standard error of the mean
SERCA	Sarco/endoplasmic reticulum Ca^{2+}-ATPase
SNAP25	Synaptosomal associated protein 25

SNARE	Soluble N-ethylmaleimide-sensitive factor attachment protein receptor
SOD	Superoxide dismutase
SVF	Stromal vascular fraction
T1D	Type 1 diabetes
T2D	Type 2 diabetes
Tg	Thapsigargin
TLR	Toll like receptor
Tm	Tunicamycin
TNF	Tumor necrosis factor
TNF-α	Tumor necrosis factor-alpha
TRAF2	Tumor necrosis factor receptor-associated factor2
TUDCA	Tauroursodeoxycholic acid
TXNIP	Thioredoxin-interacting protein
UDCA	Ursodeoxycholic acid
Ufd1	Ubiquitin-dependent degradation pathway
UPR	Unfolded protein response
UPRE	Unfolded protein response element
VAMP2	Vesicle-associated membrane protein
VAT	Visceral adipose tissue
VCP	Valosin-containing protein
VDCC	Voltage-gated calcium channels
-ve	Negative
VEGF	Vascular endothelial growth factor
Vs	Versus
WAT	White adipose tissue
Wt	Wildtype
XBP1	X-box binding protein 1
ZDF	Zucker diabetic fatty
α	Alpha
β	Beta
γ	Gamma
δ	Delta

ε	Epsilon
%	Percentage
+ve	Positive
µg	Microgram

Table of Contents

Chapter 1: Literature Review

1.1 The pancreas: composition and physiology

The pancreas is derived from the Greek words *Pan* meaning all and *Kreas* meaning flesh. The pancreas is a long flattened gland which lies in the upper abdomen behind the stomach and is surrounded by the small intestine, liver and spleen. The three main anatomical regions of the pancreas are the "head", "body" and "tail". The head is attached to the duodenum and the body and tail extends to the left side of the abdomen, with the tail positioned next to the spleen (Longnecker, 2014). The pancreas consists of two distinct cellular compartments, namely the exocrine and the endocrine pancreas. The exocrine pancreas constitutes the major part of the pancreas whereas the endocrine tissue accounts for only 1-2% of the total pancreas tissue (Sakula, 1988). The exocrine pancreas contains acinar cells that synthesise, store and secrete digestive enzymes, including proteases, amylases and lipases. These enzymes are involved in the hydrolysis of proteins, carbohydrates and fats, respectively (Leung and Ip, 2006). The endocrine part of pancreas helps to maintain glucose homeostasis. It consists of clusters of cells that form "islets" that geographically resemble "islands" amongst the exocrine or acinar tissue (Haist, 1971, Sakula, 1988). These discrete clusters of endocrine cells were first described by Paul Langerhans and are therefore called the "islets of Langerhans" (Haist, 1971). Pancreatic islet cells produce insulin, glucagon, somatostatin, pancreatic polypeptide and ghrelin. Their principal function is to regulate glucose levels in the blood.

Heterogeneity of islet cell populations exist in the head, body and tail regions in the pancreas of humans and other species such as rodents (Trimble et al., 1982). In rodents, the beta cell mass is higher in the tail and body regions compared to the head region and the body-tail region is rich in glucagon-producing alpha cells. Consequently, insulin secretion and proinsulin biosynthesis is higher in the tail region (Wang et al., 2013a, Trimble et al., 1982). Similar to rodents, the density of human islets is two-fold higher in the tail region compared to the head and body regions (Wang et al., 2013a). In contrast to rodents, human islets show no regional differences in endocrine cell composition or insulin secretion (Wang et al., 2013a, Bosco et al., 2010).

1.1.1 Islet cell populations

Islets are specialised mini-organs scattered throughout the pancreas. The islets contain endocrine cells, endothelial cells, nerves, fibroblasts, and leukocytes (lymphocytes,

macrophages and dendritic cells) (Brissova and Powers, 2008, Mattsson, 2005). The five main types of endocrine cells are called alpha (α), beta (β), delta (δ), epsilon (ε) and pancreatic polypeptide (PP) cells (**Figure 1.1**) (Wierup et al., 2002). The α cells produce the peptide hormone glucagon that increases the blood glucose levels by targeting glucagon (G-protein coupled) receptors expressed in the liver, kidney, adipose tissue, spleen and gastro-intestinal tract to release glucose in the blood by glycogenolysis and gluconeogenesis (Dunphy et al., 1998, Goke, 2008). β cells release the hormone insulin to decrease elevated blood glucose levels and maintain normoglycaemia. The δ cells produce somatostatin which regulates insulin and glucagon levels in the blood by inhibiting the secretion of insulin and glucagon from β and α cells, respectively (Hauge-Evans et al., 2009). PP cells produce pancreatic polypeptide to inhibit pancreatic enzyme secretion and the exocrine function of the pancreas (Adrian, 1978). The epsilon (ε) cells produce ghrelin which inhibits the secretion of insulin (Wierup et al., 2002, Broglio et al., 2003). Together, the endocrine islet cells regulate glucose metabolism.

1.1.2 Architecture of pancreatic islets

The architecture and composition of islets varies among species (Brissova et al., 2005). The size of islets varies from 100 to 500 μm in diameter and individual islets contain approximately 1000-3000 cells (Smith et al., 1991). In rodents, the islets are composed of ~80% β cells, 14% α cells, 6% δ cells, <5% PP cells and <1% epsilon cells. The β cells are clustered in the core of the islet and are surrounded by a mantle of α, δ and PP cells. On the other hand, human islets are composed of ~60% β cells, 30% α cells, <10% δ cells, <5% PP cells and <1% epsilon cells (Wierup et al., 2002, Brissova et al., 2005, Cabrera et al., 2006). Human islets lack mantle-core segregation and the β cells are intermingled with α and δ cells (Brissova et al., 2005). In humans, PP cells are present around the perimeter of pancreatic islets, in the parenchyma of the exocrine pancreas and the epithelium of pancreatic duct (Larsson et al., 1975, Ceranowicz et al., 2015). The characteristic architecture of islets aids in endocrine cell interactions and in regulating the secretion of the different islet hormones (Bosco et al., 2010).

Islets are highly enriched in blood vessels and generally are no further than one cell away from an intra-islet capillary (Bonner-Weir and Orci, 1982). The islet capillaries are approximately 5 μm in diameter and the density of the islet vasculature is five-times

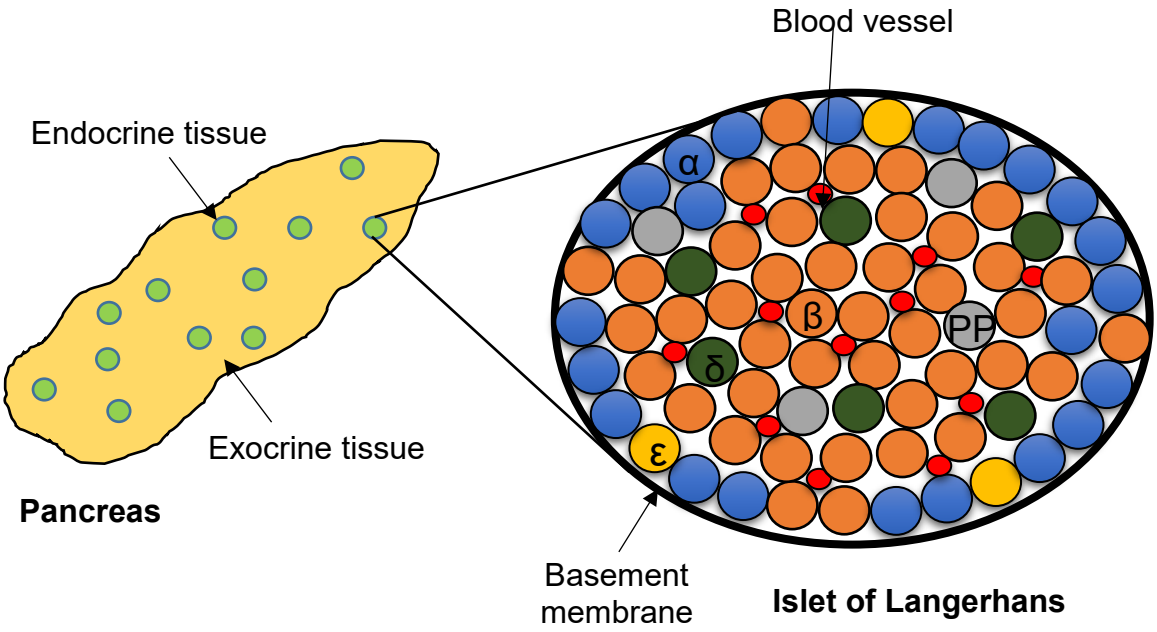

Figure 1.1: Composition of the pancreatic islet.

Each islet of Langerhans consist of five types of cells including α (blue), β (orange), δ (green), ε (yellow) and PP cells (grey) and is surrounded by a continuous basement membrane. The insulin-producing beta cells are localised in close proximity to intra-islet blood vessels or capillaries. Islets are enriched in blood vessels (red) which provide oxygen and nutrients to the endocrine cells and deliver insulin to the rest of the body.

greater than that in surrounding acinar tissue (Henderson and Moss, 1985). The intra-islet vasculature optimises oxygen and nutrient supply to the islet cells and ensures a rapid sensing of plasma glucose levels and distribution of secreted endocrine hormones (Lammert et al., 2001, Mattsson, 2005). The peri-islet basement membrane is present at the islet boundary providing structural support and acting as a barrier to cell invasion (Irving-Rodgers et al., 2008, Korpos et al., 2013).

1.2 Pancreatic islet microenvironment

The different islet endocrine cells interact with each other through extracellular spaces and gap junctions (Nepton, 2013). The extracellular matrix, neurons and endothelial cells play an important role in these cell-cell interactions.

1.2.1 Extracellular Matrix

The extracellular matrix (ECM) is an important component of the islet environment and consists of a complex network of glycoproteins and proteoglycans (Wang and Rosenberg, 1999, Laurila and Leivo, 1993). In general, the ECM functions as a cellular scaffold, a reservoir for growth factors and in cell attachment, migration, proliferation, differentiation and survival (Wang and Rosenberg, 1999, Cheng et al., 2011). Two different types of islet-associated ECM exist: the basement membrane (BM) and the interstitial matrix (IM) (Laurila and Leivo, 1993, van Deijnen et al., 1992).

BMs are highly organised sheets of ECM that separate tissues into different compartments and provide structural support (Laurila and Leivo, 1993, Wang and Rosenberg, 1999). Conventionally, the major components of BMs are type IV collagen, laminins, nidogen and perlecan. Islets contain a peri-islet BM and intra-islet BMs associated with islet capillaries. Compared to BMs, the IM consists of a more relaxed organisation of ECM components. The IM fills the space between cells in tissues and contains glycoproteins, proteoglycans and matricellular proteins (Wang and Rosenberg, 1999). The major components of the IM are collagens, fibronectin, fibrinogen and elastin. Interstitial matrices (IMs) aid in cell adhesion and migration.

1.2.2 Islet basement membrane

Islets contain a peri-islet basement membrane (BM) and sub-endothelial BMs associated with intra-islet capillaries. The mouse peri-islet BM is continuous and contains laminin chains (α 1-5, β1-3, γ1-3), collagen type IV, the heparan sulfate proteoglycan (HSPG) perlecan, and nidogens (nidogen-1 and nidogen-2) (**Figure 1.2**) (Irving-Rodgers et al., 2008). BMs are anchored to the surface of cells by integrins and beta cells, in particular, bind to collagen type IV and laminins. The composition, thickness and continuity of the islet BM is diverse amongst different species due to the presence of different forms of laminins and collagen type IV (Irving-Rodgers et al., 2008, Van Deijnen et al., 1994). The role of the islet BM is to provide structural support and to prevent cell invasion.

Collagen type IV is one of the major components of the BM and is assembled into planar hexagonal networks in the BM. *In vitro*, exogenous collagen type IV helps in the survival of intact islets and decreases insulin production and secretion by purified beta cells (Kaido et al., 2004). Laminins are biologically active components of BMs and bind to cell surface integrin and non-integrin receptors to transduce signals for proliferation, migration and differentiation. Laminins are cross-shaped or T-shaped heterotrimeric glycoproteins consisting of three polypeptide chains (α, β, γ) joined by disulfide bonds (Timpl and Brown, 1996). There are 12 laminin isoforms containing 11 laminin chains i.e., α 1-5, β1-3, γ1-3 (Jiang et al., 2002). Laminins are connected to collagen type IV by a bridging molecule called nidogen-1. Nidogen is a sulfated glycoprotein with three globular domains which contain binding sites for other ECM molecules e.g., collagen IV, laminins and perlecan (Pujuguet et al., 2000). The two isoforms of nidogen, namely nidogen-1 and nidogen-2, are present in mouse pancreatic islet BMs and act as a cell adhesive molecules that bind to integrins (Kohfeldt et al., 1998). Perlecan is a HSPG core protein present in the peri-islet BM and also in the sub-endothelial BMs of intra-islet capillaries (Irving-Rodgers et al., 2008). Perlecan in the islet BM stabilises interactions between other matrix proteins and functions as a barrier to cell invasion. In the context of the sub-endothelial BM, perlecan inhibits the extravasation of metastasizing tumour cells and leukocytes as well as leukocyte recruitment to inflammatory sites (Irving-Rodgers et al., 2008). Other extracellular HSPGs, e.g., agrin and collagen type XVIII (Iozzo, 2005) can also be found in sub-endothelial BMs (which can be 20-100 nm thick) and as a barrier against leukocyte migration (Parish, 2006, Yadav et al., 2003).

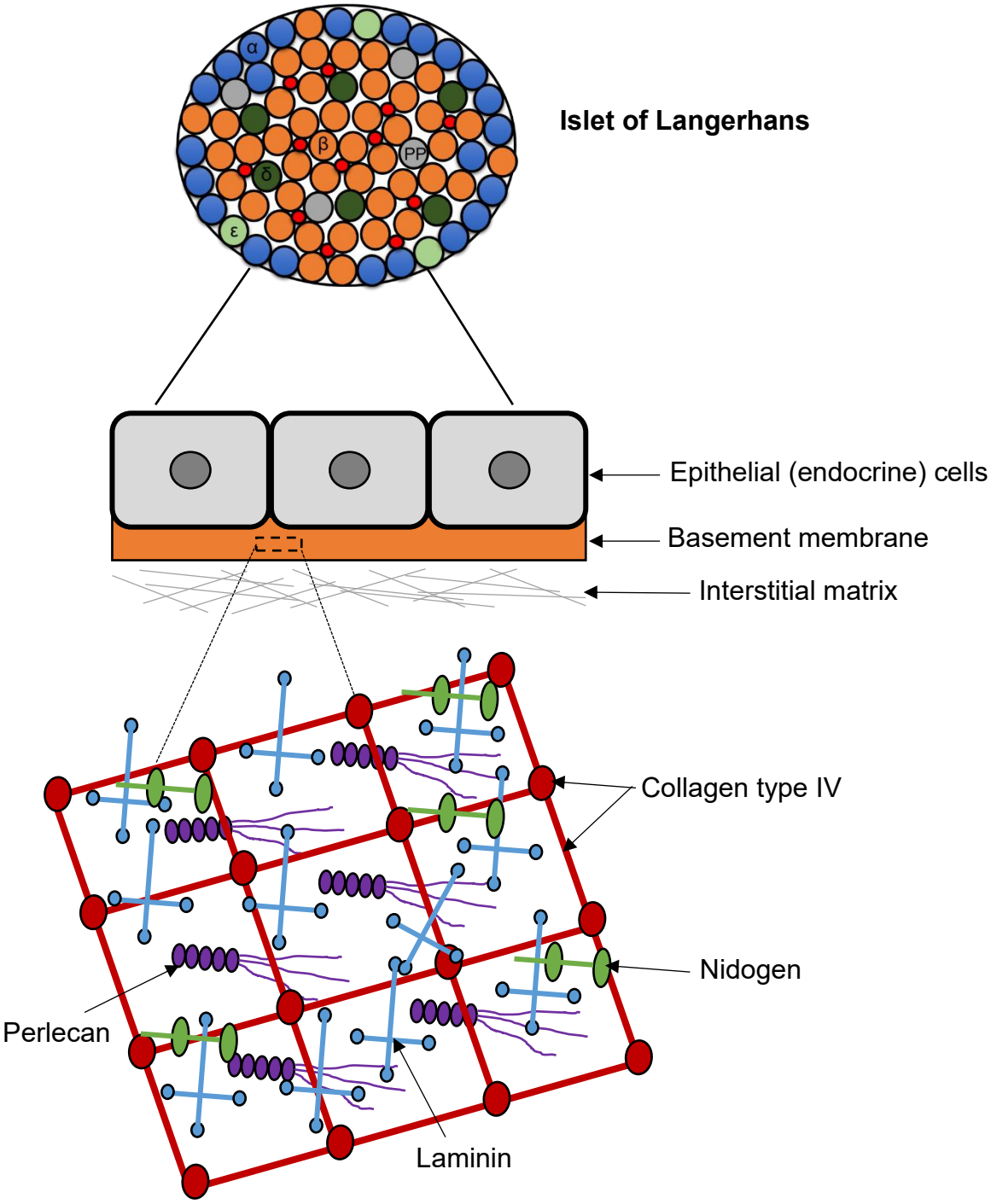

Figure 1.2: Pancreatic islet basement membrane.

The peri-islet basement membrane (BM; orange) surrounds individual islets and consists of collagen type IV (dark red), laminin (blue), perlecan (purple) and nidogen (green). The islet BM provides structural support and prevents cell invasion. Modified from Cheng et al. (2011).

Similar to the mouse peri-islet BM, the human peri-islet BM also contains perlecan, nidogen-1 and collagen IV α1/α2 (Virtanen et al., 2008, Otonkoski et al., 2008, Yurchenco, 2011). In humans, however, a double BM surrounds individual blood vessels in the islets (Virtanen et al., 2008). The inner vascular leaflet of the double BM contains laminin-411/421 and -511/521 whereas the outer leaflet which faces the endocrine cells contains only laminin-511 (Otonkoski et al., 2008). In pancreatic islets of both mouse and human, sub-endothelial BMs are rich in laminin α4 and α5 (Korpos et al., 2013).

1.2.3 Interstitial matrix (IM) in pancreas

Interstitial matrices (IMs) in the pancreas are thin layers of matrix proteins adjacent and external to the peri-islet BMs and are also localised around pancreatic ducts and blood vessels (Bogdani et al., 2014). In both human and mouse, the IM underlying the peri-islet BM contains collagen I and III, elastin, fibronectin and proteoglycans (hyaluronic acid and decorin) (Frantz et al., 2010, Korpos et al., 2013). The IM external to peri-islet BM (surrounding ducts and blood vessels in the pancreas) is also associated with hyaluronan-binding molecules such as versican, inter-alpha inhibitor and tumour necrosis factor (TNF)-stimulated gene-6 (Bogdani et al., 2014). Generally, the IM provides tensile strength and elasticity to tissues due to the presence of fibrillar collagens, and can act as a scaffold within tissues (Bonnans et al., 2014).

1.3 Islet beta cells

Islet beta cells account for 60% and 80% of the islet cell population in human and mice, respectively. The main function of the beta cell is to produce and secrete insulin in response to increased blood glucose levels, nutrients, growth factors (e.g., insulin like growth factors) and hormones (e.g., glucagon-like peptide-1 (GLP-1)) (Kulkarni, 2004). Islet beta cells synthesise proinsulin to form insulin, which is stored in intracellular granules (Haist, 1971). Beta cells co-secrete C-peptide with insulin and human beta cells also secrete islet amyloid polypeptide (IAPP, amylin) into the bloodstream (Nepton, 2013). C-peptide is released as a by-product of the cleavage of proinsulin to form mature insulin. The main function of C-peptide is to help in the synthesis of insulin and to allow correct insulin protein folding and formation of disulfide bonds (Wahren et al., 2000).

1.3.1 Insulin synthesis and storage

Insulin is a dipeptide containing A and B chains linked by disulfide bonds. The secreted form of insulin consists of 51 amino acids with 21 amino acids in chain A and 30 amino acids in chain B. The insulin gene encodes a 110 amino acid precursor known as preproinsulin (**Figure 1.3**). Preproinsulin consists of a hydrophobic N-terminal signal peptide that interacts with cytosolic ribonucleoprotein signal recognition particles (SRP) (Chan et al., 1976). The SRP helps to translocate preproinsulin from rough endoplasmic reticulum (rER) into the ER lumen (Chan et al., 1976, Lomedico and Saunders, 1977). During post-translational processing, the signal peptide is cleaved from preproinsulin by a signal peptidase to produce proinsulin (Patzelt et al., 1978), the polypeptide is folded and stabilised by the formation of three disulfide bonds (Huang and Arvan, 1995). Proinsulin consists of an amino-terminal B chain, a carboxy-terminal A chain and C-peptide, acting as a connecting peptide. In the ER, specific peptidases (prohormone convertases (PCs), PC1/3 and PC2) cleave the C-peptide chain from proinsulin to produce mature, active insulin (Steiner et al., 1996). Finally, insulin and C-peptide are packaged into secretory granules in the Golgi and are subsequently stored in the cytoplasm (Nishi et al., 1990). Insulin is also crystallised with zinc and calcium to form dense core granules during the maturation process (Hou et al., 2009). Following appropriate stimulation by glucose, insulin is secreted from the beta cells into the circulation by exocytosis (see Section 1.3.2 and 1.3.3).

1.3.2 Glucose stimulated insulin secretion

Insulin secretion is regulated by the concentration of glucose in the blood. Islet beta cells highly express specific glucose transporters (glucose transporter-2 (GLUT2) in rodents and glucose transporter-1 (GLUT1) in humans) on their cell surface for the efficient uptake of glucose in response to elevated glucose levels in the blood (Kaneto et al., 2005). GLUT2 is also expressed in the liver and to a lesser extend in the nervous system, intestine and kidney (Fu et al., 2013, Thorens, 2015). In the liver of rodents and humans, GLUT2 is a major glucose transporter; following uptake, glucose is stored as glycogen (Thorens, 2015). In other insulin-sensitive tissues (adipose tissue and skeletal muscle), GLUT4 is the predominant insulin responsive glucose transporter, facilitating the uptake of extracellular glucose into the tissues (Shan et al., 2011, Chang et al., 2004).

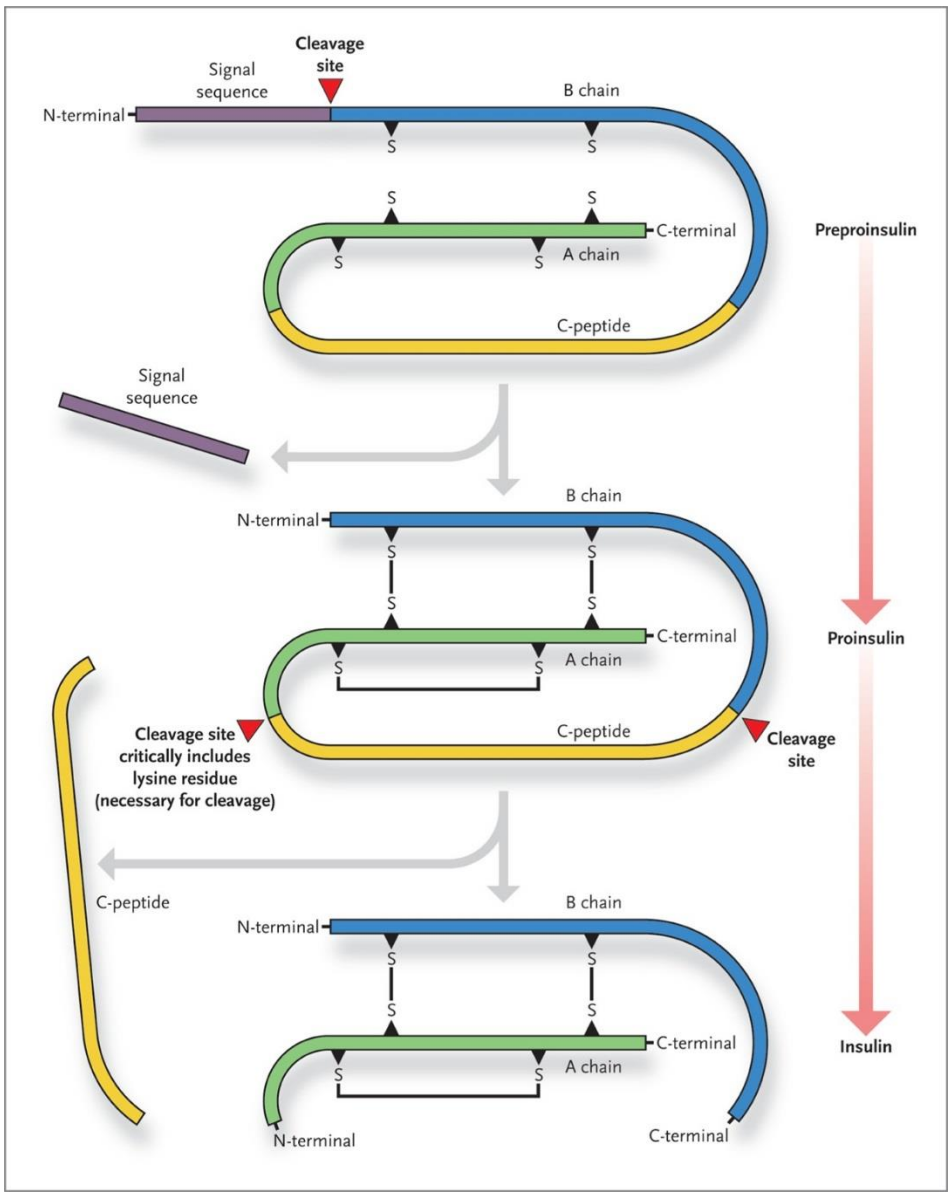

Figure 1.3: Insulin synthesis.

Insulin is synthesised as a preproinsulin in beta cells and contains chains A, B and C (C-peptide) with a signal sequence (signal peptide). The preproinsulin undergoes co-and post-translational translocation into the endoplasmic reticulum (ER) where the signal peptide is cleaved and proinsulin is produced. Proinsulin undergoes folding in the ER and forms 3 disulfide bonds. C-peptide is cleaved from proinsulin to form mature insulin with the help of prohormone convertase (PC1/3 and PC2). In the Golgi, insulin and C-peptide are packaged into secretory granules and stored in the cytoplasm (Kaufman, 2011).

Following uptake by beta cells, glucose is converted to glucose-6-phosphate by a rate-limiting enzyme, glucokinase (**Figure 1.4**). This modified glucose is trapped in the beta cells where it is further metabolised to release ATP in mitochondria. The increase in the cytosolic ATP/ADP ratio causes the closure of ATP-gated potassium channels resulting in depolarisation of the cell membrane (Rorsman et al., 2000). Eventually, this activates the voltage-gated calcium channels for transport of calcium ions into the cell. The increase in intracellular calcium ions triggers the transfer of insulin granules to the plasma membrane (**Figure 1.4**). Diffusion of insulin into the circulation reduces blood glucose levels, thereby maintaining normoglycaemia.

Glucagon like peptide-1 (GLP-1) receptors are present on the cell surface and increases insulin secretion in response to elevated glucose levels (**Figure 1.4**) (Cornu et al., 2010). GLP-1 is a growth and differentiation factor of pancreatic beta cells and after binding to its G protein-coupled receptor, activates adenylate cyclase and the production of cyclic adenosine monophosphate (cAMP). ATP in the beta cells also promotes the formation of cAMP. The increased levels of cAMP leads to the phosphorylation and activation of protein kinase A (PKA) and exchange protein directly activated by cAMP 2 (EPAC2). Together, PKA and EPAC2 increase the translation and transcription of insulin mRNA and promote pulsatile insulin secretion (Tengholm, 2012).

1.3.3 Insulin exocytosis

Insulin release is a biphasic process (Curry et al., 1968) and at least two populations of insulin secretory granules are present i.e., the readily releasable pool (RRP) and the reserve pool (**Figure 1.4**). Insulin release involves the transport of granules to the plasma membrane followed by docking, priming and fusion of the granules with the plasma membrane (Rorsman and Renström, 2003, Lang, 1999, Barg, 2003, Olofsson et al., 2002, Trexler and Taraska, 2017).

In response to increased intracellular calcium concentrations, the RRP granules come in close contact with the plasma membrane via the help of soluble N-ethylmaleimide-sensitive factor attachment protein receptor (SNARE) proteins (**Figure 1.5**) (Wang and Thurmond, 2009, Rorsman et al., 2000). The main SNARE proteins involved in insulin release are syntaxin 1, Synaptosomal-associated protein 25 (SNAP25) and vesicle

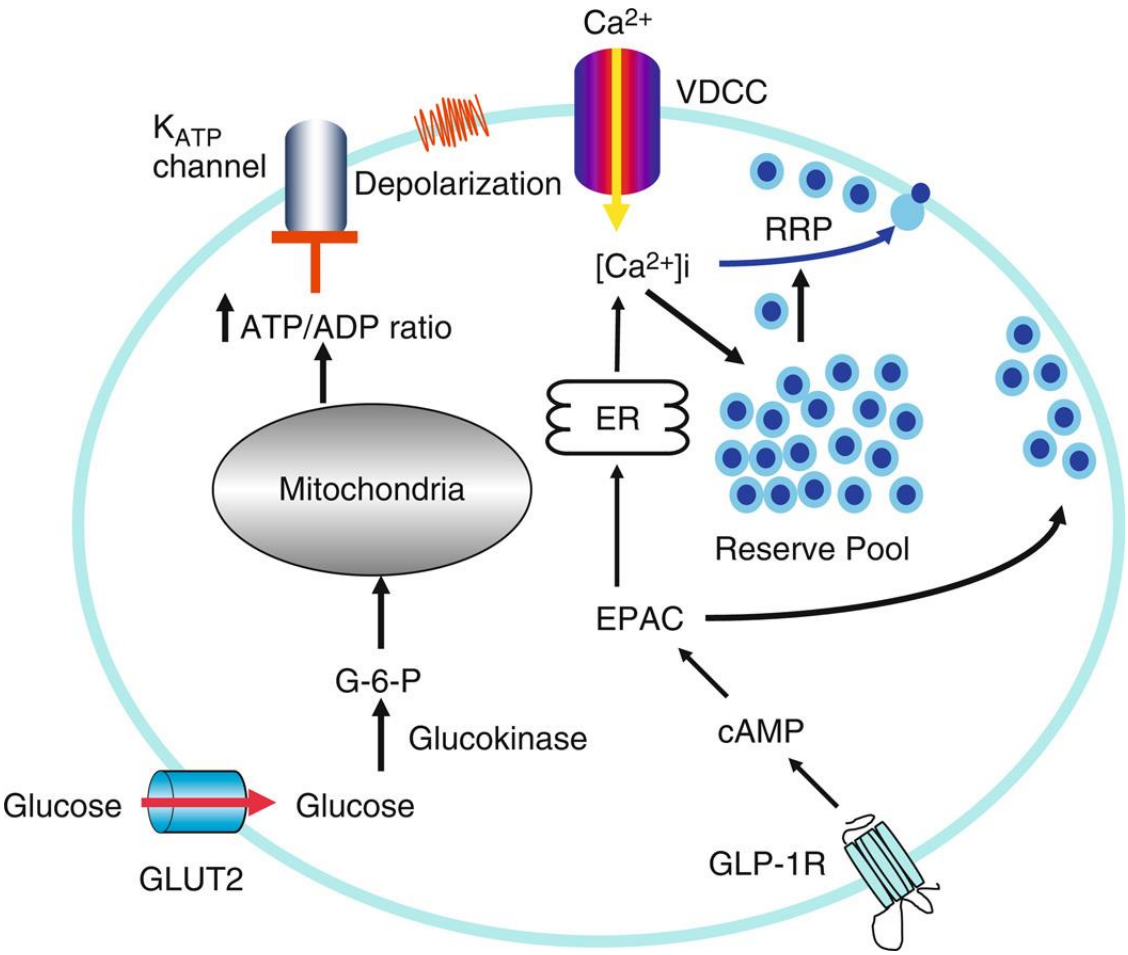

Figure 1.4: Insulin secretion pathway.

In pancreatic beta cells, elevated glucose levels (via glycolysis and mitochondrial ATP production) increases the ATP/ADP ratio. This results in the closure of ATP-sensitive K^+ (K_{ATP}) channel and plasma membrane depolarisation. This leads to an increased influx of calcium ions followed by fusion of insulin secretory granules with the plasma membrane. In addition, glucagon like peptide-1 (GLP-1) binds to its receptor to activate adenylyl cyclase and increase cAMP levels. Elevated cAMP binds and activates protein kinase A and EPAC which release intracellular calcium ions from the endoplasmic reticulum (ER) and increase the number of insulin granules at the plasma membrane. cAMP, adenosine-3', 5'-cyclic monophosphate; EPAC, exchange protein directly activated by cAMP; VDCC, voltage-dependent calcium channel; RRP, readily releasable pool of insulin granules (Hou et al., 2009).

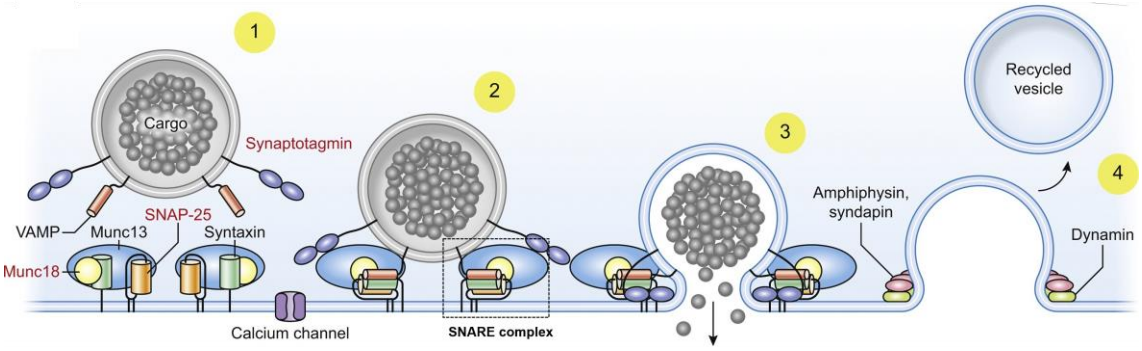

Figure 1.5: Insulin exocytosis process.

The key steps involved in insulin exocytosis are docking, priming and granule fusion. (1) The insulin granule is translocated and tethered to the plasma membrane where the exocyst complex is formed. (2) Insulin granule docking and priming involves trans-SNARE complex formation along with co-factors like Munc13, Munc18 and synaptotagmin. Munc18 binds to syntaxin to prevent binding with vesicle-associated membrane protein (VAMP). During priming, conformational changes lead to formation of the soluble N-ethylmaleimide-sensitive factor attachment protein receptor (SNARE) complex. This complex is bound to calcium channels and forms an excitosome. (3) The granule is held close to the plasma membrane and increased calcium influx allows fusion of granules to take place. (4) Recycling can occur in a kiss and run or cavicapture exocytosis where dynamin and other canonical endocytotic proteins close the fusion pore to recapture the insulin granule. SNAP25, Synaptosomal-associated protein 25. Modified from Trexler and Taraska, (2017).

associated membrane protein 2 (VAMP2). Syntaxin 1A and SNAP25 are uniformly distributed in the beta cell plasma membrane (Low et al., 2014). They function not only in membrane fusion but also in forming complexes that firmly attach the granules to the membrane and to the calcium ion channel (forming the excitosome) (Rorsman and Renström, 2003). Small GTP-binding Rab proteins interact with adhesion factors during vesicle transport and promote SNARE and vesicle fusion with the target membrane (Xiong et al., 2017). The mammalian uncoordinated-18 (Munc 18) protein regulates the SNARE complex by binding to syntaxin and forming a "closed" conformation. During priming, Munc18 interacts with Munc13 which results in the "open" conformation of syntaxin (Gaisano, 2014). This results in the formation of a "partially zipped" state where the insulin secretory granule is close to the plasma membrane. The calcium binding synaptotagmin complex is also formed and the fusion of the two membranes occurs due to the increased influx of calcium ions. Insulin is then released into the blood stream. There are three types of fusion processes: complete fusion, kiss and run, and cavicapture (Galli and Haucke, 2001, Hou et al., 2009). The complete fusion involves complete integration of the granule membrane with the plasma membrane. The kiss and run process allows partial or full granule content to be released between the granule membrane and plasma membrane through the opening of a transient pore. The cavicapture or selective "kiss and run" process is where the granule content is partially released before the membrane pore closes.

Once the readily releasable pools (RRPs) of insulin granules have been depleted, the reserve pool is used for prolonged insulin secretion (Hou et al., 2009). The reserve pool granules undergo a series of ATP, calcium, time and temperature-dependent reactions, commonly referred as priming/mobilisation to gain competence for insulin release (Rorsman and Renström, 2003). This is followed by interactions with the SNARE complex, identical to the release of insulin from RRPs.

In vitro studies revealed that beta cells within intact islets secrete more insulin than isolated pancreatic beta cells (Thorn et al., 2004, Thorn et al., 2016). Using a two-photon extracellular imaging based quantification (TEPIQ) to track exocytosis, it was found that glucose recruits individual beta cells for exocytosis, increases the number of fusion events per beta cell and activates oscillatory exocytotic activity (Low et al., 2013, Behrendorff

et al., 2010, Takahashi et al., 2002). In addition, these studies revealed that the insulin granule is dispersed towards the vasculature and away from the region of glucose uptake (Low et al., 2014) i.e., glucose-induced insulin granule exocytosis is biased toward the blood vessels (Gan et al., 2017, Low et al., 2014). Insulin secretion was therefore found to be influenced by beta cell-vasculature interactions as well as beta cell-beta cell interactions (Low et al., 2014).

1.3.4 Insulin signalling in the normal state

Insulin acts by binding to its cell surface receptor, a glycoprotein consisting of two distinct subunits, α and β, connected by disulfide bonds (**Figure 1.6**). The number of insulin receptors expressed on cells varies among different cell types (Flier, 1983). In peripheral tissues (adipose tissue and muscle), insulin binds to the extracellular α subunit causing a conformational change which allows ATP to bind to the intracellular β subunit (**Figure 1.6**). The bound ATP triggers phosphorylation of the β subunit conferring tyrosine kinase activity and recruitment of insulin receptor substrate (IRS) (Hubbard, 1997). IRS is a key element in insulin action and exists in four forms i.e., IRS-1, IRS-2, IRS-3 and IRS-4 (Kahn and White, 1988). IRS-1 accounts for insulin action in muscle and IRS-2 contributes to insulin signalling in liver (Previs et al., 2000). The C-terminus of IRS contains tyrosine and serine phosphorylation sites that bind to phosphatidylinositol 3-kinase (PI3K). The recruitment of PI3K to the plasma membrane releases the catalytic subunit of PI3K which converts phosphatidylinositol 4,5-bisphosphate (PIP2) to phosphatidylinositol (3,4,5)-trisphosphate (PIP3) (Czech, 2000). The major targets of PIP3 are protein kinase B (Akt), protein kinase C (PKC) and PI-dependent kinase 1 (PDK1). Akt binds to phosphorylated PIP3 causing its activation (Alessi et al., 1996). Activated Akt mediates insulin-stimulated glucose uptake by phosphorylating and inhibiting Rab-GTPase activating protein (Sano et al., 2003). As a result, glucose transporter protein is translocated to the cell surfaces promoting glucose uptake, glycogen, lipid, and protein synthesis, and the control of hepatic gluconeogenesis (Kahn and White, 1988).

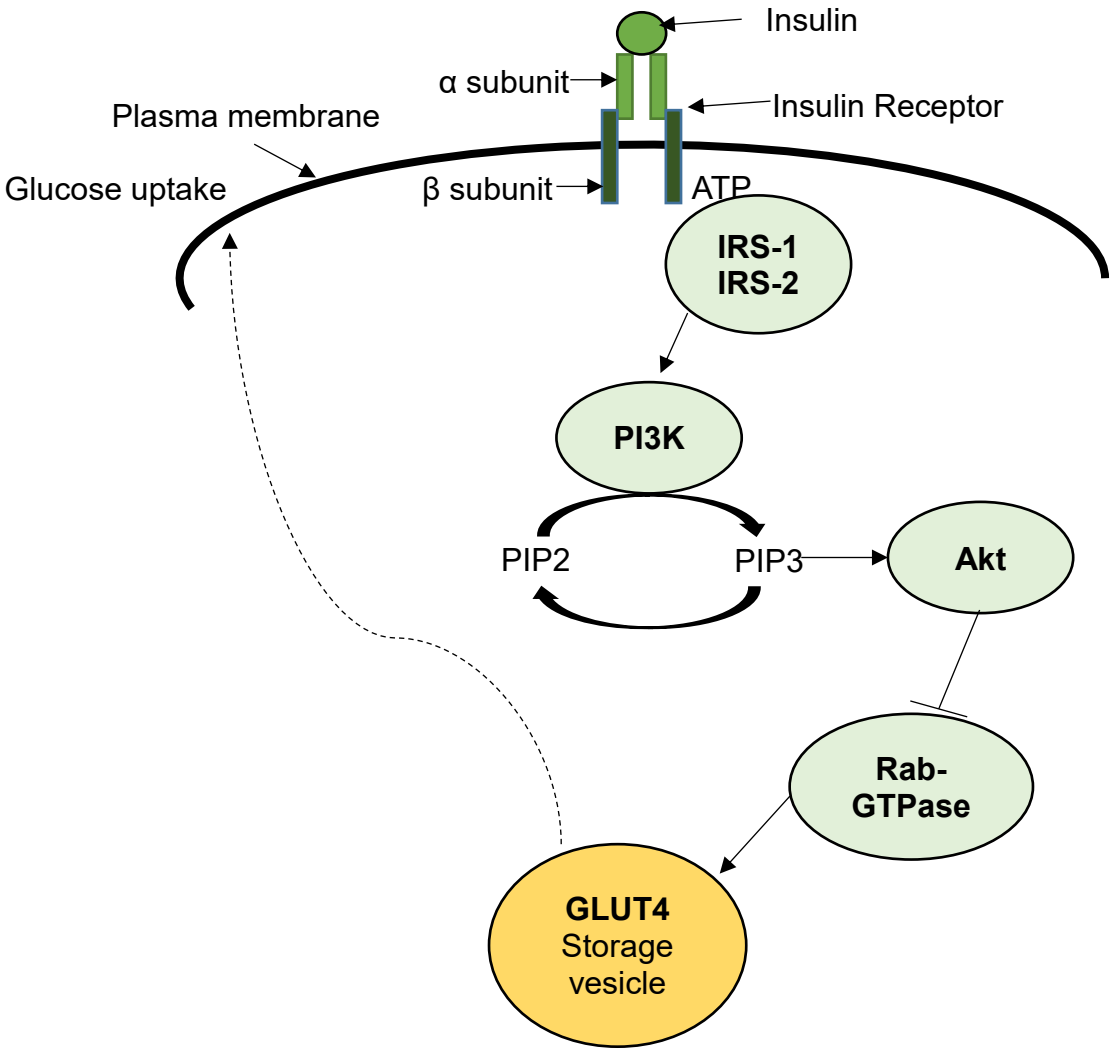

Figure 1.6: Insulin signalling.

Insulin and ATP binds to the α and β subunits of insulin receptor, respectively. ATP triggers phosphorylation of the β subunit, recruiting insulin receptor substrates (IRS) to the intracellular β subunit of the insulin receptor in target tissues (adipose tissue and muscle). This activates phosphatidylinositol-4,5-bisphosphate 3-kinase (PI3K), resulting in protein kinase B (PKB; also know as Akt) activation and the translocation of glucose transporter 4 (GLUT4) to the plasma membrane. PIP2, phosphatidylinositol-4,5-biphosphate; PIP3, phosphatidylinositol-3,4,5-triphosphate and ATP, adenosine triphosphate.

1.4 Diabetes Mellitus

Diabetes mellitus is derived from the Greek word *diabetes (siphon)* meaning to "pass through" and the Latin word *mellitus* meaning honey/sweet. It was first discovered by the ancient Egyptians around 1500 B.C and was described as a condition in which a person urinated frequently (MacCracken and Hoel, 1997). Diabetes was diagnosed by the sweet taste of the urine in suspected individuals. In the 1800s, a chemical test to detect the presence of sugar in the urine was developed (Ahmed, 2002). In 1889, Joseph Von Mering and Oskar Minkowski discovered the role of the pancreas in diabetes. They found that dogs in whom the pancreas was removed, developed symptoms of diabetes and died soon after (Minkowski, 1892). This provided the first evidence that the pancreas was important in regulating glucose levels in the body.

Diabetes mellitus is a metabolic disorder characterised by hyperglycaemia (elevated blood glucose levels). The condition is caused by defects in insulin secretion, insulin action or both that induce disturbances in the metabolism of carbohydrate, fat and protein (Alberti and Zimmet, 1998). The characteristic symptoms of diabetes mellitus are polyuria (excessive urination), polydipsia (excessive thirst), weight loss and blurred vision. The long-term complications of diabetes mellitus include: retinopathy with potential loss of vision; nephropathy resulting in renal failure; peripheral neuropathy with risk of foot ulcers, limb amputations and charcot joints; and nephropathy (Nathan 1993). Diabetes increases the incidence of atherosclerotic cardiovascular, peripheral arterial, and cerebrovascular disease, hypertension and abnormal lipoprotein metabolism (Alberti and Zimmet, 1998, American Diabetes, 2009). There are two main types of diabetes namely, type 1 diabetes (T1D) and type 2 diabetes (T2D). The processes involved in diabetes development include autoimmune destruction of the islet beta cells leading to insulin deficiency (T1D) and metabolic abnormalities leading to insulin resistance (T2D), respectively.

Type 1 diabetes (T1D) commonly referred to as insulin-dependent diabetes mellitus accounts for about 5-10% of all cases. It is an autoimmune disease caused by the immunological destruction of insulin-secreting pancreatic beta cells (Mathis et al., 2001b). In non-obese diabetic (NOD) mice, a commonly used model of spontaneous autoimmune T1D, the disease is characterised by two main stages: (i) the non-destructive phase where

inflammatory leukocytes, including macrophages, dendritic cells, CD4 T cells, CD8 T cells and B cells accumulate around the islet periphery (peri-islet insulitis) (Anderson and Bluestone, 2005, Willcox et al., 2009, Bach, 1994) and (ii) a destructive phase where the leukocytes invade the islets and destroy the beta cells, eventually reducing the insulin content of the pancreas to <10% of normal levels (Bluestone et al., 2010). In contrast to NOD mice, T1D patients show much less pronounced accumulation of cells around the islet periphery, mild infiltration, and, at clinical onset, the insulin content is reduced to 20-30% of normal pancreas (In't Veld, 2014).

Type 2 diabetes (T2D) is the most common form of diabetes and represents about 90% of all cases. It is characterised by a metabolic syndrome, reduced insulin action and eventually insulin deficiency (Marchetti et al., 2007). It is generally associated with obesity.

1.4.1 Clinical diagnosis of Type 2 Diabetes

The prevalence of diabetes is increasing dramatically; in 2011 there were over 366 million people with diabetes (including T1D and T2D) and this number is expected to increase to 552 million by 2030 (Olokoba et al., 2012). The diagnosis of T2D in humans is determined by measuring blood glucose levels (e.g., fasting plasma glucose (FPG)), after challenge with a fixed dose of glucose (e.g., oral glucose tolerance test (OGTT)) and can be monitored in the long-term by also measuring glycated haemoglobin A1c (HbA1c; **Table 1.1**) (American Diabetes association, 2010).

FPG levels are measured after at least 8 hrs of fasting. An OGTT in humans involves the oral administration of 75 g anhydrous glucose dissolved in water, followed by measuring plasma glucose levels after 2 hrs. Diabetes is diagnosed when glucose levels are ≥ 7.0 mmol/L in the fasting state or ≥ 11.1 mmol/L following a glucose load **(Table 1.1**). Individuals with impaired glucose tolerance (IGT) or impaired fasting glucose (IFG) i.e., with glucose levels between 7.8 mmol/L and 11.0 mmol/L after a glucose load (OGTT) or between 5.6 mmol/L to 6.9 mmol/L (FPG) are identified as "pre-diabetes" and have a high risk of developing diabetes (American Diabetes association, 2010). Haemoglobin A1c (HbA1c) levels are measurements of glycated haemoglobin which is formed by a non-enzymatic reaction between haemoglobin and glucose

Table 1.1: The diagnostic criteria for human diabetes (T1D and T2D).

Test	**Glucose levels**[¶]
HbA1c	≥ 6.5% or 48 mmol/mol
FPG	≥ 126 mg/dL or ≥ 7 mmol/L
OGTT 2-hr plasma glucose	≥ 200 mg/dL or ≥ 11.1 mmol/L
Random plasma glucose	≥ 200 mg/dL or ≥ 11.1 mmol/L

[¶]HbA1c, glycated haemoglobin A1c; FPG, fasting plasma glucose; and OGTT, oral glucose tolerance test. Adapted from (American Diabetes Association, 2010).

(Bookchin and Gallop, 1968, Goldstein et al., 2004). HbA1c is formed by chemical glycation of the N-terminal lysine and valines of haemoglobin A (Bookchin and Gallop, 1968). The rate of HbA1c formation is directly proportional to the blood or plasma glucose concentrations and reflects chronic glycaemia over the previous 120 days (12 weeks). HbA1c measurements can therefore be used to diagnose diabetes and to monitor disease progression (American Diabetes Association, 2010). HbA1c levels ≥ 6.5% indicate diabetes and can be up to two-fold higher than non-diabetic patients (normal range < 6%) (Rahbar et al., 1969).

T2D is a metabolic syndrome disease. Metabolic syndrome (also known as insulin resistance syndrome) is defined as a cluster of clinical and biological abnormalities which includes glucose intolerance, obesity, hypertension and dyslipidaemia (Magliano et al., 2006, Tenenbaum et al., 2003, Ginsberg and MacCallum, 2009) and is a predictor of T2D (Shin et al., 2013).

1.4.2 T2D pathogenesis

T2D is a complex disease influenced by both environmental and genetic factors. T2D develops due to lack of physical activity, increase in caloric intake, decrease in energy expenditure and increase in nutrient composition (specially increased amount of dietary fats and saturated fat) in individuals that are genetically predisposed to both insulin resistance and beta cell dysfunction (Hu et al., 2001, Prentki and Nolan, 2006, Kahn et al., 2014). Insulin resistance (IR; an impaired response to insulin) and beta cell dysfunction precede hyperglycaemia (elevated blood glucose levels) in T2D individuals (Prentki and Nolan, 2006). Longitudinal studies have demonstrated that due to insulin resistance, circulating insulin levels are increased during the normoglycaemic/prediabetic phase to compensate for growing glucose intolerance (Leahy et al 2005). Beta cell dysfunction develops due to amyloid toxicity, glucotoxicity, lipotoxicity, inflammation, ER stress and oxidative stress, ultimately leading to beta cell failure.

During the early stages of T2D development, obesity (Section 1.5) leads to inflammation in adipose tissue (Section 1.6), IR (Section 1.5) and glucose intolerance. Initially, in response to IR, beta cells increase their production of insulin. Eventually, this response and/or the chronic exposure to elevated glucose levels (glucotoxicity; Section 1.7) leads

to the accumulation of misfolded proinsulin in the endoplasmic reticulum (ER) and ER stress (**Figure 1.7; Section 1.9**). In parallel, beta cells increase the production of reactive oxygen species via the electron transport chain and by non-enzymatic glycation reactions, resulting in oxidative stress (Section 1.11)**.** In addition, apoptotic adipose cells release free fatty acids (FFAs) resulting in lipidaemia and lipotoxicity (Section 1.8) in beta cells, also exacerbating ER stress and oxidative stress. To protect the beta cells from ER stress, eukaryotic cells activate a defence system referred to as the "unfolded protein response" (UPR) or the ER stress response. The UPR maintains ER homeostasis by reducing protein translation, increasing ER chaperones and inducing ERAD pathway. The failure of the UPR to relieve ER stress contributes to beta cell failure, hyperglycaemia and overt T2D. In addition, the islets of T2D patients are characterised by amyloid deposits (see Section 1.13.4), which are insoluble fibrils formed by the aggregation of islet amyloid polypeptide (IAPP) (Haataja et al., 2008). IAPP is a 37-amino acid polypeptide which is co-expressed and co-secreted with insulin by β-cells (Butler et al., 1990). Amyloid accumulation has been shown to cause beta cell toxicity and can lead to islet inflammation in human T2D (Clark and Nilsson, 2004a, Butler et al., 2003).

1.5 Insulin resistance and obesity

IR is a metabolic condition where insulin produced by beta cells fails to facilitate glucose uptake by target peripheral tissues such as adipose tissue, liver and muscle. This metabolic abnormality results in glucose intolerance and leads to hyperglycaemia. Eventually the beta cells demonstrate impaired insulin secretion, dysfunction and eventually failure (Prentki and Nolan, 2006).

IR initially develops in adipose tissue. Adipose tissue normally plays an important role in metabolic regulation by releasing free fatty acids (FFAs) to reduce glucose uptake in muscle, insulin secretion from beta cells, and to increase glucose production from liver (Coelho et al., 2013). The main function of adipocytes is to store lipids and to secrete hormones known as adipokines, which influence metabolism, energy expenditure and insulin sensitivity. Two hypotheses have been proposed to relate obesity with insulin resistance: the "adipokine hypothesis" and the "inflammation hypothesis" (Hussain et al., 2010). The adipokine hypothesis proposed that the altered secretion of adipose tissue

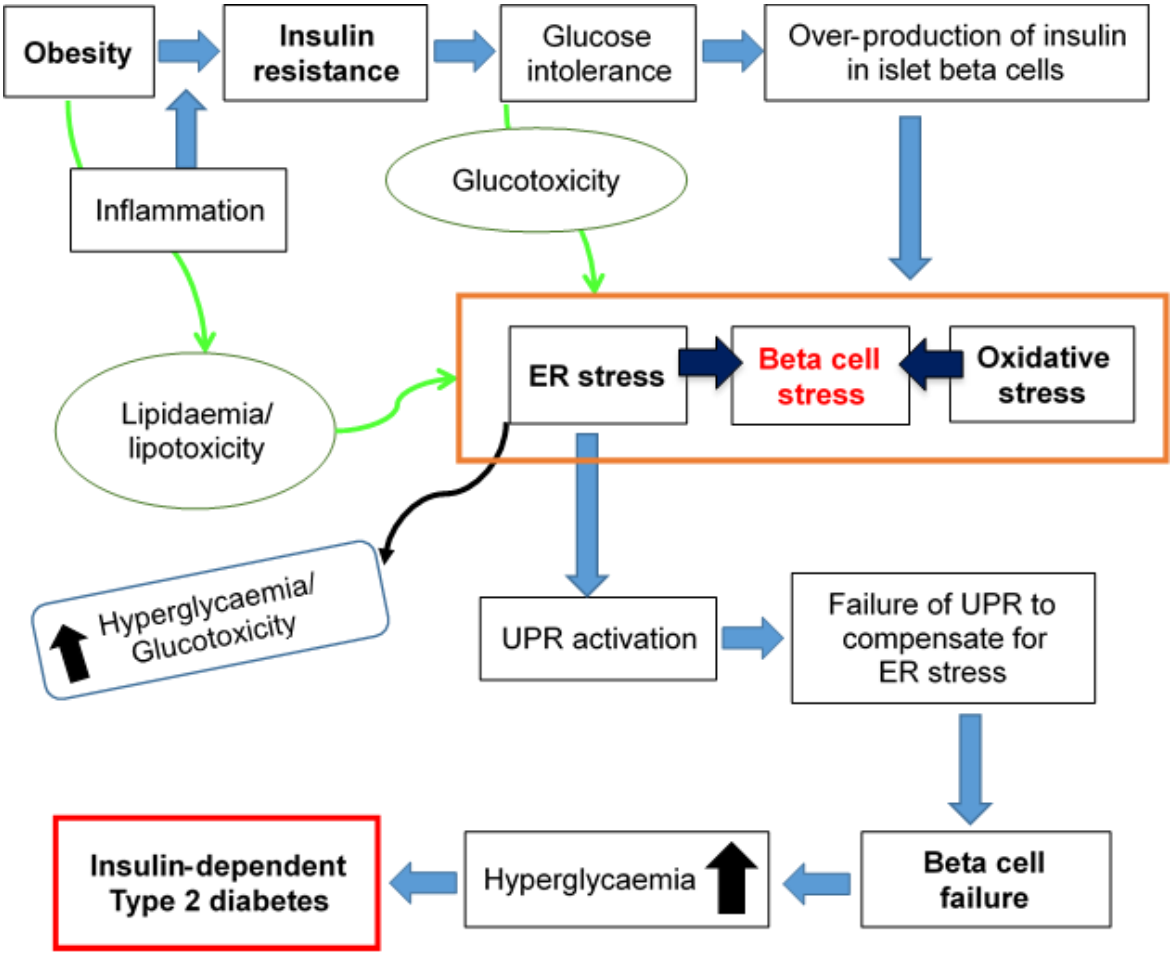

Figure 1.7: ER stress in Type 2 Diabetes.

Obesity in a subset of individuals induces insulin resistance, glucose intolerance, the over-production of insulin and lipidaemia. This process creates a biosynthetic over-load on the endoplasmic reticulum (ER) inducing ER stress and activation of the unfolded protein response (UPR) pathway. ER stress is conventionally accompanied by oxidative stress. Beta cell failure and overt hyperglycaemia, i.e., T2D, ensues when the UPR fails to compensate for ER stress.

hormones such as leptin and adiponectin, results in insulin resistance. The hormone leptin is a cytokine that acts on receptors in the central nervous system to inhibit food intake and promote energy expenditure. In ob/ob and db/db mice, IR occurs as a result of leptin deficiency and leptin resistance, respectively (Coleman, 1978). In ob/ob mice, the exogenous adminstration of leptin improves glucose tolerance and insulin sensitivity, irrespective of changes in food intake (Halaas et al., 1995, Shimomura et al., 1999). Another hormone, adiponectin, regulates glucose homeostasis and fatty acid oxidation. The levels of adiponectin are reduced in T2D mouse models (db/db and KKAγ mice (A^y mutation on KK strain)) and obese humans. Treatment of db/db and KKAγ mice with exogenous adipokine decreases insulin resistance, FFAs and the triglyceride content of muscle and liver and increases the expression of genes involved in fatty acid oxidation and energy expenditure (Yamauchi et al., 2001). Insulin resistance in PPAR-$\gamma^{+/-}$ (peroxisome proliferator-activated receptor γ) obese mice was completely reversed by combined treatment with both adiponectin and leptin, and was only partially relieved when either was adminstered alone (Yamauchi et al., 2001).

The inflammation hypothesis postulates that obesity increases chemokine secretion from the adipocytes, promoting macrophage activation and recruitment (Hussain et al., 2010). In addition, adipocytes respond to a high nutrient overload by enlarging in size via hypertrophy (**Figure 1.8**). This leads to adipocyte apoptosis, the activation and recruitment of macrophages and the local release of cytokines such as tumour necrosis factor-α (TNF-α) and chemokines (Hotamisligil et al., 1993, Xu et al., 2003, McNelis and Olefsky, 2014). Other adipocytes respond to TNF by increasing lipolysis and this results in the release of FFAs in to the circulation. FFAs bind to toll-like receptor-4 (TLR4) and TNF receptors on adipocytes, resulting in the activation of nuclear factor kappa-light-chain-enhancer of activated B cells (NF-kB; via IKKβ) and c-Jun N-terminal kinases (JNK) signalling pathways (Dasu and Jialal, 2011, McNelis and Olefsky, 2014) (**Figure 1.9**). As a consequence, IRS-1 becomes phosphorylated inhibiting insulin signalling and inducing insulin resistance (Hotamisligil et al., 1996, Dasu and Jialal, 2011).

1.6 Inflammation in type 2 diabetes

Inflammation provides a link between obesity and insulin resistance in T2D. In T2D in both mice and humans, inflammation is observed in adipose tissue, liver, muscle and pancreas. At these sites, infiltrating macrophages play a crucial role in the production of pro-inflammatory cytokines such as TNF-α, IL-6 and IL-1β which in turn activate JNK and NF-κB pathways. These signalling pathways increases transcription of inflammatory genes and phosphorylates IRS-1, causing down-regulation of insulin signalling and contributing to insulin resistance (**Figure 1.9**).

1.6.1 Adipose tissue inflammation

Adipose tissue (AT) is made up of adipocytes (the major constituent) as well as preadipocytes, endothelial cells and immune cells (known as the stromal vascular fraction (SVF) *in vitro*). A prime function of AT is to insulate and cushion internal organs and to store excess energy in the form of triglycerides. In addition, AT plays an important endocrine role, secreting adipokines and cytokines into the circulation. Inflammation in AT was first reported by Hotamisligil and colleagues who demonstrated the increased expression and production of TNF-α in obese individuals (Hotamisligil et al., 1993). This evidence was pivotal in identifying a role for inflammation in obesity-induced insulin resistance (see Section 1.5).

During obesity, white adipose tissue (WAT) initially responds to nutrient overload by fat deposition as well as the growth of adipocytes (**Figure 1.8**) (Chmelar et al., 2013, Despres et al., 2008). AT expansion is generally associated with adipocyte hypertrophy, free fatty acid flux, vascularisation, increased leptin secretion, hypoxia, ER stress, oxidative stress and adipocyte cell death. Furthermore, the expansion of WAT is accompanied by compensatory angiogenesis and also triggers an inflammatory response which is characterised by the recruitment of macrophages with pro-inflammatory and pro-angiogenic properties (McNelis and Olefsky, 2014). Activated macrophages enter WAT to phagocytose dead or dying adipocytes which release FFAs (Xu et al., 2003, Weisberg et al., 2003). They also secrete pro-inflammatory cytokines and chemokines such as TNF-α, IL-6, IL-1β and monocyte chemotactic protein 1 (MCP-1) (McNelis and Olefsky, 2014), the production of which is regulated by IKKβ-NF-κB and JNK pathways. Receptor-bound cytokines (e.g., TNF) and free fatty acids at the cell surface also induce

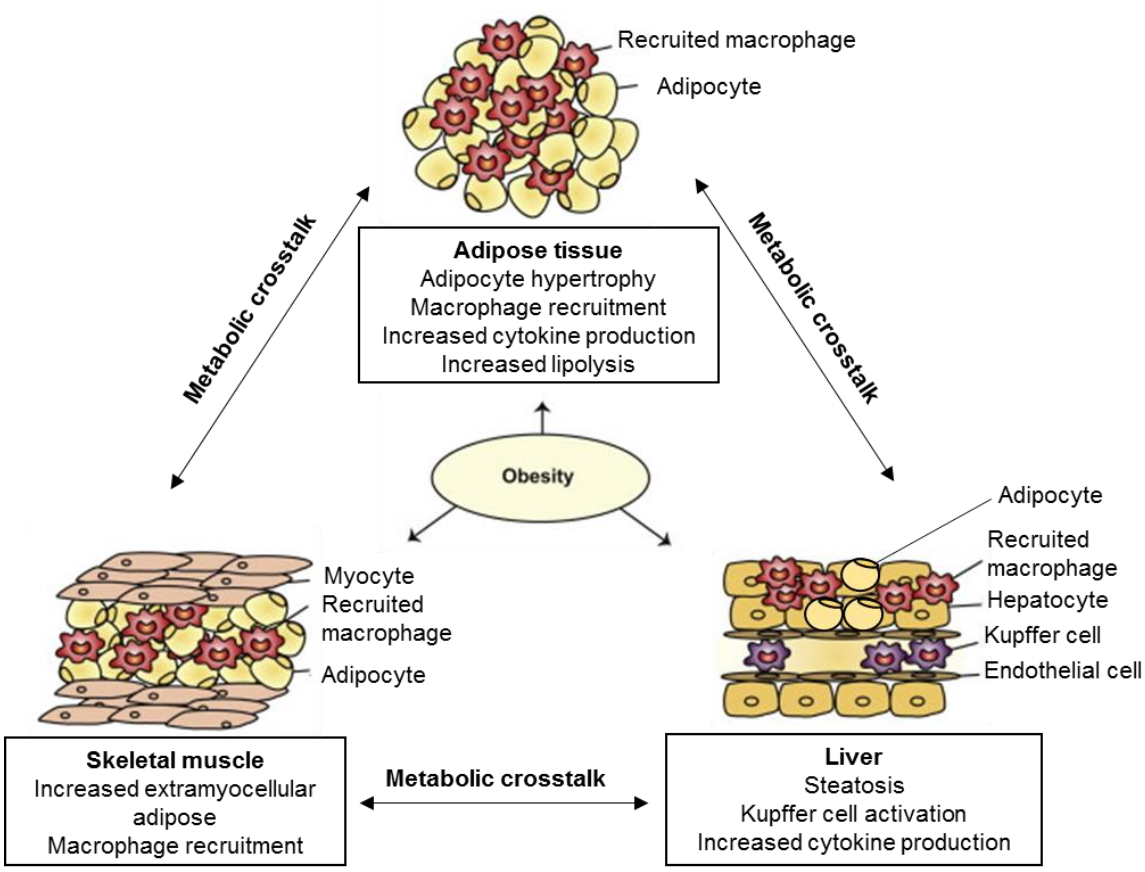

Figure 1.8: Obesity induced inflammation in the peripheral tissues.

Adipocyte enlargement and apoptosis results in the local recruitment and accumulation of macrophages. Activated macrophages secrete cytokine/chemokines stimulating viable adipocytes to release FFAs (via lipolysis) into the circulation. Similar processes occur in skeletal muscle and liver. Modified from (McNelis and Olefsky, 2014)

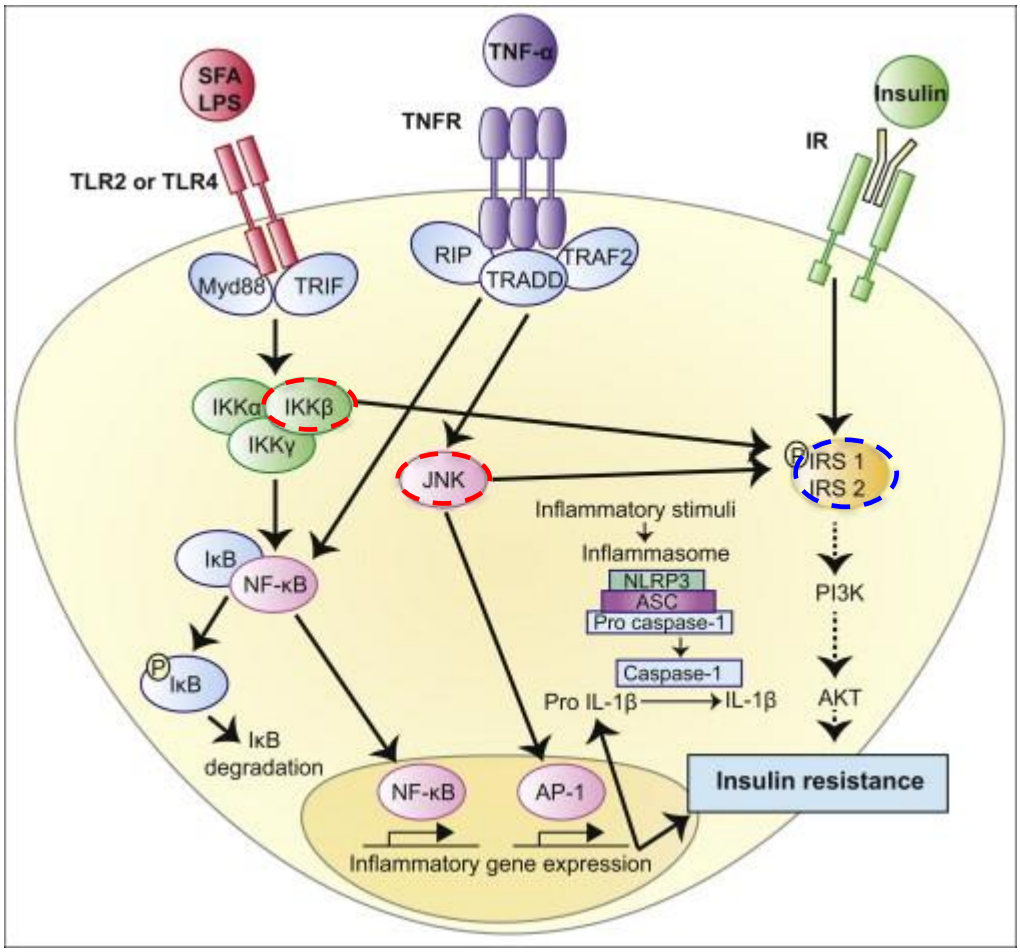

Figure 1.9: Insulin resistance-induced by inflammation.

Elevated free fatty acids (FFAs) and tumour necrosis factor (TNF) bind to their receptors on adipocytes to activate nuclear factor kappa-light-chain-enhancer of activated B cells (NF-κB) and c-Jun N-terminal kinases (JNK) signalling. The phosphorylation of IRS-1 by IKKβ and JNK inhibits insulin signalling. NF-κB and JNK signalling also increases inflammatory gene expression further contributing to insulin resistance. TLR, toll like receptor; IR, insulin receptor; PI3K, phosphatidylinositol 3-kinase; AKT, protein kinase B; IL-1β, interleukin-1 beta; TRAF2, TNF receptor-associated factor 2; TRIF, Toll/interleukin-1 receptor) domain-containing adaptor protein inducing interferon beta; TRADD, Tumor necrosis factor receptor type 1-associated death domain protein and Myd88, Myeloid differentiation primary response 88. Modified from (McNelis and Olefsky, 2014).

the expression of inflammatory genes (**Figure 1.9**) (Olefsky and Glass, 2010, Ozcan et al., 2004). In addition, the nucleotide binding domain, leucine rich-containing family, pyrin domain-containing 3 (NLRP3) inflammasome is activated in adipocytes, promoting the maturation of pro IL-1β to IL-1β and pro IL-18 to IL-18 via caspase 1 (**Figure 1.9**).

The activation of IKKβ and phosphorylation of the inhibitor of NF-κB, IκB, initiates IKKβ-NF-κB signalling (**Figure 1.9**). Under normal conditions, NF-κB is associated with IκB; upon an inflammatory stimulus (e.g., TNF), phosphorylated IκB dissociates from NF-κB. The free NF-κB translocates to the nucleus where it binds to cognate DNA response elements and activates the transcription of inflammatory genes (Shoelson et al., 2003). Similarly, inflammatory mediators phosphorylate and activate c-Jun N-terminal kinase (JNK), resulting in inflammatory gene expression. Moreover, the lack of JNK1 in $Jnk1^{-/-}$ mice prevents the development of insulin resistance and diabetes in both genetic (ob/ob) and dietary mouse models of obesity, confirming the critical role of JNK in blocking insulin signalling (Hirosumi et al., 2002).

The proinflammatory environment triggers the further recruitment of inflammatory leukocytes such as macrophages, mast cells, neutrophils, dendritic cells and lymphocytes (Weisberg et al., 2003, Talukdar et al., 2012). These leukocyte sub-populations are discussed below in detail.

(a) Adipose tissue macrophages (ATMs)

Macrophages are a major contributor to adipose tissue (AT) inflammation. Generally, the main function of macrophages is to aid in tissue development, immune responses, surveillance and tissue homeostasis. Monocytes are macrophage precursors found in the blood, bone marrow and spleen. When recruited to tissues, monocytes differentiate into inflammatory macrophages. In contrast, tissue resident macrophages aid in tissue development, tissue homeostasis and the resolution of inflammation. C-C chemokine ligand 2/chemokine receptor 2 (CCL2/CCR2) function in recruiting monocytes from the blood to tissues.

Macrophages are categorised into two distinct phenotypes: “classically activated macrophages” termed “M1” and “alternatively activated macrophages” called “M2”

(Mantovani et al., 2002, Martinez and Gordon, 2014). In obese AT, M1 macrophages are characterised by cell surface expression of CD11c and absence of both CD206 (mannose receptor) and macrophage galactose-type C-type lectin 1 (MGL1). M1 macrophages secrete cytokines such as TNF-α, IL-6 and IL-1β and produce high levels of inducible nitric oxide synthase (iNOS) that reduce insulin signaling in various tissues (e.g., adipose tissue) and contributes to insulin resistance and T2D development (Wentworth et al., 2010, Lumeng et al., 2007b, Lumeng et al., 2008, Shaul et al., 2010). In contrast, M2 macrophages are characterised by the scavenger receptors CD206 and MGL1. M2 macrophages produce cytokines such as IL-10, a potent anti-inflammatory cytokine and are involved in tissue repair, remodeling and maintenance of insulin sensitivity in lean adipose tissue (Lumeng et al., 2007a). The balance between M1/M2 determines the net inflammatory effect and degree of insulin sensitivity. Various factors that affect the M1/M2 balance include a high fat diet, free fatty acids, and fetuin-A. M2 macrophages are predominantly found in lean AT, whereas during obesity, M1 macrophages are recruited to WAT, and accumulate around dying adipocytes in ring-like formation called crown-like structures (CLSs) (Cinti et al., 2005). Macrophages are therefore a major component of the chronic low-grade inflammation in obese WAT.

(b) Neutrophils

Neutrophils circulate in the resting state and characteristically are the first immune cells to be recruited to inflamed tissues. Upon activation, neutrophils secrete antimicrobial factors such as proinflammatory cytokines and serine proteases such as neutrophil elastase. Recent studies have demonstrated that neutrophil elastase degrades IRS-1 and impairs insulin signaling (Talukdar et al., 2012). Furthermore, neutrophil elastase contributes to AT inflammation via activation of downstream signaling of TLR-4 (**Figure 1.9**) and induction of inflammatory gene expression (Talukdar et al., 2012). In addition, neutrophils promote the subsequent recruitment of monocytes to AT by producing MCP-1, IL-8 and other cytokines (Soehnlein et al., 2008).

(c) Eosinophils

In contrast to neutrophils, eosinophils serve as a negative regulator of AT inflammation. Eosinophils are present in lean AT and assist in glucose homeostasis by regulating anti-inflammatory M2 macrophages (Wu et al., 2011). In the lean state, WAT eosinophils

reduce inflammation by producing IL-4 and IL-13 which induce peroxisome proliferator activated receptor gamma (PPARγ) and delta (PPARδ) to maintain macrophage polarisation (Kang et al., 2008, Odegaard et al., 2007, Desvergne, 2008). However, in obesity, the levels of WAT eosinophils are reduced, promoting inflammation.

(d) B cells

The main function of B cells is to promote humoral immunity by producing antibodies specific for foreign antigens. In addition, B cells are able to recognise certain pathogen-associated patterns via TLRs (LeBien and Tedder, 2008) and can act as antigen presenting cells. The number of B cells are highly increased in the WAT of obese animals and contributes to WAT inflammation and insulin resistance (Winer et al., 2011). IgG2c antibodies are present in CLSs, suggesting their possible role in the clearance of dying adipocytes (Mraz and Haluzik, 2014). The recruitment of B cells (as well as T cells) precedes ATMs in adipose tissue, suggesting that B cells may play a role in ATM polarisation (Duffaut et al., 2009). In further support of this notion, mice deficient in B cells showed reduced levels of M1-polarised ATMs.

(e) T cells

T cells play a role in WAT inflammation by interacting with macrophages and regulating the inflammatory cascade. Previous studies demonstrated that the number of $CD8^+$ T cells was increased in the epididymal adipose tissue of obese mice whereas the number of $CD4^+$ T cells was reduced (Nishimura et al., 2009, Winer et al., 2011). This finding suggests that $CD4^+$ T cells may play a suppressive role in the development of obesity-induced inflammation and insulin resistance and that the relative expression of $CD8^+$ T cells might be responsible for the polarisation of macrophage from the M2 to M1 phenotype (Winer et al., 2009). The accumulation of $CD8^+$ T cells in WAT prior to macrophages supports this notion. Furthermore, both the immunological and genetic depletion of T cells reduced the infiltration of WAT macrophages, decreased adipose tissue inflammation and improved insulin resistance (Nishimura et al., 2009).

(f) Dendritic cells

Dendritic cells (DCs) are antigen presenting leukocytes of myeloid origin and play a critical role in innate as well as adaptive immunity (Wu and Liu, 2007). DCs are

categorised into two groups: plasmacytoid DC (pDC) and conventional DC (cDC). Previous studies have shown that cDCs are increased in the WAT of obese (ob/ob) and diet-induced obesity (DIO)-mice and are involved in the accumulation and activation of macrophages in inflamed AT (Dominguez and Ardavin, 2010, Stefanovic-Racic et al., 2012, Zhong et al., 2013, Chen et al., 2014). The number of cDCs in the circulation are increased in obese T2D patients and DC-deficient mice showed protection from obesity, insulin resistance as well as reduced macrophage accumulation in AT (Chmelar et al., 2013). These studies indicate that cDCs play a role in the recruitment of macrophages in WAT.

1.6.2 Islet inflammation

The pathogenesis of islet inflammation in human T2D involves mild leukocyte recruitment and infiltration, cytokine production, beta cell apoptosis, amyloid deposition and islet fibrosis (Donath et al., 2009). Immunohistochemical analysis of the infiltrating leukocytes in the pancreatic islets of T2D rodents and human patients revealed an increased number of islet macrophages (Larsen et al., 2007, Ehses et al., 2007, Richardson et al., 2009). In particular, recruited/activated macrophages secrete pro-inflammatory cytokines within the islets which can further expand the inflammatory response (Banaei-Bouchareb et al., 2004).

The major mechanism by which islet macrophages contribute to beta cell dysfunction is via the secretion of IL-1β (**Figure 1.10**). Various factors stimulate islet macrophages to secrete IL-1β *in vivo*, including: human islet amyloid polypeptide (hIAPP), palmitate, glucose and endocannabinoid (Eguchi and Nagai, 2017). These complex interactions can exacerbate islet inflammation and T2D. The exposure of beta cells to elevated glucose levels increases their metabolic activity and leads to the increased formation of reactive oxygen species (ROS). Increased glucose levels also cause dissociation of thioredoxin interacting protein (TXNIP) from thioredoxin and allow it to bind to the NLRP3 inflammasome (**Figure 1.10**) (Chen et al., 2008, Donath and Shoelson, 2011, Oslowski et al., 2012). In addition, ROS and ER stress promote activation of the NLRP3 inflammasome. Interactions with the NLRP3 inflammasome result in the processing and activation of cysteine protease caspase 1 which then converts inactive pro IL-1β to mature IL-1β (Zhou et al., 2009). Mature IL-1β, binds to IL-1R on the cell surface and activates

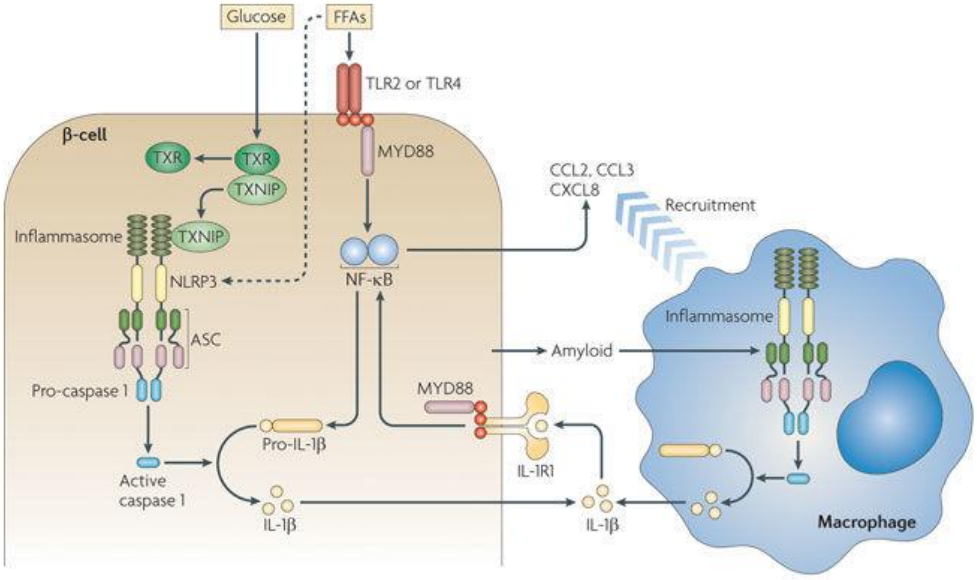

Figure 1.10: Islet inflammation in T2D.

Elevated glucose levels promote production of interleukin-1β (IL-1β) by beta cells via the dissociation of thioredoxin-interacting protein (TXNIP) from thioredoxin. This results in the activation of NOD-, LRR- and pyrin domain-containing 3 (NLRP3) inflammasome. Furthermore, free fatty acids (FFAs) can also induce inflammasome activation. This activates caspase 1 and causes formation of mature IL-1β from inactive pro-IL-1β. Mature IL-1β induces the production of several chemokines and cytokines by activating nuclear factor-kappa B (NF-κB). NF-κB activation is also enhanced by FFA-induced activation of toll-like receptors (TLRs) e.g., TLR2 or TLR4. This leads to the recruitment of macrophages to the beta cells, eventually establishing a vicious cycle of IL-1β-induced beta cell inflammation (Donath and Shoelson, 2011).

nuclear factor-kappa B (NF-κB), inducing the production cytokines and chemokines e.g., IL-6, IL-8 (in humans), TNF and MCP-1. Furthermore, free fatty acids (FFAs) bind to TLR-4 expressed on the beta cells causing nuclear translocation of NF-κB and the induction of inflammatory signals (e.g., activation of IL-1β gene). These responses lead to the recruitment of macrophages and other immune cells to the islets (Igoillo-Esteve et al., 2010), enhancing islet inflammation.

Blockade of IL-1β by treatment with IL-1 receptor antagonist restored beta cell function in both T2D rodents and humans *in vivo* and *in vitro* (Ehses et al., 2009, Sauter et al., 2008, Larsen et al., 2007, Rissanen et al., 2012). A clinical trial in which T2D patients were treated with Anakinra (an IL-1R anatagonist) for 13 weeks demonstrated an improvement in glucose metabolism, as observed by reduced HbA1c levels and increased C-peptide secretion as well as reduced levels of systemic inflammatory marker IL-6 (Larsen et al., 2007). Subsequent monitoring over a period of 39 weeks showed a sustained reduction in inflammatory markers and an improvement in beta cell function (lower proinsulin/insulin ratio) (Larsen et al., 2009). However, short-term clinical trials testing IL-1β blockade using IL-1β neutralising antibodies (LY2189102 and gevokizumab) showed only a slight improvement in HbA1c levels (Cavelti-Weder et al., 2012, Sloan-Lancaster et al., 2013). Furthermore, recent clinical trials with the anti-IL-1β antibody canakinumab demonstrated an initial reduction in HbA1c levels in the first 6-9 months but this effect was lost over time (Lytrivi et al., 2018, Everett et al., 2018). Based on these clinical studies, the role of IL-1β inhibition in improving beta cell function in T2D is unclear and warrants further investigation.

A shift in the polarisation of macrophages from the M2- to M1-like phenotype was observed in the islets of two T2D mouse models i.e., db/db mice and KKAy mice (Ehses et al., 2007, Richardson et al., 2009). This study used flow cytometry analysis of CD206 and CD301 surface markers for M2 macrophages and CD68 and F4/80 for M1 macrophages (Eguchi et al., 2012). Clodronate-loaded liposome-mediated inhibition of macrophage recruitment to the islets of db/db mice and KKAy mice improved insulin secretion in oral glucose tolerance tests. The isolated islets from these mice exhibited increased glucose stimulated-insulin secretion (GSIS) as well as increased insulin and

PDX-1 mRNA levels. Collectively these studies suggest that macrophages participate in islet inflammation and contributes to beta cell dysfunction.

While there is an established role for WAT inflammation in T2D (see Section 1.6.1), islet inflammation has only recently been identified as a contributing factor to T2D development (Ehses et al., 2007, Richardson et al., 2009, Eguchi et al., 2012, Marchetti, 2016, Eguchi and Nagai, 2017).

1.7 Hyperglycaemia/Glucotoxicity

The detrimental effect of elevated plasma glucose levels on beta cells is known as glucotoxicity (Kaiser et al., 2003). In response to high glucose levels, various types of cells reduce the transport of glucose to the cytoplasm to maintain a constant intracellular glucose concentration; however, this process fails in some cells (e.g., pancreatic beta cells, neuronal cells and endothelial cells), resulting in high intracellular glucose levels (Brownlee, 2005). Pancreatic beta cells are highly sensitive to changes in blood glucose concentrations and altered glucose homeostasis both *in vivo* and *in vitro* impacts beta cell function. The chronic exposure to increased blood glucose concentrations affects insulin synthesis/secretion, insulin sensitivity and beta cell survival, resulting in hyperglycaemia (Robertson et al., 2004). Upon entry into beta cells, glucose is metabolised, resulting in increased ATP production in mitochondria (**Figure 1.4**). However, prolonged exposure of glucose can exceed the capacity of mitochondria to convert glucose metabolites to ATP (Campos, 2012). Increased metabolic flux into the mitochondria induces the excessive generation of ROS leading to oxidative stress (Robertson et al., 2003). Treatment of db/db mice with the antioxidant N-acetylcysteine, showed enhanced insulin secretion, improved insulin content and reduced beta cell apoptosis (Kaneto et al., 1999). Glucose stimulated insulin secretion (GSIS) is impaired along with insulin gene expression in T2D humans and rodent islets. The prolonged exposure to elevated blood glucose levels in Zucker diabetic fatty (ZDF) rats and HIT-TI5 cells also causes a reduction in insulin promoter activity and PDX-1 expression, leading to decreased insulin gene expression (Kim and Yoon, 2011). These outcomes were partially improved by treating ZDF rats with troglitazone (a thiazolidinedione drug) or with the antioxidants N-acetylcysteine or aminoguanidine. In both T2D human and rodent islets, moderately high glucose

concentrations induce ER stress in beta cells due to an increased demand for insulin synthesis in the ER (Marchetti et al., 2007, Wang et al., 2005).

1.8 Lipotoxicity

The toxic effects of persistently high FFA levels on beta cells is called lipotoxicity. FFAs are a major source of energy in muscle, liver and kidney. FFAs are also a key substrate in the liver for triglyceride production (Hussain et al., 2010). Under normal physiological conditions, FFAs are important for maintaining GSIS (Stein et al., 1996). In both humans and rodents, the exposure of beta cells to elevated FFAs results in impaired *Ins* gene transcription and GSIS. Eventually prolonged exposure to FFAs can lead to beta cell apoptosis (Shimabukuro et al., 1998, Sako and Grill, 1990, Zhou and Grill, 1994). These effects are observed in the presence of increased blood glucose levels. In addition, increased FFAs can lead to the accumulation of fatty acid (FA) metabolites, affecting beta cells directly or indirectly through lipid derived signals (van Raalte et al., 2011). *In vitro*, prolonged exposure of isolated rat islets and MIN6 cells to palmitate (a saturated FFA) inhibits insulin gene expression. Palmitate also exerts toxic effects on non-diabetic human and rat pancreatic islets by reducing beta cell proliferation and hypertrophy and inducing oxidative stress and beta cell apoptosis (Kusminski et al., 2009, Briaud et al., 2001, Maedler et al., 2003, El-Assaad et al., 2003). Elevated extracellular FFAs also contribute to insulin resistance in peripheral tissues such as adipose tissue; in addition, the intracellular accumulation of FA metabolites (diacylglycerol and fatty acyl coenzyme A) impairs insulin signalling and glucose uptake (Cusi, 2010). Importantly, an increase in FFA metabolism in MIN6 cells was found to result in ER stress, defects in vesicular trafficking and apoptosis (Boslem et al., 2011).

1.9 Endoplasmic reticulum (ER) stress

The ER of eukaryotic cells is a membrane-bound organelle where proteins and lipids are synthesised. The ER produces secretory and membrane proteins as well as lipids for most cells and plays a central role in metabolism and a variety of signalling processes. The ER also plays an important role in Ca^{2+} storage and signalling (Araki et al., 2003). The Ca^{2+}

concentration inside the ER is three to four times higher than cytoplasmic Ca^{2+}; this gradient is generated by the sarcoplasmic (endoplasmic) reticulum Ca^{2+} ATPase (SERCA) proteins (Berridge, 2002). The ability of the ER to store and release Ca^{2+} allows the ER to control various processes such as organogenesis, transcriptional activity, stress responses and apoptosis (Eizirik et al., 2008).

Under normal conditions, the nascent proteins synthesised in the ER undergo conformational changes to achieve a correct or mature structure, which is often stabilised by the formation of disulfide bonds. ER chaperones and foldases (folding catalysts) increase the rate of protein folding and help to maintain protein solubility (Scheuner and Kaufman, 2008, Gething and Sambrook, 1992). The properly folded mature proteins are then transported to the Golgi apparatus, after which they can function as membrane or secretory proteins (Hammond and Helenius, 1994). ER homeostasis and function can be influenced by the lack of chaperones to promote protein folding, inhibition of protein glycosylation, calcium depletion from the ER, disruption of the redox state, protein mutations and reduced disulfide bond formation. Such perturbations lead to the accumulation of misfolded proteins in the ER lumen (Yoshida, 2007, Eizirik et al., 2008). These misfolded/unfolded proteins are normally retrotranslocated to the cytoplasm by the ER-associated degradation (ERAD) pathway and degraded by the proteasome (Ahner and Brodsky, 2004). Both ER chaperones and ERAD deal with nascent proteins in the ER. When the ER folding capacity and ERAD machinery capacity are impaired due to excessive demand, unfolded/misfolded proteins accumulate in the ER and this condition is known as “ER stress” (Yoshida, 2007, Ariyasu et al., 2017). To protect the cells from ER stress, eukaryotic cells activate a defence system referred to as the “unfolded protein response” (UPR) or the ER stress response. The UPR maintains ER homeostasis by different pathways: reducing protein translation, increasing ER chaperones, inducing ERAD and by apoptosis (**Figure 1.11**); each are discussed below.

1.9.1 ER chaperones

The proper conformation of nascent proteins in the ER is both aided and monitored by a variety of chaperones. The ER contains ER chaperones which help in the folding of nascent proteins and to establish the correct folding of misfolded or unfolded proteins (Schroder and Kaufman, 2005). ER chaperones include molecular chaperones and folding

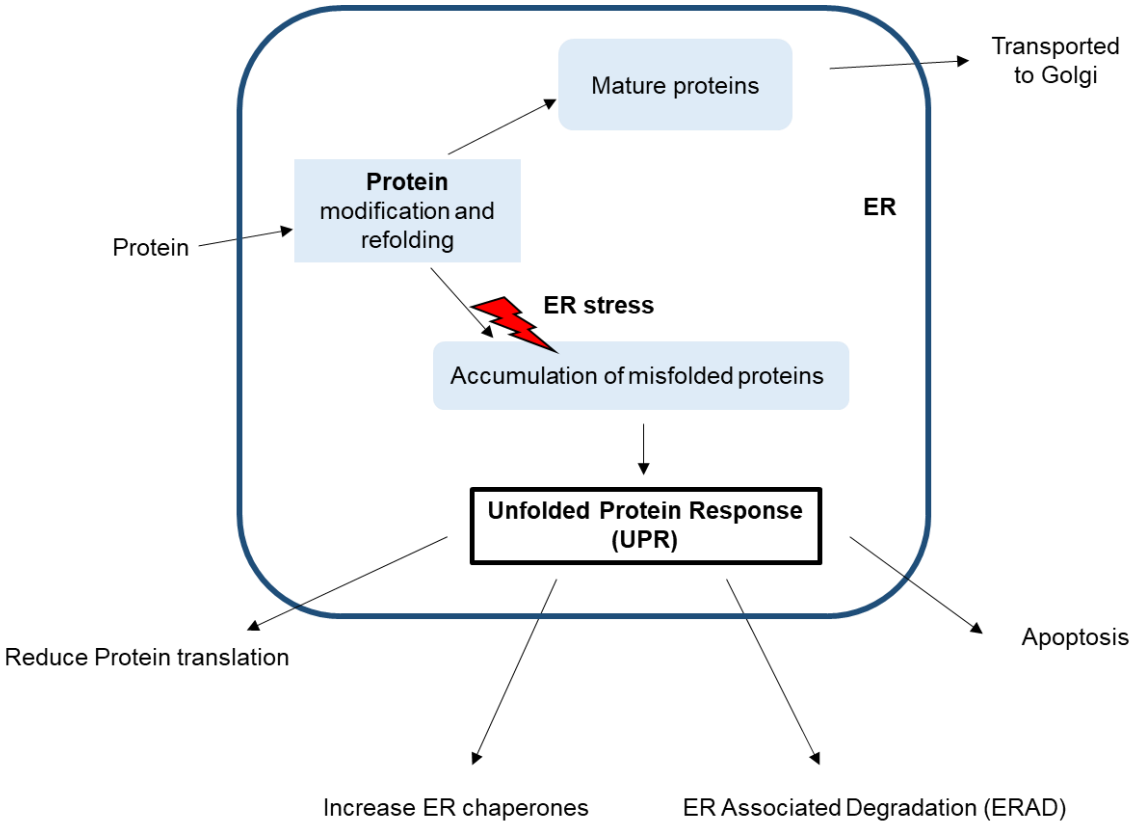

Figure 1.11: ER stress pathways.

In the ER, proteins undergo modification and refolding to become mature proteins which are then transported to the Golgi apparatus. However, the excessive accumulation of misfolded proteins in the lumen of the ER results in ER stress. To maintain homeostasis in the ER, cells adopt a compensatory pathway called the "unfolded protein response" (UPR). The UPR maintains homeostasis by decreasing protein translation, increasing ER chaperones, inducing the ERAD pathway and by apoptosis.

enzymes.

The major molecular chaperones in the ER are immunoglobulin heavy-chain binding protein (BiP; also known as GRP78 and HSPA5), BiP-associated protein (BAP), calnexin and calreticulin (Ma and Hendershot, 2004). The molecular chaperones aid in protein translocation, protein folding and protein degradation to maintain ER homeostasis. The ER chaperone, BiP, also known as glucose regulated protein 78 (GRP78), is a central regulator of ER stress with anti-apoptotic properties (Lee, 2005). BiP is the ER resident protein that binds to the hydrophobic region of unfolded proteins via a substrate binding domain (Gething, 1999). This facilitates folding through a conformational change evoked by the hydrolysis of ATP by the ATPase domain. BiP is an indicator of misfolded proteins in the ER and ER stress. In addition, BiP has the ability to control apoptosis by impairing interactions between caspases 7 and 12 (Rao et al., 2002, López et al., 2017). Heat shock protein 40 (HSP40) chaperones e.g., P58IPK, ER dnaJ 1(ERdj1), ERdj3, ERdj4 and ERdj5 modulate the function of BiP (as a co-chaperone) by regulating its ATPase (Yoshida, 2007). BAP modulates the function of BiP by enhancing nucleotide exchange and is involved in the general folding process of secretory proteins (Chung et al., 2002). Calnexin and calreticulin are molecular chaperones that belong to the class of lectin-like chaperones and are involved in the folding of glycoproteins (Ellgaard and Helenius, 2001). Proteins with an Asn-X-Ser/Thr sequence synthesised in the ER are attached with a mannose type oligosaccharide which is trimmed during protein maturation (Schrag et al., 2001, Buck et al., 2007). The glycoproteins are trimmed by glucosidase I or II and the polypeptides are folded by the calnexin cycle (Kornfeld and Kornfeld, 1985). The mannose peptide residues of polypeptides that are not folded by the calnexin cycle are cleaved by mannosidase and removed by the ERAD machinery.

Protein disulfide isomerase (PDI) and glucose regulated protein 58/ER resident protein 57 (GRP58/ERp57) are folding enzymes that help to form appropriate disulfide bonds by oxidising relevant cysteine residues of nascent proteins (Yoshida, 2007). These enzymes are also involved in protein folding as well as recognising and targeting aberrant proteins for ERAD (Nishikawa et al., 2005, Jordan and Gibbins, 2006).

1.9.2 ERAD pathway

ERAD plays an important role in maintaining ER homeostasis and in preventing diseases caused by the accumulation of proteins in the ER. The four main steps in the ERAD pathway are recognition, retrotranslocation, ubiquitination and degradation (Yoshida, 2007). Following recognition of misfolded proteins by ER molecular chaperones and lectin-like proteins, the ERAD machinery traps the misfolded proteins so that ER resident reductases can cleave the disulfide bonds to facilitate retrograde transport to the cytoplasm (Hoseki et al., 2010). The retrotranslocated proteins are then ubiquitinated and degraded by the proteasome in the cytoplasm.

Mannose type oligosaccharides are attached to most proteins in the ER. However, the glycoproteins that are not properly folded by calnexin bind to the ER degradation enhancing α mannosidase like protein (EDEM; **Figure 1.12**) (Eriksson et al., 2004). The three EDEMs involved in the ERAD pathway are EDEM1, EDEM2 and EDEM3. EDEM1 is an ER membrane protein whereas EDEM2 and EDEM3 are luminal proteins (Hirao et al., 2006, Mast et al., 2005). Other ERAD proteins responsible for the recognition of misfolded proteins include OS9 (Szathmary et al., 2005). The proteins then associate with protein disulfide isomerase (PDI) and BiP to allow cleavage of disulfide bonds and to unfold the partially folded proteins (Kabani et al., 2003, Nishikawa et al., 2001). Derlin forms a translocation channel in the ER membrane and binds to the cytosolic ATPase p97 through an adapter protein valocin-containing protein (VCP)-interacting membrane protein 1 (VIMP1) (Ye et al., 2005). p97 is a cytosolic AAA-ATPase and recruits unfolded ER proteins to the cytosol in association with ubiquitin fusion degradation 1 (ufd1) and nuclear protein localisation proteins 4 (Npl4) (Byun et al., 2014, Ye et al., 2003, Rabinovich et al., 2002). The retrotranslocated proteins are ubiquitinated by the activation enzymes (E1s)-conjugation enzymes (E2s)-ligation enzymes (E3s) ubiquitin system present in the cytoplasm (Eletr et al., 2005, Chaugule and Walden, 2016). Derlin binds to an ubiquitin ligase complex that consists of HMG-CoA reductase degradation protein 1 (HRD1) and suppressor of lin-12 like protein 1 (SEL1L) (Hosokawa et al., 2008). Ubiquitin is firstly conjugated to enzyme E2 by E1 and then transferred to the ERAD substrate by E3. The retrotranslocated and ubiquitinated proteins are deglycosylated by peptide N-glycanase before their degradation by the proteasome.

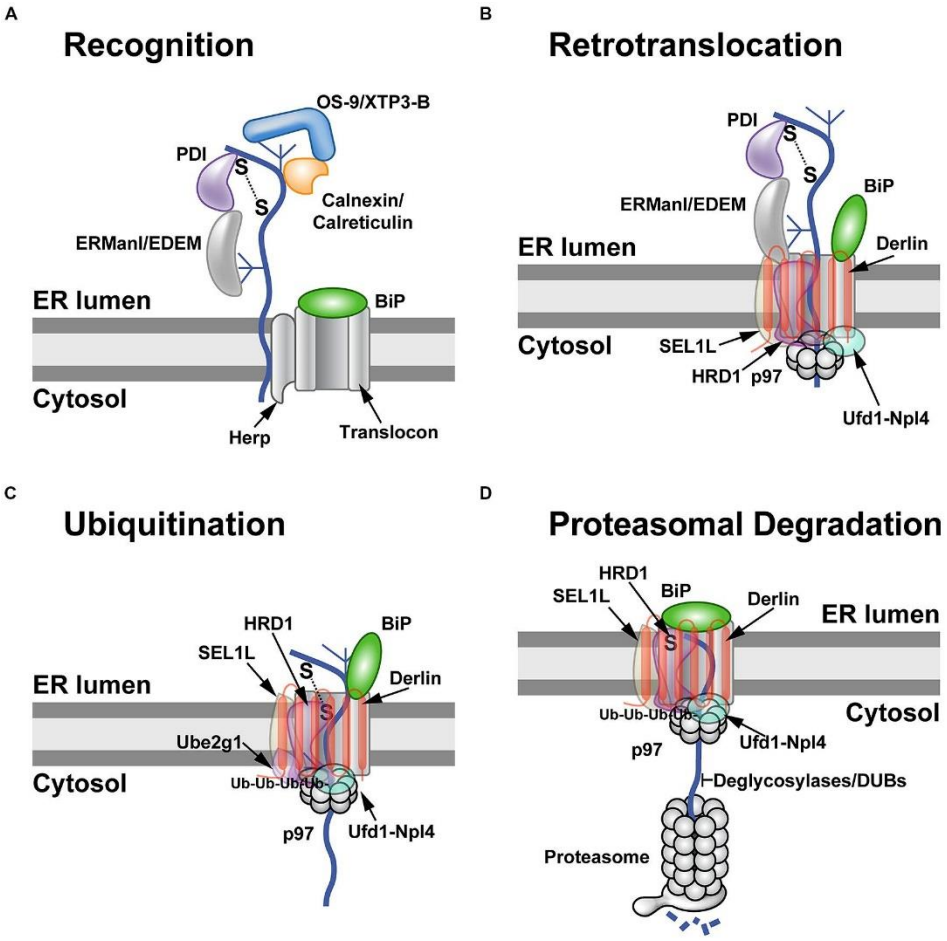

Figure 1.12: ERAD pathway.

The four main steps of ERAD pathway are recognition (a), retrotranslocation (b), ubiquitination (c) and degradation (d). (a) During recognition, misfolded protein binds to the ER degradation enhancing α-mannosidase like protein (EDEM) and OS9. In addition, misfolded protein associates with protein disulfide isomerase (PDI) to partially unfold the protein. (b) Recognition of misfolded protein results in the assembly of retrotranslocon (with the help of homocysteine-induced ER protein (Herp) and BiP). Retrotranslocon contains derlin, HMG-CoA reductase degradation protein-1 (HRD1) and suppressor of lin-12 like protein 1 (SEL1L). This complex recruit cytosolic ATPase p97 and its associated proteins ubiquitin fusion degradation 1 (ufd1) and nuclear protein localisation proteins 4 (Npl4). PDI and EDEM then disengage and the misfolded protein passes through the translocon. (c) In the cytosol, ubiquitination of the protein takes place followed by (d) proteasomal degradation of protein; BiP then binds to the luminal side of the translocon. Adapted from (Byun et al., 2014).

In the ERAD pathway for unglycosylated proteins, BiP interacts with the partially oxidised form of the protein and prevents the formation of the fully oxidised form (Hoseki et al., 2010). The protein is then transferred to a complex containing homocysteine-induced ER protein (HERP) and Derlin-1. Thereafter, like the pathway for glycosylated proteins, p97 and HRD1 assist in guiding the proteins to the proteasome for degradation.

1.9.3 Unfolded protein response

The UPR is a signal transduction system that links the ER lumen with the cytoplasm and nucleus. The aim of the UPR is to relieve ER stress, maintain ER homeostasis and prevent cell death. There are three main UPR sensors in mammals: protein kinase RNA (PKR)-like endoplasmic reticulum kinase (PERK), activating transcription factor 6 (ATF6) and inositol requiring ER to nucleus signal kinase 1 (IRE1) (**Figure 1.13**). These transmembrane proteins work together to: i) prevent entry of nascent proteins into the ER lumen and to degrade misfolded and aggregated proteins that have accumulated in the ER; ii) increase the expression of ER chaperones to improve the folding capacity of the ER; iii) increase the transport of misfolded proteins to the cytoplasm for degradation by the proteasomes; and iv) trigger apoptosis in situations where the UPR fails to compensate for ER stress (Eizirik et al., 2008).

Under "unstressed" or basal conditions, the UPR is present in an inactive state and the ER chaperone BiP is found bound to the luminal domain of the three ER transmembrane sensor protein PERK, ATF6 and IRE1 (Bertolotti et al., 2000). BiP activates these ER transmembrane sensors via a binding release mechanism (Back and Kaufman, 2012) i.e., BiP binding to the sensors prevents their activation and vice versa. In the "stressed" state, BiP senses unfolded or misfolded proteins and binds to them, resulting in dissociation from the UPR sensor and activation of UPR signalling (Zhang and Kaufman, 2008a).

1.9.3.1 PERK pathway

PERK is a transmembrane protein which is localised on the ER membrane and senses the accumulation of misfolded proteins in the ER lumen (Harding et al., 1999). The luminal portion of PERK detects unfolded proteins whereas the cytoplasmic portion of PERK contains a serine/threonine kinase domain (Shi et al., 1998).

Figure 1.13: UPR signalling pathways.

ER stress causes release of the BiP chaperone from the UPR membrane proteins (PERK, IRE1 and ATF6). PERK and IRE1 undergo phosphorylation and oligomerisation which causes inactivation of eIF2α for translational attenuation and splicing of XPB1 mRNA to enhance prosurvival genes (e.g., ERAD), respectively. In addition, the RNase activity of IRE1 degrades prosurvival mRNAs via a process called IRE1-dependent decay of mRNA (RIDD). Active ATF6 is translocated to the Golgi apparatus where it is cleaved and increases the transcription of ER chaperones and XBP1. These pathways maintain ER homeostasis and reduce ER stress. In the case of prolonged ER stress, three main apoptotic pathways are induced i.e., the UPR sensors PERK and ATF6 regulate the expression of CCAAT-enhancer-binding protein homologous protein (CHOP). CHOP is present downstream of ATF4 and activates pro-apoptotic genes such as ATF3 and GADD34. IRE1-mediated activation of TNF-receptor associated factor 2 (TRAF2)-apoptosis signal regulating kinase 1 (ASK1) results in activation of c-Jun N-terminal kinase (JNK) or NF-κB, leading to apoptosis or inflammation, respectively. Activation of caspase 12 activates the caspase cascade, resulting in apoptosis. Adapted from Deldicque (2013).

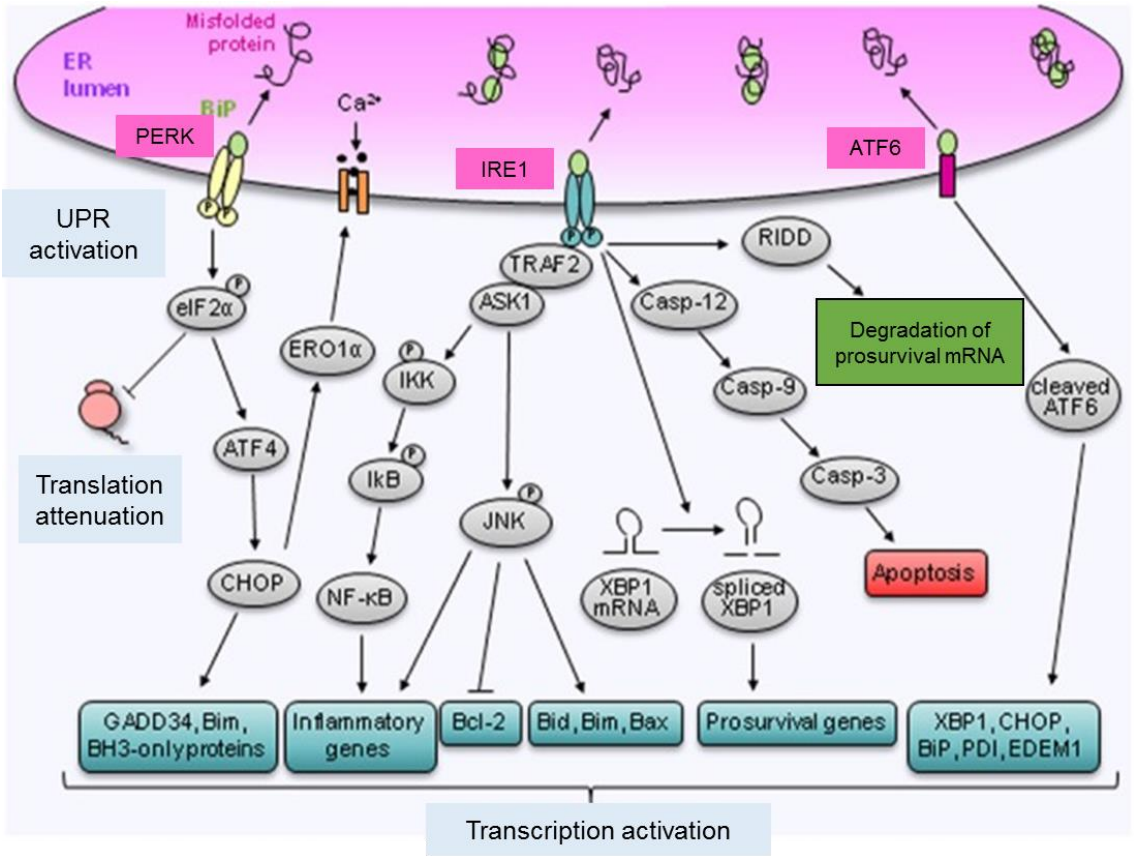
Misfolded protein
ER lumen
BiP
PERK
Ca2+
IRE1
ATF6
UPR activation
TRAF2
RIDD
ASK1
Casp-12
eIF2α
ERO1α
IKK
Degradation of prosurvival mRNA
Casp-9
cleaved ATF6
ATF4
Translation attenuation
IkB
Casp-3
JNK
XBP1 mRNA
spliced XBP1
Apoptosis
CHOP
NF-κB
GADD34, Bim, BH3-only proteins
Inflammatory genes
Bcl-2
Bid, Bim, Bax
Prosurvival genes
XBP1, CHOP, BiP, PDI, EDEM1
Transcription activation

Under normal conditions, BiP is bound to the luminal domain of PERK and remains in its inactive form (**Figure 1.13**). Under stressed conditions, misfolded proteins bind to the canonical substrate binding domain of BiP, releasing PERK and resulting in PERK activation via trans-phosphorylation and oligomerisation. Activated PERK phosphorylates and inactivates the α subunit of the eukaryotic translational initiation factor 2 (eIF2α), causing "general" (global) translation to be attenuated (Harding et al., 1999) and the protein folding load in the ER to be reduced. This process is transient because the protein is dephosphorylated by specific phosphatases including constitutive repressor of eIF2α phosphorylation (CReP), protein phosphatase 2C-GADD34 and p58IPK (Kojima et al., 2003, Brush et al., 2003). Phosphorylated eIF2α selectively activates the translation of the transcription factor ATF4 (Xu et al., 2005). ATF4 upregulates genes that are involved in amino acid import, metabolism and resistance to oxidative stress, i.e., with cytoprotective effects. In contrast, the activation of C/EMP-homologous protein (CHOP) is involved in apoptosis (Hinnebusch, 1993, Harding et al., 2000). The PERK pathway can therefore have either cytoprotective or apoptotic effects.

1.9.3.2 ATF6 pathway

The second UPR transmembrane protein in the ER is ATF6 which is a type II transmembrane protein with a basic-leucine zipper motif (bZIP) type domain and transcription factor domain (Haze et al., 1999, Todd et al., 2008). The two isoforms of ATF6, ATF6α and ATF6β, are ubiquitously expressed in mammals (Haze et al., 2001). ATF6α is responsible for the induction of the UPR.

In the presence of ER stress, ATF6α is released from BiP and translocates to the Golgi where it undergoes regulated intramembrane proteolysis (RIP) by site 1 proteases (S1P) and site 2 proteases (S2P) (**Figure 1.13**) (Ye et al., 2000, Chen et al., 2002). SP1 is a serine protease which cleaves the luminal domain of ATF6α whereas SP2 is a metalloproteinase that cleaves the N-terminal part of ATF6α. The N-terminal cytoplasmic domain of ATF6 is then translocated to the nucleus where ATF6 binds to the ER stress response element (ERSE) and activates the transcription of ER chaperone genes such as BiP (**Figure 1.13**) (Okada et al., 2002). This pathway helps to improve protein folding capacity in the ER.

1.9.3.3 IRE1 pathway

The third UPR transmembrane protein is IRE1. It is the most fundamental ER stress sensor because of its conservation among eukaryotic cells. The luminal domain of IRE1 is similar to PERK and is also responsible for detecting misfolded proteins in the ER. The cytoplasmic domain contains a kinase domain and a ribonuclease (RNase) domain (Yoshida, 2007, Tirasophon et al., 2000). IRE1 exists in two isoforms i.e., IRE1α and IRE1β. IRE1β is mainly present in gastrointestinal tract epithelial cells, whereas IRE1α is highly expressed in pancreatic cells (Bertolotti et al., 2001, Tirasophon et al., 1998).

During ER stress, BiP releases IRE1α for its activation via trans-phosphorylation and oligomerisation (**Figure 1.13**). Activated IRE1 converts x-box binding protein 1 (XBP1) pre-mRNA to a mature spliced XBP1 mRNA by unconventional process of splicing (Calfon et al., 2002). The splicing removes a 26-base intron from the mRNA encoding the bZip-containing XBP1, resulting in the translation of active XBP1 (Chen and Brandizzi, 2013). The XBP1 is then translocated to the nucleus and binds to the unfolded response element (UPRE) to increase the expression of prosurvival genes encoding chaperones, folding catalysts and ERAD machinery such as EDEM, EDEM2/3, Derlins-1–3, and HRD1 (Lee et al., 2003, Sriburi et al., 2004).

In addition, IRE1α RNase activity is involved in a mechanism known as regulated IRE1-dependent decay of mRNA (RIDD) (Hollien and Weissman, 2006). RIDD selectively degrades proteins (secretory or membrane) in the ER to reduce the ER load (Hollien et al., 2009).

1.9.4 ER stress-induced apoptosis

The excessive accumulation of misfolded proteins in the ER is toxic to cells. When the UPR pathway fails to suppress ER stress, apoptotic pathways are triggered to terminate the cells. Apoptosis is derived from a Greek word ἀπόπτωσις meaning “falling off”. Apoptosis is a type of cell death that eliminates unwanted or harmful cells and is characterised by the activation of caspases (cysteine proteases). Apoptosis occurs during the development and ageing of cells as well as when cells are damaged. Cells undergoing apoptosis are morphologically different from normal cells. Apoptotic cells are round or

oval due to cell shrinkage and have dense eosinophilic cytoplasm with tightly packed organelles (Elmore, 2007). The main characteristic feature of apoptosis is the condensation of chromatin at the nuclear periphery. This is accompanied by the disassembly of nuclear scaffold proteins and the formation of apoptotic bodies (Toné et al., 2007, Prokhorova et al., 2015). The three well characterised apoptotic pathways associated with ER stress are the CCAAT-enhancer-binding protein homologous protein (CHOP) pathway, IRE1-TRAF2-ASK1 pathway and the caspase pathway (**Figure 1.13**) (Yoshida, 2007).

Production of the transcription factor CHOP is induced by the ATF6 and PERK pathways during ER stress (**Figure 1.13**). CHOP is also known as growth arrest and DNA damage 153 (GADD153). Activated ATF4 translocates to the nucleus and binds to the amino acid response element (AARE) and to the ERSE in the promoter region of the CHOP gene to increase its expression (Oyadomari and Mori, 2004). CHOP activates the expression of proapoptotic factors such as death receptor 5 (DR5) and ER oxidoreductin 1 (ERO1). DR5 is a transmembrane receptor and a member of the TNF receptor family. DR5 is a cell surface death receptor that activates the caspase cascade (Yamaguchi and Wang, 2004). ERO1 and ER oxidase cause the ER a more hyper-oxidizing environment (Marciniak et al., 2004). Furthermore, $CHOP^{-/-}$ mice are protected from renal toxicity when ER stress is induced by tunicamycin (Marciniak et al., 2004), suggesting that CHOP induces cell death during chronic ER stress. In line with this, CHOP deletion in rodents (db/db mice and heterozygous Akita mice) protects from ER stress-induced beta cell death induced by the accumulation of misfolded proinsulin and by oxidative stress (Song et al., 2008, Oyadomari et al., 2001, Oyadomari et al., 2002b).

The IRE1-TRAF-ASK1 pathway is signalled through the IRE1-dependent activation of mitogen-activated protein kinases (MAPK) cascade (**Figure 1.13**). Activated IRE1 binds to an adaptor protein tumor necrosis factor receptor associated factor 2 (TRAF2) and forms a complex with apoptosis signal regulating kinase 1 (ASK1) which phosphorylates and activates JNK (Nishitoh et al., 2002, Urano et al., 2000). In beta cells, activation of the JNK pathway results in decreased pancreatic PDX-1 activity, suppression of insulin gene transcription and ultimately, beta cell death. Conversely, suppression of insulin gene expression by the JNK pathway can protect beta cells from oxidative stress (Zhang and

Kaufman, 2008). Furthermore, the IRE1-TRAF2-ASK1 complex phosphorylates IKK, resulting in activation of NF-κB pathway and the expression of inflammatory genes.

Caspases are proapoptotic components which are also induced by ER stress. Caspases are expressed constitutively in healthy cells and are synthesised as procaspases. The caspase family is divided into two groups: initiator caspases (caspase-8, 9, and 12) and effector caspases (caspase-3, 6, and 7) (Morishima et al., 2002). The initiator caspases, activated in response to apoptotic signals, process the precursors of the effector caspases. Caspase-12 in rodents and caspase-4 in humans is present on the ER membrane and is activated by ER stress (Martinez et al., 2010, Binet et al., 2010). Caspase-12/4 activates caspase-9 which in turn activates the caspase-3-mediated apoptotic pathway leading to beta cell death (**Figure 1.13**) (Morishima et al., 2002). Previous studies have shown that caspase-12 is induced in PC12 cells and fibroblast cells by ER stress inducers (e.g., tunicamycin, thapsigargin). Furthermore, embryonic fibroblast cells of caspase-12 null mutant mice are resistant to ER stress inducers (tunicamycin/thapsigargin), suggesting that caspase-12 is essential for ER stress-induced apoptosis (Nakagawa et al., 2000).

1.9.5 ER stress-associated inflammation

ER stress together with oxidative stress generates inflammatory signals. ER stress triggers inflammation in the hypothalamus, pancreatic beta cells, adipocytes and hepatocytes in response to increased fatty acid levels and/or nutrient overload. The ER stress sensors PERK and IRE1 and their pathways regulate the expression of thioredoxin interacting protein (TXNIP) which binds to thioredoxin to inhibit oxidant scavenging and thiol-reducing capacity (Hasnain et al., 2012). In addition, oxidative stress activates NF-κB in beta cells via TXNIP, resulting in inflammasome activation, IL-1β secretion and local inflammation (Menu et al., 2012). Thus, TXNIP provides a direct link between regulation of ER stress and oxidative stress (Oslowski et al., 2012, Hasnain et al., 2016, Menu et al., 2012). Alternatively, high levels of cytosolic Ca^{2+} and ROS can induce NF-κB signalling independently of the UPR pathway (Hasnain et al., 2016).

NF-κB is a master regulator of inflammation in beta cells. For example, IRE1/TRAF2 activation can induce AKT and JNK signalling (**Figure 1.13**) and PERK/eIF2α pathway

activates NF-κB, inducing cytokine and chemokine gene transcription and subsequent inflammation (Deng et al., 2004, Jiang et al., 2003, Urano et al., 2000). Local inflammation results in the activation of intra-islet resident macrophages, dendritic cells, T cells and endothelial cells as well as in increased leukocyte recruitment from the blood (Coppieters et al., 2012, Toyama et al., 2003).

1.9.6 ER stress inducers

The profile of ER stress markers and the UPR in different cell types suggest that different ER stress inducers activate the UPR in a distinct manner. ER stress and activation of the UPR can be induced by certain pharmacological and physiological agents. Pharmacological agents that induce ER stress include: tunicamycin, thapsigargin, brefedin A and dithiothreitol (DTT). Physiological inducers, on the other hand, include palmitate, cytokines (IL-1β and IFN-γ) and chronic exposure to high glucose (Oslowski and Urano, 2011, Cardozo et al., 2005, Cunha et al., 2008a, Åkerfeldt et al., 2008). The concentration of ER stress inducers and the duration of treatment varies among different systems. In this project, thapsigargin and tunicamycin were used as pharmacological or chemical ER stress agents in *in vitro* studies, and the saturated free fatty acid palmitate was chosen as a physiological ER stress inducer.

Tunicamycin is an antibiotic derived from *Streptomyces lysosuperificus* and inhibits N-linked glycosylation (Takatsuki et al., 1971). Tunicamycin is an inhibitor of the UDP-N-acetylglucosamine-dolichol phosphate N-acetylglucosamine-1-phosphate transferase (GPT) which blocks the initial step of glycoprotein synthesis in the ER (**Figure 1.14(a)**) (Dorner et al., 1990). Treatment with tunicamycin causes an accumulation of unfolded glycoproteins in the ER and ER stress. Tunicamycin treatment of MIN6 cells has been reported to induce the UPR and beta cell death (Srinivasan et al., 2005, Engin et al., 2013, Gao et al., 2014).

Thapsigargin is a specific inhibitor of the sarcoplasmic/endoplasmic reticulum Ca^{2+}-ATPase (SERCA) (Lytton et al., 1991). The resulting disturbance in the Ca^{2+} levels in the ER causes ER stress (**Figure 1.14(b)**). Treatment of MIN6 cells with thapsigargin results in a decline in ER calcium levels which in turn impairs the activity of the calcium-ion

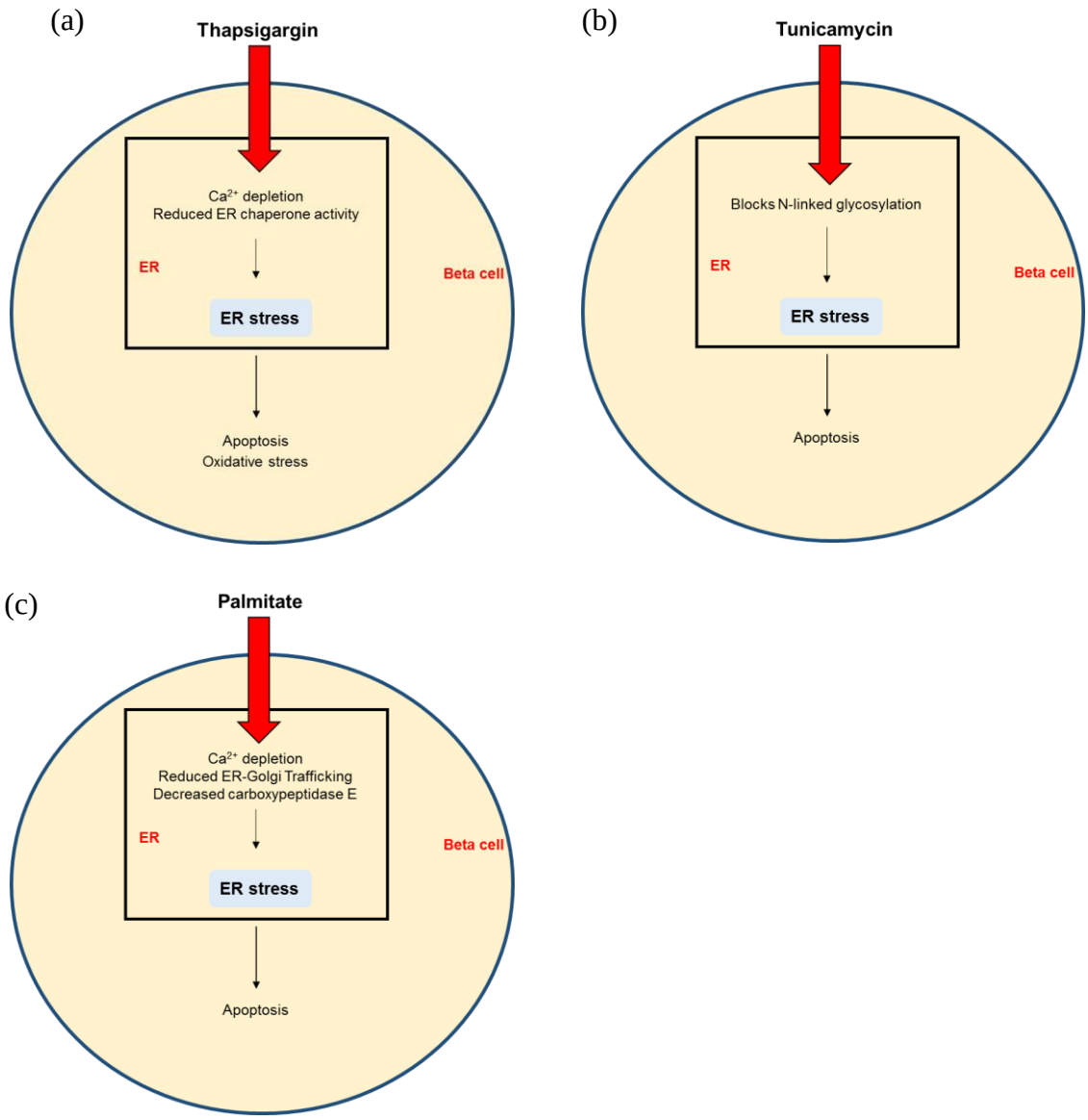

Figure 1.14: Mechanism of ER stress inducers.

(a) Tunicamycin is an antibiotic which inhibits N-linked glycosylation in the ER. Glycosylation is important for protein folding and disruption of this process results in misfolding and the accumulation of proteins in the ER causing ER stress. (b) The pharmacological ER stress agent thapsigargin decreases Ca^{2+} levels in the ER and impairs protein folding capacity by reducing the activity of ER chaperones i.e., resulting in misfolded proteins. This causes ER stress which can lead to oxidative stress and apoptosis. (c) The saturated free fatty acid palmitate results in depletion of Ca^{2+} from the ER, reduction in ER-Golgi trafficking and reduction in carboxypeptidase E, causing accumulation of misfolded proteins in the ER and ER stress. Failure of beta cells to adapt to ER stress, results in apoptosis/cell death.

dependent ER chaperones such as calnexcin and BiP, and impacts protein folding capacity in the ER leading to ER stress (Yoshida, 2007, Werno et al., 2008, Zhou et al., 1998). In *in vitro*, thapsigargin treatment of rodent islets and MIN6 cells induce increased production of ROS, enhanced expression of ER stress-associated genes and beta cell apoptosis (Srinivasan et al., 2005, Ueda et al., 2005, Zhou et al., 1998, Wali et al., 2014, Kaufman, 1999).

Palmitate is a long chain saturated FFA and is toxic for beta cells *in vivo* and *in vitro* (**Figure 1.14(c)**) (Zhang and Kaufman, 2008a). For *in vitro* studies, palmitate is usually coupled to bovine serum albumin (BSA) to increase its solubility. Exposure of pancreatic beta cells to palmitate induces ER stress by a number of different mechanisms. Elevated levels of palmitate deplete Ca^{2+} in the ER and hamper ER-to-Golgi protein trafficking, thereby contributing to the build-up of protein in the ER (Preston et al., 2009, Cunha et al., 2008b). In addition, palmitate contributes to the accumulation of long chain acyl-coenzyme A or lipid derivatives as well as to the activation of PKC-δ, resulting in beta cell dysfunction (Back et al., 2012). Palmitate exposure also promotes the degradation of carboxypeptidase E, an enzyme involved in insulin processing. This leads to the accumulation of misfolded proinsulin in the ER, culminating in ER stress (Jeffrey et al., 2008, Fonseca et al., 2011). Palmitate has also been shown to activate the UPR in INS-1E (rat) and MIN6 (mouse) insulinoma cells as well as in primary rodent and human islets (Kharroubi et al., 2004, Laybutt et al., 2007) as a consequence of ER stress, and induce beta cell apoptosis (Eizirik et al., 2008).

1.10 ER stress and type 2 diabetes

Endocrine cells are highly susceptible to ER stress because peptide hormones require a complex three-dimensional protein structure. Furthermore, the requirement for hormone secretion changes rapidly. In pancreatic beta cells, the folding and processing of newly synthesised proinsulin is carried out in the ER followed by trafficking of proinsulin to the Golgi apparatus. The increased demand in insulin and protein synthesis poses a burden on the ER that results in ER stress, beta cell dysfunction, beta cell failure and eventually diabetes.

ER stress in beta cells can be caused by chronic exposure to elevated levels of FFAs (see Section 1.8) and/or glucose (see Section 1.7), obesity (see Section 1.5), insulin resistance (see Section 1.5) and elevated levels of pro-inflammatory cytokines (Cunha et al., 2008b, Matveyenko et al., 2009, Bensellam et al., 2012, Hasnain et al., 2014). Furthermore, islet amyloid accumulation contributes to ER stress in humans with T2D.

In T2D, beta cells increase the production of proinsulin to compensate for insulin resistance in peripheral tissues. This creates an over-load in the ER causing ER dysfunction. The increased demand for protein folding in the ER creates an imbalance between the protein folding load and the ER's protein folding capacity. As a consequence, unfolded or misfolded proteins accumulate in the ER lumen causing ER stress and activation of the UPR (Zhang and Kaufman, 2008a). In response, beta cells increase their cell mass and processing capacity in order to synthesise and secrete more insulin - this is referred to as "beta cell adaptation" or "compensation" (**Figure 1.15**). When beta cells fail to adapt to an increased demand for insulin, insulin deficiency, beta cell dysfunction and ultimately diabetes ensues (**Figure 1.15**).

1.10.1 Role of the UPR in beta cell compensation

The UPR machinery is important for ER homeostasis and beta cell integrity. The UPR sensors in the ER play a critical role in regulating ER folding capacity, increasing the degradation of misfolded proteins and in reducing mRNA translation (Rabhi et al., 2014). Various transgenic mouse models and rodent models of obesity and insulin resistance have provided valuable insights into the positive role of the UPR in the adaptation of beta cells to an increased burden for proinsulin synthesis and in the mechanism of beta cell compensation.

For example, IRE1α/XBP1 stimulates proinsulin synthesis in beta cells (Lipson et al., 2006) and beta cell specific deletion of XBP1 in mice causes beta cell failure, suggesting that IRE1α-XBP1 signalling is important for beta cell function (Lee et al., 2011).

Furthermore, the conditional deletion of IRE1α in pancreatic beta cells of mice and insulinoma beta cells (INS-1 and MIN6 cells) resulted in diabetes (Lipson et al., 2006, Hassler et al., 2015, Iwawaki et al., 2010, Lee et al., 2011). Perk KO mice (with

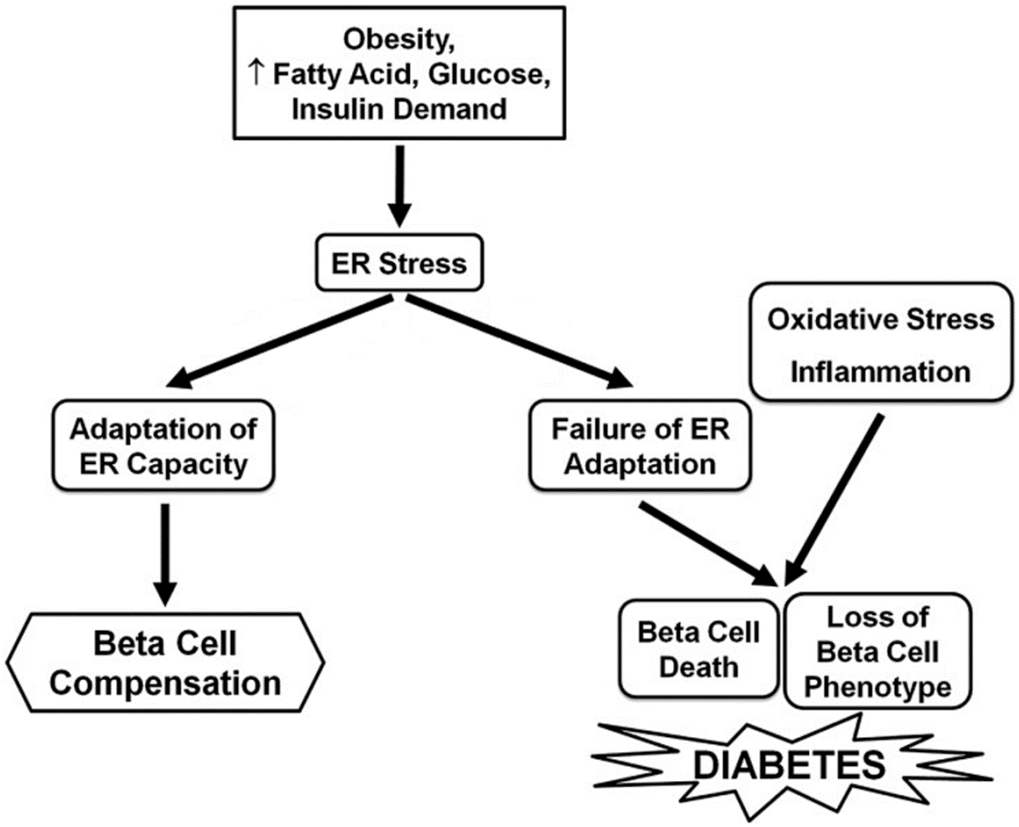

Figure 1.15: Role of ER stress in pancreatic beta cells.

Obesity and metabolic changes such as hyperlipidemia, glucose intolerance, and increased insulin demand lead to ER stress in pancreatic beta cells. Upregulation of the adaptive UPR helps to improve beta cell function by increasing beta cell mass and ER capacity. The failure of the ER to adapt to ER stress together with increased oxidative stress and inflammation results in beta cell death or loss of beta cell phenotype, causing T2D. Modified from Chan et al. (2013).

C57BL/6J or 129SvEvTac background) showed early onset of diabetes and failure tophosphorylate eIF2α and attenuate insulin translation, thus resulting in ER stress and impaired insulin secretion (Zhang et al., 2006, Harding et al., 2001). The ob/ob mice strain is leptin-deficient. Ob/ob mice become obese as well as insulin-resistant but do not develop diabetes because of beta cell compensation (Chan et al., 2013). The islets from ob/ob mice exhibit increased expression of adaptive UPR markers which accompany a compensatory increase in beta cell mass and function. In addition, BALB/c mice lacking XBP1 (BALB/c-XBP-$1^{+/-}$ mice) developed insulin resistance, suggesting that ER stress is associated with obesity and insulin resistance (Ozcan et al., 2004). Similarly, increased markers of adaptive UPR were observed in high fat diet (HFD) mice, db/db mice and ZDF rats, compared to their respective controls. Furthermore, overexpression of the ER chaperone BiP in beta cells protected RIP-*GRP78* $^{-/+}$ mice from HFD-induced diabetes (Teodoro-Morrison et al., 2013).

1.10.2 Role of the UPR in beta cell dysfunction

Chronic ER stress both *in vitro* and *in vivo* contributes to beta cell dysfunction and beta cell death by activating pro-apoptotic UPR pathways. For example, isolated islets from 6 week-old prediabetic db/db mice showed increased transcript expression for UPR markers i.e., XBP1s, ATF4, IRE1 and PERK whereas these markers were reduced in diabetic db/db mice at 16 weeks of age (Chan et al., 2013). These findings indicated that in db/db beta cells, the UPR is not able to cope sufficiently with prolonged ER stress, resulting in beta cell dysfunction. Furthermore, JNK activation following exposure of MIN6 cells to cytokines was associated with lower levels of UPR mRNAs and beta cell death, whereas inhibition of JNK in db/db islets increased UPR gene expression and reduced beta cell death (Chan et al., 2013). Although $Ins2^{WT/C96Y}$ mice represent another model of ER stress-induced diabetes, $Ins2^{WT/C96Y}$ mice crossed with $Chop^{-/-}$ mice showed delayed onset of diabetes supporting a role for CHOP in beta cell apoptosis (Oyadomari et al., 2002b). In addition, CHOP gene deletion in genetic- (db/db) and diet-induced (eIF2αS/A$Chop^{-/-}$ and STZ-treated) mouse models of insulin resistance led to improved glycaemia, reduced oxidative stress, increased beta cell mass and enhanced increase in UPR gene expression (Song et al., 2008). Conversely, beta cell lines, human islets and mouse islets exposed to pharmacological ER stress inducers such as thapsigargin and tunicamycin induced beta cell death (Eizirik et al., 2008).

In humans, a mutation in the EIF2AK3 gene which encodes for eIF2a kinase (similar to PERK) causes Wolcott-Rallison syndrome (Delepine et al., 2000). This syndrome is characterised by neonatal or early insulin-dependent diabetes caused by impaired insulin secretion. Immunohistochemical analyses of human T2D islets showed an increase in intra-islet BiP, CHOP and P58 (DNAJC3) compared to non-diabetic controls (Laybutt et al., 2007) and the ER was enlarged (Marchetti et al., 2007). These findings are consistent with prolonged ER stress contributing to beta cell dysfunction and progression of human T2D.

1.11 Oxidative stress

ER stress and oxidative stress are interconnected features of T2D (Song et al., 2008, Back et al., 2009). Oxidative stress occurs due to the excessive production or inadequate disposal of intracellular reactive oxygen species (ROS) and reactive nitrogen species (RNS) which have deleterious effects on cells. Under physiological conditions, endogenous ROS/RNS helps to maintain cell homeostasis and function (Robertson et al., 2004). Conventionally, ROS/RNS are generated in intracellular organelles including the ER and mitochondria, by oxidative phosphorylation, glyceraldehyde auto-oxidation, the formation of advanced glycation products and oxidative protein folding (Scheuner and Kaufman, 2008). High concentrations of ROS and RNS promote NF-κB activation, induce DNA damage as well as alter mitochondrial membrane potential, resulting in the release of cytochrome c and apoptosis (Lowell and Shulman, 2005). To regulate intracellular ROS and RNS levels, cells produce a wide range of antioxidant enzymes known as “free radical scavengers”, including superoxide dismutases (SODs; Cu-Zn-SOD1 (cytoplasmic); Mn-SOD2 (mitochondrial)), glutathione peroxidase, glutathione reductase, and catalase (Pham-Huy et al., 2008).

The process of oxidative protein folding involves the formation of intramolecular and intermolecular disulfide bonds and is found in the processing of proinsulin to insulin in beta cells. Oxidizing conditions are generated by two key enzymes: protein disulfide isomerase (PDI) and ER oxidoreductin 1 (ERO1) (Malhotra et al., 2008, Pollard et al., 1998). Disulfide bond formation results in the production of ROS. Firstly, PDI catalyses the oxidation of substrate polypeptides. PDI is subsequently reduced by ERO1 and the

transfer of electrons to molecular O_2 results in the generation of ROS (Tu and Weissman, 2002). In the ER, PDI also generates disulfide bonds in nascent proteins for their secretion. Additionally, reduced glutathione (GSH) reduces non-native disulfide bonds in misfolded proteins, producing oxidised glutathione and ROS (Malhotra and Kaufman, 2007). Under conditions of ER stress, this reaction would be expected to exacerbate increased ROS levels and contribute to oxidative stress.

During the production of ATP via mitochondrial respiration, superoxide (ROS) is produced by the transfer of an electron to molecular oxygen (Pham-Huy et al., 2008, Cao and Kaufman, 2014). This process is fundamental to cellular physiology and impacts calcium influx, energy demand, cellular redox state, hypoxia, ER stress, and inflammation (Cao and Kaufman, 2014).

1.11.1 ER stress-induced oxidative stress

ER stress and oxidative stress coexist and are interconnected in T2D beta cells (**Figure 1.16**). Beta cells express low levels of antioxidant enzymes and are therefore susceptible to oxidative damage (Tiedge et al., 1997, Robertson et al., 2003, Wang and Wang, 2017, Li et al., 2008a). Protein misfolding in the ER elevates ROS levels; in addition, oxidative stress can induce protein misfolding by disturbing ER homeostasis and disrupting disulfide bond formation (Scheuner and Kaufman, 2008). Hence, a vicious cycle of ER stress and oxidative stress is likely to exist in T2D beta cells.

Protein misfolding in the ER contributes to oxidative stress by increasing disulfide bond formation. GSH reduces disulfide bonds to enable proper bond formation by the PDI-ERO1 cycle. As a consequence, H_2O_2 is produced, depleting GSH levels in the ER and further increasing ROS levels. During the ER adaptive response, disulfide bonds are cleaved by disulfide reductase ERdj5 and degraded, potentially impacting the ER redox balance (Cao and Kaufman, 2014). Furthermore, CHOP activates ERO1 expression and contributes to further ROS production during ER stress. ERO1 induces inositol-1,4,5-trisphosphate receptor (IP3R)-mediated Ca^{2+} leakage from the ER which activates pro-apoptotic pathways and increases mitochondrial membrane permeability (**Figure 1.16**). Ca^{2+} released from the ER is taken up by mitochondria, exacerbating oxidative stress in cells (Tang et al., 2012). To maintain cellular redox homeostasis, the PERK pathway

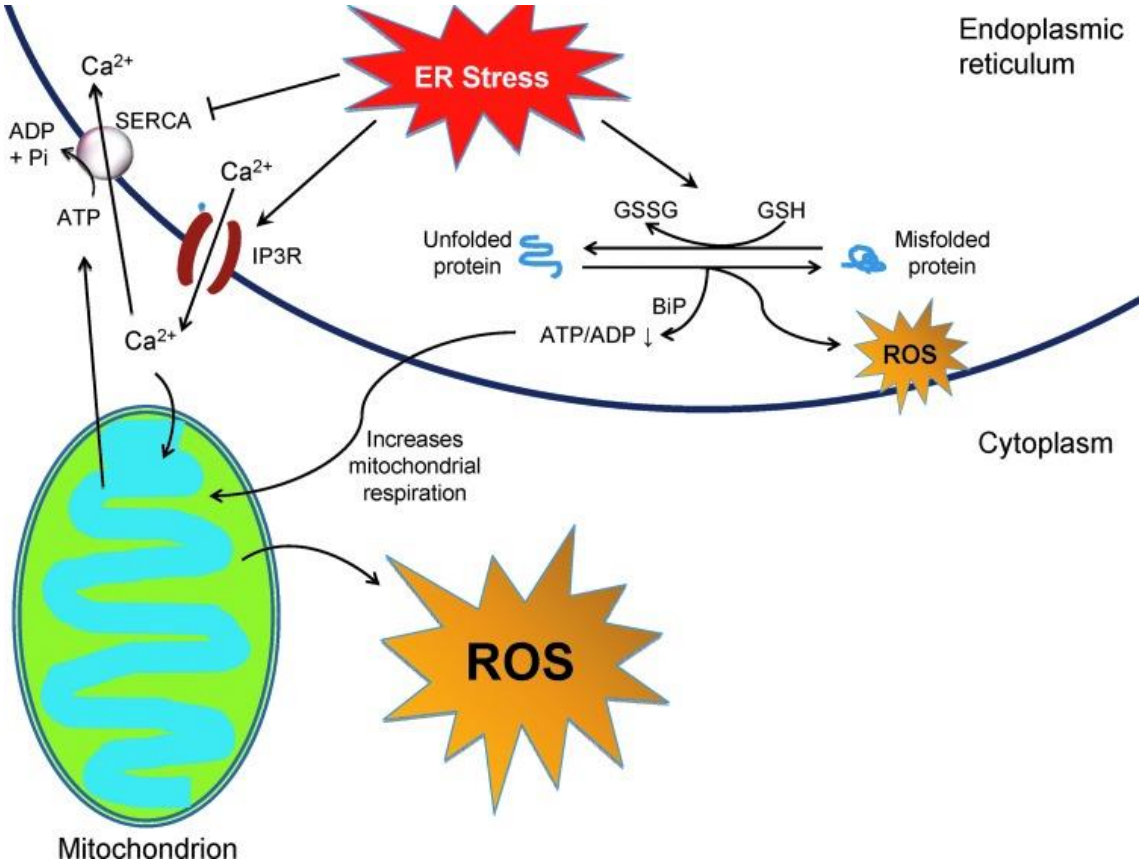

Figure 1.16: ER stress-induced ROS production in the cell.

In response to ER stress, reactive oxygen species (ROS) are generated by cellular processes including oxidative protein folding and mitochondrial respiration. This disrupts cell function and homeostasis and damages the cells. IP3R, inositol-1,4,5-trisphosphate receptor; SERCA, sarcoendoplasmic reticulum (SR) calcium transport ATPase; BiP, binding immunoglobulin protein; ATP, Adenosine triphosphate; ADP, Adenosine diphosphate; GSH, Glutathione; and GSSG, Glutathione disulfide (Cao and Kaufman, 2014).

translates mRNA that encodes for ATF4, allowing phosphorylation of NRF2 (nuclear factor-erythroid-derived 2 (NF-E2)-related factor 2 (NRF)) (Harding et al., 2003). This activation leads to the transcription of genes encoding antioxidant enzymes such as SODs, NAD(P)H quinone oxidoreductases and glutathione S-transferase to prevent intracellular ROS accumulation (Mathers et al., 2004, Zhang, 2006). In support of ROS-induced beta cell damage, *in vivo* treatment of NOD mice with antioxidants such as superoxide dismutase and catalase was shown to protect transplanted islets (Nomikos et al., 1989). Furthermore, N-acetylcysteine treatment of db/db mice displayed improved insulin content, insulin mRNA and an increase in insulin gene transcription factor PDX-1 (Kaneto et al., 1999). In addition, these antioxidants protect beta cells against glucotoxicity, oxidative stress, and AGE production and inhibit NF-κB activation (Tanaka et al., 1999, Tangvarasittichai, 2015, Ho et al., 1999, Ho and Bray, 1999).

1.12 Heparan sulfate proteoglycans

Heparan sulfate proteoglycans (HSPGs) are glycoproteins containing a core protein covalently attached to one or more heparan sulfate (HS; a type of glycosaminoglycan (GAG)) chains (**Figure 1.17**). There are five main classes of HSPGs: the syndecans, glypicans, perlecan, agrin and collagen type XVIII (**Figure 1.18**). These HSPGs always express HS chains and are therefore termed “full-time” HSPGs (Iozzo, 2001). Some HSPGs express HS chains under specific circumstances and are called “part-time” HSPGs, such as CD44, betaglycan and testican (Rops et al., 2004) (**Figure 1.18**). HSPGs are ubiquitously expressed on the surface of cells. The core proteins are attached to a transmembrane domain (syndecans) or to a glycosylphosphatidylinositol-anchored core linkage (glypicans). Extracellularly, HSPGs such as perlecan, agrin and collagen type XVIII are found in basement membranes (BMs) and extracellular matrix (ECM).

HSPGs are structurally diverse molecules due to the extensive chemical heterogeneity of the HS chains. This heterogeneity allows HS chains to bind to a wide range of bioactive molecules such as cytokines, chemokines, growth factors, cell adhesion and proteases (Parish, 2006).

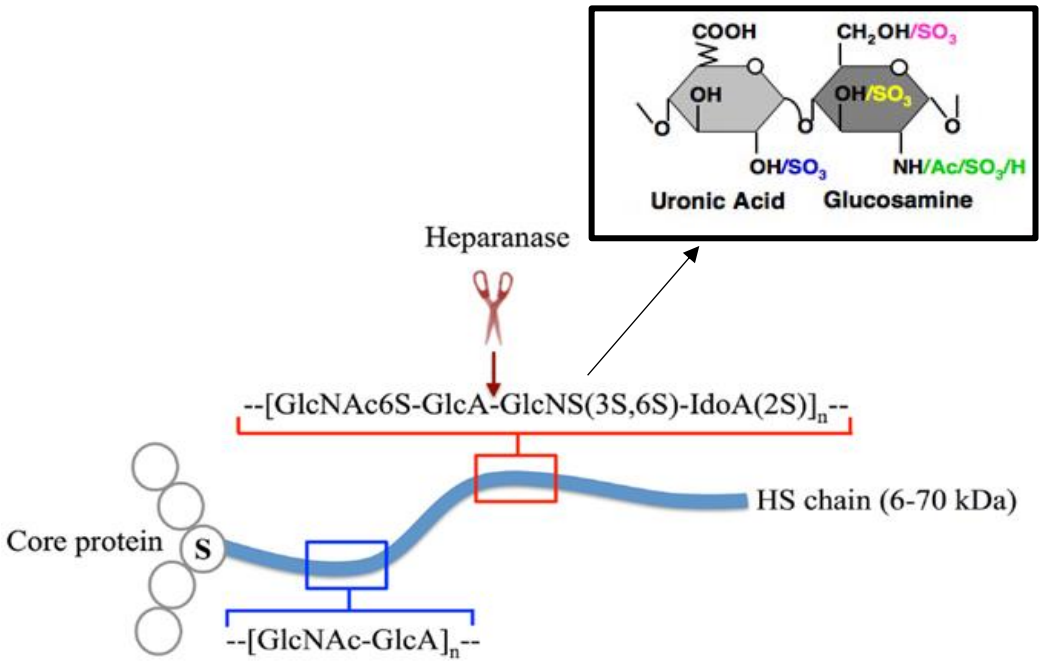

Figure 1.17: Basic structure of heparan sulfate proteoglycans.

Heparan sulfate proteoglycans (HSPGs) consist of heparan sulfate (HS) chains (thick blue line) covalently attached to a core protein. HS chains are linear polysaccharides containing repeating units of glucosamine and uronic acid (black box). The HS chains contain regions that are highly sulfated (red box). Heparanase cleaves HS chains within highly sulfated regions. Adapted from Simon Davis and Parish (2013).

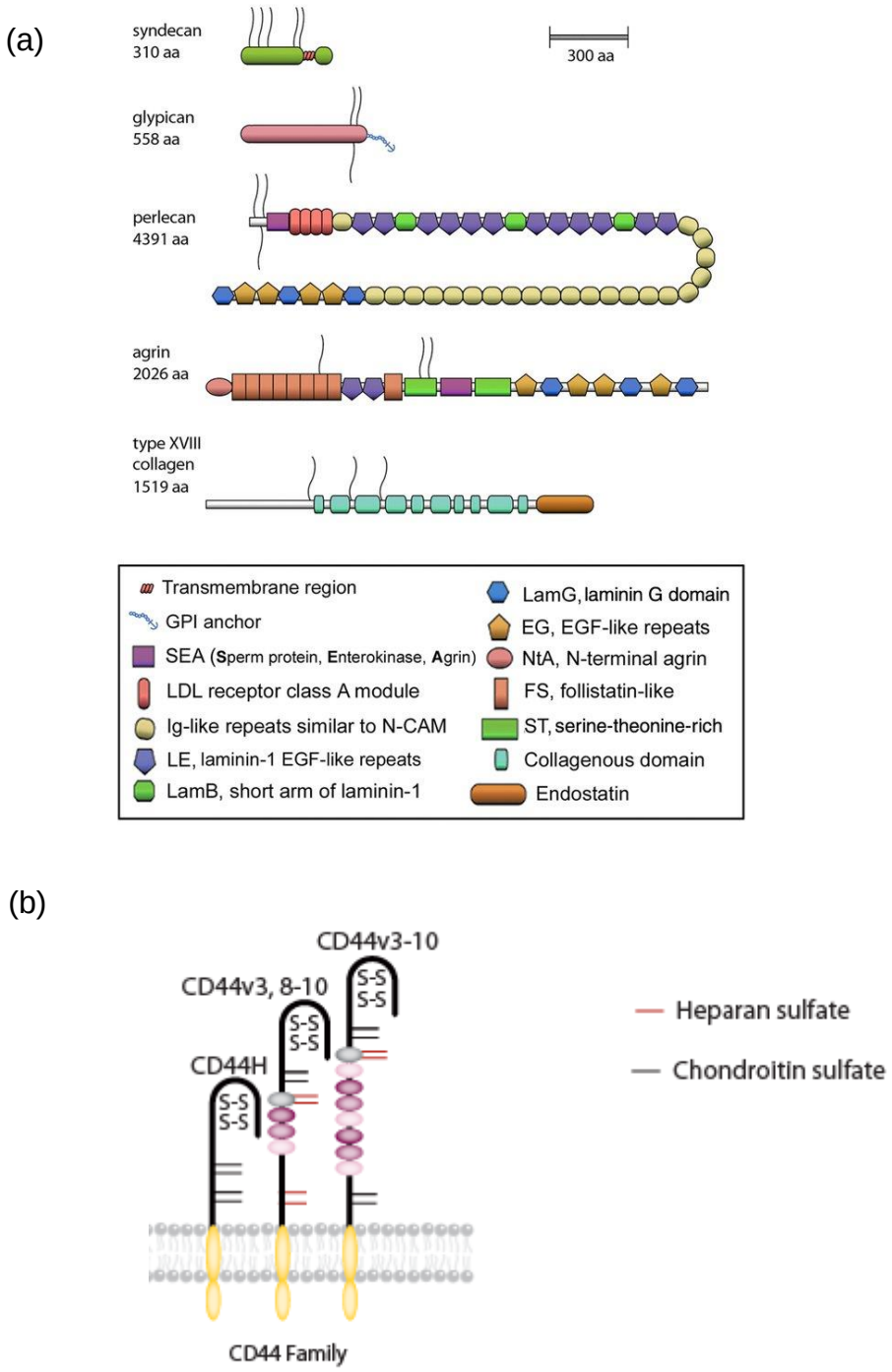

Figure 1.18: Molecular structure of different classes of HSPGs.

The five main classes of HSPGs are the syndecans, glypicans, perlecan, agrin and collagen type XVIII. Generally, syndecans and glypicans are present on the cell surface whereas perlecan, agrin and collagen type XVIII are expressed in extracellular matrix and basement membranes. (b) CD44 expresses HS chains under specific circumstances e.g., CD44 isoform with v3 exon. aa, amino acids. Modified from Iozzo (2001) and Rops et al. (2004).

1.12.1 Syndecans

Syndecans belong to a family of transmembrane proteoglycans to which HS/chondroitin sulfate (CS) chains are attached and are expressed on the cell surface. Syndecans consist of a short intracellular cytoplasmic domain, a single-span transmembrane domain with an ectodomain and an extracellular domain for attachment of GAG chains (**Figure 1.18**) (Tkachenko et al., 2005). Based on the extracellular domain structure, syndecans are categorised into four members i.e., syndecan-1 (syndecan), syndecan-2 (fibroglycan), syndecan-3 (N-syndecan) and syndecan-4 (amphiglycan) (Bernfield et al., 1992, Carey, 1997). The principal GAG chain for syndecans is HS but syndecan-1 and syndecan-3 may additionally contain CS chains (Deepa et al., 2004). The GAG chains of syndecans provide a link between the ECM and the cytoskeleton. Additionally, syndecans act as co-receptors for growth factors, interact with cytoskeleton and modulate cell interactions with the ECM. Within these context, they are involved in cell adhesion, migration, cell signalling, growth and the development of the cytoskeleton (Beauvais and Rapraeger, 2004, Ramani et al., 2012, Couchman et al., 2001).

1.12.2 Glypicans

Glypican core proteins carry 2-5 GAG chains and are bound to the cell surface via glycosyl phosphatidyl inositol (GPI) anchor (Bernfield et al., 1999, Tkachenko et al., 2005). Glypicans consist of a N-terminal signal sequence, an extracellular domain to which GAGs e.g., HS chains, are attached and a C-terminal GPI anchor (**Figure 1.18**). There are six members of glypican family: glypican-1 (glypican), glypican-2 (cerebroglycan), glypican-3 (OCI-5), glypican-4 (K-glypican), glypican-5, and glypican-6. Glypicans generally carry HS chains, with the exception of glypican-5 which contains both HS and CS chains. The glypicans play a very important role in angiogenesis, metastasis and growth regulation. Similar to syndecans, glypican HSPGs also modulate the biological activity of enzymes such as proteases and lipases.

1.12.3 Perlecan

The HSPG perlecan is a secreted HSPG, conventionally expressed in BMs. Perlecan is one of the largest single chain polypeptides found in both vertebrates and non-vertebrates (Iozzo, 1998). The perlecan core protein consists of five domains with one unique domain at the N-terminal region for attachment of HS chains and the other four domains contain

motifs that are involved in nutrient metabolism, mitogenesis and adhesion (**Figure 1.18**) (Dolan et al., 1997, Friedrich et al., 1999). Due to its abundance in BMs, perlecan plays a role in developmental and homeostatic processes, including the establishment of cartilage and the regulation of wound healing. Perlecan HS interacts with other BM components such as laminin, fibronectin and collagen to stabilise the membrane and in doing so, helps the BM to act as a physical barrier to migrating cells (Irving-Rodgers et al., 2008). Perlecan also serves as a reservoir for growth factors, cytokines and chemokines, thereby providing signals for cell activity and function.

1.12.4 Agrin

Agrin is a secreted HSPG abundantly found in BMs and ECMs. Agrin contains multiple polypeptide domains and regulates cell interactions during the development of the central nervous system (**Figure 1.18**). Agrin plays an important role in the formation, maintenance and regeneration of neuromuscular junctions (NMJs) by clustering acetylcholine receptors as well as aggregating sodium channels (Bezakova and Ruegg, 2003). Agrin represents a major component of the glomerular BM and acts as a filtration barrier (Groffen et al., 1998). Agrin found extracellularly helps in the organisation of the muscle cytoskeleton (Goldberg et al., 2009, Bezakova and Ruegg, 2003) by interacting with α-dystroglycan (which connects ECM component to cytoskeleton) (Bassat et al., 2017, Henry and Campbell, 1996).

1.12.5 Collagen type XVIII

Collagen type XVIII (Col18) is also a secreted HSPG which is found in BMs and ECM. The core protein of Col18 can carry up to four HS chains (Rehn and Pihlajaniemi, 1994, Iozzo, 2001). Col18 is a member of the multiplexin family of collagens which contains a central triple helical collagenous domain interrupted and flanked by a non-collagenous domain with extended non-collagenous N- and C-terminal domain (**Figure 1.18**). The non-collagenous domain provides a degree of flexibility between the triple helical collagenous regions and allows formation of fibril polymers. The C-terminal non-collagenous domain is further divided into three segments i.e., a proximal region which is responsible for triple helix assembly, a hinge domain which is highly susceptible to proteases and endostatin which is a proteolytic fragment with anti-angiogenic activities (Marneros and Olsen, 2005). The HS chains of Col18 aid in the migration of leukocytes

to peripheral lymph nodes and in leukocyte adhesion to blood vessels by interacting with the leukocyte receptors, L-selectin and monocyte chemotactic protein-1 (MCP-1). Col18 functions as a negative regulator of angiogenesis and has been implicated in the generation of adipose tissue and in hyperlipidaemia associated with visceral obesity and fatty liver (Seppinen and Pihlajaniemi, 2011). Col18 also functions as a growth factor reservoir, in cell adhesion to ECM and contributes to the barrier function of the glomerular BM.

1.12.6 CD44

CD44 is a part-time HSPG because it expresses HS only under specific conditions (**Figure 1.18**) (Parish, 2006). For instance, resting leukocytes do not express HSPG CD44 but upon activation induce HSPG CD44 expression. HSPG CD44 is found in various isoforms produced by splicing of up to 12 alternative exons (v2-v10) into a single site within the extracellular domain (Rops et al., 2004, Lesley et al., 1994). The standard form of CD44, CD44H or CD44S, contain exons 1-5 and 16-17 which are without HS chains; an isoform of CD44 expresses exon v3 for HS attachment (Rops et al., 2004, Bennett et al., 1995). The structure of CD44 consists of an extracellular, membrane and cytoplasmic domain. CD44 is a transmembrane protein which is typically expressed by macrophages, monocytes and endothelial cells (Henke et al., 1996). HSPG CD44 regulates leukocyte trafficking in tissues and participates in rolling interactions with hyaluronic acid (HA) on endothelial cells.

1.13 Heparan sulfate

Heparan sulfate (HS) is an anionic linear polysaccharide containing repeating disaccharides of N-acetylated or N-sulfated glucosamine and uronic acid. HSPG core proteins are modified and folded in the ER to achieve their proper or mature conformation, whereas HS chains are assembled directly onto the core proteins in the Golgi apparatus (**Figure 1.19**) i.e., HS chains are not synthesised in the absence of HSPG core proteins. HS chains are initiated at a serine residue in the core protein. Uronic acid in HS exists as either glucouronic acid or its epimer iduronic acid. Further modification of the HS disaccharides includes sulfation at the N-, 3-O or 6-O position of N-acetylamine or the 2-O position of uronic acid. Importantly, the extent of sulfation promotes the functional

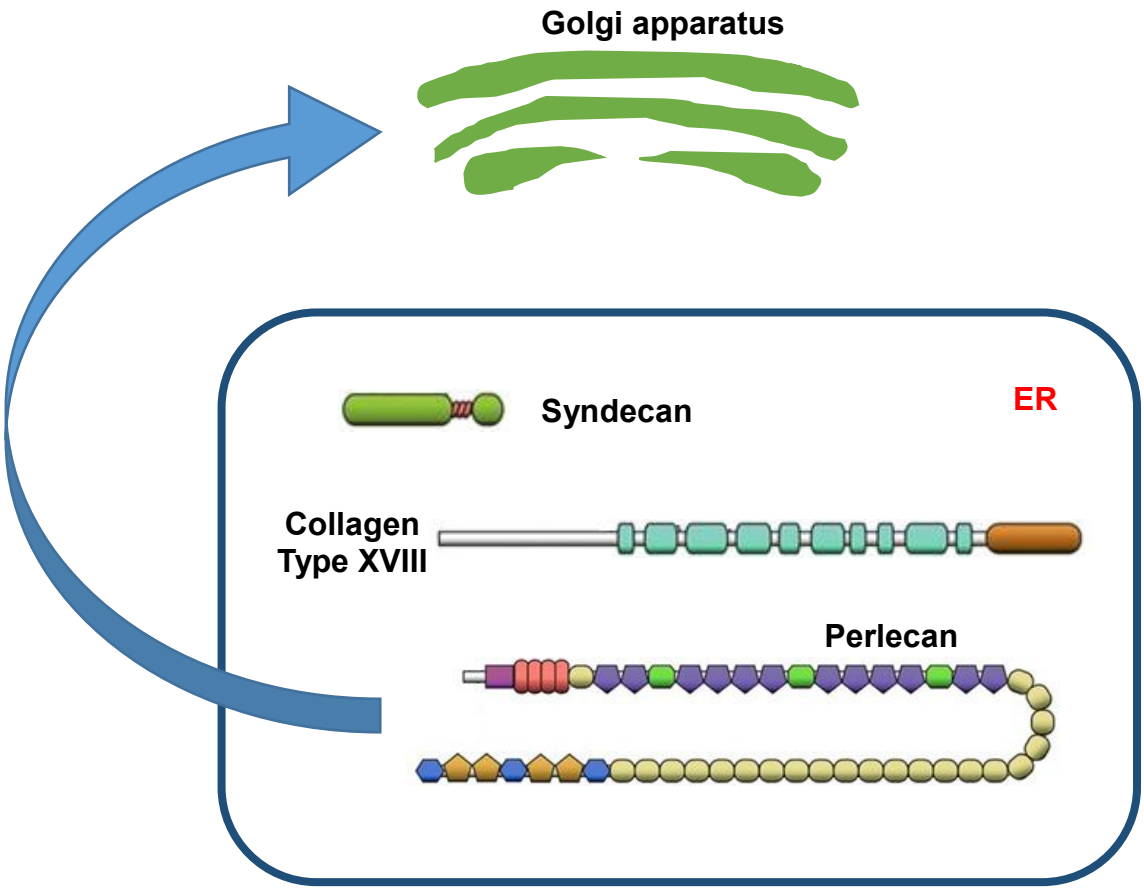

Figure 1.19: Synthesis of HSPG core proteins.

Heparan sulfate proteoglycan (HSPG) core proteins (e.g., syndecan-1, Collagen type XVIII and perlecan) are modified and folded into their proper conformation in the ER. The mature protein (containing serine residue(s)) is then transported to the Golgi apparatus for HS synthesis. Modified from Iozzo (2001).

diversity of HS chains.

1.13.1 Biosynthesis of HS

The heterogenous and complex HS structure is formed by a cascade of enzymatic reactions. HS biosynthesis involves three major steps: chain initiation, elongation and modification (**Figure 1.20**). The various enzymes involved in the process include: galactotransferases, exostosin-like glycosyltransferase (EXTL), exostosin (EXT), N-deacetylase/N-sulfotransferase (NDST), C5 epimerase and O-sulfotransferases (Esko and Lindahl, 2001).

HSPG core proteins are synthesised in the ER and transported to the Golgi apparatus for HS assembly. Within the Golgi apparatus, initially a tetrasaccharide linker protein (xylose-galactose-galactose-uronic acid) is covalently bound to a serine residue in the core protein (Bernfield et al., 1999, Iozzo, 2001). This linkage region is phosphorylated at C2 of xylose and sulfated at C4 or C6 of the galactose residue. The HS chain is then assembled by the alternate addition of N-acetylglycosamine (GlcNAc) and glucuronic acid (GlcA), followed by polymerisation of the HS disaccharides (Bernfield et al., 1999). Glucosamine residues can be sulfated by replacing the GlcNAc N-acetyl group with a sulfate group. The chain then undergoes a number of chemical modifications that includes C5 epimerization of GlcA to iduronic acid (IdoA), O-sulfation of IdoA at C2 and O-sulfation of GlcN residues at C6 (Kjellén and Lindahl, 1991).

The enzymatic modifications in the chain provide structural diversity with highly sulfated regions being interspersed with regions that are under-sulfated. The highly sulfated disaccharides make HS chains highly negatively charged or “polyanionic”. This property allows HS to interact with a vast number of proteins, thereby impacting cell physiology, inflammation and various diseases.

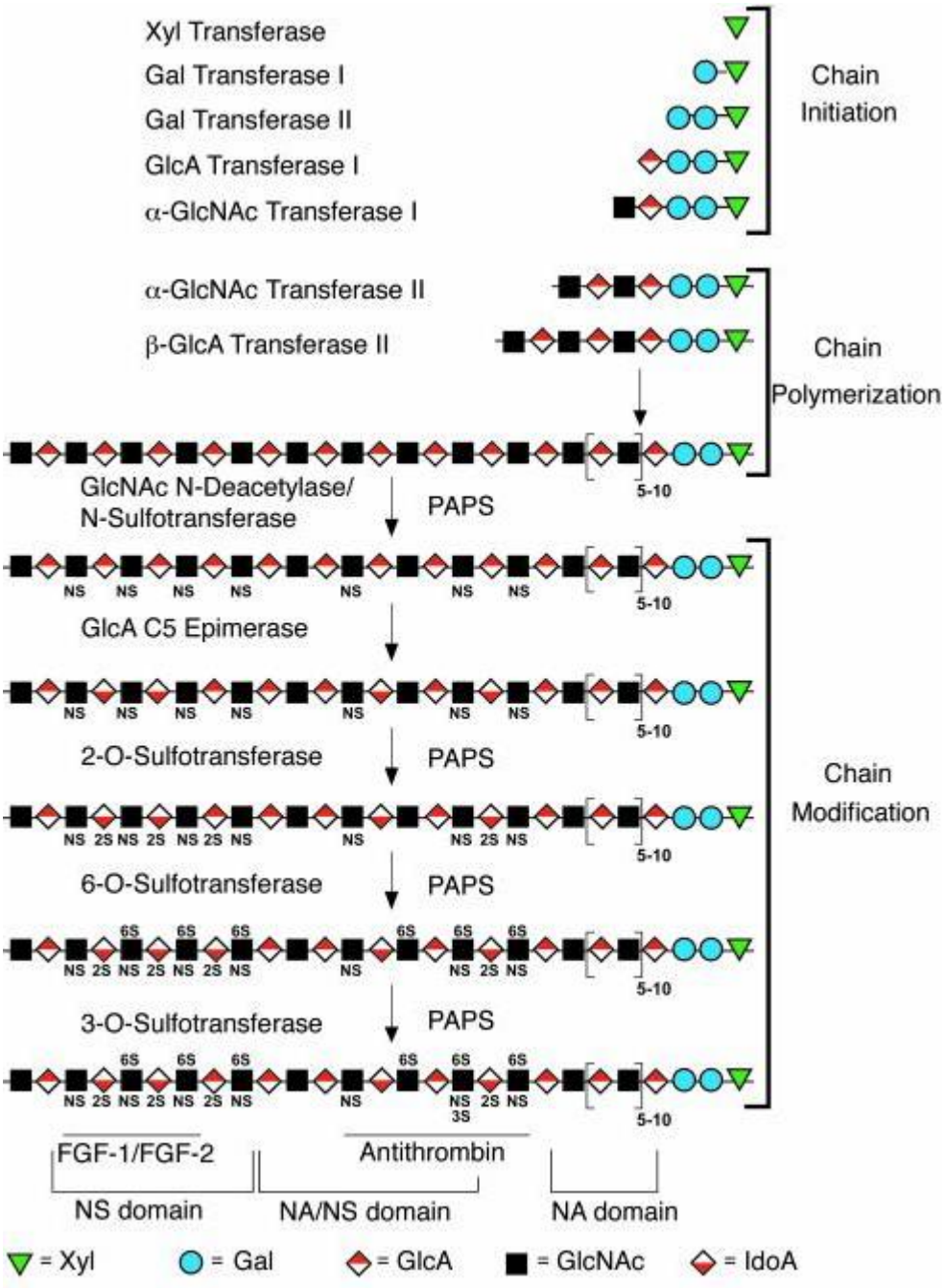

Figure 1.20: Biosynthesis of HS.

HS biosynthesis is a complex process that consists of 3 major steps: chain initiation, elongation (polymerization) and modification. Assembly of a tetrasaccharide linker protein to a serine residue present on the core protein is followed by HS chain elongation. The nascent polysaccharide undergoes chain modification by N-deacetylation/N-sulfation, C5 epimerasation, 2-O-sulfation, 6-O-sulfation and 3-O-sulfation (Esko and Lindahl, 2001).

1.13.2 Role of HS in cell physiology

The heterogeneity in HS chains and the high negative charge carried by the sulfate groups allows interaction with a number of different proteins such as growth factors, cytokines, chemokines, proteases, protease inhibitors, morphogens (a signal molecule involved in tissue development), lipases and cell-adhesion molecules (Dreyfuss et al., 2009). The anionic property of HS also allows interaction with positively charged sodium ions in the ECM and water molecules. As a result, HS is highly hydrated and provides space filing and molecular sieving properties (Parish, 2006). Additionally, HS also interacts with extracellular matrix proteins such as fibronectin and with the plasma protein antithrombin-1 via the antithrombin binding site (**Figure 1.20**) to regulate coagulation (Tkachenko et al., 2005, Liu and Pedersen, 2007). The interaction between HS and antithrombin III leads to a conformational change in the latter that increases substrate binding and accelerates the inhibition of thrombin and other clotting enzymes (Liu and Pedersen, 2007, Stringer and Gallagher, 1997). In BMs, HS acts as a physical barrier to leukocyte migration and plays a critical role in inflammation (see Section 1.13.3) (Sarrazin et al., 2011).

HS serves as a co-receptor for growth factors on the cell surface and facilitates formation of ligand-receptor complexes. For example, Hedgehog signalling, a bone morphogenic protein, wnt signalling and fibroblast growth factor (FGF) signalling are all dependent on HS interactions with their receptors (Bornemann et al., 2004). HS interacts with FGF and the FGF receptor (FGFR) in a ternary complex on the cell surface (Schlessinger et al., 2000, Pellegrini, 2001). HS stabilises this complex and increases the affinity of FGF for its receptors. Activation of FGFRs stimulate signal transduction cascades that have been implicated in embryonic development, angiogenesis, wound healing and tumour growth (Powers et al., 2000).

HS plays an essential role in the permeability of the glomerular BM (GBM) (Dreyfuss et al., 2009) and acts as an antioxidant or a free radical sink in islet beta cells to protect them from ROS-mediated damage (Ziolkowski et al., 2012, Theodoraki et al., 2015, Simeonovic et al., 2018). However, high levels of ROS depolymerise HS (Raats et al., 1997, Rota et al., 2005, Ziolkowski et al., 2012, Choong et al., 2015). HS therefore provides protection for beta cells from ROS produced during normal metabolism.

1.13.3 Role of HS in inflammation

In inflammation, the exit of leukocytes from the vasculature and passage through the underlying sub-endothelial BM to the inflammation site is a highly ordered process which involves a range of adhesion receptors and cytokines (Parish, 2005). HS serves as a scaffold for the presentation of chemokines to leukocyte receptors, modulating the rolling, adhesion and transmigration of leukocytes from blood vessels. HS therefore plays an important role in leukocyte migration and wound healing during injury and infection.

Cytokines produced by activated leukocytes such as tumour necrosis factor-α (TNF-α) and interleukin 1β (IL-1β) activate the endothelium and other leukocytes. As a result, the expression of intercellular and vascular adhesion molecules (e.g., selectins) on the endothelium are increased. HS on the endothelial cell surface directly interacts with L selectin on leukocytes to reduce their rolling and to facilitate their adhesion to the endothelium (Rops et al., 2004). The leukocytes can then interact with HS bound chemokines to activate leukocyte integrins and to achieve a more stable adhesion. The leukocytes then transmigrate across the endothelial layer via a process called transcytosis passage through the sub-endothelial BM. In order for leukocytes to traverse the BM, HS in the BM needs to be degraded by the enzyme heparanase (Hpse) which is produced by activated leukocytes and endothelial cells (Parish et al., 2001, Goldshmidt et al., 2003). Heparanase activity also releases HS-bound growth factors, cytokines and chemokines (Parish, 2006) to promote inflammatory cell responses and stimulate angiogenesis and tissue repair mechanisms.

1.13.4 Role of HS in amyloid deposition

Amyloid disease is characterised by the formation of insoluble fribillar aggregates of misfolded proteins in tissues and organs (Temussi et al., 2003). The two common amyloid diseases are Alzheimers disease (AD) and type 2 diabetes. HS promotes fribillogenesis by associating with the amyloid precursors and facilitating conformational changes required for the assembly of fibrils (van Horssen et al., 2003). In AD, HS is co-distributed with Aβ amyloid peptide in cerebral senile plaques. The HS promotes amyloid beta peptide (Aβ) fibrillisation and toxicity and also the clearance of Aβ aggregates (Zhang et al., 2012).

Islet amyloid deposition is a characteristic feature of human T2D (Kahn et al 1999). Human islet amyloid polypeptide (IAPP) is a peptide hormone which is amyloidogenic and associated with reduced beta cell mass and induction of beta cell apoptosis in T2D (Butler et al., 2003, Clark and Nilsson, 2004b). Human IAPP (hIAPP) aggregates cause beta cell and islet dysfunction and death. Therefore, overexpression of IAPP exhibit toxicity to beta cells by inducing apoptosis and amyloidogenesis. Additionally, HS co-localises with extracellular amyloid deposits in T2D humans and after islet transplantation (Young et al., 1992, Meng et al., 2007). Inhibition of HS biosynthesis in transgenic mouse islets expressing human IAPP resulted in decreased amyloid formation; furthermore, overexpression of hIAPP and Hpse also significantly reduced amyloid deposition (Hull et al., 2007). These findings indicate an important role for HS in IAPP formation.

1.13.5 Role of HS in Cancer

HS-protein interactions are important for the function of growth factors, inflammation, coagulation, ECM integrity and for modulating tumour growth and metastasis (Parish, 2006). HS chains function as a barrier to the migration of cancer cells through BMs. HS in sub-endothelial BMs is cleaved by Hpse to facilitate the movement of tumour cells from the blood to secondary sites in tissues. This degradation of BM HS is also important for angiogenesis, a process required for the growth of both the primary tumour as well as tumour metastases. HS interacts with several angiogenic factors such as vascular endothelial growth factor (VEGF), FGFs and hepatocyte growth factor (HGF), platelet derived growth factor (PDGF) that promote the vascularisation needed for tumour growth, tumour cell proliferation, and differentiation (Bogenrieder and Herlyn, 2003, Jiang and Couchman, 2003). HS therefore plays diverse roles in normal physiology and disease.

1.14 Heparanase

Heparanase exists in two forms in mammals, namely, heparanase-1 and heparanase-2. Heparanase-1 is the sole mammalian endo-β-D-glucoronidase that cleaves HS chains at specific sites, generating HS fragments that are 10-20 sugar residues in length (5-10 kDa) (Freeman and Parish, 1998, Levy-Adam et al., 2005). Heparanase-2, on the other hand,

does not exhibit HS degrading activity. Heparanase-1 (referred to as heparanase or Hpse) degrades HS at glycosidic bonds adjacent to glucuronic acid residues (Parish et al 2013). Unlike Hpse, heparitinase from bacteria extensively cleaves HS chains via a beta eliminase mechanism (or eliminative cleavage) (Vlodavsky and Friedmann, 2001). Mammalian Hpse is highly expressed by placental trophoblasts, platelets, leukocytes and tumour cells. Hpse modifies the structure and function of HSPGs by cleaving HS and contributes to the remodelling of cell surfaces and the ECM. Heparanase expression and activity is therefore tightly regulated.

1.14.1 Heparanase synthesis and release

Hpse is synthesised as a 68 kDa precursor (pre-proheparanase) which consists of an N-terminal signal peptide, a C-terminal hydrophobic peptide, 5 cysteine residues and 6 N-glycosylation sites (**Figure 1.21**) (Vreys and David, 2007). Pre-proheparanase is transported to the ER for glycosylation and cleavage of the signalling peptide to form 65 kDa inactive proheparanase. Proheparanase is directed to the Golgi apparatus, where it is packaged into vesicles and is secreted. Extracellular proheparanase interacts with cell surface HSPGs, low density lipoprotein-receptor related protein and mannose-6-phosphate receptor (MPR). The inactive enzyme is taken up by certain cells and undergoes pH-dependent proteolytic cleavage by the cysteine protease cathepsin L to produce catalytically active heparanase in a form of a heterodimer consisting of 50 kDa (human) or 48 kDa (mouse) and 8 kDa (Vlodavsky et al., 1999, Fairbanks et al., 1999, Ziolkowski et al., 2012, Simeonovic et al., 2013, Parish et al., 2013, Miao et al., 2002). Cathepsin L is found in lysosomes and is secreted by leukocytes such as macrophages (Parish et al., 2013). The maximal catalytic activity of active heparanase occurs between pH 5.5 and 6 (there is no activity outside this range) and active Hpse has a half-life of approximately 30 hrs (Gingis-Velitski et al., 2004). The active form of Hpse is then stored in lysosomes which subsequently move to the cell surface to release Hpse. Moreover, inflammatory cytokines such as TNF-α and IL-1β can also trigger Hpse release from endothelial cells and peripheral T lymphocytes (Goldberg et al., 2013, Chen et al., 2004). During leukocyte migration, cell surface Hpse which is bound to the cation-independent MPR, is activated by cathepsin L produced by macrophages. Extracellular activation of Hpse can also help to degrade HS in the ECM/BM.

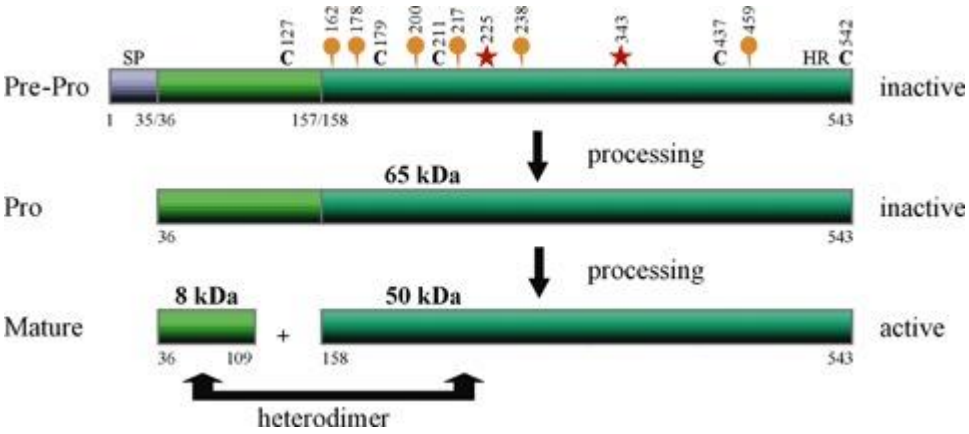

Figure 1.21: Heparanase (Hpse) structure.

Hpse is synthesised as pre-proheparanase of ~68 kDa with a N-terminal signal peptide (SP) that subsequently undergoes proteolytic cleavage in the ER and yields ~65kDa inactive proheparanase. Proheparanase undergoes proteolytic cleavage by cathepsin L to generate 50 kDa and 8 kDa subunits which forms the active heterodimer (Vreys and David, 2007).

1.14.2 Function of heparanase

Under normal conditions, the expression of heparanase by various cell types such as placental trophoblasts, blood borne cells and keratinocytes (Vreys and David, 2007) plays an important role in normal development, tissue remodelling and pathophysiology. For example, extracellular Hpse remodels BMs following injury or at inflammatory sites and regulates cell growth and differentiation by releasing growth factors bound to extracellular HS (Dempsey et al., 2000). Pathological conditions such as experimental autoimmune encephalomyelitis, diabetic nephropathy, delayed type hypersensitivity, arthritis, vascular injury, atherosclerosis and T1D have demonstrated high levels of Hpse (Parish et al., 2013, Parish, 2005, Ziolkowski et al., 2012, Li et al., 2008b, Baker et al., 2009).

Catalytically active Hpse degrades glycosidic bonds in HS at sites adjacent to N- or 6-O sulfated glucosamine at pH 5.5.-6.0 (Simeonovic et al., 2013, Ilan et al., 2006). Heparanase-mediated degradation of HS in BMs and ECMs is important for leukocyte migration and inflammation (Parish et al., 2001, Parish, 2005).

Heparanase also exhibit non-catalytic biological functions (pH 7.2-7.4), independent of its enzymatic activity (Levy-Adam et al., 2008). Cell surface heparanse promotes T cell adherence to the ECM via interaction with HSPGs expressed on the cell surface (Sotnikov et al., 2004). Heparanase enhances Akt signalling and stimulates PI3k and p38-dependent endothelial cell migration and invasion. In addition, it promotes VEGF expression via the Src pathway where it activates endothelial cells and induces a pro-angiogenic and survival response (Ilan et al., 2006, Gingis-Velitski et al., 2004, Simeonovic et al., 2013, Parish et al., 2013). Furthermore, inactive Hpse increases the expression of certain growth factors and facilitates binding of HS in the ECM and to endothelial cells *in vitro* (Gingis-Velitski et al., 2004, He et al., 2012).

During cancer progression, active heparanase contributes to the breakdown of extracellular barriers by degrading HSPGs in BMs to allow cell invasion. Hpse in this context also regulates the bioavailability and activity of growth factors. Extravasion of immune cells into non-vascular spaces is accompanied by the release of growth factors,

cytokines and chemokines bound to HS, thereby enhancing angiogenesis and tumour growth (Vlodavsky et al., 2012, Kelly et al., 2005).

During inflammation in tissues, leukocytes are recruited from the blood. Both endothelial cells and inflammatory leukocytes secrete heparanase to facilitate leukocyte migration into underlying tissues. Heparanase is highly expressed by immune cells such as macrophages, T cells, B cells, dendritic cells, neutrophils, monocytes and Langerhans cells (in the skin), as well as by platelets (Vreys and David, 2007, Vlodavsky et al., 2007, Parish, 2006). Inactive heparanase produced by endothelial cells facilitates T cell adhesion to the ECM by interacting with HSPGs on the cell surface. Thus, chemokines bound to HS in endothelium provide a chemokine gradient to direct leukocyte migration across the endothelium. The next step is for the leukocytes to migrate through the sub-endothelial BM which contains HS associated with the HSPG perlecan. Catalytically active Hpse degrades the HS in BMs and ECMs. Additionally, matrix degrading enzymes such as elastase, matrix metalloproteases, cysteine proteases, serine proteases and sulfatases are secreted by neutrophils, lymphocytes, monocytes, endothelial cells and platelets to destroy BM matrix proteins (Simeonovic et al., 2013, Parish, 2006). Cytokines (IL-4, TNF-α) secreted by inflammatory cells induce heparanase expression and the production of cathepsin L by certain leukocytes (macrophages and T cells) promotes heparanase activation (Ilan et al., 2006, Lerner et al., 2011, Gocheva et al., 2010). Collectively, these pathways facilitate the migration of leukocytes to site of inflammation. Active heparanase therefore functions as a HS degrading endoglycosidase and inactive heparanase promotes cell adhesion (at neutral pH).

1.15 Role of HS and Hpse in beta cell health and disease

The HSPG perlecan was found to be localised in the peri-islet BM where by convention it is thought to serve as a barrier to cell infiltration (Irving-Rodgers et al., 2008). Further studies particularly in the Simeonovic lab revealed that HS is intensely expressed inside pancreatic beta cells and correlates with the intracellular expression of the HSPGs collagen type XVIII, syndecan-1 and CD44 (Ziolkowski et al., 2012, Takahashi et al., 2009, Choong et al., 2015). Furthermore, during islet isolation, isolated mouse islets were

found to completely lose their peri-islet BM, partially lose their beta cell HS but retain their HSPG core proteins (Choong et al., 2015, Ziolkowski et al., 2012).

HS is essential for the survival of beta cells and plays a critical role in protecting beta cells from ROS-mediated cell death (Ziolkowski et al., 2012). Other studies also showed that beta cell-specific deletion of HS in βExtl3KO mice reduced GSIS by isolated islets and the expression of genes involved in insulin secretion (Takahashi et al., 2009). In addition, the mice showed abnormal islet morphology, and reduced beta cell proliferation during development. HS therefore also helps to regulate postnatal islet maturation and normal insulin secretion (Takahashi et al., 2009).

In T1D, the autoimmune destruction of islets in NOD/Lt mice is associated with increased Hpse expression by inflammatory (insulitis) leukocytes and loss of intra-islet HS (**Figure 1.22**). Briefly, in NOD/Lt mice, non-destructive insulitis leukocytes initially accumulate around the periphery of islets (Irving-Rodgers et al., 2008). When the insulitis switches to a destructive phenotype, the leukocytes produce catalytically active Hpse which degrades HS in the peri-islet BM (Ziolkowski et al., 2012). The disrupted islet BM allows the inflammatory cells (including T cells) to invade the islets. Within the islets, the local release of Hpse by invading leukocytes degrades intracellular HS in the beta cells, thereby contributing to beta cell death and T1D. The *in vivo* administration of a Hpse inhibitor/HS replacer, PI-88, significantly reduced the incidence of T1D by 50% in NOD/Lt mice and improved the HS content of the beta cells. These studies suggested that HS represent a critical target for autoimmune damage in beta cells and that Hpse is a novel destructive mechanism in the pathogenesis of T1D (Ziolkowski et al., 2012).

Studies of T1D in NOD mice have also identified other mechanisms of beta cell damage and destruction, including CD8 T cell-mediated cytotoxicity, programmed cell death, cytokine-induced apoptosis, ROS-mediated damage and ER stress (Rojas et al., 2018, Pirot et al., 2008). Autoreactive CD8 T cells (recognizing beta cell-specific autoantigens e.g., insulin) can kill beta cells by the perforin/granzyme pathway of cytotoxicity and/or by inducing programmed cell death via the interaction of apoptosis stimulating fragment (Fas) on beta cells and its ligand FasL on the surface of CD8+ T cells (Mathis et al., 2001, Allison et al., 2005, Mallone et al., 2011, Han et al., 2013). The secretion of pro-

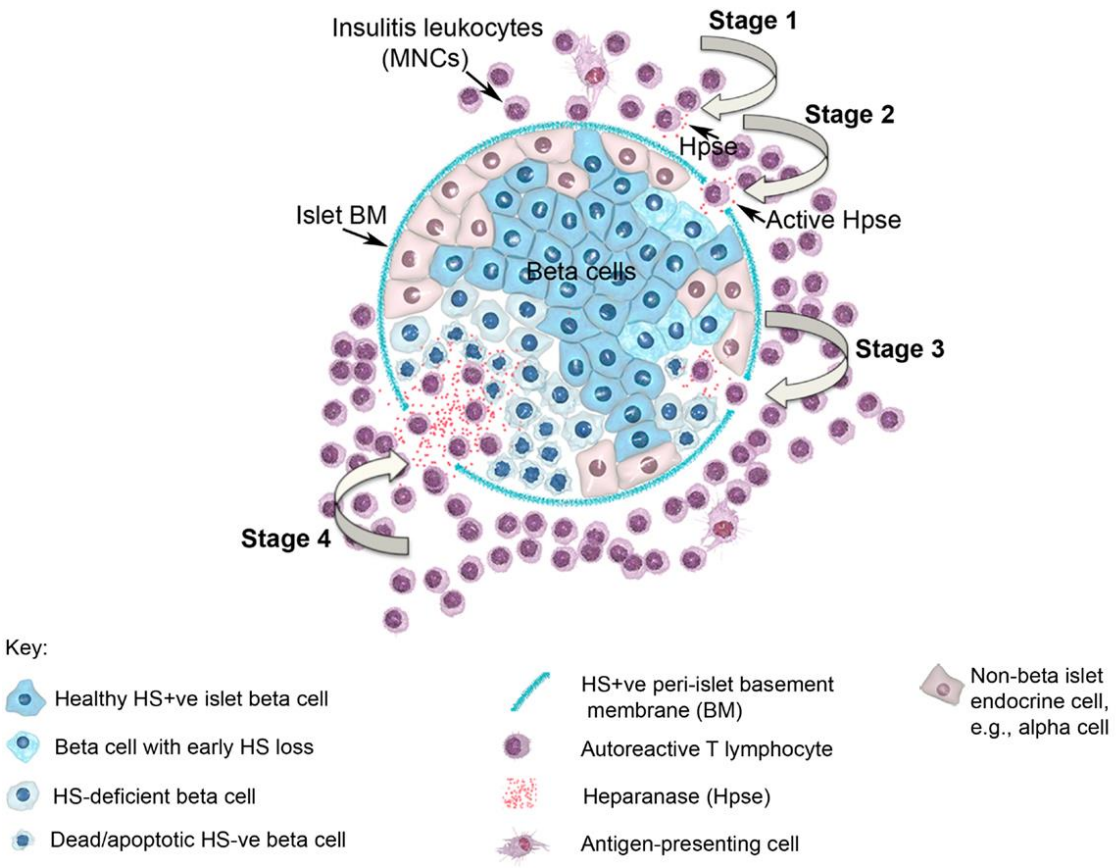

Figure 1.22: Role of islet HS and leukocyte-derived heparanase (Hpse) during different stages of T1D progression.

In stage 1 of T1D, non-destructive insulitis leukocytes produce heparanase (Hpse). During stage 2, catalytically active Hpse degrades heparan sulfate (HS) in the peri-islet basement membrane (BM). In stage 3, the damaged BM allows leukocytes to migrate into the islets. The local production of Hpse by leukocytes that have invaded the islets degrades intracellular HS inside beta cells. The depletion of intracellular HS, together with other destructive mechanisms, leads to beta cell death and subsequently T1D (Simeonovic et al., 2013).

inflammatory cytokines such as IL-1β, TNF-α, INF-γ by insulitis leukocytes also damage beta cells by (i) STAT-1-dependent induction of interferon regulatory transcription factor, iNOS expression and the subsequent production of nitric oxide and other reactive chemical species (e.g., ROS) (Mathis et al., 2001, Pirot et al., 2008) and (ii) inducing beta cell apoptosis via JAK1/2-STAT1-dependent expression of BH3-only pro-apoptotic proteins, e.g. BIM (Bcl-2-like protein), DP5 (Death Protein 5) and PUMA (p53 upregulated modulator of apoptosis) (Gurzov et al., 2016). In addition, ER stress can also contribute to beta cell damage during the development of T1D (Engin et al., 2013, Eizirik et al., 2013, Tersey et al., 2012). Thus, an array of damaging mechanisms, including the Hpse-mediated degradation of intracellular HS in the beta cells, contribute to beta cell death in T1D.

It is well established, however, that the histopathology of T1D insulitis differs in NOD mice and humans. In NOD mice, the accumulation of leukocytes around the islet periphery is pronounced and is associated with aggressive T cell infiltration. However, human T1D pancreases exhibit only mild insulitis/leukocyte infiltration. Furthermore, in humans at clinical onset, the beta cell content is reduced to 20-30% of the normal beta cell mass (In't Veld, 2014). Despite the much less aggressive islet inflammation observed in human T1D, a significant reduction in intracellular HS and HSPG core proteins in residual insulin+ve T1D human beta cells has been observed in parallel with heparanase expression by insulitis leukocytes. Furthermore, HS replacement studies in isolated human beta cells have confirmed a critical role for intracellular HS in human beta cell survival (Simeonovic et al., 2018). Similarly, NOD mouse beta cells demonstrated a loss of intracellular HS during T1D development and treatment with PI-88 (a Hpse inhibitor/HS replacer) improved the survival of beta cells by inhibiting Hpse-mediated HS degradation as well as by restoring beta cell HS (Ziolkowski et al., 2012). Together these findings highlight the clinical relevance of Hpse-mediated loss of HS to beta cell demise in T1D. However, the potential also exists for other mechanisms such as ROS-mediated depolymerisation and possibly ER stress to also contribute to the loss of beta cell HS in T1D disease.

1.16 Scope of the thesis

Recently, a ground-breaking study in the Simeonovic lab demonstrated that islet beta cells require the complex sugar heparan sulfate (HS) for their survival (Ziolkowski et al., 2012). In addition, Choong et al. demonstrated that heparan sulfate proteoglycan (HSPG) core proteins i.e., collagen type XVIII, syndecan-1 and CD44 were localised inside islet beta cells *in situ* (Choong et al., 2015). These HSPG core proteins undergo folding and maturation in the ER and HS chains are assembled on the core proteins in the Golgi apparatus (Esko and Lindahl, 2001). The presence of HSPG core proteins in beta cells supports the unique intracellular localisation of HS in islet beta cells because HS chains cannot be synthesised in the absence of HSPG core proteins. Collectively, these studies demonstrated that islet beta cells express high levels of intracellular HS and HSPG core proteins. Ziolkowski et al. (2012) showed that islet beta cells lose intracellular HS during the islet isolation process. Moreover, isolated HS-deficient beta cells were rescued from dying in culture and from ROS-induced damage by treatment with HS mimetics i.e., via HS replacement (Ziolkowski et al., 2012). These *in vitro* studies underpinned the observation in NOD mice (*in vivo*) that heparanase-mediated loss of beta cell HS contributes to beta cell death during the development of T1D (Ziolkowski et al., 2012).

Type 2 diabetes (T2D) is a metabolic syndrome disease which is characterised by insulin resistance, hyperglycaemia, lipidaemia and chronic low-grade inflammation of adipose tissue and pancreatic islets. Insulin resistance in T2D induces endoplasmic reticulum (ER) stress which results in defective protein maturation, oxidative stress and beta cell failure (Özcan et al., 2006, Laybutt et al., 2007, Hasnain et al., 2012, Eizirik et al., 2008, Schroder and Kaufman, 2005, Scheuner and Kaufman, 2008, Robertson et al., 2004, Ogihara and Mirmira, 2010, Malhotra et al., 2008, Malhotra and Kaufman, 2007, Hasnain et al., 2016). Since ER stress plays an important role in the pathogenesis of T2D, we hypothesised that ER stress in beta cells could also impair the production of HSPG core proteins, like the proteoglycan aggrecan (Domowicz et al., 2000), and subsequent HS synthesis.

This project studied the development of T2D in db/db mice to test the following hypotheses: (i) the depletion of intracellular HSPG core proteins due to ER stress-induced impaired synthesis, results in HS loss and beta cell failure/death; (ii) HS replacement rescues T2D beta cells from dying *in vitro* and (iii) the progressive loss of beta cell

function in db/db mice could be alleviated by relieving ER stress or restoring intracellular HS. This project explores whether loss of beta cell HS represents a common molecular signature for both T2D and T1D.

Aims of the project were to:

(1) Determine the expression of HSPG core proteins and HS in mouse islets of T2D-prone obese male and female db/db mice up to 20 weeks of age, compared to lean heterozygous and wildtype controls;
(2) Examine the levels of HSPG core proteins and HS expression in Akita $Ins2^{WT/C96Y}$ mice (another model of ER stress-induced diabetes) compared to wildtype $Ins2^{WT/WT}$ mice;
(3) Investigate the relationship between ER stress and the UPR to levels of HSPG core proteins, HS and intracellular Hpse in beta cells during T2D development;
(4) Ascertain whether the viability and/or function of T2D beta cells *in vitro* can be rescued by HS replacement;
(5) Establish whether HS replacement or relief from ER stress protects beta cell function in db/db mice *in vivo*;
(6) Investigate the relationship between heparanase expression by inflammatory leukocytes in the white adipose tissue (WAT) of db/db mice and T2D development.

Chapter 2: Materials and Methods

2.1 Animals

Wildtype (C57BL/KsJ; +/+), heterozygous (db/+) and homozygous db/db mice; heterozygous Akita ($Ins2^{WT/C96Y}$) and wildtype ($Ins2^{WT/WT}$) mice; and BALB/c mice were obtained from the Australian Phenomics Facility (APF), The John Curtin School of Medical Research (JCSMR), The Australian National University (ANU). Highly trained animal technicians at the APF were responsible for the general maintenance of the mice. All procedures and experiments were approved by the ANU Animal Ethics Committee and were covered under protocols A2014/51 and A2017/56.

2.1.1 db/db mice

The diabetes (db) mutation in the leptin receptor gene (*Lepr*) was identified as a recessive mutation on chromosome 4 of the C57BL/KsJ inbred mouse strain in 1966 (Hummel et al., 1966). The mice used in this project were from the BKS.Cg-$Dock7^{m}$ +/+ $Lepr^{db}$/J congenic strain (Chen et al., 1996). $Lepr^{db}$ mice which carry a homozygous mutation are commonly known as db/db mice. Db/db mice have a homozygous point mutation (G→T) in the leptin receptor (Lepr) genomic sequence in exon 19 (Chen et al., 1996). The mutation leads to defective signal transduction, resulting in hyperphagia, obesity, hyperinsulineamia, insulin resistance and hyperglycaemia (Kobayashi et al., 2000). The *misty* gene ($Dock7^{m}$; a recessive coat colour mutation) was incorporated close to the Lepr locus on chromosome 4 to distinguish between wildtype and heterozygous mice (Yaguchi et al., 2005, Coleman and Hummel, 1975). The misty gene shows misty (grey) coat colour for lean wildtype mice; black coat colour for lean heterozygous mice; and black coat colour for obese mutant db/db mice (Yaguchi et al., 2005, Jung et al., 2016). Db/db mice develop beta cell failure and type 2 diabetes (T2D). Male and female wildtype (C57BL/KsJ; wt; +/+), heterozygous (het; db/+) and db/db mice were used at 3-20 weeks of age for monitoring T2D development, pancreas harvest, islet isolation or *in vitro* treatment.

2.1.2 Akita ($Ins2^{WT/C96Y}$, $Ins2^{WT/WT}$) mice

Akita ($Ins2^{WT/C96Y}$ and $Ins2^{C96Y/C96Y}$) mice have a C57BL/NJcl background and carry a spontaneous point mutation in the *Ins2* gene where a cysteine residue is replaced by tyrosine (C96Y) (Wang et al., 1999). The mutation prevents the formation of an

intramolecular disulfide bond between insulin A and insulin B chains which results in misfolding and the accumulation of proinsulin in the ER of pancreatic beta cells, ER stress and ultimately beta cell death (Oyadomari et al., 2002b, Izumi et al., 2003, Wang et al., 1999). Homozygous $Ins2^{C96Y/C96Y}$ and heterozygous $Ins2^{WT/C96Y}$ Akita mice develop hypoinsulinemia, hyperglycaemia, polydipsia and polyuria. Homozygous $Ins2^{C96Y/C96Y}$ mice are severely hyperglycaemic by 3 weeks of age and rarely survive beyond 8-12 weeks of age (Schoeller et al., 2014). Both homozygous and heterozygous Akita ($Ins2^{WT/C96Y}$ and $Ins2^{C96Y/C96Y}$) mice develop loss of beta cell function, reduction in beta cell mass and overt hyperglycaemia by 4 weeks of age. The Akita ($Ins2^{WT/C96Y}$ and $Ins2^{C96Y/C96Y}$) mouse model is an established model of ER stress-mediated diabetes. Diabetes in $Ins2^{WT/C96Y}$ and $Ins2^{C96Y/C96Y}$ Akita mice resembles monogenic diabetes in humans e.g., maturity-onset diabetes of young (MODY); $Ins2^{WT/C96Y}$ and $Ins2^{C96Y/C96Y}$ mice exhibit no insulitis or lymphocyte infiltration in the pancreas (Yoshioka et al., 1997). The $Ins2^{WT/C96Y}$ mouse breeding colony was maintained as $Ins2^{WT/C96Y}$ mice x C57BL/6 at APF, ANU. Male and female wildtype ($Ins2^{WT/WT}$) and heterozygous ($Ins2^{WT/C96Y}$) mice were used at 4, 5, 6 and 9 weeks of age for pancreas harvest or islet isolation (see Section 2.3).

2.1.3 BALB/c mice

The BALB/c mouse strain is an albino inbred strain. BALB/c mice were obtained from APF, JCSMR, ANU. Female BALB/c mice (10-15 weeks of age) were used for islet isolation (see Section 2.3). Isolated BALB/c islets were cultured with 5 µM thapsigargin (ER stress inducer) for 3 days (see Section 2.3.1) and intracellular HSPG core proteins/HS and Hpse expression was analysed by flow cytometry on day 3 (see Section 2.8).

2.2 Metabolic studies

2.2.1 Body weight and blood glucose measurements

Body weight (Bw) of mice was measured using a digital balance (Mettler Toledo). For blood glucose (Bg) measurements, a drop of blood from the tail vein was analysed using a glucometer (Accu-Chek Go; Roche diagnostics) according to the manufacturer's instruction. Db/db mice were categorised into three groups based on their non-fasting

blood glucose levels i.e., Bg<10 mmol/L, Bg=10-15 mmol/L and Bg>15 mmol/L. The normal range for blood glucose levels, based on control mice, was determined by mean ± 2 S.D (standard deviation).

2.2.2 Intraperitoneal glucose tolerance test (ipGTT)

The glucose tolerance test (GTT) measures the clearance of a glucose load from the body and is used to identify impaired glucose tolerance (Andrikopoulos et al., 2008). Wt and db/db mice at 5-9 weeks of age were weighed and bled before fasting for 6 hours. After fasting, mice were injected intraperitoneally (i.p.) with glucose (2 g glucose/kg) and the blood glucose levels were measured over two hours at 0 (before glucose injection), 15, 30, 60, 90 and 120 mins. In parallel, 10 µl blood was collected from the tail vein using a microcap capillary (Drummond Scientific Co., Broomall, Pa, USA) into a microfuge tube containing 2 µl citrate buffer (see Appendix 1.1) to prevent blood coagulation and clot formation. The collected blood was immediately centrifuged at 2000-3000 x g for 15 mins to separate plasma. The plasma samples were stored at -20°C for measurement of plasma insulin by enzyme-linked immunosorbent assay (ELISA). The glucose dose was reduced to 0.5 g glucose/kg for obese adult female and male db/db mice to obtain fasting blood glucose levels within limits of sensitivity for the glucometer. The area under the curve (AUC) for the blood glucose plots was calculated using the trapezoid method (Purves, 1992, Andrikopoulos et al., 2008) from time 0 to 120 mins using GraphPad Prism 5 (version 5.04) software.

2.2.3 HbA1c

HbA1c levels in a drop of tail vein blood were measured using a HemoCue HbA1c 501 Analyzer, according to the manufacturer's instructions.

2.2.4 Insulin ELISA

Plasma insulin was measured using a commercial enzyme-linked immunosorbent assay (ELISA; EMD Millipore Corporation, #EZRMI-13K). The reagents were pre-warmed to room temperature and the wells of the microtiter plate were washed 3 times with diluted wash buffer (300 µl/well). Assay buffer (10 µl) was added to each well; duplicates were set up for blank, standard and sample wells. 10 µl matrix solution was then added to each well. For the standard wells, 10 µl rat insulin standard were added per well in ascending

concentration (0.2-10 ng/mL). The plasma samples were diluted (1/5) with matrix solution (10 µl) and added to sample wells. The wells were incubated with detection antibody (80 µl) for 2 hrs on an orbital microtitre plate shaker (#45000, Lomb Scientific Pty Ltd Australia) at 400-500 rpm. After 2 hrs, the solution was decanted, and the plates were washed 3 times with wash buffer (300 µl). The enzyme solution (100 µl) was added to each well and incubated for 30 mins at room temperature with continual agitation using the plate shaker at 400-500 rpm. The supernatant was decanted, and the wells were washed 6 times with wash buffer. The substrate solution (100 µl) was added to each well and incubated for 15 mins at room temperature with agitation (plate shaker, 400-500 rpm). Stop solution (100 µl/well) was added to terminate further colour development from blue to yellow. The absorbance was recorded at 450 nm (measurement wavelength) and 590 nm (reference wavelength) using a plate reader (Infinite 200Pro, Tecan i-control serial number: 1207004543). The reference wavelength absorbance was subtracted from the measurement wavelength absorbance; a standard curve was constructed and values for unknown samples were interpolated from the graph. The plasma insulin levels (ng/mL) were then adjusted to account for the dilution factor used to prepare the samples for analysis.

2.2.5 Free fatty acids

The non-esterified fatty acid (NEFA) C kit (acyl-coenzyme A-synthetase (ACS) - acyl-coenzyme A oxidase (ACOD) method, cat. # 279-75401, Wako diagnostics, Mountain view, CA, USA) was used to quantify the non-esterified free fatty acids in mouse plasma. For the assay, reagents A and B were dissolved in solvent A and B, respectively (see Appendix 1.1); all the reagents were kept on ice. Plasma samples were diluted (1/2) in Milli-Q water. The Milli-Q water blank (no sample), standards and samples (2.5 µl each) were loaded into a 96 well plate (#650180, CellStar, Greiner Bio-one, Kremsmünster, Austria) in duplicates. Reagent A (50 µl) was added to the wells using a Multipette Plus (Eppendorf, Sigma-Aldrich, St. Louis, MO, USA) and incubated for 10 mins at 37ºC. Reagent B (100 µl) was then added to each well and incubated for 10 mins at 37ºC. The plate was allowed to cool for 5 mins. The absorbance was read using a plate reader (FLUOstar OPTIMA #413-2046, BMG Labtech, Mornington, VIC, Australia) at 550 nm wavelength. The background (blank) absorbance was subtracted from the readings and a standard curve was plotted. The concentration of free fatty acids in unknown samples was

interpolated from the standard curve and adjusted for the dilution factor used to prepare the samples for analysis.

2.3 Islet isolation from mouse pancreas

Pancreatic islets were isolated as previously described (Ziolkowski et al., 2012). Donor mice were anaesthetised using i.p. avertin (0.4 ml- 0.6 ml/mouse; see Appendix 1.2). The abdominal region was sterilised using 80% ethanol and an incision was made in the skin to reveal the underlying muscle layer. An incision in the muscle layer, below the sternum and rib cage was used to expose the visceral organs. The mouse was sacrificed by exsanguination of the thoracic aorta. The liver was flipped back over the thorax and secured with sterile gauze, pre-soaked in wash medium A (see Appendix 1.2), exposing the upper abdominal region. The distal end of the common bile duct at the duodenal entry was located using a dissecting microscope (Model SDZ-P, Kyowa Optical, Tokyo, Japan) and clamped using artery forceps. A small incision was made in the proximal part of the common bile duct adjacent to the liver; collagenase P (see Appendix 1.2) solution was then slowly injected using a 30.5-gauge needle (Beckton Dickinson & Co, Franklin Lakes, NJ, USA) attached to a 3 ml syringe (Terumo Medical Corporation, Somerset, NJ, USA). The inflated pancreas was then transferred to a vial containing additional collagenase P solution (2 ml) and digested for 15 mins in a 37°C water bath (Labmaster). The pancreas digest was then hand-shaken 15-20 x over 20 seconds and then lightly vortexed. The enzymatic activity was terminated by dilution of the digest with 15 ml of medium A; the digest was then placed on ice for 5 mins. The medium (supernatant) was removed using a siliconised pasteur pipette without disturbing the sedimented, digested pancreas tissue. The digested tissue was then washed with 5 ml of medium A and placed on ice for 5 mins. The medium was then removed, and the digest was washed with approximately 2 ml of medium B (see Appendix 1.2) for 3 mins on ice. The digested tissue was resuspended in 2 ml of medium B and transferred into a sterile 10 cm glass petri dish for handpicking of the islets (**Figure 2.1**). For wildtype $Ins2^{WT/WT}$ and heterozygous $Ins2^{WT/C96Y}$ Akita pancreas tissue, the digested tissue was resuspended in 3 ml of dithizone solution (see Appendix 1.2) for 3 minutes to stain and identify the islets. Dithizone is a zinc-chelating agent which selectively stains insulin granules (Latif et al., 1988, Baskin, 2015, Kim and Jun, 2017), making the islets appear pink-red in colour. The

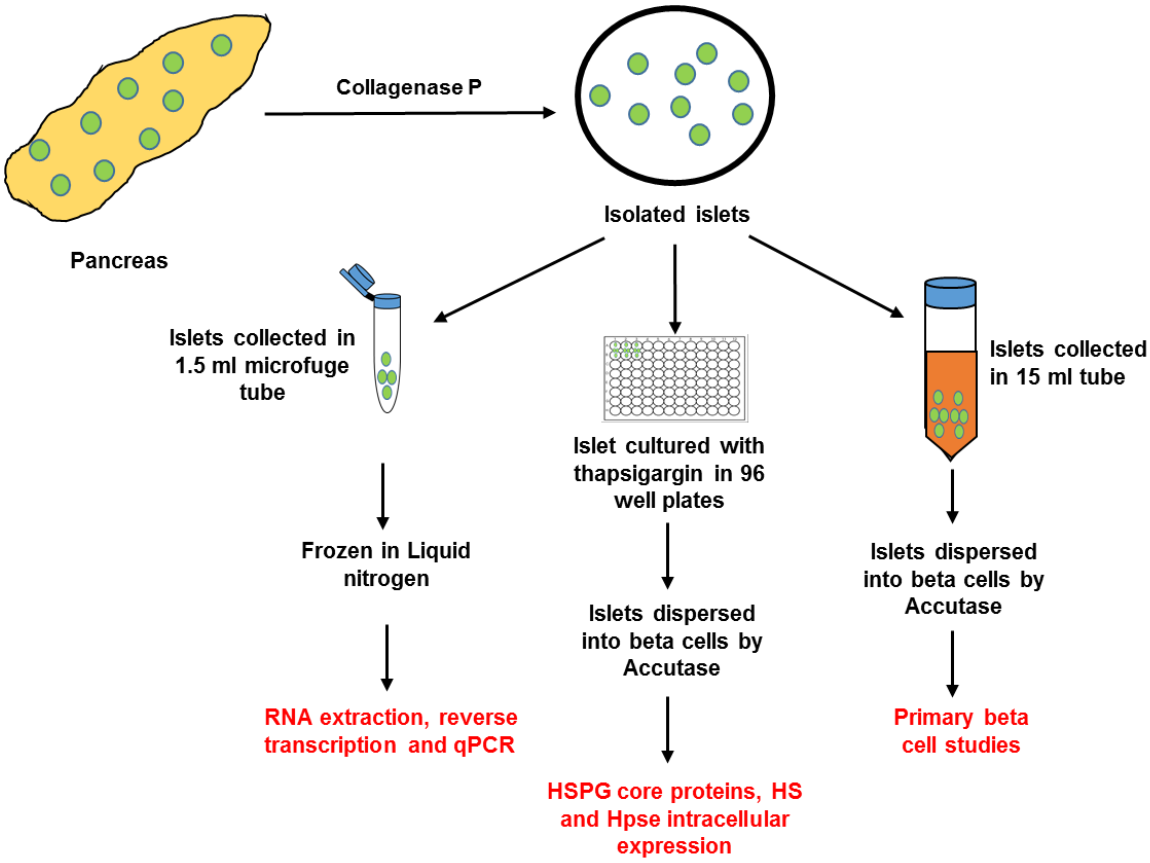

Figure 2.1: Islet isolation for experimental use.

Islets are isolated from mouse pancreases by digestion with collagenase P to separate islets from the pancreatic acinar tissue. The islets were hand-picked in a petri-dish and transferred to tubes. The islets were collected into 1.5 ml microfuge tubes, snap frozen in liquid nitrogen and stored at -80°C for RNA extraction, reverse transcription and analysis of gene expression by TaqMan qPCR (see Section 2.6.4). Alternatively, the islets were collected into a 15 ml tube and dispersed into a single cell suspension using Accutase (see Section 2.3.2). Primary isolated beta cells were used for culture and flow cytometry analysis (see Section 2.8). For some studies, whole islets were cultured with thapsigargin (see Section 2.3.1) for flow cytometry analysis intracellular levels of HSPG core proteins, HS and heparanase (Hpse) in beta cells (see Section 2.8).

islets were then hand-picked under a dissecting microscope, using a tapered Pasteur pipette attached to a 5 ml syringe via a rubber tube (**Figure 2.1**).

2.3.1 Treatment of isolated BALB/c islets with thapsigargin

Islets were isolated from BALB/c pancreas and transferred to a 96 well flat bottom plate (#142010, Thermo Fischer Scientific, Roskilde, Denmark) 10 islets/well, 12-15 wells/treatment. The islets were cultured in beta cell medium (see Section 2.4.1; **Figure 2.1**; Appendix 1.2) overnight at 37°C in a humidified gas phase of 5% CO_2/95% air. The pharmacological ER stress agent, thapsigargin (1 mM in DMSO) was diluted to 5 µM in serum-free 6 mM glucose DMEM (Invitrogen #11885; see Appendix 1.3).

The medium was removed from the over-night cultured islets and the islets were resuspended in 6 mM glucose/5 µM thapsigargin, 100 µl/well. The islets were cultured for a further 3 days at 37°C in 5% CO_2/95% air. The treated islets were then dispersed into primary beta cells (see Section 2.3.2). Thapsigargin-induced ER stress changes in the intracellular expression of HSPG core proteins, HS and Hpse were assessed by flow cytometry (see Section 2.8).

2.3.2 Dispersion of islets into primary beta cells

Isolated islets (~2 ml) were transferred into a 15 ml tube (Falcon, Corning Inc., One Riverfront plaza, NY, USA; **Figure 2.1**). PBS/EDTA solution (see Appendix 1.2) was added to 15 ml tube and centrifuged at 249 x g for 2 mins at room temperature. The supernatant was removed using a sterile glass pasteur pipette and the islets were again resuspended in PBS/EDTA. The islets were centrifuged at 249 x g for 2 mins and the supernatant was removed. A single cell suspension was obtained by incubating the islets with Accutase (250 µl/500 islets/microfuge tube; Milllipore, Temecula, CA, USA) in a 37°C water bath for 10 mins. The islets were resuspended with gentle swirling every 4 mins (Ichii et al., 2005). The islets were then dissociated by pipetting up and down for 10-15 x using a 1 ml adjustable pipette. The enzymatic activity was terminated by dilution with beta cell culture medium (see Appendix 1.2) and the cells were centrifuged at 249 x g for 5 mins. The supernatant was decanted and the islet cells were resuspended in beta cell culture medium (500 µl/500 islet equivalent). The live cells were counted by trypan

blue exclusion (see Section 2.4.3) and transferred to a 96 well plate for staining and analysis by flow cytometry (see Sections 2.8 and 2.9).

2.4 Cell culture

2.4.1 Culture of primary beta cells

Primary beta cells were cultured in RPMI 1640 (Sigma-Aldrich, St. Louis, MO, USA) supplemented with 10% heat-inactivated fetal calf serum (HIFCS), L-glutamine and antibiotics (see beta cell medium, Appendix 1.2).

2.4.2 MIN6 cells

The MIN6 cell line is derived from a C57BL/6 mouse insulinoma induced by targeted expression of the simian virus 40 T antigen gene (Miyazaki et al., 1990). MIN6 cells exhibit properties of pancreatic beta cells including the production of insulin in response to glucose, glucose transport and metabolism (Ishihara et al., 1993, Miyazaki et al., 1990) as well as susceptibility to ER stressors (Laybutt et al., 2007, Chen et al., 2013, Chan et al., 2012).

2.4.2.1 Maintenance of MIN6 cells in 25 mM glucose-DMEM

MIN6 beta cells were cultured in Dulbecco's Modified Eagle Medium (DMEM) with high glucose (GIBCO-Invitrogen #11995). The DMEM high glucose medium was supplemented with 10% heat-inactivated fetal calf serum (HIFCS), 15 mM HEPES (GIBCO-Invitrogen #15630080) and Penicillin/Steptomycin/Neomycin (PSN) antibiotics (see Appendix 1.3). The cells were maintained in T_{75} flasks (Nunc, Denmark) at 37°C in 5% CO_2/ 95% air in a humidified incubator. For sub-culturing, MIN6 cells were harvested at 70-80% confluence (approximately every 3-4 days) using trypsin (0.5 g/L; Sigma-Aldrich, St. Louis, MO, USA). The cells were collected into a 50 ml tube (Falcon, #352070, Corning Science Mexico, Reynosa, Tamaulipas, Mexico) and centrifuged at 389 x g for 3 mins (Heraeus Megafuge 1.0R, Kendro Laboratories, Hamburg, Germany). The supernatant was discarded and the pellet was resuspended in 3 ml of 25 mM glucose/DMEM medium. 1 ml of resuspended cells were transferred to a T_{75} flask

containing 20 ml of culture medium. In the context of MIN6 cells, 25 mM glucose/DMEM medium is abbreviated to 25 mM glucose.

2.4.2.2 Maintenance of MIN6 cells in 6 mM glucose-DMEM

For some experiments, MIN6 cells were cultured in a sub-stimulatory glucose concentration i.e., 6 mM glucose to simulate resting conditions and to minimise insulin secretion. The low glucose DMEM (Invitrogen, Cat. #11885) was supplemented with 10% HIFCS, 15 mM HEPES and antibiotics (see Appendix 1.3). For MIN6 studies, 6 mM glucose/DMEM medium is abbreviated to 6 mM glucose.

2.4.2.3 Subculture and harvest of MIN6 cells

The culture medium was decanted, and the adherent cells were washed with PBS to remove residual medium. The adherent cells were then treated with trypsin (0.5 g/L; Sigma-Aldrich, St. Louis, MO, USA; see Appendix 1.4) for 3 mins at 37°C. The flask was gently tapped to detach the adherent cells and 10 ml of PBS was added to terminate the trypsinisation. For each T_{75} flask, the total cell suspension was collected into a 50 ml tube (Falcon, #352070, Corning Science Mexico, Reynosa, Tamaulipas, Mexico) and centrifuged at 389 x g for 3 mins (Heraeus Megafuge 1.0R, Kendro Laboratories, Hamburg, Germany). The supernatant was decanted, and the pellet was resuspended by flicking the tube. For subsequent culture or treatment, 3 ml of fresh culture medium was added to resuspend the cells. The cell density was determined using a haemocytometer (American Optical Co., Buffalo, NY, USA) and trypan blue exclusion to identify live MIN6 cells.

2.4.3 Trypan blue exclusion for determining the density of live cells

Trypan blue is a dye which selectively stains dead cells. 10 µl cell suspension (MIN6 cells or primary beta cells) was added to 90 µl of 0.2% trypan blue solution and mixed (see Appendix 1.5). 10 µl of the stained cells was loaded into a haemocytometer and examined under a light microscope for counting. The number of viable cells (non-blue cells) were counted in the four corner grids and the mean cell number was calculated. The cell density was then calculated using the formula: mean cell count x 10^4 x 10 (dilution factor).

2.5 Treatment and analysis of MIN6 cells

2.5.1 Induction of ER stress in MIN6 cells

MIN6 cells were harvested, the cells were resuspended in 25 mM glucose (1 ml) and the cell density was assessed by trypan blue exclusion. 3 x 10^5 cells were transferred to individual wells of a 24-well plate (#3524, Costar, Corning Incorporated corning, NY, USA), 3 x 10^5 cells/1 ml/well. The cells were cultured overnight at 37°C in 5% CO_2/95% air. The pharmacological ER stress agents, thapsigargin and tunicamycin, and a physiological ER stress inducer, palmitate, were used in this study to induce ER stress in MIN6 cells.

2.5.1.1 Thapsigargin

50 nM thapsigargin was prepared by a 2-step dilution of a stock concentration of thapsigargin (1 mM in DMSO); 1 mM thapsigargin was diluted 1/200 in serum-free 6 mM glucose DMEM (Invitrogen #11885) followed by a 1/100 dilution (see Appendix 1.6).

2.5.1.2 Tunicamycin

2 μM tunicamycin was prepared by diluting a stock concentration of 6 mM tunicamycin (in DMSO); 1/100 in serum-free 6 mM glucose DMEM (Invitrogen #11885) followed by a 1/30 dilution (see Appendix 1.6).

2.5.1.3 Palmitate

Palmitate (8 mM) coupled with bovine serum albumin (BSA) was provided by Prof. Trevor Biden (The Garvan Institute of Medical Research, Sydney). Palmitate is a free fatty acid which is insoluble in aqueous solution; BSA is therefore used as a carrier. 0.4 mM palmitate/BSA was prepared by diluting (1/20) 8 mM palmitate in 6 mM glucose medium (see Appendix 1.6). This medium is referred to as 6 mM glucose + 0.4 mM palmitate in this thesis. In addition, BSA was diluted (1/20) in 6 mM glucose as a control and is referred to as 6 mM glucose + BSA.

2.5.2 Treatment with pharmacological ER stress agents

Thapsigargin and tunicamycin were prepared in 6 mM glucose medium, as previously described (see Section 2.5.1). The medium from MIN6 cells cultured overnight in a 24-well plate (see Section 2.5.1) was removed and the cells were then cultured in 25 mM glucose, 6 mM glucose, 50 nM thapsigargin or 2 μM tunicamycin (see Sections 2.5.1.1 and 2.5.1.2), 1 ml/well. Thapsigargin or tunicamycin-induced ER stress in the MIN6 cells was assessed after 20-24 hrs by qRT-PCR. Alternatively, the expression of HSPG core proteins, HS and Hpse as well as cell death were assessed by flow cytometry (see Sections 2.5.5.2 and 2.8).

2.5.3 Treatment with physiological ER stress agent

Palmitate/BSA and BSA were prepared in 6 mM glucose medium, as previously described (see Section 2.5.1.3). The culture medium from MIN6 cells cultured overnight in a 24-well plate (see Section 2.5.1) was removed from the wells and the cells were then cultured in 25 mM glucose, 6 mM glucose + BSA or 6 mM glucose + 0.4 mM palmitate/BSA, 0.5 ml/well. Palmitate-induced ER stress in MIN6 cells was assessed after 20-24 hrs by qRT-PCR. Alternatively, the expression of HSPG core proteins, HS and Hpse and cell death was assessed by flow cytometry (see Sections 2.5.5.2 and 2.8).

2.5.4 Harvest of treated MIN6 cells

Using a glass pipette, the culture medium from triplicate wells of a 24-well plate was transferred to a 15 ml tube (#352096, Corning Science Mexico, Reynosa, Tamaulipas, Mexico)). Each well was washed with PBS and the wash was transferred to the respective tubes. Diluted trypsin (see Appendix 1.4) was added to each well (0.5 ml/well) and incubated for 3 mins at 37°C, for cell detachment from the well floor. The plate was gently tapped to loosen the cells and PBS (0.5 ml/well) was added to terminate the trypsin treatment. The content of each well was mixed and transferred to the corresponding 15 ml tube using a glass pipette. The tubes were centrifuged at 693 x g for 3 mins and the supernatant was discarded. For RNA extraction, each cell pellet was resuspended in PBS (2 ml) and centrifuged at 693 x g for 3 mins. The supernatant was decanted and the pellet was resuspended in 100 μl RNA later (Qiagen #1017980) for stabilisation of the RNA. The cells were transferred to a 1.5 ml microfuge tube and stored overnight at 4°C.

Alternatively, for flow cytometry, the cell pellet was resuspended in 2 ml of 25 mM glucose and the cells were transferred to a 96 well plate for staining (see Section 2.8).

2.5.5 Analysis of MIN6 cells

2.5.5.1 Flow cytometry analysis of MIN6 cells treated with ER stress agents

MIN6 cells treated with physiological or pharmacological ER stress agents (see Sections 2.5.2 and 2.5.3) were analysed after 1-5 days of treatment. Cell death and intracellular HSPG core proteins, HS and Hpse were analysed by flow cytometry (see Sections 2.5.5.2, 2.5.5.3 and 2.8.2).

2.5.5.2 Detection of cell death by flow cytometry

Cell death was detected by flow cytometry using 7-Aminoactinomycin D (7AAD; Invitrogen). 7AAD is a fluorescent derivative of actinomycin D and is a DNA binding dye that selectively binds to GC regions in DNA (Nadine et al, 2012). 7AAD is a cell impermeable dye that is used to identify apoptotic and late apoptotic/dead cells by flow cytometry.

7AAD was diluted to 10 µg/ml in PBS (see Appendix 1.15). 0.5-2 x 10^5 cells/well were plated in individual wells of a 96-well plate (CellStar, #650180, Greiner bio-one, Frickenhausen, Germany). The cells were centrifuged at 693 x g for 3 mins and the supernatant was removed. The unstained cells (controls for background staining) were treated with 100 µl PBS; and the remaining cells were stained with 100 µl 7AAD /well (1/100 dilution). The plate was incubated for 15 mins at 37°C in 5% CO2/95% air. The cells were then washed with 100 µl PBS, centrifuged at 693 x g for 3 mins and resuspended in 100 µl PBS/well for flow cytometry analysis. The samples were run on a BD LSR Fortessa flow cytometer using FL-1 and FL-3 channels. Flow Jo software (version 10.0.7, TreeStar Inc., Ashland, OR, USA) was used to detect the % $7AAD^+$ MIN6 cells in the total population using dot plots (see Section 2.5.5.3; **Figure 2.2**).

2.5.5.3 Flow cytometry data analysis

The percentage of $7AAD^+$ cells were determined from dot plots using FlowJo Software (**Figure 2.2**). Viable MIN6 cells were gated on the basis of forward scatter (FSC) and side scatter (SSC) properties and the dead cells were excluded from the analysis. The

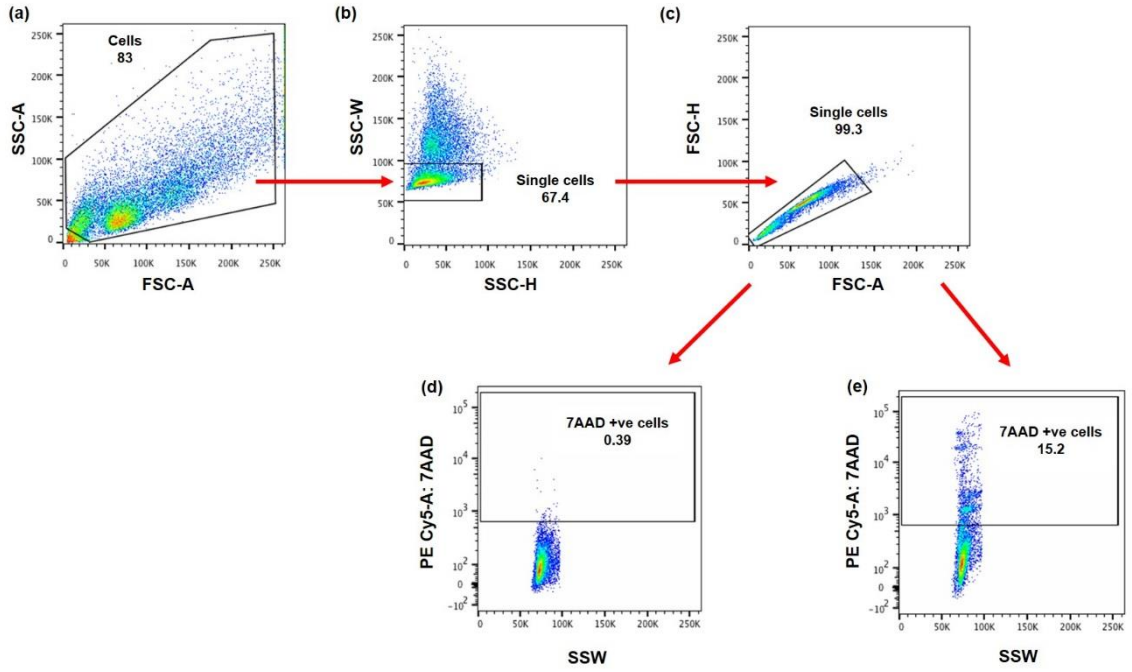

Figure 2.2: Gating strategy for quantifying damaged/dead (7AAD$^+$) MIN6 cells.
(a) Representative dot plot shows forward scatter (FSC) and side scatter (SSC) properties used to identify the viable MIN6 population and to exclude dead cells from the analysis. (b) Single cells were gated based on the SSC-W and SSC-H; (c) FSC-H and FSC-A were used to exclude doublets in the population. (d) The dot plot shows 7AAD fluorescence on y-axis and an empty channel on x-axis. The internal black rectangle was generated using unstained cells as negatively stained population (d). In this example, 15.2% MIN6 cells were 7AAD$^+$ (e). SSC-A, side scatter area; FSC-A, forward scatter area; SSC-W, side scatter width; SSC-H, side scatter height; FSC-H, forward scatter height; FSC-A, forward scatter area.

single cells were gated based on the side scatter width (SSC-W) and side scatter height (SSC-H); forward scatter height (FSC-H) and forward scatter area (FSC-A) properties were used to exclude doublets in the population. The 7AAD staining was represented on the y-axis and an empty channel on the x-axis (**Figure 2.2**). Positive staining was determined using autofluorescence of unstained cells as the negatively stained population (see gating strategy in **Figure 2.2**). The same strategy was applied for the control MIN6 cells and MIN6 cells treated with ER stressors.

The geometric mean fluorescence intensity (GMFI) of intracellular staining for HSPG core proteins, HS and Hpse was determined by flow cytometry and analysis of histograms using FlowJo software (see Section 2.8).

2.6 Quantitative real-time polymerase chain reaction

Following RNA extraction from isolated islets and MIN6 cells (see Section 2.6.2), two-step RT-PCR was performed where reverse transcription to cDNA and TaqMan real time PCR were carried out as separate steps. TaqMan real time PCR is a method used to quantify mRNA expression (**Figure 2.3**). This method uses a probe containing a reporter fluorescent dye at the 5' end and a non-fluorescent quencher at the 3' end. The close proximity of quencher to the reporter dye reduces the fluorescence emitted by the reporter dye (Arya et al., 2005). When the target sequence is present, the probe is cleaved during the extension of the PCR and the non-fluorescent quencher dye is separated from the fluorescent reporter dye resulting in increased fluorescence (**Figure 2.3**). The increase in fluorescence intensity is proportional to the amount of PCR product formed. Validated TaqMan gene expression primer/probe sets (Applied Biosystems, Foster City, CA, USA; see Appendix 1.7) were used to determine the level of expression of genes of interest in test samples, compared to corresponding controls.

2.6.1 Preparation of tissues for RNA extraction

2.6.1.1 Isolated islets

Hand-picked freshly isolated islets were transferred to a 1.5 ml microfuge tube and placed on ice for 5-10 mins (**Figure 2.1**). The supernatant was removed from the tube and the islets were frozen in liquid nitrogen for 5 mins. The islets were stored at -80°C for

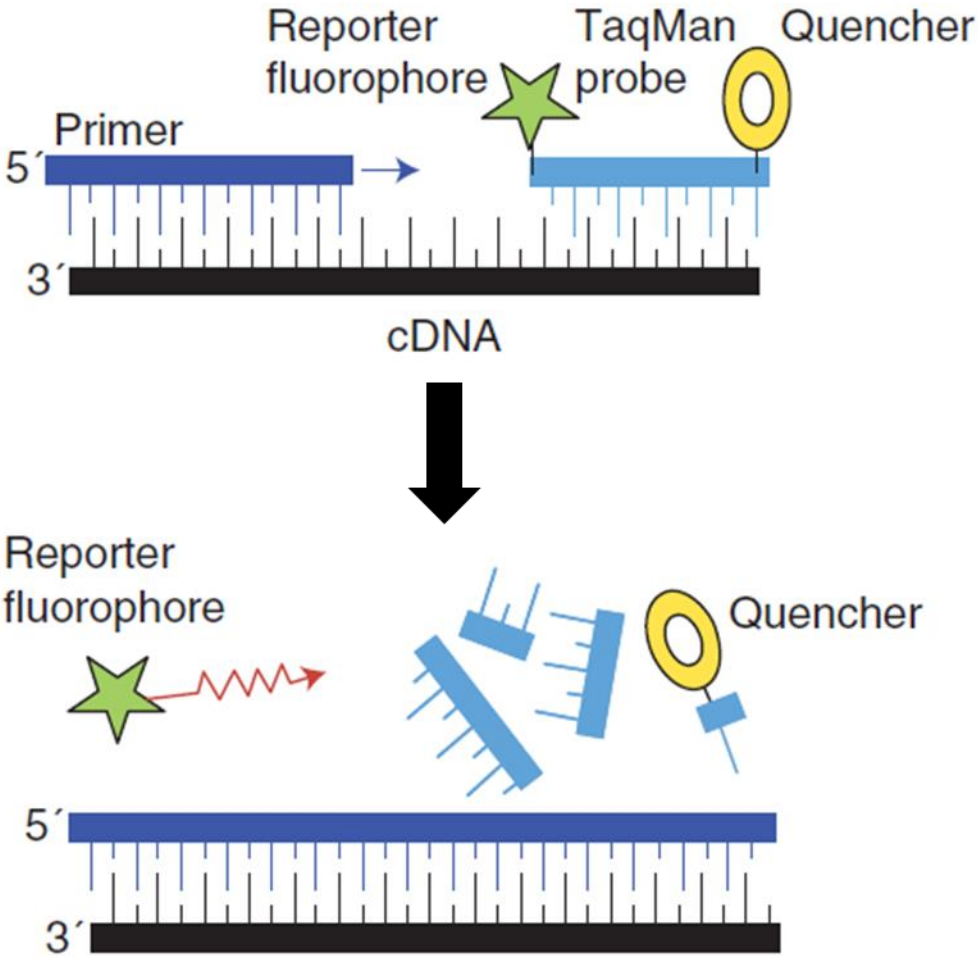

Figure 2.3: TaqMan Real Time-Polymerase chain reaction (PCR).

In TaqMan PCR, a probe (complementary nucleotide sequence to the genes of interest) contains a reporter fluorophore (F) at the 5' end of the probe and a quencher (Q) at the 3' end. The probe binds to the target sequence in the cDNA. After denaturation of the cDNA, the primer and probe hybridise to a single cDNA strand. During the extension phase, the 5' nuclease activity of Taq polymerase cleaves the probe causing separation of fluorescent reporter dye and non-fluorescent quencher dye, resulting in emission of fluorescence. The increase in fluorescence intensity is proportional to the amount of PCR product formed. Adapted from (Arya et al., 2005)

subsequent RNA extraction.

2.6.1.2 Mouse kidney tissue

Wildtype (+/+) mouse kidney was excised and segment of kidney tissue (~2-4 mm^3) were frozen in liquid nitrogen for 5 mins. The sample was stored at -80°C for subsequent RNA extraction.

2.6.2 RNA extraction from isolated islets, MIN6 cells and mouse kidney

The extraction of RNA from isolated islets and MIN6 cells (see Sections 2.5.4 and 2.6.1.1) was performed using the RNeasy Mini Kit (Qiagen #74124). Frozen pellet of islets and MIN6 cells were dislodged by flicking the tube. The cells were lysed by resuspending the pellet in RLT buffer (Qiagen #1015750). The lysed cells were mixed with 70% ethanol to aid binding of RNA to the RNeasy column. Each sample was transferred to an RNeasy spin column fitted with a 2 ml collection tube and centrifuged at 8000 x g for 15 secs ((# 540709361, Eppendorf, Netheier, Hamburg, Germany). The sample was washed with buffer RW1 and RPE to remove contaminating non-RNA. The sample was again washed with RPE buffer and then centrifuged at 8000 x g for 2 mins to evaporate residual ethanol. The RNA was eluted from RNA-bound columns by the addition of 10-30 µl RNase free water followed by centrifugation at 8000 x g for 1 min. The purity and concentration of the RNA was measured using a NanoDrop ND-1000 spectrophotometer (NanoDrop Technologies, Wilmington, DE, USA). The purity of RNA was determined by the ratio of absorbance at 260 nm/280 nm (ratio=1.8-2.1 for optimal purity). The RNA samples were then stored at -80°C.

Prior to RNA extraction of mouse kidney tissue, homogenising tubes (2 ml; Wheaton, DWK Life Sciences, Millville, NJ, USA) and pestles were pre-soaked in 10% H_2O_2/ diethylpyrocarbonate (DEPC) water overnight to remove RNases (see Appendix 1.7). The H_2O_2/DEPC water was removed from the homogenising tubes and RLT buffer containing beta-mercaptoethanol (1/100 dilution) was prepared to denature RNases. The tubes/pestles were then washed 3 x with DEPC water. Kidney tissue was added to the homogenising tube followed by addition of RLT buffer (600 µl); the tissue was homogenised manually for 1 minute. The supernatant was transferred to a microfuge tube and the lysate was centrifuged for 3 minutes at 8000 x g (# 540709361, Eppendorf,

Netheier, Hamburg, Germany). Similar to RNA extraction from islets and MIN6 beta cells, the pellet was resuspended in 70% ethanol and transferred to an RNeasy spin column fitted with a 2 ml collection tube. The sample was centrifuged at 8000 x g for 15 secs followed by washing with buffer RW1 and RPE buffer to remove non-RNA contaminants. The sample was again washed with RPE buffer and then centrifuged at 8000 x g for 2 mins to evaporate residual ethanol. RNase-free water (20 µl) was added to each column followed by centrifugation at 8000 x g for 1 min to elute the RNA. The purity and concentration of RNA was measured using a NanoDrop ND-1000 spectrophotometer (NanoDrop Technologies, Wilmington, DE). The purity of RNA was determined by the ratio of absorbance at 260 nm/280 nm (optimal ratio=1.8-2.1). The RNA samples were stored at -80°C.

2.6.3 Reverse Transcription

Total RNA (1-4 µg) was reverse transcribed in a 20 µl reaction mixture. The RNA was made up to a final volume of 11.5 µl by the addition of sterile Milli-Q water. The reaction mixture containing 1 µl of oligo dT (Cat. # 58862, Invitrogen Carlsbad, CA, USA) and 0.5 µl of dNTPs (Cat. # U1240, Promega, Madison, WI, USA) were added to the RNA sample. The samples were heated to 65°C for 5 mins for linearlisation, incubated for 2 mins on ice and then quickly spun in a microcentrifuge (Eppendorf #5417R F45-30-11) for ~20 secs. The RT mix (7 µl/tube; see Appendix 1.7) containing 5x first strand buffer (#18080093, Invitrogen, Carlsbad, CA, USA), 0.1 M dithiothreitol (DTT; #18080093, Invitrogen, Carlsbad, CA, USA), RNase OUT (#1077-019, Invitrogen, Carlsbad, CA, USA) and superscript RNase reverse transcriptase III (#18080093, Invitrogen, Carlsbad, CA, USA) was then added. Each sample was gently mixed and incubated at 50ºC for 60 mins for optimal reverse transcription activity, followed by incubation at 70ºC for 15 mins to terminate the reaction. Each cDNA sample was diluted with sterile Milli-Q water to a final concentration of 50 ng/µl and stored at -20ºC.

2.6.4 Real-time PCR

The PCR mixture (9 µl) containing 5 µl TaqMan Universal Master Mix (Ref No.: 4304437, Applied Biosystems, Foster City, CA, USA; See Appendix 1.7), 0.5-1 µl FAM-labelled TaqMan® MGB probe (TaqMan Gene Expression Assays, Applied Biosystems, Foster City, CA, USA; see Appendix 1.7) and 3-3.5 µl Milli-Q water was transferred to

each well of an ABI Prism^{TM} 384-well clear optical reaction plate (Ref No.: 4309849, Applied Biosystems, Foster City, CA, USA). 1 µl of cDNA or Milli-Q water was added to each well with each sample prepared in quadruplicates. The plate was covered with ABI Prism^{TM} optical adhesive cover (Ref No.: 4311971, Applied Biosystems, Foster City, CA, USA). The PCR was performed using a ABI7900HT real-time PCR machine with 7900HT Sequence Detection System, Version 2.2.2 2004 software program (Applied Biosystems, Foster City, CA, USA).

2.6.5 PCR data analysis

PCR data was analysed using the comparative C_T method (Popp et al., 2007, Ziolkowski et al., 2012, Livak and Schmittgen, 2001). C_T is the threshold cycle number at which the fluorescence signal generated within a reaction is greater than the minimum detection level. The level of expression of the targeted gene (PCR product) is inversely proportional to the C_T value. The mean normalised C_T value was calculated, taking into account all the biological replicates. Using the comparative C_T method, ΔC_T was calculated by subtracting the C_T value for the endogenous reference gene (i.e. Ube2d1, GAPDH or cycolphilin A) from the C_T values of the gene of interest (ATF3, CHOP, BiP and P58). The $\Delta\Delta C_T$ was calculated by subtracting the ΔC_T value of the control sample (isolated heterozygous (db/+) and wt (+/+) islets or Ins2$^{WT/WT}$ islets or kidney or 6 mM glucose MIN6 beta cells) from the ΔC_T value of the test sample (isolated db/db islets, heterozygous Ins2$^{WT/C96Y}$ islets or ER stressed MIN6 cells). The formula $2^{-\Delta\Delta CT}$ was used to obtain the fold change in the expression for each gene (Livak and Schmittgen, 2001, Schmittgen and Livak, 2008).

2.7 Immunohistochemistry and histology

2.7.1 Fixation of pancreas

Pancreases were dissected from db (wildtype, heterozygous and db/db) and Akita (wildtype and heterozygous) mice and fixed in 10% neutral-buffered formalin for at least 2 days. The fixed tissues were processed and embedded in paraffin. Unstained sections were cut at 4 µm intervals (Histopathology lab, Imaging and Cytometry Facility, JCSMR)

for staining with haemotoxylin and eosin (H&E), for histology and for immunohistochemistry.

2.7.2 Heparan sulfate proteoglycan

2.7.2.1 Collagen Type XVIII

Paraffin-embedded unstained sections of pancreas were deparaffinised in xylene, rehydrated in graded ethanols (100%, 90% and 70%) and washed in running tap water for 5 mins (see Appendix 1.8). Endogenous peroxidase activity was blocked by incubating sections with 3% hydrogen peroxide (H_2O_2) (see Appendix 1.9) for 10 mins. The sections were initially washed in PBS for 2 x 2 mins and then in running tap water for 4 mins. For antigen retrieval, the sections were incubated with 0.05% pronase (Calbiochem, EMD Millipore, Darmstadt, Germany; see Appendix 1.9) for 10 mins in a humidified mist tray (Billups Rothenberg Inc., CA, USA) at 37ºC. The sections were washed with PBS for 2 x 2 mins and incubated for an hour with Ig Blocking Reagent (M.O.M Immunodetection Kit, Vector Laboratories Inc., Burlingame, CA, USA; see Appendix 1.9) at room temperature to minimise non-specific binding of the primary mouse anti-mouse collagen type XVIII (Col18) mAb. The sections were washed 2 x 2 mins with PBS and treated with M.O.M diluent (MOM Immunodetection kit, Vector Laboratories Inc., Burlingame, CA, USA) for 5 mins to reduce background staining. The excess M.O.M diluent was then gently tipped off and the sections were incubated for 30 mins with mouse anti-mouse collagen type XVIII mAb (4 µg/ml or 8 µg/ml) or with purified mouse IgG2bκ (4 µg/ml or 8 µg/ml) as the isotype control Ig (see Appendix 1.10). The sections were then washed in PBS and incubated with horseradish peroxidase (HRP)-conjugated polyclonal rabbit anti-mouse Ig (Rabbit anti-mouse Ig-HRP, 26 µg/ml) (see Appendix 1.10) for 30 mins. After washing in PBS, the chromogen 3-amino-9-ethylcarbazole (AEC) (Sigma-Aldrich, St. Louis, MO, USA) (see Appendix 1.9) was applied to the sections for 30 mins. The sections were washed in deionised water (dH_2O) and transferred to a fresh boat of dH_2O. The sections were counterstained with Gill's Haematoxylin for 35 secs, washed in dH_2O and dipped into ammonium water (2 dips at 2 secs/dip; see Appendix 1.9), followed by washing in dH_2O. The sections were cover-slipped using DAKO glycergel mounting medium (DAKO).

2.7.2.2 Syndecan-1

Unstained formalin-fixed paraffin sections of mouse pancreas were deparaffinised in xylene, rehydrated in graded ethanols and washed in running tap water for 5 mins (see Appendix 1.8). Endogenous peroxidase activity was blocked by incubating sections with 3% H_2O_2 for 10 mins. The sections were washed in PBS (2 x 2 mins) and in running tap water (2 mins). Prior to antigen retrieval, the sections were treated with 10 mM citrate buffer (pH 6.0) for 5 mins (see Appendix 1.9). For antigen retrieval, the sections were heated in citrate buffer in a microwave (900 watts, Model No. NN-s548WA, Panasonic, Kadoma, Osaka, Japan) for 2 mins at high power, followed by 12 mins (2 x 6 mins) on low power. The sections were set aside to cool for 30 mins and then washed in PBS. The sections were incubated with Animal Free Blocker (AFB; Vector Laboratories Inc., Burlingame, CA, USA) for 10 mins. The excess AFB was tipped off and the sections were then incubated for 1 hour with the primary antibody rat anti-mouse CD138 (syndecan-1; 50 µg/ml; see Appendix 1.10) or isotype control Ig, rat IgG2aκ (50 µg/ml; see Appendix 1.10). The sections were washed with PBS and incubated with HRP-conjugated polyclonal rabbit ant-rat Ig (52 µg/ml; DAKO) as the secondary antibody for 30 mins. The sections were washed with PBS, incubated with AEC (see Appendix 1.9) for 30 mins, and then washed in deionised water (dH_2O) for 10 mins. The sections were counterstained with Gill's Haematoxylin for 35 secs, washed in dH_2O, dipped in ammonium water (2 dips at 2 secs/dip) and then washed in dH_2O. The sections were cover-slipped using DAKO glycergel mounting medium (DAKO).

2.7.2.3 CD44

Unstained formalin-fixed paraffin sections of mouse pancreas were deparaffinised in xylene, rehydrated in graded ethanols and washed in running tap water for 5 mins (see Appendix 1.8). Endogenous peroxidase activity was blocked by incubating sections with 3% H_2O_2 for 10 mins. The sections were washed in PBS (2 x 2 mins) and in running tap water (2 mins). Prior to antigen retrieval, the sections were treated with 10 mM citrate buffer (pH 6.0) for 5 mins (see Appendix 1.9). For antigen retrieval, the sections were heated in citrate buffer in a microwave (900 watts, Model No. NN-s548WA, Panasonic, Kadoma, Osaka, Japan) for 2 mins at high power, followed by 12 mins (2 x 6 mins) on low power. The sections were set aside to cool for 30 mins and then washed in PBS. The sections were incubated with Animal Free Blocker (AFB; Vector Laboratories Inc.) for

10 mins. The excess AFB was tipped off and the sections were then incubated for 1 hour with the primary antibody rat anti-mouse CD44 (CD44; 40 µg/ml) or mouse anti-human CD44v3 (10 µg/ml) mAb; alternatively, the sections were incubated with isotype control Ig (rat IgG2bκ (40 µg/ml) or mouse IgG_{2b} (10 µg/ml), respectively) (see Appendix 1.10). The sections were washed with PBS and incubated with HRP-conjugated polyclonal rabbit ant-rat Ig (52 µg/ml) or rabbit anti-mouse Ig (26 µg/ml) as the secondary antibody for 30 mins. The sections were washed with PBS, incubated with AEC (see Appendix 1.9) for 30 mins, and then washed in deionised water (dH_2O) for 10 mins. The sections were counterstained with Gill's Haematoxylin for 35 secs, washed in dH_2O, dipped in ammonium water (2 dips at 2 secs/dip) and then washed in dH_2O. The sections were cover-slipped using DAKO glycergel mounting medium (DAKO).

2.7.3 Islet endocrine hormones

2.7.3.1 Insulin and glucagon

Formalin-fixed unstained sections were de-waxed in xylene, rehydrated in graded ethanols and washed in running tap water (see Appendix 1.8). Endogenous peroxidase activity was blocked for 5 mins using 0.03% H_2O_2/methanol/sodium azide (see Appendix 1.9) and the sections were then washed in PBS for 3 x 10 mins. Sections were incubated with M.O.M Ig block reagent for 1 hour at room temperature to minimise non-specific Ig binding. Excess M.O.M Ig block was tipped off and the sections were incubated with anti-insulin mAb (ascites, 65 µg/ml or 260 µg/ml) or isotype control mouse IgG1κ (64.9 µg/ml or 227.3 µg/ml) (see Appendix 1.11). Alternatively, sections were incubated with anti-glucagon mAb (ascites, clone K79bB10, 57 µg/ml or 114 µg/ml) or corresponding isotype control mouse IgG1κ (64.9 µg/ml) for 30 mins (see Appendix 1.11). The primary antibody was washed off with PBS and the sections were incubated with the secondary, antibody biotinylated anti-mouse IgG (1/250, M.O.M Immunodetection Kit PK-2200, Vector Laboratories Inc., Burlingame, CA, USA) (see Appendix 1.11) for 10 mins. The sections were washed in PBS and incubated with VECTASTAIN Avidin-Biotin-Complex (ABC) reagent (M.O.M Immunodetection Kit, PK-2200, Vector Laboratories Inc., Burlingame, CA, USA) for 5 mins. The sections were washed in PBS and then incubated with AEC for 30 mins. The sections were then washed with dH_2O before counterstaining with Gills haematoxylin stain for 35 secs. After washing with dH_2O, the sections were

dipped in ammonium water (2 x 2 secs/dip; Appendix 1.9) and washed again with dH_2O. The slides were cover-slipped with glycergel mounting medium (DAKO).

2.7.3.2 Proinsulin

For immunostaining of proinsulin, unstained formalin-fixed paraffin sections were de-waxed in xylene, rehydrated in graded ethanols and washed in running tap water (see Appendix 1.8). Endogenous peroxidase activity was blocked for 5 mins using using 0.03% H_2O_2/methanol/sodium azide (see Appendix 1.9) and the sections were subsequently washed in PBS for 3 x 10 mins and in running tap water for 2 mins. Sections were pretreated with 10 mM citrate buffer (pH 6.0) for 5 mins to equilibrate the pH for antigen retrieval. For antigen retrieval, the sections were heated in citrate buffer for 2 mins in a microwave oven set at high power, followed by 12 mins (2 x 6 mins) on low power. The sections were set aside to cool for 30 mins, washed in PBS and then incubated with AFB for 10 mins to prevent non-specific binding of antibody. Excess AFB was removed, and the sections were then incubated for 1 hour with mouse anti-human proinsulin mAb (1/800) or isotype control mouse IgG1κ (1/8.8) (see Appendix 1.11). The primary antibody was removed by washing the sections with PBS and the sections were then incubated with the secondary antibody biotinylated anti-mouse IgG (1/250; M.O.M Immunodetection Kit, Vector Laboratories Inc., Burlingame, CA, USA; See Appendix 1.11) for 10 mins. The sections were then washed in PBS and incubated with ABC reagent for 5 mins. The sections were washed in PBS, followed by incubation with AEC for 30 mins. The sections were then washed with dH_2O before counterstaining with Gills haematoxylin stain for 35 secs. After washing with dH_2O, the sections were dipped in ammonium water (2 x 2 secs/dip) and washed again with dH_2O. The slides were cover-slipped with glycergel mounting medium (DAKO).

2.7.4 Heparan Sulfate

For immunolocalisation of heparan sulfate (HS), formalin fixed unstained paraffin sections of pancreas were deparaffinised in xylene and rehydrated in graded ethanols, followed by washing in running tap water for 5 mins (see Appendix 1.8). Endogenous peroxidase activity was blocked by incubating sections with 3% H_2O_2 (see Appendix 1.9) for 10 mins. The sections were washed in PBS for 2 x 2 mins and in running tap water for 4 mins. For antigen retrieval, the sections were incubated with 0.05% pronase (see

Appendix 1.9) for 10 mins at 37ºC in a humidified mist tray (Billups-Rothernberg Inc., CA, USA). Sections were washed with PBS for 2 x 2 mins and incubated for an hour with M.O.M Ig Blocking Reagent (M.O.M immunodetection kit, Vector Laboratories Inc., Burlingame, CA, USA; see Appendix 1.9). The sections were washed 2 x 2 mins and incubated with AFB (see Appendix 1.9) for 5 mins. The excess AFB was then gently tipped off and the sections were incubated for 1 hour with 10E4 mouse anti-human mAb (recognises highly sulfated HS; 200 µg/ml) or HepSS-1 mouse anti-human HS (recognises under-sulfated HS; 100 µg/ml) mAbs or isotype control mouse IgMκ (200 µg/ml) (see Appendix 1.12). The sections were then washed in PBS and incubated with the secondary antibody horseradish peoxidase (HRP)-conjugated polyclonal rabbit anti-mouse Ig (26 µg/ml, see Appendix 1.12) for 30 mins, followed by washing in PBS. AEC (see Appendix 1.9) was applied to the sections for 30 mins and the sections were then washed in dH_2O. Sections were counterstained in Gill's Haematoxylin for 35 secs, washed in dH_2O and dipped in ammonium water (2 dips at 2 secs/dip), followed by washing in dH_2O. The sections were cover-slipped using glycergel mounting medium (DAKO).

Alternatively, for phage display single chain anti-HS antibodies, EV3C3 anti-HS mAb and HS3A8 anti-HS mAbs were used (see Appendix 1.12). The EV3C3 anti-HS mAb stains for N-sulfation, C5 epimerisation and 2-O sulfation in HS chains; HS3A8 anti-HS mAb recognises highly sulfated HS domains i.e., 6-O and 2-O sulfation of iduronic acid (Dennissen et al., 2002, Alhasan et al., 2014). Immunolocalisation of HS by the phage display antibodies was identical to 10E4 anti-human mAb staining. The sections were stained with primary antibodies i.e., EV3C3 anti-HS (1/2) or HS3A8 anti-HS (7/10) mAbs or isotype control rabbit anti-VSV-G mAb (10 µg/ml) for 1 hour (see Appendix 1.12). The sections were washed with PBS and incubated with secondary antibody swine anti-rabbit HRP (13 µg/ml; DAKO) for 30 mins. The sections were washed and AEC was applied for 30 mins. Sections were the washed in dH_2O and counterstained in Gill's Haematoxylin for 35 secs followed by washing in dH_2O, dipping in ammonium water (2 dips at 2 secs/dip) and washing in dH_2O. The sections were cover-slipped using glycergel mounting medium (DAKO).

2.7.5 Morphometry

Normal mouse (wildtype, +/+) or Ins2$^{WT/WT}$ islets stained with HSPG core proteins (collagen type XVIII, CD44 and syndecan-1) demonstrated positive staining in the islets for primary antibodies and no or little background staining with the corresponding isotype control (**Figure 2.4**). Anti-CD44 and anti-CD44v3 mAbs showed comparable intra-islet staining. Therefore, in this thesis, CD44 expression was analysed using anti-CD44 mAb. Both 10E4 anti-HS and HepSS-1 anti-HS mAbs showed intense staining with primary antibodies and absence of background staining with the isotype controls (**Figure 2.5**). Similarly, strong staining was observed in insulin and staining in the periphery for the glucagon for primary antibodies whereas no background staining was observed with isotype controls (**Figure 2.6**). Proinsulin staining showed punctate expression in wildtype Ins2$^{WT/WT}$ mice and no background staining in the isotype control (**Figure 2.7**).

Images of immunostained sections were prepared using an Axio Observer inverted florescence microscope (Zeiss; Göttingen, Germany) at 20x maginification.

2.7.5.1 Measurement of immunostained islet area

The images were analysed to determine the percentage of islet area stained using NIH Image J software, version 1.48v software (NIH, USA) (Ziolkowski et al., 2012, Choong et al., 2015, Simeonovic et al., 2018). The threshold intensity (gray value 0-255) was set to define positive staining present in the islets of wildtype (+/+) and Ins2$^{WT/WT}$ mouse pancreas at 6-16 weeks and 9 weeks of age, respectively. When pancreatic sections showed a comparable intensity of staining in the islets, the % islet area was determined. For this measurement, the area of interest (i.e., an islet) was firstly traced to measure the total islet area; the intra-islet area of positive staining (≥ the intensity threshold) was measured and expressed as % +ve stained islet area. For each set of samples for each immunostain (e.g., for a complete time-course), the same threshold setting was applied to all samples at each time point. In contrast, for pancreas sections where the staining was variable among the islets, optical density (i.e., staining intensity) was measured using global calibration. For the latter analysis, a threshold setting is not required by the Image J program (see Section 2.7.5.2).

Figure 2.4: Localisation of HSPG core proteins in the pancreatic islets of wildtype (wt, +/+) mice.

Representative images show the immunohistochemical localisation of heparan sulfate proteoglycan (HSPG) core proteins for Col18 (a), Sdc1 (c), CD44 I and CD44v3 (g) in the islets of wt (+/+) mice at 9 weeks of age. In contrast to the strong intra-islet expression of HSPG core proteins (a, c, e and g), no background staining was observed when the primary antibody was replaced with isotype control Ig (b, d, f and h). Scale bar = 100 μm.

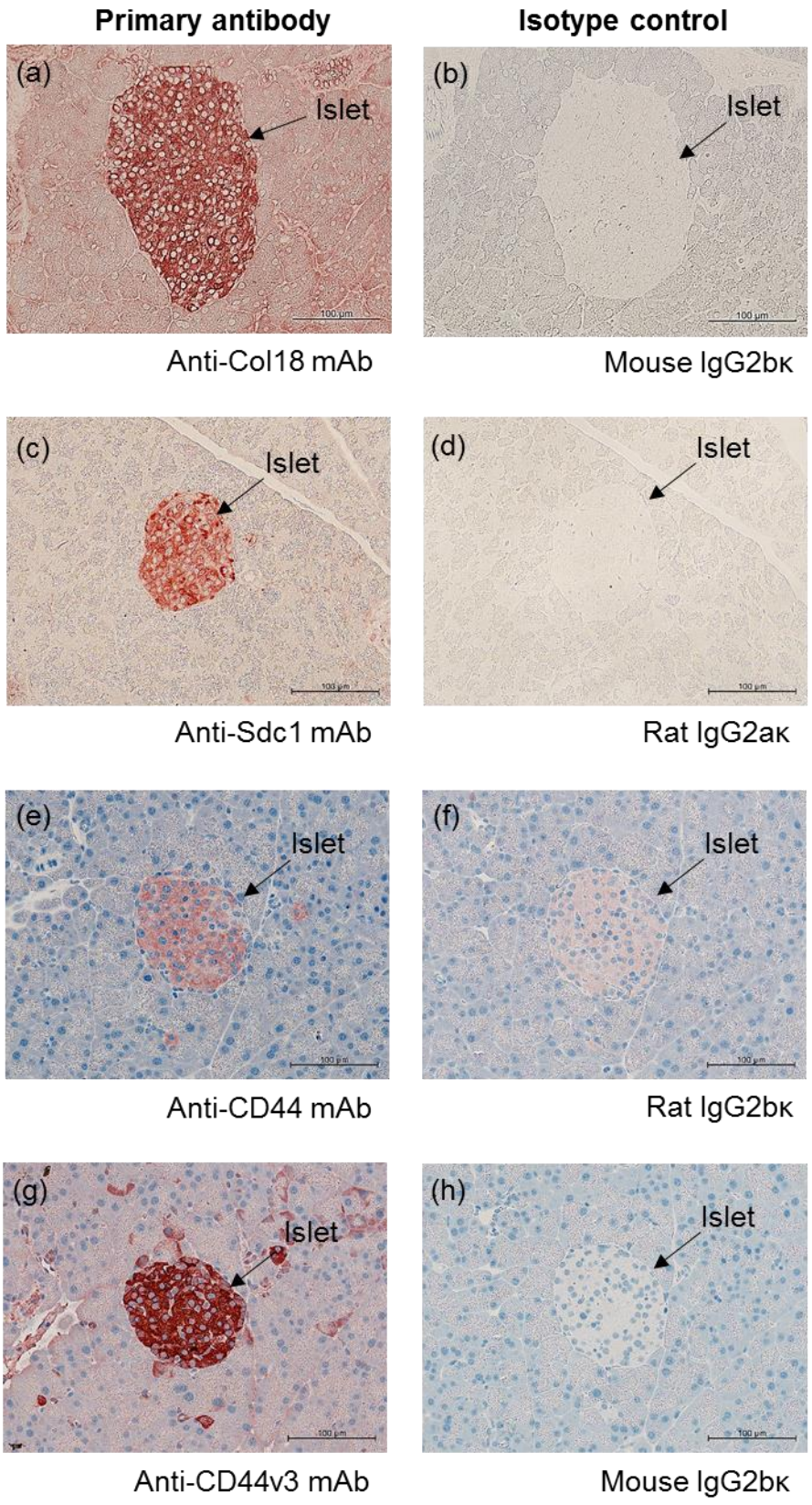
Primary antibody
Isotype control
(a)
Islet
(b)
Islet
Anti-Col18 mAb
Mouse IgG2bκ
(c)
Islet
(d)
Islet
Anti-Sdc1 mAb
Rat IgG2aκ
(e)
Islet
(f)
Islet
Anti-CD44 mAb
Rat IgG2bκ
(g)
Islet
(h)
Islet
Anti-CD44v3 mAb
Mouse IgG2bκ

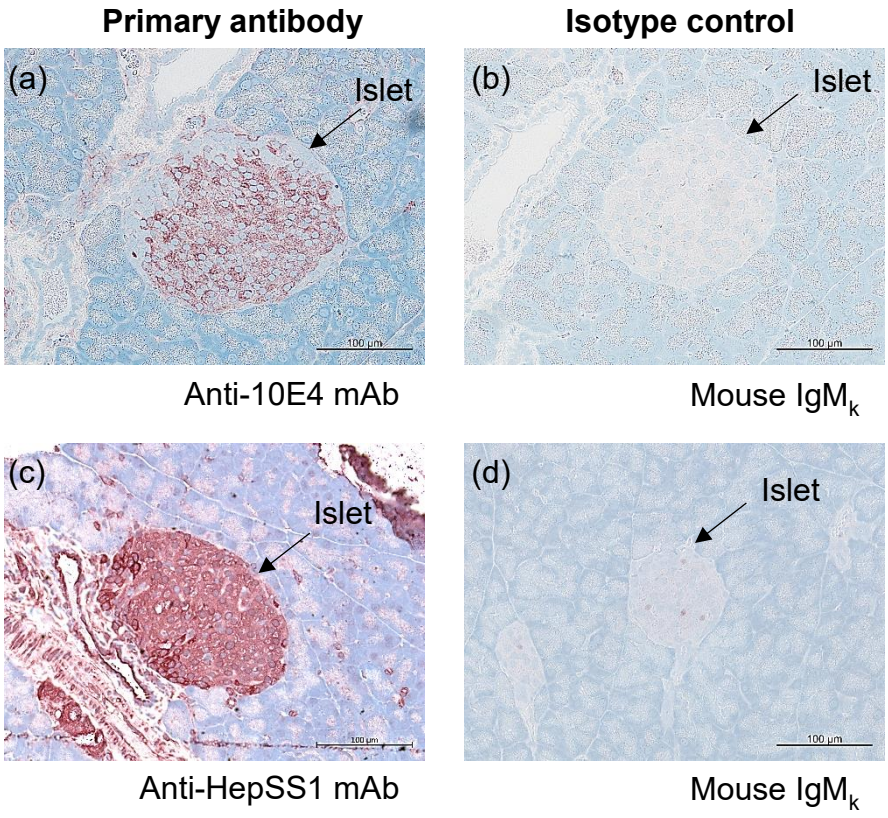

Figure 2.5: Distribution of HS in the pancreatic islets of wt (+/+) mice.

Representative images show the distribution of heparan sulfate (HS) in the islets of wt (+/+) mice at 6 weeks of age. Strong staining was observed throughout the islet with anti-10E4 mAb (a) whereas an intense staining in the periphery and strong staining inside the islet was observed with Anti-HepSS1 mAb (c). In contrast, no background staining was observed with isotype control mouse IgM_k (b, d). Scale bar = 100 μm.

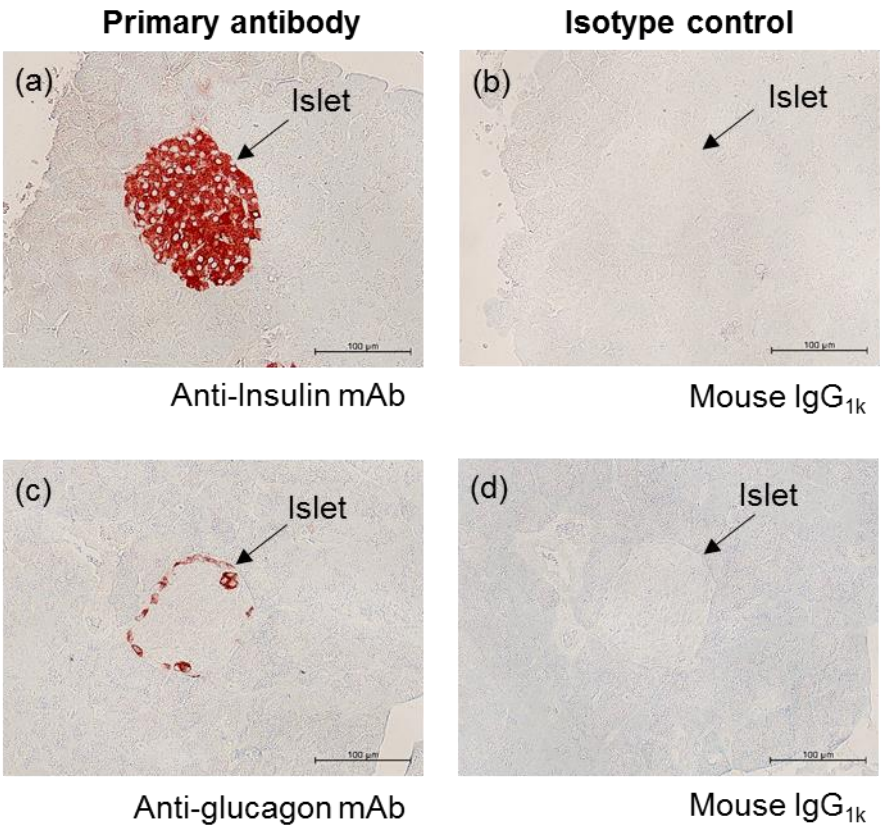

Figure 2.6: Insulin and glucagon levels in the pancreatic islets of wildtype (wt, +/+) mice.

Representative images show the distribution of insulin (a) and glucagon (d) in the islets of wt mice at 9 weeks of age. In contrast to the strong intra-islet expression of insulin (a) and glucagon (c), no background staining was observed when the primary antibody was replaced with isotype control mouse IgG_{1k} (b and d). Scale bar = 100 μm.

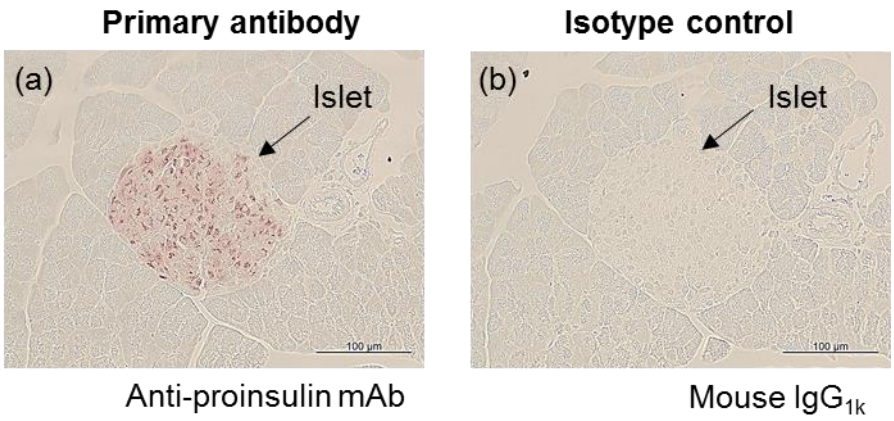

Figure 2.7: Localisation of proinsulin in the pancreatic islets of wildtype Ins2$^{WT/WT}$ mice.

Representative images show the distribution of proinsulin in the islets of Ins2$^{WT/WT}$ mice at 6 weeks of age. Punctate staining of proinsulin (a) was observed with primary antibody whereas no background staining was observed with isotype control mouse IgG$_{1k}$ (b). Scale bar = 100 µm.

For simple comparisons between two groups of adult pancreases from the same mouse strain, differences in optical density (staining intensity) analysis of islets closely resembled differences in % islet area stained (see Appendix 3). In general, for comparisons of immunostained islets between different mouse genotypes at different donor ages, the % of islet area stained was determined for the expression of HSPG core proteins and HS, while the intensity of staining in islets was analysed for endocrine hormones.

2.7.5.2 Measurement of intra-islet intensity of immunostaining

Images of immunostained sections were analysed to quantify the intensity of intra-islet staining using Image J 1.48v software (NIH, USA) (Choong et al., 2015, Ziolkowski et al., 2012). The AEC +ve component was separated from the counter-stain using a colour deconvolution plugin. The intensity of staining was determined by converting the mean pixel value of the area of interest to optical density (OD), using the calculation log10 (255/mean pixel value) (Ziolkowski et al., 2012).

2.8 Flow cytometry analysis of HS, heparanase (Hpse) and HSPG core proteins in beta cells by flow cytometry

Cell surface and intracellular fluorescence staining were determined in separate aliquots of the same cell population.

2.8.1 Cell surface staining

Primary mouse beta cells (4 x 10^4 cells/well) and MIN6 beta cells (2 x 10^5 cells/well) were distributed in a 96-well plate (#650180, CellStar, U-bottom plate, Greiner Bio-one, Kremsmünster, Austria). FACs wash buffer (see Appendix 1.13) was added to make up the volume to 200 µl/ well and the cells were centrifuged at 249 x g (primary beta cells) or 693 x g (MIN6 cells) for 3 mins. The supernatant was discarded and the plate was vortexed briefly to resuspend the cell pellet. The cells were incubated with Fc block (rat anti-mouse CD16/CD32 mAb; 5 µg/ml; see Appendix 1.14) for 10 mins on ice. Cells were then washed with FACs wash buffer and centrifuged at 249 x g or 693 x g; the supernatant was then removed. The cells were then incubated with primary antibodies

(collagen type XVIII (4 µg/ml), syndecan-1 (20 µg/ml), CD44 (40 µg/ml), 10E4 anti-HS (20 µg/ml; HS) or HP3/17 (1.5 µg/ml; Hpse)) (see Appendix 1.14) for 30 mins on ice. The cells were washed with PBS, centrifuged at 249 x g or 693 x g and the supernatant was discarded. The cells were incubated with secondary antibodies (goat anti-mouse Ig PE (5 µg/ml for Col18 and HS) or mouse anti-rat kappa PE (2 µg/ml for Sdc1 and CD44) or rat anti-mouse Ig FITC (10 µg/ml for Hpse)) (see Appendix 1.14) for 30 mins on ice, followed by washing and centrifugation at 249 x g or 693 x g. The supernatant was removed, and the cells were resuspended in 100 µl PBS. The samples were transferred to FACs cluster tubes (Axygen, Salt lake city, UT, USA) and run on a BD LSR Fortessa flow cytometer using FL-1 and FL-2 channels. The fluorochromes PE 561 and FITC were excited using a 488 nm laser. The excitation/emission wavelength maxima for PE 561 and FITC are 496-564/578 nm and 494/519 nm, respectively. The geometric mean fluorescence intensity (GMFI) of cells stained with primary antibody was determined from histograms of fluorescence staining using FlowJo software (version 10.0.7, TreeStar Inc., Ashland, OR, USA).

2.8.2 Intracellular staining

For intracellular staining, primary mouse beta cells (4 x 10^4 cells/well) and MIN6 beta cells (2 x 10^5 cells/well) were plated out in a 96-well plate (CellStar, U-bottom plate, #650180). BD wash buffer (see Appendix 1.13) was added to make up the volume to 200 µl/ well and the cells were centrifuged at 249 x g (primary beta cells) or 693 x g (MIN6 beta cells) for 3 mins. The supernatant was discarded, and the plate was vortexed briefly to resuspend the cell pellet. The cells were fixed and permeablised by treatment with 100 µl BD Fix/Perm (BD Biosciences #51-2090KZ)/sample for 10 mins on ice; 100 µl BD wash buffer was added to each well before centrifugation at 249 x g or 693 x g. The medium was removed, and the cells were incubated with Fc block (rat anti-mouse CD16/CD32 mAb; 5 µg/ml; see Appendix 1.14) for 10 mins on ice. The cells were washed with BD wash buffer, centrifuged at 249 x g or 693 x g and the supernatant was then removed. The cells were then incubated with individual primary antibody (collagen type XVIII (4 µg/ml) or syndecan-1 (20 µg/ml) or CD44 (40 µg/ml) or 10E4 anti-HS (20 µg/ml; HS) or HP3/17 (1.5 µg/ml; Hpse)) (see Appendix 1.14) for 30 mins on ice. The cells were washed with PBS, centrifuged at 249 x g or 693 x g and the supernatant was discarded. The cells were incubated with secondary antibodies (goat anti-mouse Ig PE (5

µg/ml for Col18 and HS), mouse anti-rat kappa PE (2 µg/ml for Sdc1 and CD44) or rat anti-mouse Ig FITC (10 µg/ml for Hpse)) (see Appendix 1.14) for 30 mins on ice, followed by washing with PBS and centrifugation at 249 x g or 693 x g. The supernatant was removed, and the cells were resuspended in 100 µl PBS. The samples were transferred to FACs cluster tubes (Axygen, Salt lake city, UT, USA) and run on a BD LSR Fortessa flow cytometer using FL-1 and FL-2 channels. The fluorochromes PE 561 and FITC were excited using a 488 nm laser. The excitation/emission wavelength maxima of PE 561 and FITC are 496-564/578 nm and 494/519 nm, respectively. The geometric mean fluorescence intensity (GMFI) of cells stained with primary antibody was determined from histograms of fluorescence staining using FlowJo software (version 10.0.7, TreeStar Inc., Ashland, OR, USA).

2.8.3 Gating strategy for analysis of beta cells

Viable beta cells were gated on the basis of forward scatter (FSC) and side scatter (SSC) properties, thereby excluding dead cells from the analysis. Single cells were initially identified and gated based on the SSC-W and SSC-H; gating using FSC-A and FSC-H was then done to exclude any doublets contaminating the single cell population. Histograms were generated for cell surface or intracellular staining. The gating strategy is shown in **Figures 2.8** and **2.9**. The histogram for auto-fluorescence (unstained cells) was plotted and overlayed with the histogram for cells stained with primary antibody e.g., collagen type XVIII, CD44, 10E4, syndecan-1 or HP3/17. The GMFI was calculated for stained and unstained cells using FlowJo software (version 10.0.7, TreeStar Inc., Ashland, OR, USA).

2.9 HS replacement in primary beta cells using HS mimetics

Primary beta cells were isolated from male and female wt and db/db pancreases, 4 x 10^4 cells/ml (see Section 2.3.2). The beta cells were cultured with and without HS mimetics (heparin (Celsus Laboratories, Cincinnati, OH) or PI-88 (Muparfostat; Progen Pharmaceuticals, Brisbane, Australia); 50 µg/ml) for 2 days and the cell viability was analysed by flow cytometry.

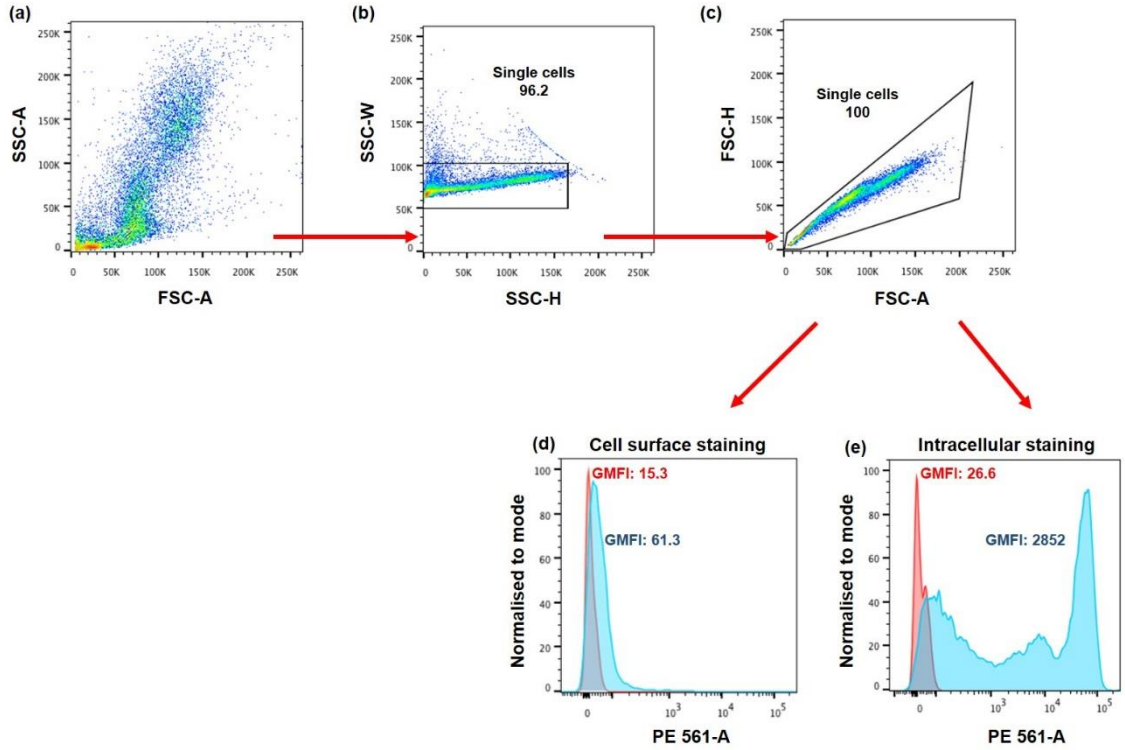

Figure 2.8: Gating strategy for measuring fluorescence staining (GMFI) in primary beta cells.

(a) Total primary islet cell population (~90% beta cells (Ziolkowski et al., 2012)) showing forward scatter (FSC) and side scatter (SSC) properties. (b) Single cells were gated based on the SSC-W and SSC-H; (c) FSC-H and FSC-A properties were used to exclude doublets (cell aggregates). Histograms showing (d) cell surface and (e) intracellular expression of collagen type XVIII (blue) versus background staining (red) in primary beta cells. The intensity of florescence staining of the population is expressed as the geometric mean fluorescence intensity (GMFI). SSC-A, side scatter area; FSC-A, forward scatter area; SSC-W, side scatter width; SSC-H, side scatter height; FSC-H, forward scatter height and FSC-A, forward scatter area.

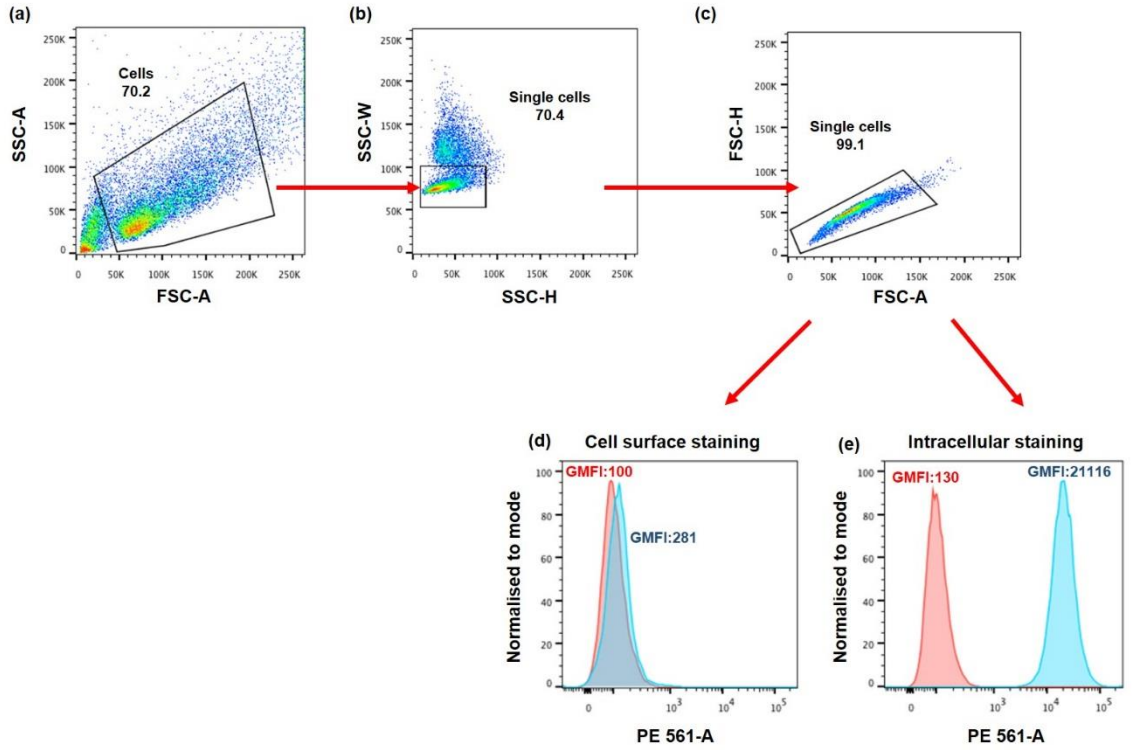

Figure 2.9: Gating strategy for measuring the intensity of fluorescence staining (GFMI) in MIN6 cells.

(a) The viable MIN6 population was gated from the total MIN6 population based on forward scatter (FSC) and side scatter (SSC) properties. Single cells were gated based on (b) SSC-W and SSC-H followed by (c) FSC-H and FSC-A to exclude doublets. (d) Representative histogram shows the number of cells normalised to mode on the Y-axis and fluorescence intensity on the X-axis for the cell surface expression of collagen type XVIII (blue) and unstained (red) MIN6 cells. (e) Representative histogram demonstrates intracellular expression of collagen type XVIII core protein (blue) in MIN6 cells, versus unstained cells (red). Fluorescence staining of the cell population is expressed as the geometric mean fluorescence intensity (GMFI). SSC-A, side scatter area; FSC-A, forward scatter area; SSC-W, side scatter width; SSC-H, side scatter height; FSC-H, forward scatter height and FSC-A, forward scatter area.

2.9.1 Analysis of cell viability using Calcein-AM and PI staining

The viability of primary beta cells was analysed by Calcein-AM and propidium iodide (PI) staining. Calcein-AM is a cell permeant dye that stains live cells. The non-fluorescent Calcein-AM is converted into fluorescent calcein following cleavage of the ester diacetate by intracellular esterase activity. PI is an impermeant fluorescent dye which only enters and stains dead cells. PI intercalates with the nucleic acid of dead cells and emits florescence. Calcein-AM was diluted to 0.04 µM in PBS (Invitrogen; see Appendix 1.15) and PI was diluted to 2.5 µg/ml in PBS (BD Biosciences; see Appendix 1.15).

Primary beta cells were plated in a 96-well plate (#650180, CellStar, Greiner Bio-one, Kremsmünster, Austria), 4-8 x 10^4/well. The plate was centrifuged at 110 – 173 x g for 3 mins and the supernatant was discarded. The cells were stained with 100 µl of 0.04 µM Calcein Acetoxymethyl (Calcein-AM; see Appendix 1.15). The unstained cells and cells to be subsequently stained with PI only were treated with 100 µl PBS. The cells were incubated for 15 mins at 37°C in 5% CO_2/95% air. The cells were then washed with 100 µl PBS and centrifuged at 110 – 173 x g for 3 mins. The supernatant was discarded, and the cells were washed again with 200 µl PBS and centrifuged. After removing the supernatant, unstained cells and cells only stained with Calcein-AM were treated with 100 µl PBS; the remaining calcein-stained wells and additional unstained wells were then stained with 2.5 µg/ml PI (100 µl/well). The plate was incubated for 15 mins at 37°C in 5% CO_2/95% air. The cells were then washed with 100 µl PBS, centrifuged and resuspended in 100 µl PBS for flow cytometry analysis. The samples were run on a BD LSR Fortessa using the FL-1 and FL-2 channels. Events were collected using BD FACS Diva software (version 8). Flow Jo software (version 10.0.7) was used to determine the % viable cells (Cal^+PI^-), dead cells (Cal^-PI^+) and damaged cells (Cal^+PI^+) in the total population using dot plots and quadrant statistics.

2.9.2 Analysis of cell viability using Sytox Green uptake

Sytox Green is an impermeant fluorescent dye used to distinguish between live and dead cells. Sytox Green specifically stains dead cells by intercalating with nucleic acids. The cells were plated at 4-8 x 10^4 cells/well in a 96-well plate (#650180, CellStar, Greiner Bio-one, Kremsmünster, Austria). The cells were centrifuged at 110 – 173 x g for 3 mins and the supernatant was discarded. The cells were either treated with 30% H_2O_2 (100

µl/well) or 100 µl PBS/well. The cells were incubated for 5 mins at 37°C in 5% CO_2/95% air. The cells were washed with 100 µl PBS and centrifuged at 110 – 173 x g for 3 mins. The cells were then stained with 31.25 nM Sytox Green (100 µl/well; see Appendix 1.15); unstained cells were treated with PBS (100 µl/well). The cells were incubated for 15 mins at 37°C in 5% CO_2/95% air and washed with PBS (100 µl/well) followed by centrifugation at 110 – 173 x g for 3 mins. The cells were resuspended in PBS (100 µl/well) and transferred to FACs cluster tubes (Axygen, Salt lake city, UT, USA) for flow cytometry analysis. The samples were run on a BD LSR Fortessa using the FL-2 channel. Events were collected using BD FACS Diva software (version 8). FlowJo software was used to determine the % dead or damaged cells in the total population from dot plots (see Section 2.9.3).

2.9.3 Flow cytometry data analysis

Flow cytometry data were generated using FlowJo Software (version 10.0.7, TreeStar Inc., Ashland, OR, USA).

2.9.3.1 Viable Calcein (Cal)+ve PI-ve population

The beta cells were separated on the basis of forward scatter (FSC) and side scatter (SSC) properties. The single cells were gated from the SSC-W and SSC-H properties; FSC-A and FSC-H was used to exclude doublets or cell aggregates according to the gating strategy in **Figure 2.10**. The Calcein (Cal^+) staining was represented on the y-axis and PI staining on the x-axis (**Figure 2.10**). The quadrants were set using unstained cells to identify the negatively stained sub-population of cells.

2.9.3.2 Dead/damaged Sytox Green +ve cells after H_2O_2 treatment

The beta cells were gated on the basis of forward scatter (FSC) and side scatter (SSC) properties. Single cells were gated based on the SSC-W and SSC-H; FSC-A and FSC-H were used to exclude doublets in the population. Sytox Green +ve staining was represented on the y-axis and SSC-W on x-axis (an empty channel) (**Figure 2.11**). The region identifying Sytox Green +ve cells was set using unstained cells to identify the region corresponding to negatively stained cells using the gating strategy as shown in the **Figure 2.11**.

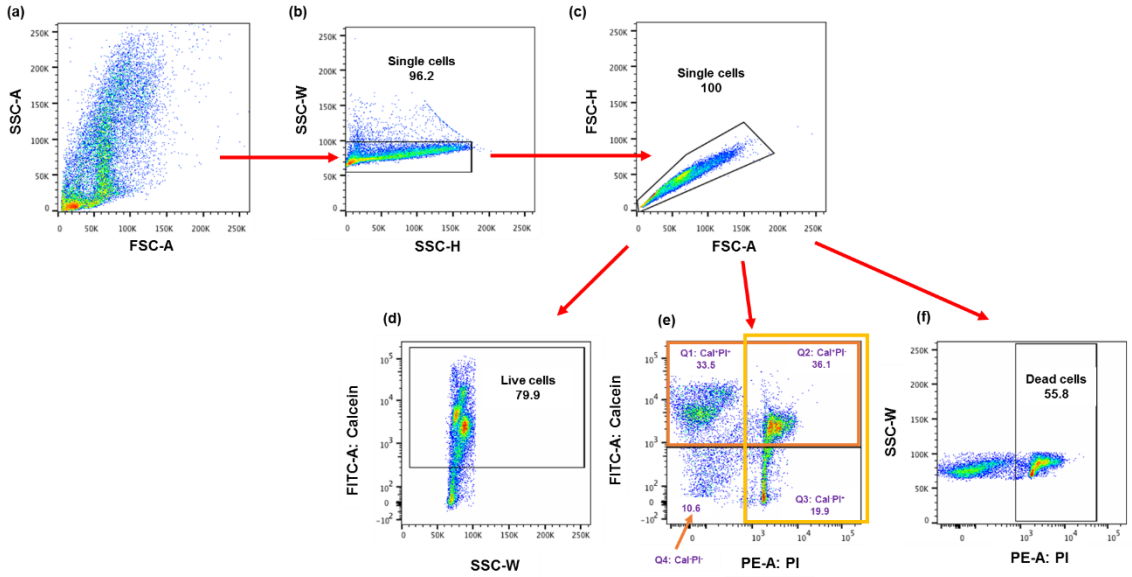

Figure 2.10: Gating strategy for measuring live (Cal^+PI^-), damaged (Cal^+PI^+) and dead (Cal^-PI^+) primary beta cells.

Representative flow cytometry dot plots for ascertaining the distribution of viable, damaged and dead beta cells show: (a) Total islet cells (~90% beta cells (Ziolkowski et al., 2012)) with forward scatter (FSC) and side scatter (SSC) properties; (b) Single cells gated on SSC-W and SSC-H; (c) FSC-H and FSC-A for exclusion of doublets; (d-f) Calcein (Cal) staining on y-axis and propidium iodide (PI) staining on x-axis. Quadrants (Q) in (e) were determined using unstained cells. Q4: Cal^-PI^- cells (cell debris); Q3: Cal^-PI^+ cells (dead cells); Q2: Cal^+PI^+ cells (damaged cells) and Q1: Cal^+PI^- cells (viable cells). Each quadrant shows data as a % of the total cell population. Single colour staining shows that 79.9% of wildtype beta cells were Calcein positive i.e., viable when analysed against an empty chanel (d). (e) Two colour staining shows that 33.5% beta cells were Cal^+PI^- (viable), 36.1% cells were Cal^+PI^+ (damaged) and 19.9% cells were Cal^-PI^+ (dead); red box shows calcein+ve cells (69.6%; $\%Cal^+Pi^- + \%Cal^+PI^+$)) and yellow box shows PI^+ cells (56.0%; $\%Cal^+PI^+ + \%Cal^-PI^+$), resembling the single colour controls in (d) and (f), respectively. (f) Single colour staining shows that 55.8% of beta cells were PI^+ when analysed against an empty chanel. Two colour staining using Calcein and PI therefore more sensitively identifies viable but undamaged cells (Cal^+PI^-). SSC-A, side scatter area; FSC-A, forward scatter area; SSC-W, side scatter width; SSC-H, side scatter height; FSC-H, forward scatter height and FSC-A, forward scatter area.

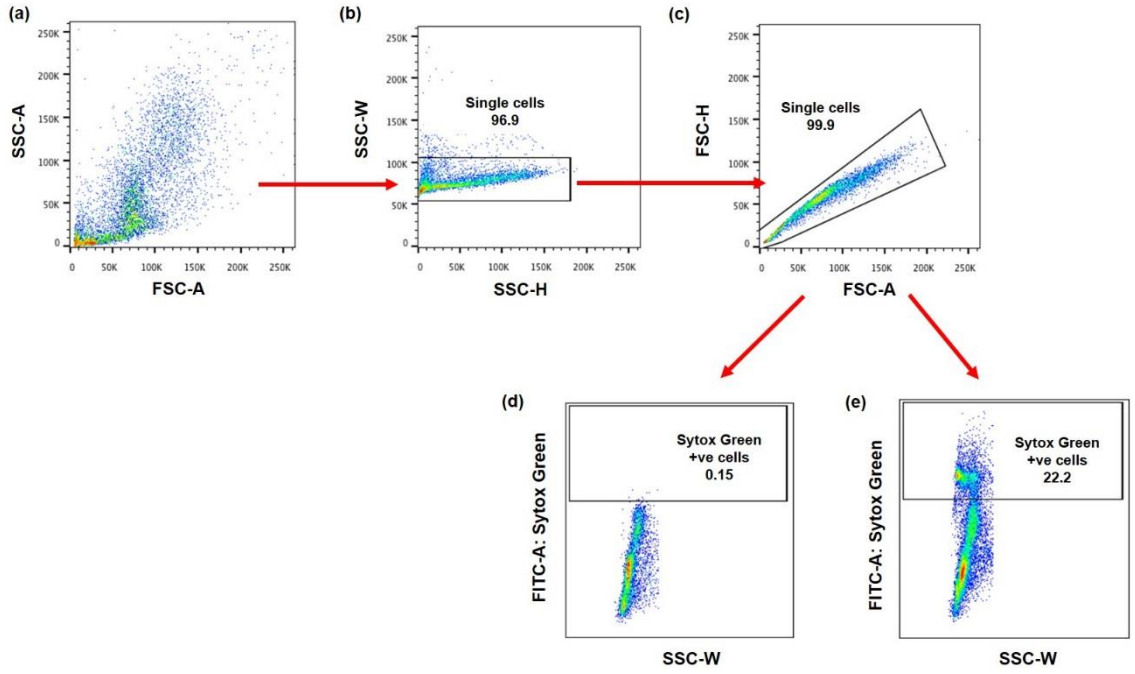

Figure 2.11: Gating strategy for determining Sytox Green positive beta cell death/damage.

(a) Representative total primary islet cells (90% beta cells) showing forward scatter (FSC) and side scatter (SSC) properties. (b) Single cells were gated based on SSC-W and SSC-H; (c) FSC-H and FSC-A were used to exclude doublets present in the population. (d) The dot plot shows Sytox Green staining on the y-axis and an empty channel for the x-axis. The black internal rectangle on the plot was generated based on exclusion of negatively stained cells in the unstained sample (d); 22.2% of treated beta cells are Sytox Green positive (+ve; (e)). SSC-A, side scatter area; FSC-A, forward scatter area; SSC-W, side scatter width; SSC-H, side scatter height; FSC-H, forward scatter height and FSC-A, forward scatter area.

2.9.4 FITC labelled HS-mimetics for HS replacement

To study the uptake of FITC-labelled heparin and FITC-labelled PI-88 in beta cells, islets were isolated from normoglycaemic db/db and wt male mice (see Section 2.3) and dispersed into a single cell suspension (see Section 2.3.2). Primary beta cells were transferred to a 96 well plate (#650180, CellStar, Greiner Bio-one, Kremsmünster, Austria), 4 x 10^4 cells/ well, and cultured with and without FITC-labelled heparin (50 µg/ml; Celsus Laboratories, Cincinnati, OH) or FITC-labelled PI-88 (50 µg/ml; Muparfostat; Progen Pharmaceuticals, Brisbane, Australia) for 2 days. Uptake of FITC-mimetic by the beta cells was analysed by confocal microscopy and with staining with 7AAD (10 µg/ml) was used to determine cell death/damage by flow cytometry.

2.9.4.1 Localisation of FITC labelled heparin and FITC labelled PI-88 by confocal microscopy

After 2 days of culture, the beta cells were spun down (110-173 x g) and washed with PBS x 2 times. PBS (10-20 µl/well) was added to the wells to resuspend the beta cells. The resuspended beta cells (10-20 µl) were then transferred to a 35 mm flat bottom dish with a 14 mm glass well (#D35-14, Cellvis, Mountain View, CA, USA) for imaging by confocal microscopy (Leica SP5 confocal microscope; 63x maginification).

2.9.4.2 Uptake of FITC-HS mimetic by flow cytometry

In parallel, the beta cells were cultured with and without 7AAD (10 µg/ml) for 15 mins (see Section 2.5.5.2). The cells were spun down at 110-173 x g, resuspended in PBS and transferred to FACs cluster tubes for flow cytometry analysis. The samples were run on a BD LSR Fortessa using the FL-3 channel. Events were collected using BD FACS Diva software (version 8). FlowJo software was used to determine the % $FITC^+7AAD^-$ (live) and $FITC^+7AAD^+$ (dead/damaged) cells from dot plots.

2.9.4.3 Analysis of flow cytometry data

The beta cells were separated on the basis of forward scatter (FSC) and side scatter (SSC) properties. The single cells were gated from the SSC-W and SSC-H properties; FSC-A and FSC-H was used to exclude doublets. Uptake of FITC heparin or FITC PI-88 was represented on the y-axis and 7AAD staining on the x-axis. The quadrants were set using unstained cells to identify negatively stained sub-population of cells (**Figure 2.12**).

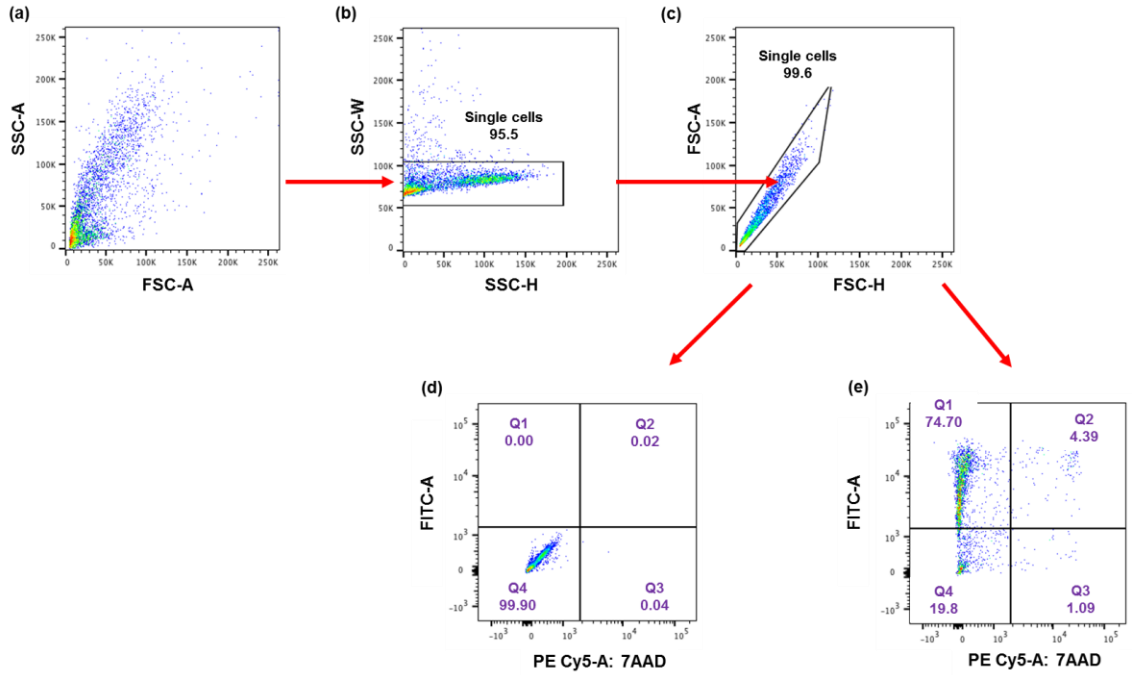

Figure 2.12: Gating strategy for the uptake of FITC-labelled HS mimetics.

(a) Representative total primary islet cells (90% beta cells) showing forward scatter (FSC) and side scatter (SSC) properties. (b) Single cells were gated based on SSC-W and SSC-H; (c) FSC-A and FSC-H were used to exclude doublets present in the population. (d) The dot plot shows FITC uptake on y-axis and 7AAD staining on x-axis. Quadrants (Q) were determined using unstained cells (d) to identify negatively stained cells. (e) 74.70% of beta cells were $FITC^{+}$ $7AAD^{-}$. SSC-A, side scatter area; FSC-A, forward scatter area; SSC-W, side scatter width; SSC-H, side scatter height; FSC-H, forward scatter height and FSC-A, forward scatter area.

2.10 Preparation of leukocyte populations from wt and db/db mice

The contribution of innate and adaptive immune cells to the white adipose tissue and peripheral blood of T2D-prone db/db and wt mice and the expression of cell surface heparanase was examined by flow cytometry.

2.10.1 Peripheral blood leukocytes

Peripheral blood (PB; 200 µl/sample) was harvested from the retro-orbital sinus of donor mice was directly into a tube containing 400 µl buffered saline glucose citrate (BSGC) buffer (see Appendix 1.16) collected by APF technical staff, JCSMR. The blood sample was left at room temperature for at least 1 hour. The sample was transferred to a 15 ml falcon tube and red blood cell lysis buffer (RCLB; see Appendix 1.16) was added to each tube (1.5 ml/tube). The samples were incubated at room temperature for 5 minutes and then centrifuged at 470 g for 5 minutes at 10°C (Heraeus Megafuge 1.0R, Kendro Laboratories, Hamburg, Germany). The supernatant was discarded, and the lysis step was repeated. The cells were then resuspended in 200 µl of FACs wash buffer for counting of live cells using trypan blue exclusion to determine the live cell density.

2.10.2 Adipose tissue isolation

Adipose tissue from male db/db and wt epididymal fat pads and female db/db and wt peri-ovarian fat pads were isolated, as previously described (Cho et al., 2014). The mouse was euthanised and the skin was disinfected with 70% ethanol. The abdominal cavity was opened to expose the abdominal organs and tissues. The peri-gonodal adipose depot was excised and the isolated fat pads were weighed using a digital balance (Mettler Toledo). The adipose tissue was then washed with PBS to remove contaminating blood and hair; and the tissue was placed in a plastic weigh tray/boat on ice.

For the isolation of stromal vascular fraction (SVF), the adipose tissue was minced using scissors in a weigh boat on ice. The tissue was then transferred to a 15 ml tube (Corning Science Mexico, Reynosa, Tamaulipas, Mexico; <1 gm) with 7 ml of cold digestion buffer containing collagenase II (1 mg/ml; see Appendix 1.16). Alternatively, for quantities of adipose tissue >1 gm, the tissue was transferred to a 50 ml falcon tube containing 10 ml cold digestion buffer/collagenase and the concentration was adjusted to

10 mg/ml (see appendix 1.16). The tubes were incubated at 37°C for 20-45 mins with vigorous agitation on a shaking platform (300-400 rpm). EDTA (0.5 M; see Appendix 1.16) was then added to the tube to achieve a final concentration of 10 mM (150-300 µl/tube) and the suspension was incubated at 37°C for 5-10 mins to terminate the digestion step and facilitate full dissociation of the SVFs. The cell slurry was transferred to a 100 µm filter (#352360, Falcon, Corning Inc., One Riverfront plaza, NY, USA) over a 50 ml Falcon tube and the filter was washed twice with FACs wash buffer (10 ml/tube/wash). The filtrate containing the SVF cells was centrifuged at 500 x g for 10 mins at 4°C to separate the adipocytes and SVFs. The pellet containing leukocytes and other SVF cells was resuspended in 0.5 ml RBC lysis buffer for 5 mins at room temperature to remove red blood cells. The FACs wash buffer (5 ml/tube) was added to terminate the lysis step and the cells were centrifuged at 500 x g for 10 mins at 4°C. The cell pellet was resuspended in 3-5 ml FACs wash buffer before determining the concentration of live cells using trypan blue exclusion.

2.10.3 Lymph node cells

Lymph nodes (LNs) from wt (+/+) mice were harvested into ~5 ml of FACs wash buffer (see Appendix 1.16) and mashed using a 3 ml syringe plunger (Terumo Co., Binan, Laguna, Philippines) over a 70 µm cell strainer (#352350, Falcon, Corning Inc., One Riverfront Plaza, NY, USA) to prepare a single cell suspension. Red cell lysis buffer (RCLB) (3 ml/tube; see Appendix 1.16) was added to the sample and incubated at room temperature for 5 minutes. The cells were then centrifuged at 389 x g for 5 minutes (Heraeus Megafuge 1.0R, Kendro Laboratories, Hamburg, Germany). The supernatant was discarded, and the cells were resuspended in 2 ml of FACs wash buffer for counting using a haemocytometer (American Optical Co., Buffalo, NY, USA; see Section 2.4.3).

2.10.4 Flow cytometry analysis of leukocyte populations

2.10.4.1 Cell surface staining

(a) Heparanase

Cells were transferred to a 96-well plate (CellStar, U-bottom plate, # 650180; 1 x 10^5-10^6 cells) and washed with FACs wash (200 µl/well) by centrifugation at 389 x g for 3 mins at 4°C. The supernatant was removed, and the cells were incubated with diluted primary human heparanase antibody HP3/17(1.5 µg/ml; see Appendix 1.17). A sample

of lymph node cells (1 x 10^6 cells/well) was also stained with HP3/17 mAb as a single colour control; FACs wash buffer was added (25 µl/well) to control unstained wells. The plate was incubated on ice for 30 mins. The cells were then washed with FACs wash buffer (200 µl/well) and centrifuged at 389 x g for 3 mins at 4°C. The supernatant was removed, and the cells were incubated with secondary antibody goat anti-mouse Ig PE (2.5 µg/ml; 25 µl/well) for 30 mins on ice in the dark. The cells were centrifuged at 389 x g for 3 mins, washed with FACs wash buffer and vortexed briefly for subsequent staining with leukocyte-specific antibodies (see Appendix 1.17).

(b) Leukocyte markers

To distinguish between sub-populations of leukocytes in the PB and SVFs, the cells were stained with a cocktail of 8 antibodies specific for a range of different leukocyte markers: CD11c, B220, Ly6G, Siglec F, CD45.2, CD11b, CD3, and Ly6C (see Appendix 1.17 for list of fluorochrome-conjugated mAbs). LN cells stained with each individual-conjugated antibody were used for compensation of the spectral overlap between different fluorochromes. The fluorescence was detected using a BD LSR II Fortessa flow cytometer with PE Texas Red, PE Cy5.5, PE Cy7, Alexa Fluor 405, APC, Alexa Fluor 700, APC-Cy7 and Qdot 605 channels. The different leukocyte sub-populations were distinguished based on the cell surface markers are shown in **Table 2.1**. Events were collected using BD FACS Diva software (version 8). Gating for analysis of heparanase expression on T cells, B cells, dendritic cells, macrophages, neutrophils and eosinophils (see Section 2.10.4.2).

2.10.4.2 Analysis of flow cytometry data

Live cells were distinguished from dead cells based on the forward scatter (FSC) and side scatter (SSC) properties. Single cells were identified using FSC-A and FSC-H and doublets were excluded based on the SSC-W and SSC-H properties. Leukocyte sub-populations were determined based on cell surface markers using the gating strategy in **Figures 2.13** and **2.14**. The geometric mean fluorescence intensity (GMFI) and geometric mean fluorescence ratio (GMFR; normalised to the Hpse expression of B lymphocytes) of cell surface Hpse (PE) staining on different leukocyte sub-populations was determined using FlowJo software (version 10.0.7, TreeStar Inc., Ashland, OR, USA).

Figure 2.13: Gating strategy for analysing leukocyte sub-populations in peripheral blood of wt mice.

Representative dot plots for peripheral blood show (a) gating of the leukocyte population using forward scatter (FSC) and side scatter (SSC) properties. (b) Single cells were gated based on FSC-A and FSC-H; (c) SSC-W versus SSC-H was used to exclude doublets. (d) The $CD45.2^{+}$ population was identified and subsequently gated for $CD11c^{+}$ and $CD11c^{-}$ expression (e). (f) From the $CD11c^{+}$ cells, conventional dendritic cells (cDCs) were gated using $Ly6C^{-}Ly6G^{-}$ staining; $CD11c^{+}Ly6C^{+}$ and $CD11c^{+}Ly6G^{+}$ leukocytes were also identified. (g) The $CD11c^{-}$ population was further divided into myeloid ($CD11b^{+}$) leukocytes and lymphocytes ($CD11b^{-}$). (h) The myeloid population was sub-divided into $Ly6C^{med\text{-}high}Ly6G^{+}$ neutrophils, $Ly6C^{high}Ly6G^{-}$ monocytes and $Ly6G^{-}Ly6C^{-}$ cells. (i) Based on Siglec F fluorescence, the $Ly6G^{-}Ly6C^{-}$ cells were divided into Siglec F^{+} eosinophils and Siglec F^{-} resident macrophages. (j) Hpse expression on leukocytes (e.g., myeloid cells) was shown using histograms of fluorescence staining (blue) versus auto-fluorescence of unstained cells (red). (k) Lymphocytes were identified as $B220^{+}$ B cells and $CD3^{+}$ T cells. FSC-A, forward scatter area; FSC-H, forward scatter height; SSC-W, side scatter width and SSC-H, side scatter height.

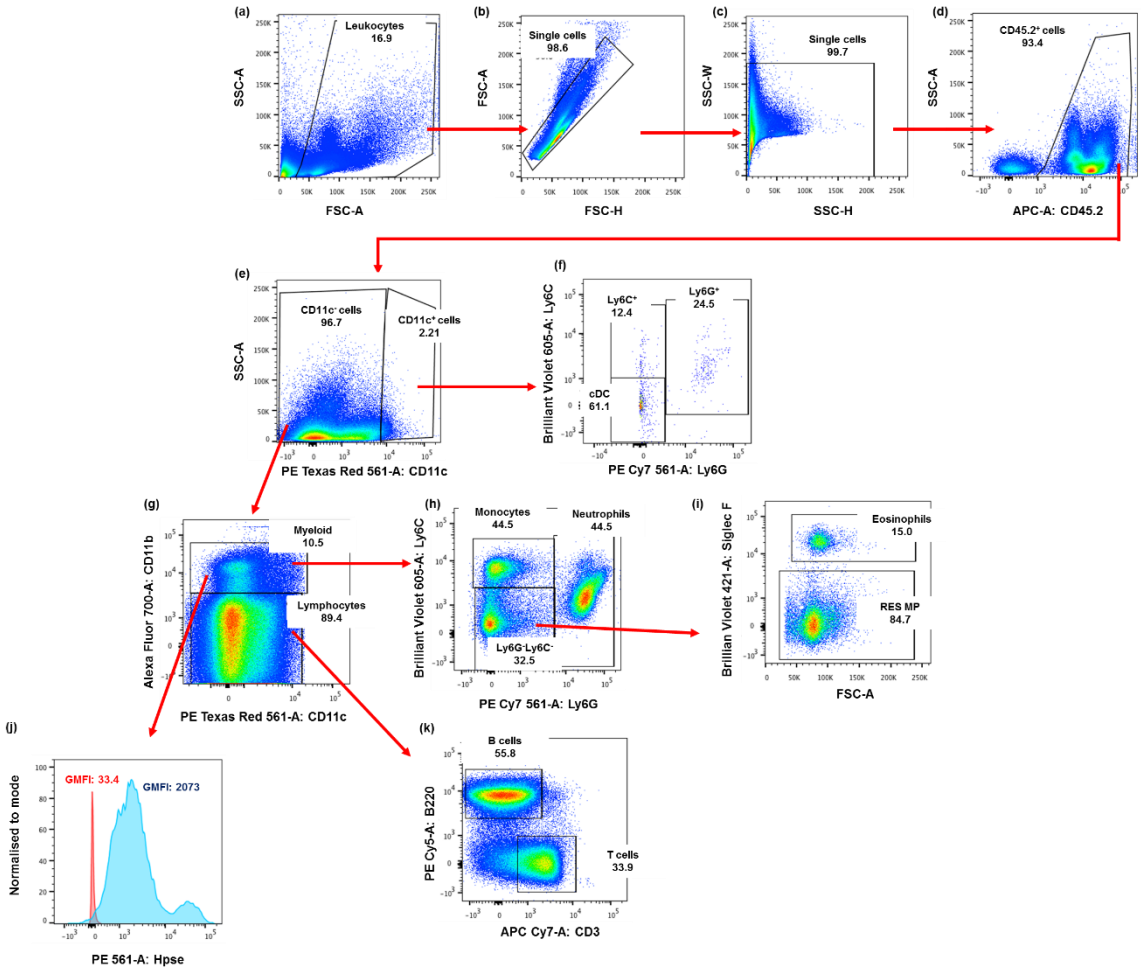
(a)
Leukocytes
16.9
SSC-A
FSC-A
(b)
Single cells
98.6
FSC-A
FSC-H
(c)
Single cells
99.7
SSC-W
SSC-H
(d)
CD45.2⁺ cells
93.4
SSC-A
APC-A: CD45.2
(e)
CD11c⁻ cells
96.7
CD11c⁺ cells
2.21
SSC-A
PE Texas Red 561-A: CD11c
(f)
Ly6C⁺
12.4
Ly6G⁺
24.5
cDC
61.1
Brilliant Violet 605-A: Ly6C
PE Cy7 561-A: Ly6G
(g)
Myeloid
10.5
Lymphocytes
89.4
Alexa Fluor 700-A: CD11b
PE Texas Red 561-A: CD11c
(h)
Monocytes
44.5
Neutrophils
44.5
Ly6G⁻Ly6C⁻
32.5
Brilliant Violet 605-A: Ly6C
PE Cy7 561-A: Ly6G
(i)
Eosinophils
15.0
RES MP
84.7
Brillian Violet 421-A: Siglec F
FSC-A
(j)
GMFI: 33.4
GMFI: 2073
Normalised to mode
PE 561-A: Hpse
(k)
B cells
55.8
T cells
33.9
PE Cy5-A: B220
APC Cy7-A: CD3

Figure 2.14: Gating strategy for analysing leukocyte sub-populations in the stromal vascular fraction of wt mice.

Epididymal adipose tissue dot plots show (a) gating of the leukocyte population using forward scatter (FSC) and side scatter (SSC) properties. (b) Single cells were gated based on FSC-A and FSC-H; (c) SSC-W versus SSC-H was used to exclude doublets. (d) The $CD45.2^+$ population was identified and subsequently gated for $CD11c^+$ and $CD11c^-$ expression (e). (f) From the $CD11c^+$ cells, conventional dendritic cells (cDCs) were gated using $Ly6C^-Ly6G^-$ staining; $CD11c^+Ly6C^+$ and $CD11c^+Ly6G^+$ leukocytes were also identified. (g) The $CD11c^-$ population was further divided into myeloid ($CD11b^+$) leukocytes and lymphocytes ($CD11b^-$). (h) The myeloid population was sub-divided into $Ly6C^{med\text{-}high}Ly6G^+$ neutrophils, $Ly6C^{high}Ly6G^-$ inflammatory macrophages (INF MP) and $Ly6G^-Ly6C^-$ cells. (i) Based on Siglec F fluorescence, the $Ly6G^-Ly6C^-$ cells were divided into Siglec F^+ eosinophils and Siglec F^- resident macrophages. (i) Hpse staining on leukocytes (e.g., myeloid cells) was demonstrated using histograms of fluorescence staining (blue) versus auto-fluorescence of unstained cells (red). (k) Lymphocytes were identified as $B220^+$ B cells and $CD3^+$ T cells. FSC-A, forward scatter area; FSC-H, forward scatter height; SSC-W, side scatter width and SSC-H, side scatter height.

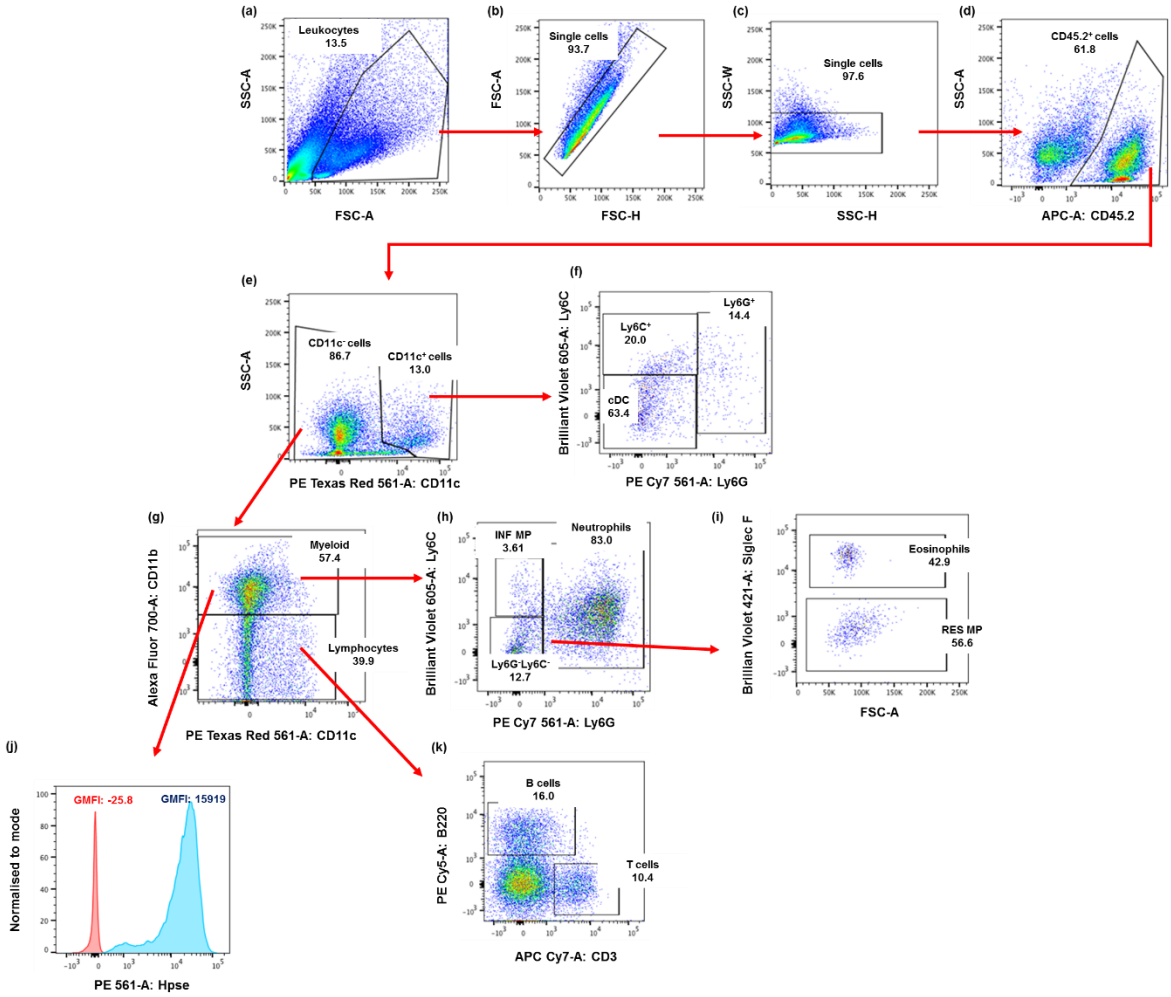
(a)
Leukocytes
13.5
SSC-A
FSC-A
(b)
Single cells
93.7
FSC-A
FSC-H
(c)
Single cells
97.6
SSC-W
SSC-H
(d)
CD45.2+ cells
61.8
SSC-A
APC-A: CD45.2
(e)
CD11c- cells
86.7
CD11c+ cells
13.0
SSC-A
PE Texas Red 561-A: CD11c
(f)
Ly6G+
14.4
Ly6C+
20.0
cDC
63.4
Brilliant Violet 605-A: Ly6C
PE Cy7 561-A: Ly6G
(g)
Myeloid
57.4
Lymphocytes
39.9
Alexa Fluor 700-A: CD11b
PE Texas Red 561-A: CD11c
(h)
INF MP
3.61
Neutrophils
83.0
Ly6G-Ly6C-
12.7
Brilliant Violet 605-A: Ly6C
PE Cy7 561-A: Ly6G
(i)
Eosinophils
42.9
RES MP
56.6
Brilliant Violet 421-A: Siglec F
FSC-A
(j)
GMFI: -25.8
GMFI: 15919
Normalised to mode
PE 561-A: Hpse
(k)
B cells
16.0
T cells
10.4
PE Cy5-A: B220
APC Cy7-A: CD3

Table 2.1: Phenotype markers for different leukocyte sub-populations.

Cell type	Cell surface marker
Leukocytes	$CD45.2^{+}$
Conventional dendritic cells (cDCs)	$CD45.2^{+}$ $CD11c^{+}$ $Ly6G^{-}$ $Ly6C^{-}$
T cells	$CD45.2^{+}$ $CD11c^{-}$ $CD11b^{-}$ $CD3^{+}$
B cells	$CD45.2^{+}$ $CD11c^{-}$ $CD11b^{-}$ $B220^{+}$
Myeloid cells	$CD45.2^{+}$ $CD11c^{-}$ $CD11b^{+}$
Neutrophils	$CD45.2^{+}$ $CD11c^{-}$ $CD11b^{+}$ $Ly6G^{+}$ $Ly6C^{med\text{-}high}$
Eosinophils	$CD45.2^{+}$ $CD11c^{-}$ $CD11b^{+}$ $Ly6G^{-}$ $Ly6C^{neg\text{-}med}$ Siglec F^{+}
Inflammatory macrophages	$CD45.2^{+}$ $CD11c^{-}$ $CD11b^{+}$ $Ly6G^{-}$ $Ly6C^{high}$
Resident macrophages	$CD45.2^{+}$ $CD11c^{-}$ $CD11b^{+}$ $Ly6G^{-}$ $Ly6C^{neg\text{-}med}$ Siglec F^{-}
Non-cDC $CD11c^{+}$ leukocytes:	$CD11c^{+}Ly6C^{+}Ly6G^{+}$
	$CD11c^{+}Ly6C^{+}Ly6G^{-}$

2.11 *In vivo* treatment of db/db mice

2.11.1 PI-88

PI-88 (phosphomannopentaose sulfate) acts as a HS replacer in beta cells (Ziolkowski et al., 2012). Previous studies in our lab showed that PI-88 (i) prevents culture-induced and ROS-induced beta cell death in mouse and human beta cells (Ziolkowski et al., 2012, Simeonovic et al., 2018) and (ii) protected ~50% of NOD mice from developing T1D (Ziolkowski et al., 2012). Male and female db/db mice were treated with PI-88 (a HS replacer/Hpse inhibitor), 10 mg/kg/day i.p. or saline (diluent control) i.p. from 3.5 weeks of age for 35 days (see Appendix 1.18).

The mice were weighed 3x/week and non-fasting blood glucose were measured 3x/week. After 35 days of treatment, HbA1c levels of mice were measured using a HemoCue Analyzer (see Section 2.2.3). The treated mice were tested for either ipGTT (see Section 2.2.2) or inflammation studies (see Section 2.10) and the pancreas tissue was collected for immunohistochemistry analysis (see Section 2.7). Additionally, plasma was separated from a 10 µl blood sample obtained from the tail vein. The blood was collected into a tube containing 2 µl of citrate buffer (see Appendix 1.1) and centrifuged at 2000-3000 x g for 15 mins. The plasma was subsequently tested for the level of free fatty acids in the circulation (see Section 2.2.5).

2.11.2 TUDCA

Tauroursodeoxycholic acid (TUDCA) is a chemical chaperone which assists in protein folding, reduces ER stress and has antioxidant and anti-apoptotic activities. TUDCA has been used *in vivo* to prevent ER stress in db/db and ob/ob mice (Özcan et al., 2006, Zhang et al., 2016). Male and female db/db mice from 4 weeks of age were treated with TUDCA, 150 mg/kg/day i.p. or saline (diluent control) i.p. for 28 days (see Appendix 1.18). The non-fasting blood glucose levels and body weight were measured 3x/week; variations in weight were used to adjust the volume of TUDCA for dosing. The HbA1c levels were measured after 28 days of treatment (see Section 2.2.3) and pancreas tissue was collected in 10% neutral-buffered formalin for histology and immunohistochemistry (see Section 2.7). For some mice, the islets were isolated from the pancreases (see Section 2.3) of TUDCA or saline treated db/db mice at 28 days and frozen in liquid nitrogen for

subsequent RNA extraction (see Section 2.6) and examination of ER stress associated genes by PCR (see Sections 2.6.4 and 2.6.5).

2.12 Statistical analyses

Statistical analysis was performed using InStat (version 3.10) and GenStat (version 18) software. A parametric statistical test was performed when the Gaussian distribution normality test was satisfied; otherwise, a non-parametric test was used. One-way ANOVA with Fischer's unprotected least significant difference (LSD), Mann-Whitney test or unpaired t-test were used for metabolic studies of treated or untreated db mice and for morphometric analyses of db and Akita mouse pancreas sections. Mann-Whitney test was also used for gene expression analysis of isolated islets. One-way ANOVA with unprotected LSD test was used for gene expression studies in MIN6 cells. Mann-Whitney, One-way ANOVA with unprotected LSD test or Two-way ANOVA with unprotected LSD test were used for flow cytometry studies of MIN6 cells, primary beta cells, peripheral blood and adipose tissue.

Chapter 3: Characterisation of islet HSPGs and HS in T2D-prone db/db mice

3.1 Introduction

Heparan sulfate proteoglycans (HSPGs) consist of a core protein with covalently attached heparan sulfate (HS) chains. HSPGs are ubiquitously expressed on the cell surface, in basement membranes (BMs) and extracellular matrix (ECM) and are distinguished by their core proteins. The five main classes of HSPG core proteins include the syndecans, glypicans as well as perlecan, agrin and collagen type XVIII (Iozzo, 2001, Parish, 2006). Both syndecans and glypicans are expressed on the cell surface but glypicans are anchored in the cell membrane via glycosylphosphatidylinositol (GPI) linkage. Perlecan, agrin and collagen type XVIII HSPGs are present in the ECM and BMs. Additionally, there are some HSPGs such as CD44, betaglycan and testican, that express HS chains under special circumstances and are therefore called part-time HSPGs (Rops et al., 2004). Whereas the core proteins of HSPGs are synthesised in the ER, the assembly of HS chains onto the core proteins occurs in the Golgi apparatus (Kreuger and Kjellen, 2012, Esko and Selleck, 2002, Leonova and Galzitskaya, 2013). HS chains are linear polysaccharides containing repeating units of glucosamine and uronic acid (Bernfield et al., 1999). During HS synthesis, the sugar residues undergo chemical modification, resulting in regions that are highly sulfated and under-sulfated. These chemical modifications impart both structural and functional heterogeneity to the HS chains.

The heterogeneity within HS chains allows them to interact with a wide range of bioactive molecules such as chemokines, cytokines, growth factors, lipases, proteases and cell-adhesion molecules (Dreyfuss et al., 2009). Furthermore, HS chains play an important role in BMs by providing stability and acting as a barrier against cell invasion. In ECM, HS can fill the intercellular space and act as a molecular sieve (Parish, 2006). HS also plays a crucial role in cell development, proliferation and differentiation as well as angiogenesis and wound healing (Vreys and David, 2007).

Recently, HS has been identified as an important regulator in post-natal islet growth; failure to synthesise HS in the beta cells of exostosin-like 3 (EXTL3) knockout mice resulted in impaired glucose-stimulated insulin secretion (Takahashi et al., 2009). Furthermore, previous studies in the Simeonovic lab showed that the high levels of HS normally expressed inside the beta cells were essential for cell survival (Ziolkowski et al., 2012). The intracellular localisation of HS is highly unusual because HS is normally

found on the surface of cells, in BMs and in ECM. During islet isolation and the subsequent culture of isolated beta cells *in vitro*, intracellular HS was found to decline and cell death increased. Moreover, this death of the beta cells could be prevented by replacing the lost HS using HS mimetics (Ziolkowski et al., 2012). Three HSPG core proteins i.e. collagen type XVIII, syndecan-1 and CD44 were shown to be expressed intracellularly in beta cells. Unlike intracellular HS, however, the HSPG core proteins were not lost during islet isolation (Choong et al., 2015). Furthermore, studies in non-obese diabetes (NOD) mice revealed that HS in the peri-islet BM and within beta cells was degraded by heparanase (Hpse), resulting in beta cell death and ultimately, type 1 diabetes (T1D) (Ziolkowski et al., 2012). A critical role for HS was therefore demonstrated in beta cell survival and the development of T1D. In this project we investigated whether beta cell HS and HSPG core proteins contribute to the progression of type 2 diabetes (T2D).

Endoplasmic reticulum (ER) stress plays an important role in the pathogenesis of T2D by causing beta cell dysfunction and death (Laybutt et al., 2007). The accumulation of misfolded proinsulin/insulin (the major protein produced by beta cells) in the ER in response to insulin resistance, leads to ER stress. Beta cell proteins, including HSPG core proteins, undergo maturation and refolding in the ER. The mature HSPG core proteins are then transported to the Golgi apparatus; at this sub-cellular site, HS chains are assembled via a complex process onto the core proteins (see Section 1.13). The activation of ER stress induces a signalling cascade i.e., the unfolded protein response (UPR) which helps to alleviate ER stress by upregulating the expression of genes that aid protein folding. However, when ER stress is prolonged pro-apoptotic pathways become activated (Yoshida, 2007). ER stress in beta cells could therefore potentially play a role in reducing the intracellular levels of HSPG core proteins, and indirectly, HS during the progression of T2D. For these studies, we used T2D-prone db/db mice which express a mutation in the leptin receptor, leading to over-eating, obesity and insulin resistance. As a result, blood glucose levels become elevated and the beta cells demonstrate reduced function and ultimately failure/death.

In this chapter, we examined the expression of HS and HSPG core proteins in the islets *in situ* in the pancreas of db/db mice during the development of T2D. The first section of

this chapter characterises T2D development in db/db mice from the JCSMR breeding colony, including glucose intolerance and insulin resistance. The next part investigates the expression of ER stress genes in islets isolated from db/db mice and wildtype controls by TaqMan real-time reverse transcriptase polymerase chain reaction (RT-PCR). Finally, immunohistochemistry is used to monitor intra-islet levels of the HSPG core proteins (collagen type XVIII, syndecan-1 and CD44) and HS during T2D development.

3.2 Results

3.2.1 Development of obesity and hyperglycaemia in male db/db mice

The body weight of male wildtype (wt), heterozygous (db/+) and homozygous db/db mice was measured at 3, 4, 5, 6, 9, 12, 16 and 20 weeks of age during the development of T2D to determine the age at which db/db mice become obese (see Section 2.2.1). In parallel, non-fasting blood glucose levels were monitored to ascertain the age at which db/db mice showed onset of hyperglycaemia.

The body weight of male wt and db/+ mice ranged from 7.85 ± 1.11 grams to 26.00 ± 0.86 grams and from 7.14 ± 0.49 grams to 30.00 ± 0.63 grams, respectively, from 3 to 20 weeks of age (**Figure 3.1(a)**). Homozygous mutant db/db mice weighed 7.72 ± 0.63 grams and 34.90 ± 3.12 grams at 3 and 20 weeks of age, respectively. The gain in body weight of male db/db mice resembled wt and db/+ mice at 3, 4 and 5 weeks of age (**Figure 3.1(a)**). The body weight of male db/db mice at 6 weeks of age was 26.00 ± 0.61 grams, 1.5-fold higher than wt mice at 17.30 ± 1.22 grams (**Figure 3.1(a)**). There was a significant 1.7-fold (weight=32.67 ± 2.18 grams), 1.6-fold (weight=34.90 ± 1.83 grams), 1.5-fold (weight=35.17 ± 1.95 grams) and 1.7-fold (weight=34.90 ± 3.12 grams) increase in the mean body weight of male db/db mice, when compared to male wt controls at 9 (weight=18.80 ± 1.63 grams), 12 (weight=21.60 ± 0.93 grams), 16 (weight=23.70 ± 0.80 grams) and 20 (weight=26.00 ± 0.86 grams) weeks of age, respectively (**Figure 3.1(a)**). Generally, the weight of wt and heterozygous db/+ mice did not differ significantly at 3-20 weeks of age, except for a 1.2-fold significant increase in the body weight of heterozygous db/+ mice at 6 weeks of age (**Figure 3.1(a)**; $P<0.01$). Male db/db mice therefore became overtly obese by 6 weeks of age, compared to lean control wt mice.

The groups of male wt, db/+ and db/db mice exhibited normal non-fasting blood glucose levels at 3, 4 and 5 weeks of age (**Figure 3.1(b)**). However by 6 weeks of age, the mean non-fasting blood glucose levels of db/db mice was significantly increased 2.5-fold to 19.63 ± 2.54 mmol/L, compared to wt mice at the same age (7.76 ± 0.69 mmol/L). The blood glucose levels were further augmented in db/db mice to 21.07 ± 2.36 mmol/L (versus wt, 7.32 ± 0.79 mmol/L), 24.28 ± 2.69 mmol/L (versus wt, 8.54 ± 0.66 mmol/L) and 24.98 ± 1.11 mmol/L (versus wt, 7.50 ± 0.36 mmol/L) at 9, 12 and 16 weeks of age, respectively. Furthermore, by 20 weeks of age, there was a 3.9-fold significant increase

(a)

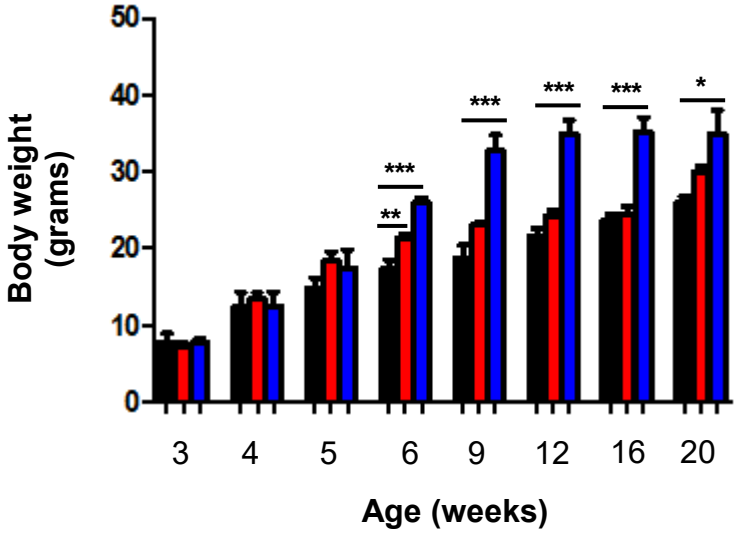

(b)

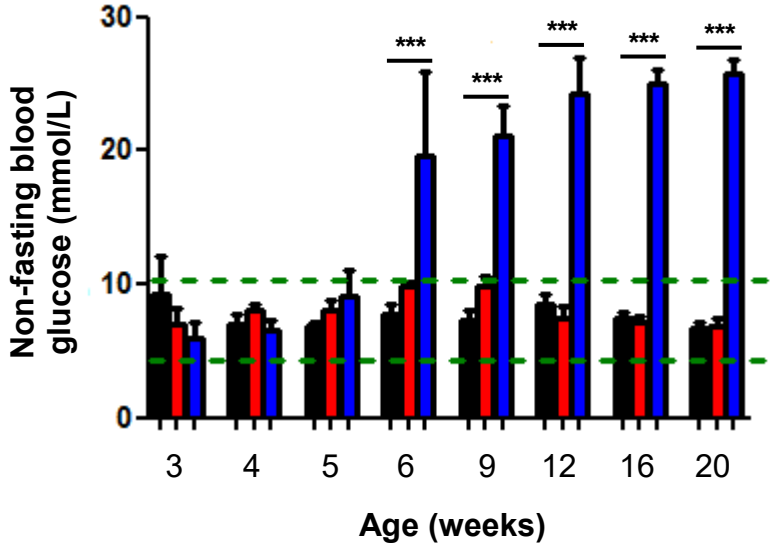

Figure 3.1: The mean body weight and non-fasting blood glucose of male wt, heterozygous db/+ and db/db mice at 3-20 weeks of age.

The body weight (a) and non-fasting blood glucose levels (b) of male wildtype (wt), heterozygous (db/+) and db/db mice were measured at 3-20 weeks of age during the development of T2D. In general, the body weight and blood glucose levels of wt, db/+ and db/db male mice were similar from 3-5 weeks of age. Obesity and hyperglycaemia in db/db mice were evident by 6 weeks. The green dotted lines define the normal blood glucose range for wt males i.e., 4.27 mmol/L to 10.83 mmol/L (see Section 2.2.1). The data represent mean ± SEM for n= 4-8 mice/group. One-way ANOVA with Fisher's unprotected LSD test; *P<0.01, **P<0.001 and ***P<0.0001.

in the non-fasting blood glucose of male db/db mice (25.72 ± 1.01 mmol/L) compared to wt controls (mean blood glucose= 6.64 ± 0.47 mmol/L). Hence, male db/db mice became hyperglycaemic by 6 weeks of age and remained overtly diabetic for up to 20 weeks of age.

Together, these data demonstrated that male db/db mice were both obese and hyperglycaemic by 6 weeks of age, marking the clinical onset of T2D.

3.2.2 Male db/db mice exhibit impaired glucose tolerance and are insulin-resistant

Male db/db mice (5-9 weeks old) were categorised into three groups based on their non-fasting blood glucose (Bg), i.e., db/db mice with Bg<10 mmol/L (normoglycaemic), db/db mice with Bg=10-15 mmol/L (mildly hyperglycaemic) and db/db mice with Bg>15 mmol/L (severely hyperglycaemic). The male db/db mice were routinely bled in the morning prior to fasting for a glucose tolerance test (GTT; on the same day) to identify their group allocation (see Sections 2.2.1 and 2.2.2).

An intraperitoneal (i.p.) GTT was performed after fasting db/db and wt mice for 6 hrs. A small droplet of blood was collected from the tail vein for blood glucose measurement at time 0 immediately before an i.p. injection of 2 g/kg glucose; subsequent blood samples were tested at 15, 30, 60, 90 and 120 minutes after challenge. The area under curve (AUC) was calculated from 0 to 120 mins. This test was performed to ascertain the capacity of db/db mice to regulate their blood glucose levels. Blood was also collected at 0, 60 and 120 mins for determining circulating plasma insulin levels using an enzyme-linked immunosorbent assay (ELISA) assay (see Section 2.2.4).

The fasting blood glucose levels at 0 mins were similar for male wt mice, normoglycaemic db/db males (Bg<10 mmol/L) and mildly hyperglycaemic db/db mice (Bg=10-15 mmol/L), i.e., 8.88-9.52 mmol/L (**Figure 3.2(a)**, **Table 3.1**). In contrast, severely hyperglycaemic db/db mice (Bg>15 mmol/L) showed significantly increased fasting blood glucose levels (Bg=16.52 ± 1.57 mmol/L) compared to wt mice (Bg=8.93 ± 0.59 mmol/L; **Figure 3.2**, **Table 3.1**). The blood glucose of wt mice was rapidly increased to 15.97 ± 1.25 mmol/L at 15 mins after glucose injection followed by a gradual

Figure 3.2: Glucose tolerance test in male wt and db/db mice.

Male wt and db/db mice were fasted for 6 hrs prior to an i.p. glucose tolerance test (ipGTT). Based on the non-fasting blood glucose levels on the test day, the db/db mice were divided into three groups i.e., Bg<10 mmol/L, Bg=10-15 mmol/L and Bg>15 mmol/L. The blood glucose levels at 0, 15, 30, 60, 90 and 120 mins were measured (a) and the area under curve was calculated (b). Blood was also collected for measurement of plasma insulin levels (c, d). (a) Whereas wt mice showed an initial rise in blood glucose levels and a subsequent decline to pre-challenge levels, the blood glucose levels of db/db mice continued to rise and remained in the hyperglycaemic range. (b) The AUC corresponding to the blood glucose profiles in (a) show a significant increase for db/db males, compared to wt mice. (c) db/db males showed higher plasma insulin levels compared wt controls i.e., db/db females were hyperinsulinaemic, prior to glucose administration. (d) AUC bar graphs, corresponding to the plasma insulin graphs in (c) illustrate that severely hyperglycaemic db/db mice were significantly hyperinsulinaemic, relative to wt males. The data represent the mean ± SEM with n= 5-10 mice/group for ipGTT and n=4-5 mice/group for plasma insulin analysis. One-way ANOVA with Fisher's unprotected LSD test; *P<0.01, **P<0.001 and ns, not significant.

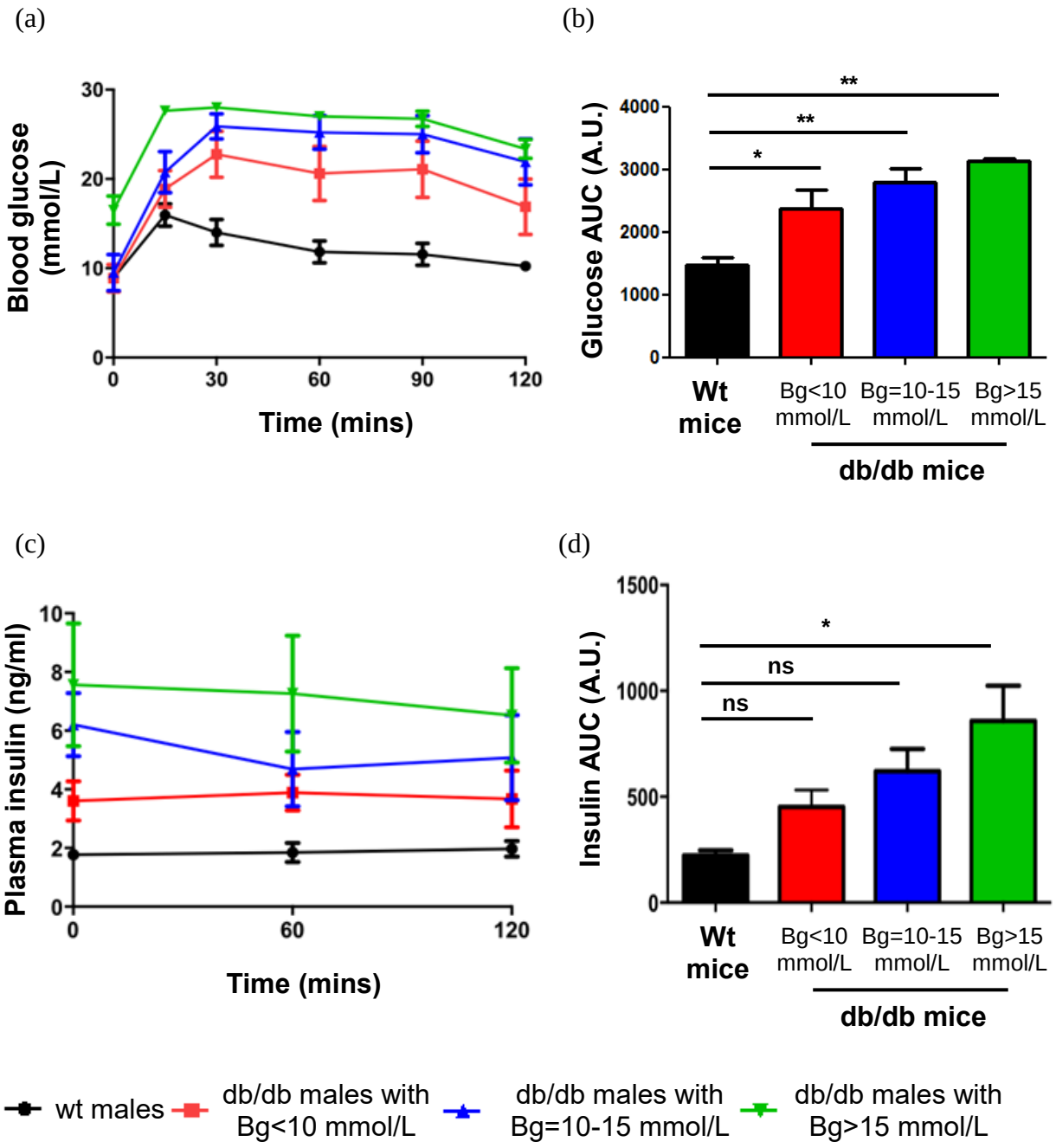
(a)
(b)
Blood glucose (mmol/L)
Time (mins)
Glucose AUC (A.U.)
Wt mice
Bg<10 mmol/L
Bg=10-15 mmol/L
Bg>15 mmol/L
db/db mice
(c)
(d)
Plasma insulin (ng/ml)
Time (mins)
Insulin AUC (A.U.)
ns
wt males
db/db males with Bg<10 mmol/L
db/db males with Bg=10-15 mmol/L
db/db males with Bg>15 mmol/L

Table 3.1: Blood glucose levels of male wt and db/db mice during ipGTT.

Time (mins)	Blood glucose (mmol/L)¶			
	Wt	db/db		
		Bg<10 mmol/L	Bg=10-15 mmol/L	Bg>15 mmol/L
0	8.93 ± 0.59	8.88 ± 1.53	9.52 ± 2.03	16.52 ± 1.57**
15	15.97 ± 1.25	18.88 ± 2.06	20.76 ± 2.30	27.65 ± 0.33***
30	14.02 ± 1.46	22.75 ± 2.58**	25.90 ± 1.41***	28.00 ± 0.00***
60	11.83 ± 1.24	20.62 ± 3.04**	25.22 ± 1.84***	27.02 ± 0.52***
90	11.55 ± 1.23	21.08 ± 3.14**	25.00 ± 2.09***	26.73 ± 0.86***
120	10.23 ± 0.52	16.90 ± 3.12#	21.92 ± 2.58**	23.35 ± 1.06***##

¶The data represent mean ± SEM. n= 5-10 male mice/group. One-way ANOVA with Fisher's unprotected LSD test; *P<0.05 and **P<0.01, ***P<0.001 represent comparisons between wt and db/db mice groups; #P<0.05, and ##P<0.01 indicates comparison between time 0 and 120 mins within groups, Unpaired t test.

decline to normal blood glucose levels by 120 mins (**Figure 3.2(a)**). Similarly, normoglycaemic and mildly hyperglycaemic db/db mice showed a rapid increase in blood glucose levels to 18.88 ± 2.06 mmol/L - 20.76 ± 2.30 mmol/L at 15 mins. Moreover, the severely hyperglycaemic db/db mice displayed significantly higher blood glucose levels (27.65 ± 0.33 mmol/L) at 15 mins compared to the wt mice ($P<0.001$). For db/db mice, the fasting blood glucose remained elevated during the ipGTT. At 120 mins, the mean blood glucose levels were 16.90 ± 3.12 mmol/L, 21.92 ± 2.58 mmol/L, and 23.35 ± 1.06 mmol/L for the db/db groups with Bg<10 mmol/L, Bg=10-15 mmol/L and Bg>15 mmol/L, respectively, and were severely elevated compared to wt mice (Bg= 10.23 ± 0.52 mmol/L; **Figure 3.2(a)**).

In summary, wt mice showed robust clearance of blood glucose as indicated by low AUC 1477.17 ± 125.29 A.U. (**Figure 3.2(b)**). There was a significant 1.6-fold (AUC=2366.50 ± 313.39 A.U.), 1.9-fold (AUC=2801.00 ± 203.24 A.U.) and 2.1-fold (AUC=3131.50 ± 49.21 A.U.) increase in the AUC for db/db mice with Bg<10 mmol/L, Bg=10-15 mmol/L and Bg>15 mmol/L, respectively, compared to wt mice (**Figure 3.2(b)**). These findings confirmed that db/db mice exhibited impaired glucose tolerance, even when normoglycaemic in the non-fasting state.

Plasma insulin levels in db/db mice belonging to the normoglycaemic (Bg<10 mmol/L) group were 2-fold higher than wt mice at 0 mins. Although this increase did not achieve statistical significance, this trend strongly suggested that normoglycaemic male db/db mice were hyperinsulinaemic (**Figure 3.2(c)**, **Table 3.2**). Plasma insulin levels remained 1.9-2.1-fold higher than corresponding wt controls in normoglycaemic db/db mice at 60 and 120 mins. Similarly, plasma insulin levels for mildly hyperglycaemic (Bg=10-15 mmol/L) db/db mice were 2.5-3.5-fold higher compared to wt mice over the time course but did not achieve statistical significance (**Figure 3.2(c)**, **Table 3.2**). The severely hyperglycaemic db/db mice showed a significant 4.3-fold, 3.9-fold and 3.3-fold higher mean plasma insulin level than wt mice at 0, 60 and 120 mins, respectively (**Figure 3.2(c)**, Table **3.2**). There was a trend for an increase in AUC of plasma insulin levels for db/db mice with Bg<10 mmol/L (AUC= 451.30 ± 80.70 A.U.) and Bg=10-15 mmol/L (AUC= 620.00 ± 105.92 A.U.) compared to controls (AUC= 222.96 ± 24.28 A.U.) but was not statistically significant. Compared to male wt mice, severely hyperglycaemic mice (

Table 3.2: The plasma insulin levels of male wt and db/db mice during ipGTT.

Time (mins)	Plasma insulin (ng/mL)¶			
	Wt	db/db		
		Bg<10 mmol/L	Bg=10-15 mmol/L	Bg>15 mmol/L
0	1.77 ± 0.16	3.61 ± 0.67	6.21 ± 1.08	7.57 ± 2.09*
60	1.84 ± 0.33	3.88 ± 0.61	4.69 ± 1.27	7.26 ± 1.98*
120	1.97 ± 0.27	3.67 ± 0.97	5.08 ± 1.46	6.52 ± 1.62*

¶The data represent mean ± SEM with n= 4-5 male mice/group. One-way ANOVA with Fisher's unprotected LSD test; *P<0.05 represent comparison between wt and db/db mice.

Bg>15 mmol/L) showed a significant 3.9-fold increase in AUC (AUC= 858.60 ± 165.49 A.U.) (**Figure 3.2(d)**). Thus, consistently high plasma insulin levels, indicating hyperinsulinaemia, were observed in db/db mice during the ipGTT, correlating with previous reports (Kobayashi et al., 2000, King, 2012, Aasum et al., 2003).

Taken together, db/db male mice displayed severe glucose intolerance despite having increased plasma insulin levels. These findings therefore confirmed that the db/db mice were insulin-resistant.

3.2.3 Pancreatic islets of db/db mice exhibit ER stress

Islets were isolated from 5-9 week old wt and hyperglycaemic db/db male mice with Bg>15 mmol/L. The mRNA was extracted using the RNeasy kit and cDNA was prepared. TaqMan PCR was performed using commercially validated primer/probes to detect transcripts for BiP (HSPA5), P58 (DNAJC3), CHOP (DDIT3), and ATF3 mRNAs (see Section 2.6), as markers of ER stress. The gene of interest was normalised to a control house-keeping gene (GAPDH) and mRNA levels of db/db islets were quantified as a fold-change of lean wt control islets.

Comparative C_T analyses revealed a 125-fold, 113-fold, 23-fold and 13-fold significant increase in the expression of the ER stress-associated genes BiP, P58, CHOP and ATF3 respectively, compared to wt islets (**Figure 3.3**). The expression of adaptive UPR genes (BiP and P58) in db/db islets was selectively increased compared to the pro-apoptotic UPR genes (CHOP and ATF3). These data confirm the existence of ER stress in the db/db islets, indicative of ER stress in the beta cells.

3.2.4 Immunohistochemical localisation of HSPG core proteins in the pancreatic islets of male wildtype, heterozygous and db/db mice

Having confirmed the induction of ER stress in male db/db islets, a condition that down-regulates protein synthesis, we next examined by immunohistochemistry the *in situ* intra-islet expression of three HSPG core proteins i.e., collagen type XVIII (Col18), syndecan-1 (Sdc1) and CD44 in pancreases of male wt, heterozygous db/+ and homozygous db/db mice at 3-20 weeks of age (see Section 2.7). Immunostaining of wt islets at 9 weeks of age confirmed the strong intra-islet expression of Col18, Sdc1 and CD44 core proteins

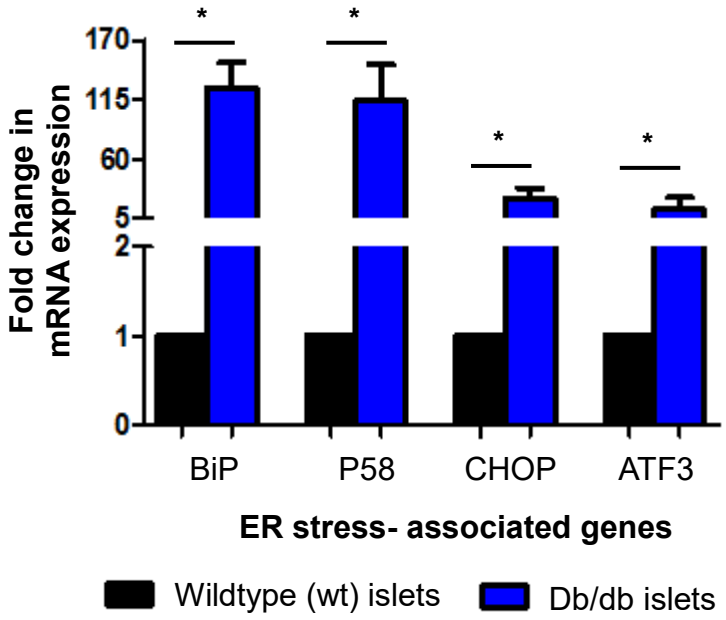

Figure 3.3: ER stress markers in male wt and db/db islets.

RNA extracted from islets isolated from male wt and hyperglycaemic db/db mice was used to prepare cDNA for TaqMan real-time PCR analysis of BiP, P58, CHOP and ATF3 transcripts. Comparative C_T analysis employing GAPDH gene expression as a reference gene for normalisation, was used to compare db/db transcript expression to wt controls. All ER stress-related genes were significantly upregulated in male db/db islets, compared to wt islets. The data represent mean ± SEM for 4 independent experiments (120-400 islets/group/experiment). Mann-Whitney test; *P<0.05.

as previously reported by the Simeonovic lab in another normal mouse strain (Choong et al., 2015); pancreas sections treated with isotype control Ig corresponding to each HSPG antibody showed no background staining (see Section 2.7, **Figure 2.4**).

(a) Collagen type XVIII

Immunohistochemical analysis of collagen type XVIII (Col18) core proteins in the pancreases of male db/db mice at 3, 4, 5, 6, 9, 12, 16 and 20 weeks of age showed substantially reduced immunostaining in db/db islets from 3 weeks of age, compared to corresponding wt control islets (**Figure 3.4**). Furthermore, intra-islet staining for Col18 was dramatically reduced in db/db islets by 5 weeks of age (prior to the onset of hyperglycaemia), compared to wt islets (**Figure 3.5**).

An early reduction in the Col18+ve area of staining in db/db islets to 80.3% ($P<0.05$) and 79.2% ($P<0.05$) of controls was observed at 3 and 4 weeks of age, respectively (**Figure 3.6**). From 4 weeks to 5 weeks of age, the Col18+ve islet area of db/db islets decreased dramatically with the levels at 5 weeks representing only ~60% of the levels at 4 weeks. The Col18+ve islet area showed a consistent reduction to 45.9%, 45.3% and 41.3% of wt islets at 5, 6 and 9 weeks of age, respectively.

A subsequent major decline in Col18 core protein expression was observed in the islets of db/db mice at 12 weeks of age when the intra-islet area was reduced to 10.5% of wt controls. Similar levels of 11.4% and 14.8% of controls were found in db/db islets at 16 and 20 weeks of age, respectively. Wt and heterozygous db/+ male mice showed significant differences at 5, 12 and 20 weeks of age; however both groups showed stronger distribution of Col18 compared to db/db mice.

Overall, this study showed that there was a progressive loss of intra-islet Col18 core protein in the islets of db/db mice during the development of T2D from 3-20 weeks of age. Striking reductions compared to corresponding wt controls were observed at 5 weeks and 12 weeks of age.

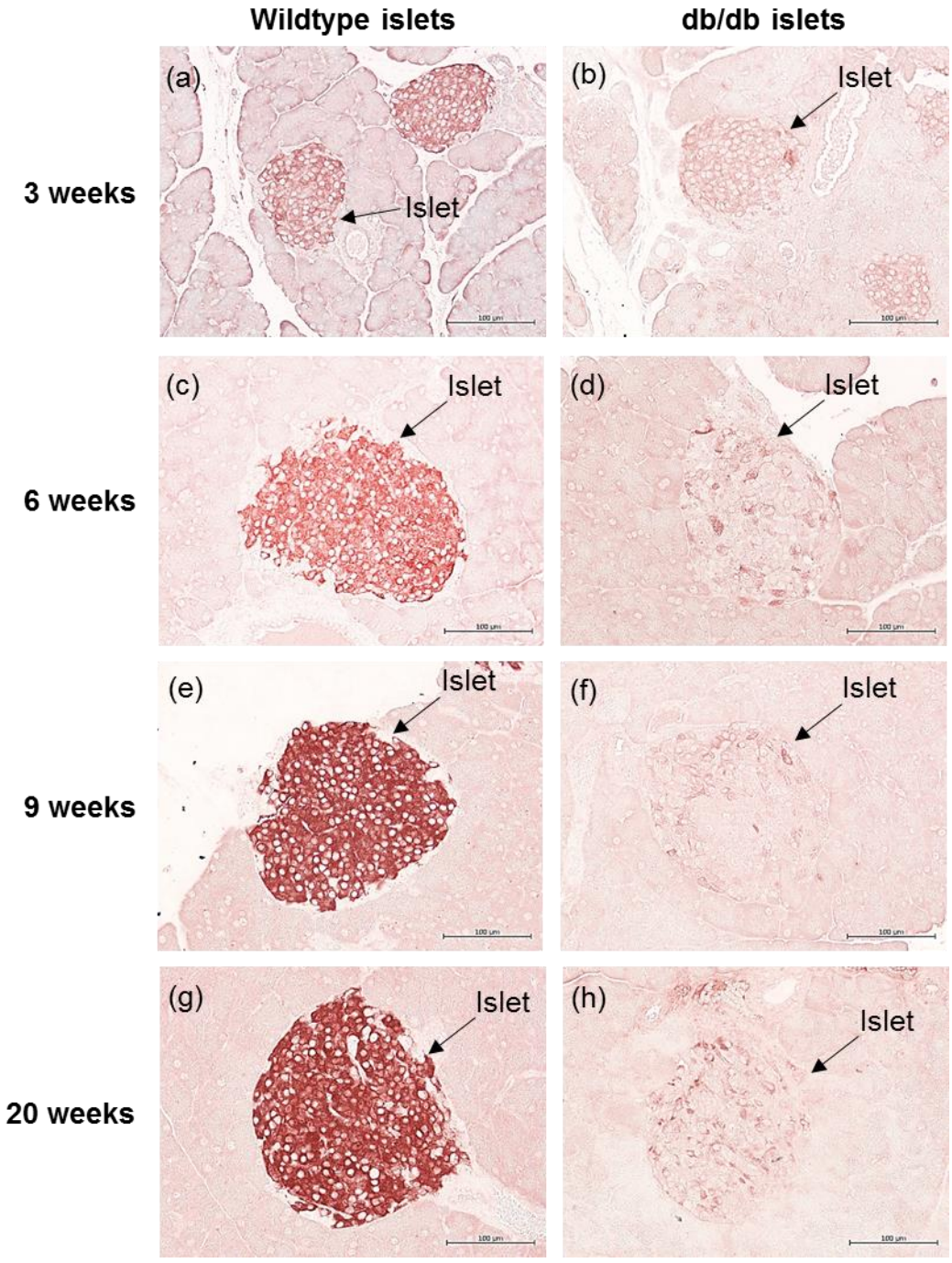

Figure 3.4: Distribution of collagen type XVIII (Col18) core protein in the pancreatic islets of male wt and db/db mice.

Representative images show the immunohistochemical localisation of Col18 core protein in the islets of db/db mice and wt mice at 3-20 weeks of age. Islets *in situ* in wildtype mouse pancreas (a, c, e, and g) showed intense Col18 staining. In contrast, db/db islets (b, d, f, and h) showed a dramatic loss of Col18 expression. Scale bar = 100 μm.

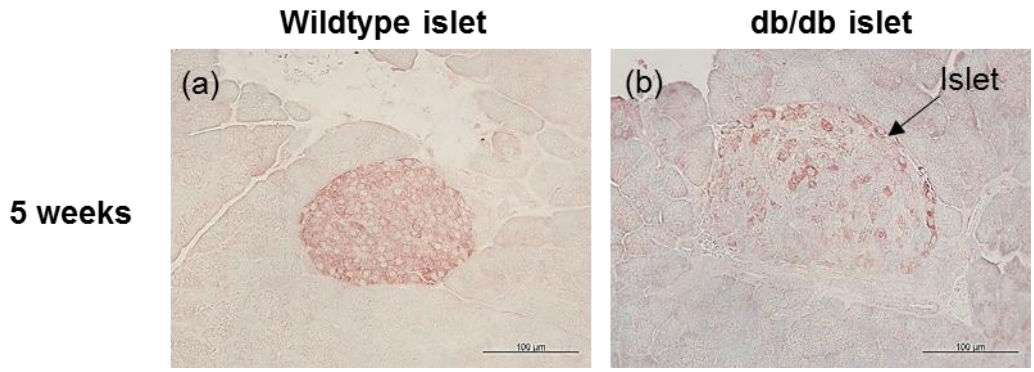

Figure 3.5: Distribution of collagen type XVIII (Col18) core protein in the pancreatic islets of male wt and db/db mice at 5 weeks of age.

Representative images show the immunohistochemical localisation of Col18 core protein in the islets of db/db mice and wt mice at 5 weeks of age. Compared to a wildtype mouse islet (a) which showed uniform Col18 staining, a dramatic loss of Col18 expression was observed in a db/db islet (b). Scale bar = 100 µm.

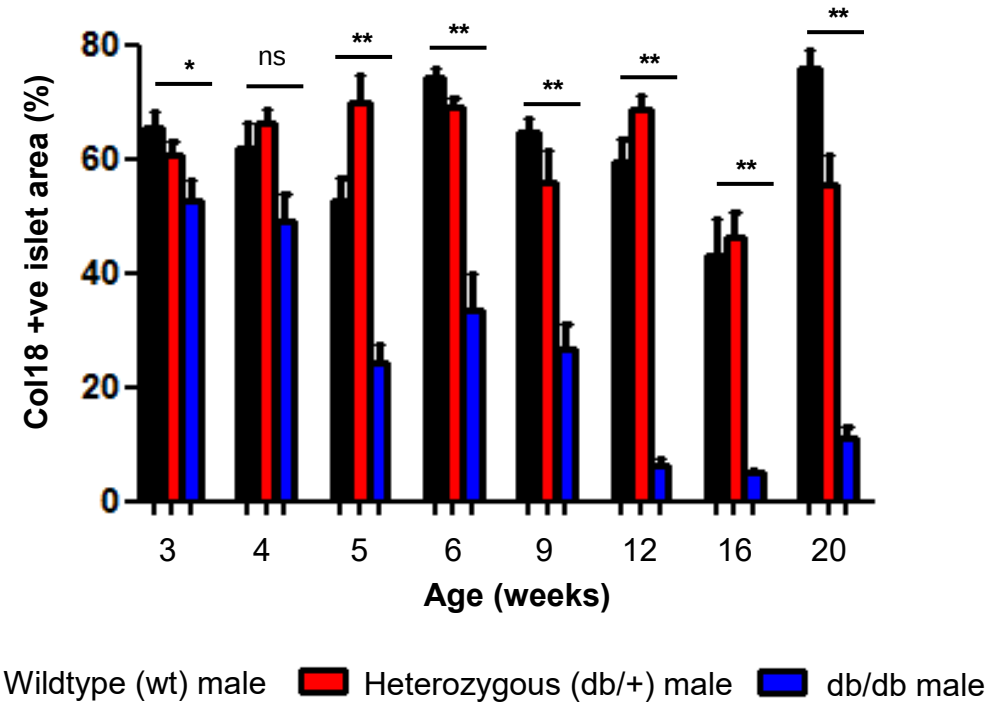

Figure 3.6: Intra-islet collagen type XVIII expression in pancreases from wt, db/+ and db/db mice at 3-20 weeks of age.

The Col18+ve islet area was assessed by immunohistochemistry and morphometry in wt, db/+ (heterozygous) and db/db pancreases from donors at 3, 4, 5, 6, 9, 12, 16 and 20 weeks of age. Intra-islet Col18 expression in db/db islets was dramatically reduced to ~45% of wt levels by 5 weeks of age; a further major decline to ~10% of wt levels was observed at 12 weeks of age. The data represent mean ± SEM for n= 3 pancreases/group with n=14-42 islets examined/group. One-Way ANOVA with Fischer's unprotected LSD test; *P<0.05, **P<0.0001 and ns, not significant.

(b) Syndecan-1

Immunohistochemistry analysis revealed a substantial decrease in the expression of intra-islet Sdc1 in db/db mice at 4 weeks of age, compared to corresponding wt controls (**Figure 3.7**). Sdc1 core protein was strongly expressed in the islets of wt mice at all ages, whereas the islets of db/db mice at 4-20 weeks of age showed little, if any, Sdc1 expression (**Figure 3.7**).

The intra-islet Sdc1 core protein expression in the islets of db/db mice and wt mice was similar at 3 weeks of age (**Figure 3.8**). A significant decline in intra-islet Sdc1 expression to 39.4% of wt islets was observed in the islets of 4 week old db/db male mice. Thereafter, the Sdc1+ve islet area was decreased to 56.7%, 22.5% and 23.6% of wt islets in db/db pancreases at 5, 6, and 9 weeks of age, respectively. Almost no intra-islet Sdc1 expression was found in db/db mice at 12, 16 and 20 weeks of age; the Sdc1+ve islet area was drastically reduced to 4.9%, 6.6% and 7.5% of wt mice, respectively.

As for intra-islet Col18, the wt and heterozygous db/+ male mice showed differences in HSPG core protein Sdc1 expression at 5-20 weeks of age. In general, however, strong intracellular expression of Sdc1 was observed in the islets of wt and heterozygous db/+ mice compared to db/db mice.

These findings demonstrate that during the development of T2D in male db/db mice there was a significant loss in the intra-islet expression of Sdc1 core protein at 4-20 weeks of age, compared to corresponding wt controls.

(c) CD44

The immunohistochemical localisation of CD44 core protein showed intracellular expression in the pancreatic islets of wt mice and predominantly cell surface staining in the islets of db/db mice from 3-20 weeks of age (**Figure 3.9**). In contrast to wt islets, db/db islets showed a striking loss of intracellular CD44 from 3 weeks of age (**Figure 3.9**).

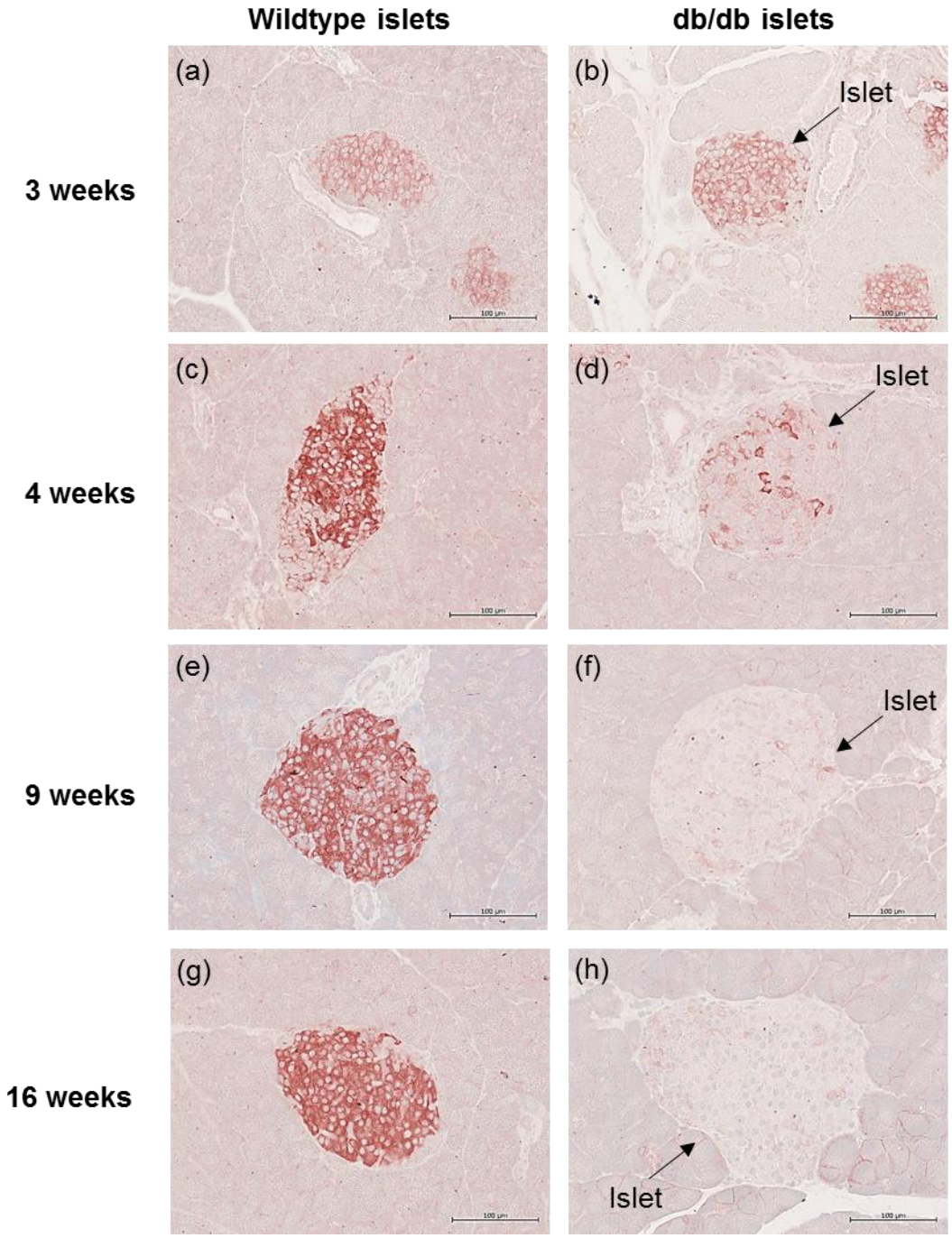

Figure 3.7: Immunohistochemical localisation of syndecan-1 (Sdc1) in the pancreatic islets of male wildtype and db/db mice.

Representative images show the localisation of Sdc1 core protein in the islets of wt (a, c, e, g) and db/db (b, d, f, h) mice at (a, b) 3 weeks, (c, d) 4 weeks, (e, f) 9 weeks and (g, h) 16 weeks of age. Islets *in situ* in wt mouse pancreas at all ages showed widespread Sdc1 staining whereas the db/db islets showed a dramatic decline in the intra-islet distribution of Sdc1 staining from 4 weeks of age (d). Scale bar = 100 μm.

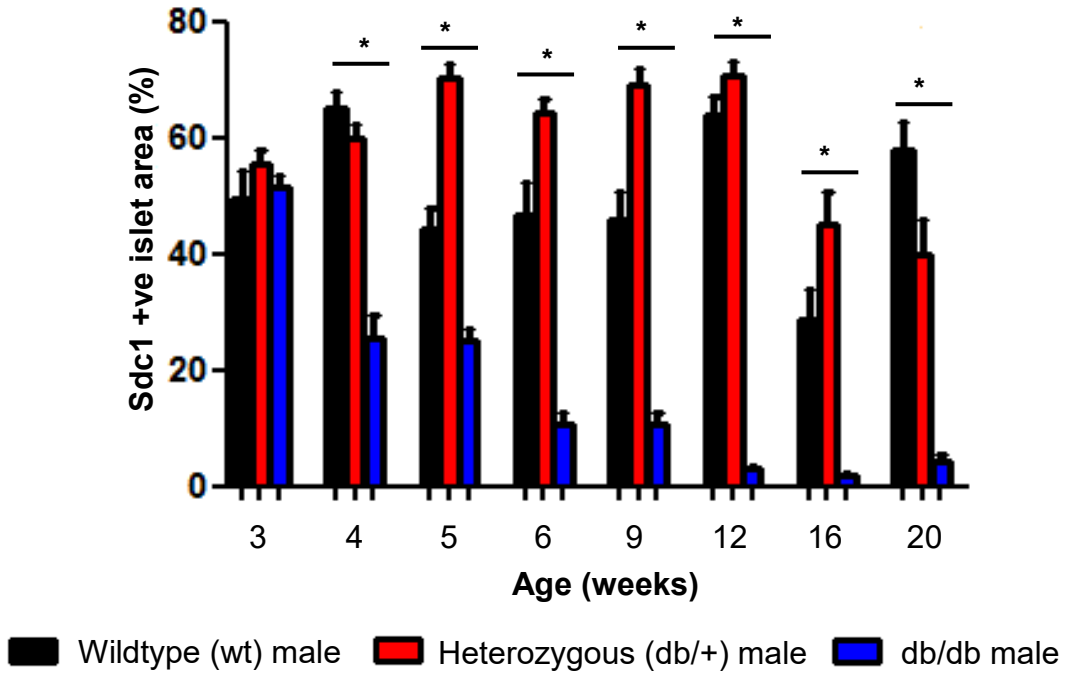

Figure 3.8: Syndecan-1 expression in pancreases from wt, db/+ and db/db mice at 3-20 weeks of age.

Morphometric analysis of the immunohistochemical staining of intra-islet Sdc1 core protein in wt, db/+ (heterozygous) and db/db pancreases from donors at 3, 4, 5, 6, 9, 12, 16 and 20 weeks of age. The Sdc1+ve islet area in db/db pancreases was significantly reduced to 39.4% of corresponding wt controls at 4 weeks of age; subsequently marked reductions were observed at 6-9 weeks of age (22.5%-23.6%) and at 12-20 weeks (4.9%-7.5%). The data represents the mean ± SEM for 3 pancreases/age group with n=15-38 islets examined/group. One-Way ANOVA with Fischer's unprotected LSD test; *P<0.0001.

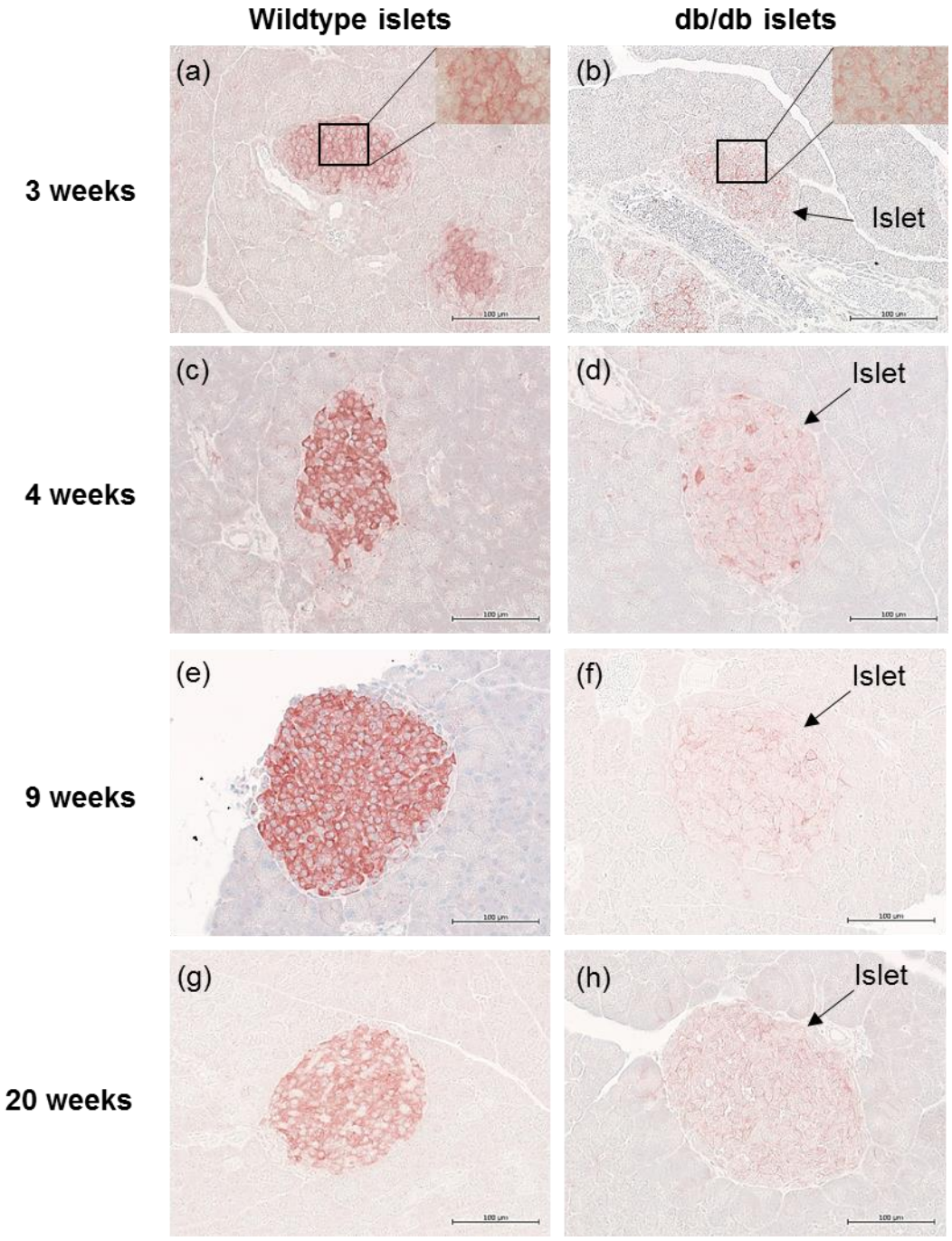

Figure 3.9: Immunohistochemical localisation of CD44 core protein in the pancreatic islets of db/db mice and wildtype mice.

Representative images show the distribution of CD44 in the islets of db/db mice (b, d, f, h) and wildtype mice (a, c, e, g) as demonstrated by immunohistochemical staining. Wildtype islets showed strong expression of CD44 and loss of staining was observed in the islets of db/db mice from 3 weeks of age (b). Scale bar = 100 μm.

Db/db islets revealed a significant decrease in the CD44+ve islet area to 60.4% of wt islets at 3 weeks of age (**Figure 3.10**). By 4 weeks of age, CD44 expression in the islets of db/db mice was further reduced to 38.3% of the corresponding wt control group. Db/db islets at 5-6 weeks of age showed 68.6% to 37.4% of the CD44+ve islet area of wt control islets. By 9-12 weeks of age, the CD44+ve islet area in db/db pancreases decreased to ~18% of corresponding wt control islets. A further decrease to 2.2-13.0% of wt controls was observed in db/db islets at 16-20 weeks of age.

While significant differences were observed between wt and heterozygous db/+ mice at 4-16 weeks of age ($P<0.05$), from a biological perspective both groups at each time point showed extensive intra-islet CD44 immunostaining compared to db/db groups. The lower intra-islet expression of CD44 at 16-20 weeks of age, in wt and db/+ pancreases compared to other time points was attributed to highly variable CD44 staining.

These data demonstrated a significant loss in the intra-islet expression of intracellular CD44 core protein in db/db islets from 3-20 weeks of age compared to corresponding wt mice.

Taken together, these immunohistochemical studies revealed a dramatic early decline in the expression of HSPG core proteins for Col18 (see Section 3.2.4 (a)), Sdc1 (see Section 3.2.4(b)) and CD44 (see Section 3.2.4(c), above) in islets from young db/db donors at 3-5 weeks of age, with CD44>Sdc1>Col18 representing highly sensitive markers of T2D progression prior to the onset of hyperglycaemia.

3.2.5 HS expression in the islets of wt and db/db mice

Since HSPG core proteins (Col18, Sdc1 and CD44) in the islets of young db/db male mice from 3-5 weeks of age, decreased dramatically and HS chains are synthesised directly onto HSPG core proteins, we next examined the intra-islet expression of HS in the pancreases of wt and db/db male mice at different ages.

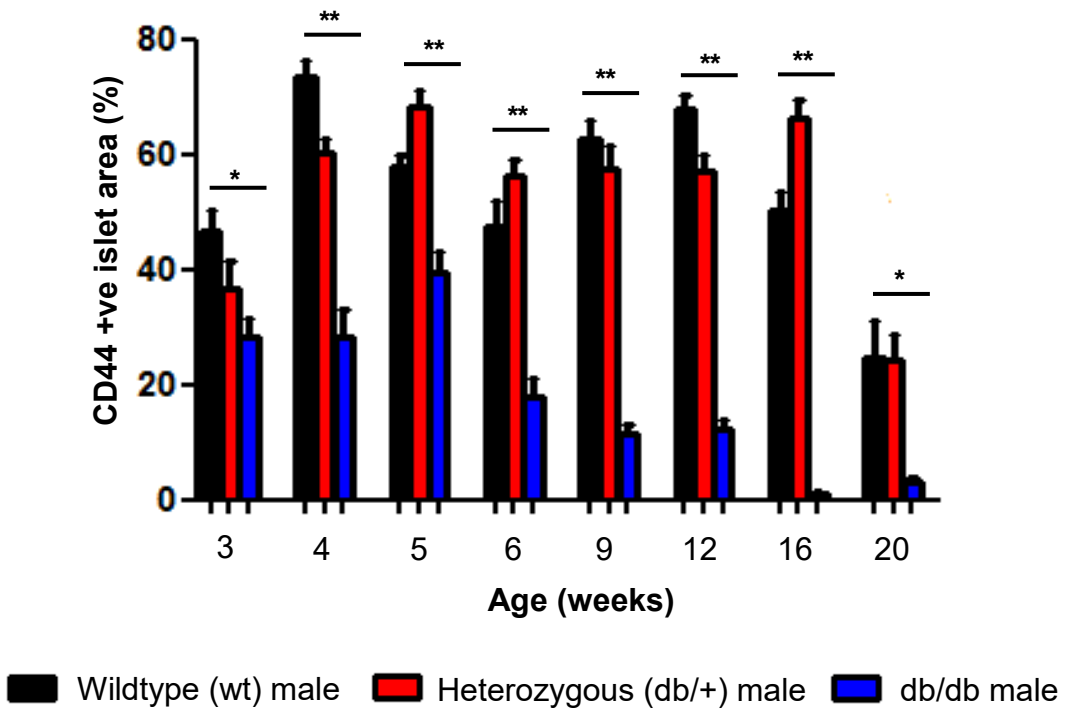

Figure 3.10: Morphometric analysis of CD44 core protein expression in pancreatic islets of wt, db/+ and db/db mice at 3-20 weeks of age.

The CD44+ve islet area in immunostained sections of wt, heterozygous db/+ and db/db pancreases was assessed using Image J software with colour deconvolution plugin. db/db islets showed a significant reduction of CD44 expression by as early as 3 weeks of age. The data represents the mean ± SEM for 3 pancreases/age group with n= 14-40 islets examined/group. One-Way ANOVA with Fischer's unprotected least significant difference (LSD) test; *P<0.01 and **P<0.0001.

The expression of HS in the islets of male db/db mice and wt mice at 4, 5, 6, and 9 weeks of age was determined by immunohistochemistry. Two different primary anti-HS antibodies i.e. anti-10E4 mAb and anti-HepSS-1 mAb were used for the analysis. The anti-10E4 mAb detects highly sulfated HS chains whereas anti HepSS-1 mAb detects less-sulfated HS chains (Ziolkowski et al., 2012, Theodoraki et al., 2015, Simeonovic et al., 2018).

Immunostaining with 10E4 anti-HS mAb resulted in a marked decrease in the HS+ve islet area in db/db pancreases by as early as 4 weeks of age, compared to lean wt mice of the same age (**Figure 3.11**). Representative images in **Figure 3.11** show strong expression of HS in wt islets and less pronounced intracellular HS in the db/db islets from 4-5 weeks of age. Furthermore, only scattered islet cells with strong positive staining were observed at 6 and 9 weeks. In contrast, immunohistochemical staining with anti-HepSS-1 mAb showed strong staining in some cells at the periphery of both wt and db/db islets in each age group (**Figure 3.12**). In parallel, a loss of intracellular HS was observed in db/db islets at 6 and 9 weeks of age compared to the widespread, intense staining in corresponding wt islets (**Figure 3.12**). Immunostaining using isotype controls corresponding to HS antibody showed no background staining (**Figure 2.5**).

The HS+ve islet area was quantified by morphometry using Image J software with colour deconvolution plugin. The threshold for positive staining was set using the strong intracellular staining observed in wt islets at 6 and 9 weeks of age. This threshold was applied to all wt and db/db specimens.

Morphometric analysis of the HS+ve islet area following immunostaining with 10E4 anti-HS mAb revealed a significant decrease in db/db islets to 48.1% of control wt islets (anti-HS wt, 50.46 ± 2.31% versus db/db, 24.27 ± 2.84%) at 4 weeks of age (**Figure 3.13(a)**). A similar marked reduction in db/db islets to 51.4% of wt controls (wt, 46.32 ± 2.56% versus db/db, 23.83 ± 2.74%) at 5 weeks of age, confirmed the early loss of highly sulfated HS from the islets prior to the onset of hyperglycaemia at 6 weeks (see Section 3.2.1). In db/db mice at 6 and 9 weeks of age, the HS+ve islet area was reduced to 33.8% and 25.7% of corresponding control wt islets (**Figure 3.13(a)**).

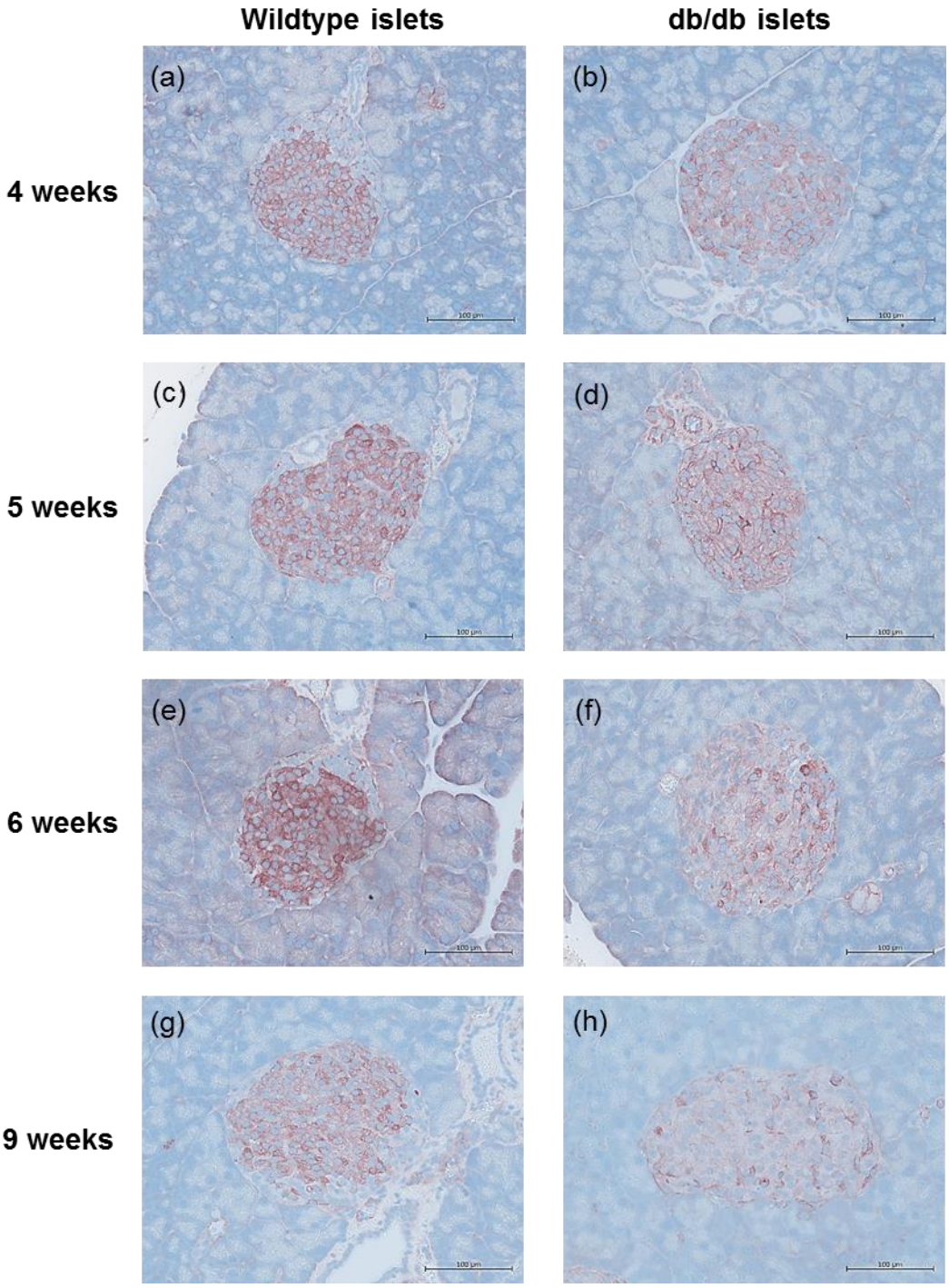

Figure 3.11: Localisation of HS in the pancreatic islets of db/db and wildtype mice at 4 to 9 weeks of age.

Representative images of the distribution of HS in the islets of db/db mice and wildtype mice as determined by immunohistochemistry using 10E4 anti-HS mAb. The islets of wildtype mice (a, c, e and f) strongly express intracellular HS whereas a progressive loss of HS was observed in db/db islets (b, d, f, and h). 10E4 anti-HS mAb; scale bar = 100 μm.

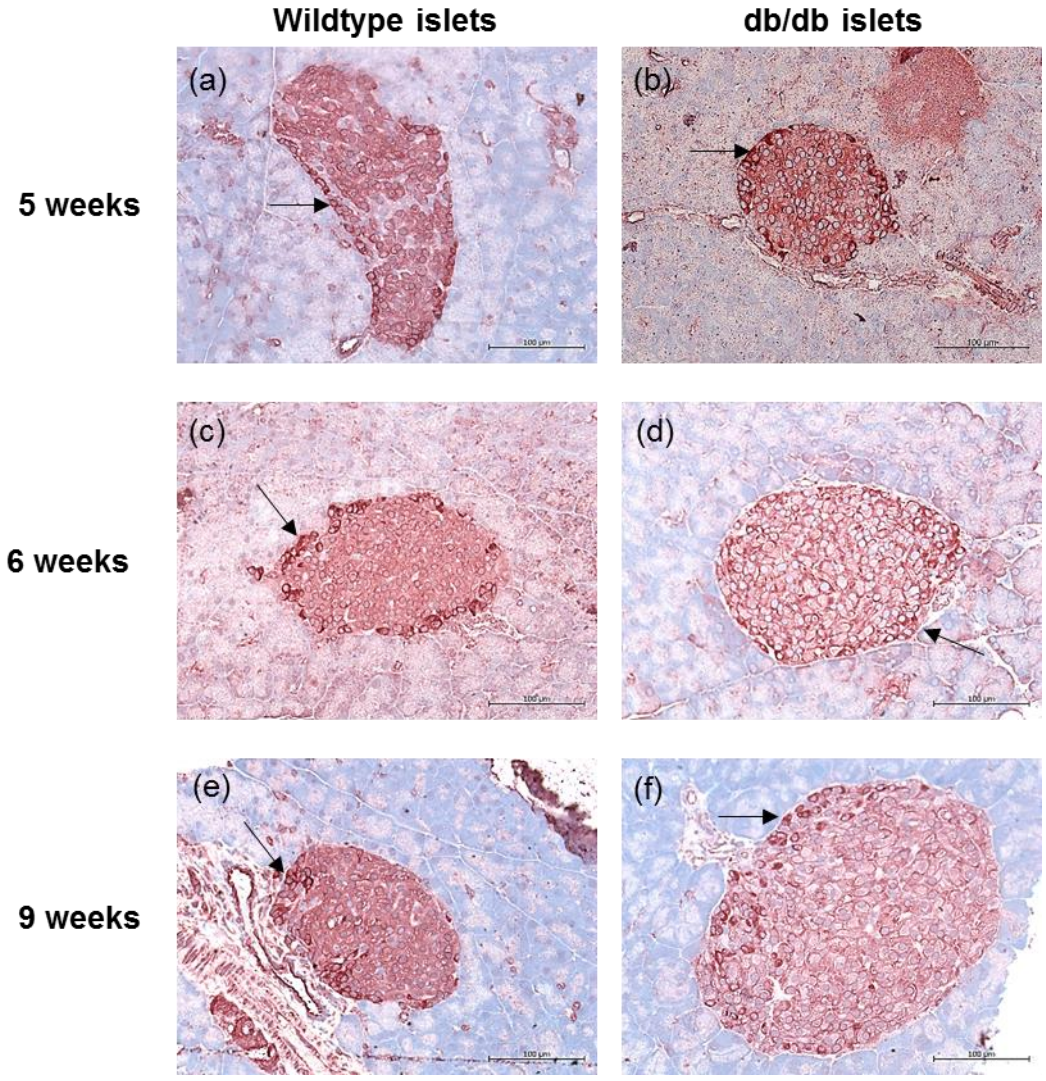

Figure 3.12: Immunohistochemical localisation of HS in the pancreatic islets of db/db and wildtype mice at 5- 9 weeks of age, using HepSS-1 anti-HS mAb.

Representative images show the distribution of HS in the islets of db/db mice and wildtype mice after immunostaining of pancreas sections with HepSS-1 anti-HS mAb. Whereas strong intracellular staining of HS was observed in some cells at the periphery of both wt and db/db islets of all ages (see arrows, a-f), db/db islets showed a marked loss of intracellular staining throughout the islet mass at 6-9 weeks of age (d, f). Scale bars =100 μm.

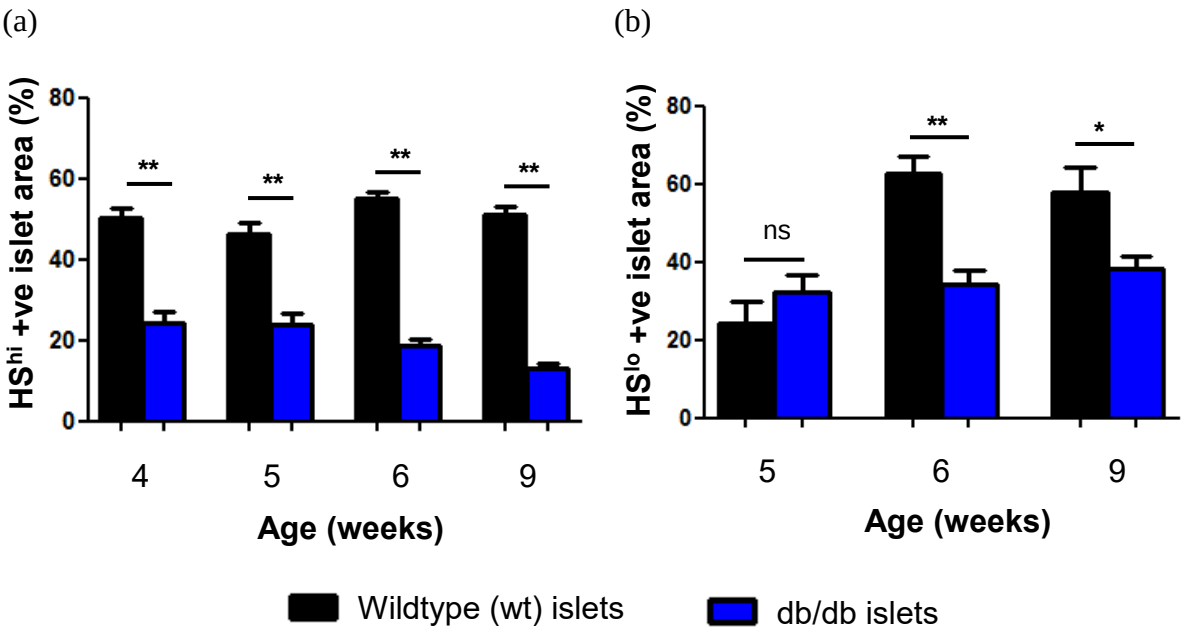

Figure 3.13: The distribution of HS in the pancreatic islets of wt and db/db mice at 4-9 weeks of age.

The relative distribution of HS in wt and db/db male pancreatic islets was determined by morphometry. The % HS+ve islet area was calculated using Image J software with colour deconvolution plugin. (a) Immunostaining with 10E4 anti-HS mAb showed that the positively stained highly sulfated HS (HS^{hi}+ve) in the db/db islets significantly decreased to 48.1% of control wt islets by 4 weeks. (b) Intracellular HS immunostaining using HepSS-1 anti-HS mAb uniformly stained islet beta cells (excluding intensely stained peripheral alpha cells) at 5 weeks. db/db islets showed a significant decline in less-sulfated (HS^{lo}+ve) expression to 54.5% of control islets by 6 weeks of age. Data show mean HS+ve islet area ± SEM for 3 pancreas specimens/age group with n=19-52 islets analysed/group for immunostaining with 10E4 mAb and n=16-40 islets analysed/group for staining with HepSS-1 mAb. Unpaired t test and Mann-Whitney test; *P<0.01, **P<0.0001 and ns, not significant.

In contrast, staining for under-sulfated HS with HepSS-1 mAb demonstrated a similar HS+ve islet area in wt islets (24.33 ± 5.63%) and db/db islets (32.20 ± 4.30%) at 5 weeks of age (**Figure 3.13 (b)**). However, by 6 weeks of age, there was a significant decrease in the intracellular distribution in db/db islets to 54.5% of control wt islets (wt, 62.73 ± 4.54% versus db/db, 34.17 ± 3.53%). Similarly, there was a significant reduction to 66.2% of wt controls in the HS+ve islet area of db/db islets at 9 weeks (wt, 57.87 ± 6.45% versus db/db, 38.30 ± 3.14%; $P<0.01$; **Figure 3.13(b)**).

Overall, db/db mice revealed a significant intra-islet loss of highly sulfated HS at the early age of 4 weeks and of under-sulfated HS by 6 weeks of age during the development of T2D.

3.2.6 Immunolocalisation of insulin and glucagon in wt and db/db pancreases

Pancreas sections of male wt and db/db mice were stained for insulin and glucagon by immunohistochemistry. Insulin staining identifies islet beta cells and glucagon staining distinguishes the islet alpha cell population.

Representative images show strong staining for insulin in the islets of wt mice from 3-20 weeks of age (**Figure 3.14**). Likewise, db/db islets showed a uniform intense expression of insulin at 3 of age (**Figure 3.14**). In contrast, there was a substantial loss of insulin in the db/db islets at 4 weeks and this reduction was maintained from 6-20 weeks of age (**Figure 3.14**)

The intensity of insulin staining was quantified using Image J software with a colour deconvolution plugin (see Section 2.7.5). The intensity of insulin staining in db/db islets showed an early significant decline to 68.7% of wt controls at 4 weeks of age (**Figure 3.15**). Although comparable staining for insulin was observed in wt and db/db islets at 5 weeks of age. The intensity of insulin staining was consistently reduced in db/db islets to 68.9% and 62.3% of wt islets at 6 and 9 weeks of age, respectively. The observed discrepancy at 5 weeks of age could be due to the fewer wt islets (n= 15) analysed compared to db/db islets (n= 30) and to unusual weaker staining of insulin in one of the three wildtype pancreas samples analysed. Insulin immunostaining was further significantly reduced to ~47-48% of corresponding controls by 12-20 weeks of age

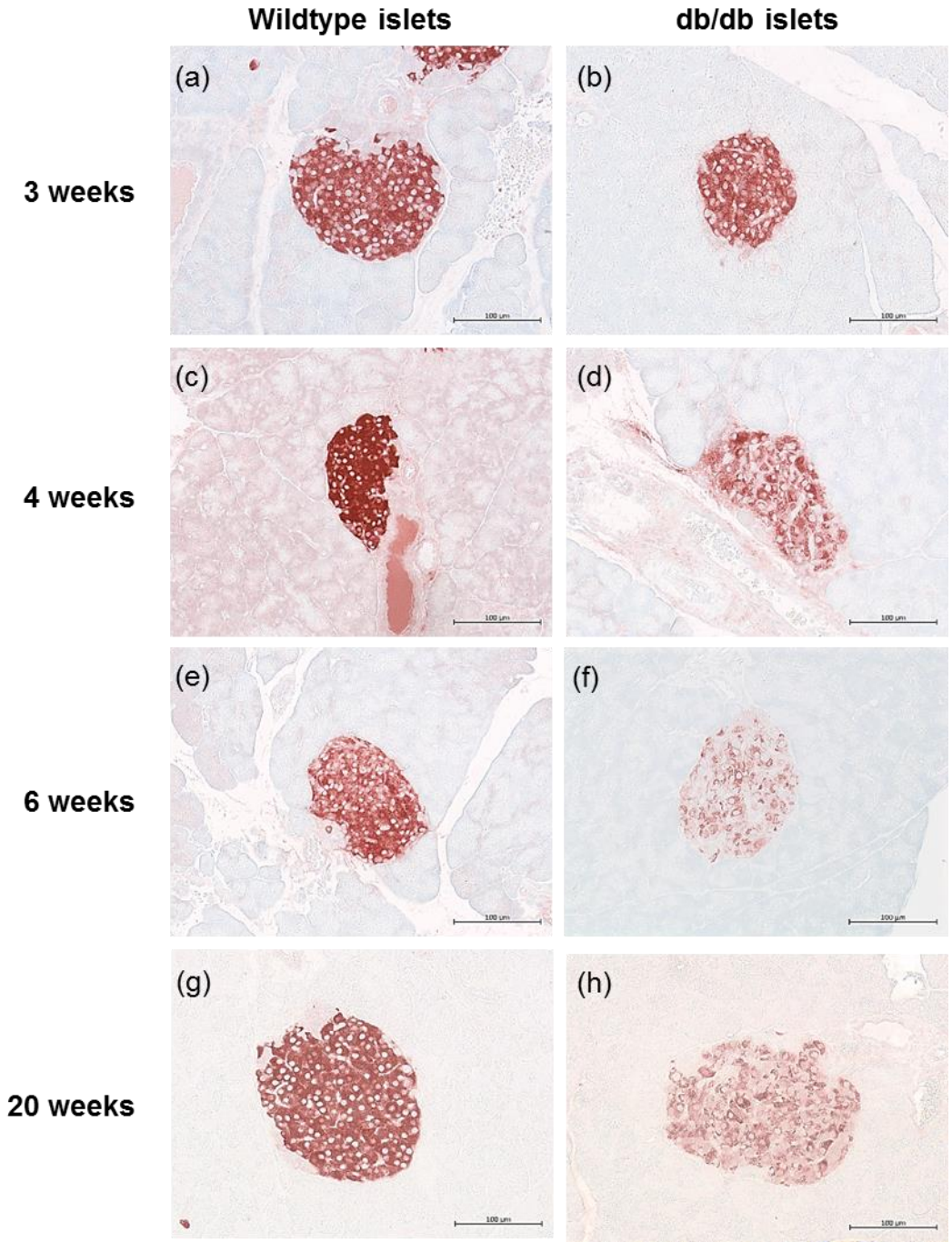

Figure 3.14: Insulin immunolocalisation in the pancreatic islets of db/db and wildtype mice at 3-20 weeks of age.

Insulin expression in the islets of db/db mice and wildtype mice, was localised by immunohistochemistry. Strong staining was observed in the islets of wildtype mice at 3, 4, 6 and 20 weeks of age (a, c, e, and g); an initial loss of staining in db/db islets was found at 4 weeks of age (b) and only scattered insulin +ve beta cells were identified in db/db islets at 6-20 weeks of age (d, f and h). Scale bar = 100 μm.

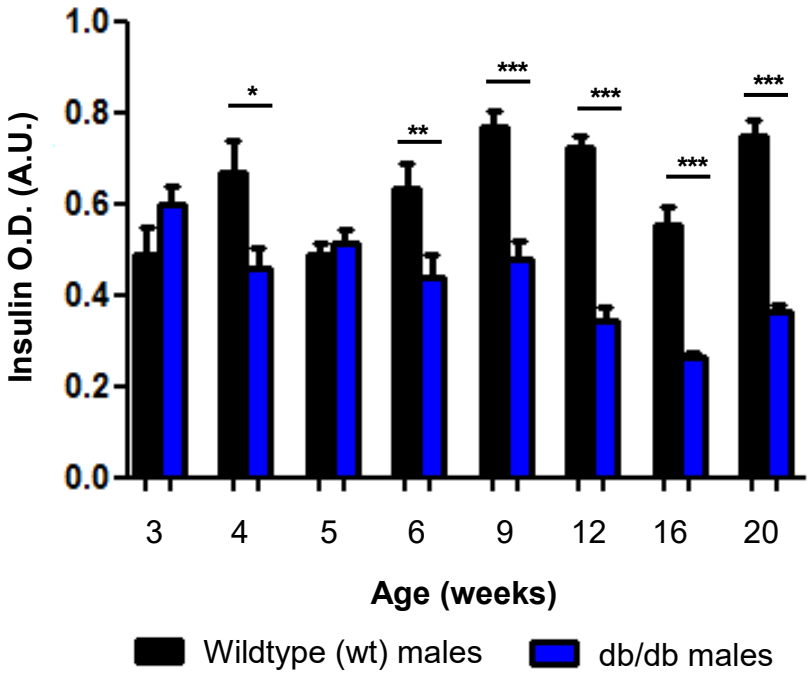

Figure 3.15: Insulin expression in the islets of db/db and wt mice.

The intensity (optical density (O.D.)) of insulin staining in pancreas section of wt and db/db mice was determined using Image J software with colour deconvolution plugin. Insulin loss was observed in two stages; an initial reduction to 68.7% of wt controls was found at 4 weeks of age followed by a loss to 47.3% of wt controls at 12 weeks of age. Data represent the mean islet intensity ± SEM for 3 pancreases/age group with n=14-37 islets examined/group. Unpaired t test and Mann-Whitney test; *P<0.05, **P<0.01 and ***P<0.0001.

($P<0.0001$).

The distribution of glucagon staining in wt and db/db islets was confined to cells at the islet periphery, identifying alpha cells (**Figure 3.16**). In general, the intensity of glucagon staining in wt and db/db islets was similar up to 20 weeks of age. A 1.4-fold increase in the glucagon+ve islet area at 16 weeks of age was observed in db/db mice compared to wt mice (**Figure 3.17**). Furthermore, by 12 weeks, the restricted localisation of alpha cells appeared to be less pronounced and the glucagon+ve islet area increased, correlating with a reduction in beta cell function (**Figure 3.15**). The statistically significant differences observed at 4, 5 and 16 weeks of age are attributed to variability in glucagon staining intensity observed between some samples.

3.2.7 Obesity and hyperglycaemia in female db/db mice

The body weight and non-fasting blood glucose levels of female wildtype (wt), heterozygous (db/+) and db/db mice were measured at 3, 4, 5, 6, 7, 8, 9, 12, 16 and 20 weeks of age (see Section 2.2.1) to establish the temporal relationship between the development of obesity and hyperglycaemia during T2D progression.

Like male db/db mice, the body weight of female wt and db/db mice was similar at 3 and 4 weeks of age. (**Figure 3.18(a)**). There was a progressive 1.4-2.0-fold significant increase in the body weight of female db/db mice from 6 weeks (21.76 ± 1.17 grams) up to 20 weeks of age (35.92 ± 4.96 grams) during the progression of T2D. Generally, the weight of wt and heterozygous db/+ mice did not differ significantly at 3-20 weeks of age, except for a 1.5-fold significant increase in the body weight of heterozygous db/+ mice (17.10 ± 0.37 grams) at 5 weeks of age compared to wt mice (11.75 ± 1.82 grams) (**Figure 3.18(a)**). This discrepancy could be due to the presence of one mutant allele in the heterozygous db/+ mice. Female db/db mice were significantly heavier than wt controls by 6 weeks of age.

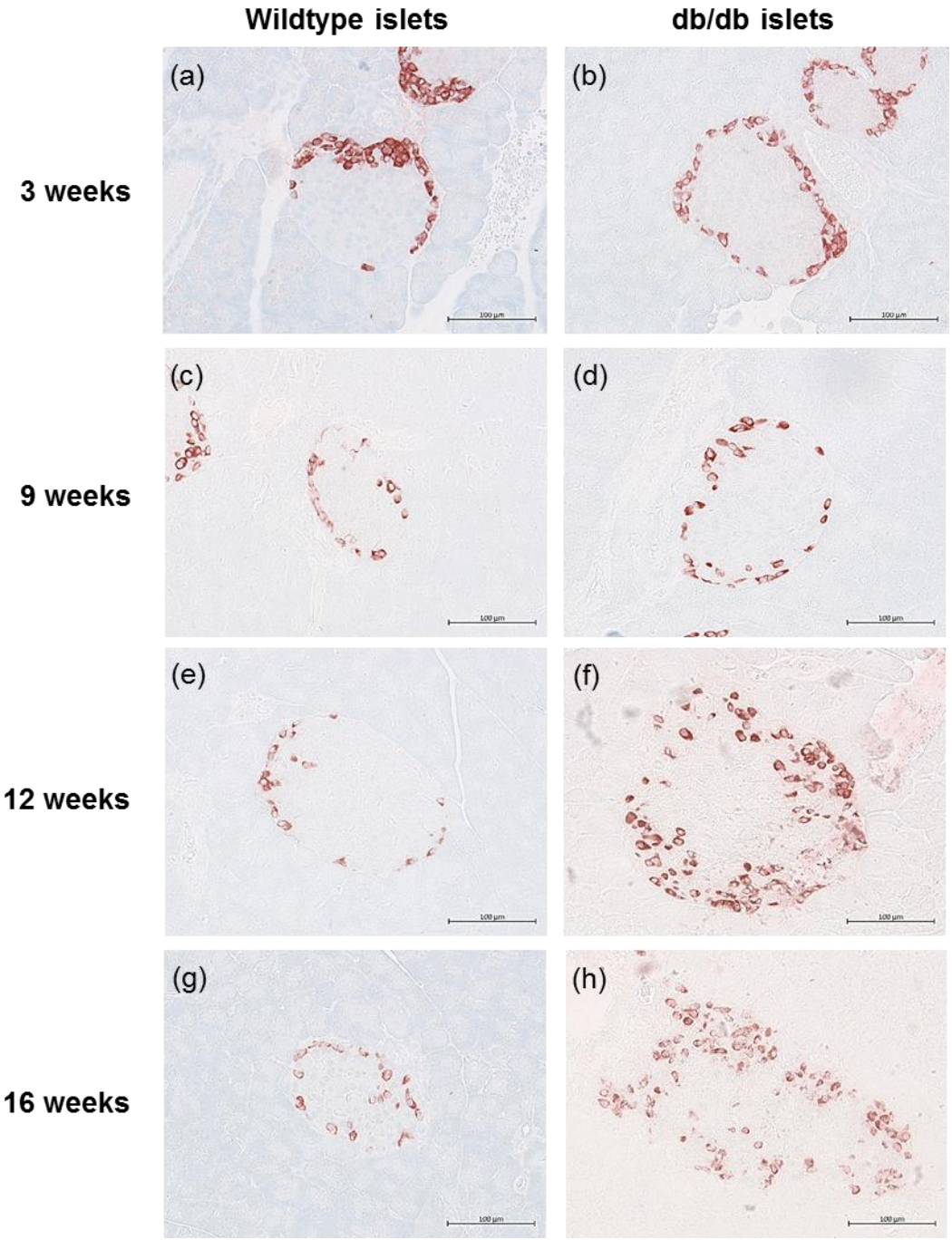

Figure 3.16: Localisation of glucagon in the pancreatic islets of db/db and wildtype mice at 3-16 weeks of age.

Glucagon expressing alpha cells were localised in the islets of db/db mice and wildtype mice. Characteristically, the islet alpha cells were found at the islet periphery in db/db pancreases from donors up to 9 weeks of age. Scale bar = 100 μm.

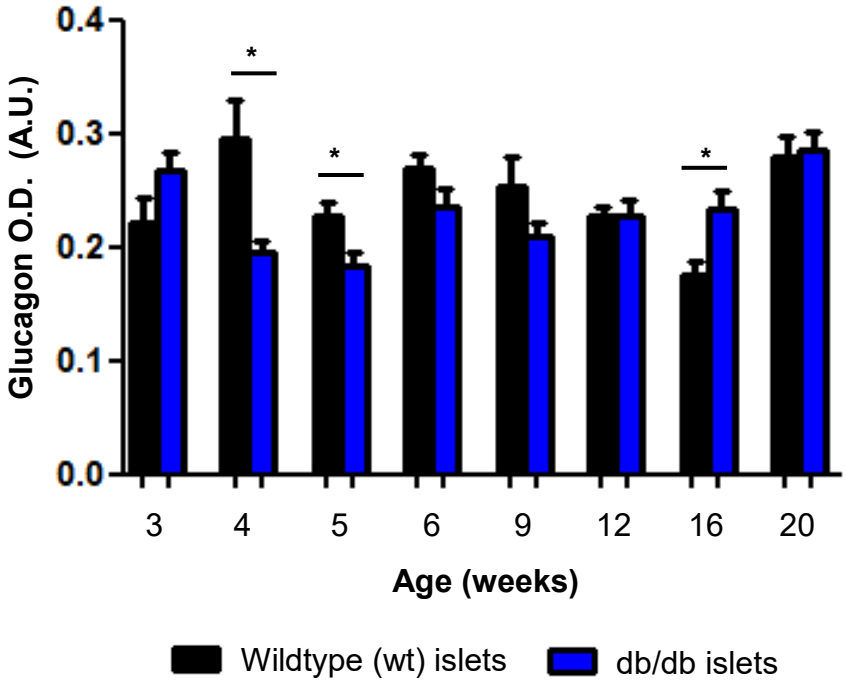

Figure 3.17: Glucagon expression in the islets of db/db and wt mice.

The intensity of glucagon immunostaining was determined in wt and db/db pancreases at 3-20 weeks of age, using Image J software with colour deconvolution plugin. In general glucagon expression was similar between wt and db/db islets up to 20 weeks of age during the development of T2D. The data shows the mean optimal density (O.D.) ± SEM for 3 pancreases/age group n=13-39 islets analysed/group. Unpaired t test and Mann-Whitney test; *P<0.05.

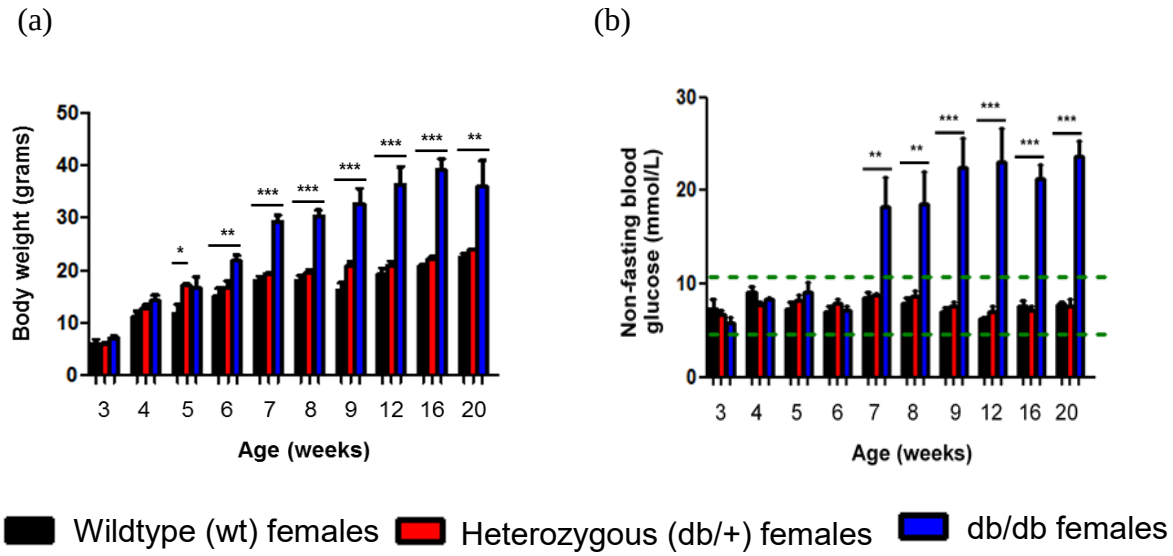

Figure 3.18: The mean body weight and non-fasting blood glucose of female wt, db/+ and db/db mice during the development of T2D.

The mean body weight and non-fasting blood glucose levels were measured in female wildtype (wt), heterozygous (db/+) and db/db mice from 3-20 weeks of age. (a) db/db females showed increased body weight from 6 weeks of age, compared to corresponding wt controls. (b) Female db/db mice demonstrated hyperglycaemia by 7 weeks of age. The green dotted lines represent the normal blood glucose range (7.55 ± 3.12 mmol/L i.e., 4.43 mmol/L-10.67 mmol/L), as assessed in 56 female wt mice (3-20 weeks of age). The data represent the mean ± SEM; n=5-8 mice/age group. One-way ANOVA with Fisher's unprotected LSD test; *P<0.05, **P<0.01 and ***P<0.001.

Female wt and heterozygous db/+ mice remained normoglycaemic for up to 20 weeks of age (**Figure 3.18(b)**). The non-fasting blood glucose levels of wt, db/+ and db/db females were maintained in the normal range (7.55 ± 3.12 mmol/L) for 3-6 weeks of age. In contrast, female db/db mice showed a significant 2.1-fold and 2.4-fold increase in non-fasting blood glucose levels at 7 weeks (18.26 ± 3.17 mmol/L) and 8 weeks (Bg, 18.60 ± 3.36 mmol/L) compared to wt controls (Bg, 7.88 ± 0.62 mmol/L). Thereafter db/db female blood glucose levels remained >20 mmol/L for up to 20 weeks of age. Thus, the onset of hyperglycaemia in female db/db mice occurred at 7 weeks of age.

Thus, female db/db mice were obese by 6 weeks of age and hyperglycaemic by 7 weeks of age during the development of T2D.

3.2.8 Female db/db mice develop glucose-intolerance and insulin-resistance

Like male db/db mice (see Section 3.2.2), female db/db mice (5-9 week old) were also categorised into three groups based on their non-fasting blood glucose, i.e., Bg<10 mmol/L (normoglycaemic), Bg=10-15 mmol/L (mildly hyperglycaemic) and Bg>15 mmol/L (severely hyperglycaemic). The db/db mice were bled in the morning and were allocated to groups prior to an i.p glucose tolerance test (ipGTT; see Section 2.2) on the same day.

Female wt blood glucose levels increased sharply and peaked at 15 mins after glucose challenge (16.80 ± 0.89 mmol/L). However, the blood glucose levels subsequently returned to pre-challenge levels of 7.76 ± 0.32 mmol/L at 120 mins (**Figure 3.19(a)**, **Table 3.3**). In contrast, the blood glucose levels of female db/db mice in each of the three groups rose sharply within 15 mins and remained elevated for up to 120 mins. The Bg<10 mmol/L and Bg=10-15 mmol/L groups showed some evidence of glycaemic control with blood glucose levels deceasing to 14.57 ± 4.59 mmol/L and 16.00 ± 1.69 mmol/L, respectively at 120 mins. In contrast, db/db females belonging to the Bg>15 mmol/L group demonstrated severe hyperglycaemia (Bg>20 mmol/L) from 30-120 mins during the observation period (**Table 3.3**).

When the ipGTT data was represented as a bar graph of AUC values for blood glucose, the AUC for db/db mice (Bg<10 mmol/L) significantly increased 1.8-fold to 2272.75 ±

Figure 3.19: ipGTT in female wt and db/db mice.

Female wt and db/db mice were fasted for 6 hrs before an i.p. glucose tolerance test (ipGTT). Based on morning non-fasting blood glucose levels, the db/db mice were divided into three groups i.e., Bg<10 mmol/L, Bg=10-15 mmol/L and Bg>15 mmol/L. (a) The blood glucose levels were measured at 0, 15, 30, 60, 90 and 120 mins after i.p. challenge (2 g/kg glucose). Following a rapid rise in blood glucose levels in all mice at 15 mins, wt females demonstrated a subsequent decline in blood glucose levels to the normal range by 120 mins; in contrast, db/db blood glucose levels remained elevated. (b) The AUC corresponding to the blood glucose profiles in (a) show a significant increase for db/db females, compared to wt mice. (c) Both wt females and db/db females of the normoglycaemic Bg<10 mmol/L group showed similar plasma insulin levels at 0 mins; mildly and severely hyperglycaemic db/db females were hyperinsulinaemic, prior to glucose administration. During the ipGTT (a) db/db females showed markedly higher plasma insulin at 60 and 120 mins, compared to wt mice (c). (d) AUC bar graphs, corresponding to the plasma insulin graphs in (c) illustrate that mildly and severely hyperglycaemic db/db groups were significantly hyperinsulinaemic, relative to wt females. The data show mean ± SEM with n=4-8 female mice/group for ipGTT and n=3 mice/group for plasma insulin analysis. One-way ANOVA with Fisher's unprotected LSD test; *P<0.001 and ns, not significant.

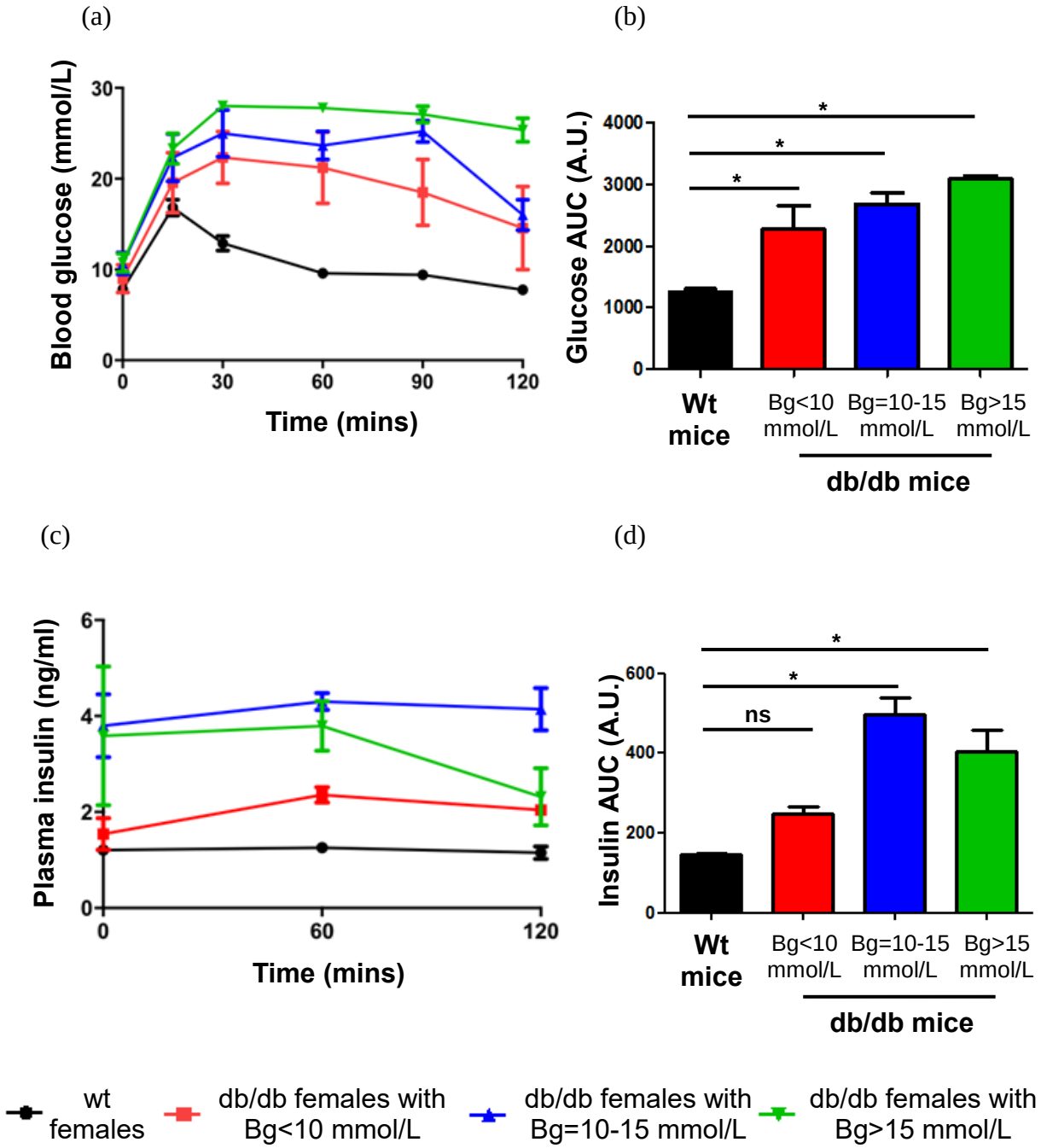
(a)
(b)
Blood glucose (mmol/L)
30
20
10
0
0
30
60
90
120
Time (mins)
Glucose AUC (A.U.)
4000
3000
2000
1000
0
*
*
*
Wt mice
Bg<10 mmol/L
Bg=10-15 mmol/L
Bg>15 mmol/L
db/db mice
(c)
(d)
Plasma insulin (ng/ml)
6
4
2
0
0
60
120
Time (mins)
Insulin AUC (A.U.)
600
400
200
0
*
*
ns
Wt mice
Bg<10 mmol/L
Bg=10-15 mmol/L
Bg>15 mmol/L
db/db mice
wt females
db/db females with Bg<10 mmol/L
db/db females with Bg=10-15 mmol/L
db/db females with Bg>15 mmol/L

Table 3.3: Blood glucose measurement during ipGTT in female db/db and wt mice.

Time (mins)	Blood glucose (mmol/L)¶			
	Wt	db/db		
		Bg<10 mmol/L	Bg=10-15 mmol/L	Bg>15 mmol/L
0	7.80 ± 0.45	8.97 ± 1.53	10.67 ± 1.20*	10.74 ± 0.99*
15	16.80 ± 0.89	19.55 ± 3.32	22.30 ± 2.61	23.32 ± 1.68*
30	12.89 ± 0.80	22.32 ± 2.85**	24.97 ± 2.58***	28.00 ± 0.00**
60	9.60 ± 0.25	21.22 ± 3.93**	23.67 ± 1.57***	27.78 ± 0.22**
90	9.41 ± 0.55	18.47 ± 3.63**	25.20 ± 1.19***	27.08 ± 0.92**
120	7.76 ± 0.32	14.57 ± 4.59*	16.00 ± 1.69*#	25.36 ± 1.30**##

¶The data represent mean ± SEM with n= 4-8 female mice/group. One-way ANOVA with Fisher's unprotected LSD test; *P<0.05, **P<0.001 represent comparisons between wt and db/db mice groups; #P<0.05 and ##P<0.001 indicate comparisons between time 0 and 120 mins within groups.

374.16 A.U., in comparison to female wt mice with AUC of 1256.13 ± 47.69 A.U. The AUC was significantly increased 2.1-fold and 2.5-fold to 2683.00 ± 178.55 A.U. and 3086.60 ± 50.96 A.U. for female db/db mice with Bg=10-15 mmol/L and Bg>15 mmol/L, respectively. Overall, a statistically significant 1.8-2.5-fold increase was observed in the AUC of db/db females compared to wt controls (**Figure 3.19(b)**), confirming that the db/db females were glucose-intolerant.

Female db/db mice in the mild and severely hyperglycaemic groups displayed increased fasting plasma insulin levels at 0 mins compared to wt mice; in contrast, db/db females in the normoglycaemic group showed similar insulin levels to wt mice (**Figure 3.19(c)**, **Table 3.4**). Plasma insulin levels were further increased in db/db mice compared to wt mice at time 60 mins and remained markedly higher over the time course. There was a trend for an increased plasma insulin AUC for db/db females with Bg<10 mmol/L (248.90 ± 17.60 A.U.), compared to wt females (146.20 ± 3.80 A.U.). AUC for db/db females with Bg=10-15 mmol/L (496.30 ± 41.90 A.U.) and Bg>15 mmol/L (404.83 ± 52.16 A.U.), were significantly higher than corresponding wt mice ($P<0.0001$; **Figure 3.19(d)**). These data indicate that female db/db mice were hyperinsulinaemic, consistent with previous studies (Kobayashi et al., 2000, Aasum et al., 2003).

Like male db/db mice (see Section 3.2.2), the failure to regulate blood glucose levels despite elevated plasma insulin in female db/db mice, confirmed the development of insulin resistance.

3.2.9 ER stress in isolated female db/db islets

ER stress markers were examined in islets isolated from female db/db mice. Comparative C_T analyses of ER stress related mRNAs in female db/db islets showed a 335.3-fold and 243.8-fold significant increase in the expression of the adaptive UPR makers BiP and P58, respectively (**Figure 3.20**; see Section 2.6). A significant 27.9-fold and 5.4-fold increase in the expression of the ER stress-associated pro-apoptotic markers CHOP and ATF3 respectively, was also observed (**Figure 3.20**). Similar to male db/db islets (see Section 3.2.3), this study demonstrated a dramatic increase in the expression of adaptive UPR genes relative to the increased expression of pro-apoptotic UPR genes. Thus, resembling male db/db mice (see Section 3.2.3), the overall increased expression of UPR genes

Table 3.4: Plasma insulin levels of wt and db/db female mice during ipGTT.

Time (mins)	Plasma insulin (ng/mL)¶			
	Wt	db/db		
		Bg<10 mmol/L	Bg=10-15 mmol/L	Bg>15 mmol/L
0	1.21 ± 0.06	1.54 ± 0.33	3.79 ± 0.65 (0.054)	3.58 ± 1.45 (0.07)
60	1.26 ± 0.11	2.36 ± 0.16*	4.30 ± 0.18**	3.79 ± 0.52**
120	1.15 ± 0.13	2.04 ± 0.02	4.14 ± 0.44**	2.32 ± 0.59 (0.06)

¶The data represent mean ± SEM with n= 3 female mice/group. One-way ANOVA with Fisher's unprotected LSD test; *P<0.05 and **P<0.001 represent comparisons between wt and db/db mice.

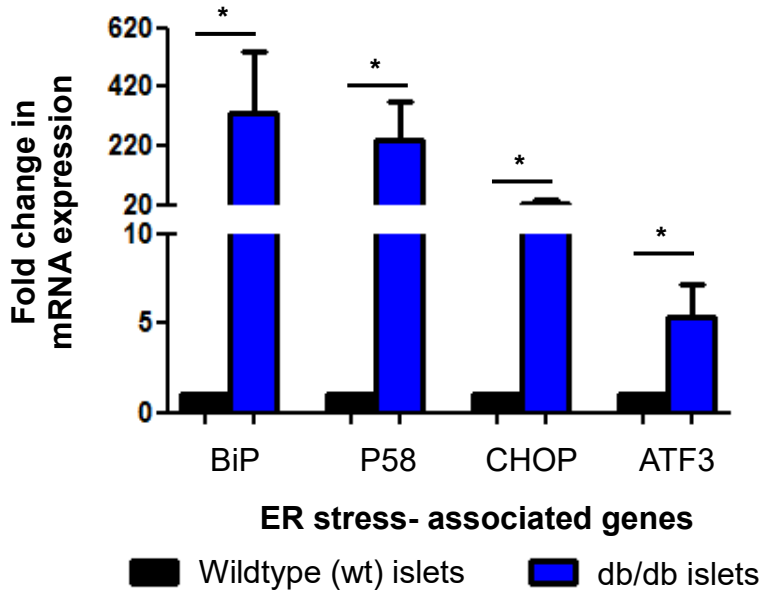

Figure 3.20: ER stress markers in female wt and db/db islets.

TaqMan real-time PCR was used to analyse mRNA expression of the ER stress-associated markers BiP, P58, CHOP and ATF3 in the islets of wt and hyperglycaemic db/db females (5-9 weeks). Comparative C_T using GAPDH gene expression as a reference for normalisation was used to compare transcript expression in db/db islets to wt controls. All ER stress-related genes were significantly upregulated in the islets of db/db donor females. The data show mean ± SEM for 4 independent experiments (n=230-341 islets/group). Mann-Whitney test; *P<0.05.

confirmed evidence of ER stress in the islets of hyperglycaemic db/db females at 5-9 weeks of age.

3.2.10 Expression of intra-islet HSPG core proteins in wildtype, heterozygous and db/db females

The intra-islet expression of three HSPG core proteins i.e., collagen type XVIII (Col18), syndecan-1 (Sdc1) and CD44 were analysed by immunohistochemistry and morphometry in the pancreas of female wildtype (wt), heterozygous (db/+) and db/db mice at 3, 4, 5, 6, 9, 12, 16 and 20 weeks of age (see Section 2.7). The sections were imaged and analysed as described in Chapter 2 (see Section 2.7.5).

Intra-islet staining for Col18 in female db/db donor pancreases at 3 weeks of age resembled corresponding wt islets (**Figure 3.21(a)**). In contrast, there was an early significant decline in Col18 expression at 4 weeks to 76.7% of wt islets. Thereafter, Col18 immunostaining progressively declined to 68.9%, 43.6%, 28.7% and 35.9% of wt islets at 5, 6, 9 and 12 weeks of age, respectively (**Figure 3.21(a)**). By 16 and 20 weeks of age, the Col18+ve islet area was only 15.2% and 26.4% of wt islets, respectively.

Analyses of the Sdc1+ve islet area in female db/db islets revealed a dramatic decrease to 32.8% and 46.3% of wt islets at 4 and 5 weeks of age, respectively ($P<0.001$; **Figure 3.21(b)**). Little, if any Sdc1 expression in db/db islets was observed from 6 weeks of age (1.3%-3.7% of wt controls; $P<0.001$).

The area of islet tissue that stained positively for CD44 in female db/db pancreases decreased markedly to 25.6% of wt control islets at 4 weeks of age (**Figure 3.21(c)**). The CD44 core protein staining was further reduced to 14.4%, 15.1% and 13.7% of control wt islets at 6, 9 and 16 weeks of age, respectively. Variability in the CD44+ve islet area observed in wt and/or db/+ islets at 5 week and 20 weeks was possibly due to biological variation in the limited sample size.

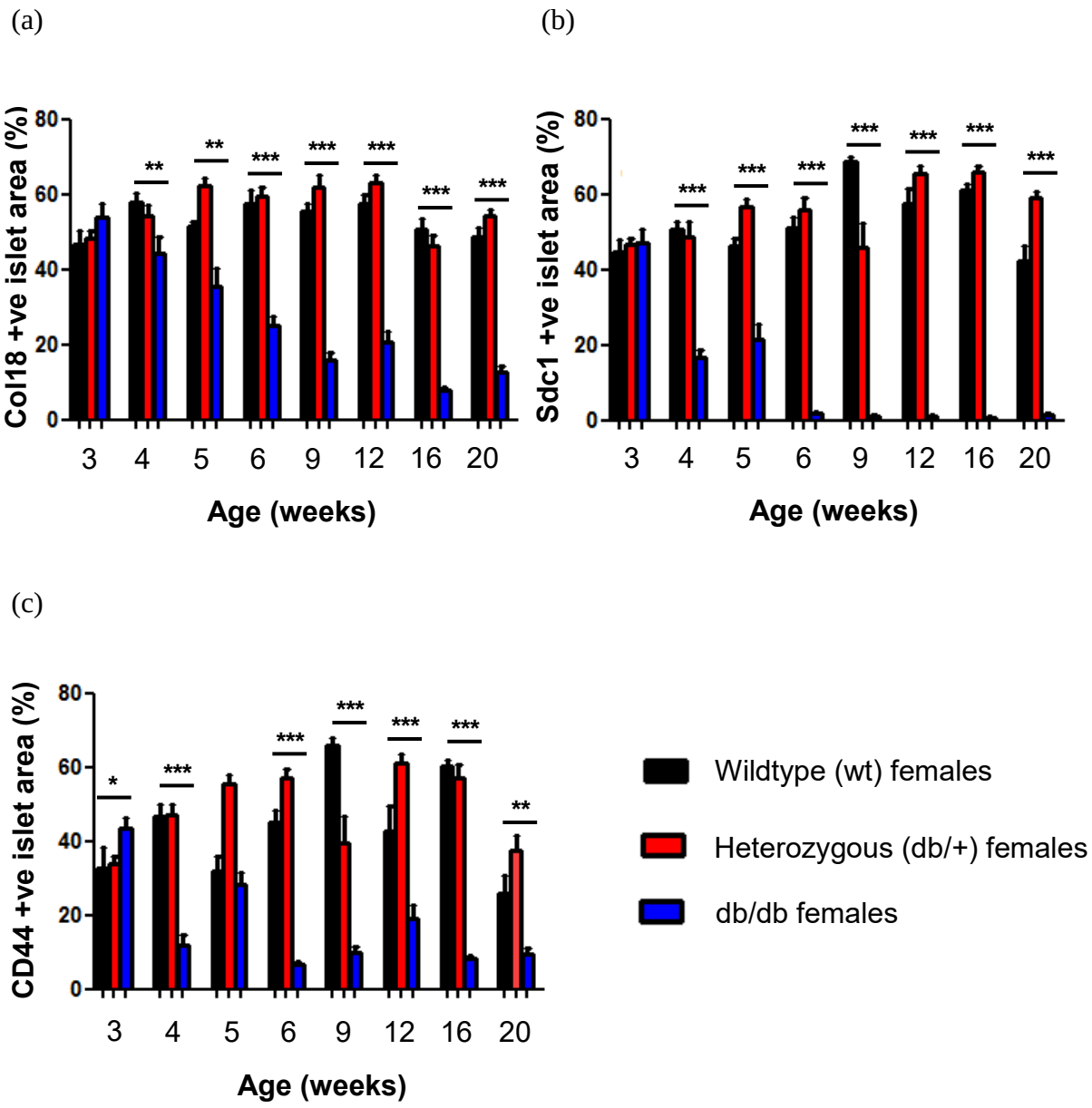

Figure 3.21: Intra-islet HSPG core protein expression in pancreases from female wt, db/+ and db/db mice at different age.

Intra-islet expression of HSPG core proteins was assessed in female wt, heterozygous (db/+) and db/db pancreases at 3, 4, 5, 6, 9, 12, 16, and 20 weeks of age by immunohistochemistry and morphometry. Data is presented as the % islet area showing positive staining for Col18 (a), Sdc1 (b) and CD44 (c). HSPG Core proteins were significantly reduced in female db/db islets from as early as 4 weeks of age. Data show mean ± SEM for 3 pancreases/age group with n=18-41 (Col18), n=16-43 (Sdc1) and n=16-35 (CD44) islets examined/group. One-Way ANOVA with Fischer's unprotected LSD test; *P<0.05, **P<0.01 and ***P<0.0001.

Female db/db mice therefore demonstrated a significant loss of intra-islet HSPG core proteins for collagen type XVIII, syndecan-1 and CD44 from 4-20 weeks of age, resembling the temporal changes observed in male db/db islets (see Section 3.2.4).

3.2.11 Insulin and glucagon localisation in female wt and db/db pancreatic islets

Pancreas sections of female wt and db/db mice were immunostained for insulin and glucagon and the intensity of the staining was quantified using Image J software with colour deconvolution plugin (see Section 2.7.5).

The intensity of insulin staining in female db/db islets was significantly increased 1.5-fold at 3 weeks of age and significantly decreased to 74.4% of wt controls by 6 weeks of age (**Figure 3.22(a)**). Intracellular insulin staining was significantly reduced further to 59.4%, 40.7%, 39.1% and 43.4% of corresponding wt controls by 9, 12, 16 and 20 weeks of age (**Figure 3.22(a)**). Hence, the intra-islet insulin was reduced in the pancreatic islets of female db/db mice from 6 weeks of age, i.e., prior to onset of non-fasting hyperglycaemia (**Figure 3.18**) and consistent with a mild level of insulinaemia (**Figure 3.19**).

There was no significant difference in the intensity of glucagon staining between wt and db/db islets except at 3-20 weeks of age, except at 4 weeks of age where a 1.4-fold increase in glucagon intensity was observed in db/db islets (**Figure 3.22(b)**). It is possible that this increase in glucagon expression could lead to a transient increase in secretion, gluconeogenesis and glycogenolysis and thereby contribute to hyperinsulinaemia and hyperglycaemia (Unger, 1971, Barbetti et al., 2016). In contrast, a previous study showed both an increased expression of glucagon+ve islet area as well as an increase in plasma glucagon levels in db/db mice, compared to heterozygous controls (Liu et al., 2011). This discrepancy could be due to differences in methodology and analysis; our immunohistochemical analysis is based on the intensity of intra-islet glucagon+ve staining whereas Liu et al. (2011) used immunofluorescence staining to analyse the glucagon+ve islet area.

(a)

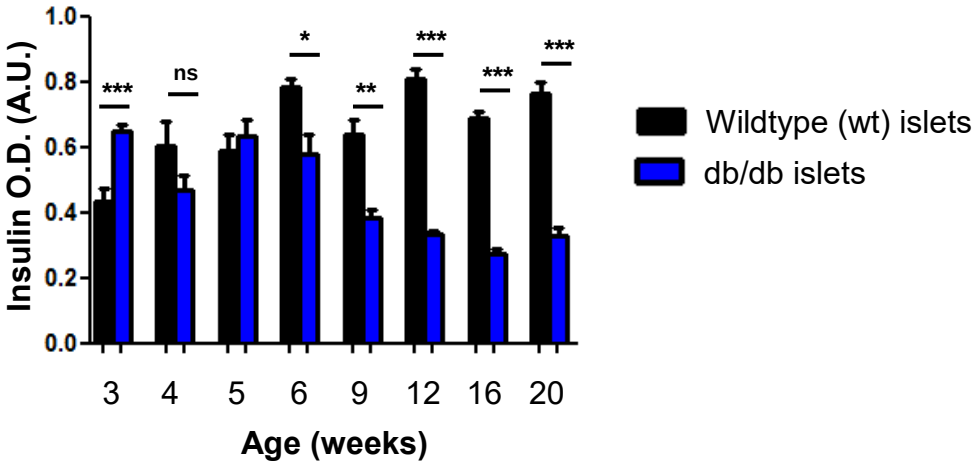

(b)

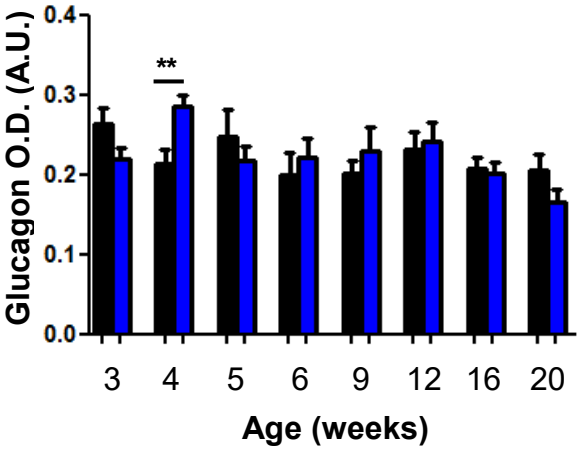

Figure 3.22: Insulin and glucagon expression in the islets of female db/db and wt mice at different ages.

The intensity (optical density (O.D.)) of immunostaining for (a) insulin and (b) glucagon was assessed in pancreas sections of female wt and db/db mice at 3-20 weeks of age by morphometry using Image J software with colour deconvolution plugin. (a) Insulin staining was significantly reduced by 6-9 weeks of age. (b) In general, glucagon expression in the islets was similar between wt and db/db mice at 3-20 weeks of age. The data represents the mean staining intensity ± SEM for 3 pancreases/age group with n=11-32 islets analysed/group (insulin) and n=8-26 islets analysed/group (glucagon). Unpaired t test and Mann-Whitney test; *P<0.05, **P<0.01, ***P<0.0001 and ns, not significant.

3.2.12 Analyses of islet area

The area of islets in pancreas sections of male and female wt and db/db mice was quantified using Image J software with colour deconvolution plugin (see Section 2.7.5).

Male db/db islets showed an initial significant increase in islet area at 4 weeks of age and a consistent increase from 6-20 weeks of age (**Figure 3.23(a)**). There was a 1.6-fold, 1.9-fold, 1.7-fold, 1.5-fold and 1.6-fold significant increase in islet area of db/db islets compared to corresponding wt controls at 4, 6, 9, 12 and 16 weeks of age, respectively. The 1.3-fold increase in the area of db/db islets at 5 weeks was not statistically significant. No significant difference was observed in the islet area of db/db males at 20 weeks of age (**Figure 3.23(b)**). Similar to male db/db islets, female db/db islets showed a significant 1.8-fold, 1.5-fold, 2.1-fold, 1.5-fold and 1.6-fold increase in the islet area compared to corresponding wt controls at 5, 9, 12, 16 and 20 weeks of age, respectively (**Figure 3.23**). A marked 1.4-fold increase in the area of islet of db/db mice was observed at 6 weeks of age compared to controls; however, this increase did not achieve statistical significance

Together, this data demonstrates that during the development of T2D in db/db mice, there is an expansion of islet mass to help maintain beta cell function, confirming previous studies (Prentki and Nolan, 2006, Dalbøge et al., 2013, Mezza et al., 2014).

3.2.13 ER stress in islets of young db/db mice

Immunohistochemistry analyses demonstrated loss of intracellular HSPG core proteins and HS in the islets of male and female db/db mice from an early age i.e., 3-4 weeks. To investigate whether the diminished levels of HSPG core proteins and HS could be due to ER stress-induced downregulation of proteins in beta cells, we examined the transcript levels of ER stress associated genes in the islets of 3.5-4.5-week old male db/db mice.

Islets were isolated from 3.5-4.5-week old heterozygous and db/db male mice. The mRNA was extracted using the RNeasy kit and cDNA was prepared (see Section 2.6). TaqMan real-time PCR was performed using commercially validated primer/probes to detect the expression of BiP (HSPA5), P58 (DNAJC3), CHOP (DDIT3), and ATF3 mRNAs (see Section 2.6.4), as markers of ER stress. The gene of interest was normalised

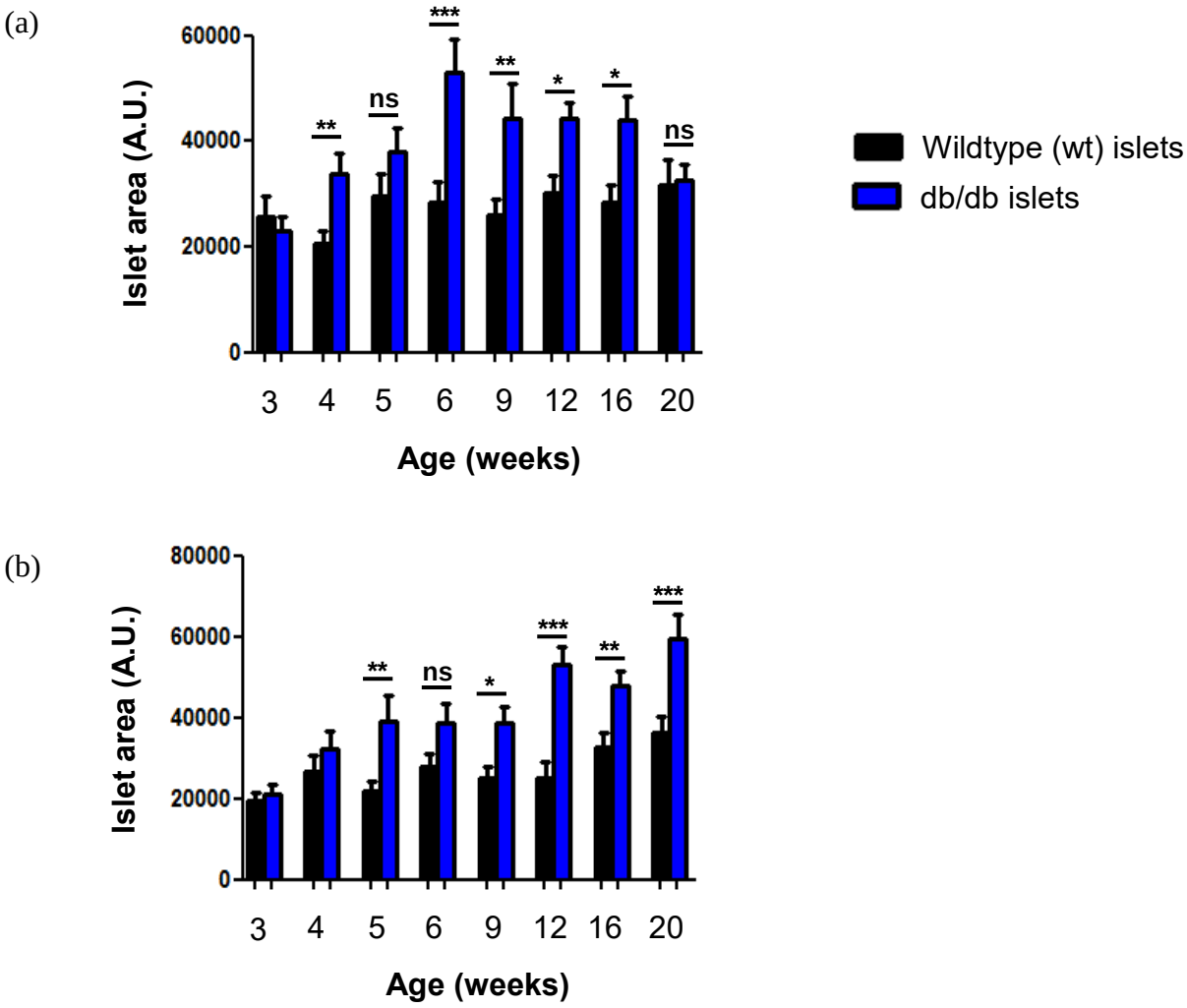

Figure 3.23: Quantification of islet area in male and female db/db and wt mice at different ages.

The area of islet tissue was analysed for both (a) male and (b) female db/db and wt mice at 3-20 weeks of age by morphometry using Image J software with colour deconvolution plugin. Male and female db/db islets showed increased islet area from at 4 weeks and 5 weeks of age, respectively. The data represents the mean ± SEM for 3 pancreases/age group with n=19-43 islets analysed/group (males) and n=14-37 islets analysed/group (females). Mann-Whitney test; *P<0.05, **P<0.01, ***P<0.001 and ns, not significant.

to a control house-keeping gene (GAPDH) and mRNA levels of db/db islets were quantified as a fold-change of their respective lean control (heterozygous db/+) islets.

Comparative C_T analyses showed a 15.9-fold ($P<0.05$), 12.9-fold, 3.8-fold and 3.5-fold increase in transcripts for BiP, P58, CHOP and ATF3, respectively, compared to controls (**Figure 3.24**). The significant ~16-fold increase in the early stress marker BiP, accompanied by a substantial ~13-fold increase in another early UPR gene P58, provide evidence for the induction of ER stress in the islets of normoglycaemic male db/db mice from as early as 3.5-4.5 weeks of age.

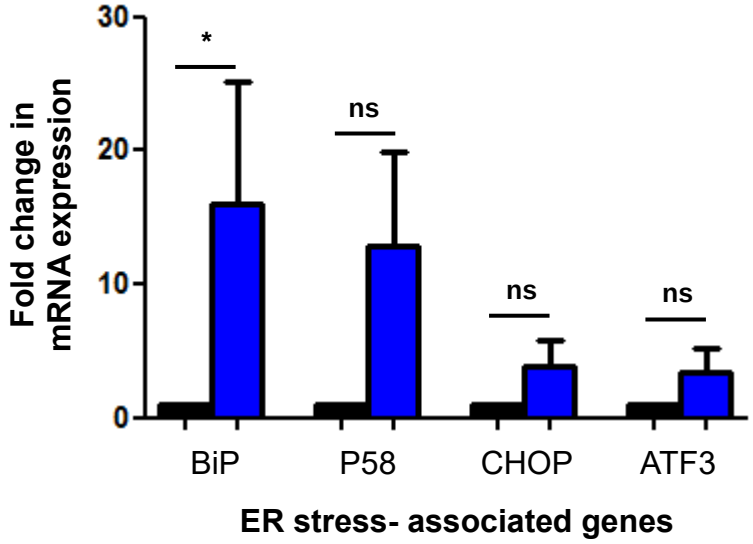

Figure 3.24: ER stress markers in male db/+ and db/db islets.

RNA extracted from islets isolated from 3.5-4.5 week old male heterozygous (db/+; black bars) and db/db (blue bars) mice was used to prepare cDNA; analysis of BiP, P58, CHOP and ATF3 transcripts was performed using TaqMan real-time PCR. Comparative C_T analysis employing GAPDH gene expression as a reference gene for normalisation, was used to compare db/db transcript expression to heterozygous controls. mRNA levels for the adaptive UPR markers BiP and P58 were highly upregulated in db/db islets from very young donors. The data show mean ± SEM for 4 independent experiments (120-350 islets/group per experiment). Mann-Whitney test; *P<0.05.

3.3 Discussion

The db/db mouse strain is a well-established model of obesity-induced type 2 diabetes (T2D) and has characteristics similar to human T2D. The db/db mice have a homozygous point mutation in the leptin receptor gene and as a result, overeat, develop obesity, insulin resistance and hyperglycaemia (Chan et al., 2011, Chen et al., 1996, Kobayashi et al., 2000, Do et al., 2016). In addition, db/db islets show a reduced number of glucose responsive beta cells and reduction in insulin exocytosis (Do et al., 2014). In fact, insulin exocytosis is restricted to only a small proportion of db/db beta cells (Low et al., 2014). Consistent with previous findings (Aasum et al., 2003, King, 2012, Kobayashi et al., 2000, Do et al., 2016), our study demonstrated that male and female db/db mice become obese and hyperglycaemic from the early age of 6-7 weeks (**Figures 3.1 and 3.18**). Male db/db mice were obese (1.5-fold heavier than corresponding wt controls) and hyperglycaemic (db/db, 19.63 ± 2.54 mmol/L vs wt, 7.76 ± 0.69 mmol/L) by 6 weeks of age whereas female db/db mice showed evidence of obesity (1.4-fold heavier than wt) by 6 weeks and were hyperglycaemic (db/db, 18.26 ± 3.17 mmol/L vs wt, 8.53 ± 0.49 mmol/L) by 7 weeks of age (**Figures 3.1 and 3.18**). These data indicate that male db/db mice develop hyperglycaemia before females. This is consistent with a previous study which reported that the onset of overt diabetes in male db/db mice precedes the onset of hyperglycaemia in female db/db mice (Aasum et al., 2003).

To further characterise and confirm the phenotype of our db/db mouse colony, we evaluated blood glucose and plasma insulin levels in wt and db/db mice in response to an intraperitoneal glucose tolerance test (ipGTT). Our data showed that male db/db mice were glucose-intolerant as they displayed consistently higher glucose levels at 30-120 mins during the ipGTT, correlating with a significantly increased glucose AUC compared to wt controls (**Figure 3.2(a, b)**). Furthermore, male db/db mice (5-9 weeks) in all three groups (normoglycaemic, mildly hyperglycaemic and severely hyperglycaemic) maintained increased insulin levels throughout the ipGTT compared to wt mice, confirming hyperinsulinaemia and insulin-resistance (**Figure 3.2(c)**). Although not statistically significant, the corresponding AUCs for the plasma insulin levels of normoglycaemic and mildly hyperglycaemic db/db males were 2.0-fold to 2.8-fold higher than wt control males (**Figure 3.2(d)**). However, severely hyperglycaemic db/db mice showed a significant 3.9-fold increase in the AUC for plasma insulin levels compared to

wt controls ($P<0.001$). Likewise, female db/db mice belonging to all three groups were glucose-intolerant and markedly insulin-resistant (**Figure 3.19**). Overall, increased blood glucose levels despite parallel increased plasma levels confirmed that both male and female db/db mice had impaired glucose tolerance due to insulin resistance.

Mouse and human islets compensate for mild insulin resistance by increasing insulin secretion (via an increase in both beta cell mass and beta cell function) (Prentki and Nolan, 2006, Dalbøge et al., 2013, Mezza et al., 2014, Saisho et al., 2013, Bernard-Kargar and Ktorza, 2001, Sone and Kagawa, 2005). Mezza et al. (2014) reported that the increase in the size of islets in insulin-resistant obese humans is due to beta cell hyperplasia (i.e., increased in number of beta cells). Other studies of male db/db mice showed an increase in beta cell area at 12 weeks of age and enhanced islet mass and beta cell proliferation at 10 weeks (but not by 24 weeks) (Dalbøge et al., 2013). Furthermore, the size of islets increased in prediabetic db/db mice, suggesting altered beta cell function (Do et al., 2016). Consistently, our study demonstrated an increase in islet area (islet size) in db/db pancreases during the development of T2D generally from 6 weeks of age (**Figure 3.23**).

Islet beta cells have a highly developed endoplasmic reticulum (ER) which is required for the folding, export and processing of newly synthesised insulin and other proteins including, HSPG core proteins (Choong et al., 2015). Disruption of chaperones which promote protein folding, inhibition of protein glycosylation, calcium depletion and certain mutations of proteins can disturb ER function and cause the accumulation of misfolded proteins in the ER lumen, a condition known as ER stress (Eizirik et al., 2008, Malhotra and Kaufman, 2007). ER stress in pancreatic beta cells can be induced by elevated free fatty acids and glucose, downstream read-outs of obesity and insulin resistance in type 2 diabetes. Prolonged ER stress initiates an adaptive programme called the unfolded protein response (UPR). This programme consists of three distinct reparative responses: translation attenuation, upregulation of ER chaperones and protein degradation via the proteasome. Collectively, these pathways relieve ER stress, help to maintain ER homeostasis and prevent cell death (Yoshida, 2007). In scenarios where the UPR fails to sufficiently counter the impact of ER stress, beta cell apoptosis is initiated. Each of these stages contributes to the pathogenesis of T2D (Laybutt et al., 2007). We therefore

evaluated the relationship between ER stress in the pancreatic islets of db/db mice to the levels of intracellular HSPGs and HS localised in beta cells.

Our data demonstrated a preferential upregulation of early adaptive UPR genes (BiP and p58) in the islets of young normoglycemic db/db mice at 3.5-4.5 weeks of age (**Figure 3.24**). This data confirms and extends a previous study showing increased BiP staining in the islets of db/db mice at 4 weeks (Sharma et al., 2015). Together these data suggest that the UPR is active from an early age in db/db beta cells. Moreover, quantitative PCR analysis of islets isolated from wt and hyperglycaemic db/db mice at 5-9 weeks of age showed the upregulated expression of both adaptive and pro-apoptotic UPR genes (**Figures 3.3 and 3.20**). Interestingly, the expression of adaptive UPR genes was higher than pro-apoptotic UPR genes, indicating that during this period of T2D development the majority of the beta cells were compensating for ER stress in order to remain viable (**Figures 3.3 and 3.20**). Our data is consistent with a previous report of increased mRNA expression of ER stress-associated adaptive (BiP, P58, Erp72, Fkbp11 and Grp94) and deleterious/pro-apoptotic (ATF3, CHOP and Trib3) UPR genes in prediabetic db/db mice at 6 weeks of age (Chan et al., 2013). In addition, ER stress has been demonstrated previously in db/db islets at 4-16 weeks of age (Kjørholt et al., 2005, Laybutt et al., 2007, Chan et al., 2015, Eizirik et al., 2008, Sharma et al., 2015). Furthermore, in humans with T2D, immunostaining showed increased intra-islet expression of CHOP, BiP and P58 proteins, compared to healthy controls (Marchetti et al., 2007, Laybutt et al., 2007). Our study therefore corroborated the induction of ER stress in islet beta cells of db/db mice.

Previous studies have identified the presence of several HSPGs in mouse islets. Takahashi et al (2009) reported mRNA expression for syndecans 2-4, glypican 1 and 4, perlecan, agrin and collagen type XVIII in 8 week old ICR (Swiss Albino) mouse islets; however, no intra-islet expression was observed for syndecan-1 or other glypicans (2, 3, 5, and 6). In another study, syndecan-4 expression was observed in islets isolated from adult male C57BL/6 mice (10-12 weeks of age) by immunofluorescence but not for syndecan-1, glypican, agrin or collagen type XVIII (Cheng et al., 2012a). This disparity in the detection of HSPG core proteins can be attributed to different antibodies and staining techniques. Recently, the Simeonovic lab identified the presence of two full time HSPGs i.e., collagen type XVIII and syndecan-1 as well as the part-time HPSG CD44 in C57BL/6

islets *in situ* and after isolation (Choong et al., 2015). Therefore, this project focused on collagen type XVIII, syndecan-1 and CD44 and the temporal changes in their intra-islet (beta cell) expression during T2D development in db/db mice.

Our study showed that the HSPG core proteins collagen type XVIII, syndecan-1 and CD44 were strongly expressed in wildtype and heterozygous islets at 3-20 weeks of age (**Figures 3.6, 3.8, 3.10 and 3.21**). Furthermore, previous studies of mouse and human islets have indicated that HSPG expression is localised in the beta cell population (Choong et al., 2015, Simeonovic et al., 2018).

A significant loss of HSPG core protein expression for Col18, Sdc1 and CD44 was observed in male db/db mice as early as 3-4 weeks of age, with levels declining to ~40-57% of normal wt controls by 4-5 weeks (**Figures 3.6, 3.8 and 3.10**). Similarly, the islets of female db/db mice demonstrated significant depletion of Col18, Sdc1 and CD44 core proteins by 4 weeks of age, with a striking progressive loss to 26%-46% of normal wt islets by 4-6 weeks (**Figure 3.21**). Interestingly, Sdc1 and CD44 showed more rapid decline than Col18 in db/db islets. This asynchrony could be due to a shorter half-life for Sdc1 and CD44, compared to collagen type XVIII. Whereas rat glomerulus basement membrane collagens have been shown to have very slow turnover *in vivo* i.e., half-life of > 100 days (Beavan et al., 1989), pulse chase experiments have revealed a rapid half-life of ~ 3-5 hours for other HSPGs in baby hamster kidney cells, glomerulus basement membrane and rat granulosa cells (Bretscher, 1985, Yanagishita and Hascall, 1984, Beavan et al., 1989, Marshall, 2016). Throughout the remainder of the observation period (9-20 weeks) the levels of HSPG core proteins fell profoundly in db/db male islets to 18%-41% at 9 weeks and 7.5-15% by 20 weeks (**Figures 3.6, 3.8 and 3.10**). Generally, a more sustained depletion to 2%-15% of normal controls was observed in female db/db islets at 9-20 weeks of age (**Figure 3.21**). Overall, the marked depletion of islet HSPGs commences at an early age in db/db mice before the onset of non-fasting hyperglycaemia and prior to or in parallel with significant loss of insulin in islet beta cells (**Figures 3.15 and 3.21(a)**). This finding together with the absence of glucagon depletion in islets alpha cells (**Figures 3.17 and 3.21(b)**) further supports the conclusion that the observed modulation of HSPG expression is occurring in islet beta cells.

Overall, HSPG core proteins were highly expressed intracellularly in beta cells of wt islets and were progressively depleted in the beta cells of db/db mice during the development of T2D. The localisation of HSPGs *inside* beta cells is unique because HSPGs are normally expressed on the cell surface or in BMs and/or ECM (Sarrazin et al., 2011).

Collagen type XVIII contains an endostatin fragment which is derived from the C-terminal NC domain. Collagen type XVIII exhibits anti-angiogenic activity through the endostatin domain and inhibits angiogenesis and tumour growth (Marneros and Olsen, 2005). However, the role of collagen type XVIII core protein in beta cells is unclear. Knock-out models of collagen type XVIII did not show abnormalities in the pancreas, a finding which could be due to other HSPG core proteins substituting for the lost core protein (Sarrazin et al., 2011).

Syndecans play a critical role in pathological processes by interacting with a wide range of ligands. Altered expression of syndecan has been observed in autoimmune disorders, cancer, HIV infection and other pathophysiological conditions (Tkachenko et al., 2005, Beauvais and Rapraeger, 2004, Agere et al., 2018). Cells surface syndecan-1 regulates cell adhesion, migration, proliferation, invasion, cell mobility and cellular signalling (Ramani et al., 2012, Elenius and Jalkanen, 1994, Zimmermann and David, 1999). *In vivo* studies have provided evidence that syndecan-1 plays a role in the clearance of lipoprotein and uptake by hepatocytes (Stanford et al., 2009). During diabetes development, it has been found that insulin promotes shedding of syndecan ectodomains, suggesting a link between insulin signalling and syndecan-mediated pathological processes (Reizes et al., 2006). A study by Cheng et al. (2012) demonstrated that intracellular syndecan-4 expression is present in mouse and rat islets as well as MIN6 cells, and with localisation to insulin positive cells but not glucagon positive cells. Recently, silencing of syndecan-4 in MIN6 cells resulted in impaired insulin secretion whereas overexpression of syndecan-4 ameliorated insulin secretion (Takahashi et al 2017). Based on these studies, it is therefore possible that intracellular syndecan-1 might play diverse roles in beta cells.

CD44 is a part-time HSPG because it displays HS chains under special circumstances. The CD44v3 is the only isoform that carries HS chains. The expression of cell surface CD44 was markedly enhanced in inflammatory renal diseases such as lupus nephritis and

anti-BM glomerulonephritis (Rops et al., 2004). Macrophages express CD44 on their cell surface and regulate growth factor action during inflammation (Jones et al., 2000). Previously, CD44 deficiency in HFD-fed C57BL/6J diabetic mice reduced immune cell infiltration in adipose tissue and improved insulin sensitivity (Kodama et al., 2012). Furthermore, Kang et al. (2013) showed that HFD-fed CD44 KO (C57BL/6J) mice have reduced susceptibility to hepatic steatosis, adipose tissue inflammation, glucose intolerance and insulin resistance. This study also revealed levels of FFA genes involved in synthesis and transport (Fasn and CD36) were reduced in CD44 KO mice (Kang et al., 2013). Additional, a recent study further revealed that CD44-expressing wildtype (female NOD) beta cells are susceptible to apoptosis whereas CD44 deficient beta cells are relatively protected (Assayag-Asherie et al., 2015). Depletion of all forms of CD44 in MIN6 cells via RNA interference improved insulin secretion and the insulin content of beta cells, suggesting that CD44 variants may inhibit insulin secretion (Kobayashi et al., 2018).

HSPGs in normal beta cells could act as intracellular reservoir for growth factors and chemokines and/or function in insulin secretion, glucose metabolism, gene transcription and homeostasis (Choong et al., 2015). The loss of core proteins in db/db beta cells could therefore contribute to reduced insulin secretion, hyperglycaemia and thus T2D. The glycosaminoglycan, HS, is synthesised directly on to HSPG core proteins in the Golgi subcellular compartment. Normally, when localised in BMs and ECM, HS interacts with a wide range of bioactive molecules such as growth factors, cytokines, chemokines, proteases and cell adhesion molecules and also helps to maintain cell integrity and function (Parish, 2006). Having observed the unusual intracellular localisation of HS in islet beta cells, Ziolkowski et al. (2012) demonstrated that HS is essential for beta cell survival and serves as a constitutive antioxidant. Thus, in view of the rapid and extensive depletion of HSPG core proteins in db/db islets during T2D development, we also examined the intra-islet expression of HS.

The expression of intra-islet HS was assessed using two antibodies, 10E4 anti-HS mAb and HepSS-1 anti-HS mAb. The anti-10E4 mAb reacts with highly sulfated HS, specifically to N-acetylated and N-sulfated glucosamine residues of HS and O-sulfated groups. On the other hand, HepSS-1 anti-HS mAb reacts with an epitope of N-sulfated

disaccharides with reduced O-sulphation (van den Born et al., 2005, Ziolkowski et al., 2012, Theodoraki et al., 2015, Simeonovic et al., 2018, Takahashi et al., 2009, Takahashi et al., 2012). HS is selectively localised in islet cell populations i.e., highly sulfated HS is observed in beta cells while under-sulfated HS is found in alpha cells (Theodoraki et al., 2015, Simeonovic et al., 2018, Ziolkowski et al., 2012). These properties correlate with the differential expression of three HS modifying enzymes i.e., heparan sulfate 6-O sulfotransferase 1 (HS6ST1), sulfatase 1 (SULF1) and sulfatase 2 (SULF2); HS6ST1 was highly expressed in the INS1 beta cells whereas SULF1 and SULF2 were abundantly present in aTC1-6 alpha cells (Theodoraki et al., 2015). These data showed an absence of 6-O sulfate groups in aTC1-6 cells compared to INS1 beta cells, suggesting beta cells express highly sulfated HS whereas alpha cells express under-sulfated HS.

As expected, wt db mice displayed high levels of intra-islet HS. This is consistent with previous reports that HS is expressed in neonatal islets and BALB/c mouse beta cells (Takahashi et al., 2009, Ziolkowski et al., 2012). We have now demonstrated by immunohistochemistry and morphometry, a progressive loss of HS in db/db islet beta cells, compared to wt islets. The decline in intracellular HS in db/db islets using 10E4 mAb was observed as early as 4 weeks of age at which time HS was reduced to ~69% of controls (**Figure 3.13(a)**). Thus, db/db beta cells underwent early loss of highly sulfated HS. Intra-islet HS levels were further reduced to 48% of controls by 9 weeks of age (**Figure 3.13(a)**). In comparison, immunostaining with HepSS-1 mAb showed that loss of under-sulfated HS in db/db islets was delayed until 6 and 9 weeks of age (**Figure 3.13(b)**).

Our study revealed that highly sulfated HS detected by 10E4 mAb was intense in normal wt (+/+) beta cells. This finding supports previous findings that highly sulfated HS is expressed in the beta cells of rodents and human islets (Ziolkowski et al., 2012, Simeonovic et al., 2018) and acts as a constitutive non-enzymatic quencher of reactive oxygen species (ROS). Replacement of HS using heparin (a highly sulfated HS analogue) preserved the viability of beta cells in *vitro* and protected the beta cells from culture- and hydrogen peroxide-induced beta cell death (Ziolkowski et al., 2012). These findings identified a critical role for HS in the survival of beta cells. HS staining with HepSS-1 mAb (which identifies under-sulfated HS) was observed more strongly at the periphery

of islets i.e., in alpha cells, and was found at moderate levels throughout the remaining islet cell mass i.e., in beta cells. These findings support the report by Theodoraki et al. (2015) that highly sulfated HS is present in beta cells and less-sulfated HS is prominent in alpha cells. Our study showed the loss of highly sulfated HS in db/db beta cells but no apparent loss of under-sulfated HS from alpha cells. Our lab has previously reported that the depletion of highly sulfated HS during islet isolation led to beta cell death *in vitro* (Ziolkowski et al., 2012). Furthermore, Theodoraki et al. (2015) demonstrated that HS desulfation rendered beta cells vulnerable to oxidative damage, supporting the report by Ziolkowski et al. (2012) that HS plays a critical role in protecting the beta cells from hydrogen peroxide-induced death. Beta cell proliferation was also reduced when INS-1 beta cells were incubated with sodium chlorate (a competitive inhibitor of 3'-phosphoadenosine 5'-phosphosulfate) which prevents 2-O and 6-O sulfation (Theodoraki et al., 2015). Collectively, these findings highlight the crucial role for intracellular highly sulfated HS in beta cell survival.

Taken together, our study has demonstrated strong intracellular expression of HSPG core proteins correlating with insulin expression in the beta cells of wildtype (+/+) mice. This property correlated with high levels of intracellular HS in islet beta cells. In contrast, a significant reduction of both HSPG core proteins and insulin, but not glucagon, was found in the islets of db/db mice during T2D development. The depletion of HSPG core proteins in db/db islets was accompanied by a significant reduction in intracellular HS in db/db beta cells. This finding is consistent with the absolute requirement of HSPG core proteins for HS synthesis (see Section 1.13) i.e., without HSPG core proteins, HS chain initiation and polymerisation cannot occur. Furthermore, the decline in HSPG core proteins and HS in db/db beta cells was observed before the mice became hyperglycaemic. These findings indicated that the trigger responsible for initiating the loss of HSPG core proteins and HS in young 3-4 week old mice was independent of non-fasting hyperglycaemia.

Beta cell dysfunction/death in T2D is generally attributed to glucotoxicity (see Section 1.7) and lipotoxicity (see Section 1.8). Briefly, chronic exposure of beta cells to high glucose levels reduces the expression of GLUT2, glucokinase and voltage-dependent calcium ion channels involved in GSIS *in vivo* and *in vitro* (Weir et al., 2001, Kaiser et al., 2003). Whereas exposure to free fatty acids (FFAs) stimulates insulin secretion,

prolonged exposure to elevated FFAs causes a reduction in GIIS (*in vitro* and *in vivo*) and beta cell apoptosis (Zhou and Grill, 1994, Shimabukuro et al., 1998, Cnop et al., 2005). A study by Laybutt et al. (2007) provided pivotal evidence that ER stress-induced beta cell apoptosis/ failure contributes to the pathogenesis of T2D. In that study, palmitate-treated MIN6 cells, T2D-db/db islets and human T2D islets showed increased mRNA expression for ER stress-associated genes (ATF4, CHOP, BiP and P58) which correlated with increased beta cell apoptosis (Laybutt et al., 2007). It is now well-recognised that ER stress can cause beta cell failure and play a critical role in T2D (Chan et al., 2013, Eizirik et al., 2008, Scheuner and Kaufman, 2008, Fonseca et al., 2011). Additionally, a complex relationship between UPR/ER stress and oxidative stress has been identified in beta cells (Song et al., 2008, Cunha et al., 2008b, Chan et al., 2013, Malhotra and Kaufman, 2007, Hasnain et al., 2016).

Beta cells undergo high levels of ER stress due to their normal secretory function (Araki et al., 2003, Eizirik et al., 2008). In response to high glucose levels, beta cells increase the synthesis of proinsulin and other secretory proteins. Following transfer to the ER, disulfide bonds are formed and correct folding of the proteins take place (Eizirik and Cnop, 2010). The increase in protein synthesis and maturation eventually induces ER stress in beta cells. To cope with this stress, beta cells activate the adaptive responses known as the unfolded protein response (UPR) which detects misfolded proteins in the ER. The three main ER sensors are IRE1, eIF2a-PERK and ATF6 (see Section 1.9). Their activation decreases the synthesis of new proteins in the ER, increases the folding capacity of the ER (by increasing the synthesis of ER chaperones) and removes misfolded proteins. When the UPR fails to maintain ER homeostasis, beta cells undergo apoptosis.

Studies by Chan et al. (2013) and Sharma et al. (2015) using immunostaining and PCR demonstrated ER stress in beta cells of db/db mice as young as 4-6 weeks of age. Furthermore, increased beta cell proliferation was observed in the presence of mild UPR activation and was reduced at 11-14 weeks of age during beta cell loss (Sharma et al., 2015). This finding suggested that mild UPR activation contributes to beta cell proliferation. These studies provide evidence that ER stress represents an early response to obesity and maintains homeostasis in beta cells. ER stress in db/db beta cells down-regulates mRNA expression to reduce general protein synthesis (Chan et al., 2013). ER

stress in the islets of ob/ob (leptin deficient) mice, which are obese and insulin resistant but do not develop diabetes, led to increased expression of adaptive UPR genes (BiP, P58, Erp72, Grp94 and Fkbp11) but not pro-apoptotic genes (ATF3, ATF4, CHOP, Trib3) at 6 and 16 weeks of age (Chan et al., 2013). The increase in adaptive UPR genes correlated with increased beta cell mass and function. Similarly, zucker rats and zucker diabetic fatty rats as well as HFD-fed mice showed increased expression of adaptive UPR markers compared to controls (Omikorede et al., 2013, Hasnain et al., 2014, Herbert and Laybutt, 2016). In contrast, db/db (leptin receptor deficient) mice, demonstrated significant upregulation of UPR genes in prediabetic db/db mice at 6 weeks of age (Chan et al., 2013). Reduced expression of the adaptive UPR and increased expression of the pro-apoptotic factor ATF3 at 16 weeks of age, correlated with reduced expression of islet-associated transcription factors and genes that optimise beta cell function in db/db mice. This study provided convincing evidence that upregulation of adaptive UPR genes provides protection from beta cell failure whereas an increase in pro-apoptotic UPR genes results in beta cell dysfunction and death.

ATF6 plays an anti-apoptotic role in ER stress (see Section 1.9.3.2). Studies have shown that reduced levels of ATF6 in ob/ob mice, HFD-mice and T2D human islets correlates with beta cell death (Engin et al., 2013), suggesting that ATF6 levels could be used as a marker for beta cell death. Interestingly, similar mRNA levels of ATF6 have been reported in db/db islets at 10-12 weeks of age compared to heterozygous controls (Laybutt et al., 2007). We propose that ATF6 protein expression in the islets of db/db mice at different ages could be determined by immunohistochemistry and western blotting to clarify the role of ATF6 during T2D development relative to other markers of ER stress and to the loss of HSPG protein expression. It is possible that a decline in ATF6 expression may more closely parallel HSPG and HS loss in db/db islets than other ER stress markers.

In our study we confirmed the induction of ER stress in the islets of db/db male and female mice at 3.5-4.5 weeks (normoglycaemic) and 5-9 weeks (hyperglycaemic). We propose that ER stress in db/db beta cells directly induces loss of intracellular HSPG core proteins which in turn results in depletion of beta cell HS. Intracellular HS has been reported to

play a critical role in protecting beta cells from oxidative damage (Ziolkowski et al., 2012). Furthermore, db/db islets at 6-20 weeks of age have been reported to show increased expression of antioxidant genes, suggesting that oxidative stress in the beta cells is enhanced (Chan et al., 2013, Hasnain et al., 2014). We therefore propose that early loss of HSPG core proteins and HS contributes to beta cell stress in T2D. Without HS, db/db beta cells are more highly susceptible to oxidative damage, beta cell failure/death and T2D.

In summary:

- Our data confirmed that db/db mice in our holding colony develop obesity, hyperglycaemia, glucose intolerance and insulin resistance.
- Our study demonstrated that islet beta cells of db/db mice exhibit ER stress as early as 3.5-4.5 weeks of age and confirmed the presence of ER stress-associated genes in hyperglycaemic db/db mice.
- We demonstrated a previously unrecognised loss of HSPG core proteins (collagen type XVIII, syndecan-1 and CD44) and HS in db/db islet beta cells during the development of T2D.
- The loss of HSPG core proteins and HS are consistent with the downstream effects of ER stress. This novel finding is further explored in Chapter 4 in the context of ER stress in heterozygous $Ins2^{WT/C96Y}$ Akita mice and pharmacologically-induced ER stress in MIN6 and primary beta cells.

Chapter 4: Loss of HS and HSPG core proteins in ER-stressed beta cells

4.1 Introduction

In Chapter 3, the pancreatic islets of male and female db/db mice over 3-20 weeks of age displayed a significant loss of intracellular heparan sulfate (HS) and heparan sulfate proteoglycan (HSPG) core proteins, collagen type XVIII, syndecan-1 and CD44, compared to age-matched lean wildtype mice. The loss of intracellular HS and HSPG core proteins in islet beta cells was observed before the mice exhibited obesity and hyperglycaemia. Additionally, we observed an upregulation of ER stress-associated genes in db/db islets, indicating that ER stress is an intrinsic property of db/db beta cells. These findings suggested that the sustained reduction in intracellular HS in islet beta cells could be due to impaired synthesis of HSPG core proteins, resulting from ER stress. To further test this hypothesis, the pancreatic islets of Akita mice were analysed at 4-9 weeks of age. In addition, MIN6 and primary beta cells were analysed after treatment with exogenous ER stress inducers *in vitro*.

The Akita mouse is a C57BL/6 mutant mouse strain discovered by Yoshioka et al. (1997; see Section 2.1.2). Both homozygous and heterozygous Akita mice spontaneously develop hyperglycaemia and display reduced beta cell mass but neither insulitis nor obesity (Wang et al., 1999, Matsuda et al., 2010, Kayo and Koizumi, 1998). Both mice and rats contain two functional insulin (*Ins*) genes, insulin gene 1 (*Ins1*) and insulin gene 2 (*Ins2*), with the latter resembling the human insulin gene (Schoeller et al., 2012, Shiao et al., 2008). Akita mice exhibit a mutation in the insulin gene 2 (*Ins2*) where a cysteine residue is replaced by tyrosine (Cys 96 Tyr; C96Y) (Wang et al., 1999). This mutation disrupts a disulfide bond normally formed between the A and B chains of proinsulin protein. As a consequence, the proinsulin protein undergoes a marked conformational change and misfolded proinsulin accumulates in the ER causing ER stress (see Section 2.1.2) (Ron, 2002b, Wang et al., 1999). The induction of ER stress-associated pro-apoptotic factor CCAAT/enhancer binding protein homologous protein (CHOP) and subsequent pancreatic beta cell apoptosis leads to reduced insulin production (Oyadomari et al., 2002b) and the rapid onset of hyperglycaemia. The Akita mouse therefore serves as a useful model of ER stress-mediated diabetes.

Both homozygous and heterozygous mutations in the *Ins2* gene cause a diabetic phenotype (see Section 2.1.2). Homozygous Akita mice are severely hyperglycaemic by

3 weeks of age and have a life span of 8-12 weeks. Additionally, the mutant mice are infertile, with male Akita mice exhibiting testicular atrophy by 5 weeks of age (Schoeller et al., 2012). In contrast, heterozygous Akita mice reproduce successfully and exhibit progressive hyperglycaemia, hypoinsulinaemia, polydipsia and polyuria, resulting in severe diabetes. In this project, we studied the effects of ER stress on beta cell HSPGs/HS in heterozygous Akita mice ($Ins2^{WT/C96Y}$) produced by interbreeding between wildtype C57BL/6 females ($Ins2^{WT/WT}$) and heterozygous $Ins2^{WT/C96Y}$ males (see Section 2.1.2).

In parallel, we used the MIN6 beta cell line to further test whether the induction of ER stress directly results in the loss of beta cell HSPGs/HS. The MIN6 beta cell line originated from an insulinoma derived from a transgenic C57BL/6 mouse expressing an insulin promotor/T-antigen construct (see Section 2.4.2). MIN6 cells express high levels of glucose transporter 2 (GLUT2) with low levels of GLUT1 and glucokinase (Miyazaki et al., 1990). Glucose enters pancreatic beta cells via GLUT2, resulting in an increase in the ATP/ADP ratio; this causes membrane depolarisation via closure of K_{ATP} channels which stimulates insulin secretion (see Section 1.3.2). Previous studies have shown that MIN6 beta cells display characteristics of normal primary beta cells including insulin secretion in response to glucose and other secretagogues (e.g., potassium chloride and L-arginine) (Ishihara et al., 1993, Miyazaki et al., 1990, Cheng et al., 2012b). MIN6 cells are therefore a useful surrogate for normal beta cells and studies of glucose-stimulated insulin secretion (GSIS).

The endoplasmic reticulum (ER) plays a major role in the maturation of newly synthesised proteins by regulating proper protein folding and post-translational modifications such as glycosylation and disulfide bond formation (see Section 1.9). ER stress can be induced by disturbances in the ER environment such as calcium homeostasis, redox status or ER function such as glycosylation and transportation to the Golgi complex (Eizirik et al., 2008, Yoshida, 2007). Previous studies have shown that ER stress can be induced in MIN6 cells by physiological metabolites (e.g., palmitate) and pharmacological ER stress agents such as thapsigargin, tunicamycin, brefeldin A and dithiothreitol (Oslowski and Urano, 2011, Laybutt et al., 2007). Thapsigargin is an inhibitor of the sarcoplasmic/endoplasmic reticulum Ca^{2+} ATPase (SERCA) pump and impairs calcium homeostasis in the ER by depleting ER calcium stores (see Section 1.9.6). Tunicamycin

suppresses N-linked glycosylation in the ER and brefeldin A inhibits protein transport from the ER-to-Golgi apparatus (see Section 1.9.6) (Dorner et al., 1990, Klausner et al., 1992). Palmitate, a saturated free fatty acid, causes depletion of ER Ca^{2+} in beta cells via translocon (Cassel et al., 2016) and hampers ER-to-Golgi protein trafficking, contributing to a build-up of protein in the ER (see Section 1.9.6). The chemical dithiothreitol impairs disulfide bond formation and causes abnormal protein folding, resulting in the accumulation of misfolded proteins in the ER and ER stress (Araki et al., 2003). Failure to restore homeostasis due to persistent, chronic ER stress can ultimately result in cell death due to apoptosis (Patil and Walter, 2001). In this study, we investigated the effects on intracellular HSPGs/HS in MIN6 beta cells induced by two pharmacological (thapsigargin and tunicamycin) ER stress-inducing agents and one physiological (palmitate) inducer.

The first part of this chapter characterises the development of hyperglycaemia in male and female $Ins2^{WT/C96Y}$ mice. In addition, ER stress was evaluated in the islets of $Ins2^{WT/C96Y}$ mice at 5-12 weeks of age by real-time RT-PCR. In parallel, the levels of intracellular HSPG core proteins and HS in both male and female $Ins2^{WT/C96Y}$ Akita and $Ins2^{WT/WT}$ mice were investigated by immunohistochemistry. In the second part of this chapter we used flow cytometry analyses to investigate the levels of intracellular and cell surface HSPG core proteins and HS in MIN6 beta cells with and without treatment with thapsigargin, tunicamycin or palmitate. In parallel, the levels of intracellular heparanase (Hpse) and cell death were also examined by flow cytometry. Finally, the third part of this chapter investigates the intracellular levels of HSPG core proteins, HS and Hpse in thapsigargin-treated primary beta cells.

4.2 Results

4.2.1 Characterisation of islet HSPG and HS in Akita mice

4.2.1.1 Development of hyperglycaemia in $Ins2^{WT/C96Y}$ mice

The non-fasting blood glucose levels of male and female $Ins2^{WT/WT}$ and $Ins2^{WT/C96Y}$ mice were measured from tail bleeds at 4, 5, 6 and 9 weeks of age (see Section 2.2.1) to ascertain the kinetics of diabetes development.

The mean non-fasting blood glucose levels of male $Ins2^{WT/WT}$ mice at 4 weeks of age was 9.26 ± 1.00 mmol/L, whereas male $Ins2^{WT/C96Y}$ mice showed a significantly 2.1-fold higher blood glucose level of 19.08 ± 1.33 mmol/L ($P<0.05$; **Figure 4.1(a)**). The mean non-fasting blood glucose level in the $Ins2^{WT/C96Y}$ mice progressively increased to 28.0 ± 0.00 mmol/L by 9 weeks of age, representing a 2.6-fold increase over corresponding age-matched control $Ins2^{WT/WT}$ males. Male $Ins2^{WT/C96Y}$ mice were therefore hyperglycaemic by 4 weeks of age.

Similarly, compared to corresponding $Ins2^{WT/WT}$ females, female $Ins2^{WT/C96Y}$ mice showed a 1.6-2.4-fold elevation in their mean non-fasting blood glucose levels from 4-9 weeks of age (**Figure 4.1(b)**). The mean non-fasting blood glucose levels in $Ins2^{WT/C96Y}$ females were 15.13 ± 0.87 mmol/L (vs $Ins2^{WT/WT}$, 9.72 ± 0.55 mmol/L), 16.53 ± 2.07 mmol/L (vs $Ins2^{WT/WT}$, 10.60 ± 1.53 mmol/L), 21.00 ± 3.47 mmol/L (vs $Ins2^{WT/WT}$, 8.85 ± 0.51 mmol/L) and 17.80 ± 2.11 mmol/L (vs $Ins2^{WT/WT}$, 9.10 ± 0.41 mmol/L) at 4, 5, 6 and 9 weeks of age, respectively. Hence, female $Ins2^{WT/C96Y}$ mice were hyperglycaemic by 4 weeks of age.

Based on these observations, both male and female $Ins2^{WT/C96Y}$ mice demonstrated hyperglycaemia as early as 4 weeks of age. Strikingly, male $Ins2^{WT/C96Y}$ mice exhibited more severe hyperglycaemia compared to female $Ins2^{WT/C96Y}$ mice.

4.2.1.2 ER stress is exhibited in male $Ins2^{WT/C96Y}$ islets

Islets were isolated from 5-12 week old male $Ins2^{WT/WT}$ and $Ins2^{WT/C96Y}$ mice (see Section 2.3) and snap frozen for RNA extraction (see Section 2.6). The islets were examined for the expression of the ER stress markers BiP (also known as HSPA5, GRP78), P58 (also known as DNAJC3), CHOP (also known as DDIT3, GADD153) and ATF3 by real time

(a)

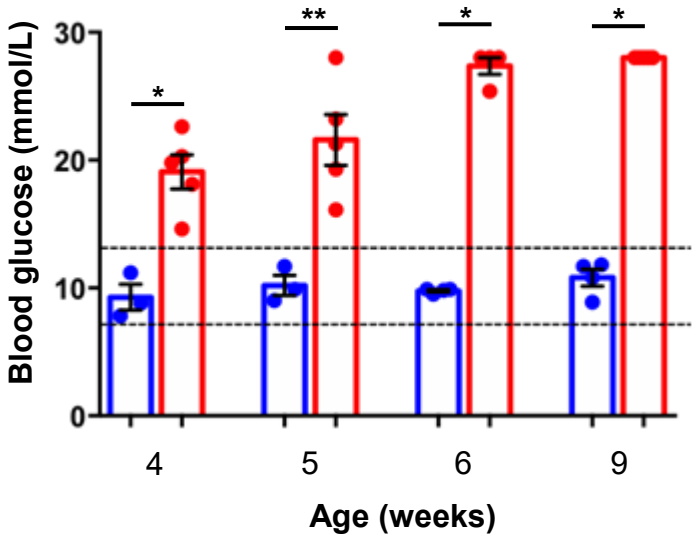

(b)

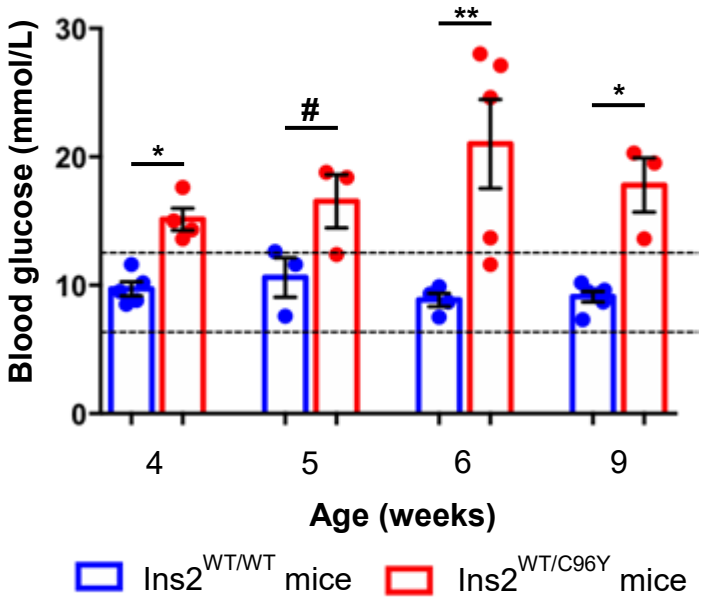

Figure 4.1: The mean non-fasting blood glucose levels of Ins2$^{WT/WT}$ and mutant Ins2$^{WT/C96Y}$ mice at 4-9 weeks of age.

The non-fasting blood glucose levels of male (a) and female (b) Ins2$^{WT/WT}$ (blue bars) and Ins2$^{WT/C96Y}$ (red bars) mice were measured at 4, 5, 6 and 9 weeks of age. The black dotted lines define the normal blood glucose range for (a) male (7.57 mmol/L-12.98 mmol/L) and (b) female (6.61 mmol/L-12.33 mmol/L) Ins2$^{WT/WT}$ mice. The data represent the mean blood glucose levels ± SEM for n=3-5 mice/group. Mann-Whitney test; *P<0.05, **P<0.01 and #P=0.06.

RT-PCR (see Section 2.6.4). The RNA was extracted using the RNeasy kit, cDNA was prepared (see Section 2.6.2) and TaqMan PCR was performed using commercially validated primer/probes (see Section 2.6.4). The gene of interest was normalised to a control house-keeping gene (GAPDH) and mRNA levels of $Ins2^{WT/C96Y}$ islets were quantified as a fold-change compared to $Ins2^{WT/WT}$ control islets.

Comparative C_T analyses showed a 382.5-fold ($P<0.05$), 286.7-fold ($P<0.05$), 32.5-fold ($P<0.05$) and 6.2-fold increase in the expression of the ER stress-associated genes BiP, P58, CHOP and ATF3 respectively, in $Ins2^{WT/C96Y}$ islets compared to control $Ins2^{WT/WT}$ islets (**Figure 4.2**). This study demonstrated a more pronounced increase in the adaptive UPR genes (BiP and P58) compared to the pro-apoptotic UPR genes (CHOP and ATF3). Overall, male $Ins2^{WT/C96Y}$ islets showed a striking upregulation of ER stress genes, confirming the presence of chronic ER stress in the beta cells.

4.2.1.3 Immunohistochemical localisation of HSPG core proteins in the pancreatic islets of male $Ins2^{WT/C96Y}$ and $Ins2^{WT/WT}$ mice

Having confirmed that the beta cells of $Ins2^{WT/C96Y}$ islets demonstrated properties of ER stress, a condition that down-regulates protein synthesis, we next examined the expression of HSPG core proteins i.e., collagen type XVIII (Col18), syndecan-1 (Sdc1) and CD44 in the pancreases of $Ins2^{WT/WT}$ and $Ins2^{WT/C96Y}$ mice by immunohistochemistry (see Section 2.7). No background islet staining was observed in pancreas sections incubated with the relevant isotype control Ig (corresponding to the monoclonal antibody for each HSPG core protein; data not shown).

Representative images showed strong intracellular staining of Col18 in $Ins2^{WT/WT}$ islets (**Figure 4.3(a)**) compared to the dramatically reduced staining in $Ins2^{WT/C96Y}$ islets (**Figure 4.3(b)**) at 6 weeks of age. Similarly, Sdc1 core protein was strongly expressed in the islets of $Ins2^{WT/WT}$ mice (**Figure 4.3(c)**) whereas the islets of $Ins2^{WT/C96Y}$ mice showed weak, scattered staining for Sdc1 (**Figure 4.3(d)**). CD44 core protein showed widespread expression in the islets of $Ins2^{WT/WT}$ mice (**Figure 4.3(e)**) but predominantly cell surface staining in $Ins2^{WT/C96Y}$ islets (**Figure 4.3(f)**).

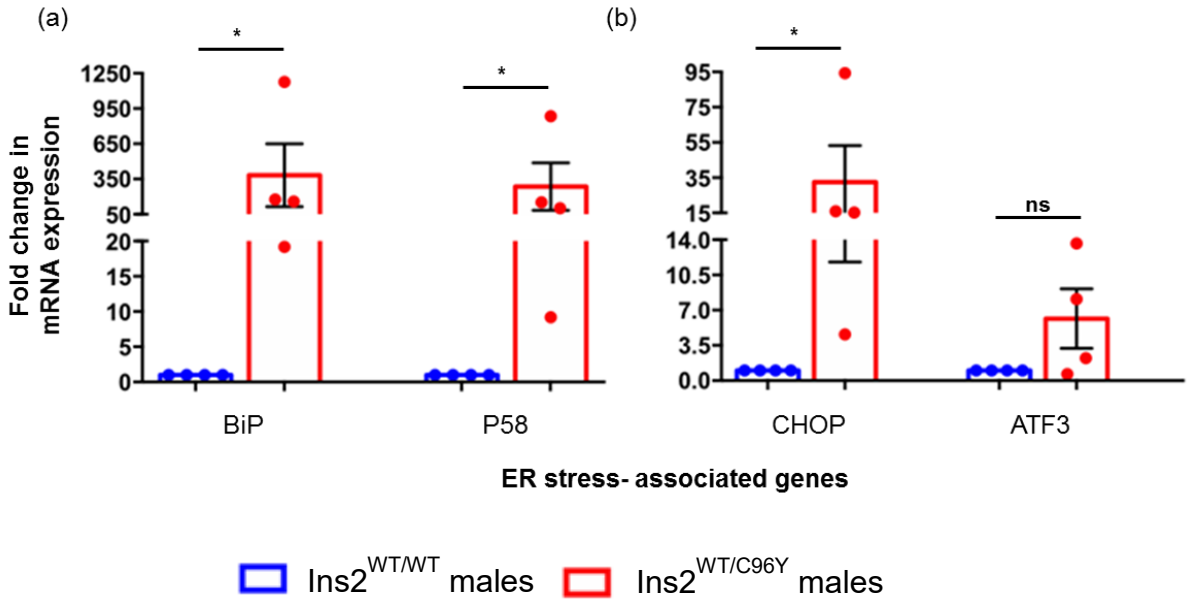

Figure 4.2: ER stress markers in male Ins2$^{WT/WT}$ and Ins2$^{WT/C96Y}$ islets.

RNA was extracted from islets of 5-12 week old male Ins2$^{WT/WT}$ and Ins2$^{WT/C96Y}$ mice to prepare cDNA for TaqMan real-time PCR analysis of (a) adaptive UPR (BiP, P58) and (b) pro-apoptotic (CHOP and ATF3) transcripts. Test transcript levels were quantified as a fold change compared to Ins2$^{WT/WT}$ control mRNA levels which were assigned a value of 1. Each of the ER stress-related genes was highly upregulated in male Ins2$^{WT/C96Y}$ islets, compared to Ins2$^{WT/WT}$ controls. The data represent the mean ± SEM for 4 independent experiments (~300 islets/group/experiment). Mann-Whitney test was used for statistical analysis; *P<0.05 and ns, not significant.

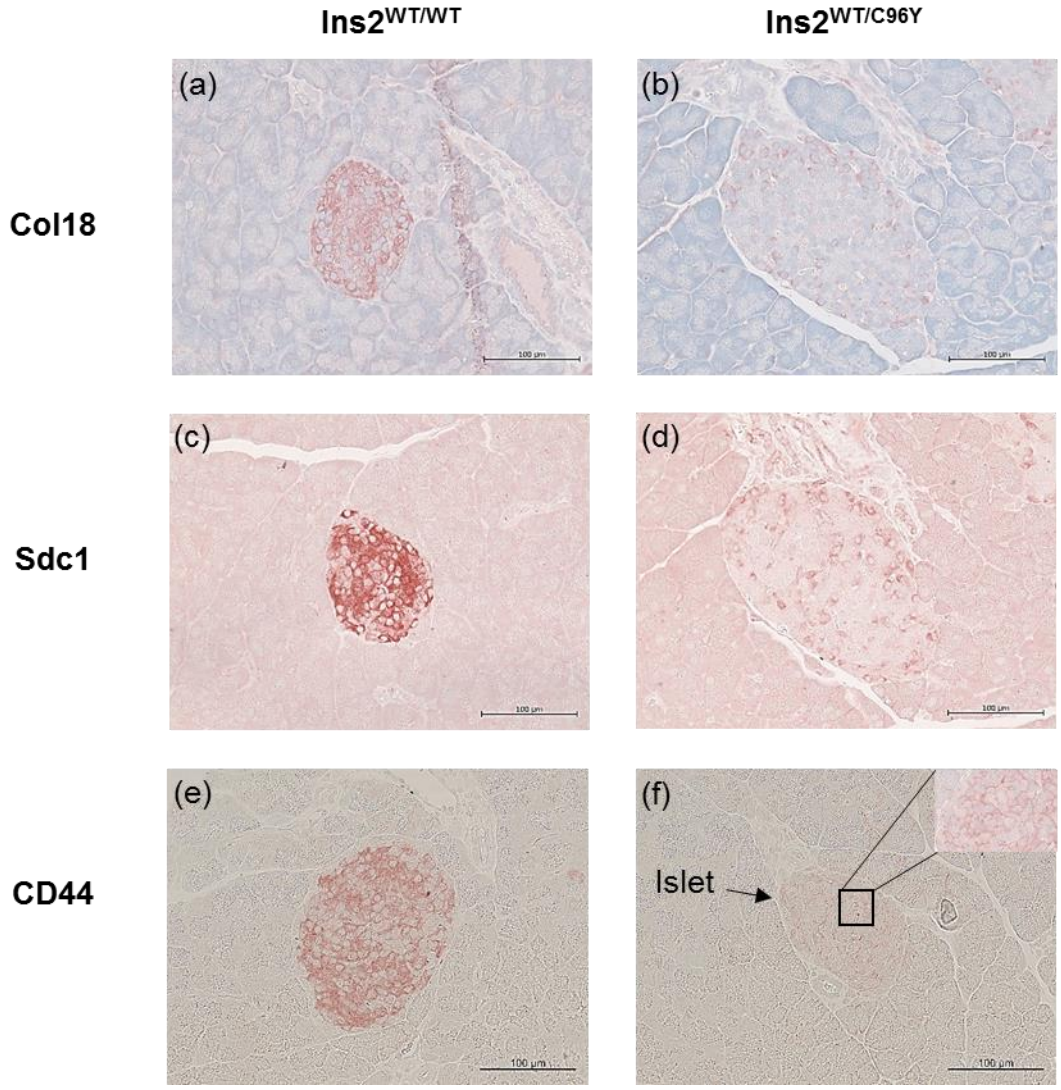

Figure 4.3: Distribution of HSPG core proteins in the pancreatic islets of male Ins2$^{WT/WT}$ and Ins2$^{WT/C96Y}$ mice at 6 weeks of age.

Representative images show the immunohistochemical localisation of Col18 (a, b), Sdc1 (c, d) and CD44 (e, f) in the islets of Ins2$^{WT/C96Y}$ mice and Ins2$^{WT/WT}$ mice at 6 weeks of age. Islets *in situ* in Ins2$^{WT/WT}$ mouse pancreas showed strong staining for Col18 (a), Sdc1 (b) and CD44 (c). In contrast, Ins2$^{WT/C96Y}$ islets (b, d and f) showed a dramatic loss of core proteins. Insert shows cell surface staining in the islet. Scale bar = 100 µm.

The HSPG core protein Col18 expression in $Ins2^{WT/WT}$ and $Ins2^{WT/C96Y}$ islets was similar at 4 weeks of age (**Figure 4.4(a)**). There was a significant decrease in the Col18+ve islet area of $Ins2^{WT/C96Y}$ islets to 24.5%, and 21.9% of corresponding $Ins2^{WT/WT}$ mice at 5 weeks and 6 weeks of age, respectively ($P<0.0001$; **Figure 4.4(a)**). Furthermore, in $Ins2^{WT/C96Y}$ mice at 9 weeks of age, the Col18+ve islet area was reduced to 9.8% of control $Ins2^{WT/WT}$ islets (**Figure 4.4(a)**). Thus, the pancreatic islets of male $Ins2^{WT/C96Y}$ mice revealed a progressive loss of Col18 from 5 weeks of age, compared to their corresponding wildtype controls.

The intra-islet Sdc1 core protein expression in $Ins2^{WT/C96Y}$ islets was significantly reduced to 17.8% of $Ins2^{WT/WT}$ islets from as early as 4 weeks of age ($P<0.0001$; **Figure 4.4(b)**). Thereafter, the Sdc1+ve islet area was further reduced to 2.8%, 8.9% and 1.9% of $Ins2^{WT/WT}$ islets by 5, 6 and 9 weeks of age, respectively (**Figure 4.4(b)**). Male $Ins2^{WT/C96Y}$ mice therefore showed a dramatic loss of intra-islet Sdc1 from 4 weeks of age, compared to their corresponding controls.

The CD44+ve islet area in $Ins2^{WT/C96Y}$ islets was reduced to 39.3% of controls at 4 weeks of age ($P<0.01$; **Figure 4.4(c)**). Moreover, intra-islet CD44 expression declined further to 7.6%, 18.7% and 11.8% of $Ins2^{WT/WT}$ controls at 5, 6 and 9 weeks of age, respectively (**Figure 4.4(c)**). However, $Ins2^{WT/WT}$ islets at 5 weeks of age showed a markedly lower expression of CD44 core protein compared to $Ins2^{WT/WT}$ islets at other time points. This was due to the weaker expression of CD44 observed in 2 out of 3 pancreases. Nevertheless, a significant difference was observed between $Ins2^{WT/C96Y}$ and $Ins2^{WT/WT}$ islets in mice at each age. Interestingly, $Ins2^{WT/C96Y}$ islets demonstrated prominent cell surface staining compared to the widespread intracellular staining in $Ins2^{WT/WT}$ islets. Hence, $Ins2^{WT/C96Y}$ mice revealed a significant reduction in CD44 expression in the pancreatic islets from 4 weeks of age, compared to their corresponding controls.

Altogether, these immunohistochemical studies revealed a dramatic early decline in the intra-islet expression of collagen type XVIII, syndecan-1 and CD44 in pancreases of male $Ins2^{WT/C96Y}$ mice from 4-5 weeks of age.

Figure 4.4: Intra-islet HSPG core protein expression in pancreases of male $Ins2^{WT/WT}$ and $Ins2^{WT/C96Y}$ mice at different ages.

Intra-islet expression of HSPG core protein was assessed in male $Ins2^{WT/WT}$ and $Ins2^{WT/C96Y}$ mice at 4, 5, 6 and 9 weeks of age by immunohistochemistry and morphometry. Data is presented as the % islet area with positive staining for Col18 (a), Sdc1 (b) and CD44 (c). Core proteins for Col18, Sdc1 and CD44 were significantly reduced in male $Ins2^{WT/C96Y}$ islets from as early as 4-5 weeks of age. Data represent mean ± SEM for n=3 pancreases/age group with n=17-28 (Col18), n=16-30 (Sdc1) and n=17-31 (CD44) islets examined/group. Mann-Whitney test; *P<0.001, **P<0.0001 and ns, not significant.

(a)

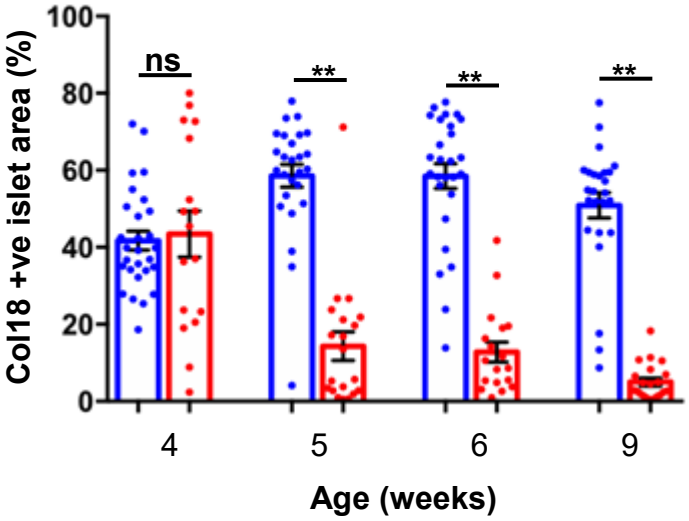
Col18 +ve islet area (%)
100
80
60
40
20
0
ns
**
**
**
4
5
6
9
Age (weeks)

(b)

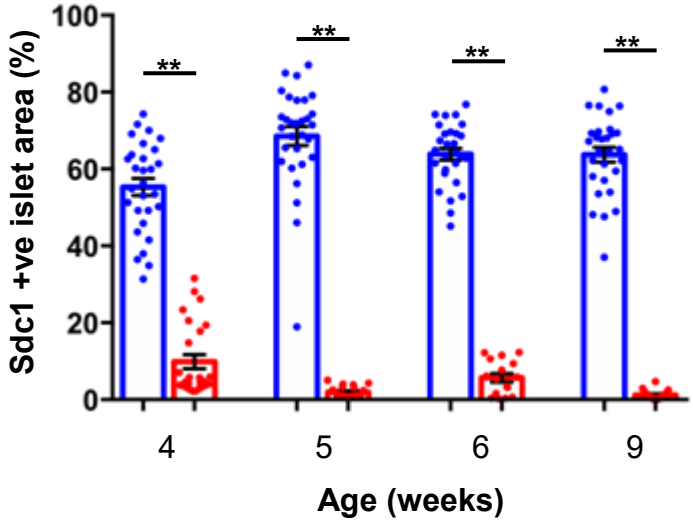
Sdc1 +ve islet area (%)
100
80
60
40
20
0
**
**
**
**
4
5
6
9
Age (weeks)

(c)

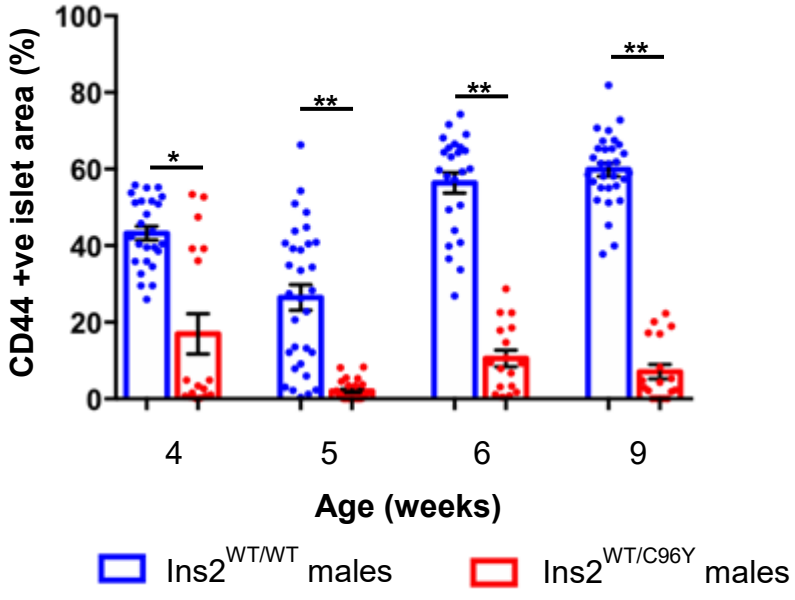
CD44 +ve islet area (%)
100
80
60
40
20
0
*
**
**
**
4
5
6
9
Age (weeks)
Ins2WT/WT males
Ins2WT/C96Y males

4.2.1.4 HS expression in the islets of $Ins2^{WT/WT}$ and $Ins2^{WT/C96Y}$ islets at 6 weeks of age

Since HS chains are attached to HSPG core proteins and we observed a reduction in HSPG core proteins in $Ins2^{WT/C96Y}$ islets, we next examined the localisation of HS in the islets of $Ins2^{WT/WT}$ and $Ins2^{WT/C96Y}$ mice at 6 weeks of age by immunohistochemistry using EV3C3 anti-HS mAb (see Section 2.7.4). The EV3C3 anti-HS mAb stains for N-sulfation, C5 epimerisation and 2-O sulphation in HS chains (Dennissen et al., 2002, Theodoraki et al., 2015). While a strong expression of HS was observed in the islets of $Ins2^{WT/WT}$ mice (**Figure 4.5(a)**), a substantial decline in intra-islet HS was found in $Ins2^{WT/C96Y}$ islets at 6 weeks of age (**Figure 4.5(b)**).

The HS+ve islet area in male $Ins2^{WT/C96Y}$ islets was significantly reduced to 58.4% of controls (25.79 ± 3.82% vs 44.13 ± 2.80%) at 6 weeks of age ($P<0.05$; **Figure 4.5(c)**). $Ins2^{WT/C96Y}$ mice therefore displayed a significant loss of intra-islet HS compared to $Ins2^{WT/WT}$ islets during the development of diabetes.

4.2.1.5 Immunostaining of insulin, proinsulin and glucagon in pancreatic islets of $Ins2^{WT/WT}$ and $Ins2^{WT/C96Y}$ male mice

Previous studies have shown that $Ins2^{WT/C96Y}$ islets exhibit a reduced insulin and proinsulin content (Wang et al., 1999, Gupta et al., 2010). We therefore investigated the distribution of insulin, proinsulin and glucagon in the islets of male $Ins2^{WT/WT}$ and $Ins2^{WT/C96Y}$ mice from 4-9 weeks of age by immunohistochemistry (see Section 2.7). The GS-9A8 antibody was used to distinguish proinsulin staining from insulin in beta cells. This antibody recognises an epitope that spans amino acids B28-30 and two arginine residues which link the B-C junction (not present in insulin protein) (Asadi et al., 2015).

Insulin was highly expressed in male $Ins2^{WT/WT}$ islets (**Figure 4.6(a)**) but showed markedly weaker expression and a scattered distribution in the islets of $Ins2^{WT/C96Y}$ mice at 6 weeks of age (**Figure 4.6(b)**). In contrast to insulin (**Figure 4.6(a)**), proinsulin staining was punctate in $Ins2^{WT/WT}$ islets (**Figure 4.6(c)**) and was essentially absent in $Ins2^{WT/C96Y}$ islets (**Figure 4.6(d)**). The distribution of glucagon staining was restricted to cells at the periphery of islets in $Ins2^{WT/WT}$ mice and was more widespread in $Ins2^{WT/C96Y}$ islets at 6 weeks of age (**Figure 4.6(e, f)**). The intensity of insulin, proinsulin and

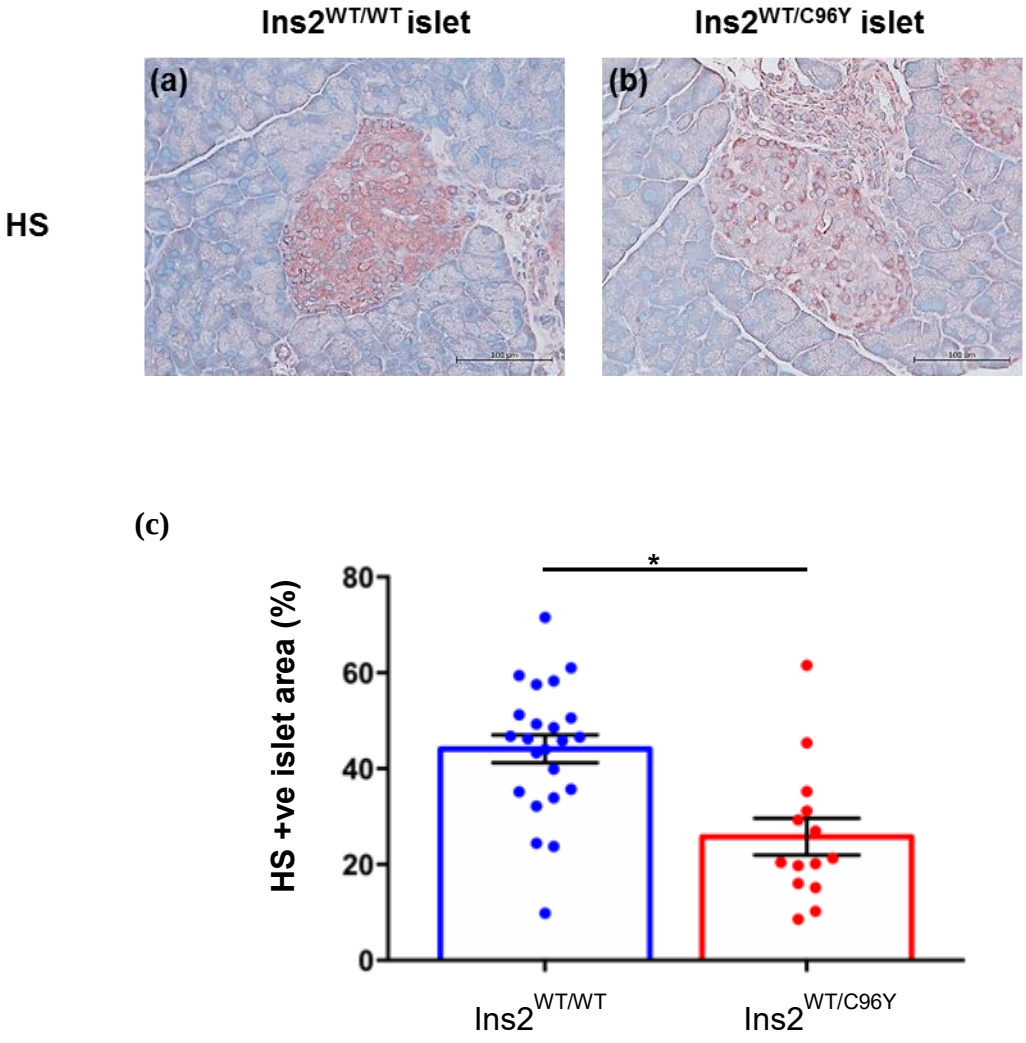

Figure 4.5: Distribution of HS in the pancreatic islets of male Ins2$^{WT/WT}$ and Ins2$^{WT/C96Y}$ islets at 6 weeks of age.

Representative images show the distribution of HS in the islets of Ins2$^{WT/C96Y}$ and Ins2$^{WT/WT}$ mice after immunostaining of pancreas sections with EV3C3 anti-HS mAb. The islets of Ins2$^{WT/WT}$ mice (a) strongly express intracellular HS whereas diminished HS staining was observed in Ins2$^{WT/C96Y}$ islets (b). (c) Immunostaining showed that the HS+ve islet area in Ins2$^{WT/C96Y}$ islets (red bars) was significantly reduced to 58.4% of controls (blue bars) at 6 weeks of age. Data represent the mean ± SEM for 3 pancreas specimens/age group with n=15-23 islets analysed/group. Unpaired t test; *P<0.001, Scale bar = 100 μm.

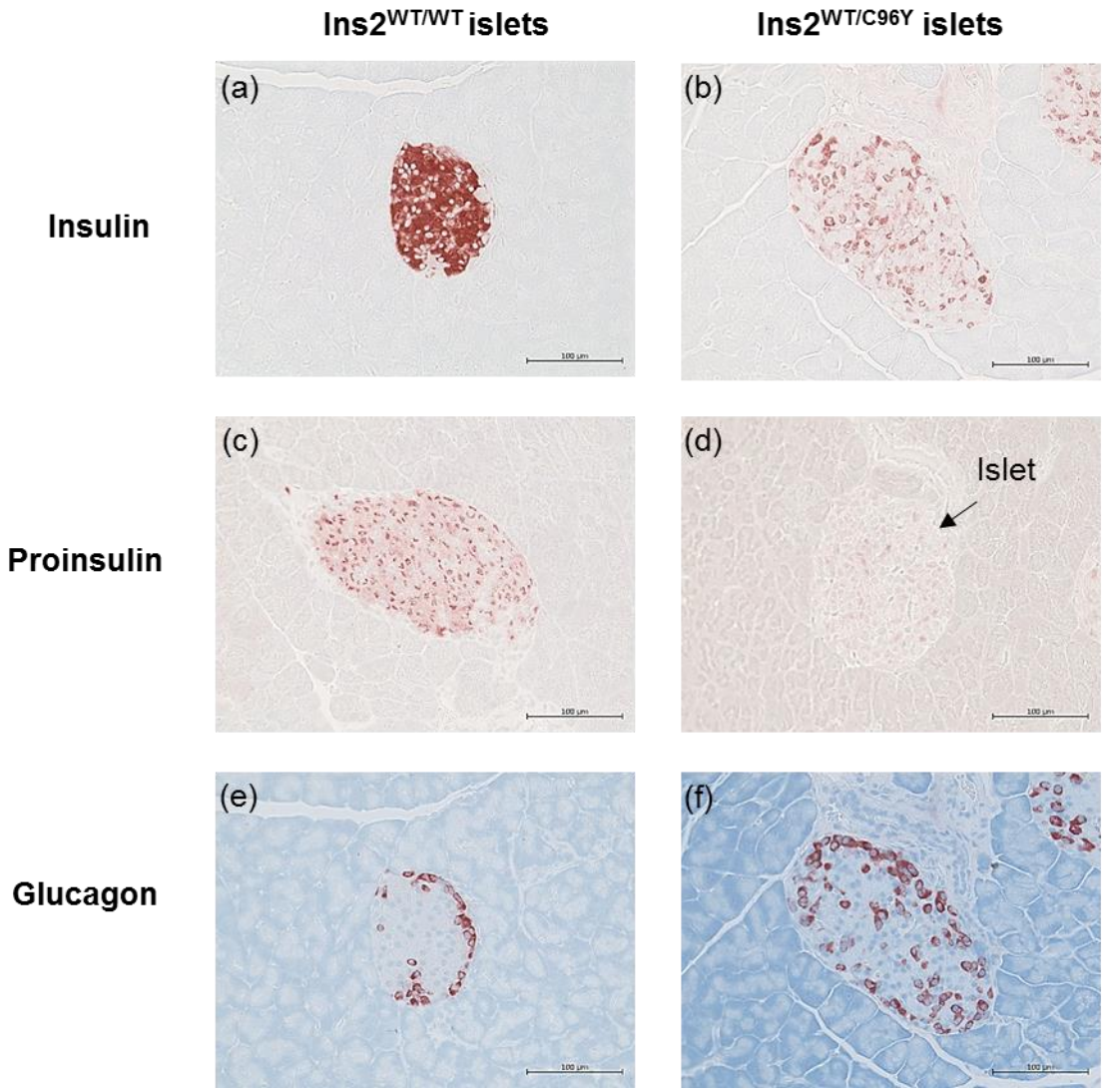

Figure 4.6: Immunolocalisation of insulin, proinsulin and glucagon in the pancreatic islets of Ins2$^{WT/WT}$ and Ins2$^{WT/C96Y}$ mice at 6 weeks of age.

Insulin, proinsulin and glucagon expression were localised in the islets of Ins2$^{WT/WT}$ and Ins2$^{WT/C96Y}$ mice by immunohistochemistry. Islets *in situ* in Ins2$^{WT/WT}$ pancreas showed strong staining of insulin (a) but only scattered insulin+ve beta cells in Ins2$^{WT/C96Y}$ islets (b). Ins2$^{WT/WT}$ mice showed punctate staining of proinsulin (c) and decreased expression in Ins2$^{WT/C96Y}$ islets (d). In general, glucagon+ve alpha cells were found at the islet periphery (e, f). Scale bar = 100 µm.

glucagon staining in $Ins2^{WT/WT}$ and $Ins2^{WT/C96Y}$ islets was quantified using Image J software with colour deconvolution plugin (see Section 2.7.5).

The intensity of insulin staining was significantly reduced to 50.8% of control $Ins2^{WT/WT}$ islets (staining intensity= 0.32 ± 0.01 vs 0.63 ± 0.03 A.U.) in $Ins2^{WT/C96Y}$ islets by 4 weeks of age ($P<0.0001$; **Figure 4.7(a)**). Insulin staining was further reduced in $Ins2^{WT/C96Y}$ islets to 34.2%, 37.3% and 38% of $Ins2^{WT/WT}$ islets at 5, 6 and 9 weeks of age respectively (**Figure 4.7(a)**). Additionally, $Ins2^{WT/C96Y}$ islets showed a significantly reduced expression of proinsulin to 31.5% of $Ins2^{WT/WT}$ controls at 6 weeks of age (**Figure 4.7(b)**). Therefore, $Ins2^{WT/C96Y}$ islets expressed a significant decline in both insulin and proinsulin expression compared to control $Ins2^{WT/WT}$ islets.

Glucagon +ve alpha cells in $Ins2^{WT/C96Y}$ islets initially showed a decrease to 72.2% of controls at 5 weeks of age; however the intensity of glucagon staining significantly increased 1.3-1.5-fold compared to $Ins2^{WT/WT}$ controls at 6-9 weeks of age ($P<0.01$; **Figure 4.7(c)**). In contrast, reduced insulin staining in beta cells was observed in the islets of $Ins2^{WT/C96Y}$ mice from 4 weeks of age.

4.2.1.6 Immunostaining of HSPG core proteins in female $Ins2^{WT/C96Y}$ islets and $Ins2^{WT/WT}$ islets

As for male heterozygous Akita mice (see Section 4.2.1.3), immunohistochemistry analysis was used to localise the HSPG core proteins, collagen type XVIII (Col18), syndecan-1 (Sdc1) and CD44 in the pancreatic islets of female $Ins2^{WT/WT}$ and $Ins2^{WT/C96Y}$ mice from 4-9 weeks of age. The intra-islet content of HSPG core proteins was quantified using Image J software with colour deconvolution plugin (see Section 2.7.5). The threshold intensity was determined by the positive staining observed in $Ins2^{WT/WT}$ pancreases at 9 weeks of age; this threshold was applied to all samples.

Immunohistochemistry analyses revealed that in female $Ins2^{WT/C96Y}$ islets the HSPG core protein Col18 was reduced from as early as 4 weeks of age. The Col18+ve islet area was significantly reduced to 61% of controls and 45-52% of corresponding $Ins2^{WT/WT}$ islets at 4 and 5-9 weeks of age, respectively (**Figure 4.8(a)**). The Sdc1+ve islet area in $Ins2^{WT/C96Y}$ mice was significantly reduced to 14-28% of $Ins2^{WT/WT}$ islets from 4-9 weeks

Figure 4.7: Insulin, proinsulin and glucagon expression in the islets of male $Ins2^{WT/WT}$ and $Ins2^{WT/C96Y}$ mice at 4-9 weeks of age.

Insulin (a) and glucagon (c) were localised in $Ins2^{WT/WT}$ and $Ins2^{WT/C96Y}$ pancreas sections (4-9 weeks of age) by immunohistochemistry and the intensity of staining was quantified using Image J software. (b) Proinsulin staining was analysed in $Ins2^{WT/WT}$ and $Ins2^{WT/C96Y}$ mice at 6 weeks of age. $Ins2^{WT/C96Y}$ mutant islets demonstrated a significant reduction in the staining intensity for insulin and proinsulin compared to $Ins2^{WT/WT}$ control islets. The data represents the mean ± SEM for n=3 pancreases/age group with n=21-36 (insulin), n=16-31 (proinsulin) and n=14-25 (glucagon) islets examined/group. Mann-Whitney test; *P<0.01, **P<0.001, ***P<0.0001 and ns, not significant.

(a)

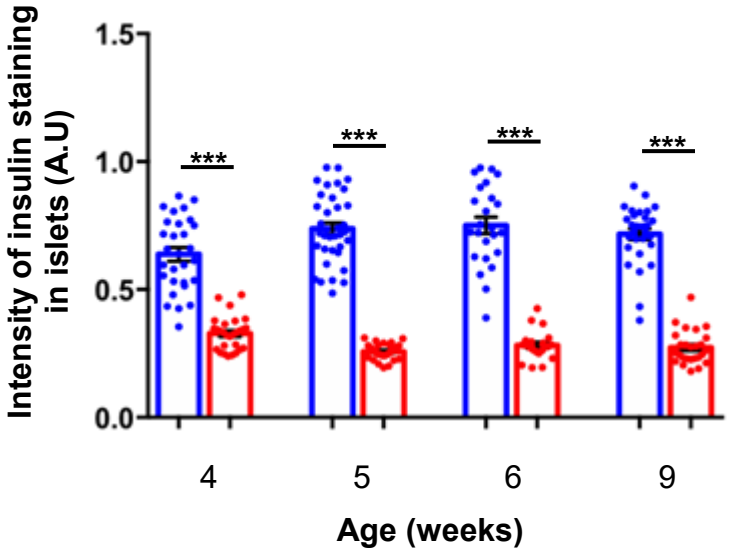
Intensity of insulin staining in islets (A.U)
1.5
1.0
0.5
0.0
***
***
***
***
4
5
6
9
Age (weeks)

(b)

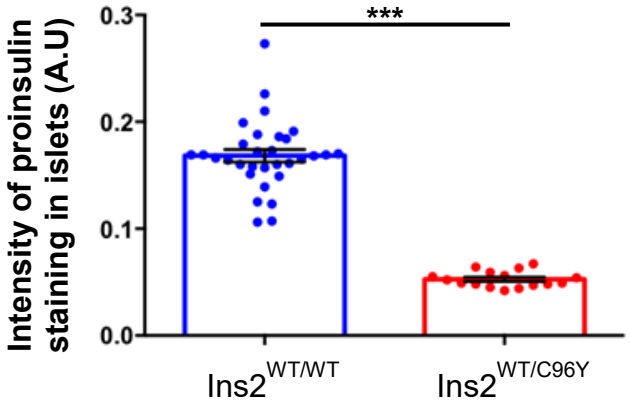
Intensity of proinsulin staining in islets (A.U)
0.3
0.2
0.1
0.0
***
Ins2WT/WT
Ins2WT/C96Y

(c)

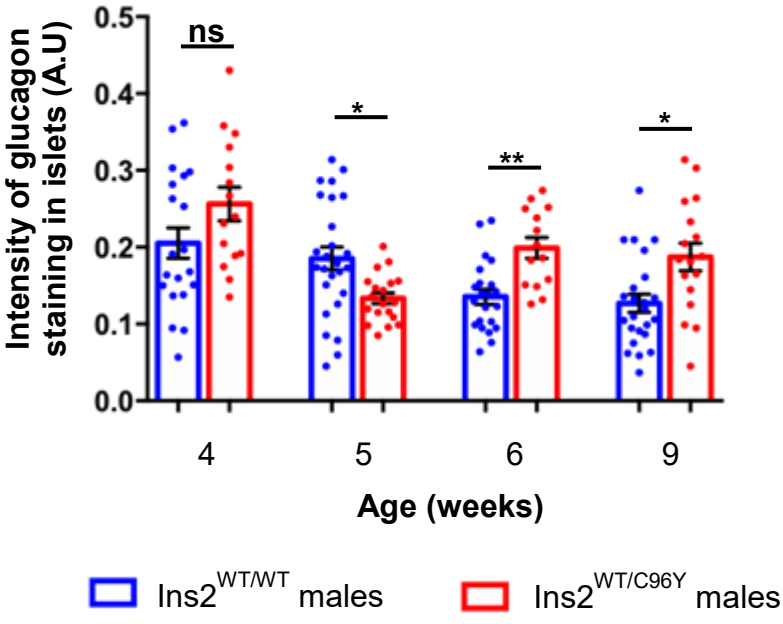
Intensity of glucagon staining in islets (A.U)
0.5
0.4
0.3
0.2
0.1
0.0
ns
*
**
*
4
5
6
9
Age (weeks)
Ins2WT/WT males
Ins2WT/C96Y males

Figure 4.8: Intra-islet HSPG core protein expression in pancreases of female $Ins2^{WT/C96Y}$ and $Ins2^{WT/WT}$ mice at 4-9 weeks of age.

The intra-islet expression of HSPG core proteins was assessed in female $Ins2^{WT/WT}$ and $Ins2^{WT/C96Y}$ mice at 4, 5, 6, and 9 weeks of age by immunohistochemistry and morphometry. The y-axis shows the % islet area stained for Col18 (a), Sdc1 (b) and CD44 (c). Core proteins for Col18, Sdc1 and CD44 were significantly reduced in female $Ins2^{WT/C96Y}$ islets from as early as 4 weeks of age. The data represent mean ± SEM for n=3 pancreases/age group with n=14-35 (Col18), n=21-38 (Sdc1) and n=18-30 (CD44) islets analysed/group. Mann-Whitney test; *P<0.001, **P<0.0001 and ns, not significant.

(a)

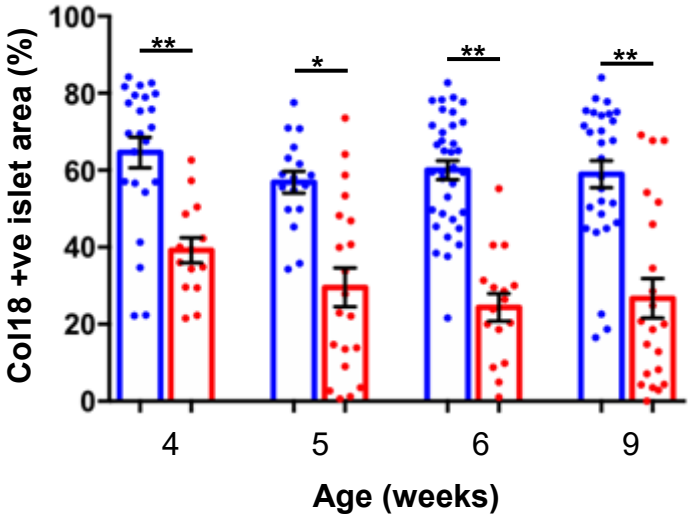
Col18 +ve islet area (%)
100
80
60
40
20
0
**
*
**
**
4
5
6
9
Age (weeks)

(b)

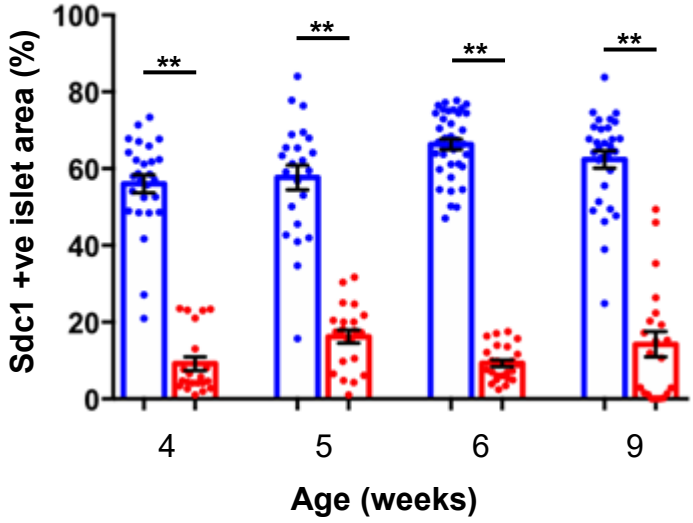
Sdc1 +ve islet area (%)
100
80
60
40
20
0
**
**
**
**
4
5
6
9
Age (weeks)

(c)

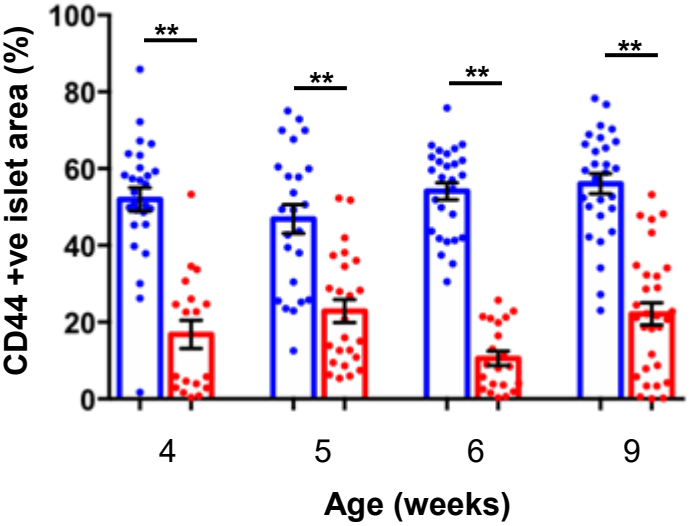
CD44 +ve islet area (%)
100
80
60
40
20
0
**
**
**
**
4
5
6
9
Age (weeks)


Ins2WT/WT females
Ins2WT/C96Y females

of age (P<0.001; **Figure 4.8(b)**). Similarly, CD44 expression was reduced to 32.3-48.8% of corresponding $Ins2^{WT/WT}$ islets in $Ins2^{WT/C96Y}$ islets by 4-5 weeks of age (P<0.001; **Figure 4.8(c)**). The mean CD44+ve islet area in $Ins2^{WT/C96Y}$ mice was 19.5% and 39.5% of controls at 6 and 9 weeks of age, respectively (P<0.001).

Similar to male $Ins2^{WT/C96Y}$ mice (see Section 4.2.1.3), female $Ins2^{WT/C96Y}$ mice demonstrated a significant reduction in the intra-islet expression of HSPG core proteins compared to $Ins2^{WT/WT}$ controls from 4 weeks of age.

4.2.1.7 Localisation of insulin, proinsulin and glucagon in the islets of female $Ins2^{WT/WT}$ and $Ins2^{WT/C96Y}$ islets by immunohistochemistry

The distribution of insulin, proinsulin and glucagon staining in female $Ins2^{WT/WT}$ and $Ins2^{WT/C96Y}$ islets was examined by immunohistochemistry. The intensity of staining was quantified using Image J software with colour deconvolution plugin (see Section 2.7.5).

The expression of insulin was significantly decreased in $Ins2^{WT/C96Y}$ islets to 48% of control $Ins2^{WT/WT}$ islets at 4 weeks of age (P<0.0001; **Figure 4.9(a)**). Similarly, the insulin levels were 62.5%, 40.5% and 58.9% of $Ins2^{WT/WT}$ islets at 5, 6 and 9 weeks of age respectively (**Figure 4.9(a)**). In $Ins2^{WT/C96Y}$ islets, the intensity of proinsulin staining was significantly reduced to 32.2% of $Ins2^{WT/WT}$ islets (P<0.0001; **Figure 4.9(b)**).

In contrast to insulin staining, glucagon expression in $Ins2^{WT/C96Y}$ islets increased 1.1-1.5-fold compared to $Ins2^{WT/WT}$ controls at 4-5 weeks of age (**Figure 4.9(c)**). However, by 9 weeks of age, the intensity of glucagon staining in $Ins2^{WT/C96Y}$ islets was reduced to 66.7% of $Ins2^{WT/WT}$ controls (**Figure 4.9(c)**).

Like male $Ins2^{WT/C96Y}$ islets (see Section 4.2.1.5), female $Ins2^{WT/C96Y}$ islets demonstrated a significant reduction in the expression of insulin and proinsulin, compared to $Ins2^{WT/WT}$ islets.

In summary, acute ER stress in $Ins2^{WT/C96Y}$ mice correlated with rapid onset of diabetes and significant loss of HSPG core proteins, HS, insulin and proinsulin. These findings resemble the loss of HS/HSPG core proteins in T2D-prone db/db mice, correlating with

Figure 4.9: Staining intensity of insulin, proinsulin and glucagon in female $Ins2^{WT/WT}$ and $Ins2^{WT/C96Y}$ islets.

Insulin (a) and glucagon (c) levels in 4-9 weeks of age female $Ins2^{WT/WT}$ and $Ins2^{WT/C96Y}$ pancreatic islets were quantified by immunohistochemistry and morphometry analysis; (b) proinsulin staining was analysed in $Ins2^{WT/WT}$ and $Ins2^{WT/C96Y}$ mice at 6 weeks of age. The intensity of staining for insulin and proinsulin was significantly reduced in $Ins2^{WT/C96Y}$ islets compared to $Ins2^{WT/WT}$ controls. The data represent mean ± SEM for n=3 pancreases/age group with n=18-36 (insulin), n=19-28 (proinsulin) and n=14-33 (glucagon) islets examined/group. Mann-Whitney test; *P<0.05, **P<0.01, ***P<0.0001 and ns, not significant.

(a)

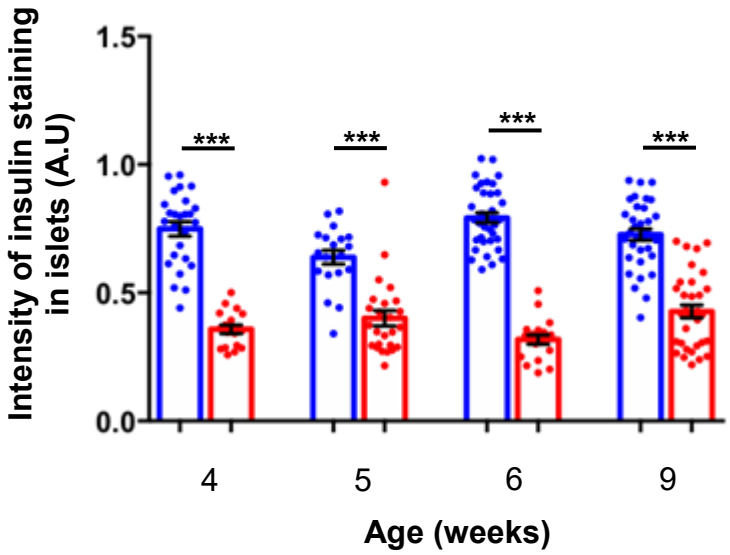
Intensity of insulin staining in islets (A.U)
1.5
1.0
0.5
0.0
***
***
***
***
4
5
6
9
Age (weeks)

(b)

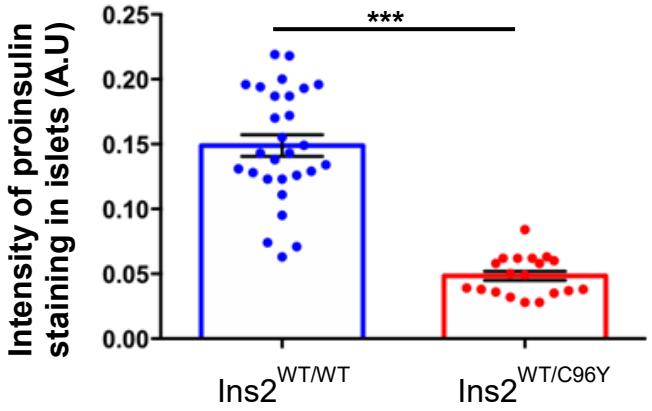
Intensity of proinsulin staining in islets (A.U)
0.25
0.20
0.15
0.10
0.05
0.00
***
Ins2WT/WT
Ins2WT/C96Y

(c)

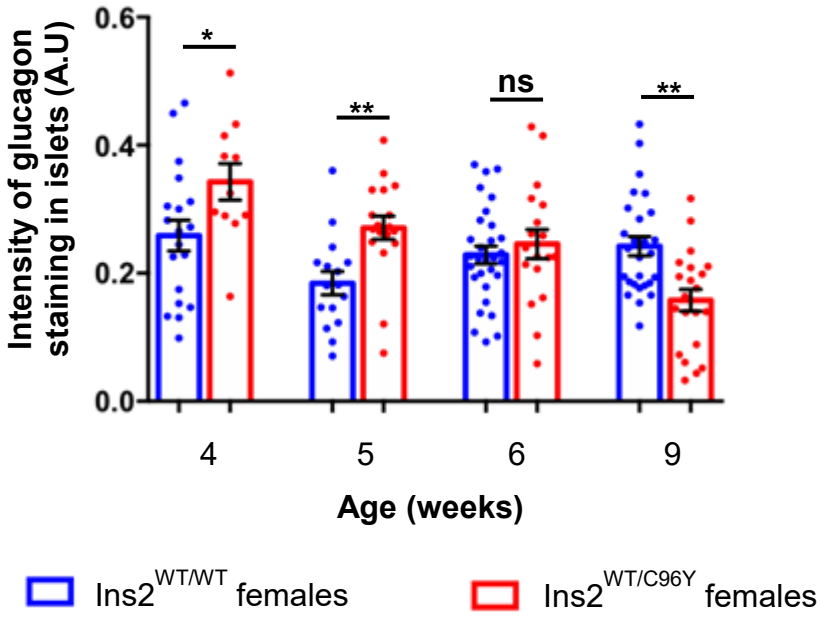
Intensity of glucagon staining in islets (A.U)
0.6
0.4
0.2
0.0
*
**
ns
**
4
5
6
9
Age (weeks)
Ins2WT/WT females
Ins2WT/C96Y females

chronic ER stress (see Chapter 3).

4.2.2 Effect of ER stress on HSPGs/HS in MIN6 beta cells

4.2.2.1 Intracellular localisation of HS and HSPG core proteins in MIN6 cells

The intracellular and cell surface expression of HS and the HSPG core proteins collagen type XVIII (Col18), syndecan-1 (Sdc1) and CD44 were analysed in freshly harvested MIN6 cells by flow cytometry (see Section 2.8). Using the gating strategy described in **Figure 2.9**, the geometric mean fluorescence intensity (GMFI) of cell surface and intracellular HSPG core proteins and HS expression was determined.

MIN6 cells demonstrated intense intracellular expression of Col18 core protein (GMFI= 42145.00 ± 10653.00) which was ~70-fold higher than at the cell surface (GMFI= 592.50 ± 55.35) (**Figures 4.10(a) and 4.11(a)**). In contrast, the intracellular expression of Sdc1 (GMFI= 2126.30 ± 585.94) and CD44 (GMFI=1559.80 ± 777.07) was not significantly

different to the corresponding cell surface expression (Sdc1 GMFI=1489.8 ± 502.62 and CD44 GMFI= 803.25 ± 195.41) (**Figure 4.11(a)**). Compared to the weak cell surface staining of HS (GMFI= 739.50 ± 243.40), MIN6 cells expressed 15.8-fold higher levels intracellularly (GMFI= 11679.00 ± 3160.08; **Figures 4.10(b) and 4.11(b)**). These data revealed that MIN6 cells express strong intracellular levels of Col18 and HS but weak cell surface expression.

The expression of heparanase (Hpse), an HS-degrading enzyme, was also examined in MIN6 cells. Hpse regulates HS turnover in cells (including beta cells) and contributes to the reduced levels of HS in the beta cells of NOD mice during T1D development (Ziolkowski et al., 2012, Bernfield et al., 1999). MIN6 cells displayed strong intracellular expression of Hpse (GMFI= 6223.00 ± 512.49) and weak cell surface expression (GMFI= 339.25 ± 18.49; **Figures 4.10(c) and 4.11(c)**). Hpse was therefore highly expressed in MIN6 cells.

Figure 4.10: Cell surface and intracellular staining of HSPG core proteins, HS and Hpse in MIN6 cells.

Representative flow cytometry histograms show the cell surface (a, c, e) and intracellular (b, d, f) expression of Col18, HS and Hpse in freshly harvested MIN6 cells. The background staining/autofluorescence is shown in red histograms and specific staining for Col18 (a, b), HS (c, d) and Hpse (e, f) is represented by blue histograms. The data show the intensity of fluorescence staining expressed as GMFI. The GMFI for intracellular staining of Col18 (b), HS (d) and Hpse (f) was 20-100-fold higher than the corresponding cell surface GMFI (a, c, e). HSPG core proteins, HS and Hpse are therefore expressed at high levels inside beta cells but at low levels on the cell surface.

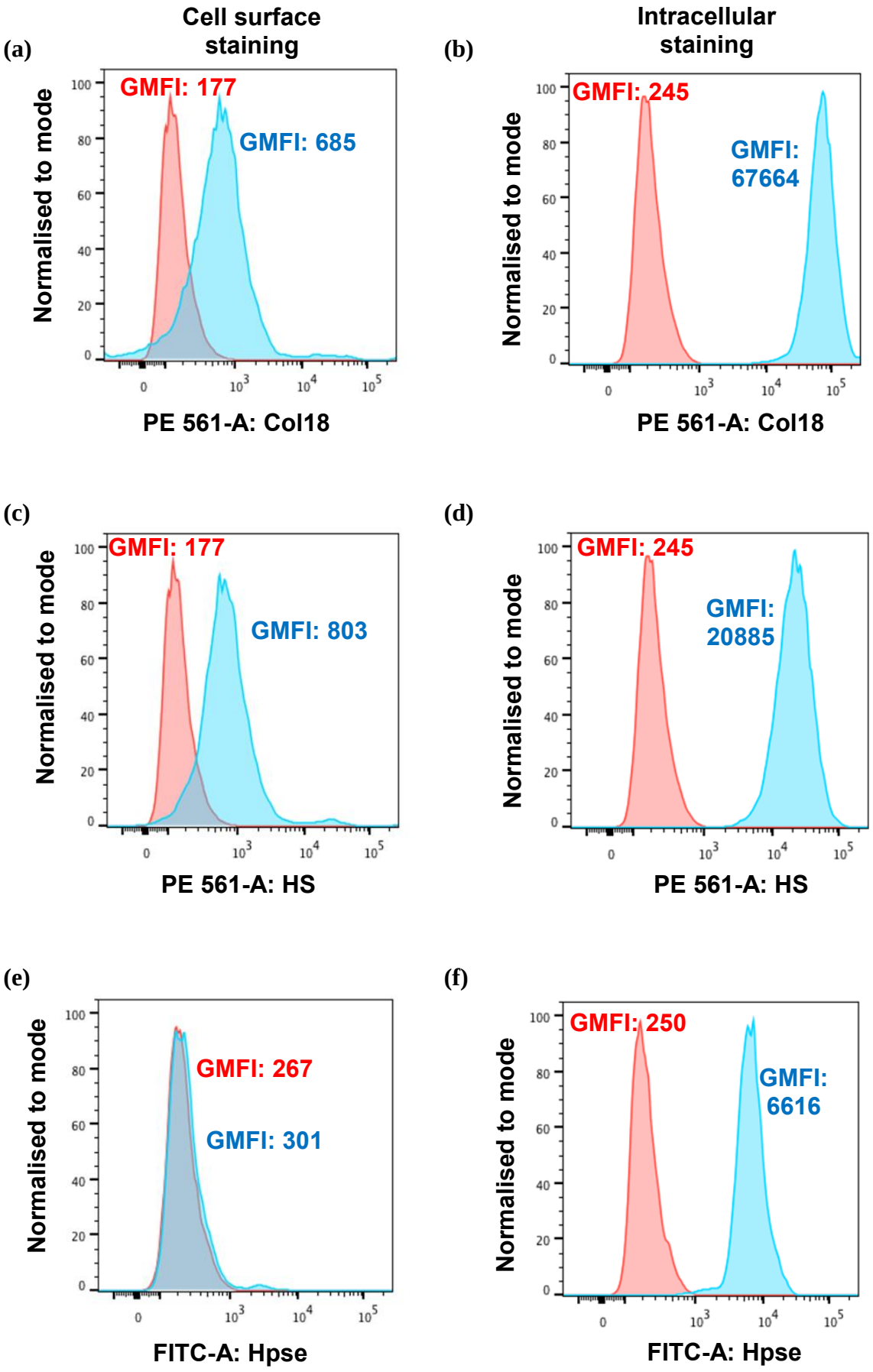
(a)
Cell surface staining
GMFI: 177
GMFI: 685
Normalised to mode
PE 561-A: Col18
(b)
Intracellular staining
GMFI: 245
GMFI: 67664
Normalised to mode
PE 561-A: Col18
(c)
GMFI: 177
GMFI: 803
Normalised to mode
PE 561-A: HS
(d)
GMFI: 245
GMFI: 20885
Normalised to mode
PE 561-A: HS
(e)
GMFI: 267
GMFI: 301
Normalised to mode
FITC-A: Hpse
(f)
GMFI: 250
GMFI: 6616
Normalised to mode
FITC-A: Hpse

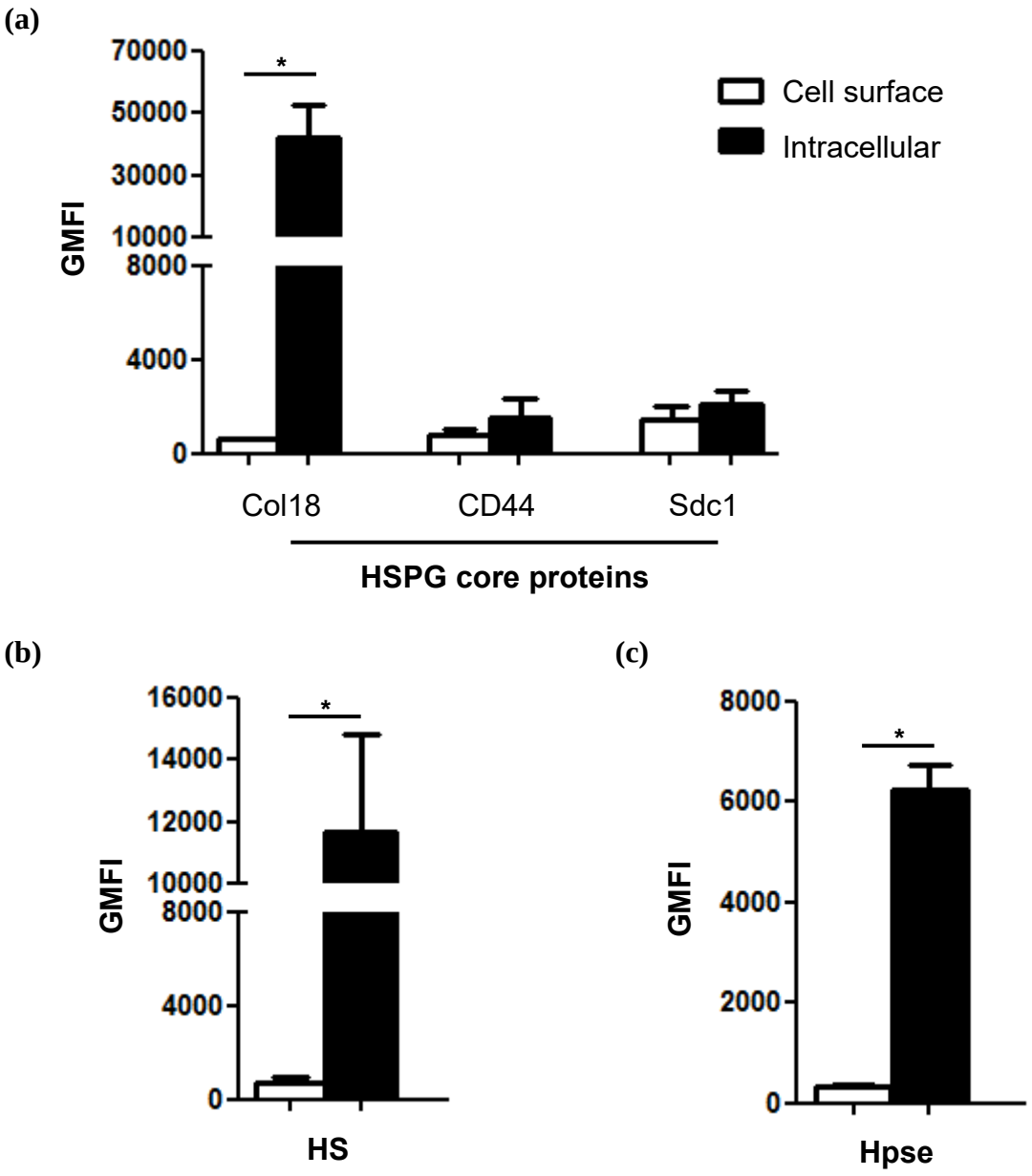

Figure 4.11: Cell surface and intracellular staining of HSPG core proteins, HS and Hpse in MIN6 cells.

Freshly harvested MIN6 cells were stained for cell surface (white bars) and intracellular (black bars) HSPG core proteins (a), HS (b) and Hpse (c) and analysed by flow cytometry. HSPG core protein Col18, HS and Hpse were expressed at significantly higher levels intracellularly than at the cell surface. The data represent GMFI ± SEM for n=4 independent experiments. Mann-Whitney test; *P<0.05.

Based on the high intracellular expression of HSPG core protein (Col18) and HS, the MIN6 beta cell line was shown to have similar properties to primary beta cells (Ziolkowski et al., 2012, Choong et al., 2015).

4.2.2.2 Induction of ER stress in MIN6 cells

ER stress in MIN6 cells was induced using physiological (palmitate, a saturated free fatty acid) and pharmacological (thapsigargin and tunicamycin) ER stress agents (see Section 2.5). Real time RT-PCR was performed to validate the induction of ER stress, using the expression of a panel of ER stress-associated genes as markers: BiP (with alternative names HSPA5, GRP78), P58 (also known as DNAJC3), CHOP (also called DDIT3) and ATF3. For thapsigargin and tunicamycin treatment, the MIN6 cells were cultured with 25 mM glucose (normal control), 6 mM glucose (treatment control) and 6 mM glucose + ER stress inducer (treatment); for palmitate treatment, the cells were treated with 25 mM glucose, 6 mM glucose/BSA (diluent for palmitate) and 6 mM glucose + palmitate/BSA. The MIN6 cells were harvested after 20-24 hrs of culture with test or control treatment (referred to as day 1). RNA was extracted from control and treated MIN6 cells using the RNeasy Mini kit to prepare cDNA for TaqMan real-time PCR studies (see Section 2.6).

MIN6 cells treated with thapsigargin showed a 2.1-fold, 1.3-fold, 3.8-fold and 10.9-fold increase in the mRNA expression of BiP, P58, CHOP and ATF3 respectively, compared to control MIN6 cells (6 mM glucose; **Figure 4.12(a)**). There was a significant increase in the expression of BiP ($P<0.05$), CHOP ($P<0.001$) and ATF3 ($P<0.001$) following thapsigargin treatment, confirming the induction of ER stress in the MIN6 cells.

For tunicamycin-treated MIN6 cells, comparative C_T analyses revealed a 2.7-fold and 3.2-fold increase in the adaptive UPR genes BiP and P58 respectively, compared to controls. Furthermore, a significant 3.8-fold and 3.4-fold increase was also observed in the expression of the pro-apoptotic genes CHOP and ATF3, respectively, compared to control MIN6 cells (6 mM glucose; $P<0.001$; **Figure 4.12(b)**).

MIN6 cells treated with palmitate/BSA showed a 1.2-fold, 1.1-fold, 1.8-fold and 4.0-fold increase in the ER stress associated genes BiP, P58, CHOP and ATF3, respectively, compared to control MIN6 cells (6 mM glucose/BSA; **Figure 4.13**). The increase in the

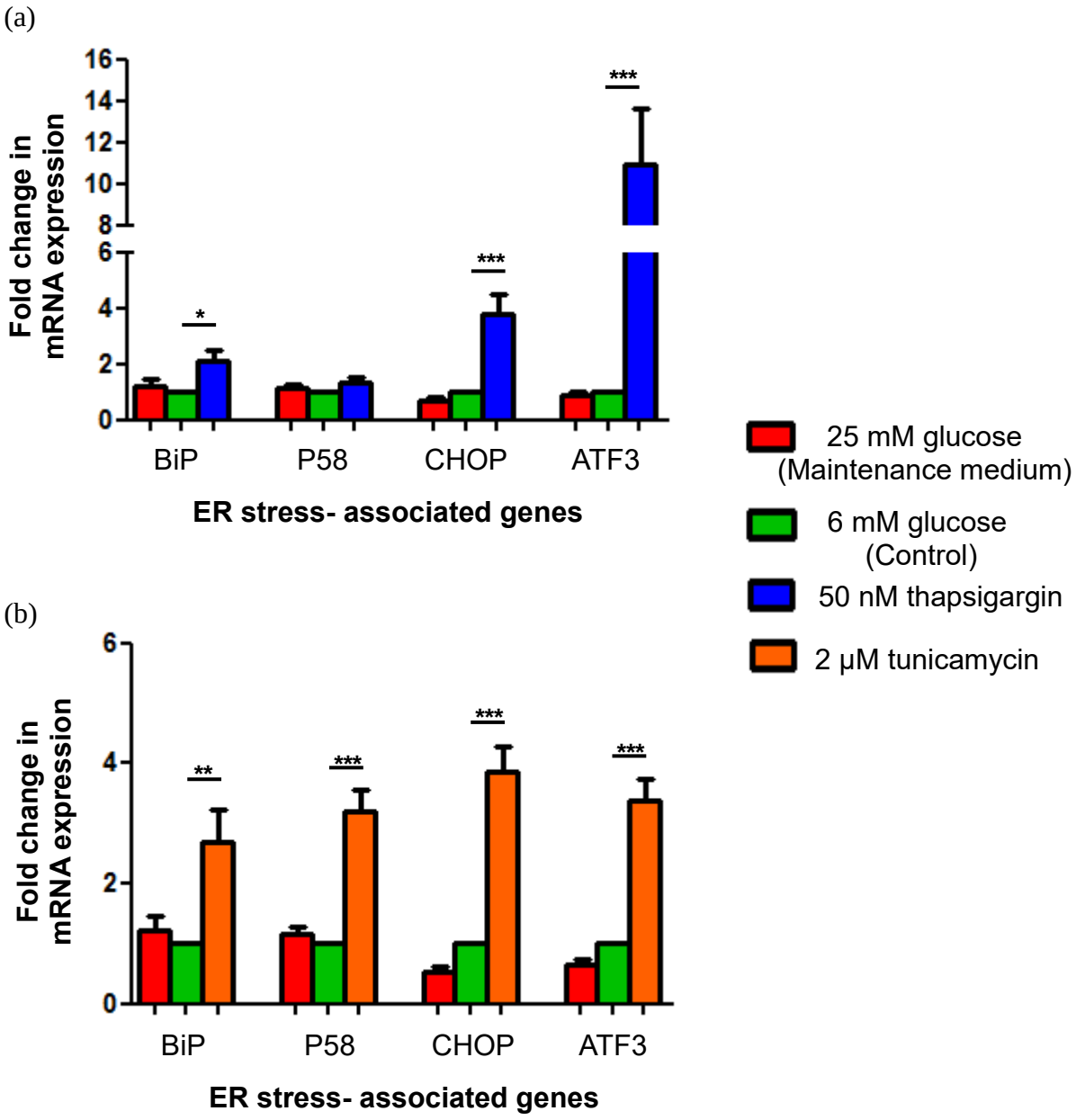

Figure 4.12: Induction of ER stress in MIN6 cells.

MIN6 cells were cultured with 25 mM glucose, 6 mM glucose and (a) 50 nM thapsigargin or (b) 2 µM tunicamycin for 20-24 hours. RNA was extracted and cDNA was prepared for TaqMan real-time PCR. Transcript levels for BiP, P58, CHOP and ATF3 were quantified as a fold change compared to 6 mM control mRNA levels which were assigned a value of 1. ER stress-related genes were upregulated in thapsigargin and tunicamycin treated MIN6 cells, relative to control cells (6 mM glucose). The data represent the mean ± SEM for n= 5 independent experiments. One-way ANOVA with Fischer's unprotected LSD test; *P<0.05, **P<0.01, ***P<0.001.

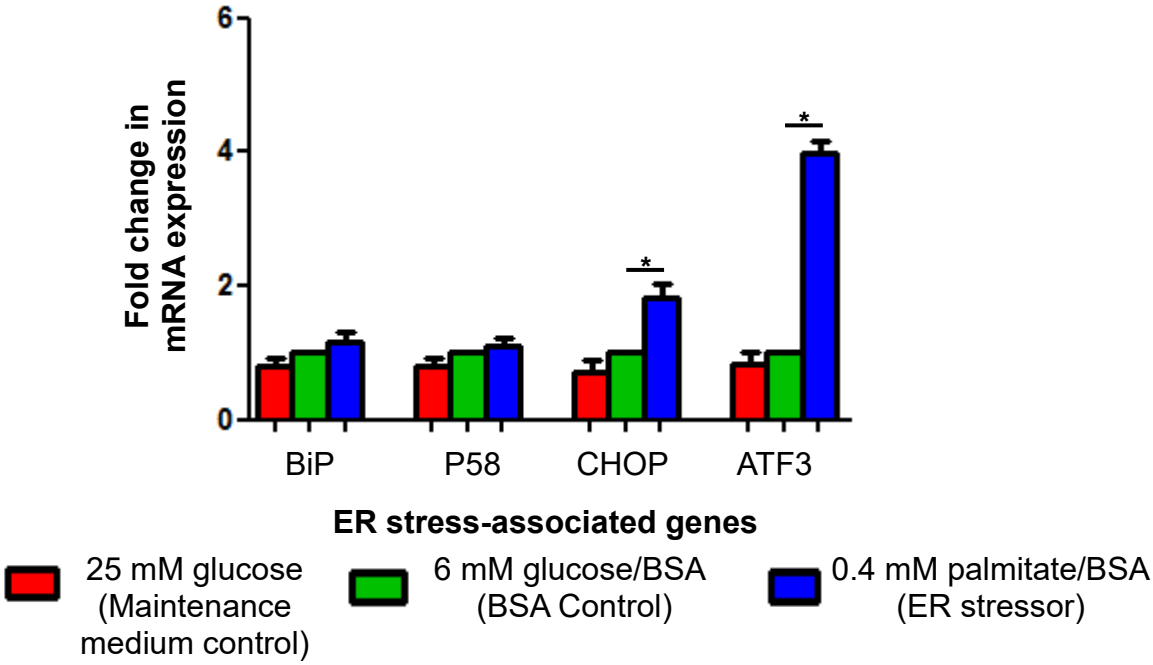

Figure 4.13: Induction of ER stress in MIN6 cells by treatment with palmitate.

MIN6 cells were cultured with 25 mM glucose medium, 6 mM glucose/BSA medium and 0.04 mM palmitate/BSA for 20-24 hrs. The cells were immediately frozen in liquid nitrogen for subsequent RNA extraction, cDNA preparation and TaqMan real-time PCR. Test transcript levels were quantified as a fold change compared to 6 mM control mRNA levels which were assigned a value of 1. CHOP and ATF3 mRNA levels were significantly elevated in ER stressed MIN6 cells, compared to controls. The data represent the mean ± SEM for n= 4 independent experiments. One-way ANOVA with Fischer's unprotected LSD test; *P<0.001.

mRNA expression for the pro-apoptotic ER stress-related genes ATF3 ($P<0.001$) and CHOP ($P<0.001$) were statistically significant when compared to control MIN6 cells (6 mM glucose/BSA).

These data confirm the induction of ER stress in MIN6 cells following acute *in vitro* treatment with pharmacological and physiological ER stress agents. Moreover, these studies showed that MIN6 cells preferentially upregulated the expression of pro-apoptotic genes (ATF3 and CHOP) compared to the adaptive UPR genes (BiP and P58) in response to ER stress.

4.2.2.3 Effect of pharmacologically-induced ER stress on HSPG core proteins, Hpse and HS in MIN6 cells

Having confirmed the acute induction of ER stress in MIN6 cells treated with thapsigargin and tunicamycin (see Section 4.2.2.2), MIN6 cells were cultured for 1-5 days in 6 mM glucose, 6 mM glucose + 50 nM thapsigargin and 6 mM glucose + 2 μM tunicamycin (see Section 2.5.2). The control and treated MIN6 cells were stained after 1, 2, 3, 4 and 5 days of culture for analysis of intracellular HSPG core proteins, Hpse and HS and analysed by flow cytometry (see Section 2.8).

4.2.2.3.1 Thapsigargin treatment of MIN6 cells

(a) HSPG core proteins

After 1 day of culture of MIN6 cells with thapsigargin, intracellular Col18 was significantly reduced to 72.2% ($P<0.01$) of controls cells (**Figure 4.14(a)**); in contrast, the intracellular expression of CD44 and Sdc1 resembled control cells (6 mM glucose; **Figure 4.14(a)**). Although the effects of thapsigargin treatment were not statistically significant on day 2, the reduction in intracellular Col18 persisted and there was a moderate decrease in intracellular Sdc1 (**Figure 4.14(b)**). By day 3, there was a significant decrease in Col18 and Sdc1 to 70.9% ($P<0.01$) and 57.5% ($P<0.05$), respectively, of control cells (**Figure 4.14(c)**), with a further decline to 50.7% ($P<0.001$) and 47.8% ($P<0.05$), respectively, by day 4 (**Figure 4.14(d)**). After 5 days of culture, no significant changes were observed in the expression of HSPG core proteins in ER stressed MIN6 cells compared to control 6 mM glucose MIN6 cells (**Figure 4.14(e)**). Interestingly, no significant change was observed in CD44 expression following thapsigargin treatment

Figure 4.14: Intracellular expression of HSPG core proteins in ER stressed MIN6 cells.

MIN6 cells were cultured with 6 mM glucose medium (control), 50 nM thapsigargin or 2 µM tunicamycin for 1-5 days and analysed for intracellular HSPG core proteins Col18, Sdc1 and CD44 by flow cytometry. The fluorescence staining is represented as GMFI. The data show mean ± SEM for n=4-11 experiments. One-way ANOVA with Fischer's unprotected LSD test; *P<0.05, **P<0.01, **P<0.001. C, control; Tg, thapsigargin; Tm, tunicamycin.

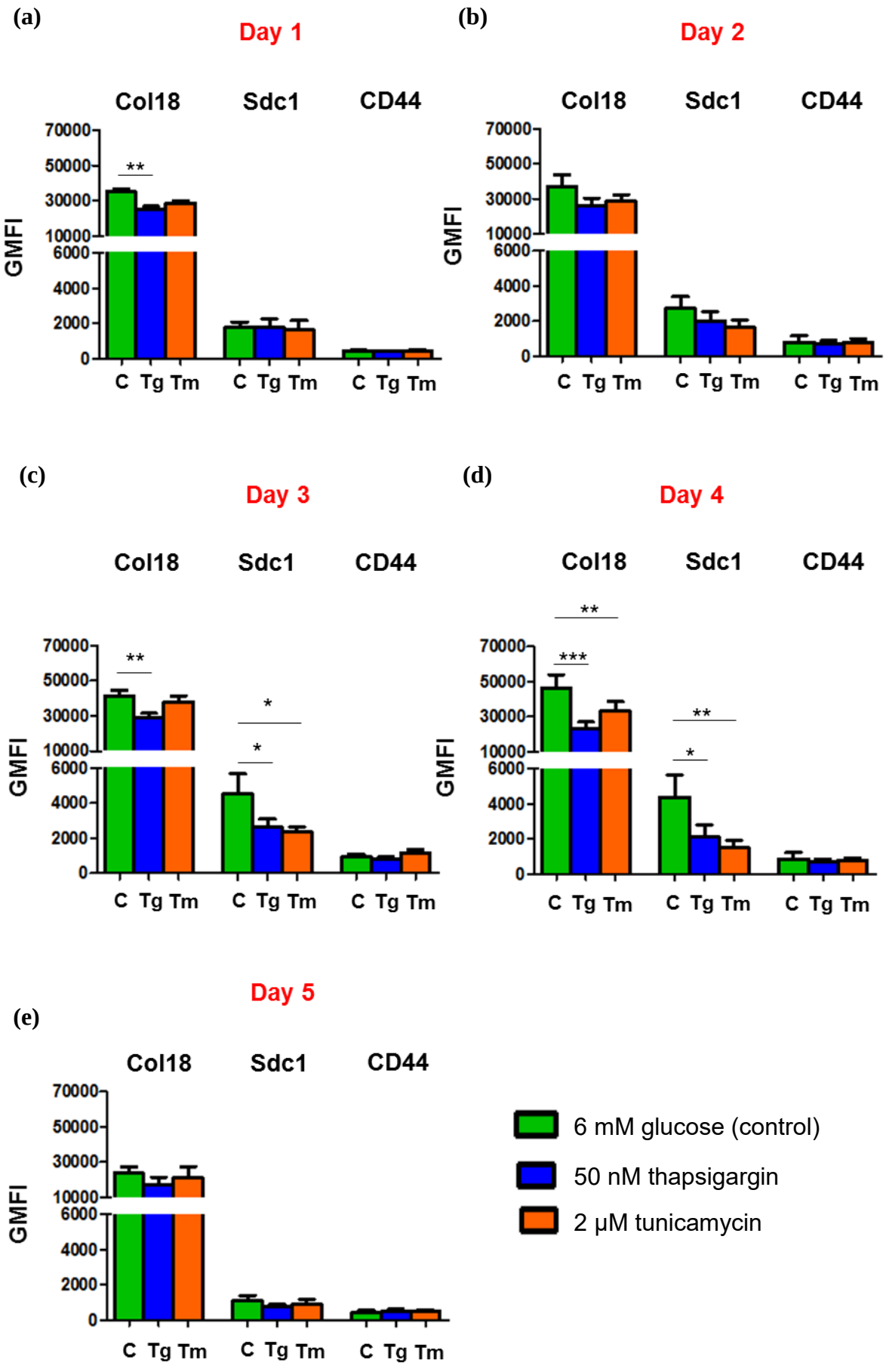
(a)
Day 1
Col18
Sdc1
CD44
GMFI
70000
50000
30000
10000
6000
4000
2000
0
**
C Tg Tm
(b)
Day 2
(c)
Day 3
*
*
(d)
Day 4
***
(e)
Day 5
6 mM glucose (control)
50 nM thapsigargin
2 µM tunicamycin

for 1-5 days (**Figure 4.14(a-e)**). Thapsigargin-mediated induction of ER stress in MIN6 cells resulted in a dramatic loss of intracellular Sdc1 core proteins and a moderate decline in intracellular Col18 core protein.

(b) HS

Thapsigargin-treated MIN6 cells showed a significant loss of intracellular HS to 79.8% ($P<0.05$) and 61.0% ($P<0.01$) of control cells at day 3 (**Figure 4.15(c)**) and day 4 (**Figure 4.15(d)**), respectively. No significant changes in HS levels were observed following thapsigargin treatment for 1, 2 or 5 days (**Figure 4.15(a, b, e)**). However, control MIN6 cells showed optimal intracellular HS on day 3 (GMFI= 17488.00 ± 2452.25), compared to day 4 (GMFI=13194.38 ± 2719.38) and day 5 (GMFI= 7283.50 ± 2391.27). The loss of intracellular HS observed in thapsigargin-treated MIN6 cells at day 3 and 4 parallels the loss of Col18 and Sdc1 HSPG core proteins.

(c) Heparanase (Hpse)

Intracellular Hpse levels were unchanged after treatment of MIN6 cells with thapsigargin for 1 day (**Figure 4.16(a)**). Thapsigargin treatment induced a significant decline in Hpse expression to 60% and 42.2% of controls (6 mM glucose) at day 2 ($P<0.05$; **Figure 4.16(b)**) and day 3 ($P<0.001$; **Figure 4.16(c)**), respectively. Intracellular Hpse decreased further to 35.8% ($P<0.001$) and 38.3% ($P<0.01$) of controls by day 4 (**Figure 4.16(d)**) and day 5, respectively (**Figure 4.16(e)**). Overall, intracellular Hpse was significantly reduced in MIN6 cells from days 2-5 after ER stress induction in MIN6 cells by treatment with thapsigargin.

4.2.2.3.2 Tunicamycin treatment of MIN6 cells

(a) HSPG core proteins

Tunicamycin treatment of MIN6 cells for 3 days resulted in a significant decrease of intracellular Sdc1 to 52% of control cells (6 mM glucose; $P<0.05$; **Figure 4.14(c)**). Although, a 1.3-fold increase in CD44 was also found, this change was not statistically significant (**Figure 4.14(c)**). After treatment for 4 days, MIN6 cells showed a significant decrease in intracellular Col18 and Sdc1 to 71.8% ($P<0.01$) and 34.1% ($P<0.01$) of controls (6 mM glucose), respectively (**Figure 4.14(d)**). No significant changes in HSPG core proteins were observed after tunicamycin treatment of MIN6 cells for 5 days (**Figure**

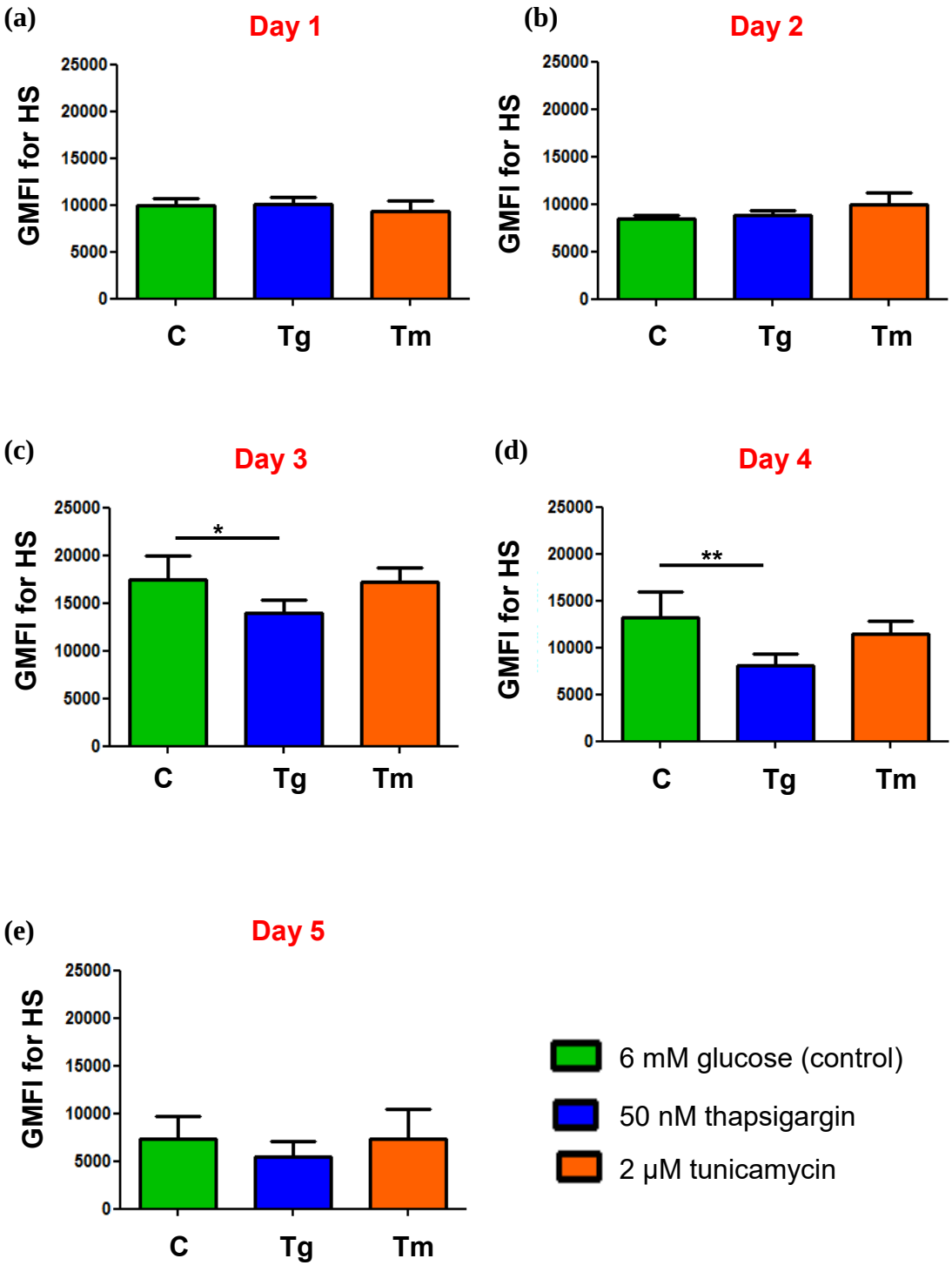

Figure 4.15: Intracellular levels of HS in ER stressed MIN6 cells.

MIN6 cells were cultured with 6 mM glucose medium (controls), 50 nM thapsigargin or 2 µM tunicamycin for 1-5 days and analysed for intracellular HS by flow cytometry. The fluorescence staining is represented as GMFI. The data show mean ± SEM for n=4-11 experiments. One-way ANOVA with Fischer's unprotected LSD test; *P<0.05, **P<0.01. C, controls; Tg, thapsigargin; Tm, tunicamycin.

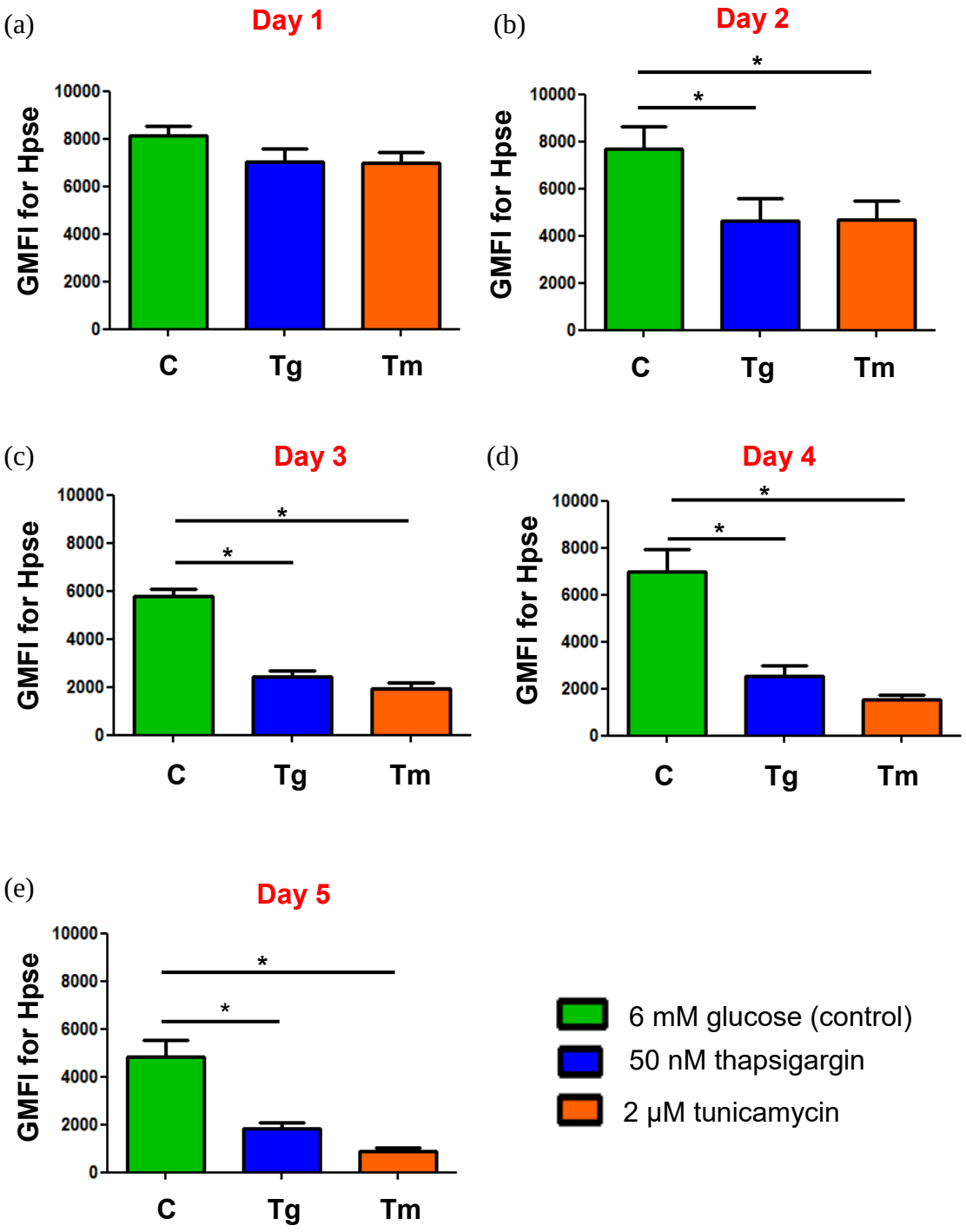

Figure 4.16: Intracellular levels of Hpse in ER stressed MIN6 cells.

MIN6 cells were cultured for 1-5 days with 6 mM glucose medium, 50 nM thapsigargin or 2 µM tunicamycin and intracellular Hpse was assessed by flow cytometry. The fluorescence staining was expressed as GMFI. The data represent mean ± SEM for n=4-11 experiments. One-way ANOVA with Fischer's unprotected LSD test; ***P<0.001. C, control; Tg, thapsigargin; Tm, tunicamycin.

4.14(e)). Overall, tunicamycin treatment of MIN6 cells for 3-4 days induced a significant loss of Sdc1 and Col18 core proteins compared to corresponding controls, with Sdc1 demonstrating more pronounced depletion, particularly on day 4.

(b) HS

Culture of MIN6 cells with tunicamycin for 1-5 days resulted in a transient decline in intracellular HS to 86.4% of controls by day 4 but no statistically significant differences were observed (**Figure 4.15**).

(c) Hpse

There was a significant decline in intracellular Hpse levels to 61% of controls after treatment of MIN6 cells for 2 days with tunicamycin ($P<0.0001$; **Figure 4.16(b)**). The levels were further reduced to 33.6%, 21.6% and 18.4% of control cells (6 mM glucose) by day 3, 4 and 5, respectively ($P<0.001$; **Figure 4.16(c-e)**). The expression of intracellular Hpse in MIN6 cells was significantly reduced by tunicamycin treatment for 2-5 days.

4.2.2.3.3 Summary

In summary, both thapsigargin- and tunicamycin-induced ER stress in MIN6 cells led to a significant loss of intracellular core proteins for Col18 and Sdc1 as well as the HS-degrading endoglycosidase, heparanase. These effects were prominent after treatment for 3-4 days. In contrast, only thapsigargin treated MIN6 cells demonstrated a significant loss of intracellular HS (day 3-4). However, since control MIN6 cells demonstrated signs of declining intracellular HS by day 4, the optimal duration of treatment with pharmacological ER stress-inducing reagents was identified as day 3. In contrast, when MIN6 beta cells were treated with the physiological ER stress inducer, palmitate for 3 days, intracellular HSPG core proteins and HS expression remained unchanged (data not shown). Overall, these findings clearly demonstrated that the pharmacological induction of ER stress in MIN6 beta cells decreases the intracellular expression of HPSG core proteins, Hpse and HS.

4.2.2.4 ER stress effects on beta cell viability

In parallel with studies of HSPG core proteins, HS and Hpse, MIN6 cells were cultured with or without pharmacological ER stress inducers (thapsigargin (50 nM) and tunicamycin (2 µM)), for 1-5 days. At daily intervals, the cells were harvested, stained with 7AAD and analysed by flow cytometry to determine the % of dead/damaged cells (see Section 2.5.2; **Figure 2.2**). These analyses were done on samples from the same MIN6 cultures used to examine intracellular HSPG core proteins, HS and Hpse.

4.2.2.4.1 Treatment of MIN6 cells with thapsigargin

Compared to control MIN6 cells, the % dead/damaged (7AAD+ve) thapsigargin-treated MIN6 cells was significantly increased 2.1-fold ($P<0.001$) and 1.5-fold ($P<0.001$) at day 2 and day 3, respectively (**Figure 4.17**). Thereafter, no further increase in the 7AAD+ve thapsigargin-treated population was observed and there was an apparent decline in cell death on days 4 and 5. It is possible that this outcome was due to the disintegration of the stressed cells during the staining and washing steps.

4.2.2.4.2 Tunicamycin-induced ER stress in MIN6 cells

The % of 7AAD+ve dying/damaged tunicamycin-treated MIN6 cells increased significantly on day 2 (1.7-fold; $P<0.01$), day 3 (2.2-fold; $P<0.001$), day 4 (1.6-fold; $P<0.001$) and day 5 (1.8-fold; $P<0.001$), compared to corresponding controls (**Figure 4.17**). In contrast to thapsigargin-induced ER stress, tunicamycin treatment resulted in a progressive increase in beta cell death over the 5-day culture period.

4.2.2.4.3 Overview of ER stress induction in MIN6 cells

In summary, ER stress-induced toxicity in MIN6 cells was pronounced by day 2 for thapsigargin and by day 3 for tunicamycin. Furthermore, ER stress-induced cell death continued to increase only in tunicamycin-treated cells up to day 5. These findings suggest that thapsigargin treatment leads to a more acute form of ER stress in MIN6 beta cells than tunicamycin, a finding which may be related to the more critical and earlier requirement for calcium ions during protein folding and maturation in the ER (Araki and Nagata, 2011, Hebert and Molinari, 2007).

Figure 4.17: Viability of ER stressed MIN6 beta cells.

MIN6 beta cells were cultured in 6 mM glucose, 50 nM thapsigargin or 2 μM tunicamycin for (a) 1, (b) 2, (c) 3, (d) 4 or (e) 5 days. At daily intervals, the cells were stained with 7AAD to determine the % 7AAD+ve cells in the total population by flow cytometry. A significant increase in cell damage/death was observed by day 2 (b) and day 3 (c). The data represents the mean GMFI ± SEM for n=4 experiments for day 1, 2 and 5; n=11 experiments for day 3 and n=8 experiments for day 4 for both thapsigargin and tunicamycin. One-way ANOVA with Fishers unprotected LSD test; *P<0.05, **P<0.01, ***P<0.001 and ns, not significant. C, control; Tg, thapsigargin; Tm, tunicamycin.

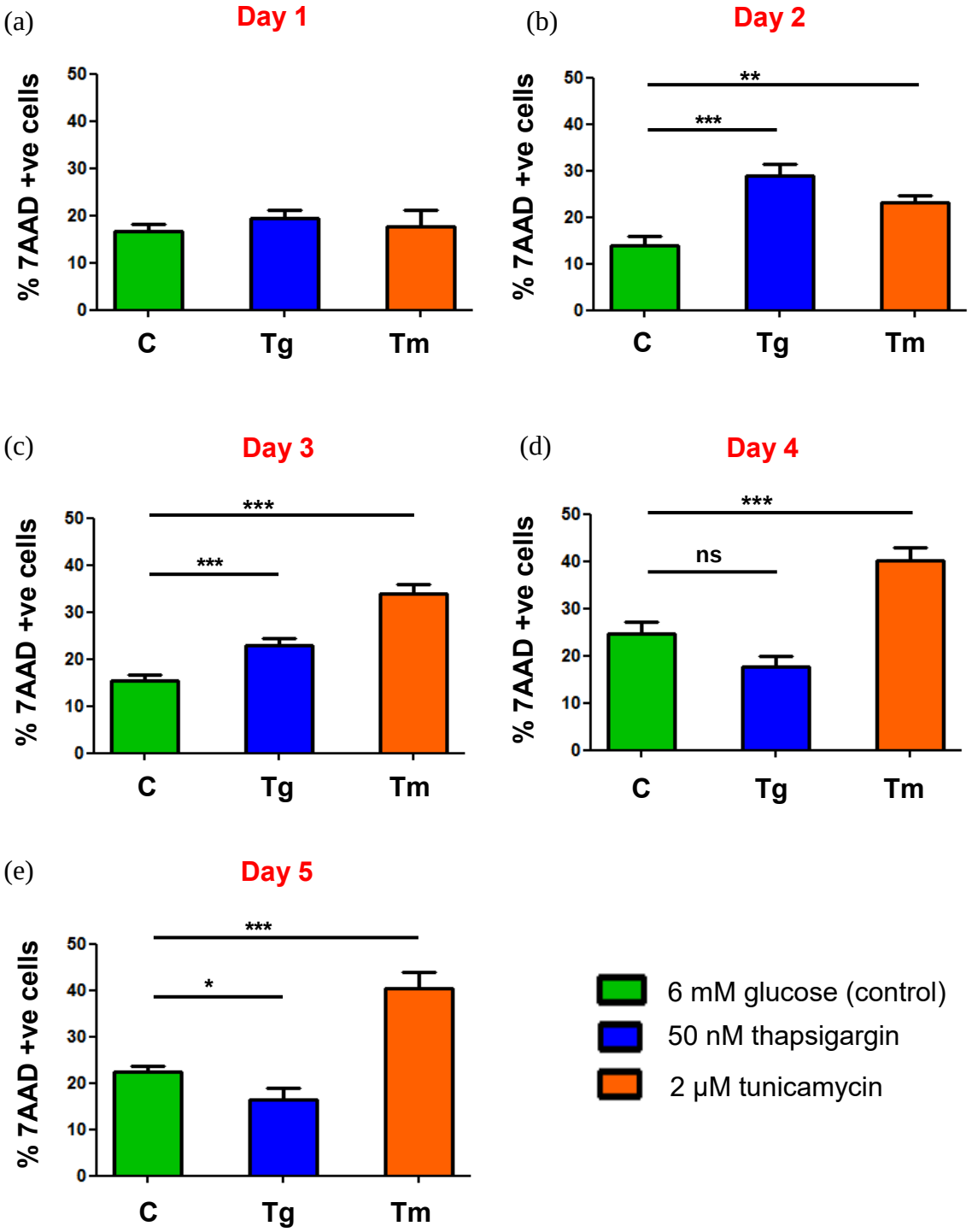
(a)
Day 1
% 7AAD +ve cells
50
40
30
20
10
0
C
Tg
Tm
(b)
Day 2
**
***
(c)
Day 3
***
***
(d)
Day 4
***
ns
(e)
Day 5
***
*
6 mM glucose (control)
50 nM thapsigargin
2 µM tunicamycin

Despite the early ~ 2-fold increase in beta cell damage/death by day 2 of thapsigargin treatment, no significant reduction in HSPG core proteins or HS was observed. Furthermore, compared to day 2, the % cell death/damage on day 3 was lower (a 1.5-fold increase over corresponding controls), a finding that correlated with a statistically significant decrease in intracellular Col18, Sdc1, HS and Hpse to ~70%, ~60%, ~80% and ~40% of controls, respectively. In addition, while there was a significant ~2-fold increase MIN6 cell damage/death by day 3 of tunicamycin treatment, no significant decline in the intensity of intracellular staining for Col18, CD44 or HS was observed, despite a significant 50% decrease in intracellular Sdc1 staining.

Taken together, ER stress-induced modulation of the intensity of staining for intracellular HSPG core proteins, HS and Hpse did not appear to be a secondary effect of early damage/death of MIN6 cells in the cultures. On this basis, we attribute the changes in these intracellular components to the experimental induction of ER stress by thapsigargin and tunicamycin.

4.2.3 Thapsigargin treatment of isolated BALB/c islets

To ascertain the relevance of ER stress effects observed in MIN6 cells for primary beta cells, isolated BALB/c islets were treated with 5 µM thapsigargin in culture for 3 days (see Section 2.3.1). At the end of the culture period, the islets were dispersed into single cells (see Section 2.3.2) and intracellular HSPG core proteins, HS and Hpse were stained and analysed by flow cytometry. A significant reduction in intracellular Sdc1 and CD44 core proteins to ~60-65% of controls ($P<0.05$) was observed (**Figure 4.18**). In addition, intracellular Col18, HS and Hpse was substantially decreased to ~70%, 80% and 80% of controls, although statistical significance in these changes was not demonstrated.

Similar to ER stress-related effects in MIN6 beta cells (see Section 4.2.2), the induction of ER stress in isolated islets/beta cells, in the absence of insulin resistance (unlike db/db beta cells (see Chapter 3)) correlated with a significant loss of HSPG core proteins and a marked reduction in intracellular HS and Hpse. The contribution of ER stress-induction and HS loss *in vivo* on beta cell viability was evaluated in db/db beta cells in Chapter 5 (Section 5.2.2).

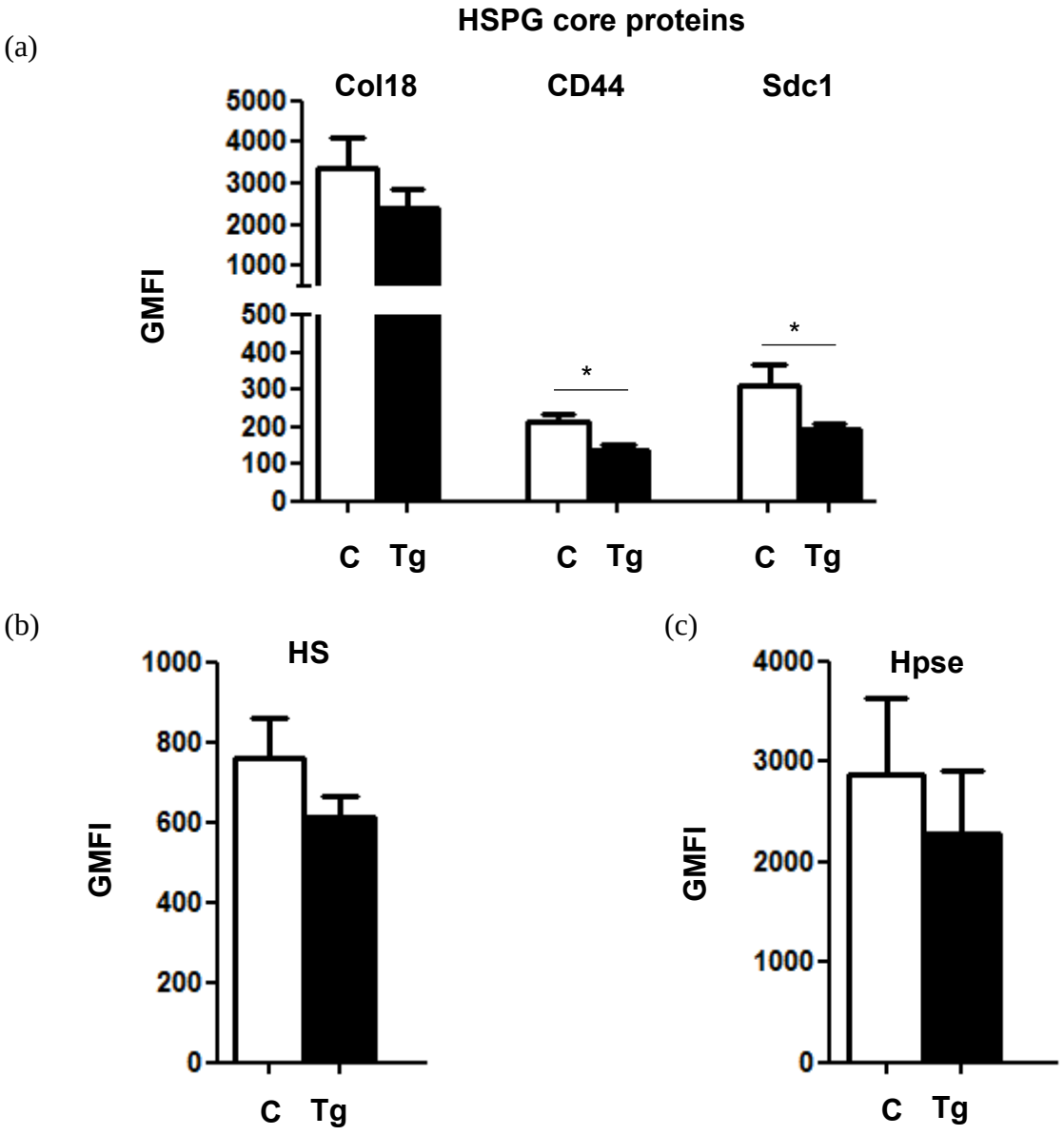

Figure 4.18: Expression of HSPG core proteins, HS and Hpse in thapsigargin treated islets.

The islets were isolated from BALB/c mice and cultured with 5 μM thapsigargin for 3 days. The islets were dispersed to single cells and the intracellular staining of HSPG core proteins, HS and Hpse were analysed by flow cytometry. Thapsigargin-treated beta cells (black bars) showed a significant decrease in intracellular CD44 and Sdc1 core proteins, compared to controls (open bars; (a)). The data represents the GMFI ± SEM for n=5 experiments/group. Unpaired t test; *P<0.05.

4.3 Discussion

In this chapter, three additional models were used to study the effects of endoplasmic reticulum (ER) stress on heparan sulfate proteoglycan (HSPG) core proteins and heparan sulfate (HS) in beta cells. The first model, heterozygous Akita ($Ins2^{WT/C96Y}$) mice, exhibits acute endogenous ER stress-induced loss of beta cell function and subsequent diabetes. In the second and third models, ER stress was experimentally induced in MIN6 beta cells and isolated islets (primary beta cells).

(i) Akita mouse model of ER stress-induced diabetes

Our studies of heterozygous Akita $Ins2^{WT/C96Y}$ mice showed overt hyperglycaemia by as early as 4 weeks of age (**Figure 4.1**). This data is consistent with previous reports of loss of beta cell function, reduction of beta cell mass and overt hyperglycaemia by 4 weeks of age (Katsuda et al., 2013, Lei et al., 2010). Additionally, we found that male $Ins2^{WT/C96Y}$ mice developed more severe hyperglycaemia than female $Ins2^{WT/C96Y}$ mice (**Figure 4.1**). This finding confirms previous reports of higher blood glucose levels in both male homozygous $Ins2^{C96Y/C96Y}$ and heterozygous $Ins2^{WT/C96Y}$ mice than in corresponding females (Lei et al., 2010, Wang et al., 1999).

Mice have two non-allelic insulin genes, *Ins1* and *Ins2*, with the *Ins2* gene producing the majority of circulating insulin. Akita mice have a C96Y mutation in the *Ins2* gene resulting in acute onset of diabetes. The single homozygous mutant $Ins1^{-/-}$ and $Ins2^{-/-}$ mouse strains do not develop diabetes and have normal plasma insulin levels (Oyadomari et al., 2002b, Leroux et al., 2001). Despite the presence of 3 normal insulin alleles (two wildtype *Ins1* alleles and one wildtype *Ins2* allele), heterozygous $Ins2^{WT/C96Y}$ mice exhibit ER stress-induced progressive loss of beta cell mass and eventually develop diabetes (Wang et al., 1999, Leroux et al., 2001, Oyadomari et al., 2002b, Eizirik et al., 2008). The C96Y mutation in the *Ins2* gene in these mice prevents the formation of a disulfide bond between the A and B chain resulting in the formation of mutant proinsulin protein in the ER (Yoshioka et al., 1997, Wang et al., 1999). The misfolded proinsulin accumulates in the ER and forms a complex with the ER chaperone BiP, inducing ER stress and subsequently beta cell apoptosis (Oyadomari et al., 2002b, Wang et al., 1999).

Electron microscopy of heterozygous Akita beta cells has revealed enlargement of ER like organelles in islet beta cells, suggesting the accumulation of mutant proinsulin in the ER (Izumi et al., 2003). The mutant proinsulin is degraded intracellularly and only properly folded proinsulin exits the ER and enters the secretory pathways (Izumi et al., 2003, Zuber et al., 2004). The initial decline in insulin secretion is due to the engagement of misfolded proinsulin with bystander proinsulin, a process which impairs the egress of wildtype proinsulin from the ER and thus blocks wildtype proinsulin production in the $Ins2^{WT/C96Y}$ beta cells (Liu M et al 2007). Initially, this accumulation of mutant protein activates the adaptive UPR to maintain homeostasis in the ER, as shown by increased expression of the ER resident chaperones, BiP and protein disulfide isomerase (Izumi et al., 2003, Oyadomari et al., 2002b). Interestingly, overexpression of BiP (via liberation of WT proinsulin from high molecular weight complexes) assisted the selective degradation of mutant proinsulin but not wildtype proinsulin in Akita mice, permitting the wildtype proinsulin to be exported from the ER for cleavage of native insulin in the secretory granules (Cunningham et al., 2017).

When ER stress is prolonged in the beta cells, the UPR shifts from "survival" mode to "apoptosis". Conventionally, the latter is characterised by the expression of CHOP protein (Pirot et al., 2007, Ma et al., 2002, Scheuner and Kaufman, 2008, Chan et al., 2015). The transcription factor CHOP induces the activation of the pro-apoptotic Bcl2 family member BIM (Puthalakath et al., 2007, Miani et al., 2013) and also plays a central role in nitric oxide-induced apoptosis in beta cells (Oyadomari et al., 2001). In addition, mutant proinsulin can also act as a "proteotoxin", exhausting the adaptive UPR and triggering multiple pro-apoptotic UPR pathways (Ron, 2002a, Liu et al., 2010, Liu et al., 2007) that result in beta cell death and diabetes (Oyadomari et al., 2002b). In summary, $Ins2^{WT/C96Y}$ beta cells are characterised by an expanded ER compartment, mutant proinsulin polypeptides associated with BiP, chronic ER stress and diminished insulin secretion culminating in decreased insulin levels in the blood (Yoshioka et al., 1997, Wang et al., 1999, Zuber et al., 2004, Izumi et al., 2003).

Consistent with previous findings (Oyadomari et al., 2002b, Chen et al., 2011, Shirakawa et al., 2013, Yamane et al., 2011), we observed a dramatic increase in mRNA levels of ER stress-associated genes in the islets of male $Ins2^{WT/C96Y}$ mice (**Figure 4.2**). Moreover,

there was a more striking upregulation in the expression of adaptive UPR genes, compared to pro-apoptotic genes. The massive ~286-383-fold increase that we observed in the transcripts for adaptive UPR genes encoding ER chaperone proteins could potentially lead to increased folding activity (e.g., mutant proinsulin protein) and help limit protein aggregation in the ER of the beta cells (Eizirik et al., 2008). However, failure of the adaptive response to compensate for ER stress would be expected to activate the expression of CHOP and ATF3, resulting in beta cell apoptosis. Consistently, our real-time RT-PCR analyses showed a ~6-33-fold increase in pro-apoptotic ER stress-related genes supporting other studies showing that hyperglycaemia in both heterozygous $Ins2^{WT/C96Y}$ and homozygous $Ins2^{C96Y/C96Y}$ Akita mice was accompanied by the induction of CHOP transcripts and beta cell apoptosis (Chen et al., 2011, Oyadomari et al., 2002a). The increased expression of adaptive UPR genes observed in our study represents a compensatory response by beta cells to overcome ER stress (Chan et al., 2013).

The Akita mouse strain is an established model of ER stress-mediated diabetes (Oyadomari et al., 2002b, Chen et al., 2011, Yoshioka et al., 1997, Ron, 2002b) and was therefore used in this study to validate whether excessive ER stress in beta cells results in loss of intracellular HS and HSPG core proteins, as observed in the ER stressed islets of db/db mice. Normally to compensate for ER stress, cells increase their protein folding activity, prevent protein aggregation, attenuate translation, and degrade misfolded proteins via the ER associated degradation (ERAD) pathway (see Section 1.9) (Araki et al., 2003, Eizirik et al., 2008). We therefore examined the expression of three HSPG core proteins, i.e., collagen type XVIII, syndecan-1 and CD44 in the pancreatic islets of $Ins2^{WT/WT}$ and $Ins2^{WT/C96Y}$ mice from 4-9 weeks of age. Choong et al. (2015) previously reported that these HSPG core proteins are highly expressed in the beta cells of normal islets. Similarly, our study demonstrated strong expression of collagen type XVIII, syndecan-1 and CD44 in the islets of $Ins2^{WT/WT}$ mice (**Figures 4.4 and 4.8**). In contrast, a dramatic loss of HPSG core proteins was revealed in the islets of very young $Ins2^{WT/C96Y}$ mice at 4 weeks of age. Immunohistochemistry analyses of male and female $Ins2^{WT/C96Y}$ islets showed a rapid loss of intra-islet Sdc1 and CD44 and a slower decline in intra-islet Col18 (**Figures 4.4 and 4.8**). Interestingly, the depletion of HSPG core proteins was more pronounced in male Akita mice than females, correlating with the more severe hyperglycaemia in males (**Figure 4.1**). Furthermore, CD44 was expressed at the cell

surface in Ins2$^{WT/C96Y}$ beta cells but largely intracellularly in control Ins2$^{WT/WT}$ beta cells. This finding could reflect a slow turnover of cell surface CD44 in Akita Ins2$^{WT/C96Y}$ beta cells or preferential export to the cell surface when the supply of CD44 protein is limiting.

In general, CD44 core protein is a ubiquitously expressed cell surface protein which plays an important role in cell aggregation, migration, activation and tumor metastasis. CD44 can also regulate hyaluronic metabolism as well as the activation of lymphocytes and subsequent release of cytokines (Lesley et al., 2000, Senbanjo and Chellaiah, 2017). In contrast to our data, a recent report revealed that CD44 (all isoforms of CD44 (panCD44) and CD44v) expression as detected by immunohistochemistry, was most prominently expressed at the cell surface of beta cells and was higher in diabetic mouse (db/db, ob/ob and Akita mice) strains compared to corresponding controls at 8-16 weeks of age (Kobayashi et al., 2018). In our studies, CD44 expression was highly expressed intracellularly in the beta cells of wildtype mice (Akita and db mice) whereas weaker and more prominent cell surface expression of CD44 was observed in the diabetic Ins2$^{WT/C96Y}$ and db/db islets. The discrepancy between the studies could be due to differences in antigen retrieval procedures. In fact, Kobayashi et al. (2018) did not describe an antigen retrieval step in their immunostaining methodology, suggesting that the immunostaining was done in the absence of antigen retrieval. Nevertheless, our finding that CD44 is preferentially localised at the cell surface in Ins2$^{WT/C96Y}$ islets does not argue against the conclusion drawn by Kobayashi et al. (2018) that cell surface CD44 can inhibit L-amino acid uptake into beta cells, thereby reducing insulin biosynthesis. This pathway could therefore contribute to ER stress relief in Akita beta cells.

We have found that ER stress-induced diabetes in non-obese Akita Ins2$^{WT/C96Y}$ mice correlated with a dramatic and early decline in intra-islet (beta cell) HSPG core proteins. Similarly, ER stress in the beta cells of obese db/db mice during T2D development correlated with a progressive reduction in both islet HSPG core proteins and HS (see Chapter 3). Since HS chains are assembled directly onto HSPG core proteins (see Section 1.13), the intra-islet expression of HS was analysed in Ins2$^{WT/C96Y}$ mice using EV3C3 phage display anti-HS Ab. This antibody detects N-sulfation, C5 epimerisation and 2-O sulfation in HS (Rops et al., 2008, Kurup et al., 2007, Dennissen et al., 2002) but not 6-O sulfation recognised by 10E4 anti-HS mAb. Due to the limited supply of the antibody,

only pancreas samples from male $Ins2^{WT/WT}$ and $Ins2^{WT/C96Y}$ donors at 6 weeks of age were examined. A striking finding was that the expression of intra-islet (beta cell) HS in $Ins2^{WT/C96Y}$ mice was reduced to 58.4% of corresponding age-matched controls (**Figure 4.5(c)**). Similar to HSPG core proteins, beta cell HS was therefore also significantly reduced in ER-stressed beta cells of Akita $Ins2^{WT/C96Y}$ mice, resembling db/db beta cells during T2D progression. Interestingly, we also observed strong HS staining in the periphery of both $Ins2^{WT/C96Y}$ and $Ins2^{WT/C96Y}$ islets i.e., in alpha cells. However, unlike beta cells that contain HS composed of highly sulfated and less sulfated regions, alpha cells contain only less-sulfated HS (Theodoraki et al., 2015) and are therefore more intensely stained with EV3C3 anti-HS Ab. Our data therefore demonstrate a selective loss of beta cell HS in the islets of $Ins2^{WT/C96Y}$ mice during the development of ER stress-induced diabetes.

Like previous studies (Shirakawa et al., 2013, Yamane et al., 2011, Nozaki et al., 2004, Gupta et al., 2010, Wang et al., 1999, Chen et al., 2017) and in contrast to $Ins2^{WT/WT}$ islets, we also found a significant decline in insulin staining of $Ins2^{WT/C96Y}$ islets to 34-63% of controls (**Figures 4.7(a) and 4.9(a)**). Furthermore, our immunohistochemical staining revealed punctate staining for proinsulin, suggesting the localisation of non-processed proinsulin in immature secretory granules in the trans-Golgi network/ER (Asadi et al., 2015). The proinsulin levels were significantly reduced to ~31-32% of controls in the islets of diabetic $Ins2^{WT/C96Y}$ mice at 6 weeks of age (**Figures 4.7(b) and 4.9(b)**), which is in line with previous studies (Kobayashi et al., 2013, Wang et al., 1999, Gupta et al., 2010). In contrast, we found evidence for increased glucagon staining in heterozygous $Ins2^{WT/C96Y}$ islets, compared to wt islets (**Figures 4.7(c) and 4.9(c)**). This data is consistent with previous findings where the circulating glucagon levels were increased at onset of diabetes in Akita mice (Barbetti et al., 2016). This increase in glucagon expression may elevate the rate of gluconeogenesis and glycogenolysis and contribute to hyperglycaemia (Unger, 1971, Barbetti et al., 2016). The action of insulin and glucagon provide exquisite control of glucose metabolism and any small change in the insulin/glucagon ratio can influence glycaemic control (Quesada et al., 2008, Jiang and Zhang, 2003). A low insulin/glucagon ratio increases the breakdown of hepatic glucose and promotes the release of free fatty acids (Barbetti et al., 2016). Increased circulating FFAs and FFA uptake by beta cells could further exacerbate ER stress in the beta cells

(Olefsky and Glass, 2010, McNelis and Olefsky, 2014). Our study confirmed a loss of insulin and proinsulin in the pancreatic islets of Akita $Ins2^{WT/C96Y}$ mice which exhibit ER stress-induced diabetes.

The reported decline in beta cell mass in Akita $Ins2^{WT/C96Y}$ mice is attributed to ER stress-induced beta cell death (Oyadomari et al., 2002a, Yamane et al., 2011, Lei et al., 2010, Izumi et al., 2003, Oyadomari et al., 2002b). In general, caspase 12, transcription factor CHOP and JNK activation are the critical effectors of ER stress-induced apoptosis in beta cells (Nakagawa et al., 2000, Oyadomari et al., 2002a, Yoshida, 2007, Ariyasu et al., 2017, Song et al., 2008, Eizirik et al., 2008, Laybutt et al., 2007). ER stress-associated activation of the transcription factor CHOP has been reported to contribute to beta cell apoptosis and diabetes in Akita mice (Oyadomari et al., 2002b, Nakagawa et al., 2000). Northern blotting and PCR analyses demonstrated that the islets of $Ins2^{WT/C96Y}$ mice display high levels of the pro-apoptotic marker CHOP (Oyadomari et al., 2002b, Winnay et al., 2014). Consistent with this property, the development of diabetes in $Ins2^{WT/C96Y}$ $Chop^{-/-}$ mice was delayed by 8-10 weeks (Oyadomari et al., 2002b). *In vitro* studies have shown that the ER of $CHOP^{-/-}$ cells is a hypo-oxidizing environment and that $CHOP^{-/-}$ cells are protected from ER stress-induced death (Marciniak et al., 2004). Beta cell protection in $Ins2^{WT/C96Y}$ $CHOP^{-/-}$ mice could also be attributed to increased resistance to nitric oxide-induced apoptosis (Wu and Kaufman, 2006). It is noteworthy, however that $Ins2^{C96Y/C96Y}$ $CHOP^{-/-}$ mice do not show any protection from diabetes (Oyadomari et al., 2002b), indicating that one or more CHOP-independent pathways exist for ER stress-induced beta cell death. Other alternative apoptosis pathways include the activation of JNK (Urano et al., 2000) and caspase-12 (Nakagawa et al., 2000).

We propose that the loss of HSPGs/HS in ER-stressed $Ins2^{WT/C96Y}$ beta cells represents a novel alternative mechanism for inducing beta cell death. Islet HS has been reported to play a critical role in postnatal islet maturation, growth and morphogenesis as well as insulin secretion (Takahashi et al., 2009). In fact, Takahashi et al. (2012) found that 3-O sulfate group of HS was necessary for maintaining normal glucose-stimulated insulin secretion by beta cells (Takahashi et al., 2012). Significantly, highly sulfated HS but not under-sulfated HS was found to preserve the survival of mouse beta cells by protecting them from oxidative damage (Ziolkowski et al., 2012). In support, Theodoraki et al. (2015)

provided evidence that desulfation of HS in rat INS1 beta cells increased their susceptibility to hydrogen peroxide-induced damage. Hence there is convincing evidence that intracellular HS plays a critical role in beta cell survival. We propose that the loss of HSPG core proteins and HS observed in $Ins2^{WT/C96Y}$ islets due to ER stress would render the beta cells highly susceptible to oxidative damage and subsequent death. Moreover, PCR analyses have revealed high levels of oxidative stress-responsive genes (Nuclear factor erythroid 2-related factor 1 (Nrf1), nuclear factor erythroid 2-related factor 1 (Nrf2), catalase, superoxide dismutase 1 (SOD1), superoxide dismutase 2 (SOD2), heme oxygenase 1 (HMOX1)) in the islets of $Ins2^{WT/C96Y}$ mice compared to $Ins2^{WT/WT}$ islets from donors at 20 weeks of age (Winnay et al., 2014). The increased expression of antioxidant markers in $Ins2^{WT/C96Y}$ islets parallels our observed loss of HSPGs/HS in $Ins2^{WT/C96Y}$ beta cells; importantly, the induced antioxidant response offers insufficient protection against the development of diabetes. Taken together, our findings provide insight into a novel mechanism where the loss of HSPGs/HS in beta cells contributes to overwhelming oxidative stress, beta cell death and diabetes in $Ins2^{WT/C96Y}$ mice.

(ii) Experimental induction of ER stress in MIN6 cells

The MIN6 cell line (derived from a mouse insulinoma) is widely used for *in vitro* studies of beta cells (Miyazaki et al., 1990). MIN6 beta cells exhibit glucose-induced insulin secretion similar to primary beta cells (Ishihara et al., 1993), and have therefore been used to study pathways regulating insulin production and secretion. Syndecan-4 in MIN6 cells was recently reported to play a role in the insulin secretory response (Takahashi et al., 2017) but other HSPG core proteins expression in MIN6 cells has not previously been reported. Our flow cytometry analyses of MIN6 beta cells demonstrated high expression of intracellular Col18 core protein and HS but low cell surface expression (**Figure 4.10**). While our findings confirm the previous report by Takahashi et al. (2012) of HS inside MIN6 cells, we identify Col18 and Sdc1 as major HSPG core proteins responsible for the localisation of HS in MIN6 cells. Furthermore, our findings are consistent with the intracellular expression of HS and HSPG core proteins in primary beta cells, previously observed by flow cytometry analyses (Ziolkowski et al., 2012, Choong et al., 2015) and western blotting (Takahashi et al., 2012). Additionally, we found that heparanase, an endoglycosidase that cleaves HS chains is highly expressed inside MIN6 cells (**Figure 4.10(c)**), like primary mouse beta cells (**Figure 4.18**). It is likely that beta cell heparanase

functions in regulating HS turnover, a homeostatic process required to maintain cellular HS, as reported for other cell types (Bernfield et al., 1999). Our demonstration of intracellular HSPG core proteins, HS and heparanase in MIN6 beta cells established this cell line as an ideal source of surrogate beta cells for directly probing the relationship between ER stress and intracellular HSPG core proteins/HS.

Initially, using TaqMan real-time RT-PCR, we confirmed the induction of ER stress-related gene expression in MIN6 cells treated with pharmacological (thapsigargin and tunicamycin) and physiological (palmitate) agents (**Figures 4.11, 4.12 and 4.13**). These data were in agreement with other reports where RT-PCR, Northern blotting and Western blotting showed increased expression of UPR genes and proteins (e.g., ATF4, BiP, P58, CHOP and ATF6) in MIN6 cells treated with thapsigargin (1 µM; 2-20 nM), tunicamycin (1-10 µg/ml; 10-100 ng/ml) and palmitate (0.4-0.5 mmol/L) for 4-48 hours (Zhou et al., 1998, Srinivasan et al., 2005, Laybutt et al., 2007, Sharma et al., 2015, Ueda et al., 2005, Hong et al., 2018, Puyal et al., 2013). We observed that unlike $Ins2^{WT/C96Y}$ (heterozygous Akita) islets and tunicamycin-treated MIN6 cells where the expression of both early and late ER stress-related genes were upregulated (**Figures 4.2 and 4.12(b)**), thapsigargin-treated MIN6 cells demonstrated a striking and selective upregulation of pro-apoptotic markers (CHOP and ATF3; **Figure 4.12(a)**), indicating that apoptosis/cell death pathways were acutely activated. These disparities could be due to differences in the range of proteins impacted by ER stress and/or specific inhibition *in vitro* of different fundamental elements or processes required for protein maturation e.g., calcium ion levels in the ER lumen (Oslowski and Urano, 2011, Urra et al., 2013).

Our *in vitro* studies of MIN6 cells revealed a significant decrease in intracellular HSPG core proteins (collagen type XVIII, syndecan-1), HS and Hpse after culture with thapsigargin for 3 days. Similarly, tunicamycin treatment of MIN6 cells resulted in a significant decline in syndecan-1 and Hpse by day 3. In contrast to thapsigargin treatment, the loss of intracellular HS was not observed with tunicamycin treatment of MIN6 cells. This could be due to the presence of other HSPG core proteins available for HS synthesis in the beta cells, such as intracellular Col18 which remained unchanged over the time course. A significant loss of intracellular Hpse was observed in ER stressed MIN6 cells after 2 days of culture indicating that Hpse is highly sensitive to ER stress and therefore

would be unlikely to contribute to diminishing intracellular HS levels in ER-stressed MIN6 cells.

Previously, ER stress in MIN6 cells has been reported to impact beta cell function and survival (Srinivasan et al., 2005, Furukawa et al., 1999, Chen et al., 2013). Srinivasan et al. (2005) demonstrated that thapsigargin- or tunicamycin-induced ER stress in MIN6 cells inhibits the phosphorylation of Akt and glucogen synthase kinase 3 beta (GSK3β) and impairs insulin receptor signalling. Furthermore, long term exposure of MIN6 cells to FFAs (such as palmitate) reduced the synthesis and post-translational modification of proinsulin and prohormone convertases 2/3 (Furukawa et al., 1999). Increased expression of the autophagy activation marker LC3-11 has also been observed in ER stressed MIN6 cells (Chen et al., 2013).

Our study demonstrated that thapsigargin was more effective in depleting intracellular Col18 and HS in MIN6 cells than tunicamycin treatment. This difference could be due to the different mechanisms by which these agents induce ER stress. Thapsigargin blocks calcium ion uptake by the ER which severely reduces the calcium-dependent protein-folding activity of ER chaperones and causes the accumulation of misfolded proteins and ER stress (Zhang and Kaufman, 2008b, Yoshida, 2007, Oslowski and Urano, 2011, Laybutt et al., 2007, Treiman et al., 1998). Thapsigargin is therefore likely to have a more severe impact on protein synthesis compared to tunicamycin which blocks N-linked glycosylation in the ER (Araki et al., 2003, Zhou et al., 1998, Ariyasu et al., 2017). Our data clearly showed that acute ER stress directly reduced intracellular HSPG core proteins in MIN6 cells, resulting in the reduced intracellular localisation of HS, presumably due to impaired HS synthesis. It should be noted that ultimately the intracellular levels of HS during acute ER stress induction will reflect the net effects of the turnover of HSPG core proteins by proteases, a homeostatic process which may vary for different HSPGs. It is noteworthy that a higher proportion of intracellular Col18 core protein was preserved relative to other HSPG core proteins in ER stressed MIN6 cells (**Figure 4.14**). Such differential effects could therefore mask the contribution of diminished Sdc1 core protein levels to the intracellular pool of HS. In any case our study has ruled out a pivotal role for heparanase in reducing intracellular HS during ER stress, with the intracellular levels of

Hpse being significantly lowered to ~20-40% of controls (**Figure 4.16**) in both thapsigargin- and tunicamycin-treated MIN6 cells.

When ER stress is prolonged, apoptotic pathways are activated via the induced transcription of CHOP and/or by the activation of JNK and caspase-12 (see Section 1.9). Thapsigargin and tunicamycin induce ER stress in MIN6 cells, in a dose and time-dependent manner, resulting in CHOP-mediated growth arrest and cell death (Zhou et al., 1998, Srinivasan et al., 2005, Oyadomari et al., 2001). Consistent with previous studies (Zhou et al., 1998, Srinivasan et al., 2005, Laybutt et al., 2007), our PCR data confirmed an increase in the expression of CHOP and ATF3 with thapsigargin, tunicamycin and palmitate treatment of MIN6 cells (**Figures 4.12 and 4.13**). The activation of CHOP as well as other pro-apoptotic pathways lead to the activation of caspase 3, indicating that ER stress signals are transmitted to mitochondria (Oyadomari and Mori, 2004). The mechanism by which CHOP stimulates cell death/apoptosis includes downregulation of the anti-apoptotic protein Bcl-2 (Eizirik et al., 2008, Fonseca et al., 2011), increased generation of cellular reactive oxygen species including the upregulation of ER oxidoreductase 1, and the upregulation of pro-apoptotic genes (Puthalakath et al., 2007, Miani et al., 2013). Our study showed a significant increase in % dead/damaged MIN6 cells (**Figure 4.19**) following acute exposure to ER stress-inducing agents.

In summary, our study of ER-stressed MIN6 cells revealed a loss of intracellular HSPGs/HS, expression of pro-apoptotic CHOP and ATF3 transcripts and increased beta cell death. Intracellular HS has been reported to protect the beta cells from reactive oxygen species; furthermore HS depletion resulted in beta cell death *in vitro* and correlated with the development of T1D in NOD mice (Ziolkowski et al., 2012). However, the significant loss of HS did not temporally correlate with an increase in 7AAD+ve MIN6 cells. This finding suggests that thapsigargin and tunicamycin treatment of MIN6 cells rapidly and directly activate the apoptotic pathways (as shown by the preferential upregulation of the pro-apoptotic UPR genes CHOP and ATF3 after ~24 hrs of culture), possibly by-passing the adaptive UPR. In support of this notion, Zhou et al. (1998) demonstrated that the depletion of intracellular Ca^{2+} stores due to thapsigargin-treatment of MIN6 cells is sufficient to trigger apoptosis. The activation of CHOP in ER-stressed MIN6 cells would be expected to upregulate the production of reactive oxygen species

(ROS) and reactive nitrogen species (Wang and Wang, 2017, Malhotra and Kaufman, 2007, Hsieh et al., 2007) which together with reduced intracellular HS, would increase the vulnerability of the cells to oxidative damage and subsequent death. Alternatively, it is possible that the acute *in vitro* treatment of MIN6 cells with thapsigargin and tunicamycin causes beta cell death in a HS-independent manner due to the rapid expression of pro-apoptotic genes. Importantly, most *in vitro* experiments are performed with potent triggers of experimental stress which induce a rapid response; in contrast, beta cells *in vivo* are more likely to encounter chronic exposure to an increasing level of ER stress during T2D development. For this reason, *in vitro* studies of ER stress should be interpreted and extrapolated with caution.

(iii) ER stress induction in isolated islets

Isolated normal BALB/c islets cultured with thapsigargin (5 µM) for 3 days, dispersed into single cells and analysed by flow cytometry (see Section 2.8), showed a significant loss of HSPG core proteins (Sdc1 and CD44) and a trend for the reduction of HS and Hpse in the beta cells (**Figure 4.18**). Other groups have demonstrated that C57BL/6 mouse islets cultured for 24 hrs with thapsigargin (2-20 nM or 1-5 µM) or tunicamycin (10-100 ng/ml or 2.5-10 µg/ml) increased the expression of the ER stress-associated genes BiP, CHOP and caspase-3, compared to controls (Sharma et al., 2015, Wali et al., 2014, Lipson et al., 2006). Furthermore, increased beta cell death was observed when the islets were cultured for 4-5 days with thapsigargin (5 µM) or tunicamycin (10 µg/ml) (Wali et al., 2014). These studies suggest that the induction of ER stress and the loss of HSPGs/HS in primary beta cells, could potentially lead to beta cell death. However, BALB/c islets may need to be treated with thapsigargin for a longer period of time (i.e., 4-5 days instead of 3 days) to observe a correlation between loss of HS/the HSPGs and ER stress-induced death. Nevertheless, our studies of ER-stress in isolated islets and the observed loss of intracellular HSPG core proteins, HS and Hpse parallel our observations in ER-stressed MIN6 cells (see Sections 4.2.2 and 4.2.3). Sharma et al. (2015) reported that treatment of C57BL/6J islets with low dose of thapsigargin or tunicamycin treatment increased the number of beta cells in a glucose-dependent manner; in contrast, high dose thapsigargin did not affect beta cell proliferation. Treatment of mouse C57BL/6J islets with cytokines (IL-1β, IL-23 or IL-24), tunicamycin or thapsigargin reduced GSIS and GLP-1 associated GSIS in the presence of ER stress and oxidative stress in beta cells

(Hasnain et al., 2014). Together, these studies suggest that ER-stressed islet beta cells could reduce islet/beta cell function.

In summary:

- Endogenously driven ER stress in Akita Ins2$^{WT/WT}$ islet beta cells was characterised by a significant reduction in islet HSPG core proteins and HS.
- The experimental induction of ER stress in MIN6 cells and primary beta cells *in vitro* also reduced the intracellular expression of HSPG core proteins/HS and increased beta cell death.
- These studies establish a plausible relationship between the depletion of islet HSPG core proteins/HS and ER stress in beta cells during T2D development in db/db mice (Chapter 3).
- Studies of alleviating ER stress and of HS replacement for rescuing db/db beta cells and preserving their viability are explored in Chapter 5.

Chapter 5: Preservation and replacement of beta cell HS

5.1 Introduction

The findings presented in Chapter 3 and 4 provide evidence that intracellular levels of HSPG core proteins (collagen type XVIII, syndecan-1 and CD44) and HS decrease dramatically in ER-stressed beta cells. These outcomes were demonstrated in T2D-prone db/db, in heterozygous Akita $Ins2^{WT/C96Y}$ islets subjected to physiological ER stress *in vivo*, as well as in MIN6 beta cells and primary isolated islets with ER stress-induced experimentally *in vitro*. Normally, nascent proteins undergo folding during their maturation in the ER with the help of ER chaperones (see Section 1.9). The accumulation of unfolded/misfolded proteins in the ER activates the ER stress cascade possibly via multiple signals, inducing increased demand for energy, elevated free fatty acids, disrupted calcium ion homeostasis, glucotoxicity and oxidative stress (see Sections 1.9 and 1.11). ER stress-induced by these metabolic disturbances results in reduced protein synthesis, increased expression of ER chaperones, activation of the unfolded protein response (UPR) and if ER stress is prolonged, apoptosis (Oslowski and Urano, 2011, Eizirik et al., 2008, Yoshida, 2007).

ER stress in beta cells *in situ* has been shown previously to contribute to insulin insensitivity or insulin resistance in adipose tissue, liver and skeletal muscle, glucose intolerance and subsequently T2D (Salvado et al., 2015, Kars et al., 2010, Ozcan et al., 2004, Özcan et al., 2006). Our studies of the experimental induction of ER stress in MIN6 beta cells *in vitro* demonstrated a loss of intracellular HSPG core proteins, HS and heparanase as well as increased beta cell death/damage (see Section 4.2.2). However, increased cell death/damage was sometimes observed before a significant decline in HSPG core proteins/HS (see Sections 4.2.2.3 and 4.2.2.4, **Figures 4.14(b), 4.15(b) and 4.17(b)**), a phenomenon which could be related to the use of an immortalised cell line and the pharmacological (unphysiological) induction of ER stress using thapsigargin and tunicamycin. To circumvent these concerns, in this chapter we set out to examine whether (i) experimentally relieving ER stress in db/db mice and (ii) replacing HS in db/db beta cells using HS mimetics restores or preserves intra-islet HS and beta cell survival, respectively.

With the first strategy, ER stress in db/db mice was alleviated using a chemical chaperone tauroursodeoxycholic acid (TUDCA) and the downstream effects on glycaemic control

and intra-islet HSPG core proteins and HS were analysed. Chemical chaperones belong to a group of low molecular weight compounds which stabilises protein conformation, improves protein folding capacity in the ER and facilitates trafficking of mutant proteins to the proteasome for disposal. These activities reduce protein aggregation in the ER and ER stress (Özcan et al., 2006, Welch and Brown, 1996, Sauer et al., 2008). The chemical 4-phenly butyric acid (PBA) also has chaperone activity and interacts with misfolded proteins via hydrophobic domains to prevent protein aggregation in the ER (Xiao et al., 2011, Mimori et al., 2012). Trimethylamine-N-oxide dehydrate (TMAO) is a natural chemical chaperone which prevents protein aggregation by binding to hydrophobic peptides to stabilise and improve protein folding (Shepshelovich et al., 2005). Similarly, endogenous bile salts and their derivatives such as ursodeoxycholic acid (UDCA), similar to TUDCA, can modulate ER function (Özcan et al., 2006, Vang et al., 2014).

TUDCA is the taurine conjugate of UDCA and is a secondary bile acid produced by intestinal bacteria (Vang et al., 2014). UDCA is a US Food and Drug Administration (FDA)-approved drug for the treatment of cholestatic liver disease because of its ability to protect hepatocytes from hydrophilic bile acids (Amaral et al., 2009, Lebensztejn, 2000, Xie et al., 2002). TUDCA has been reported to serve as an anti-apoptotic agent for neurogenerative diseases such as amyotrophic lateral sclerosis, Alzheimer's disease, Parkinson's disease and Huntington's disease (Vang et al., 2014, Elia et al., 2016, Castro-Caldas et al., 2012, Nunes et al., 2012, Amaral et al., 2009). Furthermore, TUDCA has been reported to play an important protective role in atherosclerosis, diabetes and renal disease (Vang et al., 2014). For example, PBA and TUDCA treatment restored glucose homeostasis, improved insulin sensitivity and decreased fatty liver disease in ob/ob mice (Özcan et al., 2006). TUDCA inhibits the production of free oxygen radicals, reduces ER stress and inhibits caspase activation in tissues such as liver, hypothalamus, brain and pancreatic beta cells in both db/db and ob/ob mice as well as in Huh7 cells (a human liver-derived cell line) (Özcan et al., 2006, Xie et al., 2002, Amin et al., 2012, Ozcan et al., 2009). From a mechanistic standpoint, PERK and IRE1α phosphorylation levels were lowered in the liver of ob/ob mice indicating reduced ER stress (Özcan et al., 2006). Furthermore, both liver and adipose tissue showed reduced activation of JNK and phosphorylation of IRS-1, suggesting improved insulin sensitivity (Özcan et al., 2006). Moreover, TUDCA treatment of female NOD mice preserved serum insulin levels and

islet insulin and also reduced islet inflammation (insulitis) compared to controls (Engin et al., 2013). However, obese insulin-resistant humans on TUDCA therapy showed increased hepatic and muscle insulin action, despite lack of amelioration in ER stress (Kars et al., 2010). This restoration of insulin action could have been due to improved insulin signalling caused by the inhibition of protein tyrosine phosphatase 1B (PTP1B; a negative regulator of insulin signalling) as observed in the muscles of TUDCA treated ob/ob mice (Panzhinskiy et al., 2013). Considering these findings, we assessed whether the administration of TUDCA to T2D-prone db/db mice could restore intra-islet expression of HSPG core proteins and HS by relieving ER stress in beta cells.

Our second strategy was to utilise the HS mimetics heparin (*in vitro*) and PI-88 (*in vitro* and *in vivo*) to replace the lost HS in db/db beta cells and thereby preserve beta cell survival (and hence function). HS is a glycosaminoglycan directly synthesised onto HSPG core proteins to form HSPGs; in the absence of HSPG core proteins, HS assembly cannot occur (see Section 1.13). Recently, high levels of HS were found to be localised *inside* islet beta cells and to play a critical role in post-natal islet growth and significantly, in beta cell survival (Takahashi et al., 2009, Ziolkowski et al., 2012). In Chapter 3, we demonstrated a significant loss of HSPG core proteins and HS in the beta cells of db/db mice correlating with T2D development (see Sections 3.2.4, 3.2.5 and 3.2.10). Since physiological replacement of HS by *de novo* synthesis is unfeasible in the absence of HSPG core proteins, we investigated whether replacing beta cell HS can preserve the viability of db/db beta cells *in vitro* and protect beta cell survival in db/db mice (i.e., *in vivo*), potentially ameliorating glycaemic control.

Heparin is a highly sulfated analogue of HS and is structurally related to HS (Liu and Pedersen, 2007). Heparin contains ~2.7 sulfate groups per disaccharide with molecular weight of ~15 kDa whereas HS consists of ≥ 1 sulfate group per disaccharide and weighs ~30 kDa (Shriver et al., 2012). Clinically, heparin is widely used as an anti-coagulant and anti-thrombotic drug. Heparin also binds to the catalytic site of heparanase (Hpse), inhibiting the degradation of HS i.e., heparin is a heparanase inhibitor (Vreys and David, 2007, Levy-Adam et al., 2010). Previous studies have shown that heparin administration improves the survival of cancer patients (Klerk et al., 2005, Rickles, 2006, McKenzie, 2007) and inhibits Hpse-dependent metastasis, invasion and angiogenesis in animal

models (Vlodavsky and Goldshmidt, 2001, Parish et al., 1987, Vlodavsky and Friedmann, 2001). However, heparin exhibits anti-coagulant activity which restricts its usage *in vivo*. For this reason, chemically modified heparins and sulfated oligosaccharides have been developed as alternative Hpse inhibitors (Parish, 2006). For example, glycol-split N-acetyl heparin lacks anti-coagulant activity and acts as a non-cleavable substrate for Hpse, dramatically inhibiting the catalytic activity of this enzyme (Rivara et al., 2016).

The sulfated phosphomannopentaose PI-88 (Muparfostat) is another non-cleavable inhibitor of Hpse which exhibits a low level of anti-coagulant activity (Ziolkowski et al., 2012, Parish et al., 2013, Parish et al., 1999, Simeonovic et al., 2013). PI-88 is a potent inhibitor of tumour growth (Parish et al., 1999) and has undergone clinical trials as an anti-cancer drug (Gautam et al., 2007, Liu et al., 2014). Additionally, PI-88 binds to the HS binding domains of vascular endothelial growth factor-2 (VEGF-2), fibroblast growth factor (FGF)-1 and 2, thereby reducing their functional activity and inhibiting tumour angiogenesis (Ferro et al., 2007, Kudchadkar et al., 2008). PI-88 has been shown to inhibit the primary growth of rat mammary adenocarcinoma and metastasis to the draining popliteal lymph node and to reduce the vascularity of tumours in animal models (Parish et al., 1999). Significantly, PI-88 acts as a potent HS replacer in beta cells *in vitro* (Ziolkowski et al., 2012, Simeonovic et al., 2013, Parish et al., 2013).

Ziolkowski et al. (2012) demonstrated a significant increase in the survival of isolated mouse beta cells following co-culture with HS mimetics (heparin or PI-88), identifying HS as a critical requirement for preserving beta cell viability. In addition, HS replacement with HS mimetics protected beta cells from ROS-induced cell death. Using FITC-labelled heparin and confocal microscopy, beta cell protection correlated with substantial uptake of FITC-conjugated heparin by the beta cells. Additionally, T1D onset was prevented in 50% of T1D-susceptible NOD mice and beta cell HS was preserved by *in vivo* treatment with the Hpse inhibitor/HS mimetic PI-88 (Ziolkowski et al., 2012, Simeonovic et al., 2013). Based on these findings, we set out to test whether (i) culture of T2D-prone db/db beta cells with heparin or PI-88 improves beta cell viability *in vitro*, and (ii) administration of PI-88 to young db/db mice (*in vivo*) preserves beta cell HS, improves beta cell viability and prolongs beta cell function.

Overall, in this chapter we evaluated two separate approaches for preserving and/or improving the HS content of beta cells: (i) TUDCA treatment to relieve ER stress and preserve HSPGs/HS in beta cells and (ii) HS replacement in beta cells using heparin or PI-88. For the first approach, 4 week old male db/db mice were treated with TUDCA (150 mg/kg/day) or saline intraperitoneally for 28 days to ascertain whether ER stress-relief improved intra-islet HSPG/HS expression. For the second approach, *in vitro* studies tested whether wt and db/db beta cells cultured with heparin or PI-88 demonstrated significantly increased viability. Finally, 3.5 week old db/db mice treated with the HS mimetic PI-88 (10 mg/kg/day) examined whether HS replacement delayed the progression of T2D.

5.2 Results

5.2.1 TUDCA treatment improves HSPG/HS expression in db/db beta cells

5.2.1.1 Non-fasting blood glucose levels and body weight of TUDCA-treated male db/db mice

4 week-old male db/db mice (normoglycaemic; bg<10 mmol/L) were treated with tauroursodeoxycholic acid (TUDCA; 150 mg/kg/day) or saline intraperitoneally for 28 days (see Section 2.11.2). The body weight and non-fasting blood glucose levels of the mice were determined three times/week, routinely at 9am - 10am. The TUDCA/saline dosage was adjusted, based on their body weight (see Sections 2.2.1 and 2.11.2).

The non-fasting blood glucose levels of db/db mice in the saline and TUDCA groups were similar at 4 weeks of age (**Figure 5.1(a)**). TUDCA-treated male db/db mice showed a significant reduction in the blood glucose levels to 83.1% (17.24 ± 1.14 mmol/L vs 20.74 ± 0.90 mmol/L) and 78.1% (20.06 ± 1.32 mmol/L vs 25.69 ± 0.49 mmol/L) of corresponding saline-treated controls at 6-7 weeks and 7-8 weeks of age, respectively (**Figure 5.1(a)**). A significant reduction was also observed in the body weight of TUDCA-treated males, compared to saline controls after 4 weeks of age ($P<0.01$ and $P<0.001$; **Figure 5.1(b)**). These data indicate that TUDCA treatment of db/db mice decrease blood glucose levels, reduced body weight and delayed the progression of T2D.

5.2.1.2 HbA1c levels in TUDCA-treated male db/db mice

Upon termination of treatment (day 28), glycated haemoglobin (HbA1c) levels were analysed in both saline and TUDCA-treated db/db mice, using a HemoCue HbA1c Analyzer (see Section 2.2.3). HbA1c is an integrated index of glycaemia during the previous three months (see Section 1.4.1). TUDCA treatment of male mice resulted in a significant decline in HbA1c levels to 81.6% of controls (5.24 ± 0.23% vs 6.42 ± 0.22%; **Figure 5.2**). Thus, TUDCA treatment of db/db male mice significantly improved the control of glycaemia ($P<0.01$), as determined by the independent measurements of HbA1c and weekly non-fasting blood glucose levels (see Section 5.2.1.1).

(a)

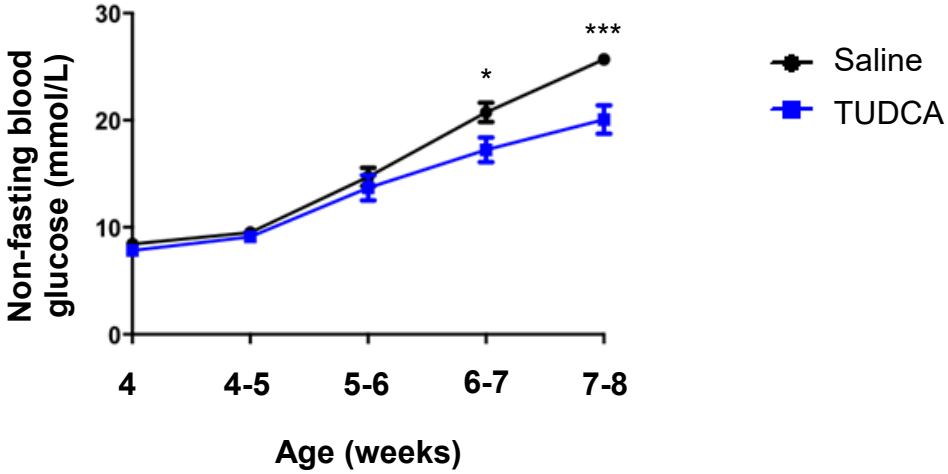

(b)

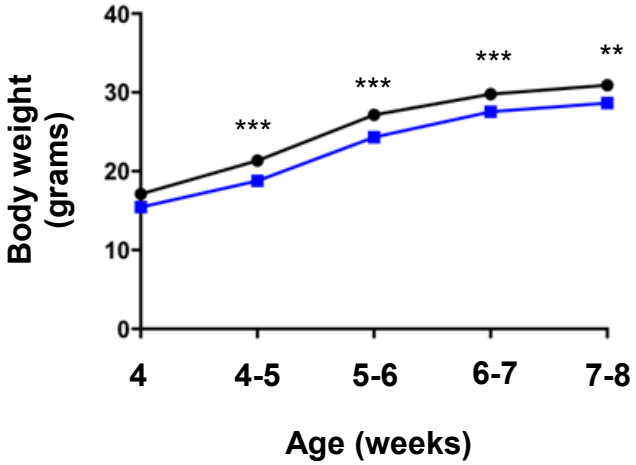

Figure 5.1: Non-fasting blood glucose levels and body weight of TUDCA-treated male db/db mice.

Male db/db mice were treated from 4 weeks of age with normal saline (black symbols) or TUDCA (150 mg/kg/day; blue symbols) i.p. for 28 days. The non-fasting blood glucose levels and body weight were monitored 3x/week. Compared to saline controls, TUDCA-treated mice showed a significant reduction in non-fasting blood glucose levels from 6-7 weeks of age (a) and a significant reduction in body weight (b). Data represent the mean of all measurements over 1 week intervals in each group ± SEM with n= 12-14 mice/group. Non-parametric Mann-Whitney test; *P<0.05, **P<0.01 and ***P<0.001.

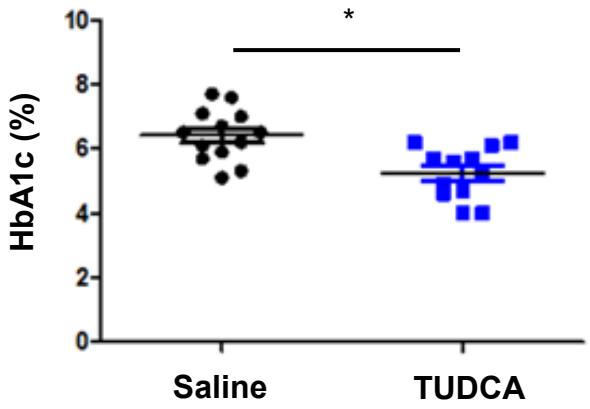

Figure 5.2: HbA1c levels in TUDCA or saline-treated male db/db mice.

4 week old male db/db mice were treated with saline (black symbols) or TUDCA (150 mg/kg/day; blue symbols) i.p. for 28 days. After termination of treatment, HbA1c levels were examined using a HemoCue HbA1c Analyzer. TUDCA-treated db/db males showed significantly lower HbA1c levels compared to controls. Data represent mean ± SEM for n= 12-13 mice/group. Unpaired t test; *P<0.01.

5.2.1.3 Expression of ER stress markers in the islets harvested from TUDCA-treated db/db males

Islets were isolated from 8 week old db/db mice that had been treated for 28 days with saline or TUDCA (see Section 2.3). Kidney tissue was harvested for use as a control to compare the C_T values between saline and PI-88 treated islets. The samples of islets and wt kidney were snap-frozen for subsequent RNA extraction and the preparation of cDNA (see Section 2.6). cDNA samples were examined for the ER stress markers: BiP (also known HSPA5, GRP78), P58 (also known DNAJC3), CHOP (also known as DDIT3, GADD153) and ATF3 by TaqMan real-time PCR. The gene of interest was normalised to a control gene (GAPDH) and mRNA levels in saline and TUDCA treated islets were quantified as a fold-change over the wt kidney sample (see Section 2.6).

Comparative C_T analyses revealed a 3.5-fold ($P<0.01$) and 3.1-fold ($P<0.01$) significant increase in the expression of the ER stress-associated adaptive UPR genes BiP and P58, respectively, in the islets of TUDCA-treated mice compared to saline controls (**Figure 5.3**). In addition, islets from TUDCA-treated mice showed a 2.3-fold ($P<0.01$) and 2.6-fold ($P<0.01$) significant increase in the expression of the ER stress-associated pro-apoptotic UPR genes, CHOP and ATF3, respectively, compared to the saline controls (**Figure 5.3**). Overall, TUDCA treatment of male db/db mice significantly upregulated the expression of adaptive and pro-apoptotic UPR markers compared to corresponding controls. These findings suggest that TUDCA elevated the UPR to further enhance beta cell compensation, maintain beta cell function and thus improve glycaemia.

5.2.1.4 Insulin immunostaining in the pancreases of db/db mice treated with TUDCA

TUDCA treatment of db/db mice upregulated the expression of a broad range of early and late genes associated with the UPR and significantly reduced blood glucose levels. In view of the known relationship between ER stress in db/db beta cells and the accumulation of misfolded insulin protein, we investigated whether TUDCA-mediated alleviation of ER stress elevated the expression of insulin in db/db islets *in situ*.

Representative images show an augmented distribution of insulin staining in the islets of TUDCA-treated db/db mice (**Figure 5.4(b)**) compared to saline-treated islets (**Figure 5.4(a)**). The intra-islet insulin content was quantified using Image J software with colour

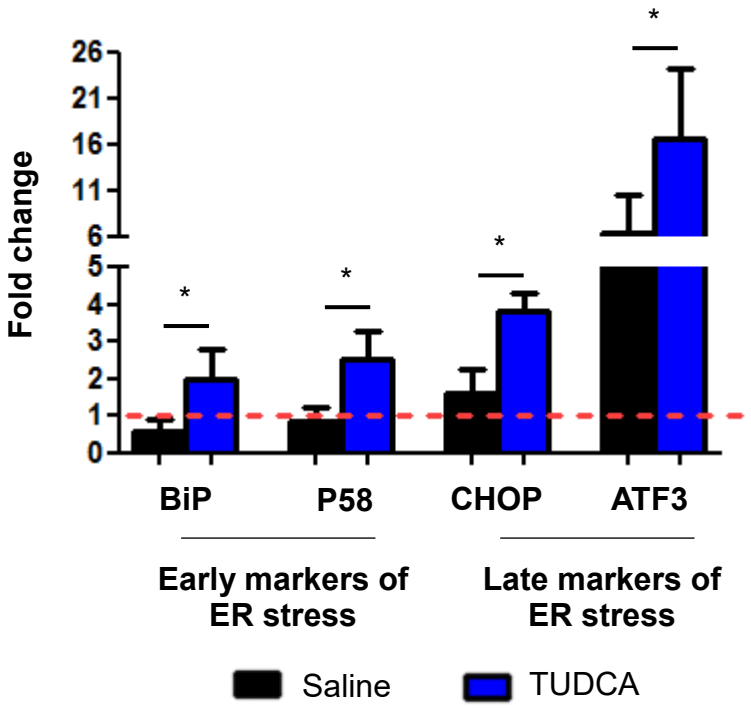

Figure 5.3: Expression of ER stress markers in the islets of TUDCA-treated db/db mice.

Islets were isolated from db/db males that had been treated for 28 days with TUDCA (150 mg/kg/day i.p.) or saline (controls). TaqMan real-time PCR showed significantly increased expression of transcripts for ER stress-associated genes in the islets from TUDCA-treated male db/db mice (blue bars) compared to saline controls (black bars). Fold-change refers to mRNA expression relative to gene expression in wt kidney (red dotted line) which is assigned a value of 1. Data represent mean ± SEM with n= 3-4 mice/group (100-140 islets/donor). Mann-Whitney test; *P<0.01.

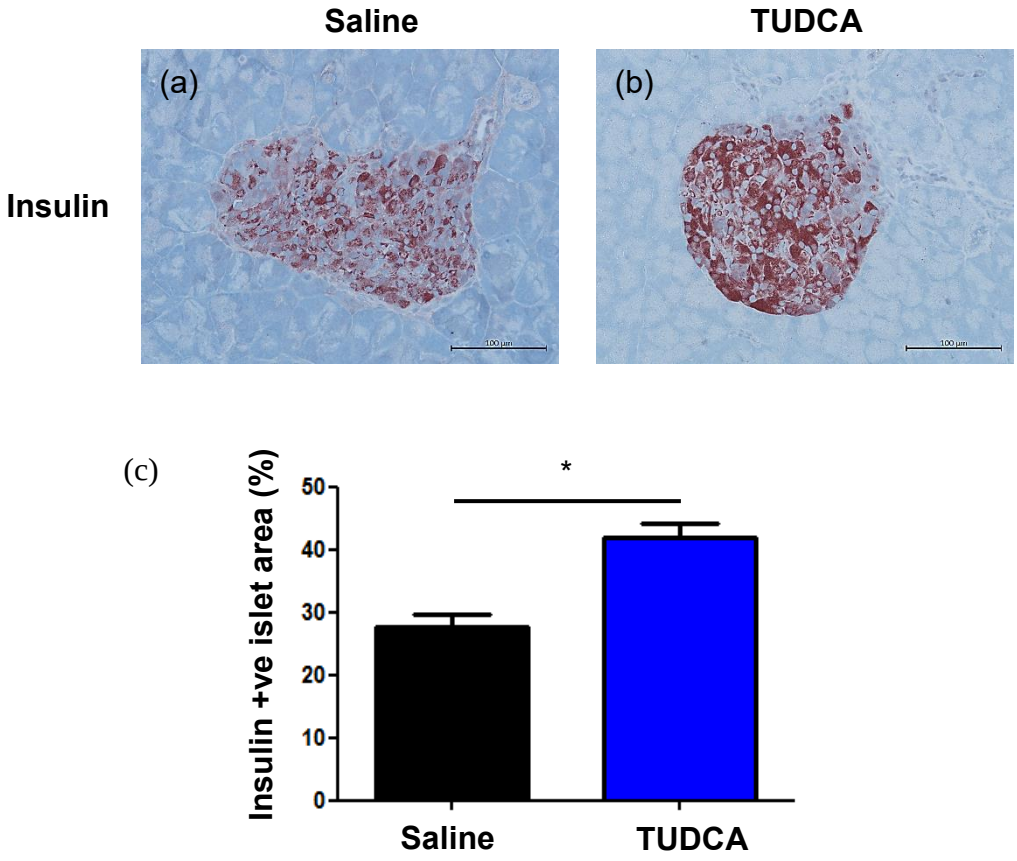

Figure 5.4: Expression of insulin in the islets of TUDCA-treated male db/db mice. 4 week old male db/db mice were treated with saline (black bar) or TUDCA (150 mg/kg/day; blue bar) i.p. for 28 days. After termination of treatment, the pancreas was harvested and insulin expression was localised in the islets by immunohistochemistry. Representative images show intense staining of insulin in TUDCA-treated db/db islets (b) and weak staining of insulin in saline controls (a). Scale bar = 100 µm. (c) Compared to saline controls, TUDCA-treated db/db islets showed a significant increase in the insulin+ve islet area of pancreatic islets. The data represent mean ± SEM for n= 8-9 pancreases/group with n= 92-105 islets analysed/group. Non-parametric Mann-Whitney test; *P<0.0001.

deconvolution plugin (see Section 2.7.5). The threshold intensity of staining was established using positive staining in saline control pancreas sections; this threshold was applied to all samples to calculate the % positive islet area.

The insulin+ve islet area showed a significant 1.5-fold increase in TUDCA-treated db/db mice compared to saline controls (41.91 ± 2.19% vs 27.66 ± 1.91%; P=0.0001; **Figure 5.4(c)**). Based on these data, TUDCA treatment led to elevated insulin expression in the pancreatic islets of db/db mice, correlating with a significant decline in blood glucose levels, albeit without re-establishing normoglycaemia. These findings provide further support for the effectiveness of TUDCA to relieve ER stress in beta cells and restore protein synthesis and/or maturation.

5.2.1.5 HSPG core protein expression in the islets of TUDCA-treated male db/db mice

Our studies confirmed that TUDCA treatment of db/db mice reduced blood glucose levels, lowered HbA1c levels and significantly increased the expression of both insulin protein and UPR markers in the treated db/db islets. We next assessed whether ER stress relief influenced the intra-islet expression of HSPG core proteins i.e., collagen type XVIII (Col18), syndecan-1 (Sdc1) and CD44 as determined by immunohistochemistry (see Section 2.7).

Representative images in **Figure 5.5** show a vast increase in the expression of Col18 core protein in the islets of TUDCA-treated mice (**Figure 5.5(b)**), compared to saline-treated control islets (**Figure 5.5(a)**). TUDCA treatment also improved islet Sdc1 expression (**Figure 5.5(c, d)**). However, little change in CD44 staining within the islets was observed (**Figure 5.5(e, f)**).

The intra-islet content of HSPG core proteins was quantified using Image J software with colour deconvolution plugin (see Section 2.7.5). The threshold intensity of staining was set to the positive staining in saline control pancreas sections; this threshold was applied to all samples to calculate the % positive islet area.

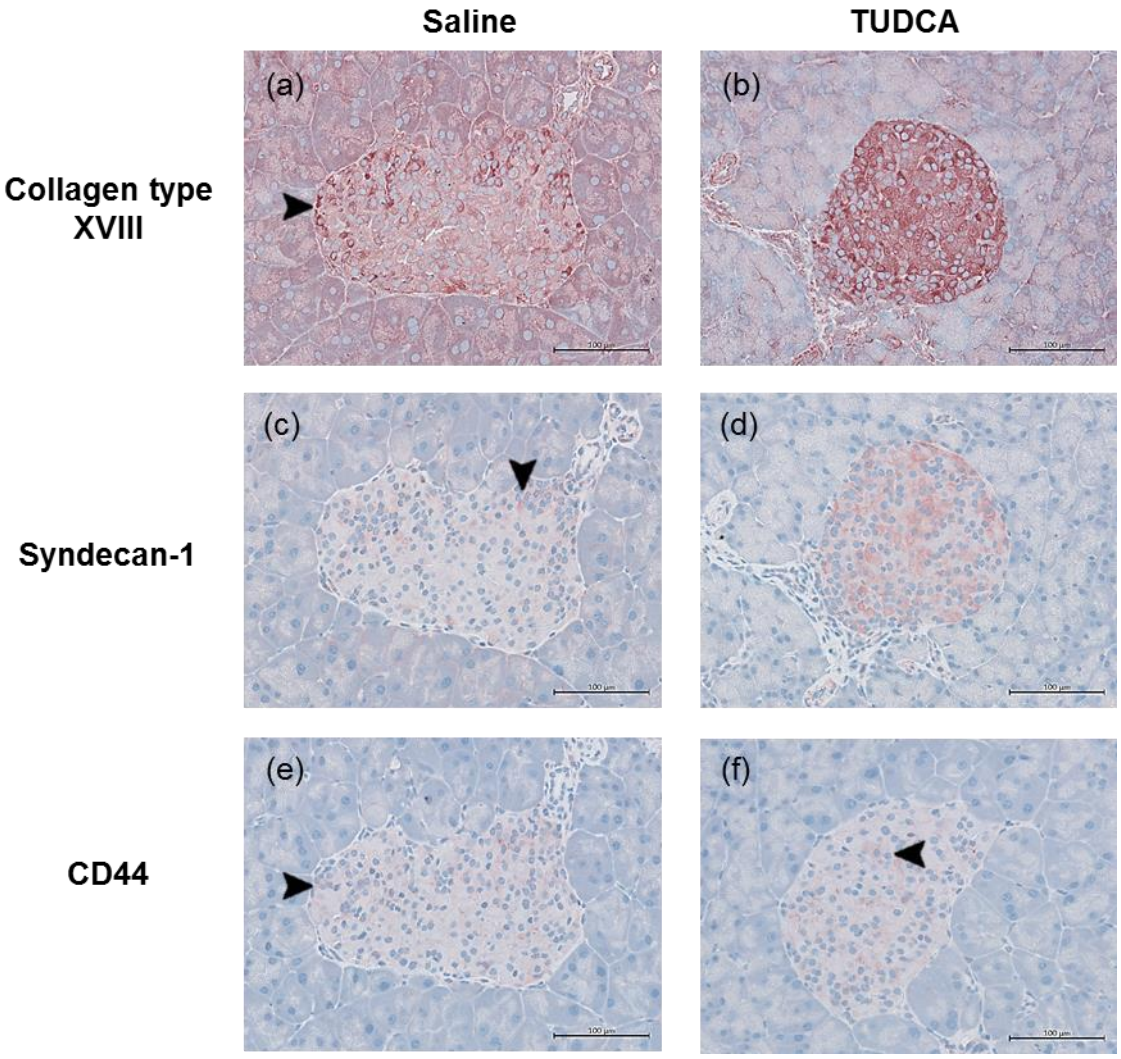

Figure 5.5: Distribution of HSPG core proteins in the pancreatic islets of db/db males.

Representative images show the immunohistochemical localisation of Col18 (a, b), Sdc1 (c, d) and CD44 (e, f) in the islets of db/db mice treated with TUDCA ((b, d, f); 150 mg/kg/day i.p.) or saline (a, c, e). Positive staining in the islets (a, c, e and f) are identified by black arrowheads. TUDCA treatment substantially increased intra-islet Col18 (b) and Sdc1 (d), compared to saline-treated controls (a, c). Scale bar = 100 µm.

The Col18+ve islet area was significantly increased by 1.7-fold in the islets of TUDCA-treated db/db mice, compared to controls (23.79 ± 2.12% vs 13.65 ± 1.17%; P<0.001; **Figure 5.6(a)**). Similarly, the Sdc1+ve islet area in TUDCA-treated pancreases increased 2.8-fold compared to saline islets, but this increase did not achieve statistical significance (6.73 ± 1.47% vs 2.38 ± 0.25%; **Figure 5.6(b)**). In contrast, TUDCA treatment did not alter the CD44+ve islet area in db/db islets (12.75 ± 1.71% vs 12.33 ± 0.98%; **Figure 5.6(c)**). In summary, the pancreatic islets of TUDCA-treated males revealed a striking increase in intra-islet HSPG core proteins, compared to controls. This improvement correlated with alleviated ER stress and improved glycaemic control in db/db mice.

5.2.1.6 Immunohistochemical staining of intra-islet HS in TUDCA-treated db/db mice

We observed recovery of intra-islet HSPG core proteins in the pancreatic islets of db/db mice treated with TUDCA compared to saline controls (see Section 5.2.1.5). HS is directly synthesised onto HSPG core proteins and is critical for the survival of beta cells (see Sections 1.13 and 1.15). We hypothesised that the observed improvement in the expression of islet HSPG core proteins could contribute to augmented synthesis of HS in beta cells, enhanced beta cell survival and hence lower blood glucose levels (see Section 5.2.1.1). We therefore examined the levels of intra-islet HS in the islets of db/db mice by immunohistochemistry (see Section 2.7). A striking increase in the HS staining of islets in TUDCA-treated db/db pancreases was observed (**Figure 5.7(b)**), compared to saline-treated islets (**Figure 5.7(a)**).

The intra-islet HS content was quantified using Image J software with colour deconvolution plugin (see Section 2.7.5). The threshold intensity of staining was set using the positive staining observed in saline control pancreases; this threshold was adopted for all samples to calculate the % positive islet area.

Treatment of male db/db mice with TUDCA resulted in a substantial 1.6-fold increase in the HS+ve islet area, compared to saline controls (24.22 ± 3.95% vs 14.80 ± 1.72%; **Figure 5.7(c)**). Although there was a trend for beta cell HS to be enhanced after TUDCA treatment, statistical significance was not established due to variation between islets in the different donors. Nevertheless, the striking improvement in beta cell HS correlated

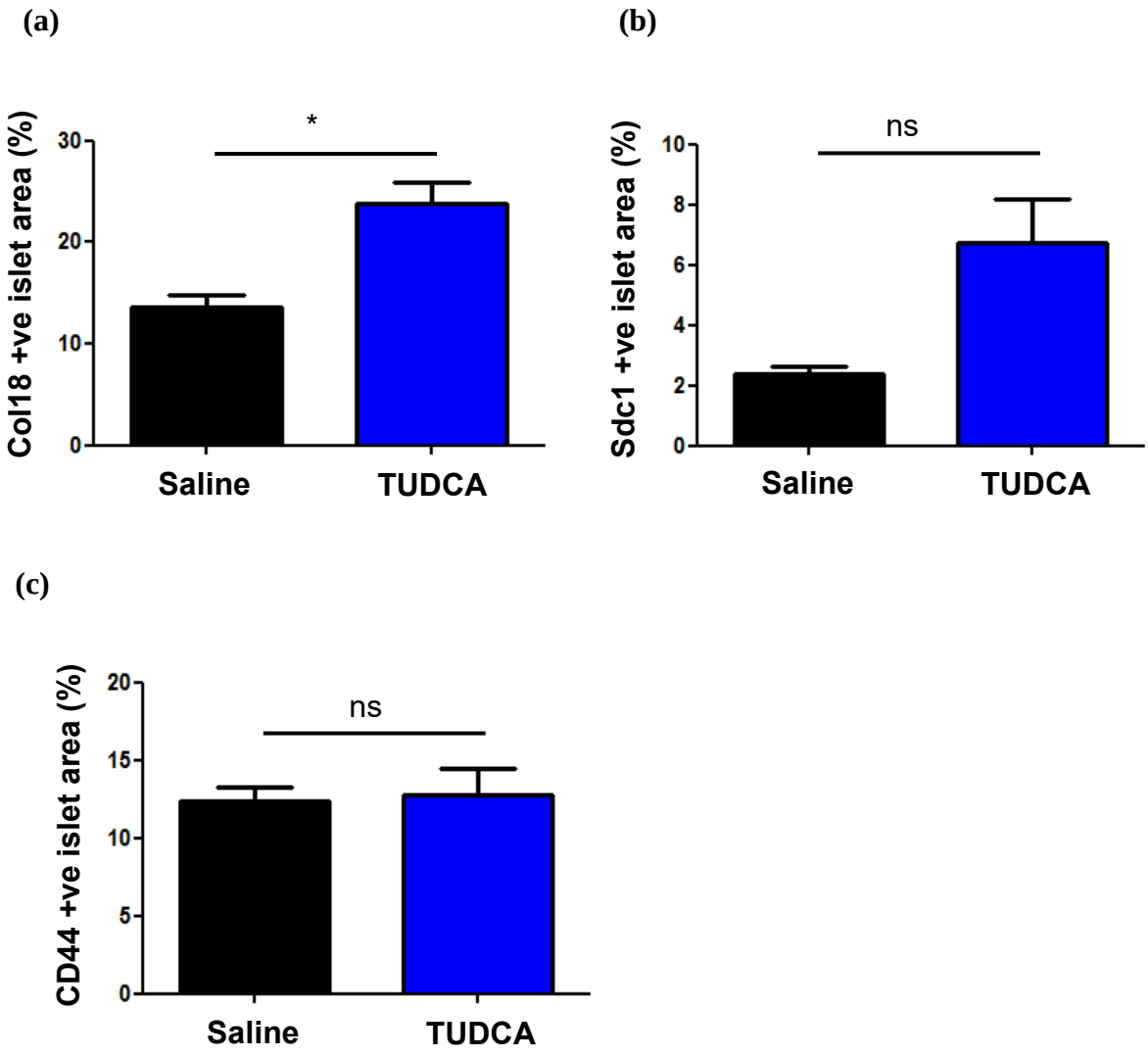

Figure 5.6: HSPG core protein expression in the islets of TUDCA-treated male db/db mice.

4 week old male db/db mice were treated with saline (black bars) or TUDCA (150 mg/kg/day; blue bars) i.p. for 28 days. The HSPG core proteins, collagen type XVIII (Col18), syndecan-1 (Sdc1) and CD44 were localised in the pancreatic islets of the db/db pancreases by immunohistochemistry. Col18 (a) and Sdc1 (b) expression in the TUDCA-treated db/db islets were increased compared to corresponding controls at 8 weeks of age but no change was observed in CD44 expression (c). The data represent mean ± SEM for n= 8-9 pancreases/group with n= 86-88 (Col18), n=92-105 (Sdc1) and n= 92-105 (CD44) islets examined/group. Mann-Whitney test; *P<0.001 and ns, not significant.

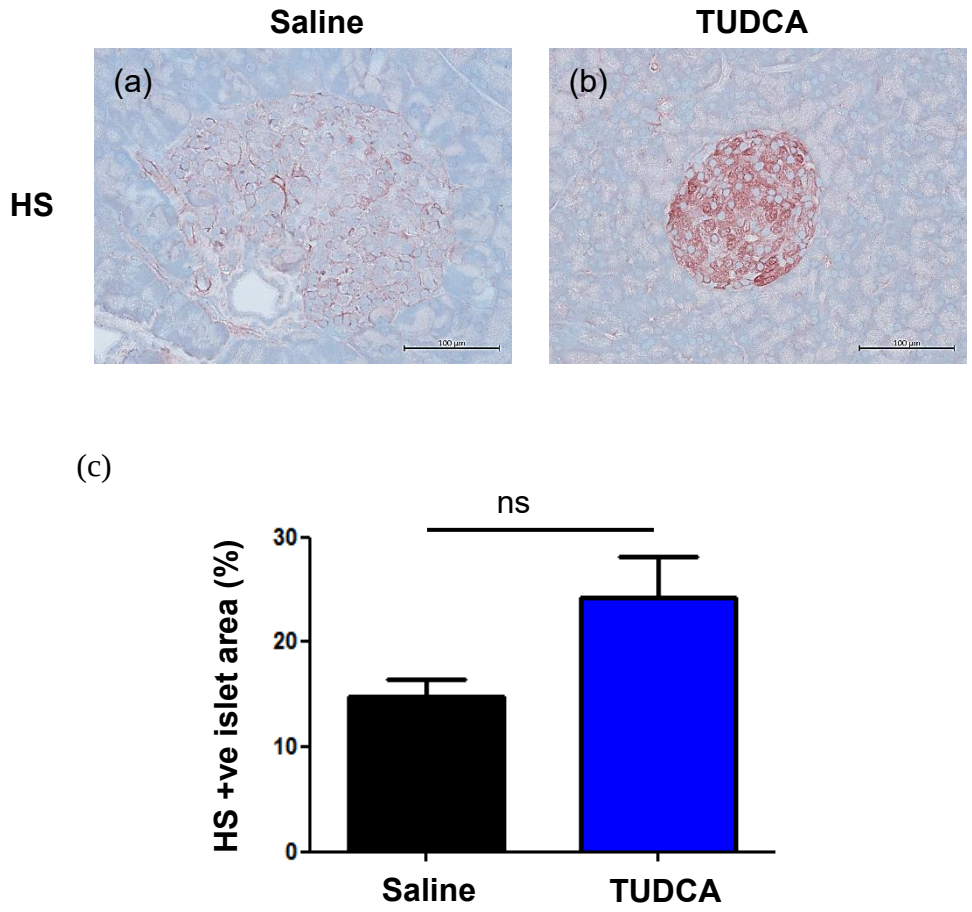

Figure 5.7: Distribution of HS in the islets of TUDCA-treated male db/db mice.

4 week old male db/db mice were treated with saline (black bar) or TUDCA (150 mg/kg/day; blue bar) i.p. for 28 days. The pancreases were harvested and intra-islet HS expression was localised by immunohistochemistry. Representative images show strong staining for intra-islet HS in TUDCA-treated male db/db mice (b); in contrast, only weak staining for HS was observed in the islets of saline-treated db/db mice (a). Scale bar = 100 µm. (c) The HS+ve islet area in TUDCA-treated db/db islets was increased compared to controls. The data represent mean ± SEM for n= 4 pancreases/group with n= 38-44 islets examined/group. Mann-Whitney test; ns, not significant.

with the significant increase in the expression of HSPG core proteins (see Section 5.2.1.5), resulting from the alleviation of ER stress in the db/db beta cells. The TUDCA-mediated modulation of these important beta cell components correlated with a significant improvement in glycaemic control (see Sections 5.2.1.1 and 5.2.1.2) and are consistent with a critical role for HS in beta cell survival (see Section 1.15).

Taken together, the long term administration of TUDCA to db/db mice confirmed an enhanced unfolded protein response which restored the maturation of insulin protein in beta cells and significantly improved non-fasting blood glucose levels. Of further significance, beta cell HSPG core proteins and HS were replenished at least in part, correlating with improved glycaemic control and mitigated T2D progression.

5.2.2 HS replacement using heparin improves beta cell viability in db/db beta cells

5.2.2.1 Intracellular expression of HSPG core proteins and HS in primary db/db beta cells

Normal or wildtype mouse islets *in situ* express high levels of intracellular HSPG core proteins and HS (Choong et al., 2015; see Sections 3.2.4, 3.2.5 and 3.2.10). However, during the isolation of islets and beta cells, intra-islet HS is selectively lost, due at least in part, to oxidative damage (Choong et al., 2015). Our earlier immunohistochemical studies identified the loss of both HSPG core proteins and HS in db/db islets *in situ* during T2D development (see Sections 3.2.4, 3.2.5 and 3.2.10). We therefore initially set out to confirm the altered distribution of HSPGs/HS in isolated db/db beta cells using flow cytometry.

(a) Male db/db and wt beta cells

Male wildtype (wt) and db/db islets were isolated from 5-9 week-old mice and dispersed into single cells (see Section 2.3). The freshly isolated beta cells were analysed for intracellular and cell surface HSPG core proteins (Collagen type XVIII (Col18), syndecan-1 (Sdc1) and CD44) and HS before and after culture for 2 days by flow cytometry (see Section 2.8). In parallel, the cell surface and intracellular expression of Hpse was examined on day 0 and day 2 (see Section 2.8).

Freshly isolated wt male beta cells demonstrated more pronounced intracellular expression of HSPG core protein, HS and Hpse (**Figure 5.8(a-c)**), than on the cell surface (**Figure 5.8(d-f)**). For the HSPG core proteins Col18, Sdc1 and CD44, the intensity of intracellular staining was 34-fold (GMFI= 3848.00 ± 575.13 vs GMFI= 112.37 ± 20.37), 3.8-fold (GMFI= 354.43 ± 89.97 vs GMFI= 93.70 ± 27.89) and 3.2-fold (GMFI= 326.17 ± 34.50 vs GMFI= 103.13 ± 7.37) higher than at the cell surface, respectively. Compared to the diminished cell surface expression of HS (GMFI= 124.47 ± 26.83) and Hpse (GMFI= 130.67 ± 10.39), wt beta cells showed an 8-fold and 12.6-fold higher expression of intracellular HS (GMFI= 1000.43 ± 129.19) and Hpse (GMFI= 1649.6 ± 180.16), respectively (**Figure 5.8**). These findings are consistent with previous studies of isolated normal beta cells (Ziolkowski et al., 2012, Choong et al., 2015).

In freshly isolated male db/db beta cells, the intracellular staining for the HSPG core protein Col18, Sdc1 and CD44 was 46% (GMFI= 1780.43 ± 148.67 vs GMFI= 3848.00 ± 575.13; $P<0.01$), 40% (GMFI= 131.11 ± 15.16 vs GMFI= 354.43 ± 89.97; $P<0.05$) and 108% (GMFI= 352.50 ± 29.89 vs GMFI= 326.17 ± 34.50) of wt beta cells, respectively (**Figure 5.8(a)**). These findings confirm the loss of Col18 and Sdc1 core proteins in db/db islets *in situ*, as determined by immunohistochemistry (see Section 3.2.4). In parallel, intracellular HS and Hpse were reduced to 82% (GMFI= 818.14 ± 95.81 vs GMFI= 1000.43 ± 129.19) and 47% (GMFI= 775.29 ± 66.17 vs GMFI= 1649.6 ± 180.16; $P<0.001$) of wt beta cells (**Figure 5.8(b, c)**). The similarity in intracellular HS in wt and db/db beta cells is likely to be attributed, at least partly, to the decline in beta cell HS that accompanies the enzymatic digestion procedures require to isolate islets and beta cells for both donor strains (Choong et al., 2015, Ziolkowski et al., 2012). Interestingly, the significant loss of Hpse in db/db beta cells is consistent with our observed decline in Hpse in ER-stressed MIN6 cells (see Sections 4.2.2.3.1 and 4.2.2.3.2). Like wt beta cells, cell surface expression of the HSPG core proteins, HS and Hpse in db/db beta cells remained substantially lower than corresponding intracellular levels (**Figure 5.8(d-f)**), with the exception of Sdc1 where the levels at both sites were similar (**Figure 5.8(a, d)**).

In general, after culture for 2 days, wt beta cells maintained higher intracellular staining (**Figure 5.9(a-c)**) than cell surface staining (**Figure 5.9(d-f)**) for HSPG core proteins (Col18, 38.6-fold; Sdc1, 3.3-fold; CD44, 1.8-fold), HS (8.0-fold) and Hpse (4.5-fold).

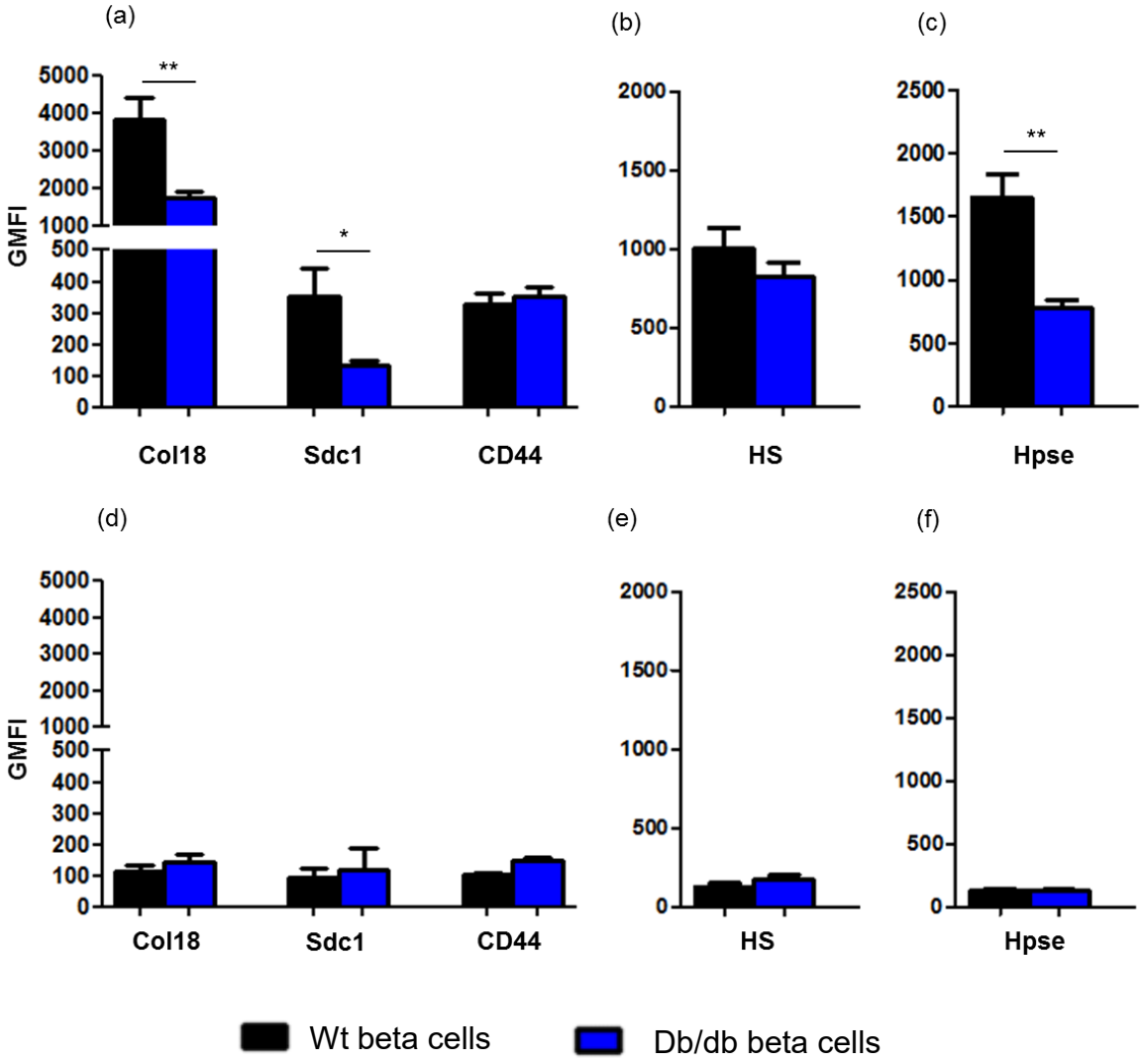

Figure 5.8: Intracellular and cell surface staining of HSPG core proteins, HS and Hpse in freshly isolated male wt and db/db beta cells.

Freshly isolated beta cells (day 0) were stained for (a-c) intracellular and (d-f) cell surface HSPG core proteins (Col18, CD44 and Sdc1), HS and Hpse and analysed by flow cytometry. Wt (black bars) and db/db (blue bars) beta cells showed strong intracellular expression for HSPG core proteins (a), HS (b) and Hpse (c) and corresponding weak cell surface expression (d-f). Intracellular Col18 (a), Sdc1 (a) and Hpse (c) were significantly reduced in db/db beta cells, compared to controls. The data represent mean GMFI ± SEM for n= 3-7 experiments/group; n= 2-4 donors/experiment. Non-parametric Mann-Whitney test; *P<0.05 and **P<0.01.

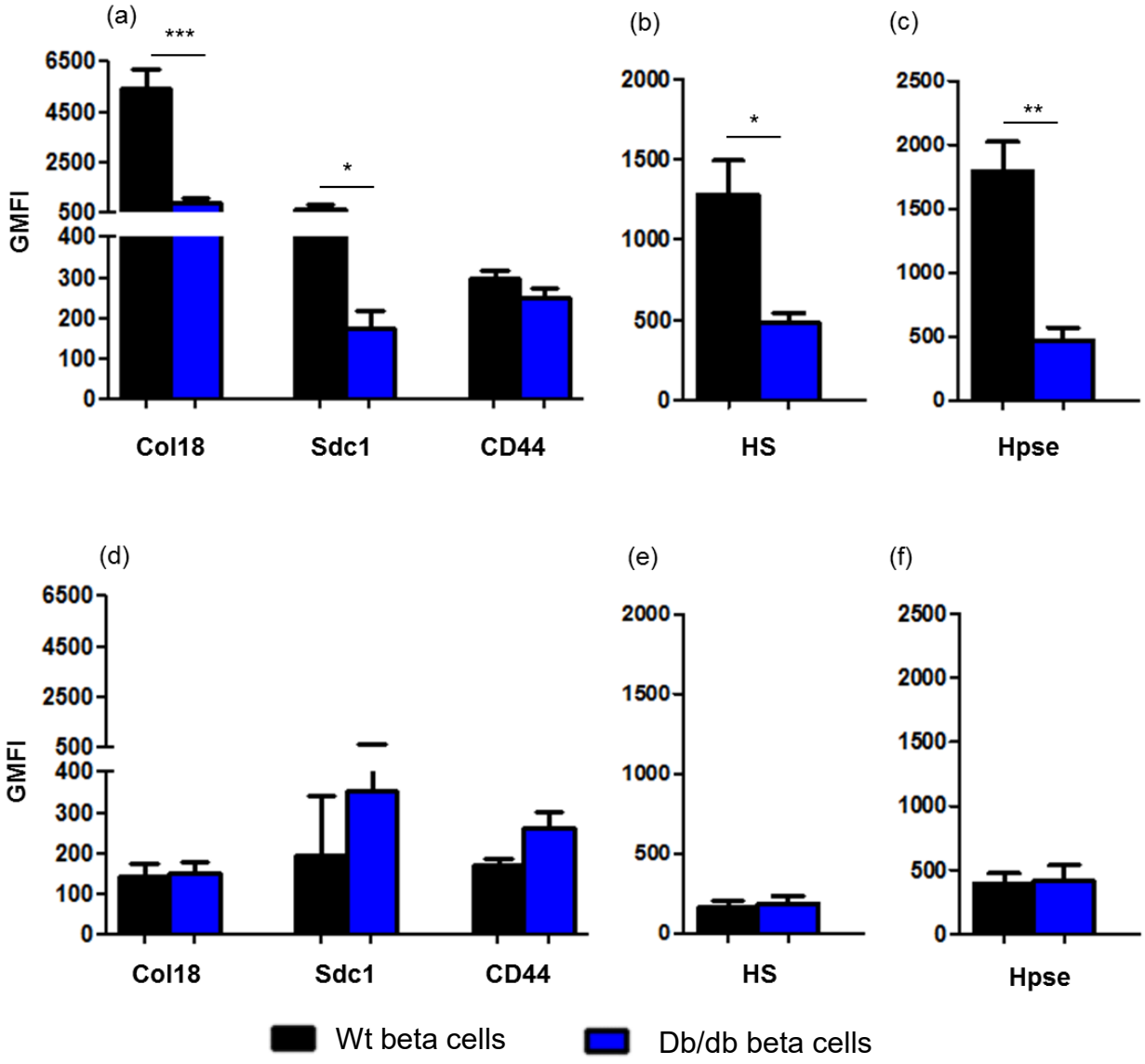

Figure 5.9: Intracellular and cell surface expression of HSPG core proteins, HS and Hpse in male wt and db/db beta cells at day 2.

Isolated beta cells were cultured for 2 days and stained for (a-c) intracellular and (d-f) cell surface HSPG core proteins (Col18, CD44 and Sdc1), HS and Hpse for flow cytometry analysis. Wt (black bars) and db/db (blue bars) beta cells showed strong intracellular expression for HSPG core proteins (a), HS (b) and Hpse (c) but weak cell surface expression (d-f). Intracellular Col18 (a), Sdc1 (a), HS (b) and Hpse (c) were significantly reduced in db/db beta cells compared to corresponding controls. The data represent the mean GMFI ± SEM for n= 3-7 experiments/group; n= 2-4 donors/experiment. Non-parametric Mann-Whitney test; *P<0.05, **P<0.01 and ***P<0.0001.

Interestingly, db/db beta cells cultured for 2 days demonstrated essentially the same level of diminished intracellular Col18 (46.3%; P<0.01), Sdc1 (36.9%; P<0.05) and Hpse (46.9%; P<0.01) relative to corresponding controls, as observed on day 0 (**Figure 5.9(a)**). A striking finding was that intracellular HS was significantly reduced to 37.5% of wt controls (P<0.05) on day 2 (**Figure 5.9(b)**); in contrast, the intracellular HS levels of db/db and wt beta cells were comparable on day 0 (**Figure 5.8(b)**). These findings indicate that intracellular levels of HSPG core proteins and Hpse in db/db and wt beta cells remain stable *in vitro*. In contrast, intracellular HS rapidly decrease in db/db beta cells *in vitro*, indicating a heightened susceptibility to damage, compared to intracellular proteins (HSPGs, Hpse).

(b) Female db/db and wt beta cells

In the case of freshly isolated female wt and db/db beta cells (day 0), no significant differences were found in the expression of intracellular HSPGs, HS and Hpse, with the exception of CD44 which increased to 1.3-fold in db/db beta cells (GMFI= 384.40 ± 20.79 vs GMFI= 288.60 ± 19.60; P<0.05) (**Figure 5.10(a)**). Although intracellular Col18, Sdc1 and Hpse was substantially reduced to 43%, 52% and 54% of corresponding wt controls, respectively, these changes were not statistically significant (**Figure 5.10**). Overall, a general trend was observed for lower intracellular HSPG core proteins and Hpse in db/db beta cells on day 0. These findings resemble the properties of male db/db beta cells (**Figure 5.8**) and the decline in intra-islet Col18 and Sdc1 observed in female db/db islets *in situ* during T2D progression (see Section 3.2.10). Like male db/db beta cells (**Figure 5.8**), no significant differences were observed in the intensity of staining for cell surface HSPG core proteins, HS or Hpse between female wt and db/db beta cells (**Figure 5.10(d-f)**). Generally, HSPGs, HS and Hpse were more highly expressed intracellularly than on the cell surface, with the exception of Sdc1 and CD44 in db/db beta cells, where the intensity of staining was similar (**Figure 5.10**).

Like cultured male db/db beta cells, intracellular HS in female db/db beta cells cultured for 2 days demonstrated a significant decline to 45% of corresponding wt beta cells (GMFI= 566.00 ± 131.68 vs GMFI= 1249.80 ± 285.24; P<0.05; **Figure 5.11(b)**). This finding was in contrast to the similar intracellular HS staining observed for wt and db/db female beta cells on day 0 (**Figure 5.10(b)**). On day 2, the intracellular levels of Col18,

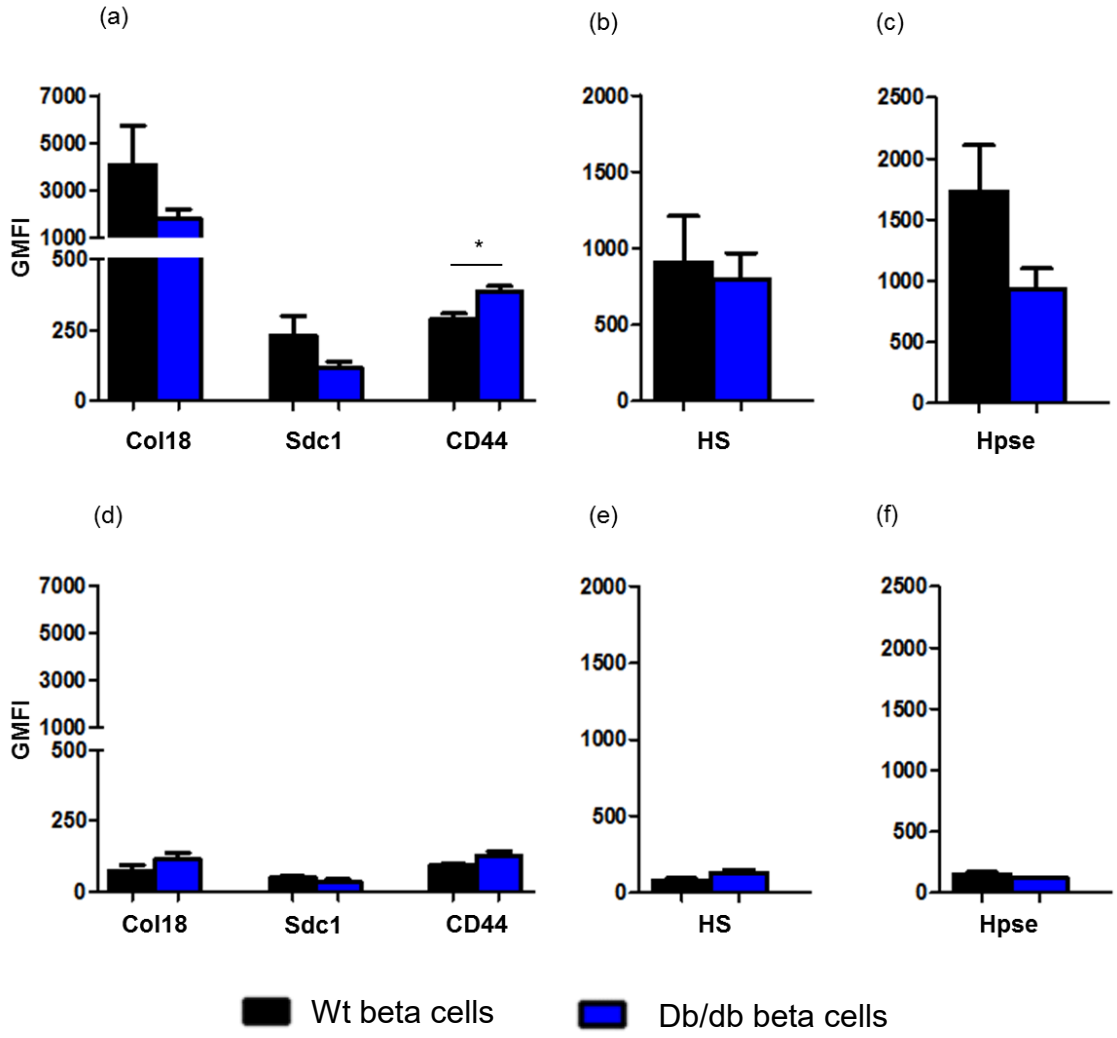

Figure 5.10: Intracellular and cell surface expression of HSPG core proteins, HS and Hpse in female wt and db/db beta cells on day 0.

Freshly isolated beta cells were prepared from female donors (5-9 weeks of age) stained for (a-c) intracellular and (d-f) cell surface HSPG core proteins (Col18, CD44 and Sdc1), HS and Hpse and analysed by flow cytometry. Wt (black bars) and db/db (blue bars) beta cells showed stronger intracellular staining for HSPG core proteins (a), HS (b) and Hpse (c) than at the cell surface (d-f). The data represent the mean GMFI ± SEM for n= 3-6 experiments/groups; n= 2-4 donors/experiment. Non-parametric Mann-Whitney test; *P<0.05.

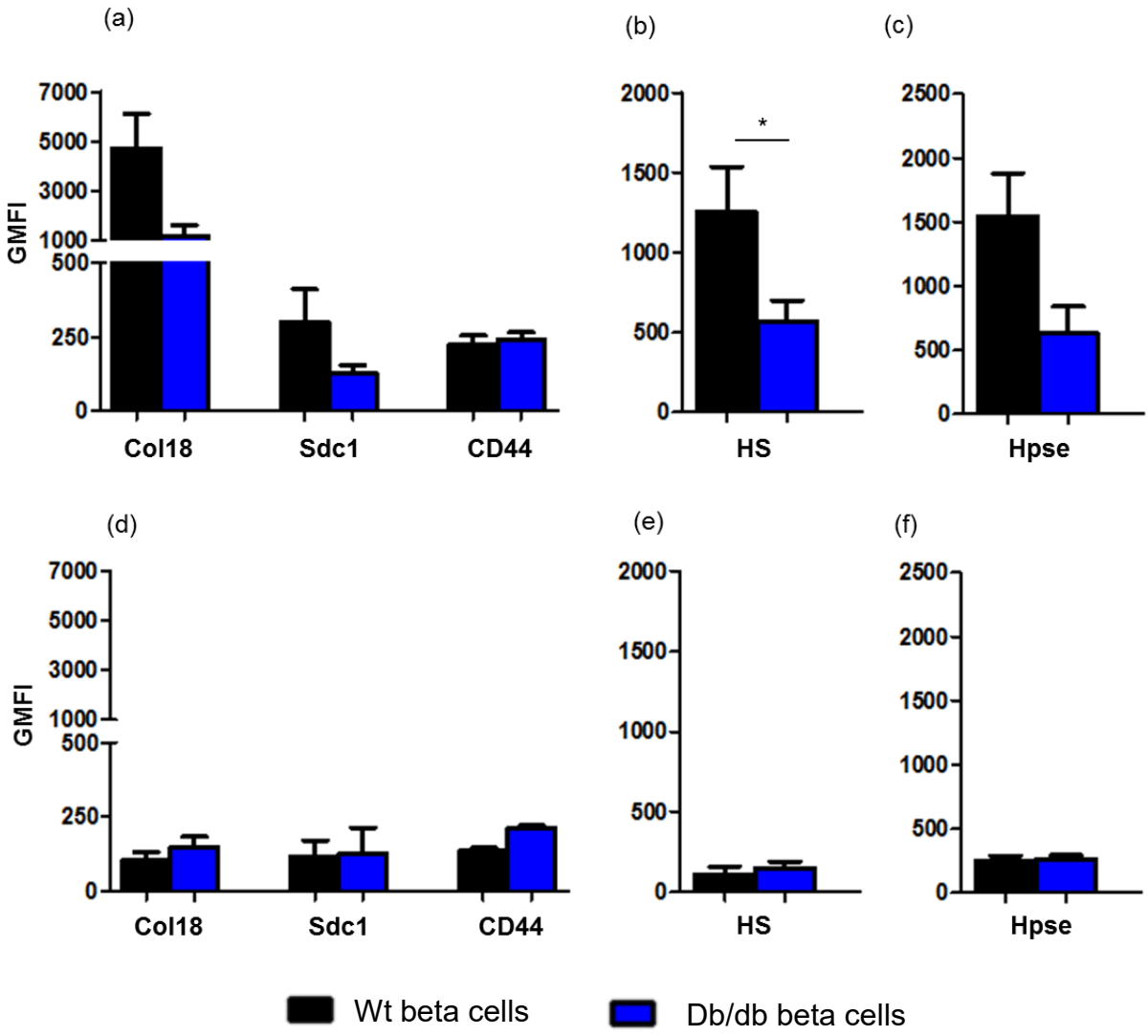

Figure 5.11: Intracellular and cell surface expression of HSPG core proteins, HS and Hpse in female wt and db/db beta cells at day 2.

Freshly isolated beta cells were cultured for 2 days, stained for (a-c) intracellular and (d-f) cell surface HSPG core proteins (Col18, CD44 and Sdc1), HS and Hpse and analysed by flow cytometry. In general, beta cells showed stronger intracellular expression of HSPG core proteins (a), HS (b) and Hpse (c) than at the cell surface expression (d-f). The data represent the mean GMFI ± SEM for n= 3-6 experiments/group with n= 2-4 donors/experiment. Non-parametric Mann-Whitney test; *P<0.05.

Sdc1 and Hpse were substantially reduced to 24.9%, 42.7% and 40.6% of corresponding wt controls (**Figure 5.11(a, c)**), in general agreement with the marked changes observed on day 0 (**Figure 5.10(a, c)**). Overall, these findings are consistent with the modulation in staining intensity observed in male db/db beta cells (**Figures 5.8 and 5.9**).

In summary, freshly isolated db/db beta cells were characterised by a marked loss of intracellular Col18 and Sdc1 core proteins and Hpse, compared to wt beta cells. In contrast, intracellular HS underwent a significant and rapid decline during culture. Previous *in vitro* studies reported by the Simeonovic lab have demonstrated that depletion of intracellular HS in beta cells correlates with loss of viability (Ziolkowski et al., 2012).

5.2.2.2 HS replacement increases the viability of db/db beta cells

Previous studies in the Simeonovic lab revealed that during the isolation of mouse islets *in vitro*, HS is largely lost from beta cells but the expression of HSPG core proteins is retained (Choong et al., 2015). Following subsequent dispersion of the islets, harvest and culture of the isolated beta cells, HS depletion was found to correlate with beta cell damage or death. Significantly, the replacement of the lost HS using HS mimetics preserved beta cell survival, clearly establishing intracellular HS as a critical requirement for beta cell health (Ziolkowski et al., 2012). Furthermore, these ground-breaking studies identified certain HS mimetics/analogues (e.g., heparin, PI-88) as "HS replacers" for beta cells. In this chapter, we confirmed the intracellular localisation for HSPG core proteins and HS in wt and db/db beta cells and detected a reduced expression of HS and HSPG core proteins in the db/db beta cells (see Section 5.2.2.1). We therefore investigated whether replacing the lost HS in db/db beta cells *in vitro* rescued them from dying and thus, significantly improved their viability.

(a) Male db/db and wt beta cells

Male db/db mice were categorised into three groups based on their non-fasting blood glucose (bg) levels i.e., mice with bg<10 mmol/L (normoglycaemic), mice with bg=10-15 mmol/L (mildly hyperglycaemic) and mice with bg>15 mmol/L (severely hyperglycaemic). Male wildtype and db/db islets were isolated and dispersed into single cells using Accutase (see Section 2.3). The Simeonovic lab previously reported that ~90%

of dispersed islet cells are ~90% insulin-positive, i.e., beta cells. Hereafter we refer to this population as beta cells (Ziolkowski et al., 2012). The viability of freshly isolated beta cells was analysed by flow cytometry using the fluorescent dyes Calcein-AM (Cal) and propidium iodide (PI) (see Section 2.9.1). Beta cell sub-populations were identified as Cal^+PI^- (viable), Cal^+PI^+ (damaged) and Cal^-PI^+ (dead) (see Section 2.9.3). In parallel, beta cells were cultured with and without heparin (HS analogue; 50 µg/ml) for 2 days at which time cell viability was assessed by flow cytometry. Representative flow cytometry dot plots show the viability of beta cells in the presence or absence of heparin for both wt and db/db beta cells (**Figure 5.12**).

Freshly isolated male wt beta cells consisted of 41.5% viable Cal^+PI^- cells, 28.4% damaged Cal^+PI^+ and 22.0% Cal^-PI^+ dead cells (**Figure 5.13(a)**). However, following culture for 2 days (Day 2), the damaged Cal^+PI^+ population increased to 2-fold, Cal^-PI^+ dead cells were reduced to ~67% and the Cal^+PI^- viable population was decreased by ~50%, compared to day 0 (**Figure 5.13(a)**). These data confirm the previous report that the viability of isolated normal beta cells deteriorates during short-term culture (Ziolkowski et al., 2012). In contrast, wt beta cells cultured with heparin for 2 days showed a significant reduction in Cal^+PI^+ damaged beta cells ($P<0.0001$) and dead cells ($P<0.0001$) to 19.6% and 10.5% of corresponding controls, respectively (**Figure 5.13(a)**). These data are consistent with a previous report of the rescue of BALB/c beta cells by HS replacement using heparin or PI-88 (Ziolkowski et al., 2012).

Isolated beta cells from db/db donors showed that ~50-60% of the cells were Cal^+PI^- on day 0 with ~17-20% Cal^+PI^+ damaged and ~7-14% Cal^-PI^+ dead cells (**Figure 5.13(b-d)**). Moreover, db/db beta cell survival decreased to ~39-43% during culture for 2 days (**Figure 5.13(b-d)**).

Like wt beta cells, the viability of beta cells (i.e., Cal^+PI^-) isolated from male normoglycaemic db/db mice (bg<10 mmol/L) significantly increased 2.8-fold ($P<0.001$) following culture with heparin (**Figure 5.13(b)**; $P<0.0001$). In addition, the population of damaged beta cells (Cal^+PI^+) and dead cells (Cal^-PI^+) were significantly reduced to 23.1% ($P<0.001$) and 27.7% of untreated controls, respectively (**Figure 5.13(b)**; $P<0.0001$). Importantly, for beta cells from mildly hyperglycaemic db/db donors (bg=10-15 mmol/L)

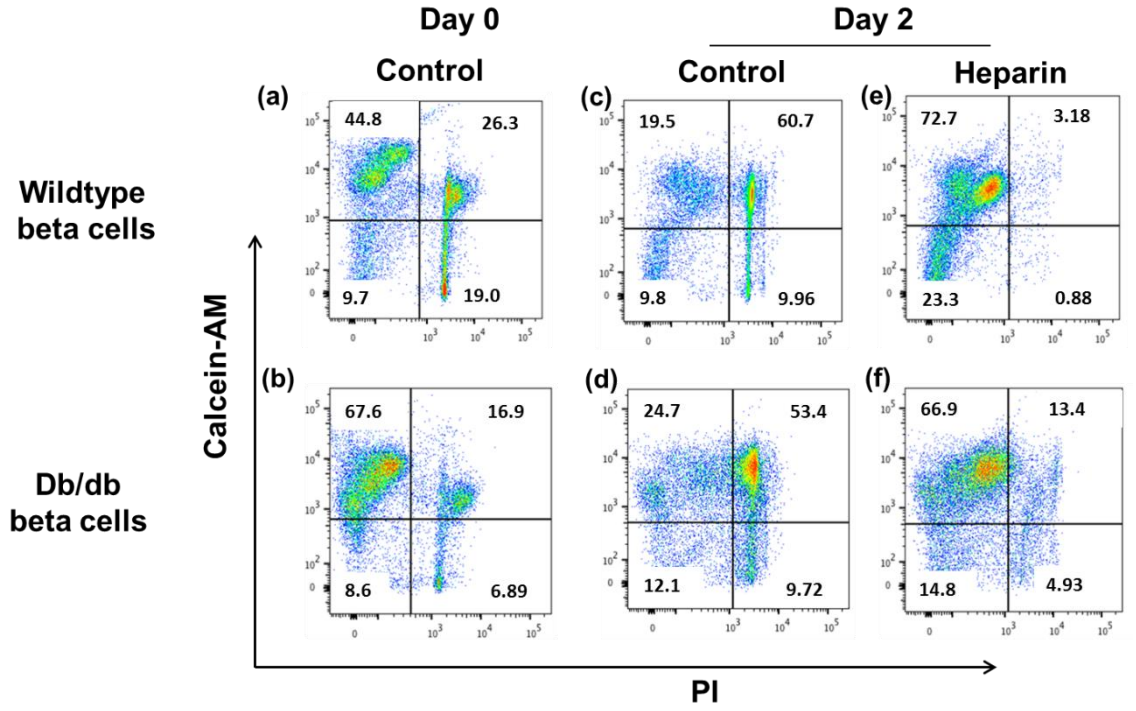

Figure 5.12: HS replacement protects db/db beta cells from dying in culture.

Wildtype and db/db female islets were isolated and dispersed into single cells. The cell viability of the beta cells was analysed by flow cytometry using the fluorescent dyes Calcein and PI. The beta cells were cultured with or without heparin (50 µg/ml) for 2 days and cell viability was analysed by flow cytometry. Representative flow cytometry dot plots show the viability (Cal^+PI^-; upper left quadrant) of wildtype (a) and db/db (b) beta cells at day 0 and after culture without (c, d) or with (e, f) heparin for 2 days. Cal^+PI^+ (upper right quadrant) identifies damaged cells; Cal^-PI^+ (lower right quadrant), dead cells; Cal^-PI^- (lower left quadrant), cell debris. Each quadrant shows data as a % of the total cell population.

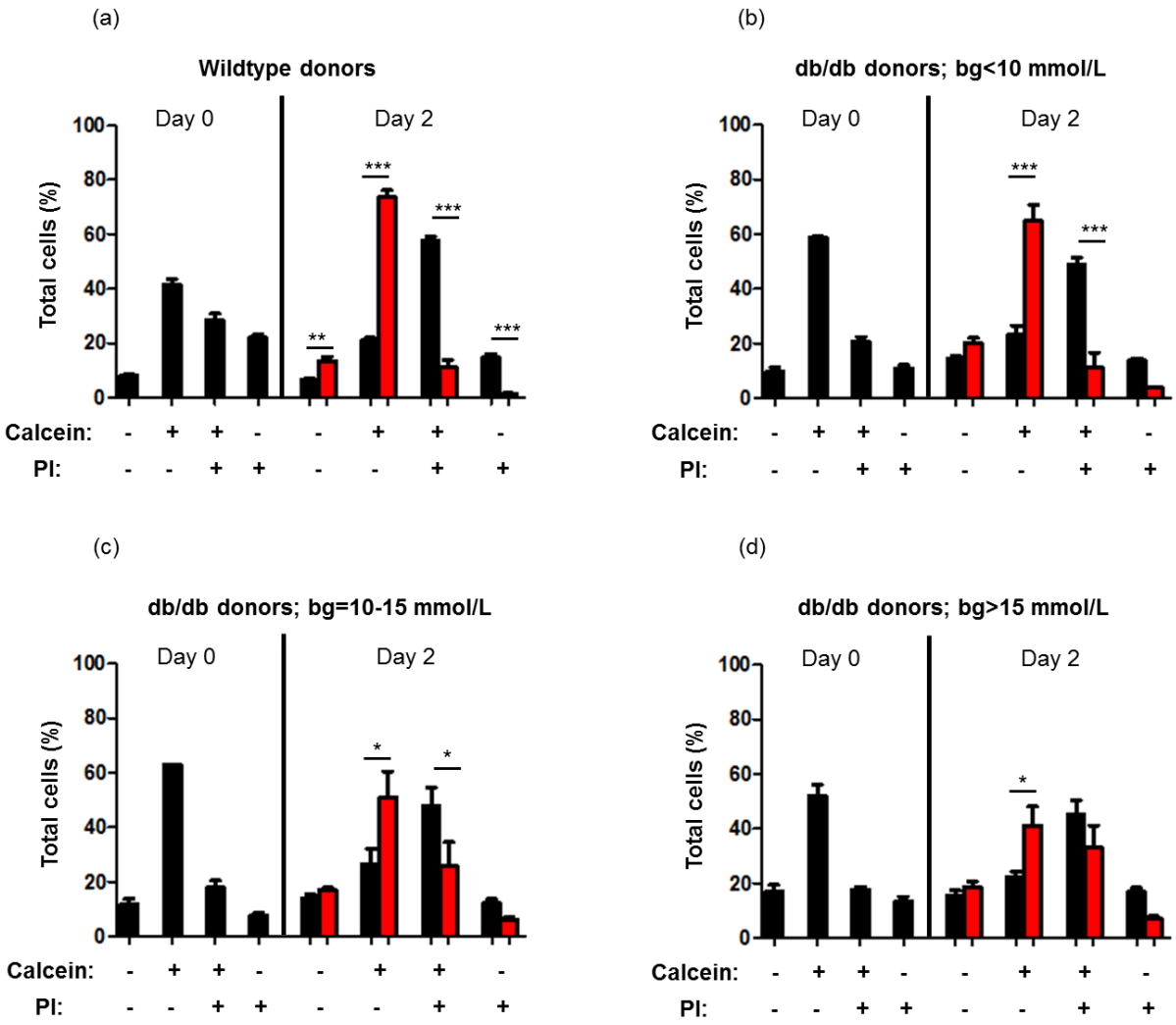

Figure 5.13: Protection of male beta cells from dying in culture by HS replacement. Islets were isolated and dispersed into single cells. The viability of male (a) wildtype and (b-d) db/db beta cells was analysed by flow cytometry using the fluorescent dyes calcein and PI. The beta cells were cultured with (red bars) and without (black bars) heparin (50 µg/ml) for 2 days and cell viability was analysed by flow cytometry. Beta cells were identified as viable (Cal^+PI^-), damaged (Cal^+PI^+) or dead (Cal^-PI^+). Wildtype (a) and db/db beta cells (b-d) treated with heparin (red bars) showed increased cell viability at day 2 compared to corresponding controls (black bars). Data represent mean ± SEM for n= 3-9 experiments/group; n= 2-3 mice/experiment. ANOVA with Fisher's unprotected LSD post-test; *P<0.05, **P<0.01 and ***P<0.0001.

treatment with heparin significantly increased the live cell (Cal^-PI^-) population by 1.9-fold ($P<0.05$); Cal^+PI^+ damaged cells and Cal^-PI^+ dead cells declined to 53.9% ($P<0.05$) and 51.5% ($P<0.05$) (**Figure 5.13(c)**). Surprisingly, db/db beta cells from hyperglycaemic donors (bg>15 mmol/L) also showed a 1.9-fold increase in live beta cells ($P<0.05$), compared to untreated control beta cells but the damaged cell population demonstrated no significant reduction (33.2% vs 45.2% for untreated controls; **Figure 5.13(d)**).

These findings clearly reveal that co-culture of db/db beta cells with heparin significantly ameliorates beta cell survival. These data reveal the capacity for HS replacement to rescue damaged db/db beta cells and restore a "viable" phenotype, even in the presence of established T2D. However, whereas the maximum survival of heparin-treated "hyperglycaemic" (bg>15 mmol/L) db/db beta cells reached 41.2% of total cells (vs 22.5% in untreated controls), 64.7% of heparin-treated "normoglycaemic" db/db beta cells were viable by day 2 (vs 23.2% in corresponding untreated control cells). Thus, conversion to a "survival phenotype" due to HS replacement, can be achieved, albeit less efficiently, in beta cells with increased pre-existing metabolic dysfunction e.g., ER stress.

(b) Female db/db and wt beta cells

As shown for male beta cells (**Figure 5.13**), freshly isolated female db/db beta cells (day 0) showed an increased proportion of viable cells (~56-63% Cal^+PI^-) compared to wt female controls (~42% Cal^+PI^-) (**Figure 5.14**). Moreover, wt and db/db beta cell survival decreased to ~50% and ~30-65% respectively during culture for 2 days (**Figure 5.14**). Furthermore, culture of wt female beta cells with heparin significantly increased the Cal^+PI^- viable population by 3.3-fold ($P<0.0001$) and significantly decreased the Cal^+PI^+ damaged and Cal^-PI^+ dead cell populations to 20.9% ($P<0.0001$) and 12.5% ($P<.0.0001$) of untreated controls (**Figure 5.14(a)**). Db/db female "normoglycaemic" and "mildly hyperglycaemic" beta cells cultured with heparin also showed a significant 2.4-fold and 2.1-fold increase, respectively, in Cal^+PI^- live beta cells (**Figure 5.14(b, c)**). In parallel, Cal^+PI^+ damaged cells were decreased to 43.6% ($P<0.01$) in "normoglycaemic" beta cells and 80.4% ($P<0.05$) in "mildly hyperglycaemic" beta cells (**Figure 5.14(b, c)**). However, in contrast to "hyperglycaemic" male db/db beta cells (**Figure 5.13(d)**), no significant changes were observed in db/db beta cells from "hyperglycaemic" female donors (**Figure 5.14(d)**). Thus, HS replacement was effective in enhancing the survival of

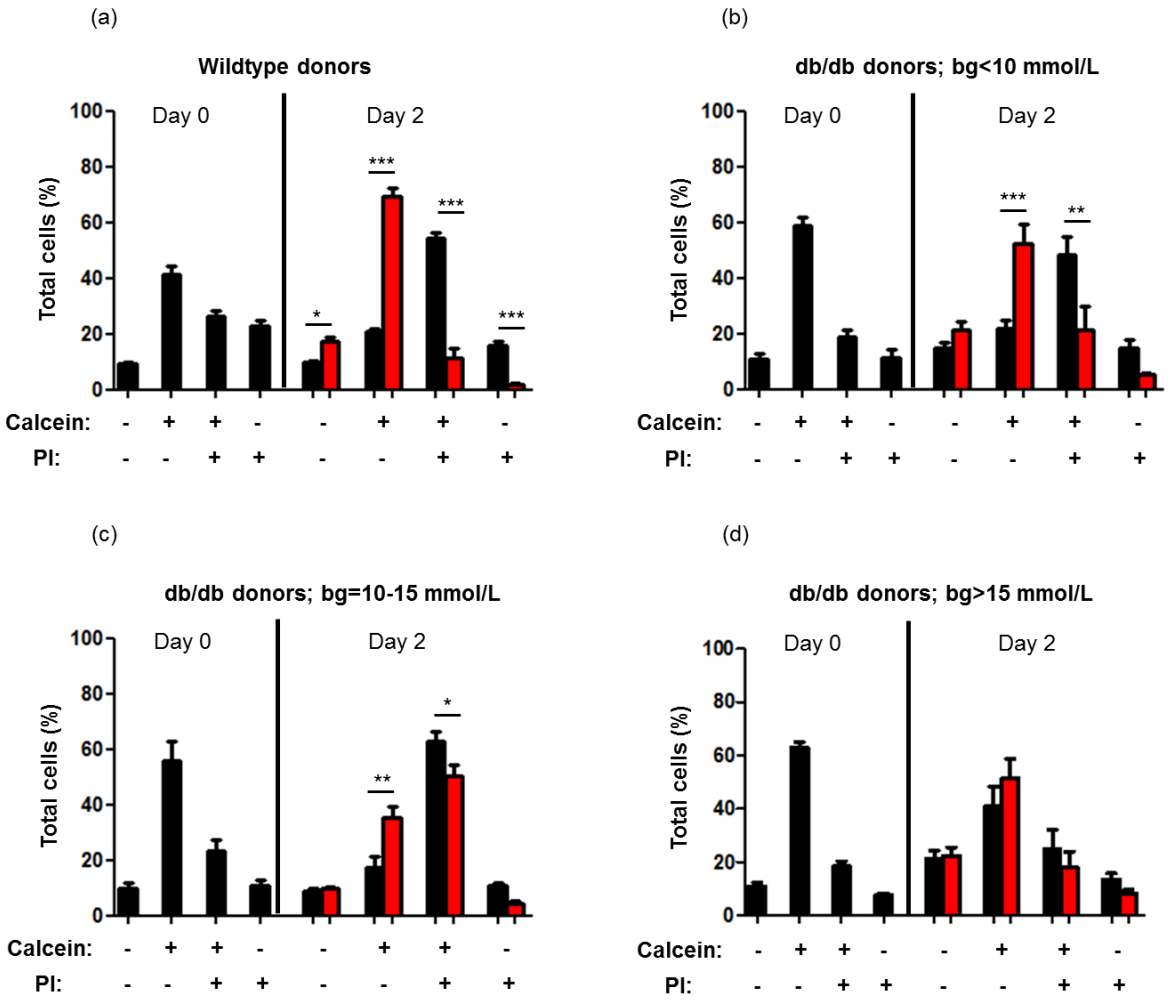

Figure 5.14: Rescue of female db/db beta cells *in vitro* by HS replacement.

Islets were isolated and dispersed into single cells. The viability of female (a) wildtype and (b-d) db/db beta cells was analysed by flow cytometry using the fluorescent dyes Calcein and PI. The female beta cells were cultured with (red bars) and without (black bars) heparin (50 µg/ml) for 2 days and cell viability was analysed by flow cytometry. Beta cells were identified as viable (Cal^+PI^-), damaged (Cal^+PI^+) or dead (Cal^-PI^+). Wildtype beta cells (a), normoglycaemic (b) and mildly hyperglycaemic (c) db/db beta cells treated with heparin (red bars) showed increased cell viability at day 2 compared to controls (black bars) but no significant change in the viability of beta cells from severely hyperglycaemic mice were found (d). Data represent mean ± SEM for n= 3-12 experiments/group; n= 2-4 mice/experiment. ANOVA with Fisher's unprotected LSD post-test; *P<0.05, **P<0.01 and ***P<0.0001.

"normoglycaemic" and "mildly hyperglycaemic" female db/db beta cells to 52.3% (vs 21.8% in untreated controls) and 35.3% (vs 17.2% in controls), respectively. Together, the *in vitro* studies of db/db beta cells confirm a critical role for HS in the survival of normal wt beta cells as well as for rescuing the viability of T2D beta cells.

5.2.2.3 HS replacement protects beta cells from oxidative damage

Ziolkowski et al. (2012) reported that HS replacement in isolated mouse beta cells not only enhanced beta cells survival in culture, but also protected the beta cells from oxidative damage. These findings suggested that *in situ* HS in beta cells may function as a non-enzymatic antioxidant or quencher of reactive oxygen species (ROS). To ascertain whether this mechanism could contribute to the rescue of db/db beta cells *in vitro*, wt and db/db beta cells were acutely exposed to hydrogen peroxide (H_2O_2) after culture for 2 days with or without heparin (50 µg/ml). Unlike previous experiments (see Section 5.2.2.2), beta cell damage/death was evaluated by flow cytometry using uptake of the non-permeant fluorescent dye Sytox Green, an intracellular esterase-independent indicator of cell viability (Sytox green -ve) and cell damage/death (Sytox green +ve) (Ziolkowski et al., 2012).

(a) Male db/db and wt beta cells

Representative flow cytometry dot plots show that both wt beta cells and db/db beta cells on day 0, demonstrate markedly increased cell death after H_2O_2 treatment (**Figure 5.15**). Significantly, treatment with the HS replacer, heparin, substantially reduced wt (**Figure 5.15(c, d, i, j)**) and db/db (**Figure 5.15(e, f, k, l)**) beta cell death in the absence (**Figure 5.15(c-f)**) and presence (**Figure 5.15(i-l)**) of hydrogen peroxide exposure on day 2.

When db/db beta cells were analysed for protection against H_2O_2-induced damage and categorised by the glycaemic status of the donor mice, beta cells freshly isolated from normoglycaemic (bg<10 mmol/L; **Figure 5.16(b)**), mildly hyperglycaemic (bg=10-15 mmol/L; **Figure 5.16(c)**) and severely hyperglycaemic (bg>15 mmol/L; **Figure 5.16(d)**) db/db male mice demonstrated a significant 2.9-fold ($P<0.01$), 4.8-fold ($P<0.001$) and 6.4-fold ($P<0.05$) increase in H_2O_2-induced cell death. Moreover, "normoglycaemic" db/db beta cells (**Figure 5.16(b)**) resembled wt beta cells on day 0 (**Figure 5.16(a)**), the latter showing a 2.7-fold increase in Sytox green +ve cell damage/death following H_2O_2-

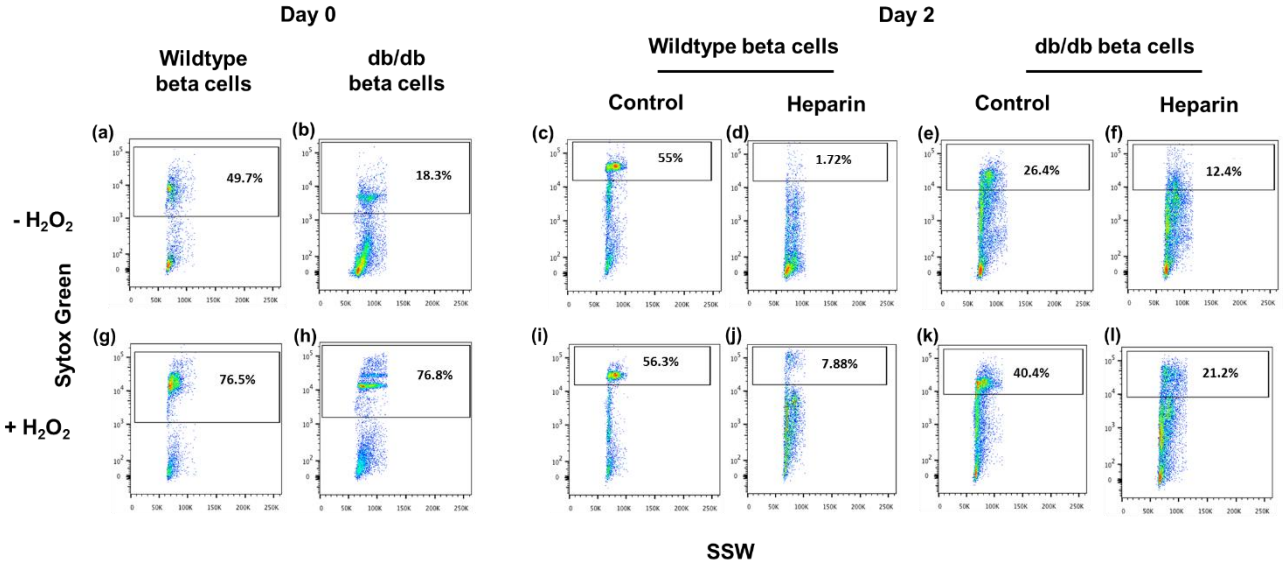

Figure 5.15: HS replacement renders male wt and db/db beta cells resistant to hydrogen peroxide (H_2O_2) induced beta cell damage.

Wildtype and db/db male islets were isolated and dispersed into single cells. The viability of the beta cells was analysed by Sytox Green uptake and flow cytometry on day 0. The beta cells were cultured with or without heparin (50 µg/ml) and cell viability was analysed on day 2. Representative flow cytometry dot plots of Sytox Green uptake (boxed regions) show that H_2O_2 treatment of freshly isolated wt (g) and db/db (h) beta cells increased beta cell damage/death. Culture with heparin for 2 days protected wt (c, d, i, j) and db/db (e, f, k, l) from culture-induced (c, d, e, f) and H_2O_2-induced (i, j, k, l) beta cell death.

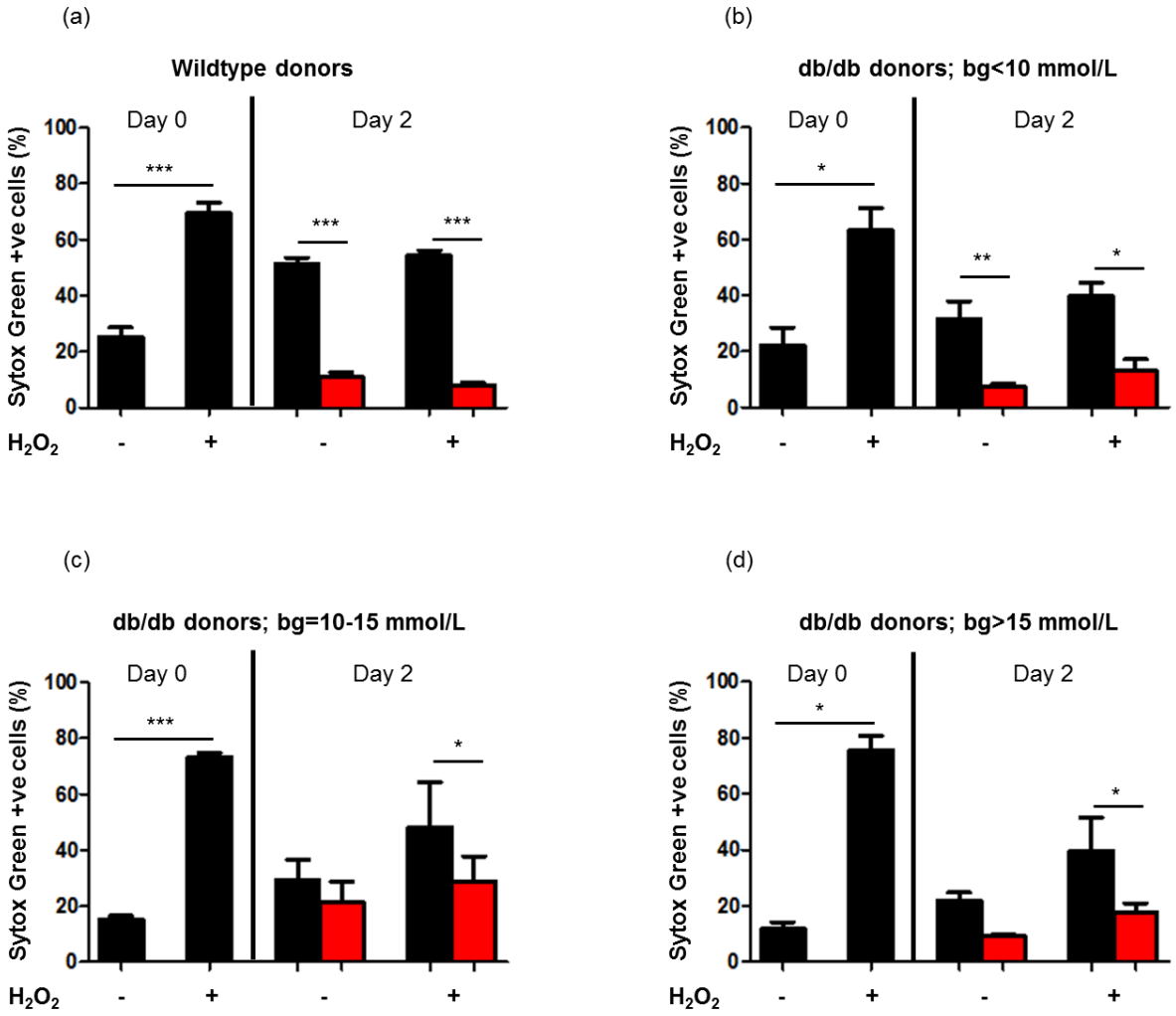

Figure 5.16: HS replacement protects male wt and db/db beta cells from ROS-induced death *in vitro*.

Male wildtype and db/db beta cells were analysed for viability and hydrogen peroxide (H_2O_2; ROS)-induced cell damage/death by flow cytometry using Sytox Green uptake on day 0. In addition, cells were cultured with (red bars) or without (black bars) heparin (50 µg/ml) for 2 days and analysed by flow cytometry. Freshly isolated wt (a), normoglycaemic (bg<10 mmol/L) db/db (b), mildly hyperglycaemic (bg=10-15 mmol/L) db/db (c) and severely hyperglycaemic (bg>15 mmol/L) db/db (d) beta cells on day 0 showed increased beta cell damage/death, respectively, after acute exposure to hydrogen peroxide. Culture of wt (a) and db/db beta cells (b-d) with heparin resulted in a significant reduction in beta cell damage/death due to hydrogen peroxide treatment. Data represent mean ± SEM for n= 3-11 experiments; n= 2-4 mice/experiment. ANOVA with Fisher's unprotected LSD post-test; *P<0.05, **P<0.01 and ***P<0.001.

treatment (P<0.05). These findings suggest that ER stress (see Section 1.9) renders hyperglycaemic db/db beta cells more sensitive to oxidative damage due to exogenous hydrogen peroxide.

As demonstrated in Section 5.2.2.2 using Calcein/PI staining, culture of wt (**Figure 5.16(a)**) and normoglycaemic db/db (**Figure 5.16(b)**) beta cells with heparin significantly decreased beta cell damage/death to 21.1% (P<0.001) and 23.4% (P<0.01) of untreated controls, i.e., increased beta cell survival. Furthermore, these heparin-rescued wt and db/db beta cells were resistant to H_2O_2-induced damage, demonstrating only ~8% (**Figure 5.16(a)**; P<0.001) and ~12-30% (**Figure 5.16(b-d)**; P<0.05) Sytox green +ve cell damage/death, respectively, compared to 54% and 39-48%, respectively, in H_2O_2-treated control beta cells. These findings are in striking contrast to the dramatic sensitivity of freshly isolated beta cells to H_2O_2-induced death (Day 0, **Figure 5.16(a-d)**). Although heparin treatment was previously shown to significantly improve the survival of "mildly" and "severely" hyperglycaemic db/db beta cells (see Section 5.2.2.2), only a trend for improved viability was observed using Sytox green uptake (Day 2, **Figure 5.16(c, d)**). However, a significant reduction in H_2O_2-mediated beta cell death to 59.9% (Day 2; **Figure 5.16(c)**; P<0.05) and 44.3% (Day 2, **Figure 5.16(d)**; P<0.05) of controls was observed after culture with heparin, confirming a robust capacity for HS replacement to improve db/db beta cell viability, even when subjected to acute oxidative stress.

(b) Female db/db and wt beta cells

Female wt and db/db beta cells treated with hydrogen peroxide immediately after their isolation showed a significant 2.9-fold (Day 0; **Figure 5.17(a)**; P<0.001) and 4.4-6.7 fold (Day 0; **Figure 5.17(b-d)**) increase in cell damage/death, compared to controls. These findings are similar to the data obtained for male db/db beta cells (Section 5.2.2.3(a)). Likewise, after culture with the HS replacer, heparin, beta cell death was reduced to 10.7% (Day 2; **Figure 5.17(a)**; P<0.001) and 55.6%-65.7% (Day 2; **Figure 5.17(b-d)**) of controls in wt and db/db beta cells, with a statistically significant decrease observed in hyperglycaemic (P<0.01) db/db beta cells, a finding not previously observed when viability was assessed using Cal^+PI^- staining (**Figure 5.14(d)**). Also like male beta cells, female wt and db/db beta cells cultured with heparin for 2 days were resistant to H_2O_2-induced death with beta cell death significantly reduced to 14.5% (Day 2; **Figure 5.17(a)**)

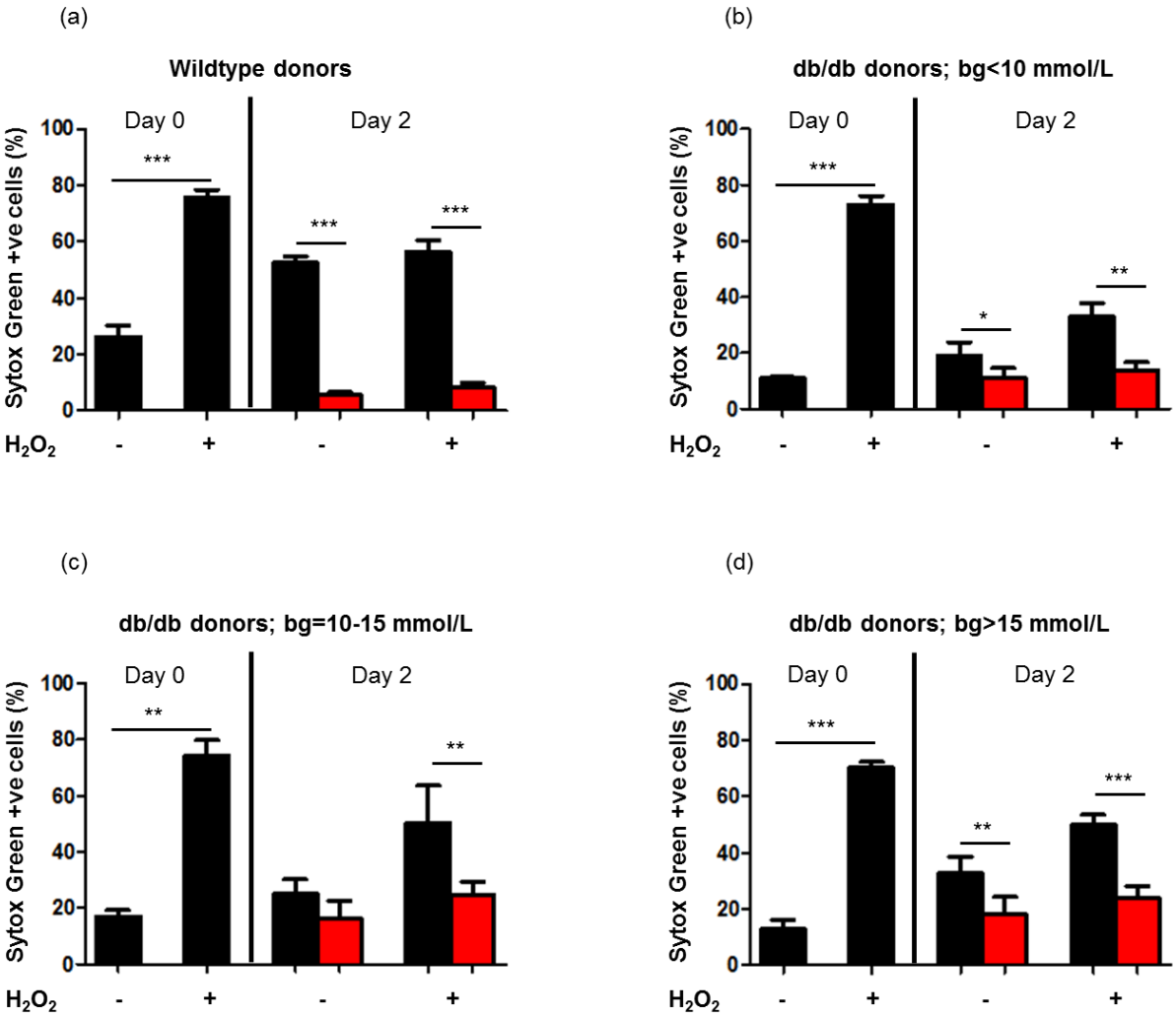

Figure 5.17: HS replacement protects female db/db beta cells from ROS-induced death *in vitro*.

Female wildtype and db/db beta cells were analysed for viability and hydrogen peroxide (H_2O_2; ROS)-induced cell damage/death by flow cytometry using Sytox Green uptake at day 0. In addition, cells were cultured with (red bars) or without (black bars) heparin (50 µg/ml) for 2 days and analysed by flow cytometry. A significant increase in the damage/death of freshly isolated wt (a), normoglycaemic db/db (b), mildly hyperglycaemic db/db (c) and severely hyperglycaemic db/db (d) beta cells was observed on day 0, after acute exposure to hydrogen peroxide. Culture with heparin for 2 days significantly reduced cell death due to acute exposure of wt and db/db beta cells to hydrogen peroxide. Data represent mean ± SEM for n= 3-11 experiments/group; n= 2-4 mice/experiment. ANOVA with Fisher's unprotected LSD post-test; *P<0.05, **P<0.01 and ***P<0.001.

and 4.7%-48.7% (Day 2; **Figure 5.17(b-d)**) of controls.

In summary, HS replacement using heparin protected wt and db/db beta cells from culture and exogenous ROS-induced beta cell death. These findings raise the possibility that culture-induced beta cell death could be mediated by ROS generated in endogenously in beta cells during culture. Despite pre-existing ER stress and most likely oxidative stress (Hasnain et al., 2014, Chan et al., 2013) in "hyperglycaemic" db/db beta cells, HS replacement protected the beta cells from hydrogen peroxide-induced death, albeit to a less pronounced extent than in wt beta cells.

5.2.3 PI-88 treatment of db/db mice

Our *in vitro* studies demonstrated that HS replacement in db/db beta cells, using heparin, protects them from both culture-induced and ROS-mediated damage/death. Since heparin is an anti-coagulant and cannot be administered long-term in mice due to the likelihood of fatal haemorrhage, we tested the efficacy of another HS replacer with minimal anti-coagulant activity, to rescue db/db beta cells *in vivo* and impede the development of hyperglycaemia. PI-88 has previously been reported to act as a potent HS replacer in beta cells isolated from normal euglycaemic BALB/c mice (Ziolkowski et al., 2012). Furthermore, treatment of adult NOD/Lt female mice with PI-88 prevented the onset of T1D in 50% of diabetes-prone mice, by acting as both a HS replacer and heparanase inhibitor (Ziolkowski et al., 2012).

We therefore treated female and male db/db mice (from 3.5 weeks of age) with PI-88 (10 mg/kg/day, i.p.) or saline (as diluent controls) for 35 days. The mice were weighed and non-fasting blood glucose was measured three times (a.m.) per week and the volume of PI-88 was adjusted, based on body weight (see Sections 2.2.1 and 2.11.1). After termination of treatment, HbA1c levels were measured (see Section 2.2.3), blood samples were collected for free fatty acid analysis (see Section 2.2.5) and ipGTTs were performed (see Section 2.2.2). In addition, the pancreases were collected for histology and/or immunohistochemical analysis of HS and insulin (see Section 2.7).

5.2.3.1 Blood glucose levels, body weight and HbA1c levels of PI-88-treated db/db mice

Female db/db mice treated with PI-88 showed a trend towards lower non-fasting blood glucose levels from 6-7 weeks of age, compared to age-matched saline controls but no statistically significant difference was established (**Figure 5.18(a)**). Similarly, male db/db mice showed no improvement in glycaemic control, based on non-fasting blood glucose levels (**Figure 5.18(b)**). No significant differences in body weight were observed between PI-88 and saline-treated db/db mice (**Figure 5.18(c, d)**). HbA1c levels measured at termination of treatment also showed no significant differences between control and PI-88 treated female (5.97 ± 0.26% vs 5.70 ± 0.26%) and male (6.24 ± 0.21% vs 5.99 ± 0.22%) db/db mice; however a trend for lower HbA1c levels was consistent for both females and males (**Figure 5.18(e, f)**). Overall, non-fasting blood glucose levels and HbA1c levels showed no improvement in PI-88-treated db/db mice.

Intraperitoneal glucose tolerance tests (ipGTTs) were performed on saline and PI-88 treated db/db mice (**Figure 5.19**). The mice were fasted for 6 hrs before receiving an intraperitoneal injection of glucose (0.5 g/kg). Blood glucose levels were measured at 0, 15, 30, 60, 90 and 120 mins (see Section 2.2.2). In addition, the area under the curve (AUC) was determined for the blood glucose profile. After 6 hrs of fasting, the blood glucose levels of saline-treated and PI-88 treated female db/db mice were 15.8 ± 3.0 mmol/L and 21.5 ± 2.9 mmol/L (**Figure 5.19(a)**); the fasting blood glucose levels of PI-88 treated and control db/db males were similar at time 0. No significant changes in blood glucose levels were subsequently observed over the 2 hour test period between saline or PI-88 treated female or male db/db mice. Hence, no significant differences were found in the AUC for saline and PI-88 treated female or male db/db mice (**Figure 5.19(c, d)**). These data revealed that PI-88 treatment for 35 days failed to improve glycaemic control in both female and male db/db mice.

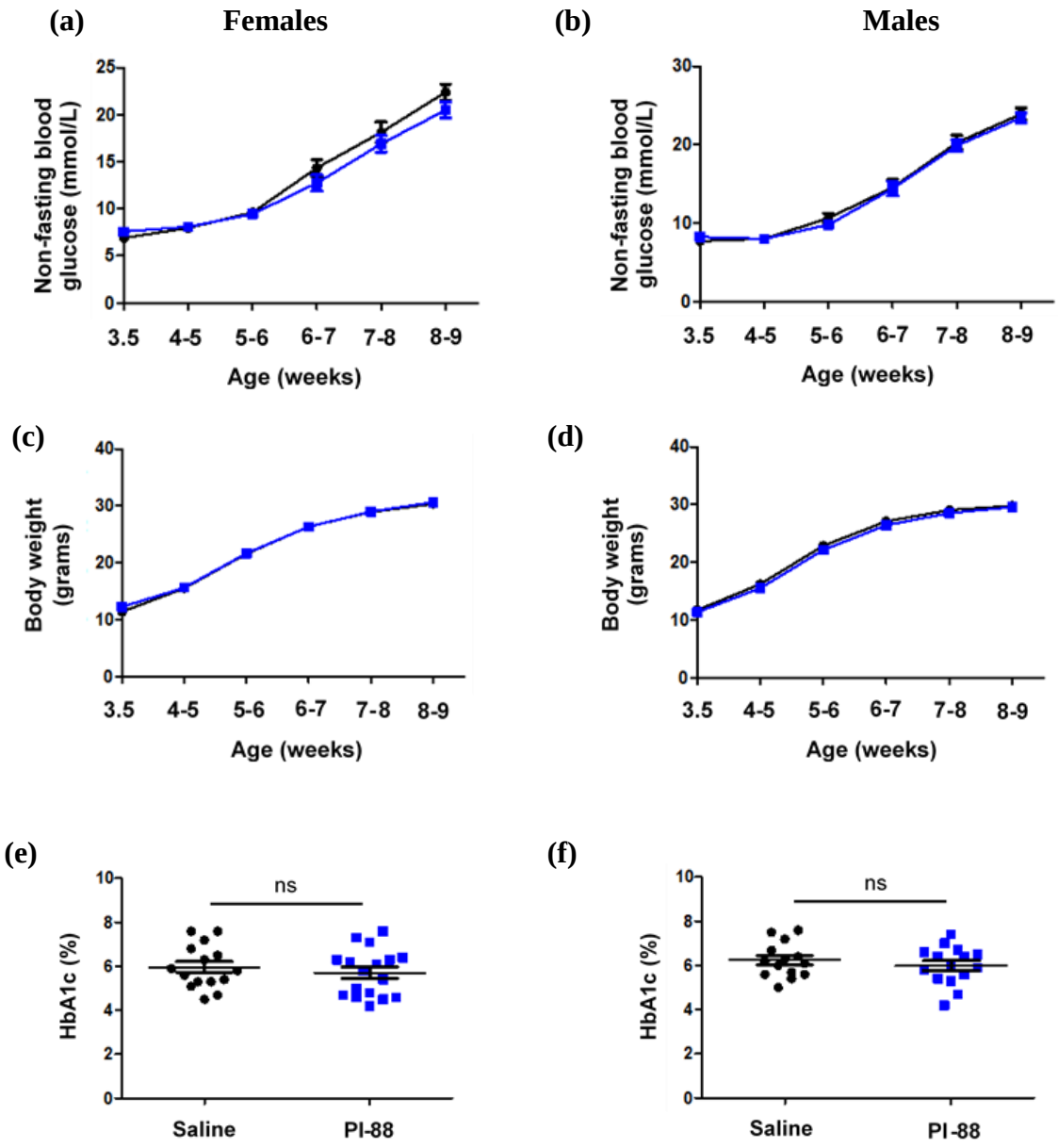

Figure 5.18: PI-88 and saline treatment of db/db mice.

Female (a, c, e) and male (b, d, f) db/db mice were treated with PI-88 (10 mg/kg/day; blue symbols) or saline (diluent controls; black symbols) i.p. from 3.5 weeks of age for 35 days. Non-fasting blood glucose levels (a, b) and body weight (c, d) were monitored 3x/week. Upon termination of treatment (1 day post-final dose), HbA1c levels were analysed using a HemoCue HbA1c Analyzer. The non-fasting blood glucose levels (a, b), body weight (c, d) and HbA1c levels (e, f) were similar for PI-88 treated and control groups within each gender. Data represent mean ± SEM for n= 8-11 mice/age group (females) or n= 14-15 mice/group (males). Non-parametric Mann-Whitney test was used for comparisons between groups for non-fasting blood glucose and body weight; Unpaired t-test was used for HbA1c; ns, not significant.

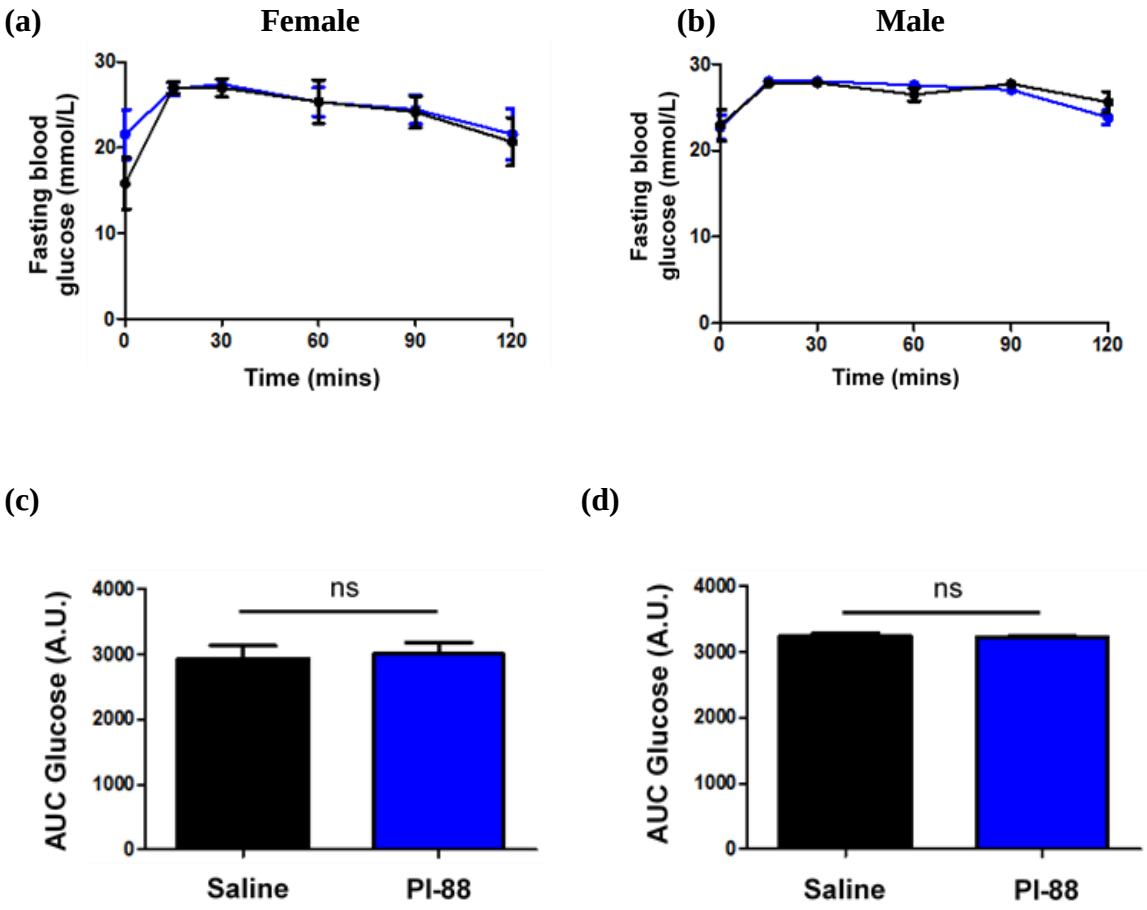

Figure 5.19: Intraperitoneal glucose tolerance test (ipGTT) in PI-88 treated and saline-treated db/db mice.

An ipGTT was performed after a 6 hour fast at 1 day after terminating treatment of female (a, c) and male (b, d) db/db mice with PI-88 (blue symbols) or saline (black symbols) for 35 days. (a, b) Fasting blood glucose levels were measured at time 0, 15, 30, 60, 90 and 120 mins. (c, d) Bar graphs show area under the curve (AUC) for blood glucose profiles. Data show mean ± SEM of 4-6 females/group and n= 9 males/group. Non-parametric Mann-Whitney test; ns, not significant.

5.2.3.2 Islet HS and insulin levels in the pancreases of PI-88 treated db/db mice

Intra-islet HS and insulin in the pancreases of PI-88 treated and control female db/db mice were localised by immunohistochemistry and quantified using Image J software with colour deconvolution plugin (see Section 2.7.5). The threshold intensity of staining was established using positive staining in pancreas sections from saline-treated mice; this threshold intensity was applied to all samples to calculate the % islet area stained.

PI-88 treatment of female db/db mice resulted in no significant increase in the HS+ve islet area (**Figure 5.20(a)**) as determined by immunohistochemical staining using HS3A8 anti-HS Ab, a phage display antibody that recognises highly sulfated HS domains (6-O and 2-O sulfation of iduronic acid) (Dennissen et al., 2002, Alhasan et al., 2014). In addition, there was a significant reduction in the insulin+ve islet area in pancreases harvested from PI-88 treated mice to 74.9% of saline controls (P=0.0014; **Figure 5.20(b)**). These data revealed that PI-88 treatment failed to improve the intra-islet expression of HS and insulin in db/db mice, compared to saline controls.

In situ, lipoprotein lipase is found bound to HS on the surface of endothelial cells (Wang et al., 2013b, Freeman et al., 2005, Parthasarathy et al., 1994). *In vitro*, PI-88 has been reported to displace and thereby inhibit lipoprotein lipase binding to the HS analogue, heparin (Freeman et al., 2005). In view of these properties, we investigated whether PI-88 treatment of db/db mice elevated the levels of circulating free fatty acids (FFAs), potentially via the release of free lipoprotein lipase into the circulation. If so, we reasoned that a potential downstream effect may be exacerbation of ER stress and dysfunction in the db/db beta cells.

The levels of non-esterified FFAs were therefore measured in the plasma of female and male db/db mice treated for 35 days with PI-88 or saline (see Section 2.2.5). PI-88 treated female and male db/db mice showed a 1.2-fold increase (0.88 ± 0.12 mM vs 0.74 ± 0.15 mM; **Figure 5.21(a)**) and 1.1-fold increase (1.17 ± 0.14 mM vs 1.04 ± 0.19 mM; **Figure 5.21(b)**) in plasma FFAs, compared to controls; however, these differences were not statistically significant. These findings indicated that the failure of PI-88 treated db/db mice to show improved glycaemic control was unlikely to be due to secondary effects on circulating free fatty acids.

(a)

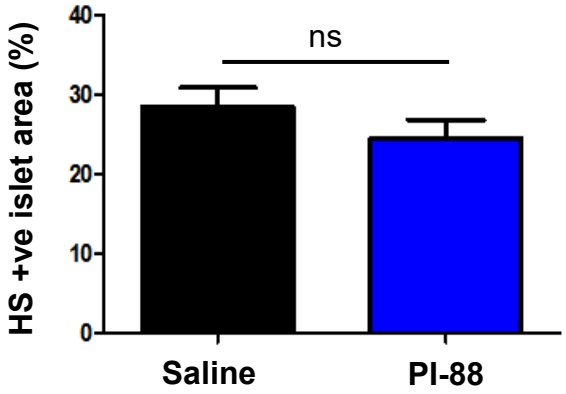

(b)

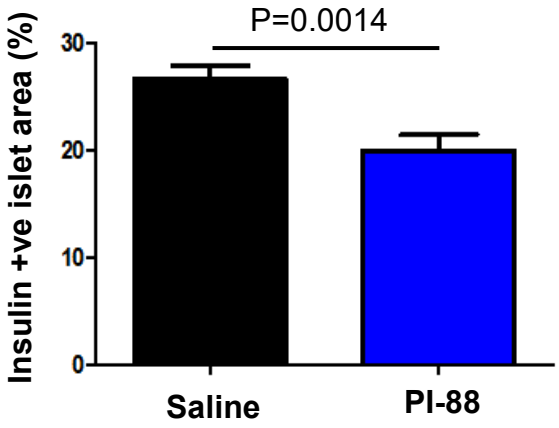

Figure 5.20: HS and insulin expression in the islets of PI-88 treated female db/db mice.

Pancreases were harvested from female db/db mice treated with PI-88 (10 mg/kg/day; blue bars) or saline (controls; black bars) i.p. on day 36 (1 day after the final dose). HS and insulin were localised in the islets by immunohistochemistry. The HS+ve islet area (a) and insulin+ve islet area (b) were determined using morphometry and Image J software. The data represent mean ± SEM for n= 4-11 pancreases/group with n= 52-55 (HS) and n= 90-151 (insulin) islets examined/group. Mann-Whitney test; ns, not significant.

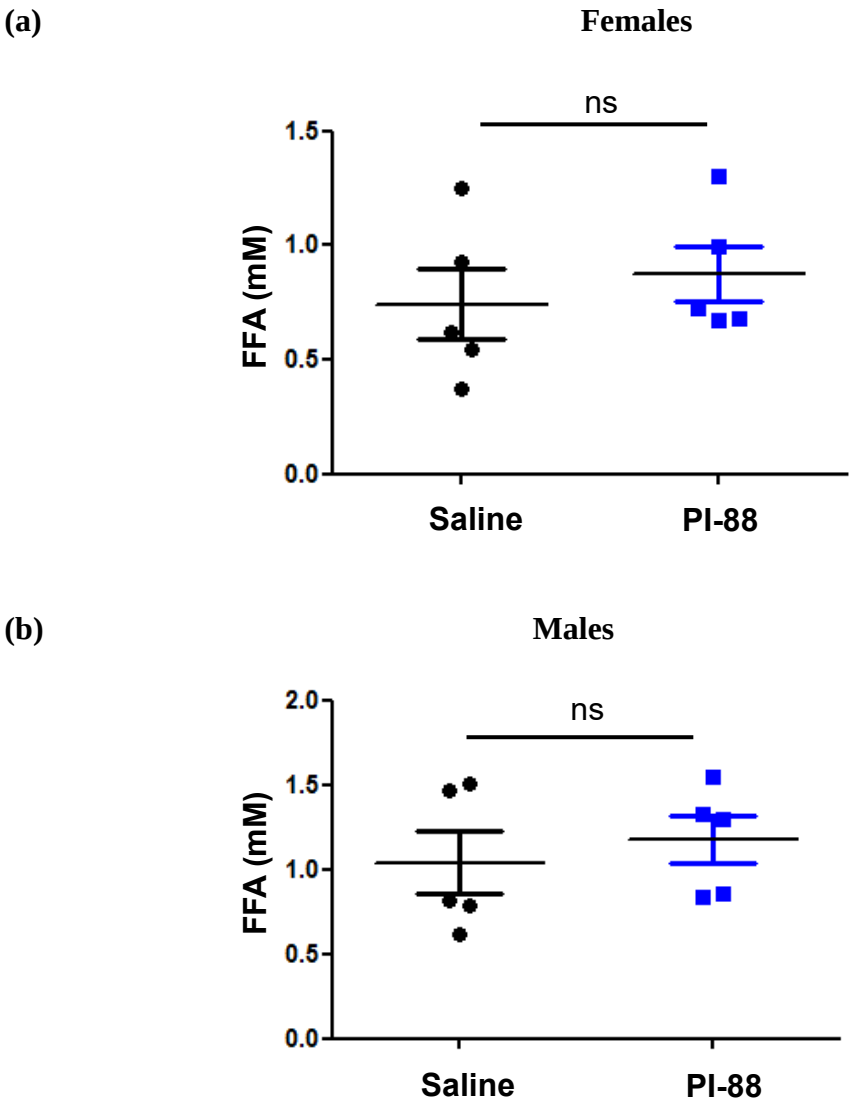

Figure 5.21: Circulating free fatty acids (FFAs) in the plasma of PI-88 and saline-treated db/db mice.

Blood samples (10 µl) were taken from (a) female and (b) male db/db mice treated for 35 days with 10 mg/kg/day PI-88 (blue symbols) i.p. or saline i.p. (black symbols). Although a trend for increased FFAs was observed on day 35 in PI-88 treated mice, no statistically significant difference was found (a, b). The data represent mean ± SEM for n= 5 mice/group. Unpaired t test; ns, not significant.

In summary, treatment of db/db mice with the HS replacer, PI-88, failed to significantly improve glycaemic control in db/db mice, based on non-fasting blood glucose levels, HbA1c levels and glucose tolerance. Surprisingly, intra-islet HS was not enhanced due to HS replacement *in vivo*. Furthermore, the insulin+ve islet area was significantly reduced, a finding that could potentially be related to the increased circulating esterified free fatty acids (Boden, 2005, Nolan et al., 2006, Cen et al., 2016). Further investigations would be required to clarify the contribution of free fatty acids to the sustained hyperglycaemia in PI-88 treated db/db mice.

5.2.3.3 HS replacement using PI-88 in db/db beta cells *in vitro*

In contrast to the report by Ziolkowski et al. (2012) that PI-88 treatment prevents the development of Type 1 diabetes (T1D) and preserves islet HS in NOD/Lt mice, our *in vivo* data showed no improvement in islet HS nor in the progression of T2D in db/db mice. To address this apparent discrepancy, we directly compared the capacity for heparin (see Section 5.2.2) and PI-88 to protect db/db beta cells from dying in culture. Male wildtype and db/db beta cells were cultured with and without heparin (50 µg/ml) or PI-88 (50 µg/ml), as heparan sulfate (HS) replacers (Ziolkowski et al., 2012), for 2 days and cell viability was analysed by flow cytometry (see Sections 2.9).

As previously demonstrated (see Section 5.2.2.2), the survival (Cal^+PI^- staining) of wt beta cells was significantly increased 2.4-fold ($P<0.001$) after culture with heparin (**Figure 5.22(a)**). Similarly, PI-88 treated wt beta cells showed a significant 2.9-fold increase in Cal^+PI^- live cells, while Cal^-PI^+ dead and Cal^+PI^+ damaged beta cells were reduced to 23.2% and 10.3% of controls respectively, resembling heparin-treated wt beta cells (**Figure 5.22(a)**). Consistent with our previous experiments (see Section 5.2.2.2), culture of db/db beta cells with heparin significantly increased their viability by 1.8-fold (Cal^+PI^- population; $P<0.001$) and Cal^+PI^+ damaged cells were significantly decreased to 45.3% of controls ($P<0.001$; **Figure 5.22(b)**). Surprisingly, while PI-88 was highly effective in protecting wt beta cells, db/db beta cells were not rescued from dying; no significant differences were observed between PI-88 treated and control live, damaged or dead beta cells (**Figure 5.22(b)**).

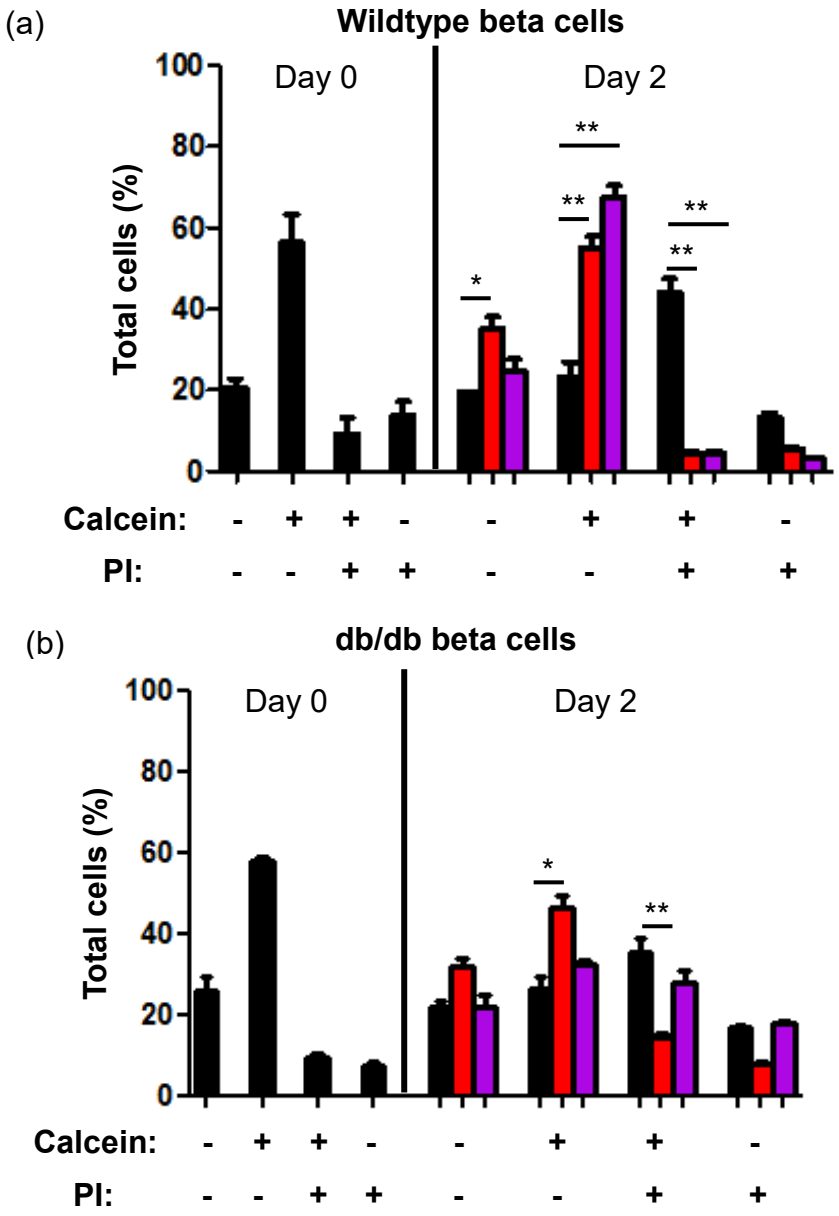

Figure 5.22: Rescue of beta cells *in vitro* using PI-88 as a HS replacer.

The viability of beta cells from (a) wildtype males and (b) db/db male mice (bg<15 mmol/L) was analysed by flow cytometry on day 0 and day 2 using the fluorescent dyes calcein and PI. The beta cells were cultured without HS replacer (black bars) or with heparin (red bars) or PI-88 (purple bars) at 50 µg/ml for 2 days and cell viability was analysed by flow cytometry. Heparin-treatment significantly increased the survival ($Cal^{+}PI^{-}$) of (a) wildtype and (b) db/db beta cells, compared to untreated controls (day 2). In contrast culture with PI-88 significantly improved the survival of wt beta cells (a) but not db/db beta cells (b). Data shows mean ± SEM; n= 3 experiments/group with n= 2-3 mice/experiment. General ANOVA with Fisher's unprotected LSD post-test; *P<0.001 and **P<0.0001.

The rescue of wt beta cells by co-culture with PI-88 (**Figure 5.22(a)**) was also accompanied by a striking resistance to cell death induced by treatment with exogenous hydrogen peroxide (**Figure 5.23**), as also demonstrated for co-culture with heparin (see Section 5.2.2.3; **Figures 5.16 and 5.17**). When tested in parallel with heparin, PI-88 treatment of wt beta cells in the absence and presence of H_2O_2 showed a significant reduction in Sytox green+ve beta cell damage/death down to 22.5% ($P<0.001$) and 24.3% ($P<0.001$) of corresponding controls, respectively (**Figure 5.23**). In the context of wt beta cells, HS replacement by PI-88, like heparin, protected against both culture-induced and ROS-induced damage/death of beta cells.

In summary, HS replacement with heparin and PI-88 preserves the viability of wt beta cells in culture and protects the beta cells from oxidative damage. Significantly, db/db beta cells treated with heparin showed improved viability and reduced beta cell death when exposed to acute hydrogen peroxide treatment. In contrast, the viability of db/db beta cells in culture was not improved by treatment with PI-88. These findings correlate with our *in vivo* studies where PI-88 treatment failed to improve the dysregulated glycaemia of db/db mice.

To further examine whether PI-88 enters db/db beta cells, beta cells were isolated from wildtype and db/db (normoglycaemic) mice. The beta cells were cultured with FITC-labelled heparin (50 µg/ml) or FITC-labelled PI-88 (50 µg/ml) for 2 days. FITC-uptake by the beta cells was examined by confocal microscopy. In parallel, flow cytometry was used to monitor FITC-heparin+ve staining and uptake of 7AAD (indicating cell damage) (see Section 2.9.4). Confocal microscopy of wt beta cells showed localisation of FITC-heparin and FITC-PI-88 staining predominantly in the cytoplasm (**Figure 5.24(a, g)**), confirming uptake by the beta cells. Flow cytometry analysis demonstrated that ~89% of beta cells were FITC-heparin+ve or FITC-PI-88+ve (**Figure 5.24(b, h)**), confirming previous studies of FITC-heparin mouse and human beta cells (Ziolkowski et al., 2012, Simeonovic et al., 2018). Similarly, we observed the intracellular uptake of both FITC-labelled heparin and FITC-labelled PI-88 in db/db beta cells and localisation in the cytoplasm (**Figure 5.24(d, j)**). In contrast to wt beta cells, FITC-heparin+ve beta cells and FITC-PI-88+ve beta cells showed that only ~43-46% of beta cells were FITC+ve, suggesting reduced uptake of heparin and PI-88 by the db/db beta cells (**Figure 5.24(e,**

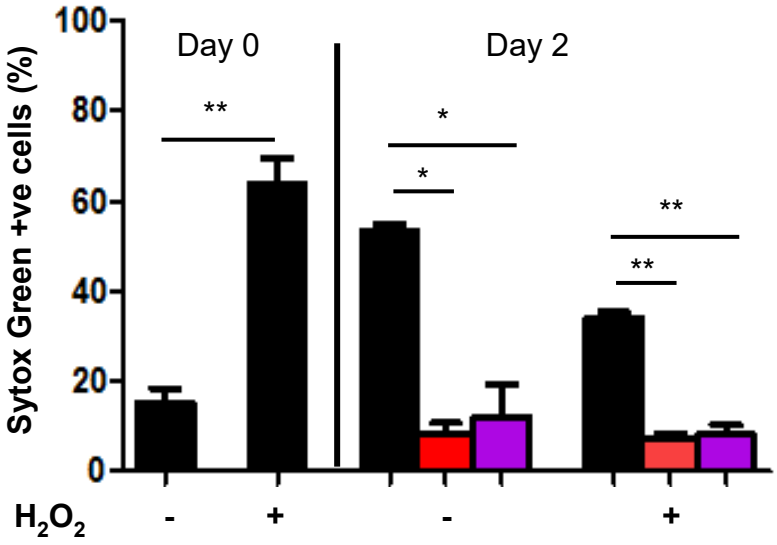

Figure 5.23: HS replacement by PI-88 protects wt beta cells from ROS-induced cell death *in vitro*.

Beta cells isolated from male wt donor mice were treated without (controls) or with 30% hydrogen peroxide (H_2O_2) on day 0 and after culture for 2 days with (red bars)/without (black bars) heparin or PI-88 (purple bars) at 50 µg/ml. Cell viability and ROS-induced cell death was examined on day 0 and day 2 by Sytox green uptake and flow cytometry. Both heparin and PI-88 treatment of wt beta cells showed protection from cell death/damage induced by H_2O_2 treatment. Data shows mean ± SEM; n= 3 experiments/group; n= 2-3 mice/experiment. General ANOVA with Fisher's unprotected LSD post-test; *P<0.001 and **P<0.0001.

Figure 5.24: Uptake of FITC-heparin and FITC-PI-88 by wildtype and db/db beta cells.

Wildtype and db/db beta cells were cultured for 2 days with FITC-heparin (a-f) or FITC-PI-88 (g-l). FITC-uptake was analysed by confocal microscopy (a, d, g, j) and flow cytometry analysis (b, e, h, k). Beta cell viability was assessed using 7AAD staining and flow cytometry (c, f, i, l). Wildtype and db/db beta cells showed substantial uptake of FITC-labelled heparin and FITC-labelled PI-88 by confocal microscopy (a, d, g, j). However, FITC-PI-88 was less effective in protecting db/db beta cells than FITC-heparin (f). n= 1 experiment and n= 2 mice/group.

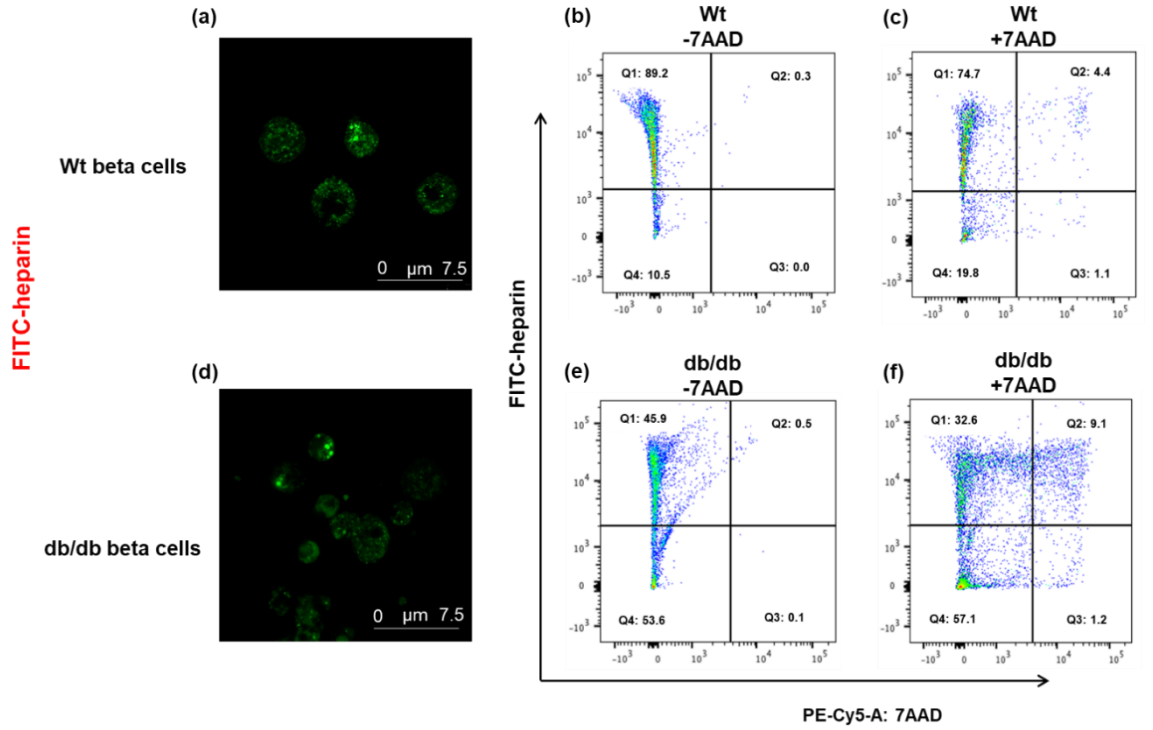
(a)
Wt beta cells
0 µm 7.5
(b)
Wt
-7AAD
Q1: 89.2
Q2: 0.3
Q4: 10.5
Q3: 0.0
(c)
Wt
+7AAD
Q1: 74.7
Q2: 4.4
Q4: 19.8
Q3: 1.1
FITC-heparin
(d)
db/db beta cells
0 µm 7.5
(e)
db/db
-7AAD
Q1: 45.9
Q2: 0.5
Q4: 53.6
Q3: 0.1
(f)
db/db
+7AAD
Q1: 32.6
Q2: 9.1
Q4: 57.1
Q3: 1.2
FITC-heparin
PE-Cy5-A: 7AAD

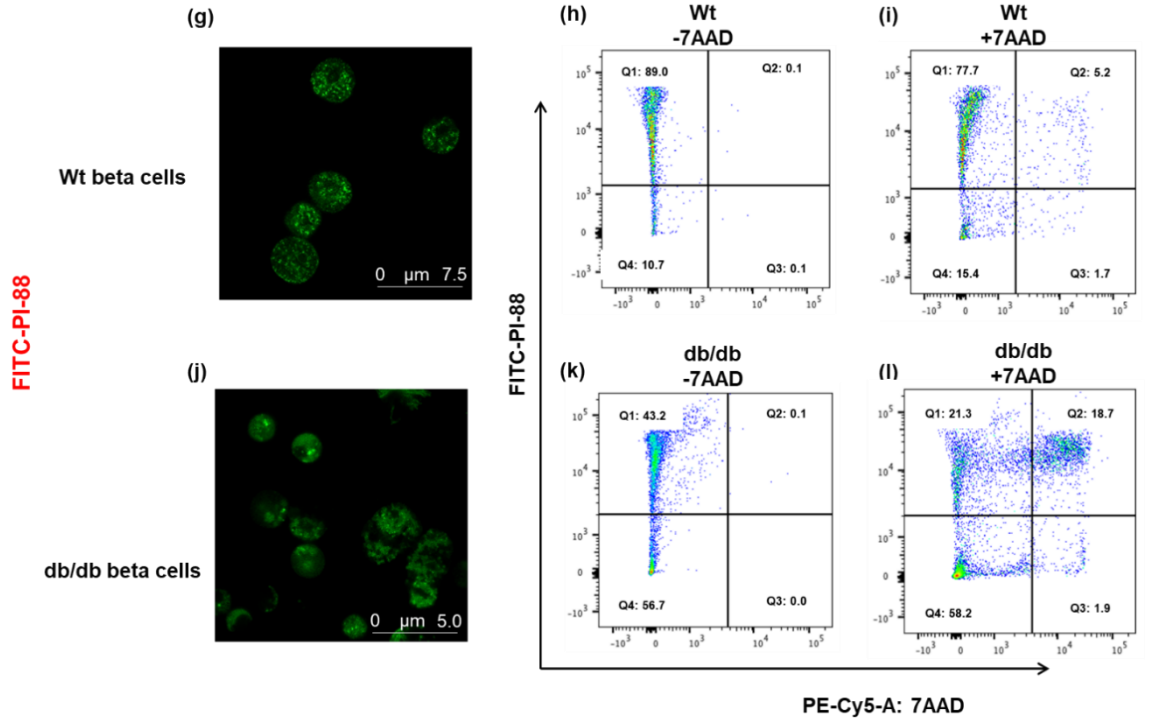
(g)
Wt beta cells
0 µm 7.5
(h)
Wt
-7AAD
Q1: 89.0
Q2: 0.1
Q4: 10.7
Q3: 0.1
(i)
Wt
+7AAD
Q1: 77.7
Q2: 5.2
Q4: 15.4
Q3: 1.7
FITC-PI-88
(j)
db/db beta cells
0 µm 5.0
(k)
db/db
-7AAD
Q1: 43.2
Q2: 0.1
Q4: 56.7
Q3: 0.0
(l)
db/db
+7AAD
Q1: 21.3
Q2: 18.7
Q4: 58.2
Q3: 1.9
FITC-PI-88
PE-Cy5-A: 7AAD

k)). Significantly, wt beta cells showed that ~80-90% were FITC-heparin+ve (Q1 + Q2 in **Figure 5.24(c)**) or FITC-PI-88+ve (Q1 + Q2 in **Figure 5.24(i)** and ~75-78% were 7AAD-ve i.e., viable (Q1, **Figure 5.24(c, i)**). While db/db beta cells showed that ~40-46% were FITC-heparin+ve (Q1+Q2 in **Figure 5.24(f)**) or FITC-PI-88+ve (Q1 + Q2 in **Figure 5.24(l)**), FITC-heparin treated beta cells demonstrated ~9% beta cell damage (Q2, **Figure 5.24(f)**), indicating that damage was ~2-fold higher in FITC PI-88-treated db/db beta cells (Q2, ~19% FITC+ve 7AAD+ve; **Figure 5.24(l)**). These data suggest that whereas HS replacement using heparin improves the survival of both wt and db/db beta cells, PI-88 is substantially less effective than heparin in providing protection for db/db beta cells. This striking difference in the capacity of HS replacers to protect db/db beta cells warrants further investigation.

5.3 Discussion

This chapter revealed that treatment of db/db mice with the chemical chaperone TUDCA improved blood glucose levels and HbA1c levels and these metabolic outcomes correlated with improved intracellular levels of HSPG core proteins and HS in islet beta cells. Secondly, primary beta cells of both wildtype and db/db mice showed strong intracellular expression of HSPG core proteins and HS; however, HS but not HSPG core proteins was lost during islet isolation. Thirdly, replacing this lost HS using heparin *in vitro* improved beta cell survival and protected the beta cells from hydrogen peroxide-induced oxidative damage. Finally, treatment of db/db mice with the dual activity HS replacer/Hpse inhibitor PI-88 did not improve the progression of T2D in db/db mice, a finding that correlated with impaired protection by PI-88 as a HS replacer in db/db beta cells *in vitro*.

(i) TUDCA treatment of db/db mice

Based on these outcomes, this Chapter (Chapter 5) evaluated whether treatment with the chemical chaperone TUDCA, previously reported to ameliorate glycaemic control in obese ob/ob mice (Özcan et al., 2006), also enhanced intra-islet HSPG/HS levels. We demonstrated improved glycaemic control in db/db mice with significantly reduced non-fasting blood glucose levels and HbA1c levels following *in vivo* treatment with the chemical chaperone TUDCA (**Figures 5.1 and 5.2**). These data are consistent with a previous study where 7-8 week old ob/ob mice treated with TUDCA (500 mg/kg/day; intraperitoneally) exhibited reduced blood glucose levels after one 1 week of treatment and the maintenance of normoglycaemia (Özcan et al., 2006). Additionally, our finding that male db/db mice treated with TUDCA showed a slight but statistically significant reduction in body weight compared to controls (**Figure 5.1(b)**) could be due to TUDCA's ability to improve insulin sensitivity, glucose tolerance and insulin clearance, as previously reported for ob/ob, db/db and HFD-mice (Ozcan et al., 2004, Özcan et al., 2006, Ozcan et al., 2009, Amin et al., 2012, Guo et al., 2015, Vettorazzi et al., 2017). Other studies have demonstrated that the body weight of TUDCA-treated ob/ob mice remain unchanged, despite reduced ER stress in host islet beta cells (Yang et al., 2010). We found that TUDCA treatment resulted in a loss of body weight in db/db males but not females, despite demonstrating ER stress relief in both male and female beta cells. This finding suggests that the impact of TUDCA on body weight could be due to sex-related effects on insulin-sensitive tissues.

ER stress in beta cells is an important mechanism that contributes to the progressive decline in beta cell function and beta cell mass in T2D (Laybutt et al., 2007, Cnop et al., 2012, Eizirik et al., 2008) as well as insulin resistance and obesity (Uppala et al., 2017, Chan et al., 2013, Engin and Hotamisligil, 2010, Özcan et al., 2006). The ER plays a critical role not only in protein maturation but also in the maintenance of intracellular calcium ion homeostasis; the storage, release and uptake of calcium ions in the cytoplasm are regulated in part by certain ER proteins (BiP, calcireticulin) (see Section 1.9). A range of factors e.g., lack of protein folding chaperones, depletion of calcium from the ER, inhibition of protein glycosylation and protein mutations, can induce an imbalance in ER/cytoplasmic calcium ion levels, thereby promoting ER stress and potentially apoptosis (see Section 1.9). TUDCA is a hydrophilic bile acid derivative, like PBA, which stabilises protein conformation by enhancing protein folding. In liver cells, downstream effects of TUDCA include blockade of calcium ion-mediated apoptosis (via reduction of calpain and decrease in calcium release from the ER) and inhibition of caspase-12 activation, with both pathways resulting in cell survival and protection (Xie et al., 2002).

In Chapter 3, our studies revealed an increase in the expression of ER-stress associated UPR genes in db/db islets compared to wt controls corroborating previous studies (Laybutt et al., 2007, Chan et al., 2013); furthermore this gene expression profile correlated with a rapid decline in islet HSPGs and HS, as demonstrated by immunohistochemistry. We therefore evaluated the expression of HSPG core proteins and HS in the islets of TUDCA-treated male db/db mice. TUDCA treatment of db/db mice demonstrated a significant increase in islet Col18 core proteins and a substantial increase in islet Sdc1 core protein compared to controls; however CD44 core protein expression remained unchanged (**Figure 5.6**). Although, a marked increase in intra-islet HS expression was also observed with TUDCA treatment, this increase did not achieve statistical significance (**Figure 5.7**). Moreover, our data showed significantly increased insulin levels in the islets of TUDCA-treated db/db mice compared to saline controls (**Figure 5.4**), resembling previous studies of TUDCA-mediated improvement in the insulin content of T1D and T2D rodent islets (Özcan et al., 2006, Engin et al., 2013, Ozcan et al., 2009). We observed that increased expression of HSPG core proteins/HS and insulin in db/db beta cells correlated with upregulated expression of UPR genes in db/db islets from TUDCA-treated mice, compared to saline controls (**Figure 5.3**). We

proposed that the enhanced UPR prolonged the ability of db/db beta cells to compensate for ER stress. As a result, beta cell HSPGs/HS and hence viability were better preserved and glycaemic control in the db/db mice was ameliorated.

Surprisingly, an increase in deleterious ER stress-associated markers (CHOP and ATF3) was also observed in the islets of db/db mice treated with TUDCA, compared to controls. c-Jun N-terminal kinase (JNK) has been reported to play an apoptotic role in beta cells and to cause beta cell dysfunction (Bonny et al., 2001, Nikulina et al., 2003). Recent studies have suggested that JNK plays a crucial role in transitioning from adaptive to apoptotic UPR during ER stress (Chan et al., 2015). During prolonged ER stress, the UPR sensor IRE1 interacts with TRAF2 to phosphorylate JNK, resulting in JNK activation (see **Figure 1.13**). Activated JNK phosphorylates its downstream target c-Jun (Brozzi et al., 2014, Brozzi et al., 2015) which activates pro-apoptotic pathways including, death protein 5 (DP5), activator protein 1 (AP-1) and CHOP. These pathways result in beta cell death (Cunha et al., 2012, Gurzov et al., 2009, Pirot et al., 2007).

TUDCA has been shown to reduce JNK- and c-Jun- induced beta cell death in the human beta cell line (EndoC-βH1) (Brozzi et al., 2015). However, IRE1-independent (i.e., ER stress-independent) JNK activation by cytokines can contribute to beta cell apoptosis (Bonny et al., 2001, Brozzi et al., 2014, Chan et al., 2011, Marroqui et al., 2014). Similarly, JNK can be activated via additional pathways, including free fatty acids (lipotoxicity) and oxidative stress (Ozcan et al., 2004, Solinas et al., 2006, Özcan et al., 2006). Thus, it is possible that the increased CHOP levels that we observed with TUDCA treatment of db/db mice are due to ER stress-independent JNK activation. To address this notion, future studies could examine phosphorylated JNK and c-Jun expression in parallel with HSPG core proteins by western blotting of islets from db/db mice treated with and without TUDCA. We also found that TUDCA treatment of db/db mice induced a 3.5-fold increase in adaptive UPR markers compared to a ~ 2.5-fold increase in terminal UPR gene expression. Increased CHOP expression has been observed in other models (zucker fatty rats, HFD mice) of beta cell adaptation, indicating that CHOP expression alone is a poor marker of maladaptive UPR (Chan et al., 2013, Herbert and Laybutt, 2016). The relative change in the expression of adaptive versus pro-apoptotic UPR genes may therefore be

more informative. In our study the preferential increase in the adaptive UPR was protective and outweighed the deleterious effects of pro-apoptotic gene expression, resulting in improved blood glucose levels in TUDCA-treated db/db mice.

Chan et al. (2013) reported that an increase in the intra-islet expression of UPR adaptive genes in ob/ob mice at 16 weeks of age, compared to 6 weeks of age was pivotal for maintaining beta cell compensation. In contrast, db/db islets at 16 weeks demonstrated reduced expression of adaptive genes, compared to islets at 6 weeks, and beta cell failure. These studies indicated that an increased adaptive UPR gene signature correlates with improved beta cell survival. Our studies extend this interpretation by showing that TUDCA-mediated enhancement of the adaptive UPR in db/db mice significantly improved beta cell HSPG content and increased intracellular beta cell HS, a property which has previously been found to maintain beta cell survival. We propose that UPR-protected synthesis of HSPG core proteins in the ER, is permissive for the assembly/synthesis of HS which in turn is essential for beta cell survival (Ziolkowski et al., 2012, Simeonovic et al., 2018), and hence function. Future studies of HS/HSPG core proteins in ob/ob islets could provide further support for this UPR-HSPG/HS pathway for beta cell viability/compensation.

In support of *in vivo* studies, isolated db/db islets (from 12-14 week donors) which had been cultured with the chemical chaperone PBA (2.5 mmol/L) for 24 hrs showed elevated expression of UPR adaptive genes (BiP, Grp94, Edem1, Fkbp11) and partial restoration of beta cell gene expression and insulin secretion (Chan et al., 2013). PBA treatment of INS-1 cells and male wistar rat islets with palmitate-induced ER stress and cytokine-induced ER stressed respectively showed diminished expression of ER stress genes (PERK, ATF4 and CHOP) (Åkerfeldt et al., 2008). Similarly thapsigargin-induced ER stress in porcine islets was alleviated by culture with TUDCA (Lee et al., 2010b). Further insight into the pathways involved have been revealed using *in vitro* studies of HepG2 cells. The activation of UPR markers in TUDCA-treated HepG2 cells correlated with a reduction in aggregated misfolded proteins (Uppala et al., 2017). These findings suggest that provision of a chemical chaperone to ER-stressed cells relieves the misfolded protein burden and prolongs the UPR to preserve ER function. Dysregulated UPR gene

expression (ATF6 and XBP1s) in beta cells has been identified in mouse models of T1D (NOD, RIP-LCMV-GP mice) mice and in T1D humans (Engin et al., 2013, Todd et al., 2008, Tersey et al., 2012, Eizirik et al., 2013, Eizirik et al., 2009, Eizirik et al., 2008, Marhfour et al., 2012, Hartman et al., 2004, Brozzi and Eizirik, 2016). Furthermore, TUDCA treatment of pre-diabetic NOD and RIP-LCMV-GP mice improved UPR markers expression in beta cell viability, reduced intra-islet leukocyte invasion and beta cell death, and thus decreased the incidence of T1D (Engin et al., 2013). These reports highlight that the impact of ER stress on beta cell dysfunction is relevant for both T2D and T1D.

TUDCA has been previously reported to ameliorate insulin resistance and insulin clearance by reducing ER stress (Vettorazzi et al., 2017, Özcan et al., 2006, Vettorazzi et al., 2016). Treatment of ob/ob mice with PBA or TUDCA revealed a decline in the expression of ER stress-associated genes, decreased levels of PERK and IRE1 phosphorylation in liver and adipose tissue, reduced insulin resistance and improved insulin sensitivity (Özcan et al., 2006). Likewise, TUDCA treatment of C57BL/6 mice fed a high fat diet (HFD) resulted in increased insulin clearance, even when treatment was restricted to 15 days (Vettorazzi et al., 2017). In addition, PBA or TUDCA treatment of mouse islets showed a reduction in ER stress (via decreasing levels of eIF2α, IRE1 and ATF6) and regulation of beta cell proliferation (Sharma et al., 2015). Nevertheless, chemical chaperones may also mediate beneficial metabolic effects independently of direct effects on ER stress. *In vitro* treatment of adipocytes and astrocytes with PBA or TUDCA, led to activation of peroxisome-proliferator activated receptor (PPAR) gamma (Nguyen et al., 2012) and alpha (Liu et al., 2002), respectively. In addition, Kars et al. (2010) reported that the administration of TUDCA *in vivo* improved insulin sensitivity in skeletal muscle and liver of obese and insulin-resistant patients by reducing JNK activation and serine phosphorylation of insulin receptor substrate 1 (IRS-1) without reducing ER stress in muscle or adipose tissue. These findings suggest that unlike beta cells, the anti-diabetogenic effect of TUDCA in some tissues can occur independently of ER stress inhibition (Salvado et al., 2015, Park and Ozcan, 2013).

Collectively, our studies demonstrated an increased expression of UPR genes in the islets of TUDCA-treated db/db mice, which correlated with improved glycaemia and the

striking recovery of intra-islet HSPGs, HS and insulin. These observations provide strong evidence that ER stress in db/db mice contributes to the loss of HSPG core proteins and impairs HS synthesis in beta cells. On this basis, HS replacement could represent an alternative approach to improving beta cell viability and function in T2D.

(ii) HS loss and HS replacement in db/db beta cells *in vitro*

Our flow cytometry data showed intracellular expression of HSPG core proteins (especially collagen type XVIII) and HS in primary beta cells isolated from both wildtype (wt) and db/db islets but weak staining on the cell surface (**Figures 5.8, 5.9, 5.10 and 5.11**). These data confirm the intracellular localisation of HSPG core proteins and HS in beta cells of wt and db/db islets, as identified *in situ* by our immunohistochemical studies (see Sections 3.2.4 and 3.2.10), as well as in MIN6 cells *in vitro* (see Section 4.2.2). The isolation of islets from pancreas tissue destroys the islet vasculature and innervation and alters the islet architecture and composition (Stendahl et al., 2009, Irving-Rodgers et al., 2014, Choong et al., 2015, Wang and Rosenberg, 1999). In particular, isolated islets lack their peri-islet basement membrane (Irving-Rodgers et al., 2008) and show significant loss of intra-islet (beta cell) HS (Ziolkowski et al., 2012, Choong et al., 2015, Simeonovic et al., 2018). Irving-Rodgers et al. (2008) demonstrated that the mouse peri-islet basement membrane contains not only collagen type IV, laminin and nidogen but also the heparan sulfate proteoglycan core protein, perlecan. Furthermore, these authors reported that following islet isolation, the peri-islet basement membrane is completely lost, including the HSPG core protein perlecan (Irving-Rodgers et al., 2014). In contrast to perlecan, Choong et al. (2015) reported that HSPG core proteins inside islet beta cells are preserved during islet isolation but there was selective depletion of HS. Our finding that Col18 and Sdc1 core proteins were expressed at substantially lower levels in isolated db/db islets, compared to isolated wt islets (**Figures 5.8, 5.9, 5.10 and 5.11**) is therefore attributed to ER stress-induced loss of these HSPGs in native db/db islets *in situ* (**Figures 3.6, 3.8, 3.10 and 3.21**; see Sections 3.2.4 and 3.2.10). Thus, the dramatic loss of HS from db/db beta cells *in vitro* is related to a combination of ER stress-induced reduction in intracellular HSPG core proteins (and hence HS), in the native donor db/db islets *in situ*, oxidative damage during the enzymatic digestion of pancreas tissue for islet harvest *in vitro*, and ER stress-related oxidative stress in db/db beta cells during culture. Consistent with this interpretation, Ziolkowski et al. (2012) demonstrated that *in vitro*, HS-depleted

BALB/c beta cells were highly susceptible to death-induced by exogenously delivered reactive oxygen species (ROS). Of utmost significance, the beta cells were protected from oxidative damage by HS replacement using HS mimetics/analogues.

Our flow cytometry studies provided evidence against a role for heparanase (Hpse) in the attrition of HS from db/db beta cells *in situ*. Like MIN6 cells (see Section 4.2.2.1), wt beta cells showed strong intracellular expression but weak cell surface expression of Hpse (**Figures 5.8(c), 5.9(c), 5.10(c) and 5.11(c)**). This finding is in agreement with the intracellular expression of Hpse in freshly isolated mouse islets (Ziolkowski et al., 2012). Beta cell Hpse is likely to function normally in the turnover of intracellular HS (Bernfield et al., 1999). Indeed HS and Hpse co-localise in endosomes and lysosomes of other cell types during HS degradation, supporting a role for Hpse in HS homeostasis (Fux et al., 2009, Gingis-Velitski et al., 2004, Yanagishita and Hascall, 1992). In contrast to wt beta cells in our study, db/db beta cells demonstrated a significant reduction in intracellular Hpse (**Figures 5.8(c), 5.9(c), 5.10(c) and 5.11(c)**). We propose that the downregulation in Hpse expression is ER stress-induced and represents a consequence of the UPR-mediated decline in "general" protein translation to reduce the accumulation of misfolded proteins in the ER (see Sections 1.9, 3.2.3 and 3.2.9). Our findings therefore strongly indicate that the loss of HS in the beta cells of db/db mice is unlikely to be due to Hpse-mediated degradation of intracellular HS.

We reasoned that the loss of intracellular HS in db/db beta cells *in situ* (see Section 3.2.5) compared to wildtype beta cells, would impair beta cell survival (Ziolkowski et al., 2012) and contribute to beta cell failure during the progression of T2D. We therefore tested whether replacing the lost HS could protect db/db beta cells from dying in culture. Co-culture with the HS replacer heparin (a highly sulfated HS analogue) significantly improved the survival of wildtype and db/db beta cells, including beta cells from hyperglycaemic db/db males (**Figures 5.13 and 5.14**). However, heparin treatment was less effective in rescuing hyperglycaemic db/db beta cells (**Figures 5.13 and 5.14**), particularly from female donors (**Figure 5.14**). This less pronounced effect could be due to an increase in the expression of antioxidant-encoding genes, as previously shown in db/db islets for protection against oxidative stress (Hasnain et al., 2014). Such a response would be consistent with extensive depletion of beta cell HS, a constitutive non-

enzymatic quencher of ROS (Ziolkowski et al., 2012). Alternatively, failure of the UPR to compensate for prolonged ER stress in hyperglycaemic db/db beta cells could reduce the synthesis and availability of heparin-binding protein(s) required for heparin uptake or intracellular transport (Simon Davis and Parish, 2013). Nevertheless, overall, these data provide convincing evidence that HS replacement using heparin preserves the viability of both wt and db/db beta cells *in vitro*. Furthermore, dual staining of heparin-treated beta cells with calcein and PI offered the advantage of identifying a shift in phenotype from damaged (Cal^+PI^+) cells to viable (Cal^+PI^-) cells, which would have been masked if only one stain had been used.

In agreement with the report by Ziolkowski et al. (2012), our flow cytometry analyses of heparin-treated wt and db/db beta cells demonstrated a general resistance to both culture-induced and ROS-induced beta cell death (**Figures 5.16 and 5.17**). In contrast to the H_2O_2-induced rapid rise in Sytox green +ve beta cell damage/death on day 0, control wt and db/db beta cells cultured for 2 days in the absence of heparin showed a minimal or less pronounced increase in damage/death in response to acute response to hydrogen peroxide. In the future, RT-PCR studies could investigate whether the loss of beta cell HS during islet/beta cell isolation and/or due to ER stress in donor islets *in situ*, results in induced or enhanced expression of antioxidant enzymes; conversely, such studies could also test whether HS replacement mitigates the induction of the antioxidant gene expression profile. Nevertheless, the death of wt beta cells *in vitro* is attributed to the excessive production of free radicals (particularly during islet/beta cell isolation) (Ziolkowski et al., 2012, Choong et al., 2015) which depolymerises intracellular HS (Raats et al., 1997, Ziolkowski et al., 2012). In the case of db/db beta cells, a pre-existing state of HS depletion due to ER stress in the donor islets *in situ* could exacerbate oxidative stress during beta cell isolation and culture. Extrapolating from these *in vitro* studies, the loss of beta cell HS in the islets of young db/db mice (see Section 3.2.13) would lead to increased oxidative stress, beta cell dysfunction and T2D development. Indeed our data are consistent with the notion that intracellular HS in normal beta cells represents a non-enzymatic mechanism for quenching or detoxifying endogenous ROS (Ziolkowski et al., 2012) normally generated via the formation of disulfide bonds during insulin biosynthesis in the ER and during oxidative phosphorylation (see Section 1.11). Thus, normal levels

of beta cell HS would compensate for the unusually low level of antioxidant enzymes (Tiedge et al., 1997).

Our studies therefore highlight intracellular HS as a previously unrecognised *critical link* between ER stress and oxidative stress in T2D beta cells i.e., ER stress dramatically reduces the synthesis of HSPG core proteins and hence HS synthesis, which in turn heightens the susceptibility of the beta cells to oxidative stress. Thus, in this context of pre-existing ER stress, oxidative stress and HS loss in beta cells in db/db mice, our data clearly reveal HS replacement as a potential intervention therapy for rescuing beta cell survival, prolonging beta cell compensation and alleviating oxidative stress.

Beta cells are highly metabolically active and therefore must rely on robust antioxidant mechanisms to neutralise the ROS produced during normal metabolism (Eizirik et al., 1994, Welsh et al., 1995). Since beta cells normally express low levels of anti-oxidant enzymes, compared to other tissues (Lenzen et al., 1996, Tiedge et al., 1997), one protective mechanism involves the induced expression of ROS scavenging enzymes, e.g., SOD2, Gpx5 (Simeonovic et al., 2018, Hasnain et al., 2014). However, the need for de novo or upregulated expression fails to provide beta cells with *immediate* protection from oxidative stress. We propose that intracellular HS acts as a *constitutive* non-enzymatic quenching agent for ROS by forming complexes with Mn^{2+} in the beta cells. Mn^{2+} is found at very high levels in pancreatic islets (Rorsman et al., 1982, Kodama et al., 1991) and *in vitro*, the formation of HS (heparin)-Mn^{2+}complexes is dependent on the sulfation of heparin disaccharides. Preliminary studies in the Simeonovic lab have demonstrated that co-culture of mouse beta cells with $MnSO_4$ and heparin substantially reduced the concentration of heparin (a HS replacer) required to improve the survival of beta cells in vitro and to protect them against acute hydrogen peroxide treatment; in contrast, culture with $MnSO_4$ alone did not provide protection. These studies suggest that HS-Mn^{2+} complexes may represent a highly novel and constitutive ROS quenching agent in beta cells.

(iii) PI-88 treatment of db/db mice

Heparin exhibits anti-coagulant activity which restricts its usage *in vivo* and therefore, chemically modified heparins and sulfated oligosaccharides have been developed as

alternative HS mimetics (Parish, 2006). The sulfated phosphomannopentaose PI-88 (Muparfostat) is a non-cleavable potent inhibitor of Hpse which exhibits a low level of anti-coagulant activity and acts as a HS replacer in beta cells *in vitro* (Ziolkowski et al., 2012, Parish et al., 2013, Parish et al., 1999, Simeonovic et al., 2013). Previously, Ziolkowski et al. (2012) demonstrated that a long term treatment (180 days) of adult female NOD mice with PI-88 (10 mg/kg/day, i.p.) significantly increased the percentage of intact islets, decreased the proportion of islets with destructive insulitis, preserved intra-islet HS and reduced the incidence of T1D by ~50%. Therefore, we sought to determine whether PI-88 could function as a HS replacer in db/db mice. Treatment of young 3.5 week db/db mice with PI-88 (10 mg/kg/day, i.p.) for 35 days, however, did not improve the non-fasting blood glucose levels (i.e., glycaemic control; **Figure 5.18(a, b)**), body weight (**Figure 5.18(c, d)**), HbA1c levels (**Figure 5.18(e, f)**), glucose tolerance (**Figure 5.19**) or the insulin+ve islet area (**Figure 5.20(b)**). In addition, no replenishment of endogenous HS in islet beta cells was observed (**Figure 5.20(a)**). The discrepancy in the effectiveness of PI-88 to prevent T1D in NOD mice but not to ameliorate T2D in db/db mice could be related to the more rapid onset of the decline in beta cell HS in db/db islets and to the shorter duration of PI-88 treatment. In addition, the therapeutic benefit in NOD mice could be due to PI-88 acting as a Hpse inhibitor, preventing leukocyte migration and the degradation of HS in the peri-islet BM and in the beta cells (Ziolkowski et al., 2012, Simeonovic et al., 2013).

To further understand the failure of PI-88 to rescue db/db mice from T2D progression, we evaluated PI-88 as a HS replacer in isolated wt and db/db beta cells *in vitro*. Treatment with heparin or PI-88 preserved the viability of wt beta cells in culture (**Figure 5.22**) and protected the beta cells from oxidative damage (**Figure 5.23**), confirming the previous report by Ziolkowski et al. (2012). Similarly, the db/db beta cells treated with heparin showed a significant improvement in viability (**Figure 5.22**), consistent with our previous HS replacement studies (see Section 5.2.2.2). In contrast to wt beta cells, however, PI-88 failed to protect db/db beta cells from dying in culture (**Figure 5.22**). Confocal microscopy of wt and db/db beta cells cultured with FITC-labelled Pi-88 or FITC-labelled heparin demonstrated uptake into the cytoplasm of the beta cells (**Figure 5.24(a, d, g, j)**). This finding dismissed the possible explanation that PI-88 failed to be taken up by the db/db beta cells. Flow cytometry analysis performed in parallel, revealed that excellent

viability was observed for wt and db/db beta cells cultured with FITC-heparin (FITC+ve 7AAD+ve damage, 5-9%; **Figure 5.24(c, f)**). However, beta cell damage was 2-fold higher in db/db beta cells cultured with FITC-PI-88 (~19%) compared to treatment with FITC heparin (~9%; **Figure 5.24(f, l)**), despite comparable uptake of FITC-heparin and FITC-PI-88 by the db/db beta cells (~43%-47% of cells were FITC+ve; **Figure 5.24(e, k)**). These findings suggest that the ability of db/db beta cells to use PI-88 as a HS replacer is defective. Nevertheless, wt beta cells incorporated ~2-fold higher levels of FITC-heparin and FITC-PI-88 than db/db beta cells (**Figure 5.24(b, e, h, k)**). Simon-Davis and Parish (2013) reported that there exist 235 HS-binding proteins in the mouse genome, with 66% of the proteins having potential to bind to HS intracellularly. It is possible, therefore, that ER stress in db/db beta cells compromises the availability of HS-binding proteins essential for cell surface binding/uptake and intracellular transport of PI-88. However, since heparin functions as a superior HS replacer to PI-88 in db/db beta cells, we propose that ER stress related effects on intracellular PI-88 have little impact on intracellular heparin, i.e., following uptake. Together these findings suggest that the failure of PI-88 treatment to ameliorate glycaemia in db/db mice is due to a defect in the uptake and intracellular distribution of PI-88 to appropriate sites of endogenous ROS production. Future confocal microscopy studies of live beta cells could investigate whether FITC-heparin and ROS identified by a fluorescent dye e.g., DCF or HYDROP co-localise better than FITC-PI-88 and ROS.

PI-88 also has the capacity to displace lipoprotein lipase from the endothelial cell surface where this enzyme is normally bound to the HSPG syndecan-1 (Wang et al., 2013b, Freeman et al., 2005). The displacement of lipoprotein lipase leads to the breakdown of lipids to free fatty acids (FFAs) (Wang and Eckel, 2009, Olivecrona, 2016). In such context of obesity and metabolic syndrome, elevated FFA levels in turn could contribute to insulin resistance, particularly in the adipose tissue and skeletal muscle, thereby exacerbating hyperglycaemia during T2D progression (see Section 1.8). Our study revealed only a slight increase (1.1-1.2-fold) in the circulating levels of FFAs in PI-88 treated db/db mice (**Figure 5.21**). This finding suggests that the failure of PI-88 to improve glycaemia in db/db mice was unlikely to be due to increased lipoprotein lipase activity.

Collectively, our data demonstrated an improved glycaemic control in db/db mice after administration of TUDCA for 28 days, correlating with improved intra-islet expression of HSPGs, HS and insulin. Our *in vitro* studies using HS analogue heparin rescued db/db beta cell viability and protected against acute oxidative damage. Since heparin is an anti-coagulant with undesired health risks *in vivo*, we tested whether another HS mimetic with minimal anti-coagulant activity PI-88, could improve glycaemia in db/db mice by preserving the viability of db/db beta cells by HS replacement. The failure of PI-88 to rescue db/db mice from T2D progression was most likely due to ER stress-induced effects on the uptake and intracellular transfer of PI-88 in db/db beta cells. RT-PCR analyses of the expression of HS-binding proteins in db/db beta cells are therefore warranted. These studies highlight the need to develop a synthetic heparin-like HS replacer that lacks anti-coagulant activity, for ameliorating beta cell compensation and glycaemia in db/db mice.

In summary:

- TUDCA treatment of db/db mice showed improved blood glucose levels and HbA1c levels correlating with improvement in beta cell HSPG core proteins and HS.
- HSPG core proteins and HS are highly expressed intracellularly in the primary beta cells of wt and db/db mice.
- HS is lost during islet isolation and HS replacement using heparin improves the survival of beta cells by protecting them from acute oxidative damage.
- *In vivo* treatment of db/db mice with a dual activity HS replacer/Hpse inhibitor PI-88 failed to improve the glycaemic control in db/db mice and could be due to ER stress-induced effects on the uptake and transfer of PI-88 in the db/db beta cells.

Chapter 6: Inflammation markers in peripheral blood and adipose tissue of db/db mice

6.1 Introduction

Type 2 diabetes (T2D) is "metabolic syndrome" disease in which chronic low-grade inflammation is associated with insulin resistance and defects in insulin secretion (Xu et al., 2003, Talukdar et al., 2012, Sell et al., 2012, Rocha et al., 2008, McArdle et al., 2013, Odegaard et al., 2007, Kintscher et al., 2008, Kahn et al., 2006, Hotamisligil et al., 1993). The first evidence of T2D-associated inflammation was reported by Hotamisligil et al. (1993). This group demonstrated increased tumour necrosis factor-alpha (TNF-α) mRNA levels in the adipose tissue (AT) of animal models of obesity and diabetes (ob/ob, db/db, zucker (fa/fa) rats, Tubby (tub/tub)) (Hotamisligil et al., 1993) as well as in the adipose tissue and liver of obese humans (Hotamisligil et al., 1995). To investigate the role of TNF-α, Zucker rats (7-9 week old) were injected with recombinant TNF-α receptor-immunoglobulin G chimeric protein (200 μg/rat) intravenously for 3 days. The neutralization of TNF-α improved glucose uptake in peripheral tissues (muscle and adipose tissues) in response to insulin, suggesting a role of TNF-α in insulin resistance. This evidence was pivotal in identifying a role for inflammation in obesity-induced insulin resistance (see Section 1.5). Subsequently, other investigations revealed that interleukin (IL)-1β, IL-22 and interferon-gamma (IFN-γ) could also modulate insulin signaling *in vitro* and *in vivo* (Sauter et al., 2008, Shaul et al., 2010, Donath and Shoelson, 2011, Hasnain et al., 2014). For example, treatment of isolated islets from male Lewis rats with proinflammatory cytokines (TNF-α, IFN-γ and IL-1β) and IL-1 receptor antagonist (IL-1RA) protected the islets from beta cell apoptosis, improved GSIS and increased the insulin content (Schwarznau et al., 2009); in addition, IL-1RA treatment of C57BL/6J mice on high fat diet (HFD) and GK rats resulted in improved glucose tolerance and insulin secretion (Sauter et al., 2008, Ehses et al., 2009). The administration of IL-22 to HFD-fed C57BL/6 mice was found to modulate oxidative stress, ER stress and inflammation and restore glucose homeostasis. Furthermore, the neutralisation of IL-23 and IL-24 partially reduced ER stress in beta cells from HFD-C57BL/6 mice and improved glucose tolerance (Hasnain et al., 2014). These studies have indicated that cytokines play a critical role in beta cell survival and function in the obese state.

Markers of obesity-associated inflammation in T2D animal models and in T2D humans, have included increased circulating levels of C-reactive protein, pro-inflammatory cytokines and chemokines (IL-6, IL-1β, TNF-α and IL-18) as well as increased

populations of immune cells (e.g., macrophages and neutrophils) in the circulation (Kolb and Mandrup-Poulsen, 2005, Donath and Shoelson, 2011, Kammoun et al., 2018, McFarlin et al., 2012), adipose tissue (Kolb and Mandrup-Poulsen, 2005, Donath and Shoelson, 2011, Ehses et al., 2009, Olefsky and Glass, 2010, McNelis and Olefsky, 2014, McFarlin et al., 2012) and islets (Ehses et al., 2007, Hasnain et al., 2014, Ehses et al., 2009, Donath and Shoelson, 2011, Maedler et al., 2004). Furthermore, treatment of T2D patients with anti-inflammatory drugs, such as salicylates and aspirin, has been found to improve insulin sensitivity, enhance glucose metabolism and improve glycaemia, as measured by HbA1c levels, hyperinsulinaemic-euglycaemic clamps, OGTT and insulin radioimmunoassays (Hundal et al., 2002, Rumore and Kim, 2010, Fleischman et al., 2008, Goldfine et al., 2008, Goldfine et al., 2013). In T2D mice, elevated levels of macrophages in the adipose (Zheng et al., 2016, Xu et al., 2003, Weisberg et al., 2003, Nagareddy et al., 2014, Shaul et al., 2010, Sartipy and Loskutoff, 2003, McFarlin et al., 2012) and T2D obese patients (Olefsky and Glass, 2010, Weisberg et al., 2003, Boutens and Stienstra, 2016, Wentworth et al., 2010) have provided strong support for adipose tissue inflammation as a potentially important driver of insulin resistance and dysregulation of glycaemia in T2D.

In insulin-resistant HFD and mutant strains of obese mice (ob/ob mice and db/db mice), the enlarged population of AT macrophages was found to correlate with an influx of bone marrow derived progenitor cells which underwent differentiation and proliferation (Xu et al., 2003, Weisberg et al., 2003, Nagareddy et al., 2014). Shaul et al. (2010) demonstrated that macrophages expressing galactose type C-type lectin ((MGL)1^+ $CD11c^+$ macrophages) were increased in the adipose tissue during HFD-induced obesity; furthermore $CD11c^+CD206^+$ macrophages were found to be associated with insulin resistance in obese humans (Wentworth et al 2010). Moreover, both the migration of monocytes from the circulation and the local proliferation of macrophages in the AT have been identified as factors that increase adipose tissue macrophages during obesity (Zheng et al., 2016). Other studies have identified a role for both innate and adaptive immune cells in T2D-associated inflammation (see Section 1.6).

Explants of adipose tissue are composed of adipocytes and the stromal vascular fraction (SVF). The SVF consists of pre-adipocytes, endothelial cells, fibroblasts and leukocytes

(see Section 1.6). The main function of adipose tissue is to store excess energy, insulate the body (i.e., provide thermoregulation) and secrete adipokines and cytokines to help regulate glucose metabolism and the local state of inflammation. These adipokines (e.g., leptin, adiponectin and resistin) and cytokines (e.g., IL-10, IL-6, IL-8 and TNF-α) exhibit either pro-inflammatory or anti-inflammatory properties (Makki et al., 2013). For example, TNF-α is a potent pro-inflammatory cytokine which is implicated in the initiation and progression of insulin resistance whereas IL-10 is an anti-inflammatory cytokine which improves insulin sensitivity and glucose transport. Leukocytes can be categorised into innate and adaptive immune cells: innate cells of the immune system include macrophages, neutrophils, eosinophils and mast cells, while the adaptive immune cells include T cells and B cells (see Section 1.6). These immune cells circulate in the blood and migrate to the tissues such as adipose tissue to establish sites of inflammation. IL-10 is produced by the macrophages, B cells and T cells which suppresses activation of macrophages and production of pro-inflammatory cytokines (Arango Duque and Descoteaux, 2014). TNF-α is secreted by the monocytic lineage cells i.e., macrophages, astroglia, microglia, Langerhans cells, Kupffer cells, and alveolar macrophages, which plays a role in development of chronic inflammatory diseases (Parameswaran and Patial, 2010).

In the lean state, adipose tissue is predominantly characterised by M2 macrophages (anti-inflammatory leukocytes), but eosinophils and lymphoid cells are also present (Martinez and Gordon, 2014, Lumeng et al., 2007a, Olefsky and Glass, 2010). M2 or "alternatively activated" macrophages are defined by their ability to antagonise prototypic inflammatory responses and gene transcription and/or protein expression of M2 markers (e.g., transmembrane glycoproteins, scavenger receptors, enzymes, growth factors, hormones, cytokines and cytokine receptors) (Martinez and Gordon, 2014, Roszer, 2015). A distinguishing property of M2 macrophages is the production of arginase which blocks inducible nitric oxide synthase activity and contributes to tissue repair (Surmi and Hasty, 2008); They can also be identified by the cell surface expression of CD163, CD206 and CD301 (Cho et al., 2014, Braune et al., 2017). M2 macrophages exhibit immunosuppressive properties and have high phagocytic capacity to maintain tissue remodelling and to resolve inflammation (Castoldi et al., 2015). Importantly M2 macrophages secrete IL-10 which limits inflammatory responses and enhance insulin

sensitivity, most likely by increasing glucose metabolism, phosphorylation of insulin receptor substrate 1 and Akt activity in muscle (Lumeng et al., 2007a, Hong et al., 2009). The secretion of IL-4, IL-13 and IL-10 by eosinophils, natural killer T cells and regulatory T cells also help to maintain an anti-inflammatory environment under normal physiological conditions. The IL-4 and IL-10 also modulate adipocyte function and maintain adipose tissue homeostasis via remodeling, in response to nutrient uptake and energy expenditure (see Section 1.6). These interactions facilitate the efficient uptake of glucose, particularly by adipocytes, thereby optimising glucose homeostasis and insulin sensitivity (Chaudhry and Rudensky, 2013, Mraz and Haluzik, 2014).

In the obese state, adipocytes in white adipose tissue (WAT) expand in response to nutrient overload (**Figure 1.8**) (Chmelar et al., 2013, Despres et al., 2008). This process is generally due to adipocyte hypertrophy caused by free fatty acid flux, increased vascularisation and elevated secretion of leptin; however, hypoxia, ER stress, oxidative stress and adipocyte cell death also accompany WAT expansion (see Section 1.6.1). Apoptotic adipocytes recruit macrophages with pro-inflammatory and pro-angiogenic properties, thereby modulating the local inflammatory reaction (Olefsky and Glass, 2010, McNelis and Olefsky, 2014). Dead or dying adipocytes release FFAs and activated macrophages involved in adipocyte phagocytosis secrete pro-inflammatory cytokines and chemokines such as TNF-α, IL-6, IL-1β and monocyte chemotactic protein 1 (McNelis and Olefsky, 2014, Xu et al., 2003, Weisberg et al., 2003). These factors exacerbate the inflammatory response by recruiting additional macrophages, mast cells, neutrophils, dendritic cells and lymphocytes (Weisberg et al., 2003, Talukdar et al., 2012). Of significance, the activation of toll like receptor 2 or 4 (TLR2/TLR4) on adipocytes by extracellular saturated free fatty acids and TNF can lead to JNK and/ IKκB-NF-κB activation causing inhibition of downstream insulin signaling and hence insulin resistance (**Figure 1.9**) and T2D (Hotamisligil et al., 1996, Dasu and Jialal, 2011, Wentworth et al., 2010, Donath and Shoelson, 2011, Mraz and Haluzik, 2014).

Heparanase (Hpse), a HS-degrading endoglycosidase, plays a vital role in cell migration, particularly in pathological conditions such as cancer, inflammatory bowel disease, experimental autoimmune encephalomyelitis, atherosclerosis and T1D (Vlodavsky and Goldshmidt, 2001, Parish et al., 2001, Simeonovic et al., 2013, Parish, 2006, Vreys and

David, 2007, McKenzie, 2007, Goldberg et al., 2013, Goldshmidt et al., 2003). Hpse is produced by macrophages, T cells, B cells, dendritic cells, neutrophils, monocytes and Langerhans cells (in the skin); Hpse is also produced at very high levels by platelets (Vreys and David, 2007). In the context of immune responses, catalytically active Hpse helps leukocytes to migrate to sites of inflammation (Parish, 2006). In response to local inflammation, circulating leukocytes extravasate between endothelial cells in the blood vessel wall. However, the sub-endothelial BM acts as a barrier to leukocyte migration, at least in part due to the HSPG perlecan (a large HSPG with a distribution restricted to BMs). Hpse secreted by endothelial cells and immune cells degrades HS in the sub-endothelial BM, relaxing the integrated network of BM matrix proteins and allowing the leukocytes to traverse and migrate into underlying tissue; this disruption of the BM architecture is further aided by proteases (e.g., cathepsins) which target and destroy BM matrix proteins. Hpse-mediated degradation of HS in the BM also liberates HS-bound chemokines and in this way assists the directed migration of leukocytes to inflammatory sites (Parish et al., 2001, Vlodavsky and Goldshmidt, 2001).

Hpse has been found to play critical roles in the pathogenesis of T1D (Simeonovic et al., 2018, Ziolkowski et al., 2012, Simeonovic et al., 2013). Initially, Hpse produced by inflammatory leukocytes and/or endothelial cells solubilize the HS chains of the HSPG perlecan in the sub-endothelial basement membrane (BM), to facilitate the passage of immune cells from the blood to underlying tissue and to sites of inflammation (Parish, 2006). Similarly, within the islet microenvironment leukocyte-derived Hpse also assists leukocyte migration across the peri-islet BM i.e., intra-islet infiltration. Significantly, within the islet mass, Hpse degrades HS within the beta cells, promoting susceptibility to oxidative damage and beta cell death (Simeonovic et al., 2013, Ziolkowski et al., 2012). Against this background, we reasoned that Hpse might play a role in the migration of leukocytes to the WAT of T2D-prone db/db mice. Furthermore, we speculated that treatment of db/db mice with PI-88, a dual activity drug that functions both as Hpse inhibitor and HS replacer, could modulate the inflammation in db/db mice, potentially improving insulin sensitivity and glycaemic control. In support of this approach, Naggareddy et al. (2014) reported that inhibition of signaling by TLR4 ligands or via the NLRP3-IL1β inflammasome, reduced obesity-induced AT inflammation and insulin resistance.

In this chapter, we investigate the relationship between the profile of innate and adaptive immune cells in the peripheral blood and white adipose tissue (WAT) of T2D-prone db/db mice. In addition, we explore the capacity for Hpse to contribute to the migration of inflammatory leukocytes to db/db WAT. Related to this and in parallel with the studies of PI-88 as a potential HS replacer in T2D (see Section 5.2.3), we assessed whether PI-88, acting as a Hpse inhibitor, can impact obesity-driven WAT inflammation in db/db mice.

6.2 Results

6.2.1 Leukocytes in the peripheral blood and WAT of female db/db mice

The populations of CD45.2$^+$ leukocytes in the peripheral blood (PB) and white adipose tissue (WAT) of 5-9 week old female db/db and wildtype (wt) mice were examined by flow cytometry (see Section 2.10). PB samples (200 µl) were obtained from the retro-orbital sinus of wt and db/db mice by highly qualified animal technicians at the Australian Phenomics Facility (APF). Following lysis of red cells (see Section 2.10.1), the leukocytes were stained for different leukocyte markers (**Table 2.1**) and analysed by flow cytometry (see Section 2.10.4). Using the gating strategy depicted in **Figures 2.12 and 2.13**, % CD45.2$^+$ cells were determined for the PB of wt and db/db females. The percentage of CD45.2$^+$ cells was not significantly different between wt and db/db PB (wt, 97.63 ± 0.53% vs 95.53 ± 0.62%; **Figure 6.1**). The circulating population of leukocytes was therefore similar for wt and db/db females.

For WAT from female wt and db/db mice, the peri-ovarian adipose depot was excised and the isolated fat pads were weighed (see Section 2.10.2). The db/db fat pads were 5.6-fold times heavier than the fat pads of wt mice (db/db, 1.29 ± 0.11 grams vs wt, 0.23 ± 0.07 grams; **Figure 6.2**), confirming the obesity of db/db mice. The WAT was digested using collagenase II and the SVF cells were separated from adipocytes (see Section 2.10.2) (Cho et al., 2014), stained for a panel of leukocyte markers (**Table 2.1**) and analysed by flow cytometry (see Section 2.10.4). The % CD45.2$^+$ cells (excluding debris and doublets) were determined for both wt and db/db females. The % CD45.2$^+$ cells (leukocytes) showed only a 1.1-fold increase in the WAT of db/db mice compared to corresponding wt mice (wt, 52.72 ± 3.65% vs db/db, 55.91 ± 2.08%; **Figure 6.1**). The total leukocyte population in female db/db WAT resembled the leukocyte load in wt WAT. Overall, our data demonstrated that wt and db/db females showed no significant differences in the leukocyte population (as % of total cells) in either PB or WAT.

6.2.2 Innate and adaptive immune cell populations in PB and WAT of wt and db/db females

We further characterised the CD45.2$^+$ cells in both WAT and PB as innate (myeloid cells and CD11c$^+$ leukocytes, e.g., conventional dendritic cells) or adaptive (lymphoid cells

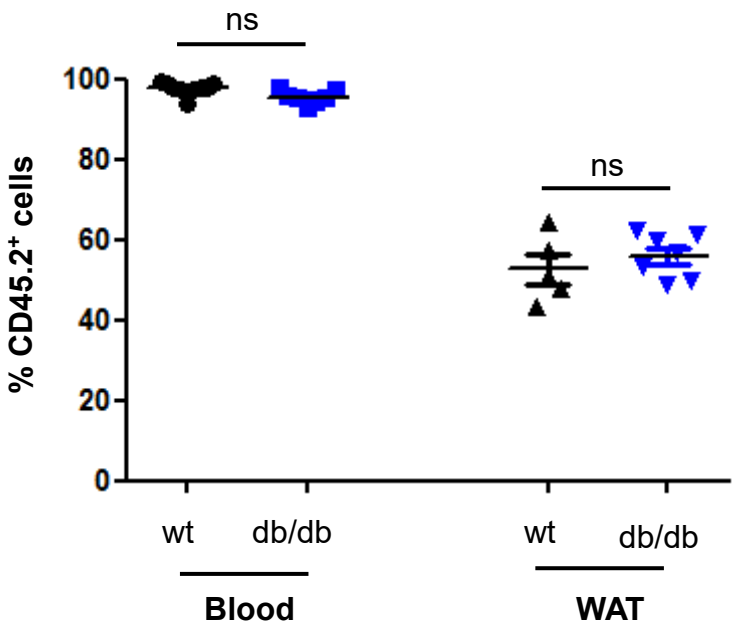

Figure 6.1: Total leukocytes in white adipose tissue (WAT) and peripheral blood (PB) of female wt and db/db mice.

Retro-orbital blood was collected from wt (black symbols) and db/db (blue symbols) female mice (5-9 weeks of age) and the peri-ovarian adipose tissue was excised and digested using collagenase II to obtain the stromal vascular fraction (SVF) containing leukocytes. Leukocyte sub-populations were identified by 9-colour flow cytometry and % $CD45.2^+$ leukocytes was determined in the total population (gated to exclude cell debris and doublets). No significant differences were observed in the PB and WAT leukocytes of wt and db/db females. The data represent the mean GMFI ± SEM for n= 5-9 mice/group. Mann-Whitney two-tailed test; ns, not significant.

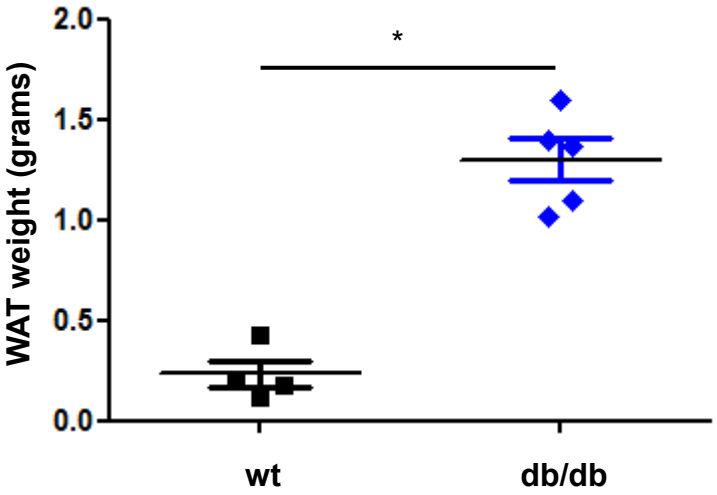

Figure 6.2: Weight of WAT in female wt and db/db mice.

Peri-ovarian WAT was excised from 5-9 week old wt (black symbols) and db/db (blue symbols) mice and the fat pads were weighed. Db/db mice showed heavier fat pads compared to wt mice. The data represent the mean ± SEM for n= 4-5 mice/group. Mann-Whitney two-tailed test; *P<0.0001.

i.e., B cells and T cells) immune cells and examined the contribution of individual leukocyte sub-populations, using the gating strategy depicted in **Figures 2.12 and 2.13**. Whereas lymphoid cells represented the largest leukocyte compartment in the PB of wt (85.1%) and db/db (78.5%) females (**Figure 6.3(a)**), the myeloid lineage represented the largest leukocyte population in wt (46.7%) and db/db (53.5%) WAT (SVF) (**Figure 6.4(a)**).

6.2.2.1 Lymphoid cells

In peripheral blood, the lymphoid lineage of $CD45^+$ leukocytes showed a slight but statistically significant reduction in db/db mice to 92.2% of corresponding controls ($P<0.05$; wt, 85.09 ± 1.00% vs db/db, 78.45 ± 2.92%; **Figure 6.3(a)**). Similarly, a marked reduction in $CD45^+$ lymphoid leukocytes to 63.9% of controls was observed in the WAT of db/db mice (wt, 39.75 ± 7.12% vs db/db, 25.40 ± 2.98%; **Figure 6.3(a)**); however, this reduction did not achieve statistical significance. The lymphoid sub-population represented by B cells showed no differences in either the peripheral blood or WAT of wt and db/db females (**Figure 6.3(b)**). In contrast, the T cell sub-population in db/db PB was significantly reduced to 77.2% of wt controls ($P<0.01$; wt, 24.26 ± 1.05% vs db/db, 18.73 ± 1.32%; **Figure 6.3(c)**). The T cell population was also markedly reduced to 65.6% of controls in db/db WAT (wt, 8.17 ± 0.72% vs db/db, 5.36 ± 0.74%; **Figure 6.3(c)**). These data demonstrated a decrease in PB lymphoid cells and a trend towards a decline in WAT lymphoid cells, specifically T cells, in db/db mice compared to wt mice. The expansion of WAT in db/db mice is therefore accompanied by a reduced T cell population particularly in the PB and to a lesser extent in WAT.

6.2.2.2 Myeloid cells

In db/db PB, there was a significant 1.5-fold increase in the population of $CD45.2^+$ myeloid leukocytes compared to wt controls ($P<0.05$; wt 12.23 ± 1.11% vs db/db, 18.78 ± 2.96%; **Figure 6.4(a)**). Specifically, the sub-population of monocytes was significantly increased 2.3-fold in db/db PB compared to wt PB ($P<0.05$; wt 2.18 ± 0.19% vs db/db, 5.11 ± 0.77%; **Figure 6.4(c)**). No significant differences were observed between wt and db/db PB neutrophils (wt, 7.41 ± 0.72% vs db/db, 9.91 ± 1.65%; **Figure 6.4(d)**), eosinophils (wt, 1.04 ± 0.18% vs db/db, 1.92 ± 0.44%; **Figure 6.4(e)**) or resident macrophages (wt, 1.49 ± 0.22% vs db/db, 1.79 ± 0.22%; **Figure 6.4(b)**).

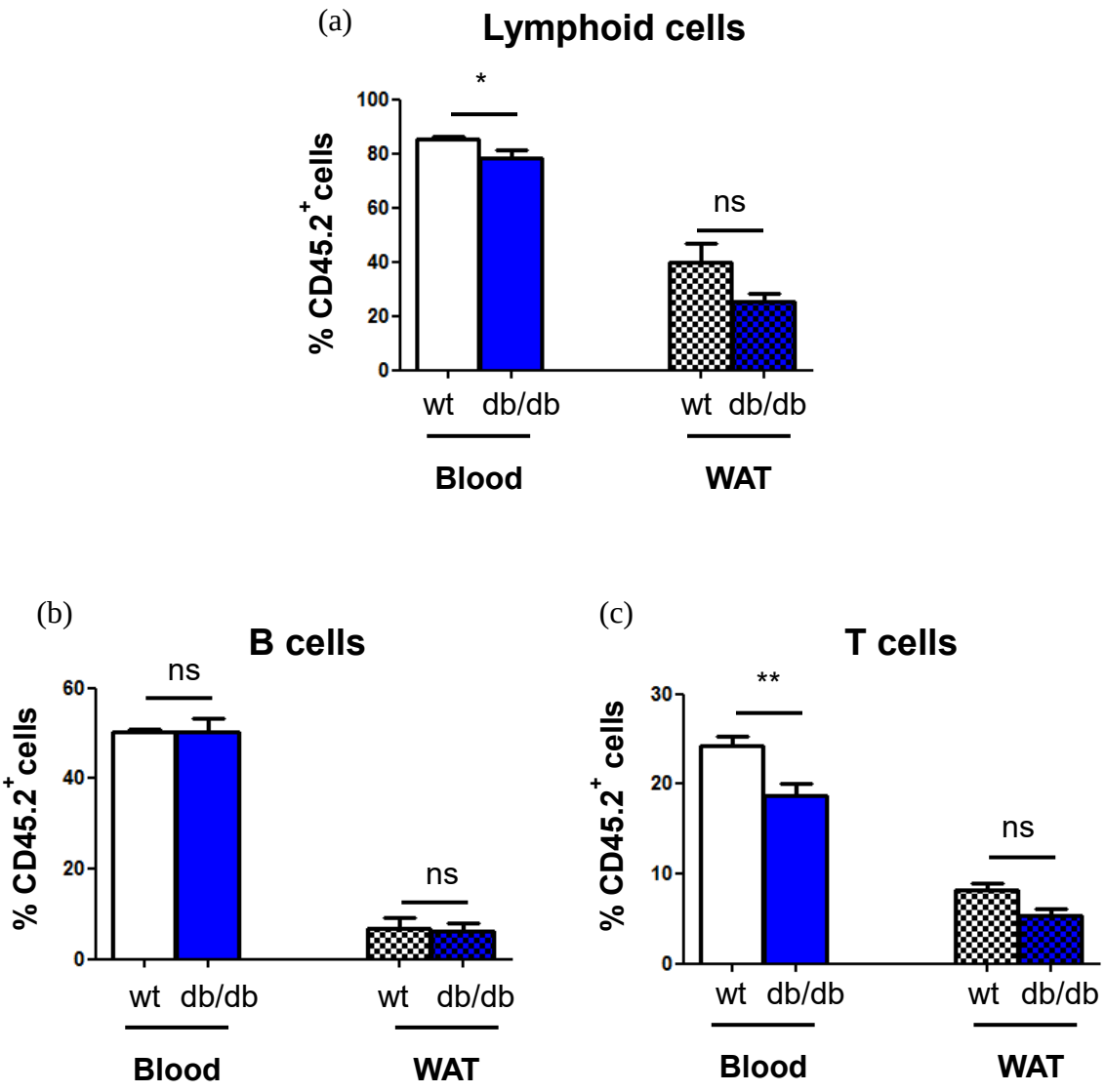

Figure 6.3: Lymphoid cells in PB and WAT of female wt and db/db mice.

Peripheral blood (PB) and the stromal vascular fraction (SVF) of peri-ovarian white adipose tissue (WAT) from female wt and db/db mice (5-9 weeks of age) were stained for leukocyte markers and analysed by flow cytometry. Using the gating strategy in Figures 2.13 and 2.14, the % of $CD45^+$ leukocytes represented by lymphoid cells (a), the B cell sub-population (b) and T cell sub-population (c) was determined. Compared to wt controls, the PB and WAT of db/db mice showed a reduction in lymphoid cells and T cells but not B cells. The data represent the mean ± SEM for n= 5-7 mice/group. Mann-Whitney two-tailed test; *P<0.05, **P<0.01 and ns, not significant.

Figure 6.4: Myeloid leukocytes and sub-populations in PB and WAT of female wt and db/db mice.

Peripheral blood (PB) and the stromal vascular fraction (SVF) of peri-ovarian white adipose tissue (WAT) from 5-9 week old female wt and db/db mice were stained for leukocyte markers and analysed by flow cytometry. Using the gating strategy in Figures 2.13 and 2.14, total myeloid cells (a), resident macrophages (b), monocytes/inflammatory macrophages (c), neutrophils (d) and eosinophils (e), expressed as a % of total $CD45.2^+$ cells, were determined for PB and WAT. Myeloid cells and the monocyte sub-population were increased in db/db PB, compared to wt controls. In parallel, inflammatory macrophages and neutrophils were increased in db/db WAT compared to wt controls. The data represent the mean ± SEM for n= 5-7 mice/group. Mann-Whitney two-tailed test; *$p<0.05$; **$p<0.01$ and ns, not significant.

(a)

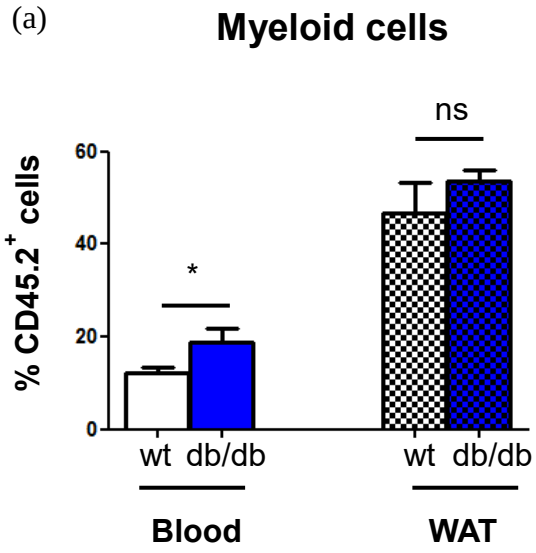
Myeloid cells
% CD45.2+ cells
60
40
20
0
*
ns
wt
db/db
wt
db/db
Blood
WAT

(b)

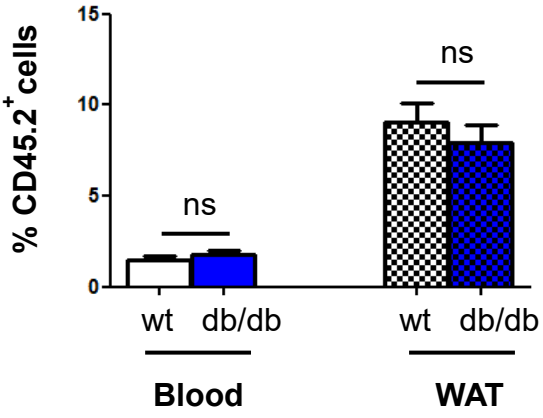
Resident macrophages
% CD45.2+ cells
15
10
5
0
ns
ns
wt
db/db
wt
db/db
Blood
WAT

(c)

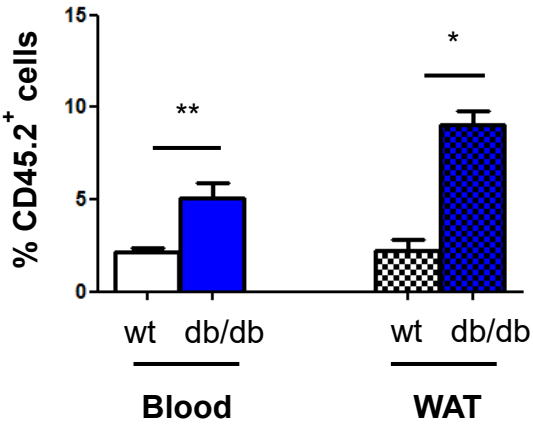
Monocytes/ inflammatory macrophages
% CD45.2+ cells
15
10
5
0
**
*
wt
db/db
wt
db/db
Blood
WAT

(d)

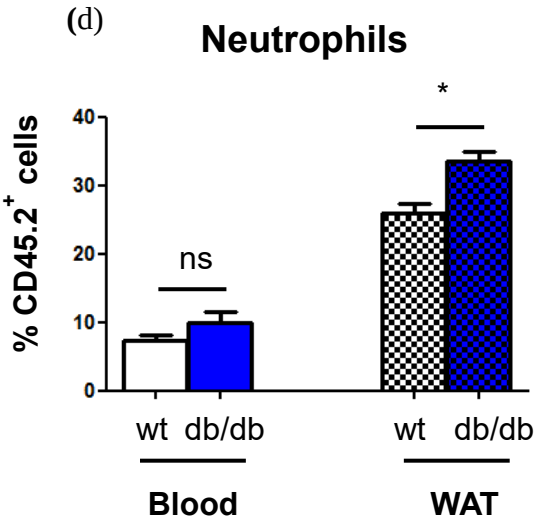
Neutrophils
% CD45.2+ cells
40
30
20
10
0
ns
*
wt
db/db
wt
db/db
Blood
WAT

(e)

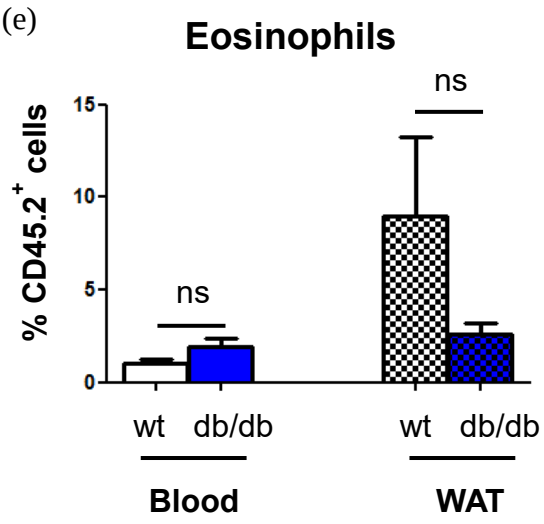
Eosinophils
% CD45.2+ cells
15
10
5
0
ns
ns
wt
db/db
wt
db/db
Blood
WAT

In contrast to PB, no significant differences were observed in the total myeloid population (represented as % total CD45.2$^+$ leukocytes) in WAT of wt and db/db female mice (wt, 46.70 ± 6.69% vs db/db, 53.48 ± 2.40%; **Figure 6.4(a)**). Inflammatory macrophages and neutrophils were significantly increased 4.1-fold (wt, 2.19 ± 0.62% vs db/db, 9.08 ± 0.72%) and 1.3-fold (wt, 25.88 ± 1.49% vs db/db 33.52 ± 1.45%), respectively, in db/db WAT compared to wt WAT (**Figure 6.4(c, d)**). However, eosinophils in db/db WAT were markedly reduced to 28.8% of controls (wt, 8.98 ± 4.24% vs db/db, 2.59 ± 0.58%; **Figure 6.4(e)**). No significant differences were observed in the resident macrophage population of db/db and wt WAT (wt, 9.08 ± 1.01% vs db/db, 7.93 ± 0.99%; **Figure 6.4(b)**).

Interestingly, myeloid cells represented 46.7% and 53.5% of CD45.2$^+$ leukocytes in wt and db/db WAT, respectively, but only 12.2% and 18.8%, respectively, in PB (**Figure 6.4(a)**). For wt WAT, the sub-populations of resident macrophages, neutrophils and eosinophils (as a % of the total leukocyte population) were 6.1-fold, 3.5-fold and 8.7-fold higher than in wt PB respectively. Similarly, db/db WAT showed a 4.4-fold and 3.4-fold increase in the populations of resident macrophages and neutrophils, respectively, compared to db/db PB. Furthermore, db/db WAT was distinguished by a 1.8-fold increase in the population of inflammatory macrophages, relative to monocytes in db/db PB (**Figure 6.4(c)**); the corresponding populations of eosinophils were comparable (**Figure 6.4(e)**). Thus, inflammatory macrophages constituted a more prominent leukocyte population in db/db WAT than wt WAT; in parallel, the monocyte population in db/db peripheral blood was significantly enlarged compared to wt blood.

6.2.2.3 CD11c$^+$ leukocytes

Previous studies have reported that CD11c$^+$ macrophages play an important role in the inflammation of white adipose tissue in obese rodents (e.g., ob/ob mice) and humans (Wentworth et al., 2010, Shaul et al., 2010, Lumeng et al., 2007a, Nguyen et al., 2007). These F4/80$^+$CD11b$^+$CD11c$^+$ macrophages release anti-inflammatory cytokines whereas F4/80$^+$CD11b$^+$CD11c$^-$ cells release pro-inflammatory cytokines (Lumeng et al., 2007a, Nguyen et al., 2007). Furthermore, the deletion of CD11c$^+$ leukocytes in obese mice (ob/ob and HFD mice) reduced local and systemic inflammation as well as improved insulin sensitivity in muscle, adipose tissue and liver (Patsouris et al., 2008). We therefore analysed CD11c$^+$ leukocyte sub-populations in our study.

(a) Conventional dendritic cells ($CD11c^+Ly6C^-Ly6G^-$ cells)

The population of conventional dendritic cells (cDCs) was similar in wt and db/db PB (wt, 0.84 ± 0.07% vs db/db, 0.79± 0.15%; **Figure 6.5(a)**). In WAT, the cDC population was significantly reduced to 65.6% of controls in WAT of db/db mice ($P<0.05$; wt, 10.23 ± 0.75% vs db/db, 6.71 ± 0.34%; **Figure 6.5(a)**). This data indicates that db/db WAT has a smaller population of cDCs (relative to the total $CD45.2^+$ leukocyte population) than in wt WAT.

(b) $CD11c^+Ly6C^+$ cells

The $CD11c^+Ly6C^+$ cells were similar in wt and db/db PB (wt, 0.15 ± 0.06% vs db/db, 0.15 ± 0.07%; **Figure 6.5(b)**). The $CD11c^+Ly6C^+$ cells were increased to 2.2-fold in WAT of db/db mice compared to wt WAT (wt, 1.10 ± 0.05% vs db/db, 2.47 ± 0.89%; **Figure 6.5(b)**). However, this increase did not achieve statistical significance. This data suggests that db/db WAT a larger population of $CD11c^+Ly6C^+$ cells compared to wt WAT.

(c) $CD11c^+Ly6G^+$ cells

The $CD11c^+Ly6G^+$ cells showed no significant difference in wt and db/db PB (wt, 0.13 ± 0.01% vs db/db, 0.19 ± 0.06%; **Figure 6.5(c)**). In db/db WAT, the $CD11c^+Ly6G^+$ cells were significantly increased 5.5-fold compared to wt WAT ($P<0.05$; wt, 1.78 ± 0.28% vs db/db, 9.73 ± 1.76%; **Figure 6.5(c)**). This data demonstrates that db/db WAT has a larger population of $CD11c^+Ly6G^+$ cells, relative to total $CD45.2^+$ leukocytes, than in wt WAT.

In summary, obesity-induced inflammation in db/db WAT was characterised by a relative increase in the sub-populations of inflammatory monocytes/macrophages and neutrophils as well as $CD11c^+Ly6G^+$ leukocyte, compared to corresponding wt controls. However, the only positive correlation observed between db/db peripheral blood and WAT was a significant increase in monocytes and inflammatory macrophages respectively.

6.2.3 Heparanase expression by innate and adaptive immune cells in PB and WAT of female db/db mice

Our data have confirmed the findings of other groups (Talukdar et al., 2012, Nguyen et al., 2007, Lumeng et al., 2007b, Xu et al., 2003, Weisberg et al., 2003, Elgazar-Carmon et al., 2008), that relative to wt WAT, inflammation in the WAT of db/db mice is marked

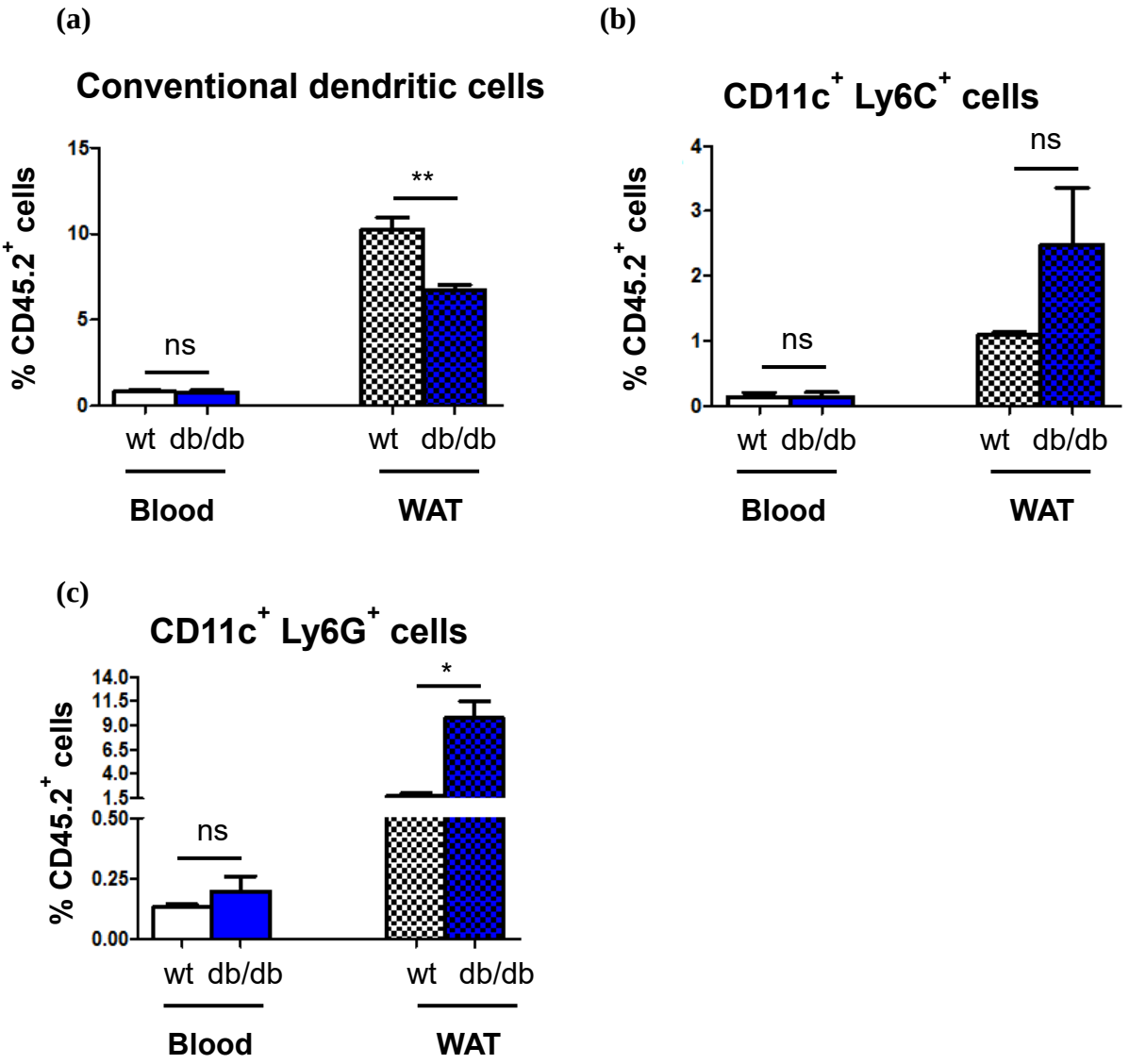

Figure 6.5: CD11c$^+$ leukocytes in PB and WAT of female wt and db/db mice.

Peripheral blood (PB) and the stromal vascular fraction (SVF) of peri-ovarian white adipose tissue (WAT) from wt and db/db female mice (5-9 week old) were stained for leukocyte markers and examined via flow cytometry. Using the gating strategy in Figures 2.13 and 2.14, the % of CD45$^+$ leukocytes represented by conventional dendritic cells (a) were found to be reduced but CD11c$^+$Ly6C$^+$ cells (b) and CD11c$^+$Ly6C$^+$ cells (c) were increased in WAT of db/db mice compared to controls; no changes were observed in the PB of wt and db/db mice. The data represent the mean ± SEM for n= 5-7 mice/group. Mann-Whitney two-tailed test; *P<0.05 and ns, not significant.

by a selective increase in myeloid leukocytes, specifically, the sub-populations of inflammatory macrophages and neutrophils. We next investigated whether the migration of inflammatory leukocytes to db/db WAT correlated with enhanced cell surface expression of Hpse (see Section 2.10.4).

In section 6.2.2.3, we found that populations of inflammatory macrophages and neutrophils were significantly increased (as a % of total $CD45.2^+$ leukocytes) in db/db WAT compared to wt WAT. Here, in parallel, we further demonstrate that cell surface Hpse on db/db WAT inflammatory macrophages was significantly increased 2.7-fold compared to db/db PB monocytes (WAT, GMFI= 4679.00 ± 430.43 vs PB, GMFI= 1759.67 ± 282.42; **Figure 6.6(c)**). Furthermore, Hpse expressed by db/db WAT neutrophils was significantly increased 8.4-fold higher than in db/db PB (WAT, GMFI= 17415.80 ± 1651.03 vs PB, GMFI= 2081.33 ± 445.48). Notably, in db/db WAT, the hierarchy for the intensity of cell surface Hpse staining on myeloid sub-populations was neutrophils>> resident macrophages> inflammatory macrophages> eosinophils.

Correlating with the enlarged populations of total myeloid cells and resident macrophages in db/db WAT compared to PB (**Figure 6.4**), Hpse expression was also elevated 3.5-fold (WAT, GMFI= 9933.40 ± 1018.84 vs PB, GMFI= 2848.17 ± 793.08) and 1.8-fold (WAT, GMFI= 6562.00 ± 251.99 vs PB, GMFI= 3637.00 ± 651.64), respectively (**Figure 6.6**). Conversely, the less prevalent populations of total lymphoid cells, B cells and T cells in db/db WAT (compared to db/db PB; **Figure 6.3**) correlated with markedly lower or comparable levels of cell surface Hpse (**Figure 6.7**). The similar populations of eosinophils in db/db WAT and PB (**Figure 6.4(e)**) was also consistent with no significant change in Hpse expression (**Figure 6.6(e)**). Surprisingly, however, the increased proportion of cDCs, $CD11c^+Ly6G^+$ cells and $CD11c^+Ly6C^+$ cells in db/db WAT (compared to db/db PB; **Figure 6.5**) did not correlate with enhanced Hpse expression (**Figure 6.8**). Interestingly, Hpse expression by $CD11c^+Ly6C^+$ cells increased 3.7-fold in db/db WAT compared to wt WAT (db/db, GMFI=18455.57 ± 7212.29 vs wt, GMFI= 5021.40 ± 865.56), but, this difference was not statistically significant (**Figure 6.8(b)**).

Figure 6.6: Hpse expression by myeloid leukocytes in PB and WAT of female wt and db/db mice.

Heparanase (Hpse) expression on total myeloid cells and myeloid sub-populations in peripheral blood (PB) and stromal vascular fraction (SVF) from peri-ovarian white adipose tissue (WAT) was determined in wt and db/db female mice at 5-9 weeks of gate by flow cytometry (see Figures 2.13 and 2.14, Section 2.10). The levels of Hpse expressed on the cell surface is indicated by the GMFI. Hpse was more highly expressed by total myeloid cells, resident macrophages, monocytes/inflammatory macrophages and neutrophils in WAT compared to PB of wt and db/db mice. The data represent the mean ± SEM for n= 5-7 mice/group. General ANOVA with Fisher's unprotected LSD post-test; *P<0.05, **P<0.01, ***P<0.001 and ns, not significant.

(a)

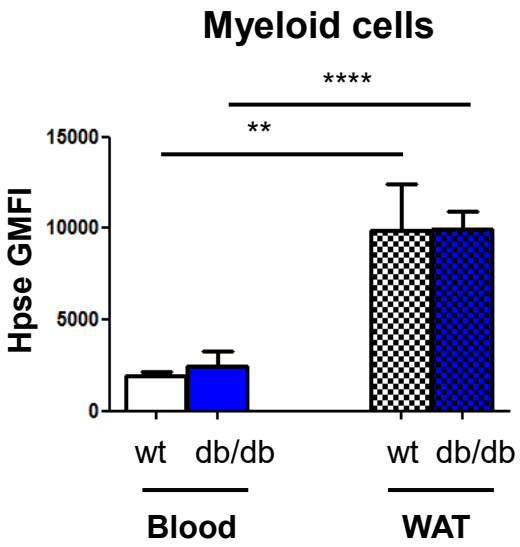
Myeloid cells
****
**
Hpse GMFI
15000
10000
5000
0
wt
db/db
wt
db/db
Blood
WAT

(b)

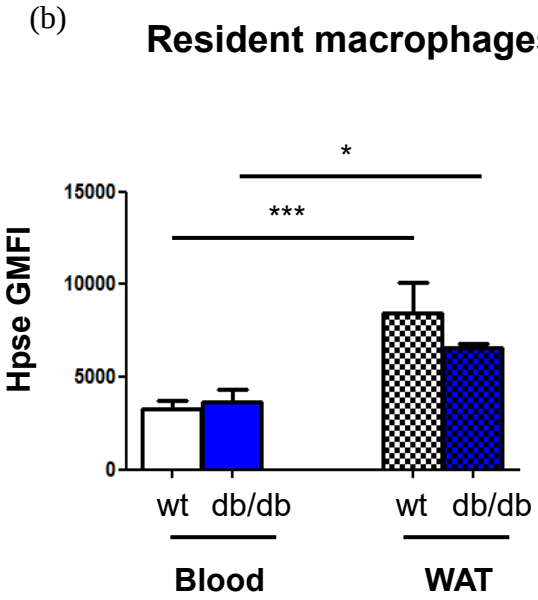
Resident macrophages
*
***
Hpse GMFI
15000
10000
5000
0
wt
db/db
wt
db/db
Blood
WAT

(c)

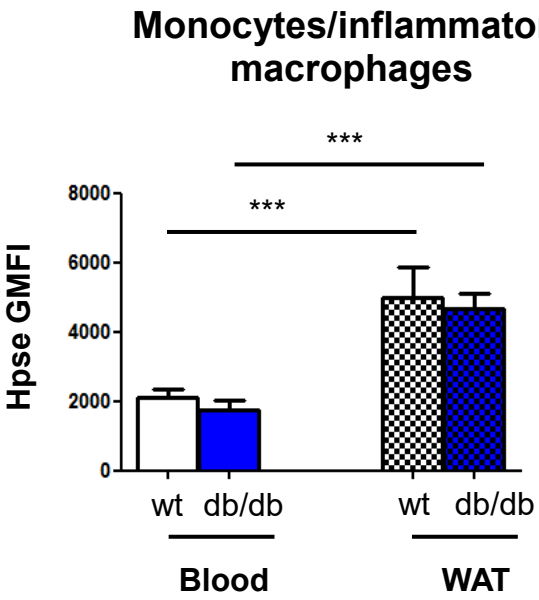
Monocytes/inflammatory macrophages
***
***
Hpse GMFI
8000
6000
4000
2000
0
wt
db/db
wt
db/db
Blood
WAT

(d)

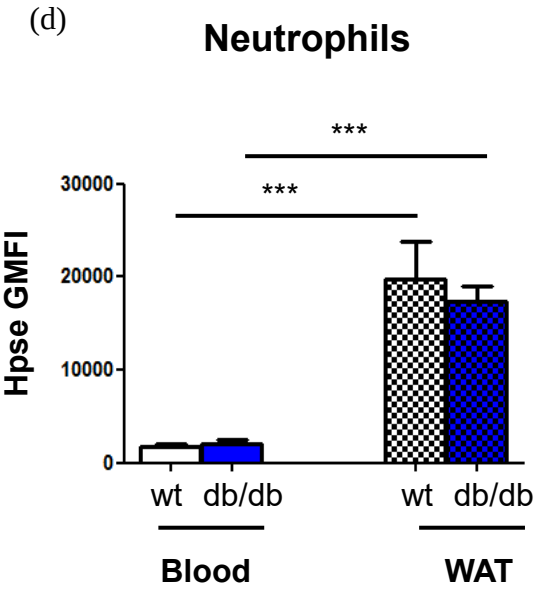
Neutrophils
***
***
Hpse GMFI
30000
20000
10000
0
wt
db/db
wt
db/db
Blood
WAT

(e)

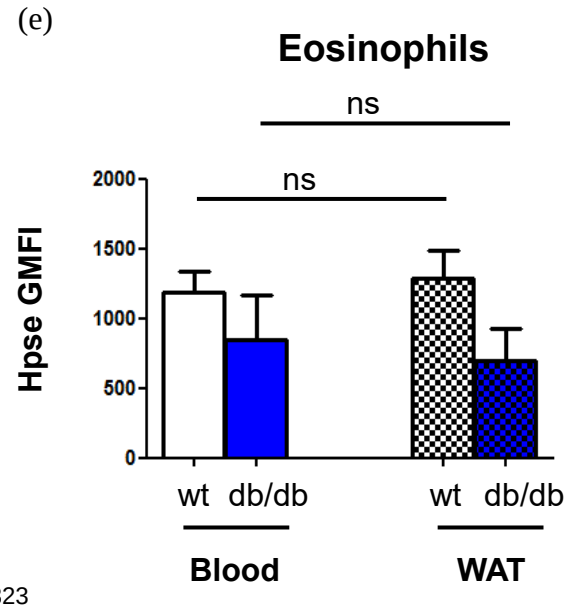
Eosinophils
ns
ns
Hpse GMFI
2000
1500
1000
500
0
wt
db/db
wt
db/db
Blood
WAT

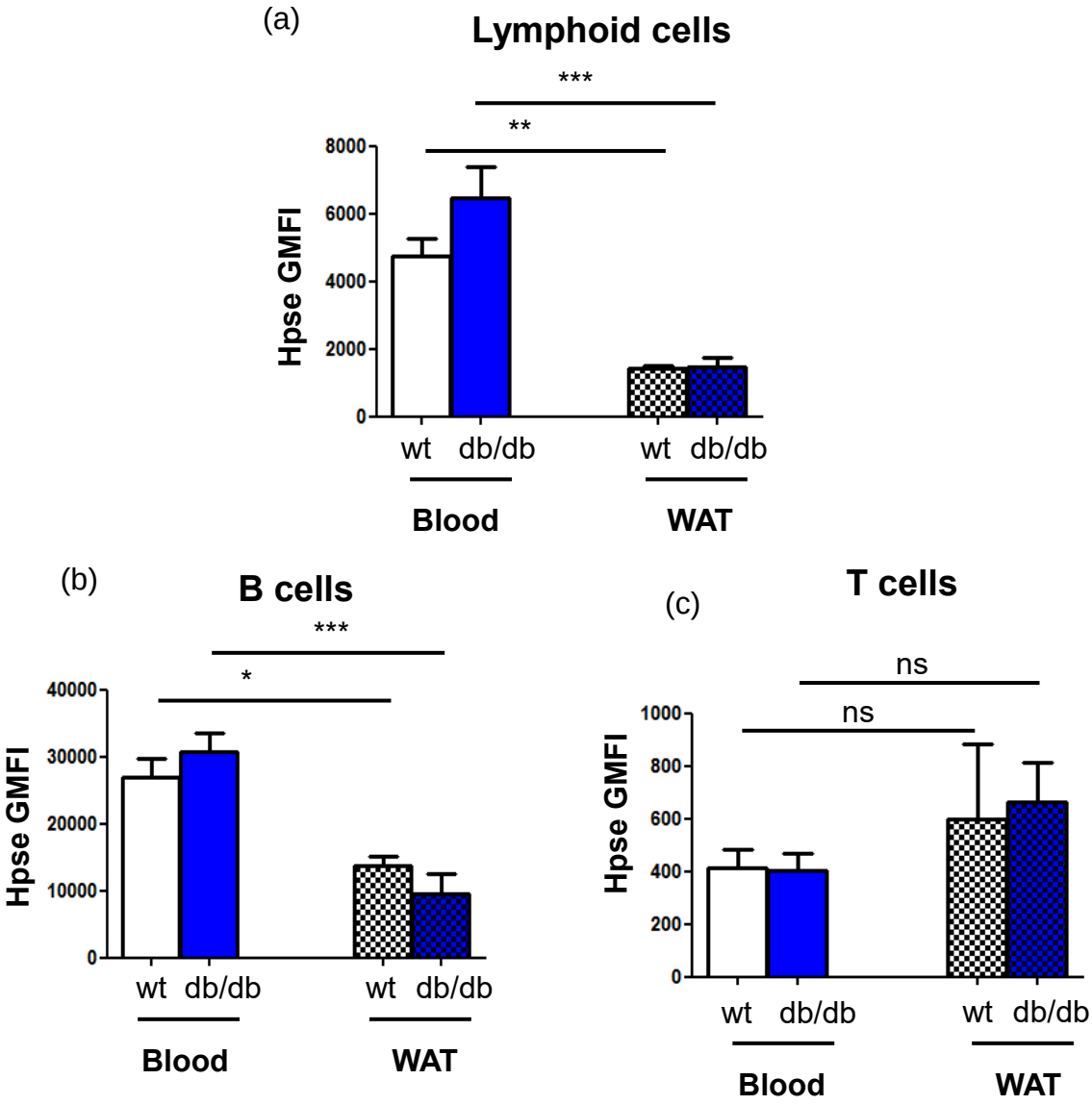

Figure 6.7: Hpse expression in lymphoid cells in PB and WAT of female wt and db/db mice.

Peripheral blood (PB) and the stromal vascular fraction (SVF) from peri-ovarian white adipose tissue (WAT) of wt and db/db female mice (5-9 weeks of age) were stained for leukocyte markers and heparanase (Hpse) and analysed by flow cytometry, using the gating strategy in Figures 2.13 and 2.14. The cell surface expression of Hpse was determined for lymphoid cells in PB and WAT of wt and db/db mice and expressed as geometric mean fluorescence intensity (GMFI). Total lymphoid cells and B cells showed reduced expression of cell surface Hpse in WAT compared to PB in wt and db/db mice. The data represent the mean ± SEM for n= 5-7 mice/group. General ANOVA with Fisher's unprotected LSD post-test; *P<0.05, **P<0.01, ***P<0.0001 and ns, not significant.

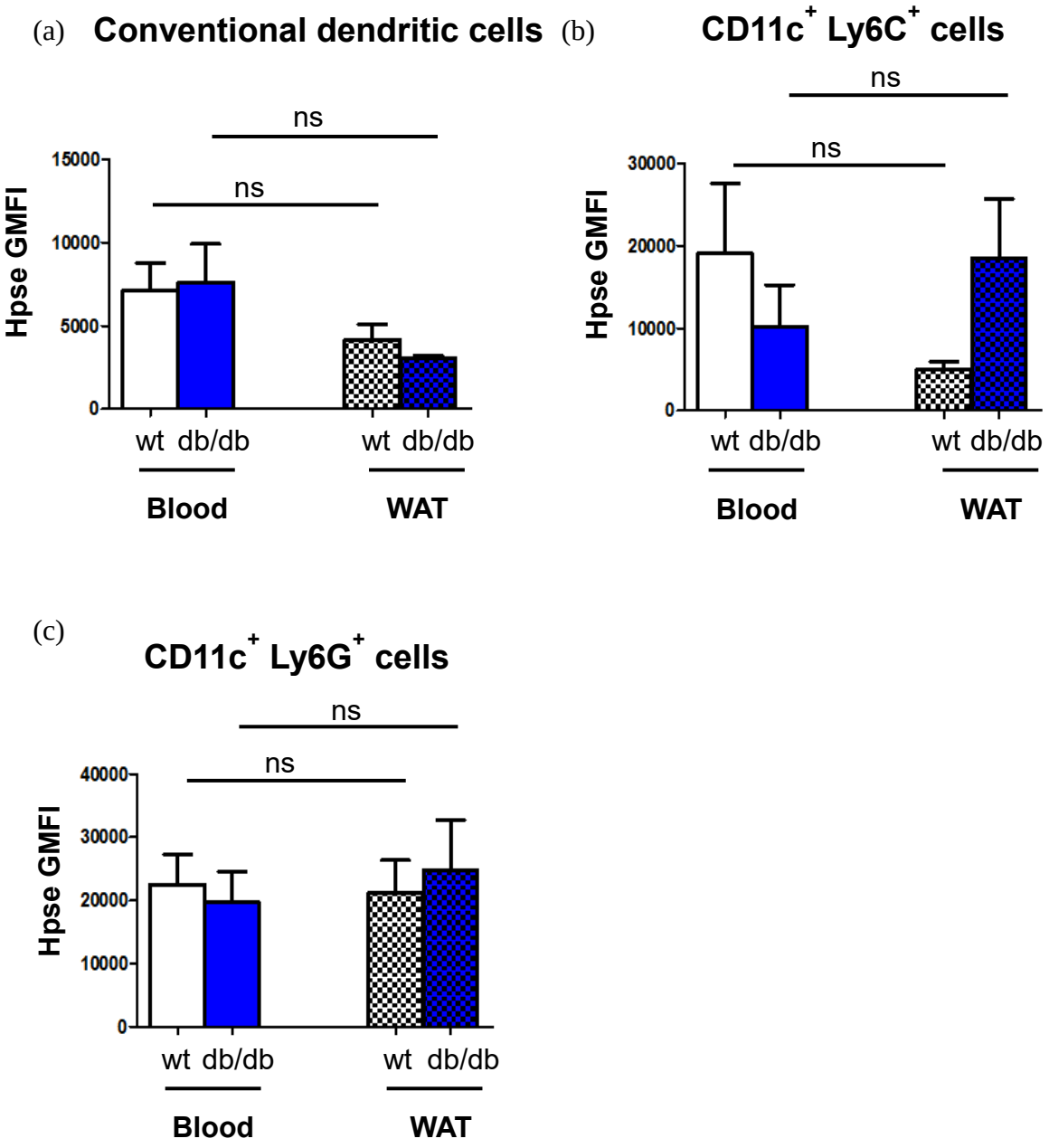

Figure 6.8: Hpse expression by CD11c$^+$ cells in PB and WAT of female wt and db/db mice.

The cell surface expression of heparanase (Hpse) on CD11c$^+$ leukocytes in peripheral blood (PB) and stromal vascular fraction (SVF) from peri-ovarian white adipose tissue (WAT) of female wt and db/db mice was determined by flow cytometry, using the gating strategy in Figures 2.13 and 2.14 (Section 2.10). Hpse expression is expressed as GMFI. No consistent trend was evident in the cell surface Hpse levels on CD11c$^+$ leukocytes in PB or WAT. The data represent the mean ± SEM for n= 5-7 mice/group. General ANOVA with Fisher's unprotected LSD post-test; ns, not significant.

Like db/db WAT, myeloid leukocytes in wt WAT also showed a significant 5.1-fold increase in Hpse expression compared to PB, respectively (WAT, GMFI= 9884.25 ± 2506.44 vs PB, GMFI= 1941.56 ± 230.95; **Figure 6.6(a)**). Hpse expressed by wt WAT inflammatory macrophages showed a significant 2.4-fold significant increase compared to PB monocytes (WAT, GMFI= 5004.50 ± 857.98 vs PB, GMFI= 2105.11 ± 243.07; **Figure 6.6(c)**). Similarly, resident macrophages and neutrophils in WAT demonstrated a significant 2.6-fold (WAT, GMFI= 8446.25 ± 1667.35 vs PB, GMFI= 3259.55 ± 467.89) and 10.7-fold (WAT, GMFI= 19725.00 ± 4129.29 vs PB, GMFI= 1816.00 ± 209.49) increase in Hpse expression, compared to wt PB (**Figure 6.6(b, d)**). No significant changes were observed in Hpse expressed by wt eosinophils in PB and WAT (**Figure 6.6(e)**). In addition like db/db WAT, Hpse expression on wt WAT total lymphoid cells and B cells were reduced to 30.2% and 50.9% respectively, of corresponding PB populations (**Figure 6.7**). The cell surface Hpse expression by cDCs and $CD11c^{+}Ly6C^{+}$ leukocytes in wt WAT was reduced to 58.8% and 26.4% of PB controls but was not statistically significant (**Figure 6.8**). No significant differences were observed in cell surface Hpse by $CD11c^{+}Ly6C^{+}$ cells in wt PB and WAT (**Figure 6.8(c)**).

Collectively, cell surface Hpse levels were significantly increased in inflammatory macrophages, resident macrophages, neutrophils and total myeloid cells of WAT in both db/db and wt mice, compared to corresponding populations in PB. A trend for an increased Hpse expression on $CD11c^{+}Ly6C^{+}$ cells in db/db WAT (only) was also observed. No significant differences in Hpse expression were found between WAT and PB for T cells, cDCs and $CD11c^{+}Ly6G^{+}$ in both db/db and wt mice; however both wt and db/db WAT B cells and total lymphoid cells showed a significant decrease in cell surface Hpse, compared to corresponding populations in PB.

Cell surface Hpse expression on immune cell sub-populations was also normalised to the corresponding level of Hpse expressed by B lymphocytes (represented as a geometric mean fluorescence ratio (GMFR)). Normalised data for female wt and db/db leukocytes confirmed highly elevated Hpse levels (relative Hpse GMFR) in total myeloid cells including inflammatory macrophages and neutrophils (see Appendix 2.1), as observed in the non-normalised data. Interestingly, the normalised data for female db/db WAT showed that the Hpse GMFR was significantly increased for total myeloid cells ($P<0.01$),

inflammatory macrophages ($P<0.05$) and neutrophils ($P<0.05$), compared to wt WAT (see Appendix 2.1).

In summary, WAT in female db/db mice showed a significant increase in inflammatory macrophages and neutrophil populations; in parallel only a significant increase in the monocyte population was found in peripheral blood. The increased expression of Hpse on both inflammatory macrophages and neutrophils in WAT suggests that this degradative enzyme may facilitate the migration of these innate immune cells from the blood to regions of inflammation in adipose tissue. However, the similar expression of Hpse by inflammatory macrophages and neutrophils in wt WAT further suggests that Hpse represents a requisite tool for their migration to white adipose tissue in both lean and obese mice.

6.2.4 Leukocytes in the peripheral blood and adipose tissue of male db/db mice

$CD45.2^+$ leukocytes were also examined in the PB and WAT of 5-9 week old male db/db and wildtype (wt) mice, as for females (see Section 6.2.1), with the exception that epididymal fat pads were analysed for WAT.

Male db/db fat pads were 5.2-fold times heavier than male wt fat pads (db/db, 1.10 ± 0.11 grams vs wt, 0.21 ± 0.02 grams; **Figure 6.9**), resembling the increased weight of db/db female WAT (**Figure 6.2**). There was no significant difference in the proportion of $CD45.2^+$ leukocytes in the total cell population in the SVF (WAT) of wt and db/db males, as demonstrated in female mice (**Figure 6.1**). Although, db/db male fat pads were significantly heavier than wt controls, no differences were observed in the leukocyte populations in wt and db/db PB or WAT (**Figure 6.10**).

6.2.5 Innate and adaptive immune cells in PB and WAT of wt and db/db males

Having observed no significant differences in the proportion of $CD45.2^+$ leukocytes between male wt and db/db PB or WAT, we next examined the sub-populations of $CD45.2^+$ cells represented by innate (myeloid cells and $CD11c^+$ leukocytes) and adaptive immune cells (lymphoid cells i.e., B and T cells) in PB and WAT of wt and db/db males (see Section 2.10).

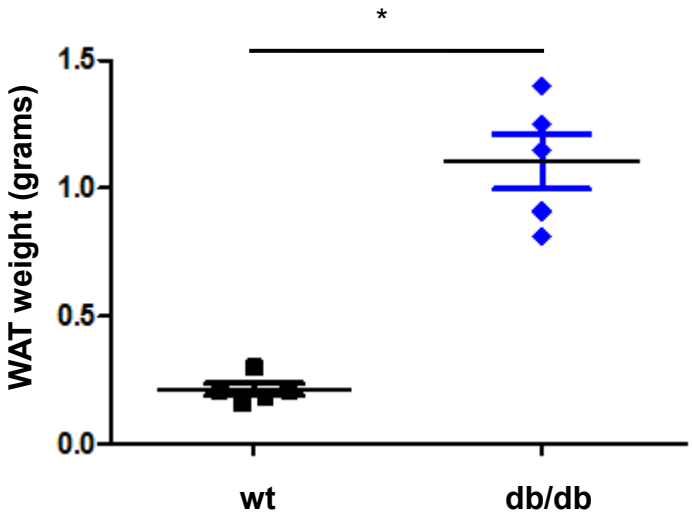

Figure 6.9: White adipose tissue (WAT) weight in male wt and db/db mice.

Epididymal adipose tissue was excised from 5-9 week old male wt and db/db mice and the fat pads were weighed. Db/db fat pads were significantly heavier compared to wt controls. The data represent the mean ± SEM for n= 5 mice/group. Mann-Whitney two-tailed test; *P<0.0001.

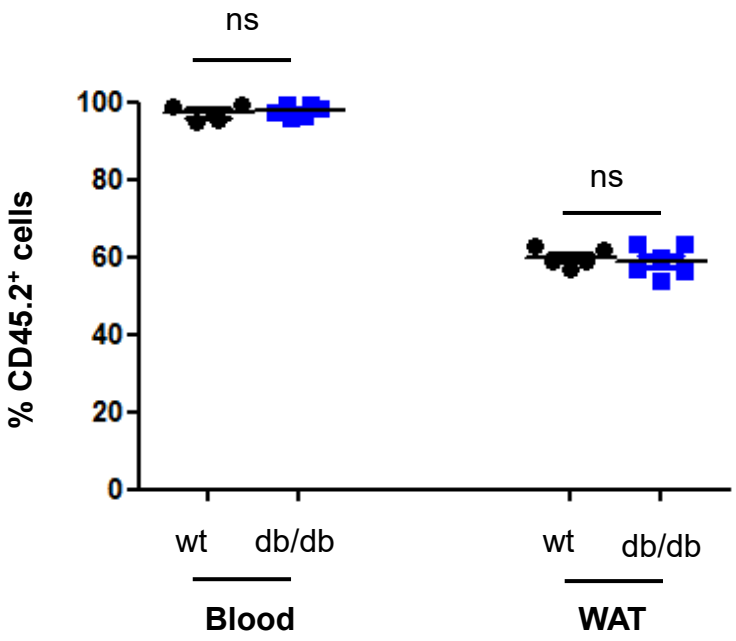

Figure 6.10: % CD45$^+$ leukocytes in male wt and db/db mice.

Retro-orbital blood (PB) was collected from 5-9 week old wt and db/db mice and the epididymal adipose tissue was excised and digested using collagenase II to obtain the stromal vascular fraction (SVF) containing leukocytes. Leukocyte sub-populations were identified by 9-colour flow cytometry and the % of the total cell population (gated to exclude cell debris and doublets) represented by CD45.2$^+$ leukocytes were determined. No significant differences in % CD45.2$^+$ leukocytes were observed between wt and db/db mice in PB or WAT. The data represent the mean GMFI ± SEM for n= 4-6 mice/group. Mann-Whitney two-tailed test; ns, not significant.

In male PB, the proportion of total lymphoid leukocytes was similar for wt (74.60 ± 10.43%) and db/db mice (78.42 ± 2.46%; **Table 6.1**). In contrast, the lymphoid cell population (represented as % of $CD45.2^+$ leukocytes) in db/db WAT was significantly reduced to 64.5% of controls (19.84 ± 1.35% vs 30.74 ± 3.05%, respectively; $P<0.05$; **Table 6.1**). No differences were observed between wt and db/db B cell and T cell populations in PB or WAT (**Table 6.1**). Overall, male db/db WAT showed a significantly reduced population of lymphoid cells, compared to male wt WAT.

The conventional dendritic cell (cDC) population was similar in wt and db/db PB (0.79 ± 0.23% vs 0.62 ± 0.19%) as well as for WAT (7.69 ± 0.53% vs 8.29 ± 0.57%; **Table 6.1**). Similarly, no significant differences were observed in the $CD11c^+Ly6C^+$ cells and $CD11c^+Ly6G^+$ cells in db/db and wt PB (**Table 6.1**). However, the proportion of $CD11c^+Ly6C^+$ cells in db/db PB was markedly increased 3-fold (wt, 0.11 ± 0.03% vs db/db, 0.33 ± 0.10%) but this difference was not statistically significant. Similarly, the $CD11c^+Ly6C^+$ leukocyte population was increased 2.1-fold in db/db WAT. The $CD11c^+Ly6G^+$ population was significantly increased 5.3-fold in db/db WAT compared to wt WAT ($P<0.001$; wt, 2.05 ± 0.44% vs db/db, 10.89 ± 0.88%); however no difference was observed in the PB. These data indicate that the proportion of $CD11c^+$ cells, particularly the $CD11c^+Ly6G^+$ leukocyte population, was increased in db/db WAT compared to wt controls.

No significant differences were observed in the total myeloid population in male PB or WAT (**Table 6.1**). However, the db/db males showed a 1.6-fold increase in myeloid leukocytes in PB (18.22 ± 2.02%), compared to wt males (11.41 ± 4.05%; **Table 6.1**). The myeloid sub-populations of monocytes and resident macrophages significantly increased 2.7-fold (4.80 ± 0.92%) and 2.5-fold (2.25 ± 0.15%) respectively in db/db PB compared to wt PB (monocytes, 1.75 ± 0.69%, $P<0.05$; RES MP, 2.25 ± 0.15%, $P<0.05$; **Table 6.1**). No significant differences were observed in PB neutrophils and eosinophils (**Table 6.1**); however there was a trend for the eosinophil population to increase 2-fold in db/db PB. Myeloid cells represented the principal leukocyte population in the WAT of male wt (54.68 ± 2.70%) and db/db (53.56 ± 1.92%) mice. However, the population of inflammatory macrophages in db/db WAT (6.98 ± 0.39%) was significantly increased 3.9-fold, compared to corresponding wt controls (1.75 ± 0.25%; $P<0.01$). In contrast, the

Table 6.1: Sub-populations of immune cell (represented as % of total CD45.2$^+$ leukocytes) in peripheral blood and WAT of wildtype and db/db male mice.

Cell type	Peripheral blood (%) ¶		WAT (%) ¶	
	wildtype	db/db	wildtype	db/db
Lymphoid	74.60 ± 10.43	78.42 ± 2.46	30.74 ± 3.05	19.84 ± 1.35*
B cell	37.85 ± 4.63	41.76 ± 1.74	3.89 ± 0.65	2.84 ± 0.75
T cell	25.20 ± 5.39	25.36 ± 2.05	6.85 ± 1.24	5.68 ± 1.48
cDC	0.85 ± 0.20	0.74 ± 0.18	8.21 ± 0.52	8.75 ± 0.83
CD11c$^+$Ly6C$^+$	0.11 ± 0.03	0.33 ± 0.10	1.97 ± 0.42	4.09 ± 0.84
CD11c$^+$Ly6G$^+$	0.19 ± 0.48	0.19 ± 0.06	2.05 ± 0.44	10.89 ± 0.88***
Myeloid	11.41 ± 4.05	18.22 ± 2.02	54.68 ± 2.70	53.56 ± 1.92
Mono/Inf Mf	1.75 ± 0.69	4.80 ± 0.92*	1.75 ± 0.25	6.98 ± 0.39**
Res Mf	0.90 ± 0.27	2.25 ± 0.15*	5.62 ± 0.79	7.94 ± 0.67
Eosinophil	0.43 ± 0.14	0.81 ± 0.13	3.40 ± 1.13	1.79 ± 0.31
Neutrophil	8.28 ± 3.07	10.24 ± 1.16	43.54 ± 1.27	36.60 ± 2.11*

¶The data represent the mean ± SEM for n=5-7 mice/group. Mann-Whitney test; *P<0.05, **P<0.01, ***P<0.0001, compared to corresponding wt control. Mono/Inf Mf, monocyte (blood)/inflammatory macrophage (WAT); and Res Mf, resident macrophages; cDC, conventional dendritic cell.

neutrophil population in db/db WAT (36.60 ± 2.11%) was significantly reduced to 84.1% of wt WAT (43.54 ± 1.27%; $P<0.05$); the eosinophil population in db/db WAT (1.79 ± 0.31%) was also reduced to 52.6% of wt eosinophils (3.40 ± 1.13%) (**Table 6.1**). There was a trend towards an increase in resident macrophages in db/db WAT but this difference did not achieve statistical significance. Overall, only monocytes/inflammatory macrophages demonstrated a significant increase in both male db/db PB and WAT, compared to wt control.

In summary, our findings revealed that for both female and male wt and db/db PB, lymphoid cells represent the major leukocyte population (~75-83%); in contrast, myeloid cells constitute the major leukocyte compartment in WAT (~50-55%). A striking feature of WAT in both female and male db/db mice was the ~4-fold increase in the relative size of the population of inflammatory macrophages, compared to corresponding wt mice. In parallel, there was a 1.6-2.3 fold elevation in circulating monocytes in db/db mice (see Section 6.2.2) Although a significant 1.3-fold increase in the neutrophil population was found in female db/db WAT, this property was not evident in male db/db WAT. Conversely, a 2.5-fold increase in the population of resident macrophages in the PB of male db/db mice was not observed in female db/db PB (see Section 6.2.2). Thus, distribution of immune cell sub-populations is altered in the peripheral blood and white adipose tissue of db/db mice. These findings suggest that aberrant inflammation of white adipose tissue in db/db mice is paralleled by an elevated level of monocytes in peripheral blood.

6.2.6 Heparanase expression by innate and adaptive immune cells in PB and WAT of male db/db mice

In parallel with our studies of the distribution of immune cell sub-populations in male db/db mice (see Section 6.2.5) on different leukocyte subsets by flow cytometry (see Section 2.10), as determined for db/db females (see Section 6.2.3). In wt and db/db mice, the level of cell surface Hpse expressed by $CD45.2^+$ leukocytes of the lymphoid lineage in WAT was significantly reduced to 28.9% and 48.4%, respectively, of the level on $CD45.2^+$ lymphoid cells in PB (**Table 6.2**). However, Hpse expression by B cells and T cells in PB and WAT showed no significant differences between wt and db/db mice (**Table 6.2**). Nevertheless, B lymphocytes in PB and WAT expressed ~40-50-fold higher

Table 6.2: Cell surface heparanase (Hpse) expression by immune cells (represented as GMFI) in peripheral blood and WAT of male wildtype and db/db mice.

Cell type	Peripheral blood (Hpse GMFI)¶		WAT (Hpse GMFI)¶	
	wildtype	db/db	wildtype	db/db
Lymphoid	1711.00 ± 240.74	1254.00 ± 139.11	496.00 ± 71.15*	607.00 ± 138.79***
B cell	9184.00 ± 1475.87	6450.60 ± 1059.73	5169.40 ± 634.61	4480.40 ± 1566.31
T cell	194.50 ± 11.78	123.32 ± 43.39	118.84 ± 21.53	108.98 ± 26.95
cDC	2624.80 ± 981.69	1960.50 ± 495.46	3514.00 ± 895.49	2468.50 ± 659.44
$CD11c^{+}Ly6C^{+}$	2396.00 ± 1243.41	16979.17 ± 7698.99	4177.40 ± 967.20	5051.33 ± 1072.35
$CD11c^{+}Ly6G^{+}$	6212.60 ± 813.78	14328.67 ± 5885.47	16068.00 ± 3185.88	13496.67 ± 2694.28
Myeloid	884.25 ± 274.14	559.80 ± 156.93	8114.20 ± 1467.82**	7011.60 ± 1498.68**
Mono/Inf Mf	744.75 ± 142.15	459.80 119.25	2283.80 ± 388.77*	2208.20 ± 433.94**
Res Mf	1032.25 ± 253.16	913.60 ± 156.46	3788.40 ± 410.04***	2776.20 ± 526.04**
Eosinophil	418.25 ± 91.95	213.78 ± 89.98	523.80 ± 69.95	570.00 ± 139.16
Neutrophil	987.25 ± 364.23	585.00 ± 183.07	11713.60 ± 2244.21**	12511.00 ± 2944.10**

¶The data represent the mean ± SEM for n=5-7 mice/group. General ANOVA with Fisher's unprotected LSD post-test for comparisons between peripheral blood and white adipose tissue of wildtype (grey) or db/db (blue) mice; *P<0.05, **P<0.01, ***P<0.001. Mono/Inf Mf, monocyte (blood)/inflammatory macrophages (WAT); Res Mf, resident macrophages; cDC, conventional dendritic cell.

levels of cell surface Hpse than T cells in the same compartments. The failure to demonstrate a significant decline in cell surface Hpse in db/db WAT B cells may be due to the small size (~3-7% of total leukocytes) of the populations in WAT (SVF; **Table 6.1**).

Conventional dendritic cells (cDCs) showed a higher expression of Hpse in the WAT of wt and db/db mice compared to PB, but these differences did not achieve statistical significance (**Table 6.2**). This finding may be due to the small populations of cDCs in PB (~0.6-0.8%) and WAT (~7.7%-8.3%). Interestingly, Hpse expression by $CD11c^{+}Ly6C^{+}$ cells were dramatically reduced to 29.8% in the WAT of db/db mice, compared to db/db PB; however statistical significance was not established (**Table 6.2**). No significant differences were observed in the cell surface expression of Hpse by $CD11c^{+}Ly6G^{+}$ cells in the WAT of db/db mice compared to PB (**Table 6.2**). In contrast, wt WAT showed 1.7-fold and 2.6-fold increase in cell surface Hpse levels on $CD11c^{+}Ly6C^{+}$ cells and $CD11c^{+}Ly6G^{+}$ cells, respectively, compared to wt PB (**Table 6.2**). Additionally, these populations expressed 2.3-7.1-fold higher levels of cell surface Hpse in db/db PB compared to wt PB (**Table 6.2**).

In wt and db/db males, myeloid leukocytes in WAT showed a significant 9.2-12.5 fold increase in cell surface Hpse compared to PB (**Table 6.2**). Hpse expressed by wt and db/db WAT inflammatory macrophages showed a significant 3.1-4.8 fold increase compared to PB monocytes (**Table 6.2**). Similarly, resident macrophages in wt and db/db WAT showed a significant 3.0-3.7 fold increase in Hpse expression, compared to wt and db/db PB (**Table 6.2**). No significant changes in Hpse expression was observed by eosinophils in peripheral blood and WAT for both wt and db/db mice (**Table 6.2**). Overall, male wt and db/db mice showed a significant increase in the expression of Hpse on total myeloid cells, resident macrophages, inflammatory macrophages and neutrophils in WAT, compared to corresponding PB.

Hpse expression on the surface of immune cell subsets in males was also normalised to the corresponding level of Hpse on B cells (i.e., GMFR). The normalised Hpse expression for male wt and db/db leukocytes (see Appendix 2.2) resembled the non-normalised data (**Table 6.2**). However, on normalisation, a trend for an increase in the GMFR for myeloid cells, inflammatory macrophages and neutrophils was observed in male db/db WAT

compared to wt WAT but these data did not achieve statistical significance (see Appendix 2.2).

In summary, cell surface Hpse levels are highly elevated in myeloid cells of WAT in wt and db/db mice, compared to PB; in contrast our studies of male wt and db/db lymphoid cells in WAT revealed a significant decline in cell surface Hpse. The high cell surface expression of Hpse on myeloid cell sub-populations correlated with the increased proportion of myeloid cells in WAT compared to blood (**Table 6.1**). Conversely, the decreased expression of Hpse on wt and db/db lymphoid cells correlated with the reduced lymphoid cell population in WAT. These same trends were also found in female wt and db/db mice, establishing cell surface Hpse as a robust marker of myeloid leukocytes (excluding eosinophils) in WAT (**Figures 6.6, 6.7 and 6.8**).

6.2.7 Leukocyte sub-populations in PB and WAT of PI-88 treated db/db mice

6.2.7.1 Female db/db mice

Based on our findings that Hpse is expressed at significantly higher levels on myeloid cells in WAT of wt and db/db mice, we evaluated whether the distribution of leukocyte sub-populations in PB and WAT was modulated in db/db mice treated with PI-88, a dual activity drug that acts not only as a HS replacer in beta cells (Ziolkowski et al., 2012) but also as a potent Hpse inhibitor (i.e., HS replacer/ Hpse inhibitor). These analyses were carried out on the same mice treated with PI-88 in Chapter 5 (see Section 5.2.3).

In Section 5.2.3, female and male db/db mice were treated with PI-88 (10 mg/kg/day, i.p.) or saline (diluent control) for 35 days. In parallel with our investigations of the effects of PI-88 treatment on glycaemia (and indirectly on beta cell survival), we analysed leukocyte sub-populations in the blood and WAT PI-88 treated db/db mice, compared to saline treated controls. Upon termination of treatment, PB and WAT were harvested, and leukocyte sub-populations as well as cell surface Hpse levels were analysed by flow cytometry (see Section 2.10).

Firstly, PI-88 treated and control saline treated female db/db mice showed no significant difference in peri-ovarian WAT weight i.e., 1.64 ± 0.29 gm vs 1.55 ± 0.25 gm, respectively (**Figure 6.11(a)**). The leukocyte population in the peripheral blood of PI-88

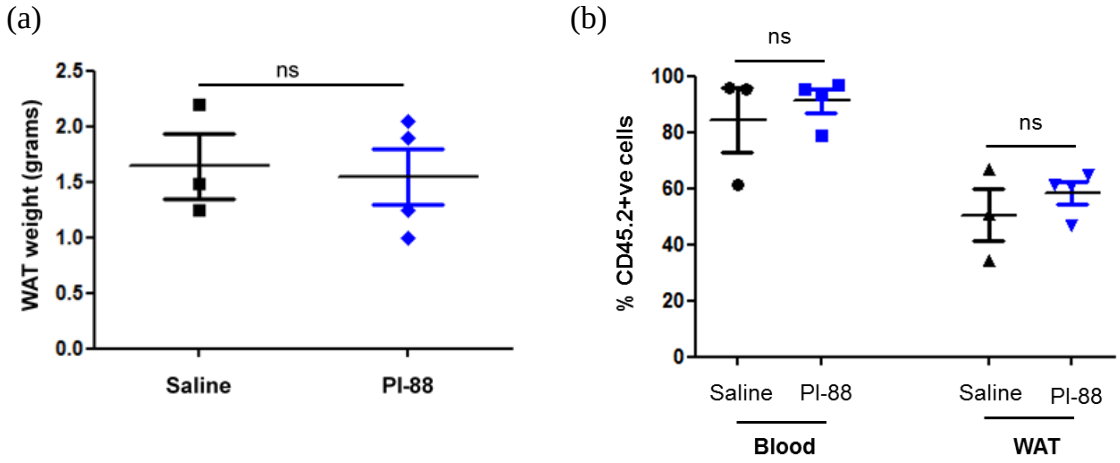

Figure 6.11: WAT weight and leukocyte content of PB and WAT in PI-88 treated and saline treated female db/db mice.

(a) The weight of peri-ovarian white adipose tissue (WAT) was determined for db/db mice treated with PI-88 (10 mg/kg/day i.p.) or i.p. saline (from Figure 5.18, Section 5.2.3). (b) Db/db fat pads as well as peripheral blood (PB) were analysed by flow cytometry for $CD45.2^+$ leukocytes. No significant differences were observed between saline- and PI-88-treated db/db mice for WAT weight and $CD45.2^+$ leukocytes as a % of the total cell population (gated to exclude cell debris and doublets) in PB or WAT. The data represent the mean GMFI ± SEM for n= 3-4 mice/group. Mann-Whitney test; ns, not significant.

treated mice increased 1.2-fold, compared to controls; however this increase was not statistically significant (**Figure 6.11(b)**). In contrast, the $CD45.2^+$ leukocyte population (as % of total cells) in WAT tissue was similar for saline and PI-88 treated mice.

When leukocyte sub-populations were examined no significant differences were observed in PB or WAT between PI-88 treated and saline-treated control mice (**Figure 6.12**). However, in WAT from PI-88 treated mice, there was a trend towards a decline in the population of inflammatory macrophages down to 72.1% of corresponding saline controls (5.24 ± 1.66 vs 7.27 ± 1.26; **Figure 6.12(j)**). Since we demonstrated that an increased inflammatory macrophage population is a distinguishing property of db/db WAT (compared to wt WAT; **Figure 6.4**), this observed trend may suggest that PI-88 treatment impaired the accumulation of inflammatory macrophages in db/db WAT. Consistent with this, no other WAT leukocyte sub-population showed marked changes due to PI-88 treatment (**Figure 6.12**). PI-88 treatment however did not significantly lower the cell surface expression of Hpse on WAT myeloid sub-populations (resident macrophages, inflammatory macrophages, neutrophils) previously found to express heightened levels of Hpse, compared to corresponding populations in PB (**Figures 6.6 and 6.13**). This finding is consistent with PI-88 acting as an inhibitor of only the catalytic activity of Hpse (Ziolkowski et al., 2012) and not the expression of Hpse protein.

6.2.7.2 Male db/db mice

Like PI-88 treated female db/db mice, PI-88 treatment of male db/db mice increased the leukocyte population in PB by 1.2-fold, compared to control db/db mice (**Table 6.3**). Within the WAT microenvironment, no significant reduction in the relative proportion of leukocyte populations was observed in PI-88 treated mice; nevertheless, there was a trend for total myeloid and neutrophil sub-populations to be lower (~88% and ~83% of corresponding saline treated control db/db mice, respectively; **Table 6.3**). Consistent with the analyses of PI-88 treated female db/db mice (see Section 6.2.7.1), PI-88 treatment did not reduce the level of cell surface Hpse on total myeloid cells or on most myeloid sub-populations (inflammatory macrophages, resident macrophages, neutrophils) in WAT (**Table 6.4**).

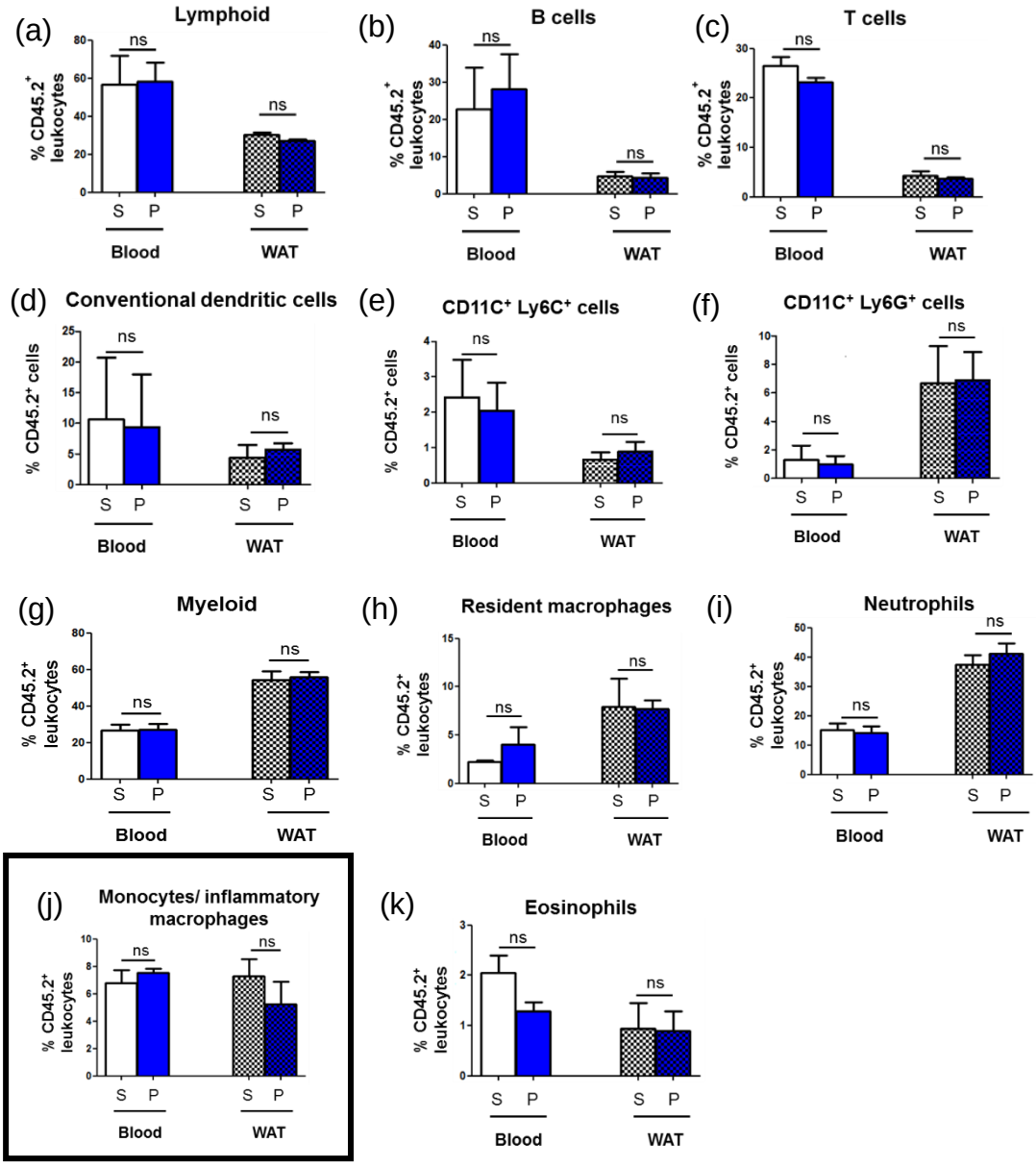

Figure 6.12: Leukocyte sub-populations in peripheral blood and WAT of db/db females treated with PI-88 or saline.

Peripheral blood (PB) and peri-ovarian white adipose tissue (WAT) were collected from db/db females treated for 35 days with PI-88 or saline (Section 5.2.3). The PB and WAT (SVF) were stained for leukocyte markers and analysed by flow cytometry. Using the gating strategy in Figures 2.13 and 2.14, leukocyte subpopulations (expressed as % of total $CD45^+$ population of leukocytes) were determined. No significant changes were observed in the leukocyte sub-populations between saline or PI-88 treated db/db mice. The data represent the mean ± SEM for n= 3-4 mice/group. Mann-Whitney test; ns, not significant. S, Saline; P, PI-88.

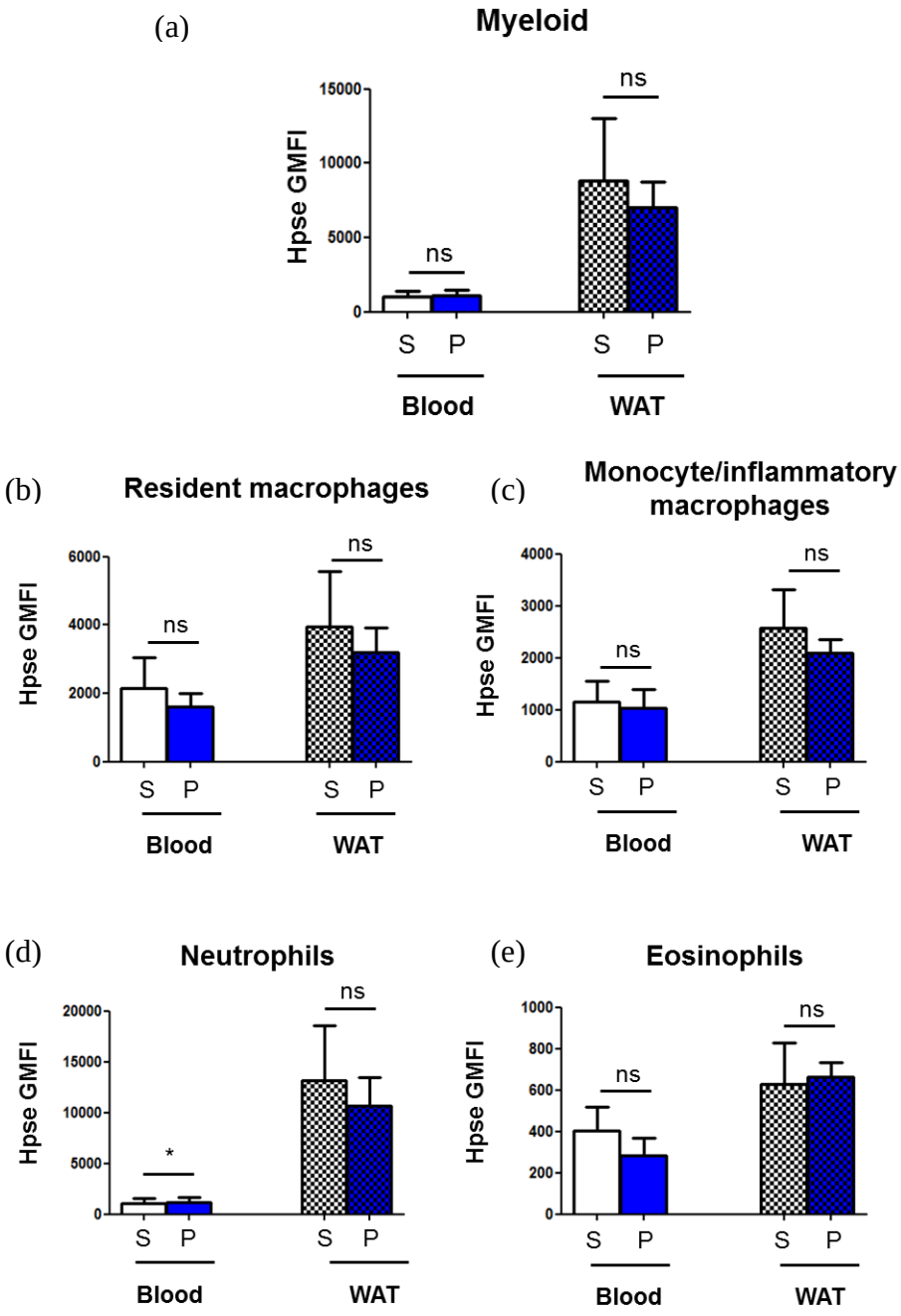

Figure 6.13: Hpse expression on myeloid sub-populations in PB and WAT of PI-88 or saline treated female db/db mice.

Upon termination of PI-88 or saline treatment of female db/db mice (from Section 5.2.3), the blood and WAT were stained for leukocyte markers and cell surface Hpse, for analysis by flow cytometry. Using the gating strategy in Figures 2.13 and 2.14, Hpse expression on the CD45.2^{+} leukocyte sub-populations was determined. Hpse expression on the cell surface was not significantly altered by PI-88 treatment. The data represent the mean ± SEM for n= 3-4 mice/group. Mann-Whitney test; ns, not significant. S, Saline; P, PI-88.

Table 6.3: Innate and adaptive immune cell populations in peripheral blood (PB) and WAT of Saline and PI-88 treated male db/db mice.

Cell type	Peripheral blood (PB)¶		WAT ¶	
	Saline	PI-88	Saline	PI-88
% $CD45^+$ cell	95.13 ± 2.17	96.88 ± 0.93	53.13 ± 2.13	63.88 ± 3.63
Lymphoid	63.97 ± 5.05	60.36 ± 4.73	26.67 ± 3.03	25.68 ± 3.59
B cell	22.33 ± 2.05	30.22 ± 4.67	5.79 ± 0.76	4.63 ± 2.35
T cell	31.03 ± 2.85	22.48 ± 0.52	5.70 ± 0.26	5.39 ± 1.09
cDC	0.57 ± 0.06	0.92 ± 0.09	4.70 ± 1.08	7.65 ± 0.82
$CD11c^+Ly6C^+$	0.29 ± 0.13	0.50 ± 0.14	0.65 ± 0.19	0.68 ± 0.37
$CD11c^+Ly6G^+$	0.35 ± 0.16	0.49 ± 0.16	9.08 ± 0.98	13.58 ± 0.89
Myeloid	32.10 ± 5.00	34.04 ± 5.29	55.53 ± 2.34	49.28 ± 2.75
Mono/Inf Mf	4.27 ± 0.90	6.74 ± 1.38	4.06 ± 0.79	3.96 ± 1.94
Res Mf	1.13 ± 0.12	2.23 ± 0.38	5.32 ± 0.88	7.77 ± 0.77
Eosinophil	1.63 ± 0.54	2.40 ± 0.85	1.17 ± 0.77	0.43 ± 0.10
Neutrophil	24.77 ± 3.64	22.34 ± 4.09	44.33 ± 2.69	36.68 ± 2.50

¶The data represent the mean ± SEM for n= 3-5 mice/group. Mann-Whitney test was performed for comparisons between peripheral blood and adipose tissue. No significant differences were observed in PB or WAT between mice that were treated with PI-88 or saline. Mono/Inf Mf, monocyte (blood)/inflammatory macrophages (WAT); Res Mf, resident macrophages; cDC, conventional dendritic cell.

Table 6.4: Cell surface heparanase (Hpse) expression by immune cells (represented as GMFI) in peripheral blood and WAT of Saline and PI-88 treated mice.

Cell type	Peripheral blood (PB; Hpse GMFI)¶		WAT (Hpse GMFI)¶	
	Saline	PI-88	Saline	PI-88
Myeloid	1286.00 ± 480.02	1325.80 ± 379.99	8858.33 ± 3479.46	8633.60 ± 1009.15
Mono/Inf Mf	1551.33 ± 641.24	1571.80 ± 529.45	2203.33 ± 883.53	2521.60 ± 419.11
Res Mf	1506.67 ± 460.07	1809.20 ± 320.19	3635.67 ± 1789.22	3859.40 ± 613.63
Eosinophils	810.67 ± 277.58	967.20 ± 292.58	606.67 ± 208.79	792.80 ± 118.93
Neutrophils	1253.33 ± 469.59	1238.00 ± 345.91	13123.67 ± 5916.58	11786.80 ± 1241.14

¶The data represent the mean ± SEM for n= 3-5 mice/group. Mann-Whitney test was performed for comparisons of PB or WAT between Saline or PI-88 treated mice. No significant differences were observed in PB or WAT between mice that were treated with PI-88 or saline. Mono/Inf Mf, monocyte (blood)/inflammatory macrophages (WAT); Res Mf, resident macrophages, cDC, conventional dendritic cell.

6.3 Discussion

Db/db mice carry a homozygous point mutation in the leptin receptor gene which results in over eating (hyperphagia) and the development of obesity, insulin resistance and hyperglycaemia (Chan et al., 2011, Chen et al., 1996, Kobayashi et al., 2000). Our data showed a significant increase (5.2-5.6-fold) in the peri-gonadal fat pads of female and male db/db mice compared to corresponding lean controls (**Figures 6.2 and 6.9**). This property is largely responsible for the increase in body weight of db/db mice during the development of T2D (**Figures 3.1 and 3.18**), as reported by other groups (Lee et al., 2010a, Boucher et al., 2005, Kim et al., 2016).

Previous studies have reported that the increased accumulation of fat in peripheral tissues (adipose tissue, liver and skeletal muscle) plays a critical role in the development of insulin resistance and T2D (Dandona et al., 2004, Weisberg et al., 2003, Sell et al., 2012, Rosen and Spiegelman, 2006, McArdle et al., 2013, Kammoun et al., 2014). Excessive nutrient intake and/or little energy expenditure contributes to the excessive accumulation of fat in adipose tissue. In turn, the altered properties of adipocytes lead to adipose tissue dysfunction (see Section 1.6) and local as well as systemic inflammation comprising innate and adaptive immune cell populations (Cildir et al., 2013, Chmelar et al., 2013, Schipper et al., 2012). Altered profiles of immune cells have also been observed in peripheral blood, spleen, liver and adipose tissue of diet-induced obesity (DIO) mouse models (Winer et al., 2011, Talukdar et al., 2012, Wu et al., 2007), mutant rodent models of T2D (Fujimoto et al., 2010, Tamura et al., 2008) as well as in humans with T2D (Kammoun et al., 2014, Donath and Shoelson, 2011, Wu et al., 2007). Interestingly, adipose tissue inflammation is not only observed during weight gain and fat accumulation but has also been observed in situations of severe weight loss, as observed in caloric restriction or post-bariatric procedures (Mraz et al., 2011, Mancuso, 2016). Obese humans (with and without T2D) with severely depleted fat reservoirs showed increased transcripts for pro-inflammatory cytokines in subcutaneous white adipose tissue (Maurizi et al., 2018). These reports suggest that rapid and extreme changes in body fat and not only weight gain, can trigger an immune response to adipose tissue (Maurizi et al., 2018, Dolezalova et al., 2007). Thus, the increase in fat pad weight observed in db/db mice is likely to contribute to adipose tissue dysfunction and trigger or exacerbate inflammation in host WAT. In this Chapter we carried out comparative studies of leukocyte sub-

populations in the circulation and white adipose tissue of db/db mice and wt (lean) controls.

(i) Leukocytes sub-populations in WAT and peripheral blood

Our data demonstrated no significant differences in the total leukocyte content (i.e., measured as % $CD45.2^+$ cells in the total cell population) in the WAT and PB of female and male db/db mice, compared to corresponding controls (**Figures 6.1 and 6.10**). These data are inconsistent with other reports showing an increase in leukocyte sub-populations in the WAT of diet-induced obesity (DIO) and mutant mouse models including db/db mice (Olefsky and Glass, 2010, Zheng et al., 2016, Xu et al., 2003, Talukdar et al., 2012, Maurizi et al., 2018, Mraz and Haluzik, 2014, Tamura et al., 2008). Such findings have supported a role for WAT inflammation in insulin resistance and T2D. To help resolve this discrepancy we further characterised leukocyte sub-populations (innate and adaptive immune cells) in the circulation and white adipose tissue of db/db mice and wt controls.

Generally, analyses of leukocytes in the circulation (Kammoun et al., 2018, Nagareddy et al., 2014, McFarlin et al., 2012) and/or in adipose tissue (Talukdar et al., 2012, Winer et al., 2011, Xu et al., 2003, Weisberg et al., 2003, Stefanovic-Racic et al., 2012, Shaul et al., 2010, Nguyen et al., 2007, Wentworth et al., 2010, Lumeng et al., 2007b, McFarlin et al., 2012) of glucose-intolerant, insulin-resistant obese mouse strains have been restricted to only a few sub-populations. Unlike previous studies of obese mice, we directly compared a range of leukocyte sub-populations in the peripheral blood and white adipose tissue of the same donor db/db (obese) and wt (lean) mice. We defined leukocyte sub-populations using cell surface markers commonly used for defining subsets in peripheral blood i.e., CD11c (+ or -), CD11b (hi or lo), Ly6C (hi or lo), Ly6G (+ or -), Siglec F (hi or lo), B220 (hi) or CD3 (hi) (see Section 2.10, **Figures 2.13 and 2.14** for the gating strategy for PB and WAT; see **Table 2.1** for the cell surface markers used to define leukocyte sub-populations). Interestingly, we found that a significant ~4-fold increase in the inflammatory macrophage ($CD11b^{hi}$ $Ly6C^{hi}$) sub-population of WAT leukocytes in both female and male db/db mice compared to wt controls, directly correlated with a significant 2.3-2.7-fold increase in the monocyte ($CD11b^{hi}$ $Ly6C^{hi}$) sub-population of peripheral blood leukocytes in the same db/db mice (**Figure 6.4 and Table 6.1**). Thus, while the overall $CD45.2^+$ leukocyte content of db/db peripheral blood was similar to lean

controls, the monocyte sub-population differed markedly. Although female and male db/db WAT was also characterised by unchanged levels in the total leukocyte population (i.e., in the SVF), a significant increase in the inflammatory macrophage sub-population was found for both female and male db/db WAT. Our study support previous report of increased levels of monocytes (in addition to WAT) in diet-induced obesity (DIO) mice model (McFarlin et al., 2012). These findings suggest that increased levels of circulating monocytes represent a peripheral biomarker of obesity-driven inflammation in WAT.

The molecular mechanism responsible for the elevated monocyte population in the circulation of obese mouse strains has been investigated by other groups. Nagareddy et al. (2014) identified an enhanced production of myeloid progenitors in the bone marrow and attributed this to systemic effects of the cytokines IL-1β produced by WAT macrophages. Furthermore, they observed that glucose-intolerant, insulin-resistant ob/ob mice, treatment with the IL-1R antagonist Anakinra improved glycaemic control following oral challenge with glucose. More recently, Kammoun et al. (2018) failed to observe an improvement in the glycaemia of db/db mice following *in vivo* treatment with MCC950, an inhibitor of IL-1β production by the NLRP3 inflammasome. They observed that monocytosis in db/db mice was not due to local effects in the islet microenvironment. Indeed these findings suggest that treatment with Anakinra, to neutralise secreted IL-1β is a more effective approach than attempts to inhibit IL-1β production via the NLRP3 inflammasome. Nevertheless, our findings in db/db WAT support reports by other groups that WAT in db/db as well as ob/ob and DIO-mice exhibit a striking increase in the population of inflammatory macrophages, compared to corresponding lean controls (Lumeng et al., 2007a, Wentworth et al., 2010, Xu et al., 2003, Weisberg et al., 2003, Kraakman et al., 2015, Tamura et al., 2008).

Studies of DIO models of insulin resistance and T2D in particular, have classified inflammatory and resident macrophage populations in obese and lean WAT using MI and M2 terminology, largely based on properties related to macrophage function. M1 macrophages are characterised by pro-inflammatory properties whereas M2 macrophages are anti-inflammatory (Kammoun et al., 2014, Kraakman et al., 2014). In lean WAT, resident macrophages express the M2 anti-inflammatory phenotype with increased IL-10 gene expression (Lumeng et al., 2007a). M2 macrophages carry the cell surface markers

CD11b, F4/80, CD301 and CD206 and via IL-10 production, promote insulin sensitivity by protecting against TNF-α induced insulin resistance (Olefsky and Glass, 2010, Lumeng et al., 2007a, Kraakman et al., 2015, Kraakman et al., 2014). This function forms an important part of their role in tissue surveillance and homeostasis. Furthermore, resident or M2 macrophages in lean WAT can be maintained by self-proliferation, most likely regulated by IL-4 produced by local eosinophils (Kraakman et al., 2014, Wu et al., 2011). However, it is currently unclear whether circulating monocytes also contribute to the resident macrophage population; this contribution may vary depending on the mouse model of T2D under investigation. IL-4 also induces the expression of peroxisome proliferator activated receptor gamma (PPARγ) and delta (PPARδ) which are required to maintain the M2 polarisation state (Odegaard et al., 2007, Desvergne, 2008, Kang et al., 2008).

In obese WAT, the relative proportion of M2 and M1 macrophages is dramatically altered, with a predominance of inflammatory M1 macrophages. These M1 macrophages carry $CD11c^{+}$, CD11b and F4/80 cell surface markers and produce TNF-α, IL-1β, IL-6 and nitric oxide (Lumeng et al., 2007a, Martinez and Gordon, 2014, Shaul et al., 2010). Specifically, inflammatory M1 macrophages have been found in crown-like structures (CLS) associated with dead or dying adipocytes resulting from nutrient excess and hypertrophy (Lumeng et al., 2007a, Nguyen et al., 2007, Lumeng et al., 2008). The local release of pro-inflammatory cytokines such as TNF-α has been proposed to promote insulin resistance in adipocytes by activating c-Jun N-terminal kinases (c-JNKs) and thereby blocking insulin signalling (Nguyen et al., 2007, Kanety et al., 1995, Zeyda and Stulnig, 2009). In support, the recruitment of M1 inflammatory macrophages has been shown to precede the elevation of plasma insulin (Xu et al., 2003, Weisberg et al., 2003). Furthermore, adipocytes in obese WAT release free fatty acids and inflammatory mediators including pro-inflammatory cytokines and MCP-1 (CCL2) in response to cellular stress, resulting in the recruitment of monocytes from the circulation. Within the adipose tissue microenvironment, monocytes differentiate into pro-inflammatory M1 macrophages which in turn are stimulated by adipocyte-derived inflammatory mediators to produce inflammatory cytokines (TNF-α, IL-6, IL-1β) (Kraakman et al., 2014, Suganami and Ogawa, 2010, Suganami et al., 2005, Oh et al., 2012). These processes

together with local hypoxia set up a "vicious cycle" of inflammation in obese adipose tissue (Suganami et al., 2005, Fujisaka et al., 2013).

In this chapter, we demonstrated no significant differences in the resident macrophage population in wt and db/db WAT. However, our studies indicate that $CD11c^{-}CD11b^{+}$ $Ly6C^{hi}$ inflammatory macrophages contribute significantly to obese WAT in db/db mice. In view of the established role for $CD11c^{+}$ inflammatory macrophages in DIO (obese) WAT (Wentworth et al., 2010, Shaul et al., 2010, Nguyen et al., 2007, Patsouris et al., 2008, Lumeng et al., 2007a), we also investigated the contribution of $CD11c^{+}$ leukocytes to the inflammatory response in db/db WAT. We found no increase in the population of conventional dendritic cells, compared to lean wt WAT. This finding disagrees with the studies of Stefanovic-Racic et al. (2012) which demonstrated a significant ~2-fold increase in conventional DCs in WAT from DIO mice. We attribute this discrepancy to the different models of T2D in db/db and DIO mice. Nevertheless, we identified enlarged populations of $CD11c^{+}Ly6C^{hi}$ and $CD11c^{+}Ly6G^{hi}$ leukocytes in db/db WAT. A significant 5.3-5.5-fold and a marked 2.1-2.2-fold increase in $CD11c^{+}Ly6G^{+}$ cells and $CD11c^{+}Ly6C^{+}$ cells, respectively, were observed in both male and female db/db WAT compared to wt WAT (**Figure 6.5 and Table 6.1**); however no significant differences were observed in the PB of wt and db/db mice. These data support a role for $CD11c^{+}$ leukocytes (excluding cDCs) in db/db WAT inflammation.

Unlike previous studies showing increased circulating neutrophils in ob/ob mice and db/db mice compared to lean controls (Kammoun et al., 2018, Nagareddy et al., 2014), we failed to observe a significant elevation in circulating neutrophils in both female and male db/db mice. This discrepancy may be due to the use of different models of obesity (Nagareddy et al., 2014) and the broader age range of db/db mice in our study, compared to 6 week db/db mice in the study by Kammoun et al. (2018). Supporting the latter explanation, Elgazor-Carman et al. (2008) reported that neutrophils are recruited early (e.g., by 3 days) to WAT in DIO mice. It is therefore possible that in db/db mice, the mobilisation and recruitment of neutrophils to obese WAT may occur at an early age (e.g., 6 weeks) and could be resolved at older ages. Although we observed a significant increase in the neutrophil population in obese WAT of female db/db mice (**Figure 6.4**), compared to wt lean controls, male db/db WAT failed to show this trend (**Table 6.1**). Studies of

DIO mice have demonstrated an important role for neutrophils in aiding the recruitment of monocytes to obese WAT and in contributing to insulin resistance via the production of neutrophil elastase (Talukdar et al., 2012). Our study, however, does not demonstrate a consistent role for neutrophils in db/db WAT inflammation. Thus a relationship between circulating neutrophils and the neutrophil population in WAT was not established in db/db mice.

We observed a trend for a reduced eosinophil population in WAT of female and male db/db mice but not in the peripheral blood (**Figure 6.4 and Table 6.1**). Similarly, Wu et al. (2011) reported a reduction in eosinophils in the obese WAT of DIO and ob/ob mice. These findings are consistent with a role of eosinophil-derived IL-4 in maintaining M2 anti-inflammatory macrophages in WAT (Wu et al., 2011, Goh et al., 2013). Furthermore, we found no significant differences in sub-populations of T cells or B cells between wt and db/db WAT in male or female mice (**Figure 6.3 and Table 6.1**).

Our findings argue against an increase in the populations of T cells and B cells, as demonstrated in the adipose tissue of DIO mouse models (Winer et al., 2011, Duffaut et al., 2009, Wu et al., 2007, Xu et al., 2003). $CD8^+$ T cells were found to be increased in the epididymal WAT of DIO obese mice whereas the number of $CD4^+$ T cells were reduced (Nishimura et al., 2009, Winer et al., 2011). These studies suggested that $CD4^+$ T cells may play a suppressive role in the development of obesity-induced inflammation and insulin resistance whereas $CD8^+$ T cells might be responsible for shifting the polarisation of macrophages from an M2 to M1 phenotype (Winer et al., 2009). Interestingly, the depletion of T cells reduced the infiltration of WAT macrophages, decreased adipose tissue inflammation and improved insulin resistance (Nishimura et al., 2009). In support, T and B cells precede the infiltration of AT by macrophages (Kintscher et al., 2008, Sell et al., 2012, Winer et al., 2009). Moreover, several studies have shown an early recruitment of B cells in visceral AT (VAT) and WAT of DIO mice, promoting T cell activation and the production of pro-inflammatory cytokines (Winer et al., 2011, DeFuria et al., 2013). A reduction in VAT inflammation was observed in DIO/HFD B^{null} mice (mμ heavy chain knockout mice) which failed to produce mature B cells. Furthermore, B cell depletion in HFD C57BL/6 mice using anti-CD20 mAb reduced blood glucose levels and improved glucose and insulin tolerance (Winer et al., 2011). T

cells and B cells can therefore modulate AT in obesity and T2D. We speculate that the apparent absence of significantly enhanced T cell and B cell populations in db/db WAT may be due to the leptin receptor deficiency in these mice. Normal mouse lymphocytes carry leptin receptors and leptin exerts direct effects on T cells *in vitro* (Lord et al., 1998). Leptin has pro-inflammatory effects on lymphocytes because of its structural similarity to pro-inflammatory cytokines like IL-6 (Fantuzzi and Faggioni, 2000), and stimulates the production of IL-6, TNF-α and MCP-1 from immune cells (Fernandez-Riejos et al., 2010). Leptin-deficient ob/ob and leptin receptor-deficient db/db mice display marked thymic atrophy and can exhibit defective immune responses (Palmer et al., 2009, Palmer et al., 2006, Mandel and Mahmoud, 1978, Fujita et al., 2002, Hick et al., 2006). Furthermore, lymphocytopenia has been reported in db/db mice (Nagareddy et al., 2014, Kimura et al., 1998), a property which would impair their significant contribution to WAT inflammation. In line with this, our study has demonstrated a trend for reduced lymphoid cell populations in the peripheral blood and adipose tissue of db/db mice compared to wt controls.

(ii) Hpse expression by leukocyte sub-populations in PB and WAT

In parallel with our studies of leukocyte sub-populations, we investigated whether the expression of Hpse, a HS-degrading endoglycosidase, correlated with the recruitment of leukocyte sub-populations from the peripheral blood to adipose tissue in lean wt and obese db/db mice. In order for leukocytes to passage from the circulation to sites of inflammation such as obese WAT, they must traverse the sub-endothelial basement membrane (BM). Conventionally, this BM consists of matrix proteins (laminin, type IV collagen and nidogen) and the heparan sulfate proteoglycan perlecan (Yurchenco, 2011, Timpl and Brown, 1996). To facilitate their migration through this BM, leukocytes produce degradative enzymes including a range of proteases (e.g., cathepsins, metalloproteases) and Hpse. Catalytically active Hpse plays a critical role by degrading the HS chains of perlecan, thereby disrupting the tightly-arranged matrix network and allowing the leukocytes to migrate to the underlying tissues (Parish, 2006). During this process, chemokines bound to HS in the BM are released to provide directional migration toward inflamed tissue sites (Parish, 2006, Vlodavsky and Friedmann, 2001, Parish et al., 2001).

Our normalised and non-normalised heparanase data showed a significant and striking elevation in the cell surface expression of heparanase by myeloid cells, including inflammatory macrophages and neutrophils in the WAT of both wildtype and db/db mice, compared to the same populations in peripheral blood (**Figure 6.6 and Table 6.2**). In contrast, lymphoid cells (including B cells and T cells) and $CD11c^+$ leukocytes in wt and db/db WAT demonstrated a significantly lower or unchanged expression of Hpse, compared to the corresponding population in peripheral blood (**Figures 6.7 and 6.8**; **Table 6.2**). Thus, only the principal myeloid cell populations that characterise both wt and obese WAT, including the enlarged population of inflammatory macrophages in db/db WAT, highly express Hpse. These findings suggest that Hpse may play an important role in facilitating the migration of myeloid leukocytes (particularly monocytes and neutrophils) to wt and obese WAT. We acknowledge, however, that the anti-Hpse mAb used in a flow cytometry analyses do not distinguish between catalytically active and inactive Hpse. It is noteworthy, however, that macrophages and monocytes have the capacity to secrete cathepsin L which converts the inactive form of Hpse (proenzyme) to its catalytically active form (Reddy et al., 1995, Lerner et al., 2011, Wood and Hulett, 2008, Boels et al., 2017).. An alternative interpretation of our data could relate to the established regulatory role for Hpse in the production of cytokines. Guttor-kapon et al. (2016) reported that macrophages deficient in Hpse produced lower levels of TNF-α, IL-1β, IL-10 and IL-6. Hpse may therefore play a role in facilitating the recruitment of myeloid cell populations to adipose tissue via the local release of HS-bound cytokines/chemokines and/or may help regulate the local production of cytokines, potentially influencing the relative levels of pro-inflammatory or anti-inflammatory cytokines in the local adipose tissue environment. Western blotting studies could be done in the future to further elucidate the role of active and inactive Hpse in the white adipose tissue of wildtype and db/db mice.

(iii) PI-88 treatment of db/db mice

Based on our Hpse expression studies, we examined whether PI-88 mediated inhibition of Hpse in db/db mice (see Chapter 5, Section 5.2.3) could modify the inflammatory response to obese white adipose tissue. While we observed a trend towards a decrease in the inflammatory macrophage population in the WAT of PI-88 treated female db/db mice, no improvement in glycaemic control was observed (see Section 5.2.3). Pulse labelling

of macrophages in HFD-fed mice has previously revealed that adipose tissue macrophages are generally replaced after 8 weeks (Lumeng et al., 2007b). It is therefore possible that extending the period of PI-88 treatment from 5 weeks to over 8 weeks may be needed in future studies to better assess the role of Hpse in modulating the recruitment of inflammatory macrophages, their cytokine production and downstream effects on insulin sensitivity in db/db WAT. For future studies, treatment of db/db and HFD-mice (prior to and during HFD-feeding) with a Hpse inhibitor could potentially prevent the progression of glucose intolerance and reduce insulin resistance by decreasing adipose tissue inflammation.

In summary:

- The population of myeloid leukocytes, specifically monocytes/inflammatory macrophages and neutrophils, was increased in the PB and WAT of db/db mice compared to lean controls. In db/db WAT, the populations of $CD11c^{+}Ly6C^{+}$ and $CD11c^{+}Ly6G^{+}$ cells were also elevated. These data suggest that inflammatory macrophages, neutrophils and $CD11c^{+}$ sub-populations play an important role in the enhanced inflammation of white adipose tissue in db/db mice.
- Elevation in the population of WAT inflammatory macrophages correlated with an increased population. Circulating levels of monocytes may therefore act as a biomarker of adipose tissue inflammation and obesity-induced insulin resistance.
- Increased expression of cell surface heparanase by the total myeloid population (including resident macrophages, inflammatory macrophages and neutrophils) in WAT of both wt and db/db mice, compared to peripheral blood, suggests that Hpse may play a critical role in the migration of leukocytes to white adipose tissue to maintain homeostasis and to establish obesity-induced inflammation, respectively.
- Short-term treatment of db/db mice with the Hpse inhibitor PI-88 did not significantly reduce the leukocyte populations in WAT; however, a trend toward a decrease in the inflammatory macrophage population was observed in the WAT of PI-88 treated db/db mice, compared to saline controls.
- Cell surface heparanase represents a marker of adipose tissue myeloid leukocytes in both lean and obese mice. Long-term treatment with a Hpse inhibitor could

potentially reduce adipose tissue inflammation and thereby improve insulin resistance and glucose tolerance.

Chapter 7: General discussion

7.1 Rationale

Heparan sulfate (HS) is a highly sulfated linear polysaccharide that contains repeating units of glucosamine and uronic acid (Iozzo, 2001, Simon Davis and Parish, 2013, Esko and Lindahl, 2001). HS chains are synthesised directly onto a heparan sulfate proteoglycan (HSPG) core protein forming a HSPG (Bernfield et al., 1999, Esko and Lindahl, 2001, Iozzo, 2001). HSPGs are characterised by their core proteins and are conventionally expressed on the cell surface (e.g., syndecans, glypicans), in basement membranes (BMs; e.g., perlecan) and in extracellular matrices (ECMs; e.g., collagen type XVIII, agrin). Due to the structural heterogeneity of HS chains, HS serves as a cell adhesion molecule and as a reservoir for a wide range of molecules including cytokines, growth factors, chemokines, proteases and lipases (Parish, 2006, Dreyfuss et al., 2009, Esko and Lindahl, 2001, Simon Davis and Parish, 2013). Furthermore, HS plays a regulatory role in various physiological processes such as development, cell proliferation and differentiation, migration, inflammation, angiogenesis and wound healing (Parish, 2006, Bishop et al., 2007, Powers et al., 2000, Parish, 2005, Rops et al., 2004).

Recent studies in the Simeonovic lab demonstrated that islet beta cells express high levels of intracellular HS *in situ*. Surprisingly, HS was found to play a critical role in the survival of beta cells (Ziolkowski et al., 2012). In addition, Choong et al. (2015) found that the HSPG core proteins collagen type XVIII, syndecan-1 and CD44 were localised inside islet beta cells *in situ*. This finding provided a basis for the unique intracellular localisation of HS in islet beta cells because HS chains cannot be synthesised in the absence of HSPG core proteins (Iozzo, 2001, Sarrazin et al., 2011, Esko and Lindahl, 2001). Together, these studies revealed that islet beta cells express unusually high levels of intracellular HS and HSPG core proteins. Furthermore, these studies showed that islet beta cells lose intracellular HS but not HSPG core proteins during the process of islet isolation *in vitro*. Moreover, certain HS mimetics preserved beta cell viability and protected the beta cells from culture- and reactive oxygen species (ROS)-induced cell death by replacing the lost intracellular HS (Ziolkowski et al., 2012). These findings suggested that HS acts as non-enzymatic antioxidant in beta cells. Progression of autoimmune disease and type 1 diabetes (T1D)-onset in non-obese diabetic (NOD) mice were characterised by depletion of beta cell HS, a finding that correlated with high expression of the HS-degrading enzyme heparanase (Hpse) by insulitis leukocytes.

Furthermore, treatment of NOD mice with the Hpse inhibitor/HS replacer PI-88 significantly reduced the incidence of T1D and improved intracellular levels of beta cell HS. Together, these findings indicated that Hpse-mediated depletion of beta cell HS contributes to beta cell death during the development of T1D (Ziolkowski et al., 2012). Therefore, this project set out to investigate the role of beta cell HSPG core proteins and HS in type 2 diabetes (T2D) in db/db mice.

7.2 ER stress contributes to the loss of HSPG core proteins and HS in T2D beta cells

Pancreatic beta cells are characterised by a highly active endoplasmic reticulum (ER) in which newly synthesised proteins (e.g., proinsulin and HSPG core proteins) undergo chemical modification and folding to achieve their mature conformation. Disruption of ER homeostasis caused by a reduction in protein-folding chaperones, inhibition of protein glycosylation, calcium depletion and certain mutations in proteins (e.g., insulin) results in the accumulation of misfolded proteins in the ER lumen and ER stress (Eizirik et al., 2008, Malhotra and Kaufman, 2007, Yoshida, 2007). A broad range of studies have provided compelling evidence for the existence of ER stress in the pancreatic islets of rodents and humans with both T2D (Marchetti et al., 2007, Laybutt et al., 2007, Chan et al., 2015, Boslem et al., 2011, Chan et al., 2013, Eizirik et al., 2008, Herbert and Laybutt, 2016, Sharma et al., 2015, Ariyasu et al., 2017, Özcan et al., 2006, Oyadomari et al., 2002b, Hasnain et al., 2016, Back and Kaufman, 2012, Araki et al., 2003, Song et al., 2008) and T1D (Engin et al., 2013, Todd et al., 2008, Tersey et al., 2012, Eizirik et al., 2013, Eizirik et al., 2009, Eizirik et al., 2008, Marhfour et al., 2012, Hartman et al., 2004, Brozzi and Eizirik, 2016).

Normally, beta cells compensate for ER stress by activating an adaptive mechanism called the “Unfolded Protein Response” (UPR). The UPR function is to increase the level of ER chaperones, reduce the synthesis of new proteins i.e., by attenuating mRNA translation to proteins, and to remove the accumulated aberrant proteins via ER-associated degradation (ERAD) (**Figure 7.1**) (Eizirik et al., 2008, Yoshida, 2007). Failure of UPR to restore ER homeostasis leads to up-regulated expression of pro-apoptotic UPR genes,

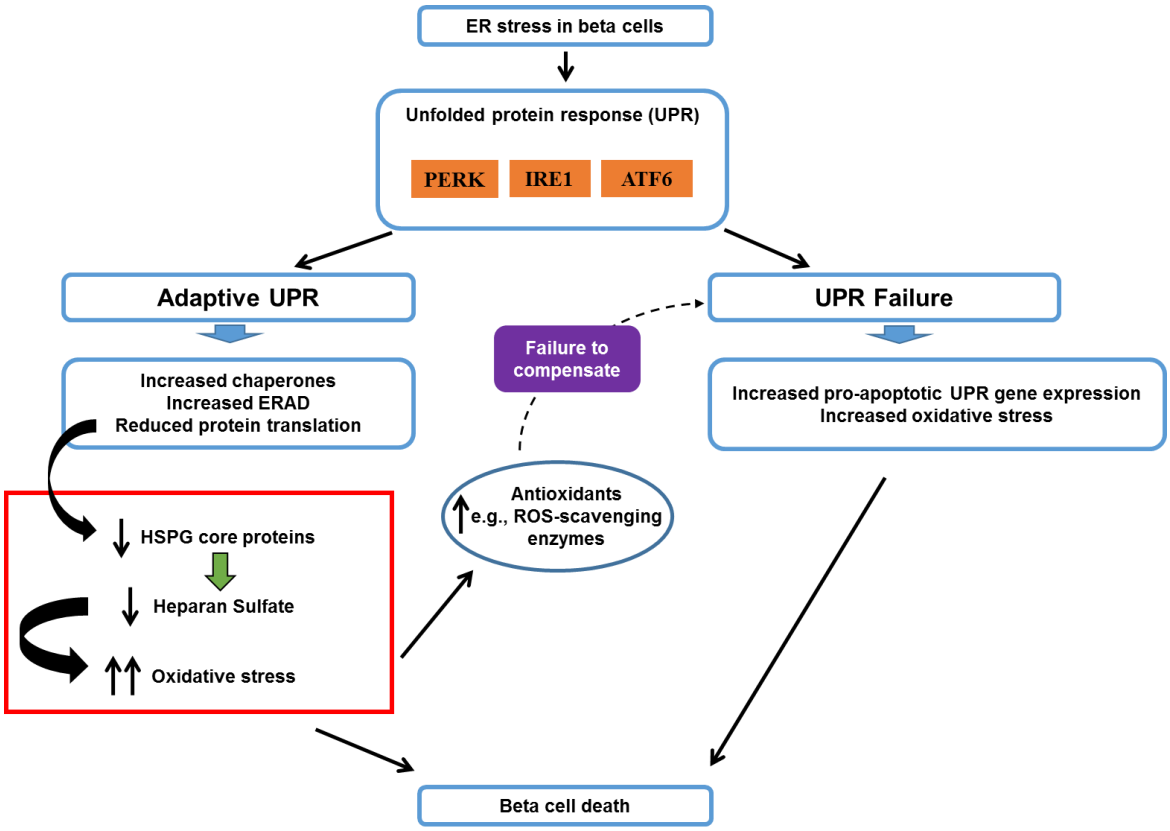

Figure 7.1: ER stress in T2D-prone beta cells.

In pancreatic beta cells, endoplasmic reticulum (ER) stress initiates the unfolded protein response (UPR) by activating the transmembrane sensors PERK, IRE1 and ATF6. Beta cells compensate for this ER stress via the adaptive UPR i.e., by increasing the molecular chaperones for protein folding, increasing ERAD and by reducing the translation of mRNAs to a range of "general" proteins. In T2D development, this reduction in protein synthesis impairs the synthesis of HSPG core proteins which in turn reduces HS synthesis. Depletion of HS in beta cells results in highly elevated oxidative stress and non-apoptotic ROS-dependent beta cell death (see red box). This represent a highly novel mechanism of beta cell death within the framework of the adaptive UPR. ER stress and oxidative stress in remaining beta cells increases the level of antioxidants to maintain beta cell homeostasis. Failure to compensate for this stress results in UPR failure, the expression of apoptotic genes and beta cell apoptosis/death. PERK, protein kinase RNA-like endoplasmic reticulum kinase; IRE1, Inositol-requiring enzyme 1; ATF6, Activation transcription factor 6; ERAD, ER-associated degradation; T2D, type 2 diabetes; HS, heparan sulfate; HSPG, heparan sulfate proteoglycan; ROS, reactive oxygen species.

increased oxidative stress and ultimately beta cell apoptosis (**Figure 7.1**) (Laybutt et al., 2007, Song et al., 2008, Chan et al., 2013, Cnop et al., 2005, Chan et al., 2015, Oyadomari et al., 2002b, Oyadomari et al., 2002a). Other studies have reported that db/db mice at 6 weeks of age showed increased transcript levels of adaptive UPR genes during beta cell compensation (Chan et al., 2013, Herbert and Laybutt, 2016). In contrast, by 16 weeks, there was a reduction in the expression of adaptive genes, an increase in the pro-apoptotic marker ATF3 and overt beta cell dysfunction (Chan et al., 2013). Similarly, islet beta cells in obese ob/ob mice expressed increased adaptive UPR markers at 6 weeks and a further increase in this adaptive gene profile at 16 weeks of age, providing protection from beta cell failure (Chan et al., 2013). The transition from adaptive to apoptotic UPR during ER stress in db/db beta cells is regulated by c-Jun N-terminal kinase (JNK) activation (Chan et al., 2015). These studies revealed that ER stress initially induces beta cell compensation to prolong beta cell function; beta cell dysfunction ensues only when the compensatory response fails to relieve ER stress (Chan et al., 2013, Eizirik and Cnop, 2010, Herbert and Laybutt, 2016, Song et al., 2008).

Our study provides a highly novel mechanism by which the adaptive UPR can contribute to beta cell death in the absence of UPR failure (**Figure 7.1**). ER stress has been previously identified in the islets of normoglycaemic db/db mice at 6 weeks of age (Chan et al., 2013); furthermore, increased BiP staining was observed in the islets of 4 week old db/db mice (Sharma et al., 2015). Our studies confirm and further extend these studies by demonstrating a preferential upregulation in early adaptive UPR genes (BiP, P58) as early as 3.5-4.5 weeks of age in the islets isolated from normoglycaemic db/db mice, compared to corresponding lean controls. In parallel at 3-4 weeks, beta cells showed a dramatic loss of HSPG core proteins and HS in the islets of db/db mice. This depletion in intracellular HS would lead to excessive oxidative stress and beta cell death. Both adaptive and pro-apoptotic UPR markers were highly expressed in the islets of older hyperglycaemic db/db mice (5-9 weeks of age), correlating with a further decline in the levels of HSPG core proteins and HS in the db/db islets. These data suggest that in the short-term, ER stress is associated with the loss of HSPG core proteins and HS in the islets of db/db mice. Future studies could use western blotting and immunofluorescence in parallel to immunohistochemistry to further confirm the changes in HSPG core protein levels and HS, respectively, during T2D development. Our observation that the loss of beta cell

HSPG core proteins and HS occurs before db/db mice become hyperglycaemic, highlights the potential for the adaptive UPR pathway to contribute to beta cell death without activating the pro-apoptotic UPR pathway.

$Ins2^{WT/C96Y}$ Akita mice represent an established model of ER stress-mediated diabetes. We confirmed that ER stress in the beta cells of $Ins2^{WT/C96Y}$ mice also correlated with a loss of intra-islet HPSG core proteins, insulin and HS, compared to corresponding controls. Recent studies of MIN6 beta cells showed intracellular expression of the HSPG syndecan-4 and HS (Takahashi et al., 2012, Takahashi et al., 2017). Our study revealed intracellular expression of the HSPG core proteins collagen type XVIII, syndecan-1 and CD44 as well as highly sulfated HS in normal MIN6 beta cells and weak expression on the cell surface. Furthermore, we observed ER stress-induced loss of both HSPG core proteins and HS, upregulated expression of late UPR (pro-apoptotic genes) and increased cell death. Our findings from these independent models of ER stress resemble the loss of intracellular HS and HSPG core proteins in db/db beta cells. Together, our data provide compelling evidence that ER stress reduces the levels of HSPG core proteins and HS in beta cells *in vitro* and *in vivo*. The chemical chaperone TUDCA has been used previously to enhance the adaptive UPR, relieve ER stress and improve beta cell survival (Xie et al., 2002, Özcan et al., 2006, Ozcan et al., 2009, Uppala et al., 2017). In support, we found that TUDCA treatment of db/db mice improved both non-fasting blood glucose levels and HbA1c levels and upregulated the expression of adaptive UPR genes; significantly, these effects correlated with increased intra-islet expression of HSPG core proteins, HS and insulin. These findings strongly indicate that ER stress plays a critical role in the expression of HSPG core proteins and that alleviating ER stress by enhancing the adaptive UPR gene response improves beta cell levels of HSPG core proteins and consequently, beta cell HS. These outcomes correlated with impaired progression of T2D in db/db mice and support a critical need for intracellular HS for beta cell survival, as demonstrated *in vitro* (see Section 5.2.2). In future studies, the HFD mouse model could be used to further validate that loss of HSPG/HS is due to ER stress and to evaluate whether early treatment with a Hpse inhibitor (commencing before the establishment of ER stress) reduces adipose tissue inflammation.

Intracellular HS has been shown previously to preserve the survival of mouse and human beta cells by serving as a non-enzymatic antioxidant for protecting the beta cells from oxidative stress (Ziolkowski et al., 2012, Simeonovic et al., 2013, Simeonovic et al., 2018). HS is lost during islet isolation and HS replacement using heparin (an HS analogue) protects mouse and human beta cells from culture-induced and ROS-induced beta cell death (Ziolkowski et al., 2012, Choong et al., 2015, Simeonovic et al., 2018). Beta cells exhibit low basal levels of antioxidant enzymes despite generating substantial amounts of ROS/RNS due to disulfide bond formation in the ER mainly during insulin biosynthesis (Yuan et al., 1999, Riemer et al., 2009, Scheuner and Kaufman, 2008, Cao and Kaufman, 2014). Basal or low levels of ROS/RNS exert beneficial effects in beta cells, including elevation of intracellular calcium ions and stimulation of insulin secretion (Hidalgo and Donoso, 2008, Feissner et al., 2009, Supale et al., 2012, Robertson et al., 2004). It has been proposed that high endogenous levels of HS protect beta cells from elevated levels of ROS generated during normal metabolism. In contrast, prolonged exposure to high levels of ROS/RNS is detrimental to beta cells (Supale et al., 2012, Collins et al., 2012, Hasnain et al., 2016) and can depolymerise HS (Rota et al., 2005, Raats et al., 1997, Ziolkowski et al., 2012, Choong et al., 2015). Both ER stress and oxidative stress co-exist in T2D-prone beta cells and unresolved chronic levels contribute to beta cell dysfunction and subsequently overt T2D. Several reports suggest that ER stress may precede oxidative stress (Oslowski et al., 2012, Tang et al., 2012, Chan et al., 2015). Furthermore, beta cell adaptation to elevated hyperglycaemia in Sprague-Dawley rats and improved beta cell survival have been correlated with increased antioxidant gene expression (Laybutt et al., 2002). We propose that normal levels of intracellular HS compensate for the low levels of antioxidant enzymes and protect beta cells from endogenous ROS (Tiedge et al., 1997, Raats et al., 1997). Indeed our *in vitro* studies demonstrated that HS replacement in wildtype (wt) and db/db beta cells protects against hydrogen peroxide-induced cell death (see Section 5.2.2.3). Consequently, during T2D development, the loss of beta cell HSPG core proteins and HS render beta cells highly vulnerable to oxidative stress.

Human beta cells have been reported to express high levels of antioxidant enzymes (e.g., superoxide dismutase (SOD), catalase) i.e., exhibit a robust antioxidant defence mechanism (Welsh et al., 1995, Eizirik et al., 1994). Nevertheless, HS replacement protects human beta cells from excessive hydrogen peroxide-induced damage, suggesting

that multiple protective pathways, including intracellular HS, operate in human beta cells to protect against oxidative damage (Simeonovic et al., 2018). An investigation of the role of intracellular HS in human T2D beta cells is therefore warranted.

Our study has identified that the intracellular loss of HS in db/db beta cells provides a highly novel mechanism by which ER stress contributes to oxidative stress in T2D (**Figure 7.1**). ER stress dramatically impairs the synthesis of HSPG core proteins in the ER due to adaptive UPR, reduces protein translation and thereby diminishes the availability of HSPG core proteins for HS synthesis. Impaired HS synthesis and hence decreased HS expression in the beta cells increases oxidative stress and thereby contributes to beta cell death and T2D development in db/db mice. A time-dependent increase in the mRNA levels of antioxidant enzymes (HO-1, GPx and catalase) was observed in the islets of db/db mice at 6 weeks and 16 weeks of age (Chan et al., 2013), suggesting that beta cells which show an early but mild loss of HS can increase the intracellular expression of antioxidant enzymes (Chan et al., 2013, Hasnain et al., 2014). However, prolonged ER stress may exceed the capacity of these inducible ROS-scavenging enzymes to cope with oxidative stress, resulting in UPR failure.

Heterogeneity exists within the total population of islet beta cells. Recent studies have revealed a role for beta cell heterogeneity in the variability of insulin responses in both human and rodent islets (Dorrell et al., 2016, Bader et al., 2016, Nasteska and Hodson, 2018). Dorrell et al. (2016) have identified four sub-populations of beta cells based on the differential expression of ST8 alpha-N-Acetyl-neuraminide alpha-2,8-sialyltransferase 1 (ST8SIA1) and CD9 i.e., $ST8SIA1^{+}CD9^{-}$, $ST8SIA1^{+}CD9^{+}$, $ST8SIA1^{-}CD9^{-}$ and $ST8SIA1^{-}CD9^{+}$ in normal human adult islets. Furthermore, these populations are altered in T2D with an increase in $ST8SIA1^{+}CD9^{-}$ and $ST8SIA1^{+}CD9^{+}$ beta cells and a decrease in $ST8SIA1^{-}CD9^{-}$ and $ST8SIA1^{-}CD9^{+}$ beta cells (Dorrell et al., 2016). *In vitro* studies have revealed that a polysialylated form of neural cell adhesion molecule (PSA-NCAM) and CDH1 (Bernard-Kargar et al., 2001, Bosco et al., 2007) is highly expressed on beta cells with high insulin secretion capacity. Bader et al (2016) showed that mouse beta cell subsets could be distinguished using the Wnt pathway target gene flattop (Fltp). $Fltp^{+}$ beta cells have improved insulin secretion and mitochondrial function whereas $Fltp^{-}$ beta cells expand during metabolic stress and T2D by

proliferation (Bader et al., 2016). Heterogeneity in secretary vesicle behaviour in rodents and humans has also been identified (MacDonald et al., 2006, Hanna et al., 2009). Insulin exocytosis is restricted to only few beta cells in the islets of db/db mice (Low et al., 2014) and 73% of the beta cells become resistant to stimulation (Do et al., 2014). These studies indicate that different subsets of beta cells exist and differ in their susceptibility to metabolic stress, proliferative capacity and differentiation. Therefore, it is possible that not all beta cells undergo the same level of ER stress i.e., some sub-populations could be more resistant to metabolic stress than others. Further studies need to be conducted to investigate the heterogeneity of db/db beta cells in response to metabolic stress to evaluate whether sub-populations can be classified based on their susceptibility to excessive oxidative stress due to HS depletion or to the pro-apoptotic UPR.

7.3 Loss of beta cell HSPGs and HS represent a common link between T1D and T2D

HS chains are commonly expressed on the cell surface, basement membranes and extracellular matrices. A novel role of HS in beta cell survival and function has recently been identified. HS has been reported to be present in the peri-islet BM (Irving-Rodgers et al., 2008, Korpos et al., 2013) where it acts as a barrier to protect islet against cell invasion. Several studies have also reported an unconventional localisation of HSPG core proteins (collagen type XVIII (Col18) and syndecan-1(Sdc1)) and HS in islet beta cells in different mouse strains (BALB/c, C57BL/6, NOD, NOD/SCID) (Ziolkowski et al., 2012, Choong et al., 2015, Takahashi et al., 2009, Theodoraki et al., 2015, Takahashi et al., 2012, Cheng et al., 2012a) and in human beta cells (Theodoraki et al., 2015, Simeonovic et al., 2018).

Intracellular HS in beta cells has been reported to play a critical role in postnatal islet maturation, insulin secretion and islet morphogenesis (Takahashi et al., 2009). Ziolkowski et al. (2012) reported that highly sulfated HS is essential for the survival of mouse beta cells by providing protection against oxidative damage. In line with this, differences in the sulfation pattern of HS in alpha and beta cells of human and rodent

islets has been reported where alpha cell HS regulates vesicle trafficking and/or hormone secretion (Theodoraki et al., 2015). HS in alpha cells is less sulfated whereas highly sulfated HS is present in the beta cells (Theodoraki et al., 2015, Ziolkowski et al., 2012, Simeonovic et al., 2018). Our studies show that HS replacement in wt and db/db beta cells *in vitro* significantly improves beta cell survival and protects the beta cells from hydrogen peroxide-induced death (see Section 5.2.2.3), as previously reported for normal isolated mouse beta cells (Ziolkowski et al., 2012). Furthermore, desulfation of HS in rat (INS1) beta cells increases their susceptibility to hydrogen peroxide-induced damage and reduces beta cell proliferation (Theodoraki et al., 2015). In addition, 3-O sulfation of HS and syndecan-4 have been reported to play a critical role in the secretion of insulin by mouse beta cells and beta cell lines (Takahashi et al., 2009, Takahashi et al., 2017, Takahashi et al., 2012). These studies suggest that HS plays diverse roles in islet beta cells, depending on sulfation pattern and in some instances, on their HSPG core proteins. Collectively, these findings provide unique insight into the critical role of HS in islet beta cells.

During the pathogenesis of T1D, non-obese diabetic (NOD) mice demonstrated a loss of beta cell HS (Ziolkowski et al., 2012) and high levels of Hpse on insulitis leukocytes. Furthermore, T1D human pancreases also demonstrated a loss of both HS and the HSPG core proteins Col18 and Sdc1 in islet beta cells (Simeonovic et al., 2018). The high cell surface levels of the HS-degrading enzyme heparanase on infiltrating leukocytes were proposed to contribute to the disruption of the peri-islet BM and the loss of HS in the islet beta cells of NOD mice and humans during T1D development (Ziolkowski et al., 2012, Simeonovic et al., 2018). Additionally, HS is also lost during the isolation of islets and this has been attributed to the generation of excessive levels of reactive oxygen species causing HS depolymerisation (Rota et al., 2005, Raats et al., 1997, Choong et al., 2015, Ziolkowski et al., 2012). This loss of HS was not readily repaired *in vitro* by de novo synthesis of HS but was partially prevented using chemical antioxidants (Choong et al., 2015). *In vitro*, HS replacement using HS mimetics (PI-88, heparin) in human and mouse beta cells significantly improved survival and provided protection from oxidative damage. These findings have supported a role for intracellular HS as non-enzymatic antioxidant. Of significance, *in vivo* treatment of NOD mice with PI-88, a Hpse inhibitor/HS replacer, reduced the incidence of diabetes by 50% and preserved beta cell HS in the pancreatic islets (Ziolkowski et al., 2012). Together, these data suggested that Hpse-mediated loss

of HS in beta cells plays a critical role in the pathogenesis of T1D by exposing the beta cells to intolerable oxidative damage.

Similar to human T1D islets, our study demonstrated a progressive decline in the expression of intracellular HSPG core proteins (Col18, Sdc1 and CD44) and HS in the pancreatic beta cells of T2D-prone db/db mice compared to the lean wildtype and heterozygous controls. Our studies provide strong support for ER stress as the responsible mechanism. In line with previous studies (Choong et al., 2015, Ziolkowski et al., 2012, Simeonovic et al., 2018), our findings support an acute loss of beta cell HS but not HSPG core proteins in both isolated db/db and wt beta cells; however further loss of HS and HSPG core proteins was observed in db/db beta cells after culture for 2 days compared to controls. This increased susceptibility to HS depletion in isolated db/db beta cells is most likely due to pre-existing ER stress-induced oxidative stress. Future studies need to examine the mRNA levels of antioxidant enzymes immediately after islet isolation and after culture for both wt and db/db islets and beta cells. Similar to T1D (Ziolkowski et al., 2012, Simeonovic et al., 2018), loss of HS precedes insulin loss in T2D, suggesting that islet beta cell HS is a sensitive marker of beta cell integrity. Furthermore, HS replacement using heparin preserves both wildtype and db/db beta cells and protects them from hydrogen peroxide-induced beta cell death *in vitro*. The expression of the HS-degrading enzyme Hpse was markedly reduced in T2D-prone db/db beta cells suggesting that the loss of beta cell HS is not due to endogenous Hpse. Supporting and extending previous studies (Kjørholt et al., 2005, Laybutt et al., 2007, Chan et al., 2015, Eizirik et al., 2008, Sharma et al., 2015, Chan et al., 2013), islets of db/db mice displayed a marked upregulation in the transcripts of ER stress-associated UPR markers (BiP, P58, CHOP and ATF3) at 3.5-4.5 weeks of age and 5-9 weeks of age. Together, these findings suggest that beta cell death in T2D, at least in part, results from HS deficiency due to ER stress-induced decline in the production of HSPG core proteins and hence impaired HS synthesis. Consistent with this notion, we have demonstrated that *in vivo* treatment with the chemical chaperone TUDCA relieves ER stress and improves intra-islet HSPG core proteins and HS levels compared to controls.

In vivo treatment of db/db mice with PI-88 (a HS replacer/Hpse replacer) did not ameliorate T2D progression. In our *in vitro* studies, confocal microscopy confirmed the

uptake of FITC-labelled PI-88 and FITC-labelled heparin into the cytoplasm of both db/db and wt beta cells. Flow cytometry analyses revealed an improvement in the survival of wt beta cells following uptake of each FITC-labelled HS mimetic; however, only db/db beta cells treated with FITC-heparin demonstrated improved survival. Furthermore, the uptake of both FITC-labelled PI-88 and FITC-labelled heparin by db/db beta cells was approximately 50% of the uptake of wt beta cells (~45% vs ~90%). This impaired uptake of FITC-labelled heparin but not FITC-labelled PI-88 in db/db beta cells still markedly increased db/db beta cell survival. There are 235 HS-binding proteins in the mouse genome and 66% of the proteins have the potential to bind HS intracellularly (Simon Davis and Parish, 2013). Therefore, it is plausible that ER stress in db/db beta cells impairs the HS-binding proteins for PI-88 and heparin uptake. We propose that the failure of PI-88 treatment to improve db/db beta cell survival as well as glycaemia in db/db (*in vitro* and *in vivo*) mice is due to a defect not only in uptake but also the intracellular distribution of PI-88 to subcellular sites of endogenous ROS production. Importantly, HS replacement using heparin in wt and db/db beta cells protects the beta cells from hydrogen peroxide-induced death *in vitro* (see Section 5.2.2.3). In future studies, RT-PCR analyses of the expression of HS-binding proteins in db/db beta cells could be investigated to resolve this discrepancy. Importantly, these studies emphasise the need to develop a synthetic heparin-like HS replacer that lacks anti-coagulant activity, for prolonging beta cell compensation and ameliorating glycaemia in db/db mice. Relieving ER stress and/or HS replacement early in T2D development could play a vital role in maintaining beta cell survival, thereby preserving the insulin-secreting function of T2D-prone islet beta cells.

In contrast to our T2D studies, treatment of NOD mice with PI-88 significantly reduced the incidence of T1D by 50%. The success of this highly innovative approach was attributed to a significant reduction in islet inflammation, reduced invasive insulitis and increased HS content of the islets, indicative of improved beta cell survival (Ziolkowski et al., 2012). Although ER stress in beta cells also accompanies beta cell demise in T1D, the NOD mice in our lab's study were treated with PI-88 from 10-11 weeks of age. Other studies have reported that NOD mice display activation of early UPR genes at 6-8 weeks of age and deleterious UPR genes at 10 weeks (Tersey et al., 2012).. It is therefore possible that PI-88 therapy during T1D development may also provide protection from ER stress via HS replacement, a notion that warrants further investigation. In db/db mice,

however, PI-88 treatment began at 3.5 weeks of age, when ER stress was already established in the islet beta cells (Chapter 3, Section 3.2.13), precluding the potential for PI-88 to impact the *induction* of ER stress. An additional discrepancy between the T1D and T2D studies is the enormous difference in the duration of treatment, with db/db and NOD mice being treated daily for 35 days and 180 days (Ziolkowski et al., 2012), respectively. It is therefore possible that the shorter treatment, existing ER stress in the beta cells and impaired PI-88 uptake/distribution in the db/db beta cells contributed to the failure of the treatment. In the future, a diet-induced obesity/T2D model where PI-88 treatment could be initiated at the same time of HFD feeding (and hence prior to the onset of ER stress) could be used to test whether PI-88 can prevent or reduce ER stress.

Our study suggests that ER stress could directly contribute to the loss of HS by impairing the synthesis of HSPG core proteins in the ER. Therefore, we speculate that a loss of HS in T1D, particularly in humans (Simeonovic et al., 2018) could also be partly due to ER stress. This would exacerbate the decline in beta cell HS due to leukocyte-derived Hpse-mediated degradation. Growing evidence suggests that ER stress plays a role in beta cell destruction during the pathogenesis of T1D (Engin et al., 2013, Todd et al., 2008, Tersey et al., 2012, Eizirik et al., 2013, Eizirik et al., 2009, Eizirik et al., 2008, Marhfour et al., 2012, Hartman et al., 2004). This ER stress pathway is most likely due to pro-inflammatory cytokines (IL-1β, TNF-γ) produced by infiltrating immune cells, resulting in calcium depletion in the ER and disruption of ER homeostasis (Eizirik et al., 2009, Cardozo et al., 2005, Engin et al., 2013, Oyadomari et al., 2001). In T1D NOD mice, Hartman et al. (2004) showed increased staining of ATF3 in islets and increased beta cell apoptosis. Furthermore, Tersey et al. (2012) reported an age-dependent increase in transcripts for ER stress markers (BiP, P58, Xbp1, Xbp1s), abnormal ER by electron microscopy and activation of NF-κB in prediabetic NOD mice, compared to controls; however, the expression of CHOP was comparable (Tersey et al., 2012). An increase in BiP but not other ER stress markers has also been observed in diabetic NOD mice compared to non-diabetic C57BL/6J controls (Åkerfeldt et al., 2008). Furthermore, female NOD beta cells showed defective expression of ATF6 and XBP1 which preceded loss of beta cell function during the progression of T1D (Engin et al., 2013). Interestingly, TUDCA treatment of NOD and RIP-LCMV-GP mice for 20 weeks and 2 weeks, respectively, reduced leukocyte infiltration in the pancreas and beta cell apoptosis,

improved the survival and morphology of beta cells, preserved insulin secretion and restored the expression of UPR markers (Engin et al., 2013). Similarly, immunostaining of human T1D islets showed increased levels of late UPR markers (CHOP and ATF3) compared to non-diabetic controls (Marhfour et al., 2012, Hartman et al., 2004) correlating with beta cell apoptosis. Defects in the expression of ATF6 and XBP1 were also found during the progression of human T1D (Engin et al., 2013). Collectively, these studies suggest that the UPR also plays a critical role in maintaining beta cells during T1D development.

Loss of intracellular HS in pancreatic beta cells therefore represents a common molecular mechanism in the pathogenesis of T1D and T2D (**Figure 7.2**).

7.4 Heparanase is a marker of myeloid leukocytes in adipose tissue inflammation

A low-grade chronic inflammation is associated with obesity and insulin resistance in T2D. Adipose tissue, liver, muscle and pancreas represent sites of inflammation in T2D in both mice and humans (Hasnain et al., 2012, Donath and Shoelson, 2011, Donath et al., 2008, Ehses et al., 2007, Marchetti, 2016, Eguchi and Nagai, 2017, Olefsky and Glass, 2010, McNelis and Olefsky, 2014).

Adipocytes act as an endocrine and paracrine organ to help regulate appetite, energy balance, immunity, insulin sensitivity, angiogenesis, blood pressure, lipid metabolism and homeostasis (Rosen and Spiegelman, 2006). In the lean state, adipose tissue is predominately characterised by M2-like macrophages, eosinophils and lymphocytes. The M2 anti-inflammatory macrophages help to maintain adipose tissue homeostasis (Wu et al., 2011, Huh et al., 2014, Goh et al., 2013, Kang et al., 2008, Molofsky et al., 2013). In contrast, in the obese state, inflammation is triggered through several pathways i.e., increased nutrient uptake, hypoxia, lipotoxicity, ER stress and TLR activation (Ozcan et al., 2004, Shi et al., 2006, Unger and Scherer, 2010, Fujisaka et al., 2013). Inflammation in obese adipose tissue is characterised by M1-like inflammatory macrophages, neutrophils, dendritic cells and lymphocytes

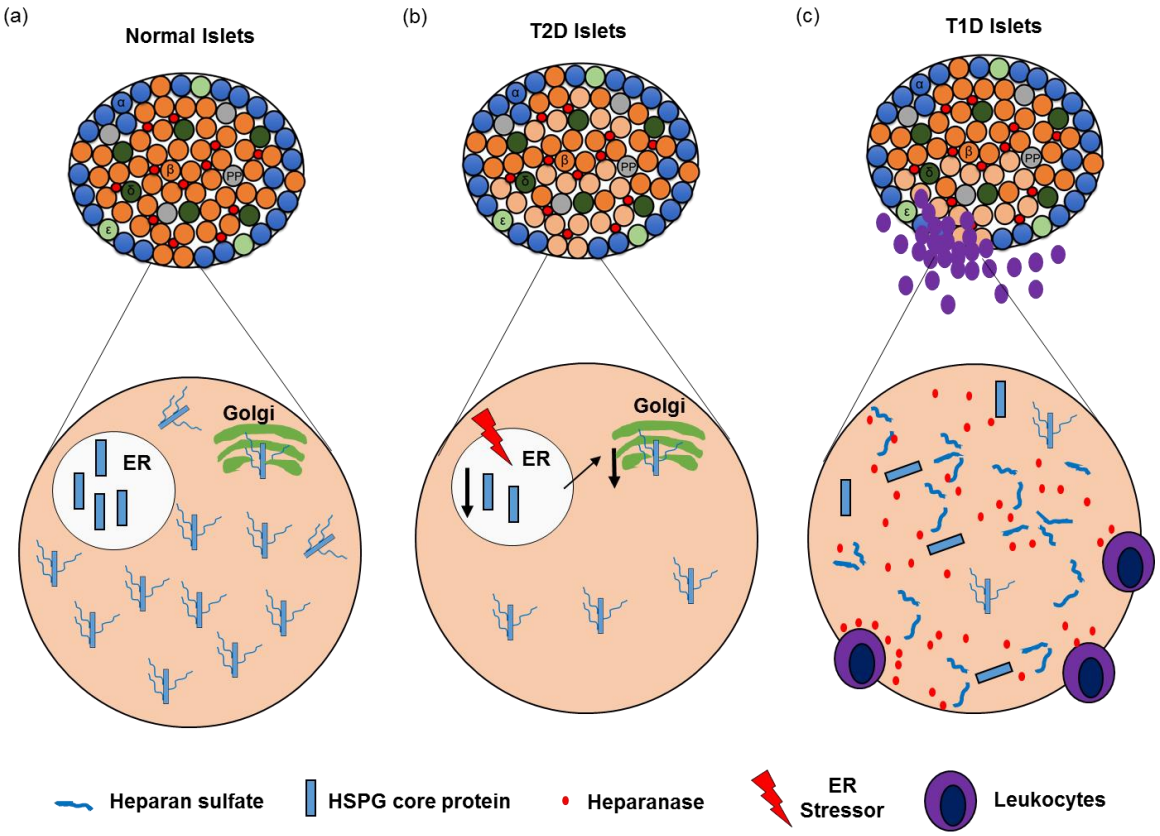

Figure 7.2: Loss of beta cell HS in T2D and T1D islets.

(a) High levels of intracellular HS are present in the beta cells of normal islets, acting as a constitutive non-enzymatic antioxidant. (b) T2D islets show impaired synthesis of HS due to ER-stress induced depletion of HSPG core proteins. (c) During T1D progression, beta cell HS is degraded by the HS-degrading enzyme heparanase produced by insulitis leukocytes. ER stress may also contribute to HS loss in T1D beta cells but to a lesser extent than in T2D. The depletion of intracellular HS via the different major pathways in (b) and (c) renders beta cells susceptible to oxidative stress/damage, resulting in beta cell death and the development of T2D and T1D, respectively. T1D, type 1 diabetes; T2D, type 2 diabetes; ER, endoplasmic reticulum; HS, heparan sulfate; HSPG, heparan sulfate proteoglycan.

(Weisberg et al., 2003, Kammoun et al., 2018, Zheng et al., 2016, Hotamisligil et al., 1993, Hotamisligil et al., 1995, Talukdar et al., 2012, Stefanovic-Racic et al., 2012, Winer et al., 2011, Wentworth et al., 2010, Shaul et al., 2010, Patsouris et al., 2008, Nguyen et al., 2007, Lumeng et al., 2007a, Xu et al., 2003, Bertola et al., 2012). Importantly, this inflammation contributes to local and systemic insulin resistance (Weisberg et al., 2003, Hotamisligil et al., 1993, Patsouris et al., 2008, Kanda et al., 2006).

Our study provides an extensive comparison of leukocyte sub-populations in peripheral blood and adipose tissue of obese T2D-prone db/db mice and lean wt mice. Importantly, we observed that the significant increase in the population of inflammatory macrophages in db/db WAT correlated with a significant increase in the circulating population of monocytes, which supports a similar finding in high fat diet (HFD)-mice (McFarlin et al., 2012). Our findings further extend these studies by demonstrating that only monocytes/inflammatory macrophages were increased in both the circulation and adipose tissue of obese db/db mice; this property was not observed in other myeloid sub-populations. The monocyte population in peripheral blood could therefore potentially act as a peripheral biomarker of increased adipose tissue inflammation and insulin resistance in obesity. We also demonstrated an increased total myeloid population (including inflammatory macrophages/monocytes, neutrophils and resident macrophages) in the white adipose tissue of db/db mice compared to wildtype mice. This finding is consistent with previous studies (Talukdar et al., 2012, Soehnlein, 2012, Elgazar-Carmon et al., 2008, Cildir et al., 2013, Nagareddy et al., 2014, Ferrante, 2013, Zheng et al., 2016, Boutens and Stienstra, 2016, Amano et al., 2014). Other studies have shown that $CD11c^+$ macrophages comprise the majority of inflammatory macrophages in obese adipose tissue (Wentworth et al., 2010, Shaul et al., 2010, Lumeng et al., 2007a, Nguyen et al., 2007, Oh et al., 2012) which could be due to increased recruitment as well as proliferation of macrophages in the adipose tissue (Lumeng et al., 2007a, Nagareddy et al., 2014, Amano et al., 2014). We demonstrated an increased proportion of $CD11c^+Ly6C^+$ and $CD11c^+Ly6G^+$ leukocytes in the white adipose tissue (WAT) of db/db mice compared to controls, contributing to the increased leukocyte accumulation in WAT. These $CD11c^+$ sub-populations need to be further characterised in the future to identify them as M1- or M2-like macrophages. Additionally, our study demonstrated a reduced proportion of eosinophils in the white adipose tissue of db/db mice providing some support for their

anti-inflammatory role (Wu et al., 2011). Db/db mice showed similar or reduced levels of lymphocytes (B cells and T cells) and conventional dendritic cells in the peripheral blood and white adipose tissue of db/db mice. This reduction in lymphocytes could be due to the mutation in the leptin receptor gene in db/db mice (Lee et al., 2010a). However, other studies have reported an increase in B and T cells in the blood and adipose tissue of db/db mice (Kintscher et al., 2008, Rausch et al., 2008, Wu and Liu, 2007). In the future, different subsets of B and T cells should be evaluated to determine their relative proportion in the blood and white adipose tissue of db/db and wt mice.

Importantly, our study identified markedly increased cell surface expression of heparanase (Hpse) on myeloid cells (resident macrophages, inflammatory macrophages and neutrophils) in white adipose tissue of wildtype and db/db mice compared to peripheral blood. This distinguishing property was not a characteristic of adipose tissue lymphocytes. It is important to note, however, that the Hpse antibody used in our experiments does not differentiate between the latent form (proheparanase) and catalytically active form of the enzyme. Future experiments could therefore use western blotting to further elucidate the role of catalytically active Hpse in white adipose tissue inflammation in wildtype and db/db mice.

Hpse is upregulated in various pathologies such as cancer-related angiogenesis and metastasis, inflammatory bowel disease, experimental autoimmune encephalomyelitis, atherosclerosis and T1D (Parish, 2006, Parish et al., 2001, Ziolkowski et al., 2012, Vlodavsky and Friedmann, 2001). Hpse has also been identified in diabetes-related complications such as nephropathy and retinopathy. In T1D, insulitis leukocytes showed increasing expression of catalytically active Hpse during T1D development in NOD mice (Ziolkowski et al., 2012, Simeonovic et al., 2013, Parish et al., 2013). This active Hpse initially degrades HS in the HSPG perlecan in sub-endothelial basement membranes (BMs) and peri-islet BMs, thereby allowing leukocyte migration from the circulation to pancreatic islets and intra-islet invasion, respectively. Significantly, leukocyte-derived Hpse subsequently degrades HS in beta cells, increasing their sensitivity to oxidative damage and death.

Similarly, we speculate that Hpse plays a critical role in the migration of monocytes from the circulation to adipose tissue where they differentiate into inflammatory macrophages (**Figure 7.3**). We propose that Hpse expressed by myeloid cells degrade HS attached to the HSPG core protein perlecan in the endothelial BMs to allow leukocytes to migrate to adipose tissue (Parish, 2006, Simon Davis and Parish, 2013, Parish et al., 2001, Vreys and David, 2007, Kjellén and Lindahl, 1991). Moreover, degradation of basement membrane HS liberates pro-inflammatory molecules bound to the HS chains (Vlodavsky et al., 2012, Kelly et al., 2005, Parish et al., 2001, Parish, 2006) and this can further promote the recruitment of immune cells to the inflamed tissue (Vlodavsky and Friedmann, 2001). In addition to the HS-degrading activity of Hpse, non-catalytic Hpse regulates the expression of genes involved in pro-inflammatory pathways (Levy-Adam et al., 2008, Kobayashi et al., 2006, Nobuhisa et al., 2007, Chen and Sanderson, 2009). Since, both wt and db/db inflammatory macrophages showed increased expression of Hpse, this marker does not discriminate between obese and lean WAT.

Previous studies have demonstrated that increased levels of inflammatory macrophages in the adipose tissue of T2D mice and humans is a potential driver of insulin resistance and eventually T2D (Zheng et al., 2016, Xu et al., 2003, Weisberg et al., 2003, Nagareddy et al., 2014, Shaul et al., 2010, Sartipy and Loskutoff, 2003, Olefsky and Glass, 2010, Boutens and Stienstra, 2016, Wentworth et al., 2010). These inflammatory macrophages secrete pro-inflammatory cytokines such as TNF-α which could activate the JNK pathway and phosphorylate insulin receptor substrate (IRS), resulting in down-regulation of insulin signaling and ultimately insulin resistance (**Figure 1.9**). In addition, activation of NF-κB caused by elevated levels of saturated free fatty acids in the circulation results in IRS phosphorylation and insulin resistance (**Figure 1.9**). Our studies demonstrated increased proportion of monocytes in the peripheral blood and inflammatory macrophages in WAT of db/db mice compared to respective wt controls. These findings correlated with adipose tissue inflammation, glucose intolerance and insulin resistance in db/db mice. The increased levels of cell surface Hpse is consistent with an important role for Hpse in facilitating the migration of monocytes from the circulation to db/db WAT. Therefore, we speculate that treatment of db/db mice with a Hpse inhibitor could modulate the inflammation in db/db mice, potentially improving insulin sensitivity and glycaemic control. Consistent with this notion, inhibition of signaling by TLR4 ligands

Figure 7.3: Role of heparanase in inflammation of WAT.

(a) In the lean state, adipose tissue contains anti-inflammatory macrophages, eosinophils and lymphocytes to help maintain homeostasis. Heparanase is highly expressed by monocytes and neutrophils, aiding their migration to adipose tissue from the circulation. (b) During obesity, white adipose tissue initially responds to nutrient overload by fat deposition and adipocyte enlargement. Adipose tissue expansion is accompanied by hypoxia, ER stress, apoptosis and release of free fatty acids (FFAs). This leads to the local recruitment and accumulation of macrophages as well as other immune cells (neutrophils, T cells) and insulin resistance. Monocytes/inflammatory macrophages express high levels of cell surface heparanase which degrade HS attached to the HSPG core protein perlecan in the sub-endothelial basement membrane (BM), allowing migration of immune cells to the inflammed tissue. Inflammatory macrophages secrete cytokines which stimulate viable adipocyte to release FFAs (via lipolysis) into the circulation. These cytokines further exacerbate the infiltration of immune cells, thereby reducing the relative proportions of anti-inflammatory macrophages and eosinophils. This cascade of events contributes to the increased inflammation of adipose tissue. ER, endoplasmic reticulum; HS, heparan sulfate; HSPG, heparan sulfate proteoglycan; WAT, white adipose tissue.

(a)

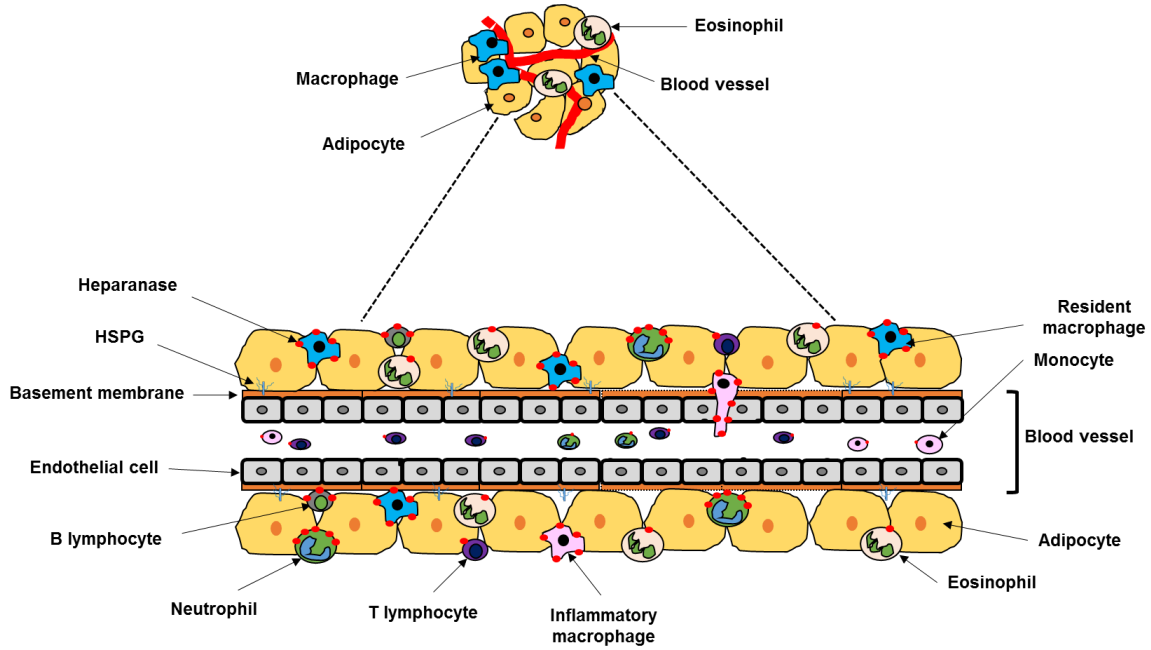
Eosinophil
Macrophage
Blood vessel
Adipocyte
Heparanase
HSPG
Basement membrane
Endothelial cell
B lymphocyte
Neutrophil
T lymphocyte
Inflammatory macrophage
Resident macrophage
Monocyte
Blood vessel
Adipocyte
Eosinophil

(b)

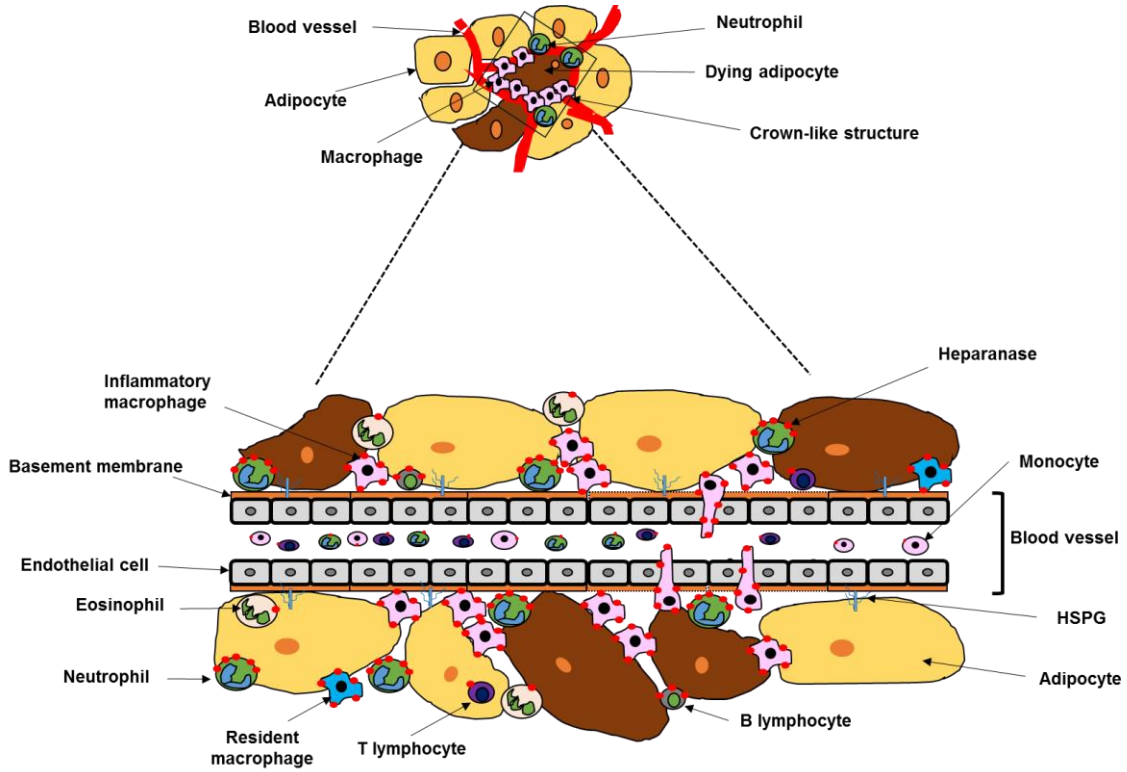
Blood vessel
Neutrophil
Dying adipocyte
Adipocyte
Crown-like structure
Macrophage
Heparanase
Inflammatory macrophage
Basement membrane
Monocyte
Blood vessel
Endothelial cell
Eosinophil
HSPG
Neutrophil
Adipocyte
B lymphocyte
Resident macrophage
T lymphocyte

Based on our Hpse expression studies, we examined whether PI-88 acting as a Hpse inhibitor (as well as a HS replacer) could modify the inflammatory response to obese white adipose tissue in db/db mice. Our data demonstrated a trend towards a decrease in the inflammatory macrophage population in the WAT of PI-88 treated female db/db mice compared to controls. However, our study failed to show an improvement in glycaemic control of PI-88 treated mice compared to controls (see Section 5.2.3). Previously, adipose tissue macrophages have been shown to be replaced after 8 weeks of HFD-feeding (Lumeng et al., 2007b). It is therefore plausible that extending the PI-88 treatment for a longer time course could allow better assessment of heparanase inhibition to modulate the recruitment of inflammatory macrophages to db/db WAT. In addition, studies of the kinetics of adipose tissue inflammation could be carried out to better define the role of leukocyte sub-populations during adipose tissue inflammation in db/db mice. Furthermore, a high fat diet (HFD)-mouse model characterised by the chronic development of insulin resistance could be employed to further evaluate the role of Hpse in leukocyte migration and WAT inflammation. Importantly, our findings highlight a need to develop a safe heparin-like HS replacer/Hpse inhibitor that could replenish beta cell HS to improve beta cell survival and reduce the adipose tissue inflammation by inhibiting Hpse activity in myeloid cells.

7.5 Conclusions

In conclusion, this project has identified that ER stress-induced decline in intra-islet HSPG core proteins correlates with HS loss in beta cells in T2D-prone db/db mice. We propose that the loss of beta cell HS is due to impaired HS synthesis. Unlike T1D where beta cell HS is largely degraded by heparanase, beta cell failure in T2D results from HS deficiency due to ER stress-mediated decline in the synthesis of HSPG core proteins. Thus, the loss of intracellular HS in beta cells represents a common pathway leading to the decline in beta cell viability for both T2D and T1D. In addition, the loss of beta cell HS contributes to oxidative stress during the development of T2D in db/db mice, revealing a novel mechanism linking ER stress and oxidative stress in T2D. Treatment with a heparin-like HS replacer/Hpse inhibitor, chemical chaperone or a combination of both could represent a clinical treatment for rescuing T2D beta cell HS, thereby

promoting beta cell survival/function and ameliorating the regulation of glycaemia. In parallel, the heparanase inhibitor activity of the drug could potentially reduce adipose tissue inflammation resulting in improved insulin sensitivity (i.e., reduced insulin resistance) and impaired T2D progression.

Bibliography

Aasum, E., Hafstad, A. D., Severson, D. L. & Larsen, T. S. 2003. Age-Dependent Changes in Metabolism, Contractile Function, and Ischemic Sensitivity in Hearts From db/db Mice. *Diabetes,* 52**,** 434-441.

Adrian, T. E. 1978. Pancreatic polypeptide. *Journal of Clinical Pathology. Supplement (Ass. Clin. Path.),* 8**,** 43-50.

Agere, S. A., Kim, E. Y., Akhtar, N. & Ahmed, S. 2018. Syndecans in chronic inflammatory and autoimmune diseases: Pathological insights and therapeutic opportunities. *J Cell Physiol,* 233**,** 6346-6358.

Ahmed, A. M. 2002. History of diabetes mellitus. *Saudi Med J,* 23**,** 373-8.

Ahner, A. & Brodsky, J. L. 2004. Checkpoints in ER-associated degradation: excuse me, which way to the proteasome? *Trends Cell Biol,* 14**,** 474-8.

Åkerfeldt, M. C., Howes, J., Chan, J. Y., Stevens, V. A., Boubenna, N., Mcguire, H. M., King, C., Biden, T. J. & Laybutt, D. R. 2008. Cytokine-Induced β-Cell Death Is Independent of Endoplasmic Reticulum Stress Signaling. *Diabetes,* 57**,** 3034-3044.

Alberti, K. G. M. M. & Zimmet, P. Z. 1998. Definition, diagnosis and classification of diabetes mellitus and its complications. Part 1: diagnosis and classification of diabetes mellitus. Provisional report of a WHO Consultation. *Diabetic Medicine,* 15**,** 539-553.

Alessi, D. R., Andjelkovic, M., Caudwell, B., Cron, P., Morrice, N., Cohen, P. & Hemmings, B. A. 1996. Mechanism of activation of protein kinase B by insulin and IGF-1. *EMBO J,* 15**,** 6541-51.

Alhasan, A. A., Spielhofer, J., Kusche-Gullberg, M., Kirby, J. A. & Ali, S. 2014. Role of 6-O-sulfated heparan sulfate in chronic renal fibrosis. *J Biol Chem,* 289**,** 20295-306.

Allison, J., Thomas, H. E., Catterall, T., Kay, T. W. & Strasser, A. 2005. Transgenic expression of dominant-negative Fas-associated death domain protein in beta cells protects against Fas ligand-induced apoptosis and reduces spontaneous diabetes in nonobese diabetic mice. *J Immunol,* 175**,** 293-301.

Amano, S. U., Cohen, J. L., Vangala, P., Tencerova, M., Nicoloro, S. M., Yawe, J. C., Shen, Y., Czech, M. P. & Aouadi, M. 2014. Local proliferation of macrophages contributes to obesity-associated adipose tissue inflammation. *Cell metabolism,* 19**,** 162-171.

Amaral, J. D., Viana, R. J., Ramalho, R. M., Steer, C. J. & Rodrigues, C. M. 2009. Bile acids: regulation of apoptosis by ursodeoxycholic acid. *J Lipid Res,* 50**,** 1721-34.

American Diabetes, A. 2009. Diagnosis and Classification of Diabetes Mellitus. *Diabetes Care,* 32**,** S62-S67.

Amin, A., Choi, S.-K., Galan, M., Kassan, M., Partyka, M., Kadowitz, P., Henrion, D., Trebak, M., Belmadani, S. & Matrougui, K. 2012. Chronic inhibition of endoplasmic reticulum stress and inflammation prevents ischaemia-induced vascular pathology in type II diabetic mice. *The Journal of pathology,* 227**,** 165-174.

Anderson, M. S. & Bluestone, J. A. 2005. The NOD mouse: a model of immune dysregulation. *Annu Rev Immunol,* 23**,** 447-85.

Andrikopoulos, S., Blair, A. R., Deluca, N., Fam, B. C. & Proietto, J. 2008. Evaluating the glucose tolerance test in mice. *Am J Physiol Endocrinol Metab,* 295**,** E1323-32.

Araki, E., Oyadomari, S. & Mori, M. 2003. Impact of endoplasmic reticulum stress pathway on pancreatic beta-cells and diabetes mellitus. *Exp Biol Med (Maywood),* 228**,** 1213-7.

Araki, K. & Nagata, K. 2011. Protein Folding and Quality Control in the ER. *Cold Spring Harbor Perspectives in Biology,* 3**,** a007526.

Arango Duque, G. & Descoteaux, A. 2014. Macrophage Cytokines: Involvement in Immunity and Infectious Diseases. *Frontiers in Immunology,* 5**,** 491.

Ariyasu, D., Yoshida, H. & Hasegawa, Y. 2017. Endoplasmic Reticulum (ER) Stress and Endocrine Disorders. *Int J Mol Sci,* 18.

Arya, M., Shergill, I. S., Williamson, M., Gommersall, L., Arya, N. & Patel, H. R. 2005. Basic principles of real-time quantitative PCR. *Expert Rev Mol Diagn,* 5**,** 209-19.

Asadi, A., Bruin, J. E. & Kieffer, T. J. 2015. Characterization of Antibodies to Products of Proinsulin Processing Using Immunofluorescence Staining of Pancreas in Multiple Species. *Journal of Histochemistry and Cytochemistry,* 63**,** 646-662.

Assayag-Asherie, N., Sever, D., Bogdani, M., Johnson, P., Weiss, T., Ginzberg, A., Perles, S., Weiss, L., Sebban, L. E., Turley, E. A., Okon, E., Raz, I. & Naor, D. 2015. Can CD44 Be a Mediator of Cell Destruction? The Challenge of Type 1 Diabetes. *PLoS ONE,* 10**,** e0143589.

Bach, J. F. 1994. Insulin-dependent diabetes mellitus as an autoimmune disease. *Endocr Rev,* 15**,** 516-42.

Back, S. H., Kang, S.-W., Han, J. & Chung, H.-T. 2012. Endoplasmic Reticulum Stress in the β-Cell Pathogenesis of Type 2 Diabetes. *Experimental Diabetes Research,* 2012**,** 11.

Back, S. H. & Kaufman, R. J. 2012. Endoplasmic Reticulum Stress and Type 2 Diabetes. *Annual review of biochemistry,* 81**,** 767-793.

Back, S. H., Scheuner, D., Han, J., Song, B., Ribick, M., Wang, J., Gildersleeve, R. D., Pennathur, S. & Kaufman, R. J. 2009. Translation attenuation through eIF2alpha phosphorylation prevents oxidative stress and maintains the differentiated state in beta cells. *Cell Metab,* 10**,** 13-26.

Bader, E., Migliorini, A., Gegg, M., Moruzzi, N., Gerdes, J., Roscioni, S. S., Bakhti, M., Brandl, E., Irmler, M., Beckers, J., Aichler, M., Feuchtinger, A., Leitzinger, C., Zischka, H., Wang-Sattler, R., Jastroch, M., Tschöp, M., Machicao, F., Staiger, H., Häring, H.-U., Chmelova, H., Chouinard, J. A., Oskolkov, N., Korsgren, O., Speier, S. & Lickert, H. 2016. Identification of proliferative and mature β-cells in the islets of Langerhans. *Nature,* 535**,** 430.

Baker, A. B., Groothuis, A., Jonas, M., Ettenson, D. S., Shazly, T., Zcharia, E., Vlodavsky, I., Seifert, P. & Edelman, E. R. 2009. Heparanase alters arterial structure, mechanics, and repair following endovascular stenting in mice. *Circ Res,* 104**,** 380-7.

Banaei-Bouchareb, L., Gouon-Evans, V., Samara-Boustani, D., Castellotti, M. C., Czernichow, P., Pollard, J. W. & Polak, M. 2004. Insulin cell mass is altered in Csf1op/Csf1op macrophage-deficient mice. *J Leukoc Biol,* 76**,** 359-67.

Barbetti, F., Colombo, C., Haataja, L., Cras-Méneur, C., Bernardini, S. & Arvan, P. 2016. Hyperglucagonemia in an animal model of insulin- deficient diabetes: what therapy can improve it? *Clinical Diabetes and Endocrinology,* 2**,** 11.

Barg, S. 2003. Mechanisms of Exocytosis in Insulin-Secreting B-Cells and Glucagon-Secreting A-Cells. *Pharmacology & Toxicology,* 92**,** 3-13.

Baskin, D. G. 2015. A Historical Perspective on the Identification of Cell Types in Pancreatic Islets of Langerhans by Staining and Histochemical Techniques. *Journal of Histochemistry and Cytochemistry,* 63**,** 543-558.

Bassat, E., Mutlak, Y. E., Genzelinakh, A., Shadrin, I. Y., Baruch Umansky, K., Yifa, O., Kain, D., Rajchman, D., Leach, J., Riabov Bassat, D., Udi, Y., Sarig, R., Sagi, I., Martin, J. F., Bursac, N., Cohen, S. & Tzahor, E. 2017. The extracellular matrix protein agrin promotes heart regeneration in mice. *Nature,* 547**,** 179-184.

Beauvais, D. M. & Rapraeger, A. C. 2004. Syndecans in tumor cell adhesion and signaling. *Reproductive biology and endocrinology : RB&E,* 2**,** 3-3.

Beavan, L. A., Davies, M., Couchman, J. R., Williams, M. A. & Mason, R. M. 1989. In vivo turnover of the basement membrane and other heparan sulfate proteoglycans of rat glomerulus. *Archives of Biochemistry and Biophysics,* 269**,** 576-585.

Behrendorff, N., Floetenmeyer, M., Schwiening, C. & Thorn, P. 2010. Protons released during pancreatic acinar cell secretion acidify the lumen and contribute to pancreatitis in mice. *Gastroenterology,* 139**,** 1711-20, 1720 e1-5.

Bennett, K. L., Jackson, D. G., Simon, J. C., Tanczos, E., Peach, R., Modrell, B., Stamenkovic, I., Plowman, G. & Aruffo, A. 1995. CD44 isoforms containing exon V3 are responsible for the presentation of heparin-binding growth factor. *J Cell Biol,* 128**,** 687-98.

Bensellam, M., Laybutt, D. R. & Jonas, J.-C. 2012. The molecular mechanisms of pancreatic β-cell glucotoxicity: Recent findings and future research directions. *Molecular and Cellular Endocrinology,* 364**,** 1-27.

Bernard-Kargar, C., Kassis, N., Berthault, M. F., Pralong, W. & Ktorza, A. 2001. Sialylated form of the neural cell adhesion molecule (NCAM): a new tool for the identification and sorting of beta-cell subpopulations with different functional activity. *Diabetes,* 50 Suppl 1**,** S125-30.

Bernard-Kargar, C. & Ktorza, A. 2001. Endocrine pancreas plasticity under physiological and pathological conditions. *Diabetes,* 50 Suppl 1**,** S30-5.

Bernfield, M., Gotte, M., Park, P. W., Reizes, O., Fitzgerald, M. L., Lincecum, J. & Zako, M. 1999. Functions of cell surface heparan sulfate proteoglycans. *Annu Rev Biochem,* 68**,** 729-77.

Bernfield, M., Kokenyesi, R., Kato, M., Hinkes, M. T., Spring, J., Gallo, R. L. & Lose, E. J. 1992. Biology of the syndecans: a family of transmembrane heparan sulfate proteoglycans. *Annu Rev Cell Biol,* 8.

Berridge, M. J. 2002. The endoplasmic reticulum: a multifunctional signaling organelle. *Cell Calcium,* 32**,** 235-49.

Bertola, A., Ciucci, T., Rousseau, D., Bourlier, V., Duffaut, C., Bonnafous, S., Blin-Wakkach, C., Anty, R., Iannelli, A., Gugenheim, J., Tran, A., Bouloumié, A., Gual, P. & Wakkach, A. 2012. Identification of Adipose Tissue Dendritic Cells Correlated With Obesity-Associated Insulin-Resistance and Inducing Th17 Responses in Mice and Patients. *Diabetes,* 61**,** 2238-2247.

Bertolotti, A., Wang, X., Novoa, I., Jungreis, R., Schlessinger, K., Cho, J. H., West, A. B. & Ron, D. 2001. Increased sensitivity to dextran sodium sulfate colitis in IRE1beta-deficient mice. *J Clin Invest,* 107**,** 585-93.

Bertolotti, A., Zhang, Y., Hendershot, L. M., Harding, H. P. & Ron, D. 2000. Dynamic interaction of BiP and ER stress transducers in the unfolded-protein response. *Nat Cell Biol,* 2**,** 326-32.

Bezakova, G. & Ruegg, M. A. 2003. New insights into the roles of agrin. *Nat Rev Mol Cell Biol,* 4**,** 295-308.

Binet, F., Chiasson, S. & Girard, D. 2010. Evidence that endoplasmic reticulum (ER) stress and caspase-4 activation occur in human neutrophils. *Biochemical and Biophysical Research Communications,* 391**,** 18-23.

Bishop, J. R., Schuksz, M. & Esko, J. D. 2007. Heparan sulphate proteoglycans fine-tune mammalian physiology. *Nature,* 446**,** 1030-7.

Bluestone, J. A., Herold, K. & Eisenbarth, G. 2010. Genetics, pathogenesis and clinical interventions in type 1 diabetes. *Nature,* 464**,** 1293-1300.

Boden, G. 2005. Free fatty acids and insulin secretion in humans. *Current Diabetes Reports,* 5**,** 167-170.

Boels, M. G. S., Koudijs, A., Avramut, M. C., Sol, W. M. P. J., Wang, G., Van Oeveren-Rietdijk, A. M., Van Zonneveld, A. J., De Boer, H. C., Van Der Vlag, J., Van Kooten, C., Eulberg, D., Van Den Berg, B. M., Ijpelaar, D. H. T. & Rabelink, T. J. 2017. Systemic Monocyte Chemotactic Protein-1 Inhibition Modifies Renal Macrophages and Restores Glomerular Endothelial Glycocalyx and Barrier Function in Diabetic Nephropathy. *The American Journal of Pathology,* 187**,** 2430-2440.

Bogdani, M., Korpos, E., Simeonovic, C. J., Parish, C. R., Sorokin, L. & Wight, T. N. 2014. Extracellular Matrix Components in the Pathogenesis of Type 1 Diabetes. *Current diabetes reports,* 14**,** 552-552.

Bogenrieder, T. & Herlyn, M. 2003. Axis of evil: molecular mechanisms of cancer metastasis. *Oncogene,* 22**,** 6524-36.

Bonnans, C., Chou, J. & Werb, Z. 2014. Remodelling the extracellular matrix in development and disease. *Nature reviews. Molecular cell biology,* 15**,** 786-801.

Bonner-Weir, S. & Orci, L. 1982. New perspectives on the microvasculature of the islets of Langerhans in the rat. *Diabetes,* 31**,** 883-9.

Bonny, C., Oberson, A., Negri, S., Sauser, C. & Schorderet, D. F. 2001. Cell-permeable peptide inhibitors of JNK: novel blockers of beta-cell death. *Diabetes,* 50**,** 77-82.

Bookchin, R. M. & Gallop, P. M. 1968. Structure of hemoglobin AIc: Nature of the N-terminal β chain blocking group. *Biochemical and Biophysical Research Communications,* 32**,** 86-93.

Bornemann, D. J., Duncan, J. E., Staatz, W., Selleck, S. & Warrior, R. 2004. Abrogation of heparan sulfate synthesis in Drosophila disrupts the Wingless, Hedgehog and Decapentaplegic signaling pathways. *Development,* 131**,** 1927-38.

Bosco, D., Armanet, M., Morel, P., Niclauss, N., Sgroi, A., Muller, Y. D., Giovannoni, L., Parnaud, G. & Berney, T. 2010. Unique Arrangement of α- and β-Cells in Human Islets of Langerhans. *Diabetes,* 59**,** 1202-1210.

Bosco, D., Rouiller, D. G. & Halban, P. A. 2007. Differential expression of E-cadherin at the surface of rat beta-cells as a marker of functional heterogeneity. *J Endocrinol,* 194**,** 21-9.

Boslem, E., Macintosh, G., Preston, Amanda m., Bartley, C., Busch, Anna k., Fuller, M., Laybutt, D. R., Meikle, Peter j. & Biden, Trevor j. 2011. A lipidomic screen of palmitate-treated MIN6 β-cells links sphingolipid metabolites with endoplasmic reticulum (ER) stress and impaired protein trafficking. *Biochemical Journal,* 435**,** 267-276.

Boucher, J., Quilliot, D., Pradère, J.-P., Simon, M.-F., Grès, S., Guigné, C., Prévot, D., Ferry, G., Boutin, J. A., Carpéné, C., Valet, P. & Saulnier-Blache, J. S. 2005. Potential involvement of adipocyte insulin resistance in obesity-associated up-regulation of adipocyte lysophospholipase D/autotaxin expression. *Diabetologia,* 48**,** 569-577.

Boutens, L. & Stienstra, R. 2016. Adipose tissue macrophages: going off track during obesity. *Diabetologia,* 59**,** 879-894.

Braune, J., Weyer, U., Hobusch, C., Mauer, J., Brüning, J. C., Bechmann, I. & Gericke, M. 2017. IL-6 Regulates M2 Polarization and Local Proliferation of Adipose Tissue Macrophages in Obesity. *The Journal of Immunology*.

Bretscher, M. S. 1985. Heparan sulphate proteoglycans and their polypeptide chains from BHK cells. *EMBO J,* 4**,** 1941-4.

Briaud, I., Harmon, J. S., Kelpe, C. L., Segu, V. B. G. & Poitout, V. 2001. Lipotoxicity of the Pancreatic β-Cell Is Associated With Glucose-Dependent Esterification of Fatty Acids Into Neutral Lipids. *Diabetes,* 50**,** 315-321.

Brissova, M., Fowler, M. J., Nicholson, W. E., Chu, A., Hirshberg, B., Harlan, D. M. & Powers, A. C. 2005. Assessment of human pancreatic islet architecture and composition by laser scanning confocal microscopy. *J Histochem Cytochem,* 53**,** 1087-97.

Brissova, M. & Powers, A. C. 2008. Architecture of Pancreatic Islets. *In:* SEINO, S. & BELL, G. I. (eds.) *Pancreatic Beta Cell in Health and Disease.* Tokyo: Springer Japan.

Broglio, F., Benso, A., Castiglioni, C., Gottero, C., Prodam, F., Destefanis, S., Gauna, C., Van Der Lely, A. J., Deghenghi, R., Bo, M., Arvat, E. & Ghigo, E. 2003. The endocrine response to ghrelin as a function of gender in humans in young and elderly subjects. *J Clin Endocrinol Metab,* 88**,** 1537-42.

Brownlee, M. 2005. The pathobiology of diabetic complications: a unifying mechanism. *Diabetes,* 54**,** 1615-25.

Brozzi, F. & Eizirik, D. L. 2016. ER stress and the decline and fall of pancreatic beta cells in type 1 diabetes. *Upsala Journal of Medical Sciences,* 121**,** 133-139.

Brozzi, F., Gerlo, S., Grieco, F. A., Nardelli, T. R., Lievens, S., Gysemans, C., Marselli, L., Marchetti, P., Mathieu, C., Tavernier, J. & Eizirik, D. L. 2014. A combined "omics" approach identifies N-Myc interactor as a novel cytokine-induced regulator of IRE1 protein and c-Jun N-terminal kinase in pancreatic beta cells. *J Biol Chem,* 289**,** 20677-93.

Brozzi, F., Nardelli, T. R., Lopes, M., Millard, I., Barthson, J., Igoillo-Esteve, M., Grieco, F. A., Villate, O., Oliveira, J. M., Casimir, M., Bugliani, M., Engin, F., Hotamisligil, G. S., Marchetti, P. & Eizirik, D. L. 2015. Cytokines induce endoplasmic reticulum stress in human, rat and mouse beta cells via different mechanisms. *Diabetologia,* 58**,** 2307-2316.

Brush, M. H., Weiser, D. C. & Shenolikar, S. 2003. Growth arrest and DNA damage-inducible protein GADD34 targets protein phosphatase 1 alpha to the endoplasmic reticulum and promotes dephosphorylation of the alpha subunit of eukaryotic translation initiation factor 2. *Mol Cell Biol,* 23**,** 1292-303.

Buck, T. M., Wright, C. M. & Brodsky, J. L. 2007. The Activities and Function of Molecular Chaperones in the Endoplasmic Reticulum. *Seminars in cell & developmental biology,* 18**,** 751-761.

Butler, A. E., Janson, J., Soeller, W. C. & Butler, P. C. 2003. Increased beta-cell apoptosis prevents adaptive increase in beta-cell mass in mouse model of type 2 diabetes: evidence for role of islet amyloid formation rather than direct action of amyloid. *Diabetes,* 52**,** 2304-14.

Butler, P. C., Chou, J., Carter, W. B., Wang, Y. N., Bu, B. H., Chang, D., Chang, J. K. & Rizza, R. A. 1990. Effects of meal ingestion on plasma amylin concentration in NIDDM and nondiabetic humans. *Diabetes,* 39**,** 752-6.

Byun, H., Gou, Y., Zook, A., Lozano, M. M. & Dudley, J. P. 2014. ERAD and how viruses exploit it. *Frontiers in Microbiology,* 5.

Cabrera, O., Berman, D. M., Kenyon, N. S., Ricordi, C., Berggren, P.-O. & Caicedo, A. 2006. The unique cytoarchitecture of human pancreatic islets has implications for islet cell function. *Proceedings of the National Academy of Sciences of the United States of America,* 103**,** 2334-2339.

Calfon, M., Zeng, H., Urano, F., Till, J. H., Hubbard, S. R., Harding, H. P., Clark, S. G. & Ron, D. 2002. IRE1 couples endoplasmic reticulum load to secretory capacity by processing the XBP-1 mRNA. *Nature,* 415**,** 92-96.

Campos, C. 2012. Chronic hyperglycemia and glucose toxicity: pathology and clinical sequelae. *Postgrad Med,* 124**,** 90-7.

Cao, S. S. & Kaufman, R. J. 2014. Endoplasmic reticulum stress and oxidative stress in cell fate decision and human disease. *Antioxid Redox Signal,* 21**,** 396-413.

Cardozo, A. K., Ortis, F., Storling, J., Feng, Y. M., Rasschaert, J., Tonnesen, M., Van Eylen, F., Mandrup-Poulsen, T., Herchuelz, A. & Eizirik, D. L. 2005. Cytokines downregulate the sarcoendoplasmic reticulum pump Ca2+ ATPase 2b and deplete endoplasmic reticulum Ca2+, leading to induction of endoplasmic reticulum stress in pancreatic beta-cells. *Diabetes,* 54**,** 452-61.

Carey, D. J. 1997. Syndecans: multifunctional cell-surface co-receptors. *Biochem J,* 327 (Pt 1)**,** 1-16.

Cassel, R., Ducreux, S., Alam, M. R., Dingreville, F., Berlé, C., Burda-Jacob, K., Chauvin, M. A., Chikh, K., Païta, L., Al-Mawla, R., Crola Da Silva, C., Rieusset, J., Thivolet, C., Van Coppenolle, F. & Madec, A. M. 2016. Protection of Human Pancreatic Islets from Lipotoxicity by Modulation of the Translocon. *PLOS ONE,* 11**,** e0148686.

Castoldi, A., Naffah De Souza, C., Câmara, N. O. S. & Moraes-Vieira, P. M. 2015. The Macrophage Switch in Obesity Development. *Frontiers in Immunology,* 6**,** 637.

Castro-Caldas, M., Carvalho, A. N., Rodrigues, E., Henderson, C. J., Wolf, C. R., Rodrigues, C. M. & Gama, M. J. 2012. Tauroursodeoxycholic acid prevents MPTP-induced dopaminergic cell death in a mouse model of Parkinson's disease. *Mol Neurobiol,* 46**,** 475-86.

Cavelti-Weder, C., Babians-Brunner, A., Keller, C., Stahel, M. A., Kurz-Levin, M., Zayed, H., Solinger, A. M., Mandrup-Poulsen, T., Dinarello, C. A. & Donath, M. Y. 2012. Effects of gevokizumab on glycemia and inflammatory markers in type 2 diabetes. *Diabetes Care,* 35**,** 1654-62.

Cen, J., Sargsyan, E. & Bergsten, P. 2016. Fatty acids stimulate insulin secretion from human pancreatic islets at fasting glucose concentrations via mitochondria-dependent and -independent mechanisms. *Nutrition & Metabolism,* 13**,** 59.

Ceranowicz, P., Cieszkowski, J., Warzecha, Z., Kuśnierz-Cabala, B. & Dembiński, A. 2015. The Beginnings of Pancreatology as a Field of Experimental and Clinical Medicine. *BioMed Research International,* 2015**,** 128095.

Chan, J. Y., Biden, T. J. & Laybutt, D. R. 2012. Cross-talk between the unfolded protein response and nuclear factor-κB signalling pathways regulates cytokine-mediated beta cell death in MIN6 cells and isolated mouse islets. *Diabetologia,* 55**,** 2999-3009.

Chan, J. Y., Cooney, G. J., Biden, T. J. & Laybutt, D. R. 2011. Differential regulation of adaptive and apoptotic unfolded protein response signalling by cytokine-induced nitric oxide production in mouse pancreatic beta cells. *Diabetologia,* 54**,** 1766-1776.

Chan, J. Y., Luzuriaga, J., Bensellam, M., Biden, T. J. & Laybutt, D. R. 2013. Failure of the Adaptive Unfolded Protein Response in Islets of Obese Mice Is Linked With Abnormalities in β-Cell Gene Expression and Progression to Diabetes. *Diabetes,* 62**,** 1557-1568.

Chan, J. Y., Luzuriaga, J., Maxwell, E. L., West, P. K., Bensellam, M. & Laybutt, D. R. 2015. The balance between adaptive and apoptotic unfolded protein responses regulates beta-cell death under ER stress conditions through XBP1, CHOP and JNK. *Mol Cell Endocrinol,* 413**,** 189-201.

Chan, S. J., Keim, P. & Steiner, D. F. 1976. Cell-free synthesis of rat preproinsulins: characterization and partial amino acid sequence determination. *Proceedings of the National Academy of Sciences,* 73**,** 1964-1968.

Chang, L., Chiang, S.-H. & Saltiel, A. R. 2004. Insulin Signaling and the Regulation of Glucose Transport. *Molecular Medicine,* 10**,** 65-71.

Chaudhry, A. & Rudensky, A. Y. 2013. Control of inflammation by integration of environmental cues by regulatory T cells. *The Journal of Clinical Investigation,* 123**,** 939-944.

Chaugule, Viduth k. & Walden, H. 2016. Specificity and disease in the ubiquitin system. *Biochemical Society Transactions,* 44**,** 212-227.

Chen, E., Tsai, T. H., Li, L., Saha, P., Chan, L. & Chang, B. H.-J. 2017. PLIN2 is a Key Regulator of the Unfolded Protein Response and Endoplasmic Reticulum Stress Resolution in Pancreatic β Cells. *Scientific Reports,* 7**,** 40855.

Chen, G., Wang, D., Vikramadithyan, R., Yagyu, H., Saxena, U., Pillarisetti, S. & Goldberg, I. J. 2004. Inflammatory cytokines and fatty acids regulate endothelial cell heparanase expression. *Biochemistry,* 43**,** 4971-7.

Chen, H., Charlat, O., Tartaglia, L. A., Woolf, E. A., Weng, X., Ellis, S. J., Lakey, N. D., Culpepper, J., More, K. J., Breitbart, R. E., Duyk, G. M., Tepper, R. I. & Morgenstern, J. P. 1996. Evidence That the Diabetes Gene Encodes the Leptin Receptor: Identification of a Mutation in the Leptin Receptor Gene in db/db Mice. *Cell,* 84**,** 491-495.

Chen, H., Zheng, C., Zhang, X., Li, J., Li, J., Zheng, L. & Huang, K. 2011. Apelin alleviates diabetes-associated endoplasmic reticulum stress in the pancreas of Akita mice. *Peptides,* 32**,** 1634-9.

Chen, J., Saxena, G., Mungrue, I. N., Lusis, A. J. & Shalev, A. 2008. Thioredoxin-interacting protein: a critical link between glucose toxicity and beta-cell apoptosis. *Diabetes,* 57**,** 938-44.

Chen, L. & Sanderson, R. D. 2009. Heparanase regulates levels of syndecan-1 in the nucleus. *PLoS One,* 4**,** e4947.

Chen, X., Shen, J. & Prywes, R. 2002. The luminal domain of ATF6 senses endoplasmic reticulum (ER) stress and causes translocation of ATF6 from the ER to the Golgi. *J Biol Chem,* 277**,** 13045-52.

Chen, Y. & Brandizzi, F. 2013. IRE1: ER stress sensor and cell fate executor. *Trends Cell Biol,* 23**,** 547-55.

Chen, Y., Tian, J., Tian, X., Tang, X., Rui, K., Tong, J., Lu, L., Xu, H. & Wang, S. 2014. Adipose tissue dendritic cells enhances inflammation by prompting the generation of Th17 cells. *PLoS One,* 9**,** e92450.

Chen, Y. Y., Sun, L. Q., Wang, B. A., Zou, X. M., Mu, Y. M. & Lu, J. M. 2013. Palmitate induces autophagy in pancreatic beta-cells via endoplasmic reticulum stress and its downstream JNK pathway. *Int J Mol Med,* 32**,** 1401-6.

Cheng, J. Y., Raghunath, M., Whitelock, J. & Poole-Warren, L. 2011. Matrix components and scaffolds for sustained islet function. *Tissue Eng Part B Rev,* 17**,** 235-47.

Cheng, J. Y., Whitelock, J. & Poole-Warren, L. 2012a. Syndecan-4 is associated with beta-cells in the pancreas and the MIN6 beta-cell line. *Histochem Cell Biol,* 138**,** 933-44.

Cheng, K., Delghingaro-Augusto, V., Nolan, C. J., Turner, N., Hallahan, N., Andrikopoulos, S. & Gunton, J. E. 2012b. High Passage MIN6 Cells Have Impaired Insulin Secretion with Impaired Glucose and Lipid Oxidation. *PLoS ONE,* 7**,** e40868.

Chmelar, J., Chung, K.-J. & Chavakis, T. 2013. *The role of innate immune cells in obese adipose tissue inflammation and development of insulin resistance*.

Cho, K. W., Morris, D. L. & Lumeng, C. N. 2014. Flow cytometry analyses of adipose tissue macrophages. *Methods Enzymol,* 537**,** 297-314.

Choong, F. J., Freeman, C., Parish, C. R. & Simeonovic, C. J. 2015. Islet Heparan Sulfate but Not Heparan Sulfate Proteoglycan Core Protein Is Lost During Islet Isolation and Undergoes Recovery Post-Islet Transplantation. *American Journal of Transplantation,* 15**,** 2851-2864.

Chung, K. T., Shen, Y. & Hendershot, L. M. 2002. BAP, a mammalian BiP-associated protein, is a nucleotide exchange factor that regulates the ATPase activity of BiP. *J Biol Chem,* 277**,** 47557-63.

Cildir, G., Akincilar, S. C. & Tergaonkar, V. 2013. Chronic adipose tissue inflammation: all immune cells on the stage. *Trends Mol Med,* 19**,** 487-500.

Cinti, S., Mitchell, G., Barbatelli, G., Murano, I., Ceresi, E., Faloia, E., Wang, S., Fortier, M., Greenberg, A. S. & Obin, M. S. 2005. Adipocyte death defines macrophage localization and function in adipose tissue of obese mice and humans. *J Lipid Res,* 46**,** 2347-55.

Clark, A. & Nilsson, M. R. 2004a. Islet amyloid: a complication of islet dysfunction or an aetiological factor in Type 2 diabetes? *Diabetologia,* 47**,** 157-169.

Clark, A. & Nilsson, M. R. 2004b. Islet amyloid: a complication of islet dysfunction or an aetiological factor in Type 2 diabetes? *Diabetologia,* 47**,** 157-69.

Cnop, M., Foufelle, F. & Velloso, L. A. 2012. Endoplasmic reticulum stress, obesity and diabetes. *Trends Mol Med,* 18**,** 59-68.

Cnop, M., Welsh, N., Jonas, J. C., Jorns, A., Lenzen, S. & Eizirik, D. L. 2005. Mechanisms of pancreatic beta-cell death in type 1 and type 2 diabetes: many differences, few similarities. *Diabetes,* 54 Suppl 2**,** S97-107.

Coelho, M., Oliveira, T. & Fernandes, R. 2013. Biochemistry of adipose tissue: an endocrine organ. *Archives of Medical Science : AMS,* 9**,** 191-200.

Coleman, D. L. 1978. Obese and diabetes: Two mutant genes causing diabetes-obesity syndromes in mice. *Diabetologia,* 14**,** 141-148.

Coleman, D. L. & Hummel, K. P. 1975. Symposium IV: Diabetic syndrome in animals. Influence of genetic background on the expression of mutations at the diabetes locus in the mouse. II. Studies on background modifiers. *Isr J Med Sci,* 11**,** 708-13.

Collins, S., Pi, J. & Yehuda-Shnaidman, E. 2012. Uncoupling and reactive oxygen species (ROS)--a double-edged sword for beta-cell function? "Moderation in all things". *Best Pract Res Clin Endocrinol Metab,* 26**,** 753-8.

Coppieters, K. T., Dotta, F., Amirian, N., Campbell, P. D., Kay, T. W. H., Atkinson, M. A., Roep, B. O. & Von Herrath, M. G. 2012. Demonstration of islet-autoreactive

CD8 T cells in insulitic lesions from recent onset and long-term type 1 diabetes patients. *The Journal of Experimental Medicine,* 209**,** 51-60.

Cornu, M., Modi, H., Kawamori, D., Kulkarni, R. N., Joffraud, M. & Thorens, B. 2010. Glucagon-like peptide-1 increases beta-cell glucose competence and proliferation by translational induction of insulin-like growth factor-1 receptor expression. *J Biol Chem,* 285**,** 10538-45.

Couchman, J. R., Chen, L. & Woods, A. 2001. Syndecans and cell adhesion. *Int Rev Cytol,* 207**,** 113-50.

Cunha, D. A., Hekerman, P., Ladriere, L., Bazarra-Castro, A., Ortis, F., Wakeham, M. C., Moore, F., Rasschaert, J., Cardozo, A. K., Bellomo, E., Overbergh, L., Mathieu, C., Lupi, R., Hai, T., Herchuelz, A., Marchetti, P., Rutter, G. A., Eizirik, D. L. & Cnop, M. 2008a. Initiation and execution of lipotoxic ER stress in pancreatic beta-cells. *J Cell Sci,* 121**,** 2308-18.

Cunha, D. A., Hekerman, P., Ladrière, L., Bazarra-Castro, A., Ortis, F., Wakeham, M. C., Moore, F., Rasschaert, J., Cardozo, A. K., Bellomo, E., Overbergh, L., Mathieu, C., Lupi, R., Hai, T., Herchuelz, A., Marchetti, P., Rutter, G. A., Eizirik, D. L. & Cnop, M. 2008b. Initiation and execution of lipotoxic ER stress in pancreatic β-cells. *Journal of Cell Science,* 121**,** 2308-2318.

Cunha, D. A., Igoillo-Esteve, M., Gurzov, E. N., Germano, C. M., Naamane, N., Marhfour, I., Fukaya, M., Vanderwinden, J. M., Gysemans, C., Mathieu, C., Marselli, L., Marchetti, P., Harding, H. P., Ron, D., Eizirik, D. L. & Cnop, M. 2012. Death protein 5 and p53-upregulated modulator of apoptosis mediate the endoplasmic reticulum stress-mitochondrial dialog triggering lipotoxic rodent and human beta-cell apoptosis. *Diabetes,* 61**,** 2763-75.

Cunningham, C. N., He, K., Arunagiri, A., Paton, A. W., Paton, J. C., Arvan, P. & Tsai, B. 2017. Chaperone-Driven Degradation of a Misfolded Proinsulin Mutant in Parallel With Restoration of Wild-Type Insulin Secretion. *Diabetes,* 66**,** 741-753.

Curry, D. L., Bennett, L. L. & Grodsky, G. M. 1968. Dynamics of insulin secretion by the perfused rat pancreas. *Endocrinology,* 83**,** 572-84.

Cusi, K. 2010. The role of adipose tissue and lipotoxicity in the pathogenesis of type 2 diabetes. *Curr Diab Rep,* 10**,** 306-15.

Czech, M. P. 2000. PIP2 and PIP3: complex roles at the cell surface. *Cell,* 100**,** 603-6.

Dalbøge, L. S., Almholt, D. L. C., Neerup, T. S. R., Vassiliadis, E., Vrang, N., Pedersen, L., Fosgerau, K. & Jelsing, J. 2013. Characterisation of Age-Dependent Beta Cell Dynamics in the Male db/db Mice. *PLOS ONE,* 8**,** e82813.

Dandona, P., Aljada, A. & Bandyopadhyay, A. 2004. Inflammation: the link between insulin resistance, obesity and diabetes. *Trends Immunol,* 25**,** 4-7.

Dasu, M. R. & Jialal, I. 2011. Free fatty acids in the presence of high glucose amplify monocyte inflammation via Toll-like receptors. *American Journal of Physiology - Endocrinology And Metabolism,* 300**,** E145-E154.

Deepa, S. S., Yamada, S., Zako, M., Goldberger, O. & Sugahara, K. 2004. Chondroitin sulfate chains on syndecan-1 and syndecan-4 from normal murine mammary gland epithelial cells are structurally and functionally distinct and cooperate with heparan sulfate chains to bind growth factors. A novel function to control binding of midkine, pleiotrophin, and basic fibroblast growth factor. *J Biol Chem,* 279**,** 37368-76.

Defuria, J., Belkina, A. C., Jagannathan-Bogdan, M., Snyder-Cappione, J., Carr, J. D., Nersesova, Y. R., Markham, D., Strissel, K. J., Watkins, A. A., Zhu, M., Allen, J., Bouchard, J., Toraldo, G., Jasuja, R., Obin, M. S., Mcdonnell, M. E., Apovian, C.,

Denis, G. V. & Nikolajczyk, B. S. 2013. B cells promote inflammation in obesity and type 2 diabetes through regulation of T-cell function and an inflammatory cytokine profile. *Proc Natl Acad Sci U S A,* 110**,** 5133-8.

Delepine, M., Nicolino, M., Barrett, T., Golamaully, M., Lathrop, G. M. & Julier, C. 2000. EIF2AK3, encoding translation initiation factor 2-alpha kinase 3, is mutated in patients with Wolcott-Rallison syndrome. *Nat Genet,* 25**,** 406-9.

Dempsey, L. A., Brunn, G. J. & Platt, J. L. 2000. Heparanase, a potential regulator of cell-matrix interactions. *Trends Biochem Sci,* 25**,** 349-51.

Deng, J., Lu, P. D., Zhang, Y., Scheuner, D., Kaufman, R. J., Sonenberg, N., Harding, H. P. & Ron, D. 2004. Translational repression mediates activation of nuclear factor kappa B by phosphorylated translation initiation factor 2. *Mol Cell Biol,* 24**,** 10161-8.

Dennissen, M. A., Jenniskens, G. J., Pieffers, M., Versteeg, E. M., Petitou, M., Veerkamp, J. H. & Van Kuppevelt, T. H. 2002. Large, tissue-regulated domain diversity of heparan sulfates demonstrated by phage display antibodies. *J Biol Chem,* 277**,** 10982-6.

Despres, J. P., Lemieux, I., Bergeron, J., Pibarot, P., Mathieu, P., Larose, E., Rodes-Cabau, J., Bertrand, O. F. & Poirier, P. 2008. Abdominal obesity and the metabolic syndrome: contribution to global cardiometabolic risk. *Arterioscler Thromb Vasc Biol,* 28**,** 1039-49.

Desvergne, B. 2008. PPARδ/β: The Lobbyist Switching Macrophage Allegiance in Favor of Metabolism. *Cell Metabolism,* 7**,** 467-469.

Do, O. H., Gunton, J. E., Gaisano, H. Y. & Thorn, P. 2016. Changes in beta cell function occur in prediabetes and early disease in the Lepr(db) mouse model of diabetes. *Diabetologia,* 59**,** 1222-1230.

Do, O. H., Low, J. T., Gaisano, H. Y. & Thorn, P. 2014. The secretory deficit in islets from db/db mice is mainly due to a loss of responding beta cells. *Diabetologia,* 57**,** 1400-9.

Dolan, M., Horchar, T., Rigatti, B. & Hassell, J. R. 1997. Identification of sites in domain I of perlecan that regulate heparan sulfate synthesis. *J Biol Chem,* 272**,** 4316-22.

Dolezalova, R., Lacinova, Z., Dolinkova, M., Kleiblova, P., Haluzikova, D., Housa, D., Papezova, H. & Haluzik, M. 2007. Changes of endocrine function of adipose tissue in anorexia nervosa: comparison of circulating levels versus subcutaneous mRNA expression. *Clin Endocrinol (Oxf),* 67**,** 674-8.

Dominguez, P. M. & Ardavin, C. 2010. Differentiation and function of mouse monocyte-derived dendritic cells in steady state and inflammation. *Immunol Rev,* 234**,** 90-104.

Domowicz, M. S., Pirok, E. W., 3rd, Novak, T. E. & Schwartz, N. B. 2000. Role of the C-terminal G3 domain in sorting and secretion of aggrecan core protein and ubiquitin-mediated degradation of accumulated mutant precursors. *J Biol Chem,* 275**,** 35098-105.

Donath, M. Y., Boni-Schnetzler, M., Ellingsgaard, H. & Ehses, J. A. 2009. Islet inflammation impairs the pancreatic beta-cell in type 2 diabetes. *Physiology (Bethesda),* 24**,** 325-31.

Donath, M. Y., Schumann, D. M., Faulenbach, M., Ellingsgaard, H., Perren, A. & Ehses, J. A. 2008. Islet Inflammation in Type 2 Diabetes. *From metabolic stress to therapy,* 31**,** S161-S164.

Donath, M. Y. & Shoelson, S. E. 2011. Type 2 diabetes as an inflammatory disease. *Nat Rev Immunol,* 11**,** 98-107.

Dorner, A. J., Wasley, L. C., Raney, P., Haugejorden, S., Green, M. & Kaufman, R. J. 1990. The stress response in Chinese hamster ovary cells. Regulation of ERp72 and protein disulfide isomerase expression and secretion. *J Biol Chem,* 265**,** 22029-34.

Dorrell, C., Schug, J., Canaday, P. S., Russ, H. A., Tarlow, B. D., Grompe, M. T., Horton, T., Hebrok, M., Streeter, P. R., Kaestner, K. H. & Grompe, M. 2016. Human islets contain four distinct subtypes of beta cells. *Nat Commun,* 7**,** 11756.

Dreyfuss, J. L., Regatieri, C. V., Jarrouge, T. R., Cavalheiro, R. P., Sampaio, L. O. & Nader, H. B. 2009. Heparan sulfate proteoglycans: structure, protein interactions and cell signaling. *An Acad Bras Cienc,* 81**,** 409-29.

Duffaut, C., Galitzky, J., Lafontan, M. & Bouloumie, A. 2009. Unexpected trafficking of immune cells within the adipose tissue during the onset of obesity. *Biochem Biophys Res Commun,* 384**,** 482-5.

Dunphy, J. L., Taylor, R. G. & Fuller, P. J. 1998. Tissue distribution of rat glucagon receptor and GLP-1 receptor gene expression. *Mol Cell Endocrinol,* 141**,** 179-86.

Eguchi, K., Manabe, I., Oishi-Tanaka, Y., Ohsugi, M., Kono, N., Ogata, F., Yagi, N., Ohto, U., Kimoto, M., Miyake, K., Tobe, K., Arai, H., Kadowaki, T. & Nagai, R. 2012. Saturated fatty acid and TLR signaling link beta cell dysfunction and islet inflammation. *Cell Metab,* 15**,** 518-33.

Eguchi, K. & Nagai, R. 2017. Islet inflammation in type 2 diabetes and physiology. *J Clin Invest,* 127**,** 14-23.

Ehses, J. A., Lacraz, G., Giroix, M. H., Schmidlin, F., Coulaud, J., Kassis, N., Irminger, J. C., Kergoat, M., Portha, B., Homo-Delarche, F. & Donath, M. Y. 2009. IL-1 antagonism reduces hyperglycemia and tissue inflammation in the type 2 diabetic GK rat. *Proc Natl Acad Sci U S A,* 106**,** 13998-4003.

Ehses, J. A., Perren, A., Eppler, E., Ribaux, P., Pospisilik, J. A., Maor-Cahn, R., Gueripel, X., Ellingsgaard, H., Schneider, M. K., Biollaz, G., Fontana, A., Reinecke, M., Homo-Delarche, F. & Donath, M. Y. 2007. Increased number of islet-associated macrophages in type 2 diabetes. *Diabetes,* 56**,** 2356-70.

Eizirik, D. L., Cardozo, A. K. & Cnop, M. 2008. The role for endoplasmic reticulum stress in diabetes mellitus. *Endocr Rev,* 29**,** 42-61.

Eizirik, D. L. & Cnop, M. 2010. ER Stress in Pancreatic β Cells: The Thin Red Line Between Adaptation and Failure. *Science Signaling,* 3**,** pe7-pe7.

Eizirik, D. L., Colli, M. L. & Ortis, F. 2009. The role of inflammation in insulitis and beta-cell loss in type 1 diabetes. *Nat Rev Endocrinol,* 5**,** 219-26.

Eizirik, D. L., Miani, M. & Cardozo, A. K. 2013. Signalling danger: endoplasmic reticulum stress and the unfolded protein response in pancreatic islet inflammation. *Diabetologia,* 56**,** 234-41.

Eizirik, D. L., Pipeleers, D. G., Ling, Z., Welsh, N., Hellerstrom, C. & Andersson, A. 1994. Major species differences between humans and rodents in the susceptibility to pancreatic beta-cell injury. *Proc Natl Acad Sci U S A,* 91**,** 9253-6.

El-Assaad, W., Buteau, J., Peyot, M.-L., Nolan, C., Roduit, R., Hardy, S., Joly, E., Dbaibo, G., Rosenberg, L. & Prentki, M. 2003. Saturated Fatty Acids Synergize with Elevated Glucose to Cause Pancreatic β-Cell Death. *Endocrinology,* 144**,** 4154-4163.

Elenius, K. & Jalkanen, M. 1994. Function of the syndecans--a family of cell surface proteoglycans. *J Cell Sci,* 107 (Pt 11)**,** 2975-82.

Eletr, Z. M., Huang, D. T., Duda, D. M., Schulman, B. A. & Kuhlman, B. 2005. E2 conjugating enzymes must disengage from their E1 enzymes before E3-dependent ubiquitin and ubiquitin-like transfer. *Nat Struct Mol Biol,* 12**,** 933-4.

Elgazar-Carmon, V., Rudich, A., Hadad, N. & Levy, R. 2008. Neutrophils transiently infiltrate intra-abdominal fat early in the course of high-fat feeding. *J Lipid Res,* 49**,** 1894-903.

Elia, A. E., Lalli, S., Monsurrò, M. R., Sagnelli, A., Taiello, A. C., Reggiori, B., La Bella, V., Tedeschi, G. & Albanese, A. 2016. Tauroursodeoxycholic acid in the treatment of patients with amyotrophic lateral sclerosis. *European Journal of Neurology,* 23**,** 45-52.

Ellgaard, L. & Helenius, A. 2001. ER quality control: towards an understanding at the molecular level. *Curr Opin Cell Biol,* 13**,** 431-7.

Elmore, S. 2007. Apoptosis: A Review of Programmed Cell Death. *Toxicologic pathology,* 35**,** 495-516.

Engin, F. & Hotamisligil, G. S. 2010. Restoring endoplasmic reticulum function by chemical chaperones: an emerging therapeutic approach for metabolic diseases. *Diabetes, Obesity and Metabolism,* 12**,** 108-115.

Engin, F., Yermalovich, A., Nguyen, T., Hummasti, S., Fu, W., Eizirik, D. L., Mathis, D. & Hotamisligil, G. S. 2013. Restoration of the unfolded protein response in pancreatic beta cells protects mice against type 1 diabetes. *Sci Transl Med,* 5**,** 211ra156.

Eriksson, K. K., Vago, R., Calanca, V., Galli, C., Paganetti, P. & Molinari, M. 2004. EDEM contributes to maintenance of protein folding efficiency and secretory capacity. *J Biol Chem,* 279**,** 44600-5.

Esko, J. D. & Lindahl, U. 2001. Molecular diversity of heparan sulfate. *J Clin Invest,* 108**,** 169-73.

Esko, J. D. & Selleck, S. B. 2002. Order out of chaos: assembly of ligand binding sites in heparan sulfate. *Annu Rev Biochem,* 71**,** 435-71.

Everett, B. M., Donath, M. Y., Pradhan, A. D., Thuren, T., Pais, P., Nicolau, J. C., Glynn, R. J., Libby, P. & Ridker, P. M. 2018. Anti-Inflammatory Therapy With Canakinumab for the Prevention and Management of Diabetes. *Journal of the American College of Cardiology,* 71**,** 2392-2401.

Fairbanks, M. B., Mildner, A. M., Leone, J. W., Cavey, G. S., Mathews, W. R., Drong, R. F., Slightom, J. L., Bienkowski, M. J., Smith, C. W., Bannow, C. A. & Heinrikson, R. L. 1999. Processing of the human heparanase precursor and evidence that the active enzyme is a heterodimer. *J Biol Chem,* 274**,** 29587-90.

Fantuzzi, G. & Faggioni, R. 2000. Leptin in the regulation of immunity, inflammation, and hematopoiesis. *J Leukoc Biol,* 68**,** 437-46.

Feissner, R. F., Skalska, J., Gaum, W. E. & Sheu, S. S. 2009. Crosstalk signaling between mitochondrial Ca2+ and ROS. *Front Biosci (Landmark Ed),* 14**,** 1197-218.

Fernandez-Riejos, P., Najib, S., Santos-Alvarez, J., Martin-Romero, C., Perez-Perez, A., Gonzalez-Yanes, C. & Sanchez-Margalet, V. 2010. Role of leptin in the activation of immune cells. *Mediators Inflamm,* 2010**,** 568343.

Ferrante, A. W., Jr. 2013. Macrophages, fat, and the emergence of immunometabolism. *J Clin Invest,* 123**,** 4992-3.

Ferro, V., Dredge, K., Liu, L., Hammond, E., Bytheway, I., Li, C., Johnstone, K., Karoli, T., Davis, K., Copeman, E. & Gautam, A. 2007. PI-88 and novel heparan sulfate mimetics inhibit angiogenesis. *Semin Thromb Hemost,* 33**,** 557-68.

Fleischman, A., Shoelson, S. E., Bernier, R. & Goldfine, A. B. 2008. Salsalate improves glycemia and inflammatory parameters in obese young adults. *Diabetes Care,* 31**,** 289-94.

Fonseca, S. G., Gromada, J. & Urano, F. 2011. Endoplasmic reticulum stress and pancreatic beta cell death. *Trends in endocrinology and metabolism: TEM,* 22**,** 266-274.

Frantz, C., Stewart, K. M. & Weaver, V. M. 2010. The extracellular matrix at a glance. *Journal of Cell Science,* 123**,** 4195-4200.

Freeman, C., Liu, L., Banwell, M. G., Brown, K. J., Bezos, A., Ferro, V. & Parish, C. R. 2005. Use of sulfated linked cyclitols as heparan sulfate mimetics to probe the heparin/heparan sulfate binding specificity of proteins. *J Biol Chem,* 280**,** 8842-9.

Freeman, C. & Parish, C. R. 1998. Human platelet heparanase: purification, characterization and catalytic activity. *Biochemical Journal,* 330**,** 1341-1350.

Friedrich, M. V., Gohring, W., Morgelin, M., Brancaccio, A., David, G. & Timpl, R. 1999. Structural basis of glycosaminoglycan modification and of heterotypic interactions of perlecan domain V. *J Mol Biol,* 294**,** 259-70.

Fu, Z., Gilbert, E. R. & Liu, D. 2013. Regulation of Insulin Synthesis and Secretion and Pancreatic Beta-Cell Dysfunction in Diabetes. *Current diabetes reviews,* 9**,** 25-53.

Fujimoto, S., Mochizuki, K. & Goda, T. 2010. Gene Expression of Inflammatory Cytokines in Peripheral Leukocytes in db/db Mice Rose with Progression of Diabetes. *Bioscience, Biotechnology, and Biochemistry,* 74**,** 1488-1490.

Fujisaka, S., Usui, I., Ikutani, M., Aminuddin, A., Takikawa, A., Tsuneyama, K., Mahmood, A., Goda, N., Nagai, Y., Takatsu, K. & Tobe, K. 2013. Adipose tissue hypoxia induces inflammatory M1 polarity of macrophages in an HIF-1alpha-dependent and HIF-1alpha-independent manner in obese mice. *Diabetologia,* 56**,** 1403-12.

Fujita, Y., Murakami, M., Ogawa, Y., Masuzaki, H., Tanaka, M., Ozaki, S., Nakao, K. & Mimori, T. 2002. Leptin inhibits stress-induced apoptosis of T lymphocytes. *Clin Exp Immunol,* 128**,** 21-6.

Furukawa, H., Carroll, R. J., Swift, H. H. & Steiner, D. F. 1999. Long-term elevation of free fatty acids leads to delayed processing of proinsulin and prohormone convertases 2 and 3 in the pancreatic beta-cell line MIN6. *Diabetes,* 48**,** 1395-401.

Gaisano, H. Y. 2014. Here come the newcomer granules, better late than never. *Trends in Endocrinology & Metabolism,* 25**,** 381-388.

Galli, T. & Haucke, V. 2001. Cycling of synaptic vesicles: how far? How fast! *Sci STKE,* 2001**,** re1.

Gan, W. J., Zavortink, M., Ludick, C., Templin, R., Webb, R., Webb, R., Ma, W., Poronnik, P., Parton, R. G., Gaisano, H. Y., Shewan, A. M. & Thorn, P. 2017. Cell polarity defines three distinct domains in pancreatic β-cells. *Journal of Cell Science,* 130**,** 143-151.

Gao, W., Fu, Y., Yu, C., Wang, S., Zhang, Y., Zong, C., Xu, T., Liu, Y., Li, X. & Wang, X. 2014. Elevation of NR4A3 expression and its possible role in modulating insulin expression in the pancreatic beta cell. *PLoS One,* 9**,** e91462.

Gautam, A., Wilson, E., Chen, P.-J., Lee, P.-H., Lin, D.-Y., Wu, C.-C., Jeng, L.-B., Lin, P.-W., Mok, K.-T., Liu, C.-J., Lee, W.-C., Yeh, H.-Z., Lai, K.-L. & Chang, S.-C. 2007. PI-88, a novel heparanase inhibitor, as adjuvant therapy for hepatocellular carcinoma: A large randomized phase II clinical trial. *Cancer Research,* 67**,** 2650-2650.

Gething, M. J. 1999. Role and regulation of the ER chaperone BiP. *Semin Cell Dev Biol,* 10**,** 465-72.

Gething, M. J. & Sambrook, J. 1992. Protein folding in the cell. *Nature,* 355**,** 33-45.

Gingis-Velitski, S., Zetser, A., Kaplan, V., Ben-Zaken, O., Cohen, E., Levy-Adam, F., Bashenko, Y., Flugelman, M. Y., Vlodavsky, I. & Ilan, N. 2004. Heparanase uptake is mediated by cell membrane heparan sulfate proteoglycans. *J Biol Chem,* 279**,** 44084-92.

Ginsberg, H. N. & Maccallum, P. R. 2009. The Obesity, Metabolic Syndrome, and Type 2 Diabetes Mellitus Pandemic: Part I. Increased Cardiovascular Disease Risk and the Importance of Atherogenic Dyslipidemia in Persons With the Metabolic Syndrome and Type 2 Diabetes Mellitus. *Journal of the cardiometabolic syndrome,* 4**,** 113-119.

Gocheva, V., Wang, H. W., Gadea, B. B., Shree, T., Hunter, K. E., Garfall, A. L., Berman, T. & Joyce, J. A. 2010. IL-4 induces cathepsin protease activity in tumor-associated macrophages to promote cancer growth and invasion. *Genes Dev,* 24**,** 241-55.

Goh, Y. P., Henderson, N. C., Heredia, J. E., Red Eagle, A., Odegaard, J. I., Lehwald, N., Nguyen, K. D., Sheppard, D., Mukundan, L., Locksley, R. M. & Chawla, A. 2013. Eosinophils secrete IL-4 to facilitate liver regeneration. *Proc Natl Acad Sci U S A,* 110**,** 9914-9.

Goke, B. 2008. Islet cell function: alpha and beta cells--partners towards normoglycaemia. *Int J Clin Pract Suppl***,** 2-7.

Goldberg, R., Meirovitz, A., Hirshoren, N., Bulvik, R., Binder, A., Rubinstein, A. M. & Elkin, M. 2013. Versatile role of heparanase in inflammation. *Matrix Biology,* 32**,** 234-240.

Goldberg, S., Harvey, S. J., Cunningham, J., Tryggvason, K. & Miner, J. H. 2009. Glomerular filtration is normal in the absence of both agrin and perlecan–heparan sulfate from the glomerular basement membrane. *Nephrology Dialysis Transplantation,* 24**,** 2044-2051.

Goldfine, A. B., Conlin, P. R., Halperin, F., Koska, J., Permana, P., Schwenke, D., Shoelson, S. E. & Reaven, P. D. 2013. A randomised trial of salsalate for insulin resistance and cardiovascular risk factors in persons with abnormal glucose tolerance. *Diabetologia,* 56**,** 714-723.

Goldfine, A. B., Silver, R., Aldhahi, W., Cai, D., Tatro, E., Lee, J. & Shoelson, S. E. 2008. Use of salsalate to target inflammation in the treatment of insulin resistance and type 2 diabetes. *Clin Transl Sci,* 1**,** 36-43.

Goldshmidt, O., Zcharia, E., Cohen, M., Aingorn, H., Cohen, I., Nadav, L., Katz, B. Z., Geiger, B. & Vlodavsky, I. 2003. Heparanase mediates cell adhesion independent of its enzymatic activity. *FASEB J,* 17**,** 1015-25.

Goldstein, D. E., Little, R. R., Lorenz, R. A., Malone, J. I., Nathan, D., Peterson, C. M. & Sacks, D. B. 2004. Tests of glycemia in diabetes. *Diabetes Care,* 27**,** 1761-73.

Groffen, A. J., Ruegg, M. A., Dijkman, H., Van De Velden, T. J., Buskens, C. A., Van Den Born, J., Assmann, K. J., Monnens, L. A., Veerkamp, J. H. & Van Den Heuvel, L. P. 1998. Agrin is a major heparan sulfate proteoglycan in the human glomerular basement membrane. *J Histochem Cytochem,* 46**,** 19-27.

Guo, Q., Shi, Q., Li, H., Liu, J., Wu, S., Sun, H. & Zhou, B. 2015. Glycolipid Metabolism Disorder in the Liver of Obese Mice Is Improved by TUDCA via the Restoration of Defective Hepatic Autophagy. *International Journal of Endocrinology,* 2015**,** 11.

Gupta, S., Mcgrath, B. & Cavener, D. R. 2010. PERK (EIF2AK3) Regulates Proinsulin Trafficking and Quality Control in the Secretory Pathway. *Diabetes,* 59**,** 1937-1947.

Gurzov, E. N., Ortis, F., Cunha, D. A., Gosset, G., Li, M., Cardozo, A. K. & Eizirik, D. L. 2009. Signaling by IL-1β+IFN-γ and ER stress converge on DP5/Hrk activation: a novel mechanism for pancreatic β-cell apoptosis. *Cell Death And Differentiation,* 16**,** 1539.

Gurzov, E. N., Stanley, W. J., Pappas, E. G., Thomas, H. E. & Gough, D. J. 2016. The JAK/STAT pathway in obesity and diabetes. *FEBS J,* 283**,** 3002-15.

Haataja, L., Gurlo, T., Huang, C. J. & Butler, P. C. 2008. Islet amyloid in type 2 diabetes, and the toxic oligomer hypothesis. *Endocr Rev,* 29**,** 303-16.

Haist, R. E. 1971. Functions of the islets of Langerhans. *Canadian Medical Association Journal,* 105**,** 956-passim.

Halaas, J. L., Gajiwala, K. S., Maffei, M., Cohen, S. L., Chait, B. T., Rabinowitz, D., Lallone, R. L., Burley, S. K. & Friedman, J. M. 1995. Weight-reducing effects of the plasma protein encoded by the obese gene. *Science,* 269**,** 543-6.

Hammond, C. & Helenius, A. 1994. Quality control in the secretory pathway: retention of a misfolded viral membrane glycoprotein involves cycling between the ER, intermediate compartment, and Golgi apparatus. *J Cell Biol,* 126**,** 41-52.

Han, S., Donelan, W., Wang, H., Reeves, W. & Yang, L.-J. 2013. Novel autoantigens in type 1 diabetes. *American journal of translational research,* 5**,** 379-392.

Hanna, S. T., Pigeau, G. M., Galvanovskis, J., Clark, A., Rorsman, P. & Macdonald, P. E. 2009. Kiss-and-run exocytosis and fusion pores of secretory vesicles in human beta-cells. *Pflugers Arch,* 457**,** 1343-50.

Harding, H. P., Novoa, I., Zhang, Y., Zeng, H., Wek, R., Schapira, M. & Ron, D. 2000. Regulated translation initiation controls stress-induced gene expression in mammalian cells. *Mol Cell,* 6**,** 1099-108.

Harding, H. P., Zeng, H., Zhang, Y., Jungries, R., Chung, P., Plesken, H., Sabatini, D. D. & Ron, D. 2001. Diabetes Mellitus and Exocrine Pancreatic Dysfunction in Perk−/− Mice Reveals a Role for Translational Control in Secretory Cell Survival. *Molecular Cell,* 7**,** 1153-1163.

Harding, H. P., Zhang, Y. & Ron, D. 1999. Protein translation and folding are coupled by an endoplasmic-reticulum-resident kinase. *Nature,* 397**,** 271-4.

Harding, H. P., Zhang, Y., Zeng, H., Novoa, I., Lu, P. D., Calfon, M., Sadri, N., Yun, C., Popko, B., Paules, R., Stojdl, D. F., Bell, J. C., Hettmann, T., Leiden, J. M. & Ron, D. 2003. An integrated stress response regulates amino acid metabolism and resistance to oxidative stress. *Mol Cell,* 11**,** 619-33.

Hartman, M. G., Lu, D., Kim, M. L., Kociba, G. J., Shukri, T., Buteau, J., Wang, X., Frankel, W. L., Guttridge, D., Prentki, M., Grey, S. T., Ron, D. & Hai, T. 2004. Role for activating transcription factor 3 in stress-induced beta-cell apoptosis. *Mol Cell Biol,* 24**,** 5721-32.

Hasnain, S. Z., Borg, D. J., Harcourt, B. E., Tong, H., Sheng, Y. H., Ng, C. P., Das, I., Wang, R., Chen, A. C. H., Loudovaris, T., Kay, T. W., Thomas, H. E., Whitehead, J. P., Forbes, J. M., Prins, J. B. & Mcguckin, M. A. 2014. Glycemic control in diabetes is restored by therapeutic manipulation of cytokines that regulate beta cell stress. *Nat Med,* 20**,** 1417-1426.

Hasnain, S. Z., Lourie, R., Das, I., Chen, A. C. & Mcguckin, M. A. 2012. The interplay between endoplasmic reticulum stress and inflammation. *Immunol Cell Biol,* 90**,** 260-70.

Hasnain, S. Z., Prins, J. B. & Mcguckin, M. A. 2016. Oxidative and endoplasmic reticulum stress in beta-cell dysfunction in diabetes. *J Mol Endocrinol,* 56**,** R33-54.

Hassler, J. R., Scheuner, D. L., Wang, S., Han, J., Kodali, V. K., Li, P., Nguyen, J., George, J. S., Davis, C., Wu, S. P., Bai, Y., Sartor, M., Cavalcoli, J., Malhi, H., Baudouin, G., Zhang, Y., Yates Iii, J. R., Itkin-Ansari, P., Volkmann, N. & Kaufman, R. J. 2015. The IRE1α/XBP1s Pathway Is Essential for the Glucose Response and Protection of β Cells. *PLOS Biology,* 13**,** e1002277.

Hauge-Evans, A. C., King, A. J., Carmignac, D., Richardson, C. C., Robinson, I. C., Low, M. J., Christie, M. R., Persaud, S. J. & Jones, P. M. 2009. Somatostatin secreted by islet delta-cells fulfills multiple roles as a paracrine regulator of islet function. *Diabetes,* 58**,** 403-11.

Haze, K., Okada, T., Yoshida, H., Yanagi, H., Yura, T., Negishi, M. & Mori, K. 2001. Identification of the G13 (cAMP-response-element-binding protein-related protein) gene product related to activating transcription factor 6 as a transcriptional activator of the mammalian unfolded protein response. *Biochem J,* 355**,** 19-28.

Haze, K., Yoshida, H., Yanagi, H., Yura, T. & Mori, K. 1999. Mammalian transcription factor ATF6 is synthesized as a transmembrane protein and activated by proteolysis in response to endoplasmic reticulum stress. *Mol Biol Cell,* 10**,** 3787-99.

He, Y. Q., Sutcliffe, E. L., Bunting, K. L., Li, J., Goodall, K. J., Poon, I. K., Hulett, M. D., Freeman, C., Zafar, A., Mcinnes, R. L., Taya, T., Parish, C. R. & Rao, S. 2012. The endoglycosidase heparanase enters the nucleus of T lymphocytes and modulates H3 methylation at actively transcribed genes via the interplay with key chromatin modifying enzymes. *Transcription,* 3**,** 130-45.

Hebert, D. N. & Molinari, M. 2007. In and Out of the ER: Protein Folding, Quality Control, Degradation, and Related Human Diseases. *Physiological Reviews,* 87**,** 1377-1408.

Henderson, J. R. & Moss, M. C. 1985. A morphometric study of the endocrine and exocrine capillaries of the pancreas. *Q J Exp Physiol,* 70**,** 347-56.

Henke, C. A., Roongta, U., Mickelson, D. J., Knutson, J. R. & Mccarthy, J. B. 1996. CD44-related chondroitin sulfate proteoglycan, a cell surface receptor implicated with tumor cell invasion, mediates endothelial cell migration on fibrinogen and invasion into a fibrin matrix. *J Clin Invest,* 97**,** 2541-52.

Henry, M. D. & Campbell, K. P. 1996. Dystroglycan: an extracellular matrix receptor linked to the cytoskeleton. *Curr Opin Cell Biol,* 8**,** 625-31.

Herbert, T. P. & Laybutt, D. R. 2016. A Reevaluation of the Role of the Unfolded Protein Response in Islet Dysfunction: Maladaptation or a Failure to Adapt? *Diabetes,* 65**,** 1472-80.

Hick, R. W., Gruver, A. L., Ventevogel, M. S., Haynes, B. F. & Sempowski, G. D. 2006. Leptin Selectively Augments Thymopoiesis in Leptin Deficiency and Lipopolysaccharide-Induced Thymic Atrophy. *Journal of immunology (Baltimore, Md. : 1950),* 177**,** 169-176.

Hidalgo, C. & Donoso, P. 2008. Crosstalk between calcium and redox signaling: from molecular mechanisms to health implications. *Antioxid Redox Signal,* 10**,** 1275-312.

Hinnebusch, A. G. 1993. Gene-specific translational control of the yeast GCN4 gene by phosphorylation of eukaryotic initiation factor 2. *Mol Microbiol,* 10**,** 215-23.

Hirao, K., Natsuka, Y., Tamura, T., Wada, I., Morito, D., Natsuka, S., Romero, P., Sleno, B., Tremblay, L. O., Herscovics, A., Nagata, K. & Hosokawa, N. 2006. EDEM3, a soluble EDEM homolog, enhances glycoprotein endoplasmic reticulum-associated degradation and mannose trimming. *J Biol Chem,* 281**,** 9650-8.

Hirosumi, J., Tuncman, G., Chang, L., Gorgun, C. Z., Uysal, K. T., Maeda, K., Karin, M. & Hotamisligil, G. S. 2002. A central role for JNK in obesity and insulin resistance. *Nature,* 420**,** 333-6.

Ho, E. & Bray, T. M. 1999. Antioxidants, NFkappaB activation, and diabetogenesis. *Proc Soc Exp Biol Med,* 222**,** 205-13.

Ho, E., Chen, G. & Bray, T. M. 1999. Supplementation of N-acetylcysteine inhibits NFkappaB activation and protects against alloxan-induced diabetes in CD-1 mice. *FASEB J,* 13**,** 1845-54.

Hollien, J., Lin, J. H., Li, H., Stevens, N., Walter, P. & Weissman, J. S. 2009. Regulated Ire1-dependent decay of messenger RNAs in mammalian cells. *J Cell Biol,* 186**,** 323-31.

Hollien, J. & Weissman, J. S. 2006. Decay of endoplasmic reticulum-localized mRNAs during the unfolded protein response. *Science,* 313**,** 104-7.

Hong, E.-G., Ko, H. J., Cho, Y.-R., Kim, H.-J., Ma, Z., Yu, T. Y., Friedline, R. H., Kurt-Jones, E., Finberg, R., Fischer, M. A., Granger, E. L., Norbury, C. C., Hauschka, S. D., Philbrick, W. M., Lee, C.-G., Elias, J. A. & Kim, J. K. 2009. Interleukin-10 Prevents Diet-Induced Insulin Resistance by Attenuating Macrophage and Cytokine Response in Skeletal Muscle. *Diabetes,* 58**,** 2525-2535.

Hong, S. W., Lee, J., Cho, J. H., Kwon, H., Park, S. E., Rhee, E. J., Park, C. Y., Oh, K. W., Park, S. W. & Lee, W. Y. 2018. Pioglitazone Attenuates Palmitate-Induced Inflammation and Endoplasmic Reticulum Stress in Pancreatic beta-Cells. *Endocrinol Metab (Seoul),* 33**,** 105-113.

Hoseki, J., Ushioda, R. & Nagata, K. 2010. Mechanism and components of endoplasmic reticulum-associated degradation. *J Biochem,* 147**,** 19-25.

Hosokawa, N., Wada, I., Nagasawa, K., Moriyama, T., Okawa, K. & Nagata, K. 2008. Human XTP3-B forms an endoplasmic reticulum quality control scaffold with the HRD1-SEL1L ubiquitin ligase complex and BiP. *J Biol Chem,* 283**,** 20914-24.

Hotamisligil, G. S., Arner, P., Caro, J. F., Atkinson, R. L. & Spiegelman, B. M. 1995. Increased adipose tissue expression of tumor necrosis factor-alpha in human obesity and insulin resistance. *J Clin Invest,* 95**,** 2409-15.

Hotamisligil, G. S., Peraldi, P., Budavari, A., Ellis, R., White, M. F. & Spiegelman, B. M. 1996. IRS-1-mediated inhibition of insulin receptor tyrosine kinase activity in TNF-alpha- and obesity-induced insulin resistance. *Science,* 271**,** 665-8.

Hotamisligil, G. S., Shargill, N. S. & Spiegelman, B. M. 1993. Adipose expression of tumor necrosis factor-alpha: direct role in obesity-linked insulin resistance. *Science,* 259**,** 87-91.

Hou, J. C., Min, L. & Pessin, J. E. 2009. Insulin Granule Biogenesis, Trafficking and Exocytosis. *Vitamins and hormones,* 80**,** 473-506.

Hsieh, Y. H., Su, I. J., Lei, H. Y., Lai, M. D., Chang, W. W. & Huang, W. 2007. Differential endoplasmic reticulum stress signaling pathways mediated by iNOS. *Biochem Biophys Res Commun,* 359**,** 643-8.

Hu, F. B., Manson, J. E., Stampfer, M. J., Colditz, G., Liu, S., Solomon, C. G. & Willett, W. C. 2001. Diet, lifestyle, and the risk of type 2 diabetes mellitus in women. *N Engl J Med,* 345**,** 790-7.

Huang, X. F. & Arvan, P. 1995. Intracellular transport of proinsulin in pancreatic beta-cells. Structural maturation probed by disulfide accessibility. *J Biol Chem,* 270**,** 20417-23.

Hubbard, S. R. 1997. Crystal structure of the activated insulin receptor tyrosine kinase in complex with peptide substrate and ATP analog. *EMBO J,* 16**,** 5572-81.

Huh, J. Y., Park, Y. J., Ham, M. & Kim, J. B. 2014. Crosstalk between Adipocytes and Immune Cells in Adipose Tissue Inflammation and Metabolic Dysregulation in Obesity. *Mol Cells,* 37**,** 365-71.

Hull, R. L., Zraika, S., Udayasankar, J., Kisilevsky, R., Szarek, W. A., Wight, T. N. & Kahn, S. E. 2007. Inhibition of glycosaminoglycan synthesis and protein glycosylation with WAS-406 and azaserine result in reduced islet amyloid formation in vitro. *Am J Physiol Cell Physiol,* 293**,** C1586-93.

Hummel, K. P., Dickie, M. M. & Coleman, D. L. 1966. Diabetes, a new mutation in the mouse. *Science,* 153**,** 1127-8.

Hundal, R. S., Petersen, K. F., Mayerson, A. B., Randhawa, P. S., Inzucchi, S., Shoelson, S. E. & Shulman, G. I. 2002. Mechanism by which high-dose aspirin improves glucose metabolism in type 2 diabetes. *J Clin Invest,* 109**,** 1321-6.

Hussain, A., Hydrie, M., Claussen, B. & Asghar, S. 2010. Type 2 diabetes and obesity: a review. *J Diabetol,* 2**,** 1-7.

Ichii, H., Inverardi, L., Pileggi, A., Molano, R. D., Cabrera, O., Caicedo, A., Messinger, S., Kuroda, Y., Berggren, P. O. & Ricordi, C. 2005. A novel method for the assessment of cellular composition and beta-cell viability in human islet preparations. *Am J Transplant,* 5**,** 1635-45.

Igoillo-Esteve, M., Marselli, L., Cunha, D. A., Ladriere, L., Ortis, F., Grieco, F. A., Dotta, F., Weir, G. C., Marchetti, P., Eizirik, D. L. & Cnop, M. 2010. Palmitate induces a pro-inflammatory response in human pancreatic islets that mimics CCL2 expression by beta cells in type 2 diabetes. *Diabetologia,* 53**,** 1395-405.

Ilan, N., Elkin, M. & Vlodavsky, I. 2006. Regulation, function and clinical significance of heparanase in cancer metastasis and angiogenesis. *Int J Biochem Cell Biol,* 38**,** 2018-39.

In't Veld, P. 2014. Insulitis in human type 1 diabetes: a comparison between patients and animal models. *Seminars in Immunopathology,* 36**,** 569-579.

Iozzo, R. V. 1998. Matrix proteoglycans: from molecular design to cellular function. *Annu Rev Biochem,* 67**,** 609-52.

Iozzo, R. V. 2001. Heparan sulfate proteoglycans: intricate molecules with intriguing functions. *J Clin Invest,* 108**,** 165-7.

Iozzo, R. V. 2005. Basement membrane proteoglycans: from cellar to ceiling. *Nat Rev Mol Cell Biol,* 6**,** 646-56.

Irving-Rodgers, H. F., Choong, F. J., Hummitzsch, K., Parish, C. R., Rodgers, R. J. & Simeonovic, C. J. 2014. Pancreatic islet basement membrane loss and remodeling after mouse islet isolation and transplantation: impact for allograft rejection. *Cell Transplant,* 23**,** 59-72.

Irving-Rodgers, H. F., Ziolkowski, A. F., Parish, C. R., Sado, Y., Ninomiya, Y., Simeonovic, C. J. & Rodgers, R. J. 2008. Molecular composition of the peri-islet basement membrane in NOD mice: a barrier against destructive insulitis. *Diabetologia,* 51**,** 1680-8.

Ishihara, H., Asano, T., Tsukuda, K., Katagiri, H., Inukai, K., Anai, M., Kikuchi, M., Yazaki, Y., Miyazaki, J. I. & Oka, Y. 1993. Pancreatic beta cell line MIN6

exhibits characteristics of glucose metabolism and glucose-stimulated insulin secretion similar to those of normal islets. *Diabetologia,* 36**,** 1139-45.

Iwawaki, T., Akai, R. & Kohno, K. 2010. IRE1alpha disruption causes histological abnormality of exocrine tissues, increase of blood glucose level, and decrease of serum immunoglobulin level. *PLoS One,* 5**,** e13052.

Izumi, T., Yokota-Hashimoto, H., Zhao, S., Wang, J., Halban, P. A. & Takeuchi, T. 2003. Dominant Negative Pathogenesis by Mutant Proinsulin in the Akita Diabetic Mouse. *Diabetes,* 52**,** 409-416.

Jeffrey, K. D., Alejandro, E. U., Luciani, D. S., Kalynyak, T. B., Hu, X., Li, H., Lin, Y., Townsend, R. R., Polonsky, K. S. & Johnson, J. D. 2008. Carboxypeptidase E mediates palmitate-induced beta-cell ER stress and apoptosis. *Proc Natl Acad Sci U S A,* 105**,** 8452-7.

Jiang, F.-X., Naselli, G. & Harrison, L. C. 2002. Distinct Distribution of Laminin and Its Integrin Receptors in the Pancreas. *Journal of Histochemistry & Cytochemistry,* 50**,** 1625-1632.

Jiang, G. & Zhang, B. B. 2003. Glucagon and regulation of glucose metabolism. *Am J Physiol Endocrinol Metab,* 284**,** E671-8.

Jiang, H. Y., Wek, S. A., Mcgrath, B. C., Scheuner, D., Kaufman, R. J., Cavener, D. R. & Wek, R. C. 2003. Phosphorylation of the alpha subunit of eukaryotic initiation factor 2 is required for activation of NF-kappaB in response to diverse cellular stresses. *Mol Cell Biol,* 23**,** 5651-63.

Jiang, X. & Couchman, J. R. 2003. Perlecan and Tumor Angiogenesis. *Journal of Histochemistry and Cytochemistry,* 51**,** 1393-1410.

Jones, M., Tussey, L., Athanasou, N. & Jackson, D. G. 2000. Heparan sulfate proteoglycan isoforms of the CD44 hyaluronan receptor induced in human inflammatory macrophages can function as paracrine regulators of fibroblast growth factor action. *J Biol Chem,* 275**,** 7964-74.

Jordan, P. A. & Gibbins, J. M. 2006. Extracellular Disulfide Exchange and the Regulation of Cellular Function. *Antioxidants & Redox Signaling,* 8**,** 312-324.

Jung, H., Nam, H. & Suh, J.-G. 2016. Rapid and efficient identification of the mouse leptin receptor mutation (C57BL/KsJ-db/db) by tetra-primer amplification refractory mutation system-polymerase chain reaction (ARMS-PCR) analysis. *Laboratory Animal Research,* 32**,** 70-73.

Kabani, M., Kelley, S. S., Morrow, M. W., Montgomery, D. L., Sivendran, R., Rose, M. D., Gierasch, L. M. & Brodsky, J. L. 2003. Dependence of Endoplasmic Reticulum-associated Degradation on the Peptide Binding Domain and Concentration of BiP. *Molecular Biology of the Cell,* 14**,** 3437-3448.

Kahn, C. R. & White, M. F. 1988. The insulin receptor and the molecular mechanism of insulin action. *Journal of Clinical Investigation,* 82**,** 1151-1156.

Kahn, S. E., Cooper, M. E. & Del Prato, S. 2014. Pathophysiology and treatment of type 2 diabetes: perspectives on the past, present, and future. *Lancet,* 383**,** 1068-83.

Kahn, S. E., Hull, R. L. & Utzschneider, K. M. 2006. Mechanisms linking obesity to insulin resistance and type 2 diabetes. *Nature,* 444**,** 840-6.

Kaido, T., Yebra, M., Cirulli, V. & Montgomery, A. M. 2004. Regulation of human beta-cell adhesion, motility, and insulin secretion by collagen IV and its receptor alpha1beta1. *J Biol Chem,* 279**,** 53762-9.

Kaiser, N., Leibowitz, G. & Nesher, R. 2003. Glucotoxicity and beta-cell failure in type 2 diabetes mellitus. *J Pediatr Endocrinol Metab,* 16**,** 5-22.

Kammoun, H. L., Allen, T. L., Henstridge, D. C., Barre, S., Coll, R. C., Lancaster, G. I., Cron, L., Reibe, S., Chan, J. Y., Bensellam, M., Laybutt, D. R., Butler, M. S., Robertson, A. a. B., O'neill, L. A., Cooper, M. A. & Febbraio, M. A. 2018. Evidence against a role for NLRP3-driven islet inflammation in db/db mice. *Molecular Metabolism*.

Kammoun, H. L., Kraakman, M. J. & Febbraio, M. A. 2014. Adipose tissue inflammation in glucose metabolism. *Rev Endocr Metab Disord,* 15**,** 31-44.

Kanda, H., Tateya, S., Tamori, Y., Kotani, K., Hiasa, K.-I., Kitazawa, R., Kitazawa, S., Miyachi, H., Maeda, S., Egashira, K. & Kasuga, M. 2006. MCP-1 contributes to macrophage infiltration into adipose tissue, insulin resistance, and hepatic steatosis in obesity. *The Journal of Clinical Investigation,* 116**,** 1494-1505.

Kaneto, H., Kajimoto, Y., Miyagawa, J., Matsuoka, T., Fujitani, Y., Umayahara, Y., Hanafusa, T., Matsuzawa, Y., Yamasaki, Y. & Hori, M. 1999. Beneficial effects of antioxidants in diabetes: possible protection of pancreatic beta-cells against glucose toxicity. *Diabetes,* 48**,** 2398-2406.

Kaneto, H., Matsuoka, T. A., Nakatani, Y., Kawamori, D., Miyatsuka, T., Matsuhisa, M. & Yamasaki, Y. 2005. Oxidative stress, ER stress, and the JNK pathway in type 2 diabetes. *J Mol Med (Berl),* 83**,** 429-39.

Kanety, H., Feinstein, R., Papa, M. Z., Hemi, R. & Karasik, A. 1995. Tumor necrosis factor alpha-induced phosphorylation of insulin receptor substrate-1 (IRS-1). Possible mechanism for suppression of insulin-stimulated tyrosine phosphorylation of IRS-1. *J Biol Chem,* 270**,** 23780-4.

Kang, H. S., Liao, G., Degraff, L. M., Gerrish, K., Bortner, C. D., Garantziotis, S. & Jetten, A. M. 2013. CD44 Plays a Critical Role in Regulating Diet-Induced Adipose Inflammation, Hepatic Steatosis, and Insulin Resistance. *PLOS ONE,* 8**,** e58417.

Kang, K., Reilly, S. M., Karabacak, V., Gangl, M. R., Fitzgerald, K., Hatano, B. & Lee, C. H. 2008. Adipocyte-derived Th2 cytokines and myeloid PPARdelta regulate macrophage polarization and insulin sensitivity. *Cell Metab,* 7**,** 485-95.

Kars, M., Yang, L., Gregor, M. F., Mohammed, B. S., Pietka, T. A., Finck, B. N., Patterson, B. W., Horton, J. D., Mittendorfer, B., Hotamisligil, G. S. & Klein, S. 2010. Tauroursodeoxycholic Acid May Improve Liver and Muscle but Not Adipose Tissue Insulin Sensitivity in Obese Men and Women. *Diabetes,* 59**,** 1899-1905.

Katsuda, Y., Ohta, T., Shinohara, M., Bin, T. & Yamada, T. 2013. Diabetic mouse models. *Open Journal of Animal Sciences,* Vol.03No.04**,** 9.

Kaufman, R. J. 1999. Stress signaling from the lumen of the endoplasmic reticulum: coordination of gene transcriptional and translational controls. *Genes Dev,* 13**,** 1211-33.

Kaufman, R. J. 2011. Beta-Cell Failure, Stress, and Type 2 Diabetes. *The New England journal of medicine,* 365**,** 1931-1933.

Kayo, T. & Koizumi, A. 1998. Mapping of murine diabetogenic gene mody on chromosome 7 at D7Mit258 and its involvement in pancreatic islet and beta cell development during the perinatal period. *Journal of Clinical Investigation,* 101**,** 2112-2118.

Kelly, T., Suva, L. J., Huang, Y., Macleod, V., Miao, H.-Q., Walker, R. C. & Sanderson, R. D. 2005. Expression of Heparanase by Primary Breast Tumors Promotes Bone Resorption in the Absence of Detectable Bone Metastases. *Cancer Research,* 65**,** 5778-5784.

Kharroubi, I., Ladriere, L., Cardozo, A. K., Dogusan, Z., Cnop, M. & Eizirik, D. L. 2004. Free fatty acids and cytokines induce pancreatic beta-cell apoptosis by different mechanisms: role of nuclear factor-kappaB and endoplasmic reticulum stress. *Endocrinology,* 145**,** 5087-96.

Kim, D. & Jun, H.-S. 2017. In Vivo Imaging of Transplanted Pancreatic Islets. *Frontiers in Endocrinology,* 8**,** 382.

Kim, J. W. & Yoon, K. H. 2011. Glucolipotoxicity in Pancreatic beta-Cells. *Diabetes Metab J,* 35**,** 444-50.

Kim, K. E., Jung, Y., Min, S., Nam, M., Heo, R. W., Jeon, B. T., Song, D. H., Yi, C.-O., Jeong, E. A., Kim, H., Kim, J., Jeong, S.-Y., Kwak, W., Ryu, D. H., Horvath, T. L., Roh, G. S. & Hwang, G.-S. 2016. Caloric restriction of db/db mice reverts hepatic steatosis and body weight with divergent hepatic metabolism. *Scientific Reports,* 6**,** 30111.

Kimura, M., Tanaka, S., Isoda, F., Sekigawa, K., Yamakawa, T. & Sekihara, H. 1998. T lymphopenia in obese diabetic (db/db) mice is non-selective and thymus independent. *Life Sci,* 62**,** 1243-50.

King, A. J. F. 2012. The use of animal models in diabetes research. *British Journal of Pharmacology,* 166**,** 877-894.

Kintscher, U., Hartge, M., Hess, K., Foryst-Ludwig, A., Clemenz, M., Wabitsch, M., Fischer-Posovszky, P., Barth, T. F., Dragun, D., Skurk, T., Hauner, H., Bluher, M., Unger, T., Wolf, A. M., Knippschild, U., Hombach, V. & Marx, N. 2008. T-lymphocyte infiltration in visceral adipose tissue: a primary event in adipose tissue inflammation and the development of obesity-mediated insulin resistance. *Arterioscler Thromb Vasc Biol,* 28**,** 1304-10.

Kjellén, L. & Lindahl, U. 1991. Proteoglycans: Structures and Interactions. *Annual Review of Biochemistry,* 60**,** 443-475.

Kjørholt, C., Åkerfeldt, M. C., Biden, T. J. & Laybutt, D. R. 2005. Chronic Hyperglycemia, Independent of Plasma Lipid Levels, Is Sufficient for the Loss of β-Cell Differentiation and Secretory Function in the db/db Mouse Model of Diabetes. *Diabetes,* 54**,** 2755-2763.

Klausner, R. D., Donaldson, J. G. & Lippincott-Schwartz, J. 1992. Brefeldin A: insights into the control of membrane traffic and organelle structure. *The Journal of Cell Biology,* 116**,** 1071-1080.

Klerk, C. P., Smorenburg, S. M., Otten, H. M., Lensing, A. W., Prins, M. H., Piovella, F., Prandoni, P., Bos, M. M., Richel, D. J., Van Tienhoven, G. & Buller, H. R. 2005. The effect of low molecular weight heparin on survival in patients with advanced malignancy. *J Clin Oncol,* 23**,** 2130-5.

Kobayashi, H., Yamazaki, S., Takashima, S., Liu, W., Okuda, H., Yan, J., Fujii, Y., Hitomi, T., Harada, K. H., Habu, T. & Koizumi, A. 2013. Ablation of Rnf213 retards progression of diabetes in the Akita mouse. *Biochem Biophys Res Commun,* 432**,** 519-25.

Kobayashi, K., Forte, T. M., Taniguchi, S., Ishida, B. Y., Oka, K. & Chan, L. 2000. The db/db mouse, a model for diabetic dyslipidemia: molecular characterization and effects of Western diet feeding. *Metabolism,* 49**,** 22-31.

Kobayashi, M., Naomoto, Y., Nobuhisa, T., Okawa, T., Takaoka, M., Shirakawa, Y., Yamatsuji, T., Matsuoka, J., Mizushima, T., Matsuura, H., Nakajima, M., Nakagawa, H., Rustgi, A. & Tanaka, N. 2006. Heparanase regulates esophageal keratinocyte differentiation through nuclear translocation and heparan sulfate cleavage. *Differentiation,* 74**,** 235-43.

Kobayashi, N., Okazaki, S., Sampetrean, O., Irie, J., Itoh, H. & Saya, H. 2018. CD44 variant inhibits insulin secretion in pancreatic β cells by attenuating LAT1-mediated amino acid uptake. *Scientific Reports,* 8**,** 2785.

Kodama, H., Shimojo, N. & Suzuki, K. T. 1991. Distribution of manganese in rat pancreas and identification of its primary binding protein as pro-carboxypeptidase B. *The Biochemical journal,* 278 (Pt 3)**,** 857-862.

Kohfeldt, E., Sasaki, T., Göhring, W. & Timpl, R. 1998. Nidogen-2: a new basement membrane protein with diverse binding properties11Edited by I. B. Holland. *Journal of Molecular Biology,* 282**,** 99-109.

Kojima, E., Takeuchi, A., Haneda, M., Yagi, A., Hasegawa, T., Yamaki, K., Takeda, K., Akira, S., Shimokata, K. & Isobe, K. 2003. The function of GADD34 is a recovery from a shutoff of protein synthesis induced by ER stress: elucidation by GADD34-deficient mice. *FASEB J,* 17**,** 1573-5.

Kolb, H. & Mandrup-Poulsen, T. 2005. An immune origin of type 2 diabetes? *Diabetologia,* 48**,** 1038-50.

Kornfeld, R. & Kornfeld, S. 1985. Assembly of asparagine-linked oligosaccharides. *Annu Rev Biochem,* 54**,** 631-64.

Korpos, É., Kadri, N., Kappelhoff, R., Wegner, J., Overall, C. M., Weber, E., Holmberg, D., Cardell, S. & Sorokin, L. 2013. The Peri-islet Basement Membrane, a Barrier to Infiltrating Leukocytes in Type 1 Diabetes in Mouse and Human. *Diabetes,* 62**,** 531-542.

Kraakman, Michael j., Kammoun, Helene l., Allen, Tamara l., Deswaerte, V., Henstridge, Darren c., Estevez, E., Matthews, Vance b., Neill, B., White, David a., Murphy, Andrew j., Peijs, L., Yang, C., Risis, S., Bruce, Clinton r., Du, X.-J., Bobik, A., Lee-Young, Robert s., Kingwell, Bronwyn a., Vasanthakumar, A., Shi, W., Kallies, A., Lancaster, Graeme i., Rose-John, S. & Febbraio, Mark a. 2015. Blocking IL-6 trans-Signaling Prevents High-Fat Diet-Induced Adipose Tissue Macrophage Recruitment but Does Not Improve Insulin Resistance. *Cell Metabolism,* 21**,** 403-416.

Kraakman, M. J., Murphy, A. J., Jandeleit-Dahm, K. & Kammoun, H. L. 2014. Macrophage Polarization in Obesity and Type 2 Diabetes: Weighing Down Our Understanding of Macrophage Function? *Frontiers in Immunology,* 5**,** 470.

Kreuger, J. & Kjellen, L. 2012. Heparan sulfate biosynthesis: regulation and variability. *J Histochem Cytochem,* 60**,** 898-907.

Kudchadkar, R., Gonzalez, R. & Lewis, K. D. 2008. PI-88: a novel inhibitor of angiogenesis. *Expert Opin Investig Drugs,* 17**,** 1769-76.

Kulkarni, R. N. 2004. The islet beta-cell. *Int J Biochem Cell Biol,* 36**,** 365-71.

Kurup, S., Wijnhoven, T. J., Jenniskens, G. J., Kimata, K., Habuchi, H., Li, J. P., Lindahl, U., Van Kuppevelt, T. H. & Spillmann, D. 2007. Characterization of anti-heparan sulfate phage display antibodies AO4B08 and HS4E4. *J Biol Chem,* 282**,** 21032-42.

Kusminski, C. M., Shetty, S., Orci, L., Unger, R. H. & Scherer, P. E. 2009. Diabetes and apoptosis: lipotoxicity. *Apoptosis,* 14**,** 1484-95.

Lammert, E., Cleaver, O. & Melton, D. 2001. Induction of pancreatic differentiation by signals from blood vessels. *Science,* 294**,** 564-7.

Lang, J. 1999. Molecular mechanisms and regulation of insulin exocytosis as a paradigm of endocrine secretion. *Eur J Biochem,* 259**,** 3-17.

Larsen, C. M., Faulenbach, M., Vaag, A., Ehses, J. A., Donath, M. Y. & Mandrup-Poulsen, T. 2009. Sustained effects of interleukin-1 receptor antagonist treatment in type 2 diabetes. *Diabetes Care,* 32**,** 1663-8.

Larsen, C. M., Faulenbach, M., Vaag, A., Volund, A., Ehses, J. A., Seifert, B., Mandrup-Poulsen, T. & Donath, M. Y. 2007. Interleukin-1-receptor antagonist in type 2 diabetes mellitus. *N Engl J Med,* 356**,** 1517-26.

Larsson, L.-I., Sundler, F. & Håkanson, R. 1975. Immunohistochemical localization of human pancreatic polypeptide (HPP) to a population of islet cells. *Cell and Tissue Research,* 156**,** 167-171.

Latif, Z. A., Noel, J. & Alejandro, R. 1988. A simple method of staining fresh and cultured islets. *Transplantation,* 45**,** 827-30.

Laurila, P. & Leivo, I. 1993. Basement membrane and interstitial matrix components form separate matrices in heterokaryons of PYS-2 cells and fibroblasts. *Journal of Cell Science,* 104**,** 59-68.

Laybutt, D. R., Kaneto, H., Hasenkamp, W., Grey, S., Jonas, J. C., Sgroi, D. C., Groff, A., Ferran, C., Bonner-Weir, S., Sharma, A. & Weir, G. C. 2002. Increased expression of antioxidant and antiapoptotic genes in islets that may contribute to beta-cell survival during chronic hyperglycemia. *Diabetes,* 51**,** 413-23.

Laybutt, D. R., Preston, A. M., Åkerfeldt, M. C., Kench, J. G., Busch, A. K., Biankin, A. V. & Biden, T. J. 2007. Endoplasmic reticulum stress contributes to beta cell apoptosis in type 2 diabetes. *Diabetologia,* 50**,** 752-763.

Lebensztejn, D. M. 2000. Application of ursodeoxycholic acid (UDCA) in the therapy of liver and biliary duct diseases in children. *Med Sci Monit,* 6**,** 632-6.

Lebien, T. W. & Tedder, T. F. 2008. B lymphocytes: how they develop and function. *Blood,* 112**,** 1570-80.

Lee, A. H., Heidtman, K., Hotamisligil, G. S. & Glimcher, L. H. 2011. Dual and opposing roles of the unfolded protein response regulated by IRE1alpha and XBP1 in proinsulin processing and insulin secretion. *Proc Natl Acad Sci U S A,* 108**,** 8885-90.

Lee, A. H., Iwakoshi, N. N. & Glimcher, L. H. 2003. XBP-1 regulates a subset of endoplasmic reticulum resident chaperone genes in the unfolded protein response. *Mol Cell Biol,* 23**,** 7448-59.

Lee, A. S. 2005. The ER chaperone and signaling regulator GRP78/BiP as a monitor of endoplasmic reticulum stress. *Methods,* 35**,** 373-381.

Lee, S.-E., Jang, I.-S., Park, J.-S., Lee, J.-H., Lee, S.-Y., Baek, S.-Y., Lee, S.-H. & Lee, H. 2010a. Systemic immunity of obese-diabetes model (db/db) mice. *Molecular & Cellular Toxicology,* 6**,** 143-149.

Lee, Y. Y., Hong, S. H., Lee, Y. J., Chung, S. S., Jung, H. S., Park, S. G. & Park, K. S. 2010b. Tauroursodeoxycholate (TUDCA), chemical chaperone, enhances function of islets by reducing ER stress. *Biochemical and Biophysical Research Communications,* 397**,** 735-739.

Lei, X., Zhang, S., Barbour, S. E., Bohrer, A., Ford, E. L., Koizumi, A., Papa, F. R. & Ramanadham, S. 2010. Spontaneous development of endoplasmic reticulum stress that can lead to diabetes mellitus is associated with higher calcium-independent phospholipase A2 expression: a role for regulation by SREBP-1. *J Biol Chem,* 285**,** 6693-705.

Lenzen, S., Drinkgern, J. & Tiedge, M. 1996. Low antioxidant enzyme gene expression in pancreatic islets compared with various other mouse tissues. *Free Radic Biol Med,* 20**,** 463-6.

Leonova, E. I. & Galzitskaya, O. V. 2013. Structure and functions of syndecans in vertebrates. *Biochemistry (Moscow),* 78**,** 1071-1085.

Lerner, I., Hermano, E., Zcharia, E., Rodkin, D., Bulvik, R., Doviner, V., Rubinstein, A. M., Ishai-Michaeli, R., Atzmon, R., Sherman, Y., Meirovitz, A., Peretz, T., Vlodavsky, I. & Elkin, M. 2011. Heparanase powers a chronic inflammatory circuit that promotes colitis-associated tumorigenesis in mice. *J Clin Invest,* 121**,** 1709-21.

Leroux, L., Desbois, P., Lamotte, L., Duvillie, B., Cordonnier, N., Jackerott, M., Jami, J., Bucchini, D. & Joshi, R. L. 2001. Compensatory responses in mice carrying a null mutation for Ins1 or Ins2. *Diabetes,* 50 Suppl 1**,** S150-3.

Lesley, J., Hascall, V. C., Tammi, M. & Hyman, R. 2000. Hyaluronan binding by cell surface CD44. *J Biol Chem,* 275**,** 26967-75.

Lesley, J., Howes, N., Perschl, A. & Hyman, R. 1994. Hyaluronan binding function of CD44 is transiently activated on T cells during an in vivo immune response. *J Exp Med,* 180**,** 383-7.

Leung, P. S. & Ip, S. P. 2006. Pancreatic acinar cell: Its role in acute pancreatitis. *The International Journal of Biochemistry & Cell Biology,* 38**,** 1024-1030.

Levy-Adam, F., Abboud-Jarrous, G., Guerrini, M., Beccati, D., Vlodavsky, I. & Ilan, N. 2005. Identification and characterization of heparin/heparan sulfate binding domains of the endoglycosidase heparanase. *J Biol Chem,* 280**,** 20457-66.

Levy-Adam, F., Feld, S., Cohen-Kaplan, V., Shteingauz, A., Gross, M., Arvatz, G., Naroditsky, I., Ilan, N., Doweck, I. & Vlodavsky, I. 2010. Heparanase 2 Interacts with Heparan Sulfate with High Affinity and Inhibits Heparanase Activity. *The Journal of Biological Chemistry,* 285**,** 28010-28019.

Levy-Adam, F., Feld, S., Suss-Toby, E., Vlodavsky, I. & Ilan, N. 2008. Heparanase facilitates cell adhesion and spreading by clustering of cell surface heparan sulfate proteoglycans. *PLoS One,* 3**,** e2319.

Li, N., Frigerio, F. & Maechler, P. 2008a. The sensitivity of pancreatic beta-cells to mitochondrial injuries triggered by lipotoxicity and oxidative stress. *Biochem Soc Trans,* 36**,** 930-4.

Li, R. W., Freeman, C., Yu, D., Hindmarsh, E. J., Tymms, K. E., Parish, C. R. & Smith, P. N. 2008b. Dramatic regulation of heparanase activity and angiogenesis gene expression in synovium from patients with rheumatoid arthritis. *Arthritis Rheum,* 58**,** 1590-600.

Lipson, K. L., Fonseca, S. G., Ishigaki, S., Nguyen, L. X., Foss, E., Bortell, R., Rossini, A. A. & Urano, F. 2006. Regulation of insulin biosynthesis in pancreatic beta cells by an endoplasmic reticulum-resident protein kinase IRE1. *Cell Metab,* 4**,** 245-54.

Liu, C.-J., Chang, J., Lee, P.-H., Lin, D.-Y., Wu, C.-C., Jeng, L.-B., Lin, Y.-J., Mok, K.-T., Lee, W.-C., Yeh, H.-Z., Ho, M.-C., Yang, S.-S., Yang, M.-D., Yu, M.-C., Hu, R.-H., Peng, C.-Y., Lai, K.-L., Chang, S. S.-C. & Chen, P.-J. 2014. Adjuvant heparanase inhibitor PI-88 therapy for hepatocellular carcinoma recurrence. *World Journal of Gastroenterology : WJG,* 20**,** 11384-11393.

Liu, J. & Pedersen, L. C. 2007. Anticoagulant Heparan Sulfate: Structural Specificity and Biosynthesis. *Applied microbiology and biotechnology,* 74**,** 263-272.

Liu, M., Hodish, I., Haataja, L., Lara-Lemus, R., Rajpal, G., Wright, J. & Arvan, P. 2010. Proinsulin misfolding and diabetes: mutant INS gene-induced diabetes of youth. *Trends Endocrinol Metab,* 21**,** 652-9.

Liu, M., Hodish, I., Rhodes, C. J. & Arvan, P. 2007. Proinsulin maturation, misfolding, and proteotoxicity. *Proceedings of the National Academy of Sciences,* 104**,** 15841-15846.

Liu, N., Qiang, W., Kuang, X., Thuillier, P., Lynn, W. S. & Wong, P. K. Y. 2002. The peroxisome proliferator phenylbutyric acid (PBA) protects astrocytes from ts1 MoMuLV-induced oxidative cell death. *Journal of NeuroVirology,* 8**,** 318-325.

Liu, Z., Kim, W., Chen, Z., Shin, Y.-K., Carlson, O. D., Fiori, J. L., Xin, L., Napora, J. K., Short, R., Odetunde, J. O., Lao, Q. & Egan, J. M. 2011. Insulin and Glucagon Regulate Pancreatic α-Cell Proliferation. *PLOS ONE,* 6**,** e16096.

Livak, K. J. & Schmittgen, T. D. 2001. Analysis of relative gene expression data using real-time quantitative PCR and the 2(-Delta Delta C(T)) Method. *Methods,* 25**,** 402-8.

Lomedico, P. & Saunders, G. 1977. Cell-free modulation of proinsulin synthesis. *Science,* 198**,** 620-622.

López, I., Tournillon, A.-S., Prado Martins, R., Karakostis, K., Malbert-Colas, L., Nylander, K. & Fåhraeus, R. 2017. p53-mediated suppression of BiP triggers BIK-induced apoptosis during prolonged endoplasmic reticulum stress. *Cell Death and Differentiation,* 24**,** 1717-1729.

Lord, G. M., Matarese, G., Howard, J. K., Baker, R. J., Bloom, S. R. & Lechler, R. I. 1998. Leptin modulates the T-cell immune response and reverses starvation-induced immunosuppression. *Nature,* 394**,** 897-901.

Low, J. T., Mitchell, J. M., Do, O. H., Bax, J., Rawlings, A., Zavortink, M., Morgan, G., Parton, R. G., Gaisano, H. Y. & Thorn, P. 2013. Glucose principally regulates insulin secretion in mouse islets by controlling the numbers of granule fusion events per cell. *Diabetologia,* 56**,** 2629-2637.

Low, J. T., Zavortink, M., Mitchell, J. M., Gan, W. J., Do, O. H., Schwiening, C. J., Gaisano, H. Y. & Thorn, P. 2014. Insulin secretion from beta cells in intact mouse islets is targeted towards the vasculature. *Diabetologia,* 57**,** 1655-63.

Lowell, B. B. & Shulman, G. I. 2005. Mitochondrial dysfunction and type 2 diabetes. *Science,* 307**,** 384-7.

Lumeng, C. N., Bodzin, J. L. & Saltiel, A. R. 2007a. Obesity induces a phenotypic switch in adipose tissue macrophage polarization. *J Clin Invest,* 117**,** 175-84.

Lumeng, C. N., Delproposto, J. B., Westcott, D. J. & Saltiel, A. R. 2008. Phenotypic Switching of Adipose Tissue Macrophages With Obesity Is Generated by Spatiotemporal Differences in Macrophage Subtypes. *Diabetes,* 57**,** 3239-3246.

Lumeng, C. N., Deyoung, S. M., Bodzin, J. L. & Saltiel, A. R. 2007b. Increased inflammatory properties of adipose tissue macrophages recruited during diet-induced obesity. *Diabetes,* 56**,** 16-23.

Lytrivi, M., Igoillo-Esteve, M. & Cnop, M. 2018. Inflammatory stress in islet beta-cells: therapeutic implications for type 2 diabetes? *Curr Opin Pharmacol,* 43**,** 40-45.

Lytton, J., Westlin, M. & Hanley, M. R. 1991. Thapsigargin inhibits the sarcoplasmic or endoplasmic reticulum Ca-ATPase family of calcium pumps. *J Biol Chem,* 266**,** 17067-71.

Ma, Y., Brewer, J. W., Diehl, J. A. & Hendershot, L. M. 2002. Two distinct stress signaling pathways converge upon the CHOP promoter during the mammalian unfolded protein response. *J Mol Biol,* 318**,** 1351-65.

Ma, Y. & Hendershot, L. M. 2004. ER chaperone functions during normal and stress conditions. *Journal of Chemical Neuroanatomy,* 28**,** 51-65.

Maccracken, J. & Hoel, D. 1997. From ants to analogues. Puzzles and promises in diabetes management. *Postgrad Med,* 101**,** 138-40, 143-5, 149-50.

Macdonald, P. E., Braun, M., Galvanovskis, J. & Rorsman, P. 2006. Release of small transmitters through kiss-and-run fusion pores in rat pancreatic β cells. *Cell Metabolism,* 4**,** 283-290.

Maedler, K., Oberholzer, J., Bucher, P., Spinas, G. A. & Donath, M. Y. 2003. Monounsaturated Fatty Acids Prevent the Deleterious Effects of Palmitate and High Glucose on Human Pancreatic β-Cell Turnover and Function. *Diabetes,* 52**,** 726-733.

Maedler, K., Sergeev, P., Ehses, J. A., Mathe, Z., Bosco, D., Berney, T., Dayer, J.-M., Reinecke, M., Halban, P. A. & Donath, M. Y. 2004. Leptin modulates β cell expression of IL-1 receptor antagonist and release of IL-1β in human islets. *Proceedings of the National Academy of Sciences of the United States of America,* 101**,** 8138-8143.

Magliano, D. J., Shaw, J. E. & Zimmet, P. Z. 2006. How to best define the metabolic syndrome. *Ann Med,* 38**,** 34-41.

Makki, K., Froguel, P. & Wolowczuk, I. 2013. Adipose Tissue in Obesity-Related Inflammation and Insulin Resistance: Cells, Cytokines, and Chemokines. *ISRN Inflammation,* 2013**,** 139239.

Malhotra, J. D. & Kaufman, R. J. 2007. Endoplasmic reticulum stress and oxidative stress: a vicious cycle or a double-edged sword? *Antioxid Redox Signal,* 9**,** 2277-93.

Malhotra, J. D., Miao, H., Zhang, K., Wolfson, A., Pennathur, S., Pipe, S. W. & Kaufman, R. J. 2008. Antioxidants reduce endoplasmic reticulum stress and improve protein secretion. *Proc Natl Acad Sci U S A,* 105**,** 18525-30.

Mallone, R., Brezar, V. & Boitard, C. 2011. T cell recognition of autoantigens in human type 1 diabetes: clinical perspectives. *Clin Dev Immunol,* 2011**,** 513210.

Mancuso, P. 2016. The role of adipokines in chronic inflammation. *ImmunoTargets and Therapy,* 5**,** 47-56.

Mandel, M. A. & Mahmoud, A. a. F. 1978. Impairment of Cell-Mediated Immunity in Mutation Diabetic Mice (db/db). *The Journal of Immunology,* 120**,** 1375-1377.

Mantovani, A., Sozzani, S., Locati, M., Allavena, P. & Sica, A. 2002. Macrophage polarization: tumor-associated macrophages as a paradigm for polarized M2 mononuclear phagocytes. *Trends Immunol,* 23**,** 549-55.

Marchetti, P. 2016. Islet inflammation in type 2 diabetes. *Diabetologia,* 59**,** 668-672.

Marchetti, P., Bugliani, M., Lupi, R., Marselli, L., Masini, M., Boggi, U., Filipponi, F., Weir, G. C., Eizirik, D. L. & Cnop, M. 2007. The endoplasmic reticulum in pancreatic beta cells of type 2 diabetes patients. *Diabetologia,* 50**,** 2486-94.

Marciniak, S. J., Yun, C. Y., Oyadomari, S., Novoa, I., Zhang, Y., Jungreis, R., Nagata, K., Harding, H. P. & Ron, D. 2004. CHOP induces death by promoting protein synthesis and oxidation in the stressed endoplasmic reticulum. *Genes Dev,* 18**,** 3066-77.

Marhfour, I., Lopez, X. M., Lefkaditis, D., Salmon, I., Allagnat, F., Richardson, S. J., Morgan, N. G. & Eizirik, D. L. 2012. Expression of endoplasmic reticulum stress markers in the islets of patients with type 1 diabetes. *Diabetologia,* 55**,** 2417-20.

Marneros, A. G. & Olsen, B. R. 2005. Physiological role of collagen XVIII and endostatin. *FASEB J,* 19**,** 716-28.

Marroqui, L., Santin, I., Dos Santos, R. S., Marselli, L., Marchetti, P. & Eizirik, D. L. 2014. BACH2, a candidate risk gene for type 1 diabetes, regulates apoptosis in

pancreatic beta-cells via JNK1 modulation and crosstalk with the candidate gene PTPN2. *Diabetes,* 63**,** 2516-27.

Marshall, C. B. 2016. Rethinking glomerular basement membrane thickening in diabetic nephropathy: adaptive or pathogenic? *American Journal of Physiology-Renal Physiology,* 311**,** F831-F843.

Martinez, F. O. & Gordon, S. 2014. The M1 and M2 paradigm of macrophage activation: time for reassessment. *F1000Prime Rep,* 6**,** 13.

Martinez, J. A., Zhang, Z., Svetlov, S. I., Hayes, R. L., Wang, K. K. & Larner, S. F. 2010. Calpain and caspase processing of caspase-12 contribute to the ER stress-induced cell death pathway in differentiated PC12 cells. *Apoptosis,* 15**,** 1480-93.

Mast, S. W., Diekman, K., Karaveg, K., Davis, A., Sifers, R. N. & Moremen, K. W. 2005. Human EDEM2, a novel homolog of family 47 glycosidases, is involved in ER-associated degradation of glycoproteins. *Glycobiology,* 15**,** 421-36.

Mathers, J., Fraser, J. A., Mcmahon, M., Saunders, R. D., Hayes, J. D. & Mclellan, L. I. 2004. Antioxidant and cytoprotective responses to redox stress. *Biochem Soc Symp***,** 157-76.

Mathis, D., Vence, L. & Benoist, C. 2001a. beta-Cell death during progression to diabetes. *Nature,* 414**,** 792-8.

Mathis, D., Vence, L. & Benoist, C. 2001b. [beta]-Cell death during progression to diabetes. *Nature,* 414**,** 792-798.

Matsuda, T., Kido, Y., Asahara, S.-I., Kaisho, T., Tanaka, T., Hashimoto, N., Shigeyama, Y., Takeda, A., Inoue, T., Shibutani, Y., Koyanagi, M., Hosooka, T., Matsumoto, M., Inoue, H., Uchida, T., Koike, M., Uchiyama, Y., Akira, S. & Kasuga, M. 2010. Ablation of C/EBPβ alleviates ER stress and pancreatic β cell failure through the GRP78 chaperone in mice. *The Journal of Clinical Investigation,* 120**,** 115-126.

Mattsson, G. 2005. The endothelial cells in islets of langerhans. *Ups J Med Sci,* 110**,** 1-15.

Matveyenko, A. V., Gurlo, T., Daval, M., Butler, A. E. & Butler, P. C. 2009. Successful Versus Failed Adaptation to High-Fat Diet–Induced Insulin Resistance. *The Role of IAPP-Induced β-Cell Endoplasmic Reticulum Stress,* 58**,** 906-916.

Maurizi, G., Guardia, L. D., Maurizi, A. & Poloni, A. 2018. Adipocytes properties and crosstalk with immune system in obesity ‐ related inflammation. *Journal of Cellular Physiology,* 233**,** 88-97.

Mcardle, M., Finucane, O., Connaughton, R., Mcmorrow, A. & Roche, H. 2013. Mechanisms of Obesity-Induced Inflammation and Insulin Resistance: Insights into the Emerging Role of Nutritional Strategies. *Frontiers in Endocrinology,* 4.

Mcfarlin, B. K., Carpenter, K. C., Strohacker, K. & Breslin, W. L. 2012. Comparison of Blood Monocytes and Adipose Tissue Macrophages in a Mouse Model Diet-Induced Weight Gain. *Comparative Medicine,* 62**,** 462-465.

Mckenzie, E. A. 2007. Heparanase: a target for drug discovery in cancer and inflammation. *British Journal of Pharmacology,* 151**,** 1-14.

Mcnelis, Joanne c. & Olefsky, Jerrold m. 2014. Macrophages, Immunity, and Metabolic Disease. *Immunity,* 41**,** 36-48.

Meng, F., Abedini, A., Song, B. & Raleigh, D. P. 2007. Amyloid Formation by Pro-Islet Amyloid Polypeptide Processing Intermediates: Examination of the Role of Protein Heparan Sulfate Interactions and Implications for Islet Amyloid Formation in Type 2 Diabetes. *Biochemistry,* 46**,** 12091-12099.

Menu, P., Mayor, A., Zhou, R., Tardivel, A., Ichijo, H., Mori, K. & Tschopp, J. 2012. ER stress activates the NLRP3 inflammasome via an UPR-independent pathway. *Cell Death &Amp; Disease,* 3**,** e261.

Mezza, T., Muscogiuri, G., Sorice, G. P., Clemente, G., Hu, J., Pontecorvi, A., Holst, J. J., Giaccari, A. & Kulkarni, R. N. 2014. Insulin Resistance Alters Islet Morphology in Nondiabetic Humans. *Diabetes,* 63**,** 994-1007.

Miani, M., Barthson, J., Colli, M. L., Brozzi, F., Cnop, M. & Eizirik, D. L. 2013. Endoplasmic reticulum stress sensitizes pancreatic beta cells to interleukin-1β-induced apoptosis via Bim/A1 imbalance. *Cell Death &Amp; Disease,* 4**,** e701.

Miao, H. Q., Navarro, E., Patel, S., Sargent, D., Koo, H., Wan, H., Plata, A., Zhou, Q., Ludwig, D., Bohlen, P. & Kussie, P. 2002. Cloning, expression, and purification of mouse heparanase. *Protein Expr Purif,* 26**,** 425-31.

Mimori, S., Okuma, Y., Kaneko, M., Kawada, K., Hosoi, T., Ozawa, K., Nomura, Y. & Hamana, H. 2012. Protective effects of 4-phenylbutyrate derivatives on the neuronal cell death and endoplasmic reticulum stress. *Biol Pharm Bull,* 35**,** 84-90.

Miyazaki, J., Araki, K., Yamato, E., Ikegami, H., Asano, T., Shibasaki, Y., Oka, Y. & Yamamura, K. 1990. Establishment of a pancreatic beta cell line that retains glucose-inducible insulin secretion: special reference to expression of glucose transporter isoforms. *Endocrinology,* 127**,** 126-32.

Molofsky, A. B., Nussbaum, J. C., Liang, H. E., Van Dyken, S. J., Cheng, L. E., Mohapatra, A., Chawla, A. & Locksley, R. M. 2013. Innate lymphoid type 2 cells sustain visceral adipose tissue eosinophils and alternatively activated macrophages. *J Exp Med,* 210**,** 535-49.

Morishima, N., Nakanishi, K., Takenouchi, H., Shibata, T. & Yasuhiko, Y. 2002. An endoplasmic reticulum stress-specific caspase cascade in apoptosis. Cytochrome c-independent activation of caspase-9 by caspase-12. *J Biol Chem,* 277**,** 34287-94.

Mraz, M. & Haluzik, M. 2014. The role of adipose tissue immune cells in obesity and low-grade inflammation. *J Endocrinol,* 222**,** R113-27.

Mraz, M., Lacinova, Z., Drapalova, J., Haluzikova, D., Horinek, A., Matoulek, M., Trachta, P., Kavalkova, P., Svacina, S. & Haluzik, M. 2011. The effect of very-low-calorie diet on mRNA expression of inflammation-related genes in subcutaneous adipose tissue and peripheral monocytes of obese patients with type 2 diabetes mellitus. *J Clin Endocrinol Metab,* 96**,** E606-13.

Nagareddy, P. R., Kraakman, M., Masters, S. L., Stirzaker, R. A., Gorman, D. J., Grant, R. W., Dragoljevic, D., Hong, E. S., Abdel-Latif, A., Smyth, S. S., Choi, S. H., Korner, J., Bornfeldt, K. E., Fisher, E. A., Dixit, V. D., Tall, A. R., Goldberg, I. J. & Murphy, A. J. 2014. Adipose tissue macrophages promote myelopoiesis and monocytosis in obesity. *Cell metabolism,* 19**,** 821-835.

Nakagawa, T., Zhu, H., Morishima, N., Li, E., Xu, J., Yankner, B. A. & Yuan, J. 2000. Caspase-12 mediates endoplasmic-reticulum-specific apoptosis and cytotoxicity by amyloid-beta. *Nature,* 403**,** 98-103.

Nasteska, D. & Hodson, D. J. 2018. The role of beta cell heterogeneity in islet function and insulin release. *Journal of Molecular Endocrinology,* 61**,** R43-R60.

Nathan , D. M. 1993. Long-Term Complications of Diabetes Mellitus. *New England Journal of Medicine,* 328**,** 1676-1685.

Nepton, S. 2013. Beta-Cell Function and Failure. *In:* ESCHER, A. P. & LI, A. (eds.) *Type 1 Diabetes.* Rijeka: InTech.

Nguyen, M. T., Favelyukis, S., Nguyen, A. K., Reichart, D., Scott, P. A., Jenn, A., Liu-Bryan, R., Glass, C. K., Neels, J. G. & Olefsky, J. M. 2007. A subpopulation of macrophages infiltrates hypertrophic adipose tissue and is activated by free fatty acids via Toll-like receptors 2 and 4 and JNK-dependent pathways. *J Biol Chem,* 282**,** 35279-92.

Nguyen, M. T. A., Chen, A., Lu, W. J., Fan, W., Li, P.-P., Oh, D. Y. & Patsouris, D. 2012. Regulation of Chemokine and Chemokine Receptor Expression by PPARγ in Adipocytes and Macrophages. *PLOS ONE,* 7**,** e34976.

Nikulina, M. A., Sandhu, N., Shamim, Z., Andersen, N. A., Oberson, A., Dupraz, P., Thorens, B., Karlsen, A. E., Bonny, C. & Mandrup-Poulsen, T. 2003. The JNK binding domain of islet-brain 1 inhibits IL-1 induced JNK activity and apoptosis but not the transcription of key proapoptotic or protective genes in insulin-secreting cell lines. *Cytokine,* 24**,** 13-24.

Nishi, Y., Uryu, M., Yamanaka, S., Watanabe, K., Kitamura, N., Iguchi, M. & Mitsuhashi, S. 1990. The structure and mechanical properties of sheets prepared from bacterial cellulose. *Journal of Materials Science,* 25**,** 2997-3001.

Nishikawa, S.-I., Fewell, S. W., Kato, Y., Brodsky, J. L. & Endo, T. 2001. Molecular Chaperones in the Yeast Endoplasmic Reticulum Maintain the Solubility of Proteins for Retrotranslocation and Degradation. *The Journal of Cell Biology,* 153**,** 1061-1070.

Nishikawa, S., Brodsky, J. L. & Nakatsukasa, K. 2005. Roles of molecular chaperones in endoplasmic reticulum (ER) quality control and ER-associated degradation (ERAD). *J Biochem,* 137**,** 551-5.

Nishimura, S., Manabe, I., Nagasaki, M., Eto, K., Yamashita, H., Ohsugi, M., Otsu, M., Hara, K., Ueki, K., Sugiura, S., Yoshimura, K., Kadowaki, T. & Nagai, R. 2009. CD8+ effector T cells contribute to macrophage recruitment and adipose tissue inflammation in obesity. *Nat Med,* 15**,** 914-20.

Nishitoh, H., Matsuzawa, A., Tobiume, K., Saegusa, K., Takeda, K., Inoue, K., Hori, S., Kakizuka, A. & Ichijo, H. 2002. ASK1 is essential for endoplasmic reticulum stress-induced neuronal cell death triggered by expanded polyglutamine repeats. *Genes Dev,* 16**,** 1345-55.

Nobuhisa, T., Naomoto, Y., Okawa, T., Takaoka, M., Gunduz, M., Motoki, T., Nagatsuka, H., Tsujigiwa, H., Shirakawa, Y., Yamatsuji, T., Haisa, M., Matsuoka, J., Kurebayashi, J., Nakajima, M., Taniguchi, S. I., Sagara, J., Dong, J. & Tanaka, N. 2007. Translocation of heparanase into nucleus results in cell differentiation. *Cancer Science,* 98**,** 535-540.

Nolan, C. J., Madiraju, M. S. R., Delghingaro-Augusto, V., Peyot, M.-L. & Prentki, M. 2006. Fatty Acid Signaling in the β-Cell and Insulin Secretion. *Diabetes,* 55**,** S16-S23.

Nomikos, I. N., Wang, Y. & Lafferty, K. J. 1989. Involvement of O2 radicals in 'autoimmune' diabetes. *Immunol Cell Biol,* 67 (Pt 1)**,** 85-7.

Nozaki, J., Kubota, H., Yoshida, H., Naitoh, M., Goji, J., Yoshinaga, T., Mori, K., Koizumi, A. & Nagata, K. 2004. The endoplasmic reticulum stress response is stimulated through the continuous activation of transcription factors ATF6 and XBP1 in Ins2+/Akita pancreatic beta cells. *Genes Cells,* 9**,** 261-70.

Nunes, A. F., Amaral, J. D., Lo, A. C., Fonseca, M. B., Viana, R. J. S., Callaerts-Vegh, Z., D'hooge, R. & Rodrigues, C. M. P. 2012. TUDCA, a Bile Acid, Attenuates Amyloid Precursor Protein Processing and Amyloid-β Deposition in APP/PS1 Mice. *Molecular Neurobiology,* 45**,** 440-454.

Odegaard, J. I., Ricardo-Gonzalez, R. R., Goforth, M. H., Morel, C. R., Subramanian, V., Mukundan, L., Red Eagle, A., Vats, D., Brombacher, F., Ferrante, A. W. & Chawla, A. 2007. Macrophage-specific PPARgamma controls alternative activation and improves insulin resistance. *Nature,* 447**,** 1116-20.

Ogihara, T. & Mirmira, R. G. 2010. An islet in distress: β cell failure in type 2 diabetes. *Journal of Diabetes Investigation,* 1**,** 123-133.

Oh, D. Y., Morinaga, H., Talukdar, S., Bae, E. J. & Olefsky, J. M. 2012. Increased macrophage migration into adipose tissue in obese mice. *Diabetes,* 61**,** 346-54.

Okada, T., Yoshida, H., Akazawa, R., Negishi, M. & Mori, K. 2002. Distinct roles of activating transcription factor 6 (ATF6) and double-stranded RNA-activated protein kinase-like endoplasmic reticulum kinase (PERK) in transcription during the mammalian unfolded protein response. *Biochem J,* 366**,** 585-94.

Olefsky, J. M. & Glass, C. K. 2010. Macrophages, inflammation, and insulin resistance. *Annu Rev Physiol,* 72**,** 219-46.

Olivecrona, G. 2016. Role of lipoprotein lipase in lipid metabolism. *Curr Opin Lipidol,* 27**,** 233-41.

Olofsson, C. S., Gopel, S. O., Barg, S., Galvanovskis, J., Ma, X., Salehi, A., Rorsman, P. & Eliasson, L. 2002. Fast insulin secretion reflects exocytosis of docked granules in mouse pancreatic B-cells. *Pflugers Arch,* 444**,** 43-51.

Olokoba, A. B., Obateru, O. A. & Olokoba, L. B. 2012. Type 2 Diabetes Mellitus: A Review of Current Trends. *Oman Medical Journal,* 27**,** 269-273.

Omikorede, O., Qi, C., Gorman, T., Chapman, P., Yu, A., Smith, D. M. & Herbert, T. P. 2013. ER stress in rodent islets of Langerhans is concomitant with obesity and beta-cell compensation but not with beta-cell dysfunction and diabetes. *Nutr Diabetes,* 3**,** e93.

Oslowski, Christine m., Hara, T., O'sullivan-Murphy, B., Kanekura, K., Lu, S., Hara, M., Ishigaki, S., Zhu, Lihua j., Hayashi, E., Hui, Simon t., Greiner, D., Kaufman, Randal j., Bortell, R. & Urano, F. 2012. Thioredoxin-Interacting Protein Mediates ER Stress-Induced β Cell Death through Initiation of the Inflammasome. *Cell Metabolism,* 16**,** 265-273.

Oslowski, C. M. & Urano, F. 2011. Measuring ER stress and the unfolded protein response using mammalian tissue culture system. *Methods in enzymology,* 490**,** 71-92.

Otonkoski, T., Banerjee, M., Korsgren, O., Thornell, L. E. & Virtanen, I. 2008. Unique basement membrane structure of human pancreatic islets: implications for beta-cell growth and differentiation. *Diabetes Obes Metab,* 10 Suppl 4**,** 119-27.

Oyadomari, S., Araki, E. & Mori, M. 2002a. Endoplasmic reticulum stress-mediated apoptosis in pancreatic β-cells. *Apoptosis,* 7**,** 335-345.

Oyadomari, S., Koizumi, A., Takeda, K., Gotoh, T., Akira, S., Araki, E. & Mori, M. 2002b. Targeted disruption of the Chop gene delays endoplasmic reticulum stress-mediated diabetes. *J Clin Invest,* 109**,** 525-32.

Oyadomari, S. & Mori, M. 2004. Roles of CHOP/GADD153 in endoplasmic reticulum stress. *Cell Death Differ,* 11**,** 381-9.

Oyadomari, S., Takeda, K., Takiguchi, M., Gotoh, T., Matsumoto, M., Wada, I., Akira, S., Araki, E. & Mori, M. 2001. Nitric oxide-induced apoptosis in pancreatic beta cells is mediated by the endoplasmic reticulum stress pathway. *Proc Natl Acad Sci U S A,* 98**,** 10845-50.

Ozcan, L., Ergin, A. S., Lu, A., Chung, J., Sarkar, S., Nie, D., Myers, M. G. & Ozcan, U. 2009. Endoplasmic Reticulum Stress Plays a Central Role in Development of Leptin Resistance. *Cell Metabolism,* 9**,** 35-51.

Ozcan, U., Cao, Q., Yilmaz, E., Lee, A. H., Iwakoshi, N. N., Ozdelen, E., Tuncman, G., Gorgun, C., Glimcher, L. H. & Hotamisligil, G. S. 2004. Endoplasmic reticulum stress links obesity, insulin action, and type 2 diabetes. *Science,* 306**,** 457-61.

Özcan, U., Yilmaz, E., Özcan, L., Furuhashi, M., Vaillancourt, E., Smith, R. O., Görgün, C. Z. & Hotamisligil, G. S. 2006. Chemical Chaperones Reduce ER Stress and Restore Glucose Homeostasis in a Mouse Model of Type 2 Diabetes. *Science (New York, N.Y.),* 313**,** 1137-1140.

Palmer, G., Aurrand-Lions, M., Contassot, E., Talabot-Ayer, D., Ducrest-Gay, D., Vesin, C., Chobaz-Péclat, V., Busso, N. & Gabay, C. 2006. Indirect Effects of Leptin Receptor Deficiency on Lymphocyte Populations and Immune Response in db/db Mice. *The Journal of Immunology,* 177**,** 2899-2907.

Palmer, G., Talabot‐Ayer, D., Lamacchia, C., Toy, D., Seemayer, C. A., Viatte, S., Finckh, A., Smith, D. E. & Gabay, C. 2009. Inhibition of interleukin‐33 signaling attenuates the severity of experimental arthritis. *Arthritis & Rheumatism,* 60**,** 738-749.

Panzhinskiy, E., Ren, J. & Nair, S. 2013. Protein Tyrosine Phosphatase 1B and Insulin Resistance: Role of Endoplasmic Reticulum Stress/Reactive Oxygen Species/Nuclear Factor Kappa B Axis. *PLOS ONE,* 8**,** e77228.

Parameswaran, N. & Patial, S. 2010. Tumor Necrosis Factor-α Signaling in Macrophages. *Critical reviews in eukaryotic gene expression,* 20**,** 87-103.

Parish, C. R. 2005. Heparan sulfate and inflammation. *Nat Immunol,* 6**,** 861-2.

Parish, C. R. 2006. The role of heparan sulphate in inflammation. 6**,** 633.

Parish, C. R., Coombe, D. R., Jakobsen, K. B., Bennett, F. A. & Underwood, P. A. 1987. Evidence that sulphated polysaccharides inhibit tumour metastasis by blocking tumour-cell-derived heparanases. *International Journal of Cancer,* 40**,** 511-518.

Parish, C. R., Freeman, C., Brown, K. J., Francis, D. J. & Cowden, W. B. 1999. Identification of sulfated oligosaccharide-based inhibitors of tumor growth and metastasis using novel in vitro assays for angiogenesis and heparanase activity. *Cancer Res,* 59**,** 3433-41.

Parish, C. R., Freeman, C. & Hulett, M. D. 2001. Heparanase: a key enzyme involved in cell invasion. *Biochim Biophys Acta,* 1471**,** M99-108.

Parish, C. R., Freeman, C., Ziolkowski, A. F., He, Y. Q., Sutcliffe, E. L., Zafar, A., Rao, S. & Simeonovic, C. J. 2013. Unexpected new roles for heparanase in Type 1 diabetes and immune gene regulation. *Matrix Biol,* 32**,** 228-33.

Park, S. W. & Ozcan, U. 2013. Potential for therapeutic manipulation of the UPR in disease. *Seminars in Immunopathology,* 35**,** 351-373.

Parthasarathy, N., Goldberg, I. J., Sivaram, P., Mulloy, B., Flory, D. M. & Wagner, W. D. 1994. Oligosaccharide sequences of endothelial cell surface heparan sulfate proteoglycan with affinity for lipoprotein lipase. *J Biol Chem,* 269**,** 22391-6.

Patil, C. & Walter, P. 2001. Intracellular signaling from the endoplasmic reticulum to the nucleus: the unfolded protein response in yeast and mammals. *Curr Opin Cell Biol,* 13**,** 349-55.

Patsouris, D., Li, P.-P., Thapar, D., Chapman, J., Olefsky, J. M. & Neels, J. G. 2008. Ablation of CD11c-positive cells normalizes insulin sensitivity in obese insulin resistant animals. *Cell metabolism,* 8**,** 301-309.

Patzelt, C., Labrecque, A. D., Duguid, J. R., Carroll, R. J., Keim, P. S., Heinrikson, R. L. & Steiner, D. F. 1978. Detection and kinetic behavior of preproinsulin in pancreatic islets. *Proc Natl Acad Sci U S A,* 75**,** 1260-4.

Pellegrini, L. 2001. Role of heparan sulfate in fibroblast growth factor signalling: a structural view. *Curr Opin Struct Biol,* 11**,** 629-34.

Pham-Huy, L. A., He, H. & Pham-Huy, C. 2008. Free Radicals, Antioxidants in Disease and Health. *International Journal of Biomedical Science : IJBS,* 4**,** 89-96.

Pirot, P., Cardozo, A. K. & Eizirik, D. L. 2008. Mediators and mechanisms of pancreatic beta-cell death in type 1 diabetes. *Arq Bras Endocrinol Metabol,* 52**,** 156-65.

Pirot, P., Ortis, F., Cnop, M., Ma, Y., Hendershot, L. M., Eizirik, D. L. & Cardozo, A. K. 2007. Transcriptional regulation of the endoplasmic reticulum stress gene chop in pancreatic insulin-producing cells. *Diabetes,* 56**,** 1069-77.

Pollard, M. G., Travers, K. J. & Weissman, J. S. 1998. Ero1p: a novel and ubiquitous protein with an essential role in oxidative protein folding in the endoplasmic reticulum. *Mol Cell,* 1**,** 171-82.

Popp, S. K., Mann, D. A., Milburn, P. J., Gibbs, A. J., Mccullagh, P. J., Wilson, J. D., Tonjes, R. R. & Simeonovic, C. J. 2007. Transient transmission of porcine endogenous retrovirus to fetal lambs after pig islet tissue xenotransplantation. *Immunol Cell Biol,* 85**,** 238-48.

Powers, C. J., Mcleskey, S. W. & Wellstein, A. 2000. Fibroblast growth factors, their receptors and signaling. *Endocr Relat Cancer,* 7**,** 165-97.

Prentki, M. & Nolan, C. J. 2006. Islet beta cell failure in type 2 diabetes. *J Clin Invest,* 116**,** 1802-12.

Preston, A. M., Gurisik, E., Bartley, C., Laybutt, D. R. & Biden, T. J. 2009. Reduced endoplasmic reticulum (ER)-to-Golgi protein trafficking contributes to ER stress in lipotoxic mouse beta cells by promoting protein overload. *Diabetologia,* 52**,** 2369-2373.

Previs, S. F., Withers, D. J., Ren, J. M., White, M. F. & Shulman, G. I. 2000. Contrasting effects of IRS-1 versus IRS-2 gene disruption on carbohydrate and lipid metabolism in vivo. *J Biol Chem,* 275**,** 38990-4.

Prokhorova, E. A., Zamaraev, A. V., Kopeina, G. S., Zhivotovsky, B. & Lavrik, I. N. 2015. Role of the nucleus in apoptosis: signaling and execution. *Cell Mol Life Sci,* 72**,** 4593-612.

Pujuguet, P., Simian, M., Liaw, J., Timpl, R., Werb, Z. & Bissell, M. J. 2000. Nidogen-1 regulates laminin-1-dependent mammary-specific gene expression. *J Cell Sci,* 113 (Pt 5)**,** 849-58.

Purves, R. D. 1992. Optimum numerical integration methods for estimation of area-under-the-curve (AUC) and area-under-the-moment-curve (AUMC). *Journal of Pharmacokinetics and Biopharmaceutics,* 20**,** 211-226.

Puthalakath, H., O'reilly, L. A., Gunn, P., Lee, L., Kelly, P. N., Huntington, N. D., Hughes, P. D., Michalak, E. M., Mckimm-Breschkin, J., Motoyama, N., Gotoh, T., Akira, S., Bouillet, P. & Strasser, A. 2007. ER stress triggers apoptosis by activating BH3-only protein Bim. *Cell,* 129**,** 1337-49.

Puyal, J., Petremand, J., Dubuis, G., Rummel, C. & Widmann, C. 2013. HDLs protect the MIN6 insulinoma cell line against tunicamycin-induced apoptosis without inhibiting ER stress and without restoring ER functionality. *Mol Cell Endocrinol,* 381**,** 291-301.

Quesada, I., Tuduri, E., Ripoll, C. & Nadal, A. 2008. Physiology of the pancreatic alpha-cell and glucagon secretion: role in glucose homeostasis and diabetes. *J Endocrinol,* 199**,** 5-19.

Raats, C. J., Bakker, M. A., Van Den Born, J. & Berden, J. H. 1997. Hydroxyl radicals depolymerize glomerular heparan sulfate in vitro and in experimental nephrotic syndrome. *J Biol Chem,* 272**,** 26734-41.

Rabhi, N., Salas, E., Froguel, P., Annicotte, J.-S., #Xe9 & Bastien 2014. Role of the Unfolded Protein Response in β Cell Compensation and Failure during Diabetes. *Journal of Diabetes Research,* 2014**,** 11.

Rabinovich, E., Kerem, A., Frohlich, K. U., Diamant, N. & Bar-Nun, S. 2002. AAA-ATPase p97/Cdc48p, a cytosolic chaperone required for endoplasmic reticulum-associated protein degradation. *Mol Cell Biol,* 22**,** 626-34.

Rahbar, S., Blumenfeld, O. & Ranney, H. M. 1969. Studies of an unusual hemoglobin in patients with diabetes mellitus. *Biochem Biophys Res Commun,* 36**,** 838-43.

Ramani, V. C., Pruett, P. S., Thompson, C. A., Delucas, L. D. & Sanderson, R. D. 2012. Heparan sulfate chains of syndecan-1 regulate ectodomain shedding. *J Biol Chem,* 287**,** 9952-61.

Rao, R. V., Peel, A., Logvinova, A., Del Rio, G., Hermel, E., Yokota, T., Goldsmith, P. C., Ellerby, L. M., Ellerby, H. M. & Bredesen, D. E. 2002. Coupling endoplasmic reticulum stress to the cell death program: role of the ER chaperone GRP78. *FEBS Lett,* 514**,** 122-8.

Rausch, M. E., Weisberg, S., Vardhana, P. & Tortoriello, D. V. 2008. Obesity in C57BL/6J mice is characterized by adipose tissue hypoxia and cytotoxic T-cell infiltration. *Int J Obes (Lond),* 32**,** 451-63.

Reddy, V. Y., Zhang, Q. Y. & Weiss, S. J. 1995. Pericellular mobilization of the tissue-destructive cysteine proteinases, cathepsins B, L, and S, by human monocyte-derived macrophages. *Proceedings of the National Academy of Sciences of the United States of America,* 92**,** 3849-3853.

Rehn, M. & Pihlajaniemi, T. 1994. Alpha 1(XVIII), a collagen chain with frequent interruptions in the collagenous sequence, a distinct tissue distribution, and homology with type XV collagen. *Proceedings of the National Academy of Sciences,* 91**,** 4234-4238.

Reizes, O., Goldberger, O., Smith, A. C., Xu, Z., Bernfield, M. & Bickel, P. E. 2006. Insulin Promotes Shedding of Syndecan Ectodomains from 3T3-L1 Adipocytes: A Proposed Mechanism for Stabilization of Extracellular Lipoprotein Lipase. *Biochemistry,* 45**,** 5703-5711.

Richardson, S. J., Willcox, A., Bone, A. J., Foulis, A. K. & Morgan, N. G. 2009. Islet-associated macrophages in type 2 diabetes. *Diabetologia,* 52**,** 1686-8.

Rickles, F. R. 2006. If heparanase is the answer, what is the question? *J Thromb Haemost,* 4**,** 557-9.

Riemer, J., Bulleid, N. & Herrmann, J. M. 2009. Disulfide formation in the ER and mitochondria: two solutions to a common process. *Science,* 324**,** 1284-7.

Rissanen, A., Howard, C. P., Botha, J. & Thuren, T. 2012. Effect of anti-IL-1beta antibody (canakinumab) on insulin secretion rates in impaired glucose tolerance or type 2 diabetes: results of a randomized, placebo-controlled trial. *Diabetes Obes Metab,* 14**,** 1088-96.

Rivara, S., Milazzo, F. M. & Giannini, G. 2016. Heparanase: a rainbow pharmacological target associated to multiple pathologies including rare diseases. *Future Med Chem,* 8**,** 647-80.

Robertson, R. P., Harmon, J., Tran, P. O. & Poitout, V. 2004. Beta-cell glucose toxicity, lipotoxicity, and chronic oxidative stress in type 2 diabetes. *Diabetes,* 53 Suppl 1**,** S119-24.

Robertson, R. P., Harmon, J., Tran, P. O., Tanaka, Y. & Takahashi, H. 2003. Glucose toxicity in beta-cells: type 2 diabetes, good radicals gone bad, and the glutathione connection. *Diabetes,* 52**,** 581-7.

Rocha, V. Z., Folco, E. J., Sukhova, G., Shimizu, K., Gotsman, I., Vernon, A. H. & Libby, P. 2008. Interferon-gamma, a Th1 cytokine, regulates fat inflammation: a role for adaptive immunity in obesity. *Circ Res,* 103**,** 467-76.

Rojas, J., Bermudez, V., Palmar, J., Mart, #X00ed, Nez, M., #X00ed, Sof, A., #X00ed, Olivar, L. C., Nava, M., Tomey, D., Rojas, M., Salazar, J., Garicano, C. & Velasco, M. 2018. Pancreatic Beta Cell Death: Novel Potential Mechanisms in Diabetes Therapy. *Journal of Diabetes Research,* 2018**,** 19.

Ron, D. 2002a. Proteotoxicity in the endoplasmic reticulum: lessons from the Akita diabetic mouse. *The Journal of Clinical Investigation,* 109**,** 443-445.

Ron, D. 2002b. Proteotoxicity in the endoplasmic reticulum: lessons from the Akita diabetic mouse. *J Clin Invest,* 109**,** 443-5.

Rops, A. L., Van Den Hoven, M. J., Baselmans, M. M., Lensen, J. F., Wijnhoven, T. J., Van Den Heuvel, L. P., Van Kuppevelt, T. H., Berden, J. H. & Van Der Vlag, J. 2008. Heparan sulfate domains on cultured activated glomerular endothelial cells mediate leukocyte trafficking. *Kidney Int,* 73**,** 52-62.

Rops, A. L. W. M. M., Van Der Vlag, J., Lensen, J. F. M., Wijnhoven, T. J. M., Van Den Heuvel, L. P. W. J., Van Kuppevelt, T. H. & Berden, J. H. M. 2004. Heparan sulfate proteoglycans in glomerular inflammation. *Kidney International,* 65**,** 768-785.

Rorsman, P., Berggren, P. O. & Hellman, B. 1982. Manganese accumulation in pancreatic beta-cells and its stimulation by glucose. *The Biochemical journal,* 202**,** 435-444.

Rorsman, P., Eliasson, L., Renstrom, E., Gromada, J., Barg, S. & Gopel, S. 2000. The Cell Physiology of Biphasic Insulin Secretion. *News Physiol Sci,* 15**,** 72-77.

Rorsman, P. & Renström, E. 2003. Insulin granule dynamics in pancreatic beta cells. *Diabetologia,* 46**,** 1029-1045.

Rosen, E. D. & Spiegelman, B. M. 2006. Adipocytes as regulators of energy balance and glucose homeostasis. *Nature,* 444**,** 847-853.

Roszer, T. 2015. Understanding the Mysterious M2 Macrophage through Activation Markers and Effector Mechanisms. *Mediators Inflamm,* 2015**,** 816460.

Rota, C., Liverani, L., Spelta, F., Mascellani, G., Tomasi, A., Iannone, A. & Vismara, E. 2005. Free radical generation during chemical depolymerization of heparin. *Anal Biochem,* 344**,** 193-203.

Rumore, M. M. & Kim, K. S. 2010. Potential Role of Salicylates in Type 2 Diabetes. *Annals of Pharmacotherapy,* 44**,** 1207-1221.

Saisho, Y., Butler, A. E., Manesso, E., Elashoff, D., Rizza, R. A. & Butler, P. C. 2013. beta-cell mass and turnover in humans: effects of obesity and aging. *Diabetes Care,* 36**,** 111-7.

Sako, Y. & Grill, V. E. 1990. A 48-hour lipid infusion in the rat time-dependently inhibits glucose-induced insulin secretion and B cell oxidation through a process likely coupled to fatty acid oxidation. *Endocrinology,* 127**,** 1580-9.

Sakula, A. 1988. Paul Langerhans (1847-1888): a centenary tribute. *Journal of the Royal Society of Medicine,* 81**,** 414-415.

Salvado, L., Palomer, X., Barroso, E. & Vazquez-Carrera, M. 2015. Targeting endoplasmic reticulum stress in insulin resistance. *Trends Endocrinol Metab,* 26**,** 438-48.

Sano, H., Kane, S., Sano, E., Miinea, C. P., Asara, J. M., Lane, W. S., Garner, C. W. & Lienhard, G. E. 2003. Insulin-stimulated phosphorylation of a Rab GTPase-activating protein regulates GLUT4 translocation. *J Biol Chem,* 278**,** 14599-602.

Sarrazin, S., Lamanna, W. C. & Esko, J. D. 2011. Heparan Sulfate Proteoglycans. *Cold Spring Harbor Perspectives in Biology,* 3**,** a004952.

Sartipy, P. & Loskutoff, D. J. 2003. Monocyte chemoattractant protein 1 in obesity and insulin resistance. *Proc Natl Acad Sci U S A,* 100**,** 7265-70.

Sauer, T., Patel, M., Chan, C.-C. & Tuo, J. 2008. Unfolding the Therapeutic Potential of Chemical Chaperones for Age-related Macular Degeneration. *Expert review of ophthalmology,* 3**,** 29-42.

Sauter, N. S., Schulthess, F. T., Galasso, R., Castellani, L. W. & Maedler, K. 2008. The antiinflammatory cytokine interleukin-1 receptor antagonist protects from high-fat diet-induced hyperglycemia. *Endocrinology,* 149**,** 2208-18.

Scheuner, D. & Kaufman, R. J. 2008. The unfolded protein response: a pathway that links insulin demand with beta-cell failure and diabetes. *Endocr Rev,* 29**,** 317-33.

Schipper, H. S., Nuboer, R., Prop, S., Van Den Ham, H. J., De Boer, F. K., Kesmir, C., Mombers, I. M. H., Van Bekkum, K. A., Woudstra, J., Kieft, J. H., Hoefer, I. E., De Jager, W., Prakken, B., Van Summeren, M. & Kalkhoven, E. 2012. Systemic inflammation in childhood obesity: circulating inflammatory mediators and activated CD14++ monocytes. *Diabetologia,* 55**,** 2800-2810.

Schlessinger, J., Plotnikov, A. N., Ibrahimi, O. A., Eliseenkova, A. V., Yeh, B. K., Yayon, A., Linhardt, R. J. & Mohammadi, M. 2000. Crystal structure of a ternary FGF-FGFR-heparin complex reveals a dual role for heparin in FGFR binding and dimerization. *Mol Cell,* 6**,** 743-50.

Schmittgen, T. D. & Livak, K. J. 2008. Analyzing real-time PCR data by the comparative CT method. *Nature Protocols,* 3**,** 1101.

Schoeller, E. L., Albanna, G., Frolova, A. I. & Moley, K. H. 2012. Insulin Rescues Impaired Spermatogenesis via the Hypothalamic-Pituitary-Gonadal Axis in Akita Diabetic Mice and Restores Male Fertility. *Diabetes,* 61**,** 1869-1878.

Schoeller, E. L., Chi, M., Drury, A., Bertschinger, A., Esakky, P. & Moley, K. H. 2014. Leptin Monotherapy Rescues Spermatogenesis in Male Akita Type 1 Diabetic Mice. *Endocrinology,* 155**,** 2781-2786.

Schrag, J. D., Bergeron, J. J. M., Li, Y., Borisova, S., Hahn, M., Thomas, D. Y. & Cygler, M. 2001. The Structure of Calnexin, an ER Chaperone Involved in Quality Control of Protein Folding. *Molecular Cell,* 8**,** 633-644.

Schroder, M. & Kaufman, R. J. 2005. ER stress and the unfolded protein response. *Mutat Res,* 569**,** 29-63.

Schwarznau, A., Hanson, M. S., Sperger, J. M., Schram, B. R., Danobeitia, J. S., Greenwood, K. K., Vijayan, A. & Fernandez, L. A. 2009. IL-1β Receptor Blockade Protects Islets Against Pro-inflammatory Cytokine Induced Necrosis and Apoptosis. *Journal of cellular physiology,* 220**,** 341-347.

Sell, H., Habich, C. & Eckel, J. 2012. Adaptive immunity in obesity and insulin resistance. *Nat Rev Endocrinol,* 8**,** 709-16.

Senbanjo, L. T. & Chellaiah, M. A. 2017. CD44: A Multifunctional Cell Surface Adhesion Receptor Is a Regulator of Progression and Metastasis of Cancer Cells. *Frontiers in Cell and Developmental Biology,* 5**,** 18.

Seppinen, L. & Pihlajaniemi, T. 2011. The multiple functions of collagen XVIII in development and disease. *Matrix Biol,* 30**,** 83-92.

Shan, W.-F., Chen, B.-Q., Zhu, S.-J., Jiang, L. & Zhou, Y.-F. 2011. Effects of GLUT4 expression on insulin resistance in patients with advanced liver cirrhosis. *Journal of Zhejiang University. Science. B,* 12**,** 677-682.

Sharma, R. B., O'donnell, A. C., Stamateris, R. E., Ha, B., Mccloskey, K. M., Reynolds, P. R., Arvan, P. & Alonso, L. C. 2015. Insulin demand regulates β cell number via the unfolded protein response. *The Journal of Clinical Investigation,* 125**,** 3831-3846.

Shaul, M. E., Bennett, G., Strissel, K. J., Greenberg, A. S. & Obin, M. S. 2010. Dynamic, M2-like remodeling phenotypes of CD11c+ adipose tissue macrophages during high-fat diet--induced obesity in mice. *Diabetes,* 59**,** 1171-81.

Shepshelovich, J., Goldstein-Magal, L., Globerson, A., Yen, P. M., Rotman-Pikielny, P. & Hirschberg, K. 2005. Protein synthesis inhibitors and the chemical chaperone TMAO reverse endoplasmic reticulum perturbation induced by overexpression of the iodide transporter pendrin. *Journal of Cell Science,* 118**,** 1577-1586.

Shi, H., Kokoeva, M. V., Inouye, K., Tzameli, I., Yin, H. & Flier, J. S. 2006. TLR4 links innate immunity and fatty acid-induced insulin resistance. *J Clin Invest,* 116**,** 3015-25.

Shi, Y., Vattem, K. M., Sood, R., An, J., Liang, J., Stramm, L. & Wek, R. C. 1998. Identification and characterization of pancreatic eukaryotic initiation factor 2 alpha-subunit kinase, PEK, involved in translational control. *Mol Cell Biol,* 18**,** 7499-509.

Shiao, M.-S., Liao, B.-Y., Long, M. & Yu, H.-T. 2008. Adaptive Evolution of the Insulin Two-Gene System in Mouse. *Genetics,* 178**,** 1683-1691.

Shimabukuro, M., Zhou, Y. T., Levi, M. & Unger, R. H. 1998. Fatty acid-induced beta cell apoptosis: a link between obesity and diabetes. *Proc Natl Acad Sci U S A,* 95**,** 2498-502.

Shimomura, I., Bashmakov, Y., Ikemoto, S., Horton, J. D., Brown, M. S. & Goldstein, J. L. 1999. Insulin selectively increases SREBP-1c mRNA in the livers of rats with streptozotocin-induced diabetes. *Proceedings of the National Academy of Sciences,* 96**,** 13656-13661.

Shin, J. A., Lee, J. H., Lim, S. Y., Ha, H. S., Kwon, H. S., Park, Y. M., Lee, W. C., Kang, M. I., Yim, H. W., Yoon, K. H. & Son, H. Y. 2013. Metabolic syndrome as a predictor of type 2 diabetes, and its clinical interpretations and usefulness. *Journal of Diabetes Investigation,* 4**,** 334-343.

Shirakawa, J., Togashi, Y., Sakamoto, E., Kaji, M., Tajima, K., Orime, K., Inoue, H., Kubota, N., Kadowaki, T. & Terauchi, Y. 2013. Glucokinase Activation Ameliorates ER Stress–Induced Apoptosis in Pancreatic β-Cells. *Diabetes,* 62**,** 3448-3458.

Shoelson, S. E., Lee, J. & Yuan, M. 2003. Inflammation and the IKK beta/I kappa B/NF-kappa B axis in obesity- and diet-induced insulin resistance. *Int J Obes Relat Metab Disord,* 27 Suppl 3**,** S49-52.

Shriver, Z., Capila, I., Venkataraman, G. & Sasisekharan, R. 2012. Heparin and Heparan Sulfate: Analyzing Structure and Microheterogeneity. *Handbook of experimental pharmacology***,** 159-176.

Simeonovic, C. J., Popp, S. K., Starrs, L. M., Brown, D. J., Ziolkowski, A. F., Ludwig, B., Bornstein, S. R., Wilson, J. D., Pugliese, A., Kay, T. W. H., Thomas, H. E., Loudovaris, T., Choong, F. J., Freeman, C. & Parish, C. R. 2018. Loss of intra-

islet heparan sulfate is a highly sensitive marker of type 1 diabetes progression in humans. *PLoS ONE,* 13**,** e0191360.

Simeonovic, C. J., Ziolkowski, A. F., Wu, Z., Choong, F. J., Freeman, C. & Parish, C. R. 2013. Heparanase and Autoimmune Diabetes. *Frontiers in Immunology,* 4**,** 471.

Simon Davis, D. A. & Parish, C. R. 2013. Heparan Sulfate: A Ubiquitous Glycosaminoglycan with Multiple Roles in Immunity. *Frontiers in Immunology,* 4**,** 470.

Sloan-Lancaster, J., Abu-Raddad, E., Polzer, J., Miller, J. W., Scherer, J. C., De Gaetano, A., Berg, J. K. & Landschulz, W. H. 2013. Double-blind, randomized study evaluating the glycemic and anti-inflammatory effects of subcutaneous LY2189102, a neutralizing IL-1beta antibody, in patients with type 2 diabetes. *Diabetes Care,* 36**,** 2239-46.

Smith, F. E., Rosen, K. M., Villa-Komaroff, L., Weir, G. C. & Bonner-Weir, S. 1991. Enhanced insulin-like growth factor I gene expression in regenerating rat pancreas. *Proc Natl Acad Sci U S A,* 88**,** 6152-6.

Soehnlein, O. 2012. Multiple roles for neutrophils in atherosclerosis. *Circ Res,* 110**,** 875-88.

Soehnlein, O., Zernecke, A., Eriksson, E. E., Rothfuchs, A. G., Pham, C. T., Herwald, H., Bidzhekov, K., Rottenberg, M. E., Weber, C. & Lindbom, L. 2008. Neutrophil secretion products pave the way for inflammatory monocytes. *Blood,* 112**,** 1461-71.

Solinas, G., Naugler, W., Galimi, F., Lee, M. S. & Karin, M. 2006. Saturated fatty acids inhibit induction of insulin gene transcription by JNK-mediated phosphorylation of insulin-receptor substrates. *Proc Natl Acad Sci U S A,* 103**,** 16454-9.

Sone, H. & Kagawa, Y. 2005. Pancreatic beta cell senescence contributes to the pathogenesis of type 2 diabetes in high-fat diet-induced diabetic mice. *Diabetologia,* 48**,** 58-67.

Song, B., Scheuner, D., Ron, D., Pennathur, S. & Kaufman, R. J. 2008. Chop deletion reduces oxidative stress, improves beta cell function, and promotes cell survival in multiple mouse models of diabetes. *J Clin Invest,* 118**,** 3378-89.

Sotnikov, I., Hershkoviz, R., Grabovsky, V., Ilan, N., Cahalon, L., Vlodavsky, I., Alon, R. & Lider, O. 2004. Enzymatically Quiescent Heparanase Augments T Cell Interactions with VCAM-1 and Extracellular Matrix Components under Versatile Dynamic Contexts. *The Journal of Immunology,* 172**,** 5185-5193.

Sriburi, R., Jackowski, S., Mori, K. & Brewer, J. W. 2004. XBP1: a link between the unfolded protein response, lipid biosynthesis, and biogenesis of the endoplasmic reticulum. *J Cell Biol,* 167**,** 35-41.

Srinivasan, S., Ohsugi, M., Liu, Z., Fatrai, S., Bernal-Mizrachi, E. & Permutt, M. A. 2005. Endoplasmic Reticulum Stress–Induced Apoptosis Is Partly Mediated by Reduced Insulin Signaling Through Phosphatidylinositol 3-Kinase/Akt and Increased Glycogen Synthase Kinase-3β in Mouse Insulinoma Cells. *Diabetes,* 54**,** 968-975.

Stanford, K. I., Bishop, J. R., Foley, E. M., Gonzales, J. C., Niesman, I. R., Witztum, J. L. & Esko, J. D. 2009. Syndecan-1 is the primary heparan sulfate proteoglycan mediating hepatic clearance of triglyceride-rich lipoproteins in mice. *The Journal of Clinical Investigation,* 119**,** 3236-3245.

Stefanovic-Racic, M., Yang, X., Turner, M. S., Mantell, B. S., Stolz, D. B., Sumpter, T. L., Sipula, I. J., Dedousis, N., Scott, D. K., Morel, P. A., Thomson, A. W. & O'doherty, R. M. 2012. Dendritic cells promote macrophage infiltration and

comprise a substantial proportion of obesity-associated increases in CD11c+ cells in adipose tissue and liver. *Diabetes,* 61**,** 2330-9.

Stein, D. T., Esser, V., Stevenson, B. E., Lane, K. E., Whiteside, J. H., Daniels, M. B., Chen, S. & Mcgarry, J. D. 1996. Essentiality of circulating fatty acids for glucose-stimulated insulin secretion in the fasted rat. *J Clin Invest,* 97**,** 2728-35.

Steiner, D. F., Rouille, Y., Gong, Q., Martin, S., Carroll, R. & Chan, S. J. 1996. The role of prohormone convertases in insulin biosynthesis: evidence for inherited defects in their action in man and experimental animals. *Diabetes Metab,* 22**,** 94-104.

Stendahl, J. C., Kaufman, D. B. & Stupp, S. I. 2009. Extracellular Matrix in Pancreatic Islets: Relevance to Scaffold Design and Transplantation. *Cell transplantation,* 18**,** 1-12.

Stringer, S. E. & Gallagher, J. T. 1997. Heparan sulphate. *Int J Biochem Cell Biol,* 29**,** 709-14.

Suganami, T., Nishida, J. & Ogawa, Y. 2005. A paracrine loop between adipocytes and macrophages aggravates inflammatory changes: role of free fatty acids and tumor necrosis factor alpha. *Arterioscler Thromb Vasc Biol,* 25**,** 2062-8.

Suganami, T. & Ogawa, Y. 2010. Adipose tissue macrophages: their role in adipose tissue remodeling. *J Leukoc Biol,* 88**,** 33-9.

Supale, S., Li, N., Brun, T. & Maechler, P. 2012. Mitochondrial dysfunction in pancreatic beta cells. *Trends Endocrinol Metab,* 23**,** 477-87.

Surmi, B. K. & Hasty, A. H. 2008. Macrophage infiltration into adipose tissue: initiation, propagation and remodeling. *Future lipidology,* 3**,** 545-556.

Szathmary, R., Bielmann, R., Nita-Lazar, M., Burda, P. & Jakob, C. A. 2005. Yos9 protein is essential for degradation of misfolded glycoproteins and may function as lectin in ERAD. *Mol Cell,* 19**,** 765-75.

Takahashi, I., Noguchi, N., Nata, K., Yamada, S., Kaneiwa, T., Mizumoto, S., Ikeda, T., Sugihara, K., Asano, M., Yoshikawa, T., Yamauchi, A., Shervani, N. J., Uruno, A., Kato, I., Unno, M., Sugahara, K., Takasawa, S., Okamoto, H. & Sugawara, A. 2009. Important role of heparan sulfate in postnatal islet growth and insulin secretion. *Biochem Biophys Res Commun,* 383**,** 113-8.

Takahashi, I., Ohashi, K. & Nata, K. 2012. Involvement of heparan sulfate 3‐O‐sulfotransferase isoform‐1 in the insulin secretion pathway. *Journal of Diabetes Investigation,* 3**,** 362-370.

Takahashi, I., Yamada, S. & Nata, K. 2017. Effects of heparan sulfate proteoglycan syndecan-4 on the insulin secretory response in a mouse pancreatic beta-cell line, MIN6. *Mol Cell Endocrinol*.

Takahashi, N., Kishimoto, T., Nemoto, T., Kadowaki, T. & Kasai, H. 2002. Fusion Pore Dynamics and Insulin Granule Exocytosis in the Pancreatic Islet. *Science,* 297**,** 1349-1352.

Takatsuki, A., Arima, K. & Tamura, G. 1971. Tunicamycin, a new antibiotic. I. Isolation and characterization of tunicamycin. *J Antibiot (Tokyo),* 24**,** 215-23.

Talukdar, S., Oh, D. Y., Bandyopadhyay, G., Li, D., Xu, J., Mcnelis, J., Lu, M., Li, P., Yan, Q., Zhu, Y., Ofrecio, J., Lin, M., Brenner, M. B. & Olefsky, J. M. 2012. Neutrophils mediate insulin resistance in mice fed a high-fat diet through secreted elastase. *Nat Med,* 18**,** 1407-12.

Tamura, Y., Sugimoto, M., Murayama, T., Ueda, Y., Kanamori, H., Ono, K., Ariyasu, H., Akamizu, T., Kita, T., Yokode, M. & Arai, H. 2008. Inhibition of CCR2 ameliorates insulin resistance and hepatic steatosis in db/db mice. *Arterioscler Thromb Vasc Biol,* 28**,** 2195-201.

Tanaka, Y., Gleason, C. E., Tran, P. O. T., Harmon, J. S. & Robertson, R. P. 1999. Prevention of glucose toxicity in HIT-T15 cells and Zucker diabetic fatty rats by antioxidants. *Proceedings of the National Academy of Sciences,* 96**,** 10857-10862.

Tang, C., Koulajian, K., Schuiki, I., Zhang, L., Desai, T., Ivovic, A., Wang, P., Robson-Doucette, C., Wheeler, M. B., Minassian, B., Volchuk, A. & Giacca, A. 2012. Glucose-induced beta cell dysfunction in vivo in rats: link between oxidative stress and endoplasmic reticulum stress. *Diabetologia,* 55**,** 1366-79.

Tangvarasittichai, S. 2015. Oxidative stress, insulin resistance, dyslipidemia and type 2 diabetes mellitus. *World Journal of Diabetes,* 6**,** 456-480.

Temussi, P. A., Masino, L. & Pastore, A. 2003. NEW EMBO MEMBER'S REVIEW: From Alzheimer to Huntington: why is a structural understanding so difficult? *The EMBO Journal,* 22**,** 355-361.

Tenenbaum, A., Fisman, E. Z. & Motro, M. 2003. Metabolic syndrome and type 2 diabetes mellitus: focus on peroxisome proliferator activated receptors (PPAR). *Cardiovascular Diabetology,* 2**,** 4-4.

Tengholm, A. 2012. Cyclic AMP dynamics in the pancreatic β-cell. *Upsala Journal of Medical Sciences,* 117**,** 355-369.

Teodoro-Morrison, T., Schuiki, I., Zhang, L., Belsham, D. D. & Volchuk, A. 2013. GRP78 overproduction in pancreatic beta cells protects against high-fat-diet-induced diabetes in mice. *Diabetologia,* 56**,** 1057-1067.

Tersey, S. A., Nishiki, Y., Templin, A. T., Cabrera, S. M., Stull, N. D., Colvin, S. C., Evans-Molina, C., Rickus, J. L., Maier, B. & Mirmira, R. G. 2012. Islet beta-cell endoplasmic reticulum stress precedes the onset of type 1 diabetes in the nonobese diabetic mouse model. *Diabetes,* 61**,** 818-27.

Theodoraki, A., Hu, Y., Poopalasundaram, S., Oosterhof, A., Guimond, S. E., Disterer, P., Khoo, B., Hauge-Evans, A. C., Jones, P. M., Turnbull, J. E., Van Kuppevelt, T. H. & Bouloux, P. M. 2015. Distinct patterns of heparan sulphate in pancreatic islets suggest novel roles in paracrine islet regulation. *Mol Cell Endocrinol,* 399**,** 296-310.

Thorens, B. 2015. GLUT2, glucose sensing and glucose homeostasis. *Diabetologia,* 58**,** 221-232.

Thorn, P., Fogarty, K. E. & Parker, I. 2004. Zymogen granule exocytosis is characterized by long fusion pore openings and preservation of vesicle lipid identity. *Proc Natl Acad Sci U S A,* 101**,** 6774-9.

Thorn, P., Zorec, R., Rettig, J. & Keating, D. J. 2016. Exocytosis in non-neuronal cells. *Journal of Neurochemistry,* 137**,** 849-859.

Tiedge, M., Lortz, S., Drinkgern, J. & Lenzen, S. 1997. Relation between antioxidant enzyme gene expression and antioxidative defense status of insulin-producing cells. *Diabetes,* 46**,** 1733-42.

Timpl, R. & Brown, J. C. 1996. Supramolecular assembly of basement membranes. *Bioessays,* 18**,** 123-32.

Tirasophon, W., Lee, K., Callaghan, B., Welihinda, A. & Kaufman, R. J. 2000. The endoribonuclease activity of mammalian IRE1 autoregulates its mRNA and is required for the unfolded protein response. *Genes Dev,* 14**,** 2725-36.

Tirasophon, W., Welihinda, A. A. & Kaufman, R. J. 1998. A stress response pathway from the endoplasmic reticulum to the nucleus requires a novel bifunctional protein kinase/endoribonuclease (Ire1p) in mammalian cells. *Genes Dev,* 12**,** 1812-24.

Tkachenko, E., Rhodes, J. M. & Simons, M. 2005. Syndecans: new kids on the signaling block. *Circ Res,* 96**,** 488-500.

Todd, D. J., Lee, A. H. & Glimcher, L. H. 2008. The endoplasmic reticulum stress response in immunity and autoimmunity. *Nat Rev Immunol,* 8**,** 663-74.

Toné, S., Sugimoto, K., Tanda, K., Suda, T., Uehira, K., Kanouchi, H., Samejima, K., Minatogawa, Y. & Earnshaw, W. C. 2007. Three Distinct Stages of Apoptotic Nuclear Condensation Revealed by Time-Lapse Imaging, Biochemical and Electron Microscopy Analysis of Cell-Free Apoptosis. *Experimental cell research,* 313**,** 3635-3644.

Toyama, H., Takada, M., Tanaka, T., Suzuki, Y. & Kuroda, Y. 2003. Characterization of islet-infiltrating immunocytes after pancreas preservation by two-layer (UW/perfluorochemical) cold storage method. *Transplantation Proceedings,* 35**,** 1503-1505.

Treiman, M., Caspersen, C. & Christensen, S. B. 1998. A tool coming of age: thapsigargin as an inhibitor of sarco-endoplasmic reticulum Ca(2+)-ATPases. *Trends Pharmacol Sci,* 19**,** 131-5.

Trexler, A. J. & Taraska, J. W. 2017. Regulation of insulin exocytosis by calcium-dependent protein kinase C in beta cells. *Cell Calcium,* 67**,** 1-10.

Trimble, E. R., Halban, P. A., Wollheim, C. B. & Renold, A. E. 1982. Functional differences between rat islets of ventral and dorsal pancreatic origin. *J Clin Invest,* 69**,** 405-13.

Tu, B. P. & Weissman, J. S. 2002. The FAD- and O(2)-dependent reaction cycle of Ero1-mediated oxidative protein folding in the endoplasmic reticulum. *Mol Cell,* 10**,** 983-94.

Ueda, K., Kawano, J., Takeda, K., Yujiri, T., Tanabe, K., Anno, T., Akiyama, M., Nozaki, J., Yoshinaga, T., Koizumi, A., Shinoda, K., Oka, Y. & Tanizawa, Y. 2005. Endoplasmic reticulum stress induces Wfs1 gene expression in pancreatic beta-cells via transcriptional activation. *Eur J Endocrinol,* 153**,** 167-76.

Unger, R. H. 1971. Glucagon and the insulin: glucagon ratio in diabetes and other catabolic illnesses. *Diabetes,* 20**,** 834-8.

Unger, R. H. & Scherer, P. E. 2010. Gluttony, sloth and the metabolic syndrome: a roadmap to lipotoxicity. *Trends Endocrinol Metab,* 21**,** 345-52.

Uppala, J. K., Gani, A. R. & Ramaiah, K. V. A. 2017. Chemical chaperone, TUDCA unlike PBA, mitigates protein aggregation efficiently and resists ER and non-ER stress induced HepG2 cell death. *Scientific Reports,* 7**,** 3831.

Urano, F., Wang, X., Bertolotti, A., Zhang, Y., Chung, P., Harding, H. P. & Ron, D. 2000. Coupling of stress in the ER to activation of JNK protein kinases by transmembrane protein kinase IRE1. *Science,* 287**,** 664-6.

Urra, H., Dufey, E., Lisbona, F., Rojas-Rivera, D. & Hetz, C. 2013. When ER stress reaches a dead end. *Biochimica et Biophysica Acta (BBA) - Molecular Cell Research,* 1833**,** 3507-3517.

Van Deijnen, J. H. M., Hulstaert, C. E., Wolters, G. H. J. & Van Schilfgaarde, R. 1992. Significance of the peri-insular extracellular matrix for islet isolation from the pancreas of rat, dog, pig, and man. *Cell and Tissue Research,* 267**,** 139-146.

Van Deijnen, J. H. M., Van Suylichem, P. T. R., Wolters, G. H. J. & Van Schilfgaarde, R. 1994. Distribution of collagens type I, type III and type V in the pancreas of rat, dog, pig and man. *Cell and Tissue Research,* 277**,** 115-121.

Van Den Born, J., Salmivirta, K., Henttinen, T., Ostman, N., Ishimaru, T., Miyaura, S., Yoshida, K. & Salmivirta, M. 2005. Novel heparan sulfate structures revealed by monoclonal antibodies. *J Biol Chem,* 280**,** 20516-23.

Van Horssen, J., Wesseling, P., Van Den Heuvel, L. P. W. J., De Waal, R. M. W. & Verbeek, M. M. 2003. Heparan sulphate proteoglycans in Alzheimer's disease and amyloid‐related disorders. *The Lancet Neurology,* 2**,** 482-492.

Van Raalte, D. H., Brands, M., Van Der Zijl, N. J., Muskiet, M. H., Pouwels, P. J., Ackermans, M. T., Sauerwein, H. P., Serlie, M. J. & Diamant, M. 2011. Low-dose glucocorticoid treatment affects multiple aspects of intermediary metabolism in healthy humans: a randomised controlled trial. *Diabetologia,* 54**,** 2103-12.

Vang, S., Longley, K., Steer, C. J. & Low, W. C. 2014. The Unexpected Uses of Urso- and Tauroursodeoxycholic Acid in the Treatment of Non-liver Diseases. *Global Advances in Health and Medicine,* 3**,** 58-69.

Vettorazzi, J. F., Kurauti, M. A., Soares, G. M., Borck, P. C., Ferreira, S. M., Branco, R. C. S., Michelone, L. D. S. L., Boschero, A. C., Junior, J. M. C. & Carneiro, E. M. 2017. Bile acid TUDCA improves insulin clearance by increasing the expression of insulin-degrading enzyme in the liver of obese mice. *Scientific Reports,* 7**,** 14876.

Vettorazzi, J. F., Ribeiro, R. A., Borck, P. C., Branco, R. C. S., Soriano, S., Merino, B., Boschero, A. C., Nadal, A., Quesada, I. & Carneiro, E. M. 2016. The bile acid TUDCA increases glucose-induced insulin secretion via the cAMP/PKA pathway in pancreatic beta cells. *Metabolism,* 65**,** 54-63.

Virtanen, I., Banerjee, M., Palgi, J., Korsgren, O., Lukinius, A., Thornell, L. E., Kikkawa, Y., Sekiguchi, K., Hukkanen, M., Konttinen, Y. T. & Otonkoski, T. 2008. Blood vessels of human islets of Langerhans are surrounded by a double basement membrane. *Diabetologia,* 51**,** 1181-91.

Vlodavsky, I., Beckhove, P., Lerner, I., Pisano, C., Meirovitz, A., Ilan, N. & Elkin, M. 2012. Significance of heparanase in cancer and inflammation. *Cancer Microenviron,* 5**,** 115-32.

Vlodavsky, I. & Friedmann, Y. 2001. Molecular properties and involvement of heparanase in cancer metastasis and angiogenesis. *Journal of Clinical Investigation,* 108**,** 341-347.

Vlodavsky, I., Friedmann, Y., Elkin, M., Aingorn, H., Atzmon, R., Ishai-Michaeli, R., Bitan, M., Pappo, O., Peretz, T., Michal, I., Spector, L. & Pecker, I. 1999. Mammalian heparanase: gene cloning, expression and function in tumor progression and metastasis. *Nat Med,* 5**,** 793-802.

Vlodavsky, I. & Goldshmidt, O. 2001. Properties and function of heparanase in cancer metastasis and angiogenesis. *Haemostasis,* 31 Suppl 1**,** 60-3.

Vlodavsky, I., Ilan, N., Naggi, A. & Casu, B. 2007. Heparanase: structure, biological functions, and inhibition by heparin-derived mimetics of heparan sulfate. *Curr Pharm Des,* 13**,** 2057-73.

Vreys, V. & David, G. 2007. Mammalian heparanase: what is the message? *J Cell Mol Med,* 11**,** 427-52.

Wahren, J., Ekberg, K., Johansson, J., Henriksson, M., Pramanik, A., Johansson, B. L., Rigler, R. & Jornvall, H. 2000. Role of C-peptide in human physiology. *Am J Physiol Endocrinol Metab,* 278**,** E759-68.

Wali, J. A., Rondas, D., Mckenzie, M. D., Zhao, Y., Elkerbout, L., Fynch, S., Gurzov, E. N., Akira, S., Mathieu, C., Kay, T. W., Overbergh, L., Strasser, A. & Thomas, H. E. 2014. The proapoptotic BH3-only proteins Bim and Puma are downstream of

endoplasmic reticulum and mitochondrial oxidative stress in pancreatic islets in response to glucotoxicity. *Cell Death Dis,* 5**,** e1124.

Wang, H. & Eckel, R. H. 2009. Lipoprotein lipase: from gene to obesity. *American Journal of Physiology-Endocrinology and Metabolism,* 297**,** E271-E288.

Wang, H., Kouri, G. & Wollheim, C. B. 2005. ER stress and SREBP-1 activation are implicated in β-cell glucolipotoxicity. *Journal of Cell Science,* 118**,** 3905-3915.

Wang, J., Takeuchi, T., Tanaka, S., Kubo, S. K., Kayo, T., Lu, D., Takata, K., Koizumi, A. & Izumi, T. 1999. A mutation in the insulin 2 gene induces diabetes with severe pancreatic beta-cell dysfunction in the Mody mouse. *J Clin Invest,* 103**,** 27-37.

Wang, J. & Wang, H. 2017. Oxidative Stress in Pancreatic Beta Cell Regeneration. *Oxidative Medicine and Cellular Longevity,* 2017**,** 1930261.

Wang, R. N. & Rosenberg, L. 1999. Maintenance of beta-cell function and survival following islet isolation requires re-establishment of the islet-matrix relationship. *J Endocrinol,* 163**,** 181-90.

Wang, X., Misawa, R., Zielinski, M. C., Cowen, P., Jo, J., Periwal, V., Ricordi, C., Khan, A., Szust, J., Shen, J., Millis, J. M., Witkowski, P. & Hara, M. 2013a. Regional Differences in Islet Distribution in the Human Pancreas - Preferential Beta-Cell Loss in the Head Region in Patients with Type 2 Diabetes. *PLoS ONE,* 8**,** e67454.

Wang, Y., Zhang, D., Chiu, A. P., Wan, A., Neumaier, K., Vlodavsky, I. & Rodrigues, B. 2013b. Endothelial heparanase regulates heart metabolism by stimulating lipoprotein lipase secretion from cardiomyocytes. *Arterioscler Thromb Vasc Biol,* 33**,** 894-902.

Wang, Z. & Thurmond, D. C. 2009. Mechanisms of biphasic insulin-granule exocytosis – roles of the cytoskeleton, small GTPases and SNARE proteins. *Journal of Cell Science,* 122**,** 893-903.

Weir, G. C., Laybutt, D. R., Kaneto, H., Bonner-Weir, S. & Sharma, A. 2001. Beta-cell adaptation and decompensation during the progression of diabetes. *Diabetes,* 50**,** S154.

Weisberg, S. P., Mccann, D., Desai, M., Rosenbaum, M., Leibel, R. L. & Ferrante, A. W., Jr. 2003. Obesity is associated with macrophage accumulation in adipose tissue. *J Clin Invest,* 112**,** 1796-808.

Welch, W. J. & Brown, C. R. 1996. Influence of molecular and chemical chaperones on protein folding. *Cell Stress Chaperones,* 1**,** 109-15.

Welsh, N., Margulis, B., Borg, L. A., Wiklund, H. J., Saldeen, J., Flodström, M., Mello, M. A., Andersson, A., Pipeleers, D. G. & Hellerström, C. 1995. Differences in the expression of heat-shock proteins and antioxidant enzymes between human and rodent pancreatic islets: implications for the pathogenesis of insulin-dependent diabetes mellitus. *Molecular medicine (Cambridge, Mass.),* 1**,** 806-820.

Wentworth, J. M., Naselli, G., Brown, W. A., Doyle, L., Phipson, B., Smyth, G. K., Wabitsch, M., O'brien, P. E. & Harrison, L. C. 2010. Pro-inflammatory CD11c+CD206+ adipose tissue macrophages are associated with insulin resistance in human obesity. *Diabetes,* 59**,** 1648-56.

Werno, C., Zhou, J. & Brune, B. 2008. A23187, ionomycin and thapsigargin upregulate mRNA of HIF-1alpha via endoplasmic reticulum stress rather than a rise in intracellular calcium. *J Cell Physiol,* 215**,** 708-14.

Wierup, N., Svensson, H., Mulder, H. & Sundler, F. 2002. The ghrelin cell: a novel developmentally regulated islet cell in the human pancreas. *Regul Pept,* 107**,** 63-9.

Willcox, A., Richardson, S. J., Bone, A. J., Foulis, A. K. & Morgan, N. G. 2009. Analysis of islet inflammation in human type 1 diabetes. *Clinical & Experimental Immunology,* 155**,** 173-181.

Winer, D. A., Winer, S., Shen, L., Wadia, P. P., Yantha, J., Paltser, G., Tsui, H., Wu, P., Davidson, M. G., Alonso, M. N., Leong, H. X., Glassford, A., Caimol, M., Kenkel, J. A., Tedder, T. F., Mclaughlin, T., Miklos, D. B., Dosch, H. M. & Engleman, E. G. 2011. B cells promote insulin resistance through modulation of T cells and production of pathogenic IgG antibodies. *Nat Med,* 17**,** 610-7.

Winer, S., Chan, Y., Paltser, G., Truong, D., Tsui, H., Bahrami, J., Dorfman, R., Wang, Y., Zielenski, J., Mastronardi, F., Maezawa, Y., Drucker, D. J., Engleman, E., Winer, D. & Dosch, H. M. 2009. Normalization of obesity-associated insulin resistance through immunotherapy. *Nat Med,* 15**,** 921-9.

Winnay, J. N., Dirice, E., Liew, C. W., Kulkarni, R. N. & Kahn, C. R. 2014. p85alpha deficiency protects beta-cells from endoplasmic reticulum stress-induced apoptosis. *Proc Natl Acad Sci U S A,* 111**,** 1192-7.

Wood, R. J. & Hulett, M. D. 2008. Cell surface-expressed cation-independent mannose 6-phosphate receptor (CD222) binds enzymatically active heparanase independently of mannose 6-phosphate to promote extracellular matrix degradation. *J Biol Chem,* 283**,** 4165-76.

Wu, D., Molofsky, A. B., Liang, H. E., Ricardo-Gonzalez, R. R., Jouihan, H. A., Bando, J. K., Chawla, A. & Locksley, R. M. 2011. Eosinophils sustain adipose alternatively activated macrophages associated with glucose homeostasis. *Science,* 332**,** 243-7.

Wu, H., Ghosh, S., Perrard, X. D., Feng, L., Garcia, G. E., Perrard, J. L., Sweeney, J. F., Peterson, L. E., Chan, L., Smith, C. W. & Ballantyne, C. M. 2007. T-cell accumulation and regulated on activation, normal T cell expressed and secreted upregulation in adipose tissue in obesity. *Circulation,* 115**,** 1029-38.

Wu, J. & Kaufman, R. J. 2006. From acute ER stress to physiological roles of the Unfolded Protein Response. *Cell Death Differ,* 13**,** 374-84.

Wu, L. & Liu, Y. J. 2007. Development of dendritic-cell lineages. *Immunity,* 26**,** 741-50.

Xiao, C., Giacca, A. & Lewis, G. F. 2011. Sodium Phenylbutyrate, a Drug With Known Capacity to Reduce Endoplasmic Reticulum Stress, Partially Alleviates Lipid-Induced Insulin Resistance and β-Cell Dysfunction in Humans. *Diabetes,* 60**,** 918-924.

Xie, Q., Khaoustov, V. I., Chung, C. C., Sohn, J., Krishnan, B., Lewis, D. E. & Yoffe, B. 2002. Effect of tauroursodeoxycholic acid on endoplasmic reticulum stress-induced caspase-12 activation. *Hepatology,* 36**,** 592-601.

Xu, C., Bailly-Maitre, B. & Reed, J. C. 2005. Endoplasmic reticulum stress: cell life and death decisions. *J Clin Invest,* 115**,** 2656-64.

Xu, H., Barnes, G. T., Yang, Q., Tan, G., Yang, D., Chou, C. J., Sole, J., Nichols, A., Ross, J. S., Tartaglia, L. A. & Chen, H. 2003. Chronic inflammation in fat plays a crucial role in the development of obesity-related insulin resistance. *J Clin Invest,* 112**,** 1821-30.

Yadav, R., Larbi, K. Y., Young, R. E. & Nourshargh, S. 2003. Migration of leukocytes through the vessel wall and beyond. *Thromb Haemost,* 90**,** 598-606.

Yaguchi, H., Togawa, K., Moritani, M. & Itakura, M. 2005. Identification of candidate genes in the type 2 diabetes modifier locus using expression QTL. *Genomics,* 85**,** 591-599.

Yamaguchi, H. & Wang, H. G. 2004. CHOP is involved in endoplasmic reticulum stress-induced apoptosis by enhancing DR5 expression in human carcinoma cells. *J Biol Chem,* 279**,** 45495-502.

Yamane, S., Hamamoto, Y., Harashima, S. I., Harada, N., Hamasaki, A., Toyoda, K., Fujita, K., Joo, E., Seino, Y. & Inagaki, N. 2011. GLP‐1 receptor agonist attenuates endoplasmic reticulum stress‐mediated β‐cell damage in Akita mice. *Journal of Diabetes Investigation,* 2**,** 104-110.

Yamauchi, T., Kamon, J., Waki, H., Terauchi, Y., Kubota, N., Hara, K., Mori, Y., Ide, T., Murakami, K., Tsuboyama-Kasaoka, N., Ezaki, O., Akanuma, Y., Gavrilova, O., Vinson, C., Reitman, M. L., Kagechika, H., Shudo, K., Yoda, M., Nakano, Y., Tobe, K., Nagai, R., Kimura, S., Tomita, M., Froguel, P. & Kadowaki, T. 2001. The fat-derived hormone adiponectin reverses insulin resistance associated with both lipoatrophy and obesity. *Nat Med,* 7**,** 941-6.

Yanagishita, M. & Hascall, V. C. 1984. Metabolism of proteoglycans in rat ovarian granulosa cell culture. Multiple intracellular degradative pathways and the effect of chloroquine. *J Biol Chem,* 259**,** 10270-83.

Yang, J.-S., Kim, J. T., Jeon, J., Park, H. S., Kang, G. H., Park, K. S., Lee, H. K., Kim, S. & Cho, Y. M. 2010. Changes in hepatic gene expression upon oral administration of taurine-conjugated ursodeoxycholic acid in ob/ob mice. *PloS one,* 5**,** e13858-e13858.

Ye, J., Rawson, R. B., Komuro, R., Chen, X., Dave, U. P., Prywes, R., Brown, M. S. & Goldstein, J. L. 2000. ER stress induces cleavage of membrane-bound ATF6 by the same proteases that process SREBPs. *Mol Cell,* 6**,** 1355-64.

Ye, Y., Meyer, H. H. & Rapoport, T. A. 2003. Function of the p97–Ufd1–Npl4 complex in retrotranslocation from the ER to the cytosol: dual recognition of nonubiquitinated polypeptide segments and polyubiquitin chains. *The Journal of Cell Biology,* 162**,** 71-84.

Ye, Y., Shibata, Y., Kikkert, M., Van Voorden, S., Wiertz, E. & Rapoport, T. A. 2005. Recruitment of the p97 ATPase and ubiquitin ligases to the site of retrotranslocation at the endoplasmic reticulum membrane. *Proc Natl Acad Sci U S A,* 102**,** 14132-8.

Yoshida, H. 2007. ER stress and diseases. *FEBS J,* 274**,** 630-58.

Yoshioka, M., Kayo, T., Ikeda, T. & Koizumi, A. 1997. A novel locus, Mody4, distal to D7Mit189 on chromosome 7 determines early-onset NIDDM in nonobese C57BL/6 (Akita) mutant mice. *Diabetes,* 46**,** 887-94.

Young, I. D., Ailles, L., Narindrasorasak, S., Tan, R. & Kisilevsky, R. 1992. Localization of the basement membrane heparan sulfate proteoglycan in islet amyloid deposits in type II diabetes mellitus. *Arch Pathol Lab Med,* 116**,** 951-4.

Yuan, Y., Wang, Z. H. & Tang, J. G. 1999. Intra-A chain disulphide bond forms first during insulin precursor folding. *Biochem J,* 343 Pt 1**,** 139-44.

Yurchenco, P. D. 2011. Basement membranes: cell scaffoldings and signaling platforms. *Cold Spring Harb Perspect Biol,* 3.

Zeyda, M. & Stulnig, T. M. 2009. Obesity, Inflammation, and Insulin Resistance – A Mini-Review. *Gerontology,* 55**,** 379-386.

Zhang, D. D. 2006. Mechanistic studies of the Nrf2-Keap1 signaling pathway. *Drug Metab Rev,* 38**,** 769-89.

Zhang, H., Ma, Q., Zhang, Y.-W. & Xu, H. 2012. Proteolytic processing of Alzheimer's β-amyloid precursor protein. *Journal of Neurochemistry,* 120**,** 9-21.

Zhang, J., Fan, Y., Zeng, C., He, L. & Wang, N. 2016. Tauroursodeoxycholic Acid Attenuates Renal Tubular Injury in a Mouse Model of Type 2 Diabetes. *Nutrients,* 8.

Zhang, K. & Kaufman, R. J. 2008a. From endoplasmic-reticulum stress to the inflammatory response. *Nature,* 454**,** 455-462.

Zhang, K. & Kaufman, R. J. 2008b. From endoplasmic-reticulum stress to the inflammatory response. *Nature,* 454**,** 455-62.

Zhang, W., Feng, D., Li, Y., Iida, K., Mcgrath, B. & Cavener, D. R. 2006. PERK EIF2AK3 control of pancreatic beta cell differentiation and proliferation is required for postnatal glucose homeostasis. *Cell Metab,* 4**,** 491-7.

Zheng, C., Yang, Q., Cao, J., Xie, N., Liu, K., Shou, P., Qian, F., Wang, Y. & Shi, Y. 2016. Local proliferation initiates macrophage accumulation in adipose tissue during obesity. *Cell Death Dis,* 7**,** e2167.

Zhong, J., Rao, X., Deiuliis, J., Braunstein, Z., Narula, V., Hazey, J., Mikami, D., Needleman, B., Satoskar, A. R. & Rajagopalan, S. 2013. A Potential Role for Dendritic Cell/Macrophage-Expressing DPP4 in Obesity-Induced Visceral Inflammation. *Diabetes,* 62**,** 149-157.

Zhou, R., Tardivel, A., Thorens, B., Choi, I. & Tschopp, J. 2009. Thioredoxin-interacting protein links oxidative stress to inflammasome activation. *Nature Immunology,* 11**,** 136.

Zhou, Y. P. & Grill, V. E. 1994. Long-term exposure of rat pancreatic islets to fatty acids inhibits glucose-induced insulin secretion and biosynthesis through a glucose fatty acid cycle. *J Clin Invest,* 93**,** 870-6.

Zhou, Y. P., Teng, D., Dralyuk, F., Ostrega, D., Roe, M. W., Philipson, L. & Polonsky, K. S. 1998. Apoptosis in insulin-secreting cells. Evidence for the role of intracellular Ca2+ stores and arachidonic acid metabolism. *Journal of Clinical Investigation,* 101**,** 1623-1632.

Zimmermann, P. & David, G. 1999. The syndecans, tuners of transmembrane signaling. *FASEB J,* 13 Suppl**,** S91-S100.

Ziolkowski, A. F., Popp, S. K., Freeman, C., Parish, C. R. & Simeonovic, C. J. 2012. Heparan sulfate and heparanase play key roles in mouse β cell survival and autoimmune diabetes. *The Journal of Clinical Investigation,* 122**,** 132-141.

Zuber, C., Fan, J. Y., Guhl, B. & Roth, J. 2004. Misfolded proinsulin accumulates in expanded pre-Golgi intermediates and endoplasmic reticulum subdomains in pancreatic beta cells of Akita mice. *FASEB J,* 18**,** 917-9.

Appendix 1: Solutions and reagents

1.1 Free fatty acid analysis

Reagents	Content
0.1 M trisodium citrate	29.4 mg trisodium citrate (Cat. #10242, Merck Pty Ltd., Kilsyth, Vic, Australia) 1 ml dH_2O
Solvent A	Dissolve one bottle of colour A with 10 ml of solvent A
Solvent B	Dissolve one bottle of colour B with 20 ml of solvent B

1.2 Reagents used in islet isolation

Solution	Content
Hanks 10X	100 g/L sodium chloride (Cat. #10241.3000, BDH, Poole, Dorset, UK) 5 g/L potassium chloride (Cat. #7447-48-7, Fronine, AR) 1.25 g/L magnesium sulfate (Cat. #302-500G, Ajax Chemicals, Univar, Syd, Australia) 1.25 g/L magnesium chloride (Cat. # 8147330500, Merck, Darmstadt, Germany) 1.4 g/L calcium chloride (Cat. #10070-500G, BDH, Poole, Dorset, UK) 12.5 g/L Glucose (Cat. #10117.4Y-500G, BDH, Poole, Dorset, UK) Make up to 1L with dH_2O
1 M HEPES	25 g HEPES (Cat. #11344-041, GIBCO, Life Technologies, Carlsbad, CA, USA) 100 ml Hanks balanced salt solution Adjust pH to 7.4
Avertin	70 mM 2, 2, 2, Tribomoethanol (Cat. #T48402, Sigma- Aldrich, St. Louis, MO, USA) 2% (v/v) 2-methyl-2-2 butanol (Fluka Chemie AG, Buch, Switzerland) Made in warm tap water and sterile filtered
Penicillin-Streptomycin-Neomycin (PSN) x 1000	80.7 mM Penicillin G (Cat. #02104537, MP Biomedicals, Santa Ana, CA, USA)

	68.6 mM Streptomycin sulphate (Cat. #S9137, Sigma-Aldrich, St Louis, MO, USA) 5 mM Neomycin sulphate (Cat. #N6386, Sigma-Aldrich, St Louis, MO, USA)
Bovine serum albumin (BSA)	15 g BSA fraction V IgG Free (Cat. # 30063-481, GIBCO, Life Technologies, Carlsbad, CA, USA) 100 ml Hanks balanced salt solution (1x) Sterile filter
Wash medium A	500 ml Hanks 1X 10 ml 1M HEPES 5 ml BSA 1 ml PSN 5 mg DNAse (Cat. # D5025, Sigma-Aldrich, St. Louis, MO, USA)
Wash medium B	90 ml Hanks 1X 2 ml 1M HEPES 10 ml HIFCS (Serana, Bunbury, WA, Australia) 0.2 ml PSN
Collagenase P	12.5 mg Collagenase P (Cat. #11213873001, Roche Diagnostic, Mannheim, Germany) 5 ml wash medium A
Stock dithizone solution	20 mg dithizone (Cat. #D5130-10G, Sigma-Aldrich, St. Louis, MO, USA) 0.6 ml 95% ethanol 1-2 drops of ammonium hydroxide (Ajax Chemicals, Syd, Australia)
Final dithizone solution	0.3 ml stock dithizone solution Up to 100 ml with PBS Adjust pH to 7.4 by 1N HCl
Islet culture medium- Primary beta cell culture medium	40 ml RPMI-1640 (Invitrogen, Carlsbad, CA, USA) 4 ml Heat inactivated fetal calf serum (HIFCS; Sigma-Aldrich, St. Louis, MO, USA) 0.8 ml L-Glutamine (Cat. #25030081, GIBCO, Life Technologies, Carlsbad, CA, USA)

	160 µl PSN
PBS/EDTA	116 mg EDTA (Cat. #180, UNIVAR, Auburn, NSW, Australia) 100 ml PBS

1.3 MIN6 cell line culture medium

Solution	Content
MIN6 culture medium (25 mM glucose)	Dulbecco's modified eagles medium (DMEM) high glucose medium (Cat. #11995, GIBCO, Life Technologies, Carlsbad, CA, USA) 10% HIFCS (Serana, Bunbury, WA, Australia) 15 mM HEPES (#1670218, GIBCO, Life Technologies, Carlsbad, CA, USA) 0.1% (v/v) PSN
6 mM glucose medium	Dulbecco's modified eagles medium (DMEM) low glucose medium (Cat. # 11885 GIBCO, Life Technologies, Carlsbad, CA, USA) 10% HIFCS (Serana, Bunbury, WA, Australia) 15 mM HEPES (#1670218, GIBCO, Life Technologies, Carlsbad, CA, USA) 0.1% (v/v) PSN

1.4 MIN6 Cell harvest treatment

Solution	Content
Trypsin-EDTA (0.5 g/l)	90% (v/v) PBS 10% (v/v) 5 g/l Trypsin (#T4174, Sigma-Aldrich, ST. Louis, MO, USA)

1.5 Trypan blue

Solution	Content
Trypan blue	8 ml 0.5% trypan blue (Fluka, Chemie AG, Buch, Switzerland) 12 ml Saline

1.6 ER stress inducers

Agents	Stock concentration	Working concentration
Thapsigargin (Cat. #T9033-1MG, Sigma-Aldrich, ST. Louis, MO, USA)	1 mM	5 µM or 50 nM prepared in 6 mM glucose medium
Tunicamycin (Cat. #T7765-5MG, Sigma-Aldrich, ST. Louis, MO, USA)	6 mM	2 µM prepared in 6 mM glucose medium
Palmitate/BSA (provided by Dr. Trevor Biden and Dr. Viviane Delghingaro-Augusto)	8 mM (20x concentration)	0.4 mM (1x) prepared in 6 mM glucose medium

1.7 Reagents for real-time RT PCR

Reagents	Content
Diethyl pyrocarbonate (DEPC) water	500 µl DEPC (Cat. # D5758, Sigma-Aldrich, ST. Louis, MO, USA) 500 ml MilliQ water
TaqMan Universal Master Mix	TaqMan 2X Universal Master Mix (Cat. #4318157, Applied Biosystems, Life technologies Ltd., Warrington, UK)
TaqMan Primer/Probes (Applied Biosystems, Foster City, CA, USA)	**Reference genes:** UBC- Mm02525934_g1 GAPDH- Mm99999915_g1 PPIA- Mm02342430_g1 **ER stress genes:** BiP- Mm00517691_m1 P58-Mm01226332_m1 CHOP- Mm01135937_g1 ATF3- Mm00476033_m1
RT mix	4 µl 5x FS buffer (Cat. #18080093, Invitrogen, Carlsbad, CA, USA) 1 µl DTT (Cat. #18080093, Invitrogen, Carlsbad, CA, USA) 1 µl RNase OUT (Cat. #1077-019, Invitrogen, Carlsbad, CA, USA) 1 µl Superscript III (Cat. #18080093, Invitrogen, Carlsbad, CA, USA)

1.8 Steps to deparaffinise and dehydrate pancreas sections

Xylene	**Xylene**	**Absolute ethanol**	**Absolute ethanol**	**90% ethanol**	**70% ethanol**	**Running tap water**
1 min	1 min	10 dips	10 dips	10 dips	10 dips	5 mins or 2 mins

1.9 Reagents used in immunohistochemistry

Solution	**Content**
0.1 N acetic acid	2.9 ml glacial acetic acid (Cat. #10235, BDH, Poole, Dorset, UK) 500 ml dH_2O
0.1 M Sodium acetate	0.68 g anhydrous sodium acetate (Cat. #D3247, UNIVAR, Ajax Chemicals, Syd, Australia) 500 ml dH_2O
0.1 M Acetate buffer	10.5 ml 0.1N acetic acid 39.5 ml 0.1M sodium acetate (Cat. #679, UNIVAR, Auburn, NSW, Australia)
3% H_2O_2	25 ml 30% H_2O_2 (Cat. # HA154, Chem-Supply Pty. Ltd, Gillman, SA, Australia) 225 ml Methanol (EMSURE, Merck, Darmstadt, Germany)
Peroxidase block (stock)	10 µl 30% H_2O_2 10 ml Methanol
Peroxidase block (working solution)	5 ml of H_2O_2/Methanol solution (Stock peroxidase block) 28 µl 18% sodium azide (Sigma-Aldrich, St. Louis, MO, USA)
AEC stock solution	40 mg AEC (Cat. #A5754, Sigma-Aldrich, St. Louis, MO, USA) 5 ml N-N-dimethyl formamide (Cat. #D158550, Sigma-Aldrich, St. Louis, MO, USA)
AEC working solution	4.75 ml acetate buffer 0.25 ml AEC stock solution 25 µl 3% H_2O_2 (Cat. #HA154-500M, Chem Supply, Bedford St., SA, Australia) Sterile filter a 0.2 µm CR filter
Ammonium H_2O	100 µl concentrated ammonium 250 ml dH_2O

Pronase	2.5 mg Pronase (Cat. #537088, Calbiochem, EMD Millipore, Darmstadt, Germany) 5 ml dH_2O
M.O.M Ig block	2.5 ml PBS 2 drops of M.O.M Ig blocking reagent (PK-2200, Vector Laboratories Inc., Burlingame, CA, USA)
Animal Free block (AFB)	0.5 ml AFB 5X 2 ml dH_2O
M.O.M diluent	2.5 ml PBS 200 µl M.O.M protein concentrate (PK-2200, Vector Laboratories Inc., Burlingame, CA, USA)
Citrate buffer (10 mM)	1.05 g citric acid (Cat. #CA014, Chem Supply, Gillman, SA, Australia) 500 ml dH_2O Adjust pH to 6 using 10 M and 2.5 M sodium hydroxide (Ajax Chemicals, Syd, Australia) solution
MOM VECTASTAIN ABC reagent (PK-2200, Vector Laboratories Inc., Burlingame, CA, USA)	2.5 ml PBS 2 drops of reagent A 2 drops of reagent B

1.10 Antibodies used for HSPG core proteins immunohistochemistry

Common name	Specific name	Catalogue number	Stock concentration	Company	Dilution used
Syndecan-1	Purified Rat anti-mouse CD138 mAb	#553712	0.5 mg/ml	BD Biosciences	1/10 (50 µg/ml)
Rat IgG_{2ak}	Purified Rat IgG_{2ak}, isotype control	#559073	0.5 mg/ml	BD Biosciences	1/10 (50 µg/ml)
CD44	Purified NA/LE Rat anti-mouse CD44	#553130	1 mg/ml	BD Biosciences	1/25 (40 µg/ml)
Rat IgG_{2bk}	Purified NA/LE Rat IgG_{2bk}, isotype control	#555845	1 mg/ml	BD Biosciences	1/25 (40 µg/ml)
CD44v3	Human CD44v3 Monoclonal Mouse IgG_{2b} Clone # 3G5	#BBA11	0.5 mg/ml	R&D systems	1/50 (10 µg/ml)
Mouse IgG_{2b}	Purified mouse IgG_{2bk}, isotype control	#557351	0.5 mg/ml	BD Pharmingen	1/50 (10 µg/ml)
Collagen type XVIII	Collagen type XVIII sc-32720 mouse monoclonal IgG_{2b}	#COL18A1 (1837-46)	200 µg/ml	Santa Cruz Biotechnology	1/25 (8 µg/ml) 1/50 (4 µg/ml)
Mouse IgG_{2b}	Purified mouse IgG_{2bk}, isotype control	#557351	0.5 mg/ml	BD Pharmingen	1/62.5 (8 µg/ml) 1/125 (4 µg/ml)
Rabbit anti-rat Ig-HRP	Polyclonal rabbit anti-rat immunoglobulins/ HRP	#P0450	1.3 g/L	DAKO	1/50 (26 µg/ml) 1/25 (52 µg/ml)
Rabbit anti-mouse Ig-HRP	Polyclonal rabbit anti-mouse immunoglobulins/ HRP	#P0161	1.3 g/L	DAKO	1/50 (26 µg/ml)

1.11 Antibodies used for Hormone stain

Common name	Specific name	Catalogue number	Stock concentration	Company	Dilution used
Insulin	Monoclonal anti-insulin	#I2018	32.5216 mg/ml	Sigma	1/500 (65 µg/ml) or 1/125 (260 µg/ml)
Glucagon	Monoclonal anti-glucagon clone K79bB10	#G2654	57.0539 mg/ml	Sigma	1/500 (114 µg/ml) or 1/1000 (57 µg/ml)
Mouse IgG_{1k}	Purified mouse IgG_{ik}, isotype control, clone P3	#14-4714-85	0.5 mg/ml	eBioscience	1/7.7 (64.9 µg/ml) or 1/8.8 (227.3 µg/ml)
M.O.M biotinylated anti-mouse IgG	Vector M.O.M immunodetection kit	#PK-2200	unknown	Vector Laboratories Inc.	1/250
Proinsulin	Recombinant human proinsulin coupled to bovine thyroglobulin GS-9A8-C	unknown	212 µg/µl	Developmental Studies Hybridoma Bank (DSHB) by Madsen, O.D.	1/800

1.12 Antibodies used for HS immunohistochemistry

Common name	Specific name	Catalogue number	Stock concentration	Company	Dilution used
10E4	Clone F58-10E4	#370255-1	1 mg/ml	Amsbio	1/5 (200 µg/ml)
HepSS-1	Clone HepSS-1	#270426-1	1 mg/ml	Seikagaku	1/10 (100 µg/ml)
Mouse IgM	Purified mouse IgM_k isotype control	#550340	250 µg/ml	BD Pharmingen	1/1.25 (200 µg/ml)
Rabbit anti-mouse IgHRP	Polyclonal rabbit anti-mouse immunoglobulins/HRP	#P0161	1.3 g/L	DAKO	1/50 (26 µg/ml)
EV3C3	It was a gift from Dr. Toin Van Kuppevelt, University of Nijmegen, The Netherlands				1/2
Rabbit anti-VSV-G	Vesicular Stomatitis Virus glycoprotein (VSV-G) antibody produced in rabbit	#V4888	1 mg/ml	Sigma-Aldrich	1/100 (10 µg/ml)
Swine anti-rabbit HRP	Polyclonal swine anti-rabbit immunoglobulin/HRP	#P0217	1.3 g/L	DAKO	1/100 (13 µg/ml)
HS3A8	It was a gift from Dr. Toin Van Kuppevelt, University of Nijmegen, The Netherlands				7/10

1.13 Buffers used in immunofluorescence staining for flow cytometry

Solution	Content
FACs wash buffer	Phosphate buffered saline (PBS) 5% (v/v) HIFCS
BD wash buffer (Cat. #554714, BD Biosciences, Dickinson, San Diego, CA, USA)	90% (v/v) deionised water 10% (v/v) 10x stock BD wash solution

1.14 Antibodies used for cell surface and intracellular staining

Antibody/Dye	Stock concentration	Working concentration	company	Catalogue
Purified rat anti-mouse CD16/CD32 (mouse Fc block)	0.5 mg/ml	5 µg/ml (1/100)	BD Biosciences	553142
Purified Rat anti- mouse CD138 (syndecan-1) mAb	0.5 mg/ml	20 µg/ml (1/25)	BD Biosciences	553712
Purified NA/LE Rat anti-mouse CD44 (CD44)	1 mg/ml	40 µg/ml (1/25)	BD Biosciences	553130
Anti-heparan sulfate F58-10E4 (HS)	1 mg/ml	20 µg/ml (1/50)	(i) Seikagaku corporation (ii) Amsbio	370255-1
Collagen type XVIII	0.2 mg/ml	4 µg/ml (1/50)	Santa Cruz Biotechnology	1837-46
HP3/17 (Hpse)	150 µg/ml	1.5 µg/ml (1/100)	Insight biopharmaceuticals Ltd.	INS-26-1-0000-12
Goat anti-Mouse Ig PE	0.25 mg/ml	5 µg/ml (1/50)	Southern Biotech	1012-09
Mouse anti-rat kappa PE Rat	0.1 mg/ml	2 µg/ml (1/50)	Southern Biotech	3090-09
Rat anti- Mouse Ig FITC	0.5 mg/ml	10 µg/ml (1/50)	BD Biosciences	553395

*The working concentration of mAbs was prepared either in FACs wash buffer for cell surface staining or in BD wash buffer for intracellular staining.

1.15 Fluorescent dyes used in flow cytometry

Antibody/Dye	Stock concentration	Working concentration	company	Catalogue
7-aminoactinomycin D (7AAD)	1 mg/ml	10 µg/ml prepared in PBS	Life Technologies	A1310
Calcein AM	0.5 mM	0.04 µM prepared in PBS	Life Technologies	C3100MP
Propidium iodide	50 µg/ml	2.5 µg/ml prepared in PBS	BD Biosciences	51-66211E
Sytox Green	5 mM	31.25 nM prepared in PBS	Life technologies	S7020

1.16 Reagents for preparing adipose and peripheral blood leukocytes

Reagents	Content
FACs wash buffer	Phosphate buffered saline (PBS) 5% (v/v) HIFCS
Red cell lysis buffer (RCLB)	4.17 g ammonium chloride (Cat. #04217, Ajax Chemicals Ltd., Sydney, Australia) 0.0185 g EDTA (Cat. # 180, UNIVAR, Auburn, NSW, Australia) 0.5 g NAHCo3 (Cat. #D3247, Ajax Chemicals Ltd., Sydney, Australia) Upto 500 ml with dH_2O pH: 7.3 and sterile filter
Buffered saline glucose citrate (BSGC)	116 mM sodium chloride (Cat. #SA046, Chem Supply Pty. Ltd., Gillman SA, Australia) 13.6 mM trisodium citrate (Cat. #10242, Merck Pty Ltd., Kilsyth, Vic, Australia) 8.6 mM Na2HPO4 (Cat. #310537, Ajax Chemicals Ltd., Sydney, Australia) 1.6 mM KH2PO4 (Cat. #391-500MG, Ajax Finechem, Thermo Fischer Scientific, NSW, Australia) 0.9 mM EDTA (Cat. # 180, UNIVAR, Auburn, NSW, Australia) 11.1 mM Glucose (Cat. #783-500MG, Ajax Finechem, Thermo Fischer Scientific, NSW, Australia) Up to 500 ml with dH_2O and sterile filter
Digestion Buffer	1 ml 0.5% BSA (Cat. # 30063-481, GIBCO, Life technologies, Carlsbad, CA, USA) 100 ml Hanks
Collagenase Solution (Cat. #C6885, Sigma-Aldrich, ST. Louis, MO, USA)	10 mg/ml in digestion buffer Sterile filter Final concentration 1 mg/ml
EDTA	0.5 M EDTA (Cat. # 180, UNIVAR, Auburn, NSW, Australia)

1.17 Antibodies/fluorochromes used for analyzing heparanase expression in leukocyte sub-populations

Antibody/Dye	Stock concentration	Working concentration	Company	Catalogue
Purified rat anti-mouse CD16/CD32 (mouse Fc block)	0.5 mg/ml	5 µg/ml (1/100)	BD Biosciences	553142
HP3/17 (Hpse)	150 µg/ml	1.5 µg/ml (1/100)	Insight Biopharmaceuticals Ltd.	INS-26-1-0000-12
Goat α Mouse Ig PE	0.25 mg/ml	2.5 µg/ml (1/100)	Southern Biotech	1012-09
PE-CF 594 Hamster ant-mouse CD11c	0.2 mg/ml	2 µg/ml (1/100)	BD Biosciences	562454
PerCP-Cy5.5 rat anti-mouse CD45R/B220	0.2 mg/ml	2 µg/ml (1/100)	BD Biosciences	552771
PE-Cy7 rat anti-mouse Ly6G	0.2 mg/ml	2 µg/ml (1/100)	BD Biosciences	560601
BV-421 rat anti- mouse Siglec F	0.2 mg/ml	2 µg/ml (1/100)	BD Biosciences	562681
APC Anti-mouse CD45.2	0.2 mg/ml	2 µg/ml (1/100)	eBioscience	17-0454-82
Alexa Fluor 700 rat anti-mouse CD11b	0.2 mg/ml	2 µg/ml (1/100)	BD Biosciences	557960
APC-Cy7 hamster anti-mouse CD3e	0.2 mg/ml	4 µg/ml (1/50)	BD Biosciences	557596
BV 605 rat anti-mouse Ly6C	0.2 mg/ml	2 µg/ml (1/100)	BD Biosciences	563011

1.18 Reagents for *in vivo* treatment

Treatment	Stock	Volume
PI-88 (10 mg/kg/day, i.p.) (Progen Pharmaceuticals Ltd., Brisbane, Australia)	2 mg/ml in 0.9% saline	Mouse weight= w (g) Volume of PI-88= w x 0.01 mg/g/day x (1000 µl/2mg) =5w (µl) Example: For 25 g mouse, dose (volume) of PI-88= 5 x 25= 125 µl
TUDCA (150 mg/kg/day, i.p.) (Cat. #580549, Calbiochem, EMD Millipore, Darmstadt, Germany)	30 mg/ml in 0.9% saline	Mouse weight= w (g) Volume of TUDCA= w x 0.15 mg/g/day x (1000 µl/30 mg) =5w (µl) Example: For 25 g mouse, dose (volume) of TUDCA= 5 x 25= 125 µl

Appendix 2: Cell surface heparanase expression on immune cells

Appendix 2.1: Normalised cell surface heparanase expression on immune cells of female db/db mice

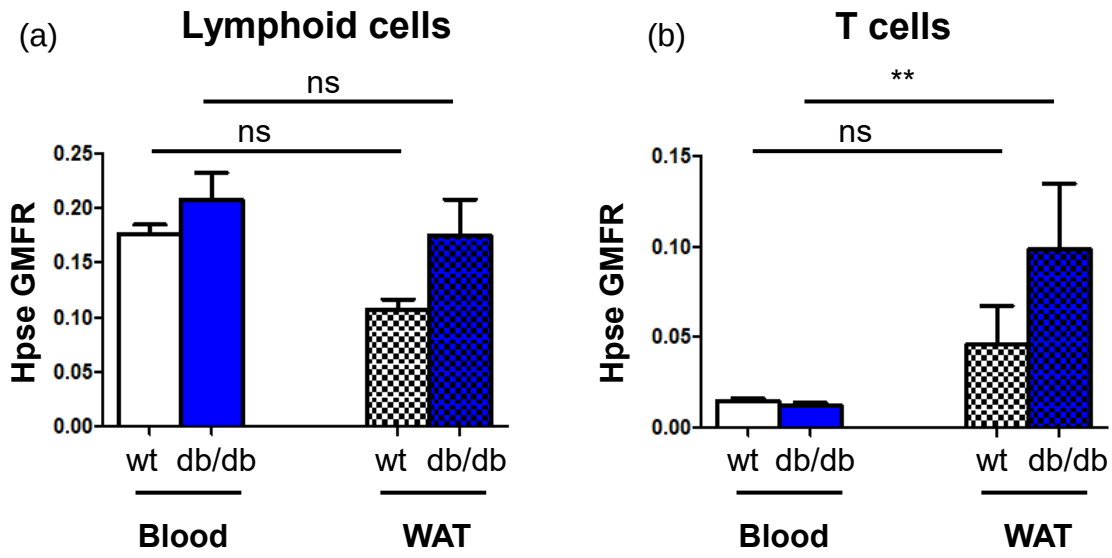

Figure 2.1.1: Hpse expression in lymphoid cells in PB and WAT of female wt and db/db mice.

Peripheral blood (PB) and the stromal vascular fraction (SVF) from peri-ovarian white adipose tissue (WAT) of wt and db/db female mice (5-9 weeks of age) were stained for leukocyte markers and heparanase and analysed by flow cytometry, using the gating strategy in Figures 2.13 and 2.14. The cell surface expression of Hpse for lymphoid cells in PB and WAT of wt and db/db mice was normalised to the levels of Hpse expressed by B lymphocytes. Relative Hpse expression is shown as the geometric mean fluorescence ratio (GMFR). T cells showed an increase in Hpse GMFR in db/db WAT compared to blood. The data represent the mean ± SEM for n= 5-7 mice/group. General ANOVA with Fisher's unprotected LSD post-test; *P<0.05, **P<0.01, ***P<0.0001 and ns, not significant.

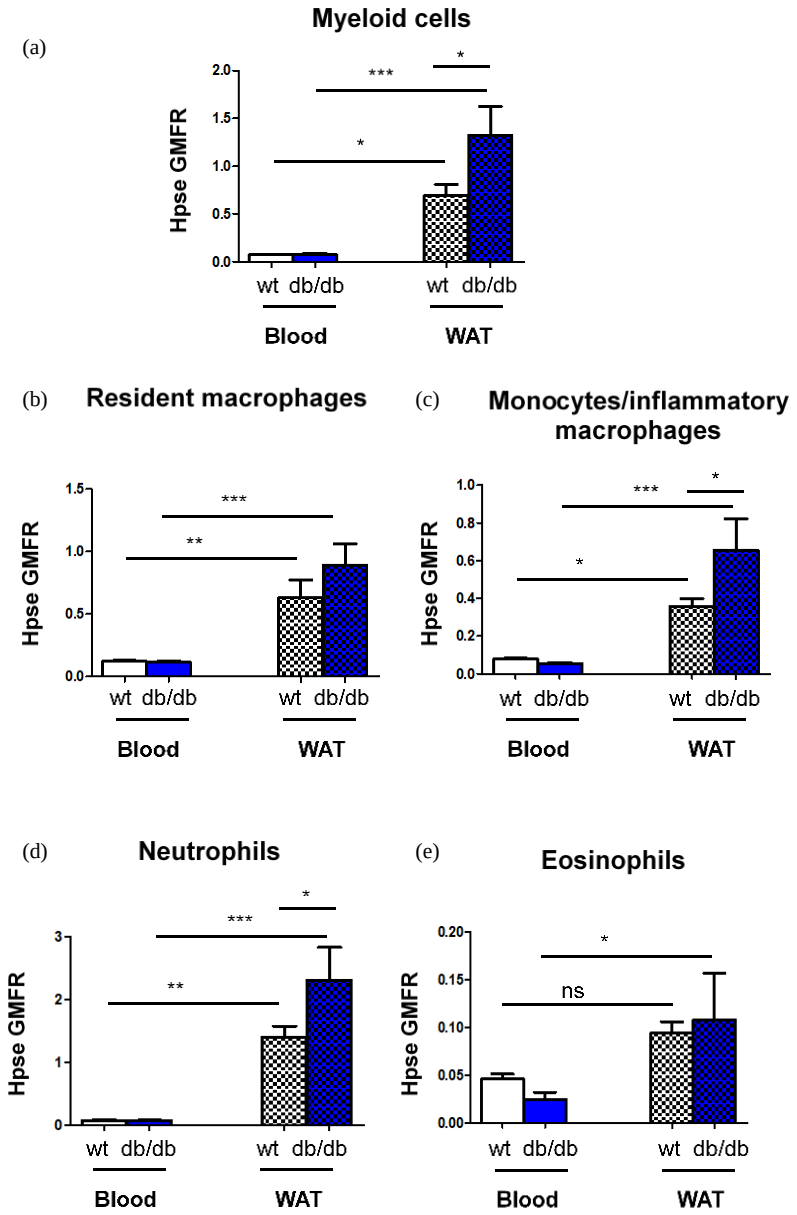

Figure 2.1.2: Hpse expression by myeloid leukocytes in PB and WAT of female wt and db/db mice.

Heparanase expression on total myeloid cells and myeloid sub-populations in peripheral blood (PB) and stromal vascular fraction (SVF) from peri-ovarian white adipose tissue (WAT) was determined in wt and db/db female mice at 5-9 weeks of gate by flow cytometry (see Figures 2.13 and 2.14, Section 2.10). The cell surface Hpse expression was normalised to the levels of Hpse expressed by B lymphocytes and is shown as the geometric mean fluorescence ratio (GMFR). Hpse GMFR was highly expressed by total myeloid cells in WAT compared to PB of wt and db/db mice. The data represent the mean ± SEM for n= 5-7 mice/group. General ANOVA with Fisher's unprotected LSD post-test; *P<0.05, **P<0.01, ***P<0.001 and ns, not significant.

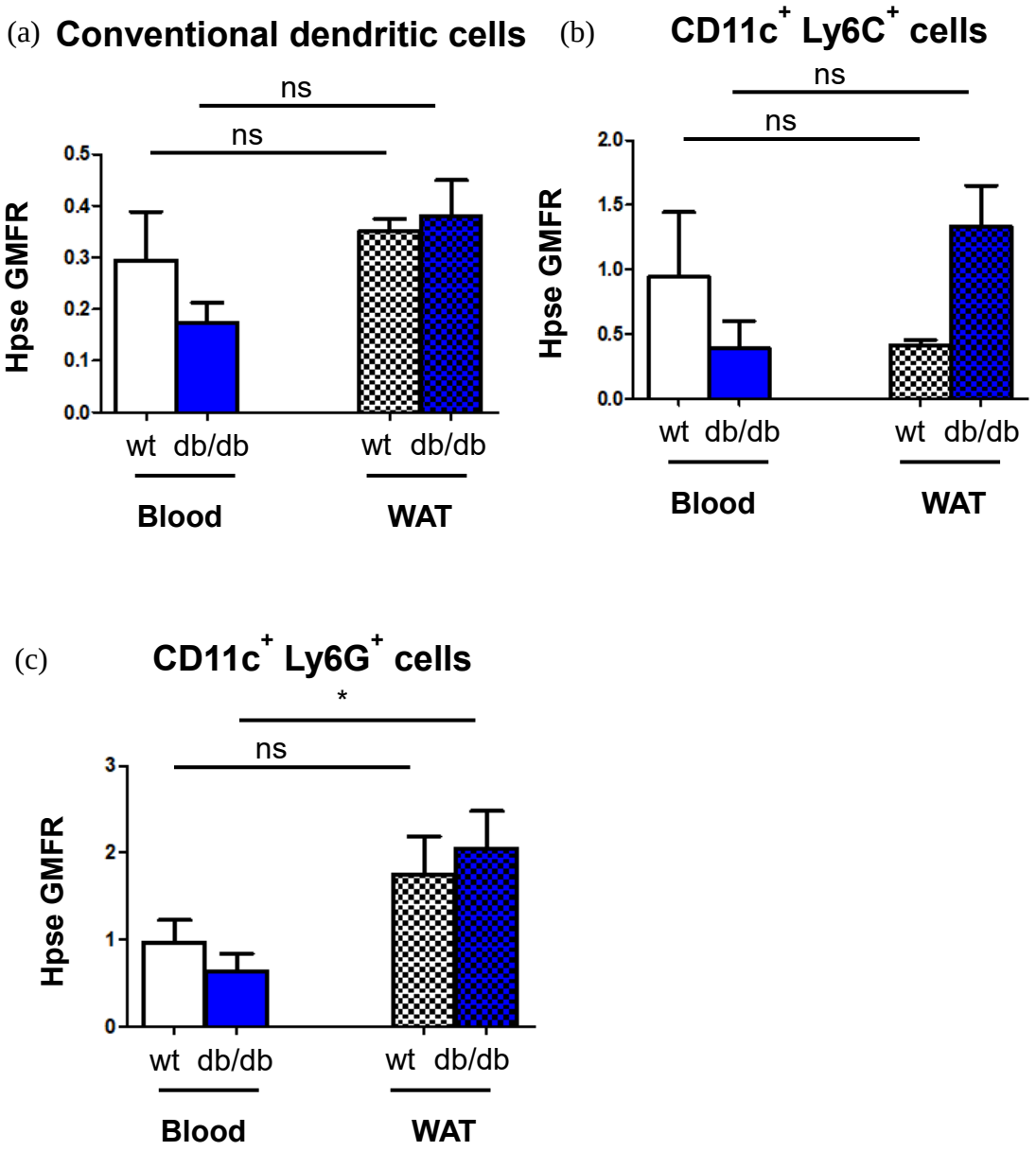

Figure 2.1.3: Hpse expression by CD11c$^+$ cells in PB and WAT of female wt and db/db mice.

The cell surface expression of heparanase (Hpse) on CD11c$^+$ leukocytes in peripheral blood (PB) and stromal vascular fraction (SVF) from peri-ovarian white adipose tissue (WAT) of female wt and db/db mice was determined by flow cytometry, using the gating strategy in Figure 2.13 and 2.14, (Section 2.10). Hpse expression was normalised to Hpse levels expressed by B lymphocytes and the data is shown as the geometric mean fluorescence ratio (GMFR). Hpse GMFR by CD11c$^+$Ly6G$^+$ cells were increased in db/db WAT compared to blood. The data represent the mean ± SEM for n= 5-7 mice/group. General ANOVA with Fisher's unprotected LSD post-test; ns, not significant.

Appendix 2.2: Cell surface heparanase (Hpse) expression by immune cells (represented as GMFR) in peripheral blood and WAT of male wildtype and db/db mice.

Cell type	Peripheral blood (Hpse GMFR)¶		WAT (Hpse GMFR)¶	
	wildtype	db/db	wildtype	db/db
Lymphoid	0.19 ± 0.02	0.20 ± 0.01	0.09 ± 0.00	0.19 ± 0.05
T cell	0.02 ± 0.00	0.02 ± 0.00	0.02 ± 0.01	0.03 ± 0.01
cDC	0.31 ± 0.18	0.28 ± 0.08	0.74 ± 0.26	1.00 ± 0.49
$CD11c^{+}Ly6C^{+}$	0.33 ± 0.23	3.79 ± 2.08	0.88 ± 0.28	2.76 ± 1.91
$CD11c^{+}Ly6G^{+}$	0.72 ± 0.18	2.19 ± 0.82	3.58 ± 1.07	7.54 ± 5.26
Myeloid	0.10 ± 0.02	0.08 ± 0.01	1.58 ± 0.19***	1.98 ± 0.34***
Mono/Inf Mf	0.09 ± 0.02	0.07 ± 0.01	0.45 ± 0.07*	0.68 ± 0.14***
Res Mf	0.12 ± 0.03	0.14 ± 0.02	0.75 ± 0.07**	0.83 ± 0.17***
Eosinophil	0.05 ± 0.01	0.03 ± 0.01	0.10 ± 0.01	0.18 ± 0.05*
Neutrophil	0.11 ± 0.03	0.08 ± 0.01	2.29 ± 0.31***	3.35 ± 0.46***

¶The data represent the mean ± SEM for n= 5-7 mice/group. Cell surface Hpse on immune cells was normalised to the Hpse expression of B lymphocytes. The data show the geometric mean fluorescence ratio (GMFR). General ANOVA with Fisher's unprotected LSD post-test for comparisons between peripheral blood and white adipose tissue of wildtype (grey) or db/db (blue) mice; *P<0.05, **P<0.01, ***P<0.001. GMFR, geometric mean fluorescence ratio; Mono/Inf Mf, monocyte (blood)/inflammatory macrophages (WAT); Res Mf, resident macrophages; cDC, conventional dendritic cell.

Appendix 3: Comparison of optical density and % islet area stained in TUDCA-treated db/db islets

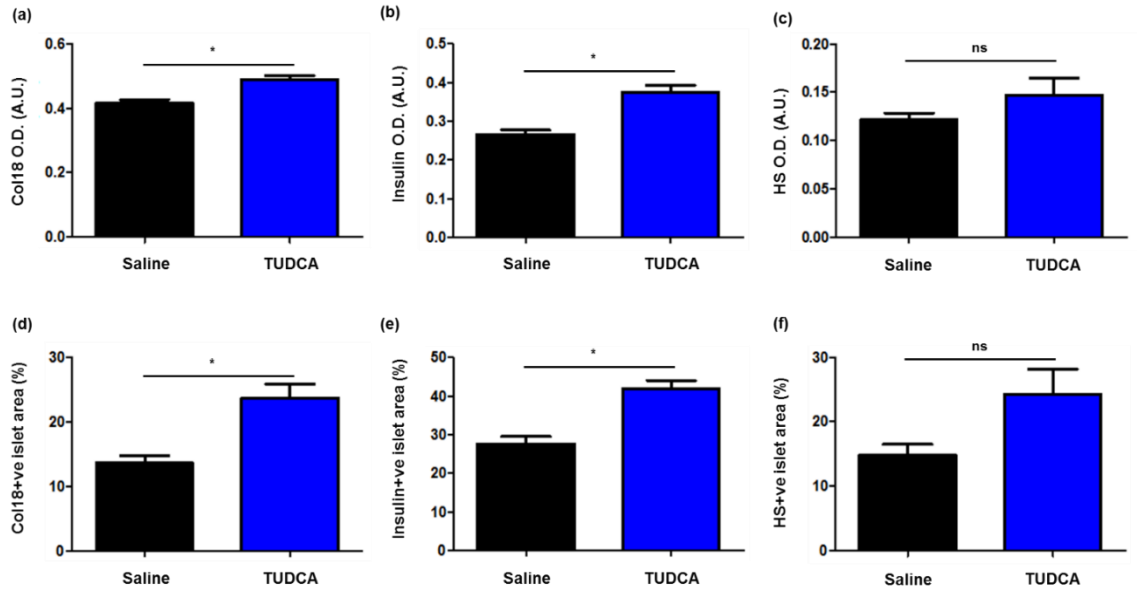

Appendix 3: Expression of intra-islet collagen type XVIII, insulin and HS in pancreases from saline and TUDCA treated db/db mice.

4 week old male db/db mice were treated with saline (black bar) or TUDCA (150 mg/kg/day; blue bar) i.p. for 28 days. After termination of treatment, the pancreas was harvested and collagen type XVIII (Col18), insulin and heparan sulfate (HS) expression were localised in the islets by immunohistochemistry. Bar graphs show significant differences between groups using optical density (O.D./staining intensity) analysis (a-c) or threshold-based analysis of % islet area stained (d-f). Compared to saline controls, TUDCA-treated db/db islets showed a significant increase in the staining intensity of Col18 (a) and insulin (b) which was confirmed by the corresponding analysis of % islet area stained (d, e). No significant difference was observed between optimal density/staining intensity (c) or threshold-based % islet area stained (f) when the comparison was performed within same mouse strain (db/db). The data represent mean ± SEM for n= 8-9 pancreases/group with n= 86-88 (Col18) and n= 92-105 (insulin) islets analysed/group; 4 pancreases/group with n=38-44 islets analysed/group for HS. Non-parametric Mann-Whitney test; *P<0.0001 and ns, not significant.